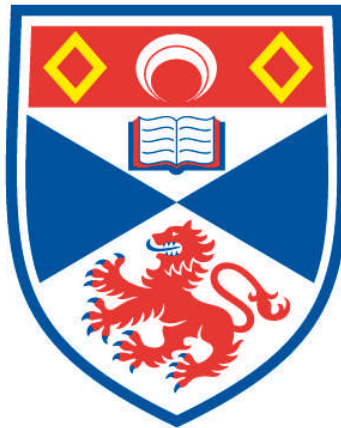


**A THEORETICAL STUDY OF THE R. CORONAE
BOREALIS GROUP OF VARIABLE STARS**

GRAHAM A. P. WILLINGALE

**A Thesis Submitted for the Degree of PhD
at the
University of St Andrews**



1990

**Full metadata for this item is available in
Research@StAndrews:FullText
at:**

<http://research-repository.st-andrews.ac.uk/>

Please use this identifier to cite or link to this item:

<http://hdl.handle.net/10023/4656>

This item is protected by original copyright

**This item is licensed under a
Creative Commons License**

A THEORETICAL STUDY OF THE
R CORONAE BOREALIS
GROUP OF VARIABLE STARS

BY

GRAHAM P. H. WILLINGALE

A thesis submitted to the university of St. Andrews in application for
the degree of doctor of philosophy.

April, 1989.



BEST COPY

AVAILABLE

PAGE NUMBERS AND
TEXT CUT OFF IN
ORIGINAL THESIS

To my parents, without whom this thesis
would never have come to fruition.

The glory of the stars makes the beauty
of the sky, a brilliant decoration to
the heights of the Lord. At the words
of the Holy One they stand as he
decrees, and never grow slack of their
watch.

Ecclesiasticus 43, verses 9-11.

Certificate

I hereby certify that the candidate has fulfilled the conditions of the resolution and regulations appropriate to the degree of Ph. D. of the University of St. Andrews and that he is qualified to submit this thesis in application for that degree.



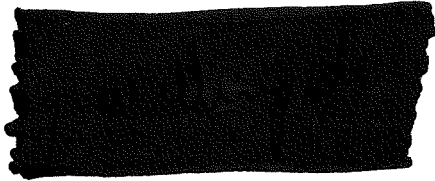
T. R. CARSON

(Supervisor)

Declaration

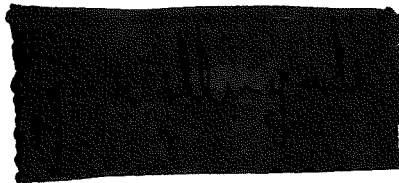
I, Graham Percy Henry Willingale, hereby certify that this thesis, which is approximately 65,000 words in length, has been written by me, and that it has not been submitted in any previous application for a higher degree.

I was admitted as a research student under Ordinance No. 12 on the 1st. October, 1984 and as a candidate for the degree of Ph. D. on the 1st. October, 1985; the higher study for which this is a record was carried out in the University of St. Andrews between 1984 and 1988.



G. P. H. WILLINGALE

In submitting this thesis to the university of St. Andrews I understand that I am giving permission for it to be made available for use in accordance with the regulations of the University Library for the time being in force, subject to the copyright vested in the work not being affected thereby. I also understand that the title and abstract will be published, and that a copy of the work may be made and supplied to any BONA FIDE library or research worker.



G. P. H. WILLINGALE

Abstract

A theoretical study of the R Coronae Borealis group of variables is presented. A modified Christy code is used for the non-linear calculations and Dr Worrell's codes are used for the linear calculations. These codes are used in conjunction with both Carson and Los Alamos opacity tables, following the work of Saio on the linear analysis of Hydrogen deficient Carbon stars. 630 linear models are presented in 3 surveys along with 10 non-linear models of RCB stars and 20 incidental models used for comparison purposes.

A study of the observations, given in the literature showed that the masses and luminosities of these stars are poorly defined. A linear analysis of 7 of these stars, in conjunction with observations given in literature, has allowed luminosity limitations to be placed on seven of these stars, and for the two stars which also have spectroscopic data a rough mass was calculable. The spectroscopic mass and luminosity limits of R CrB are $(0.96 \pm 0.07)M_{\odot}$ and $(9,500 - 16,500)L_{\odot}$ and for RY Sgr are $(0.95 \pm 0.06)M_{\odot}$ and $(9,000 - 13,000)L_{\odot}$. A non-linear model of RY Sgr using the best mass and luminosity produced a light curve that agreed well with the overall characteristics of the observations, i.e., period, amplitude and semi-regularity. Another of the non-linear models showed a 7^m drop in its luminosity curve, which lasted for about twenty days. This is greatly short of the months to years seen in the observations, but could be suggestive of the initiation of the 'deep minimum' phenomenon. It was followed by the rapid outward movement of all the outer zones, which could indicate a method of ejecting carbon grains. Further research needs to be done before any conclusions can be drawn.

The non-linear analysis of the 5,000K and 6,000K models may indicate that the effective temperatures given in the literature for these stars are too low, as a value nearer 7,000K seems to give better results. From this analysis, it seems that the majority of the RCB group of stars have masses in the range $(0.8 - 1.2)M_{\odot}$, which is consistent with the evolutionary analysis of Weiss.

CONTENTS

1 INTRODUCTION

- 1.1 What is a Variable Star ?1- 1
- 1.2 Aims, Hopes and Aspirations.....1- 4

REVIEW

2 OBSERVATIONS OF THE RCB GROUP

- 2.1 Introduction.....2- 1
- 2.2 Review of the RCB Group
 - 2.2.1 Definitions and distribution.....2- 1
 - 2.2.2 Abundances and effective temperature.....2- 5
 - 2.2.3 Luminosity and mass.....2- 7
 - 2.2.4 Variability of some RCB stars.....2- 8
 - 2.2.5 Deep Minima.....2- 9
 - 2.2.6 Infra-red excesses.....2-11
- 2.3 Individual Stars
 - 2.3.1 Variable RCB stars
 - 2.3.1.1 R Coronae Borealis.....2-13
 - 2.3.1.2 RY Sagittarii.....2-21
 - 2.3.1.3 S Apodis.....2-26
 - 2.3.1.4 UW Centauri.....2-28
 - 2.3.1.5 LR Scorpii.....2-30
 - 2.3.1.6 XX Camelopardis.....2-30
 - 2.3.2 Other RCB stars
 - 2.3.2.1 UV Cassiopeiae.....2-30
 - 2.3.2.2 SU Tauri.....2-34
 - 2.3.2.3 W Mensae.....2-35
 - 2.3.2.4 WX Coronae Australis.....2-35
 - 2.3.2.5 RS Telescopii.....2-36
 - 2.3.2.6 RZ Normae.....2-38
 - 2.3.2.7 U Aquarii.....2-38
 - 2.3.3 Hot RCB stars
 - 2.3.3.1 DY Centauri.....2-40
 - 2.3.3.2 V348 Sagittarii.....2-40
 - 2.3.3.3 MV Sagittarii.....2-42
- 2.4 Review of Linear Models.....2-44
- 2.5 Review of Non-Linear Models.....2-52
- 2.6 Evolution of the RCB Group.....2-55
- 2.7 Summary of RCB Observations.....2-59

CONTENTS

THEORY

3 PULSATION THEORY

3.1 Introduction.....	3- 1
3.2 Assumptions and Definitions.....	3- 4
3.3 Conservation of Mass.....	3- 6
3.4 Conservation of Momentum.....	3- 7
3.5 Conservation of Energy.....	3- 9
3.6 Transport Equations.....	3-12
3.7 Boundary Conditions.....	3-13
3.8 Shocks and Profiles.....	3-15

4 THE PHYSICS

4.1 The Equation of State

4.1.1 General Overview of the Problem.....	4- 1
4.1.2 Diatomic Molecules.....	4- 4
4.1.3 Triatomic Molecules.....	4- 7
4.1.4 Free Ions.....	4-11

4.2 Stellar Opacities.....	4-14
----------------------------	------

COMPUTATIONAL SHEMES

5 DIFFERENCING THE NON-LINEAR EQUATIONS

5.1 Preliminaries.....	5- 1
5.2 Differencing The Continuity Equation.....	5- 3
5.3 Differencing The Momentum Equation.....	5- 3
5.4 Differencing The Energy Equation.....	5- 5
5.5 The Luminosity Interpolation.....	5- 6
5.6 Solving The Differenced Energy Equations.....	5- 7
5.7 Time Step.....	5-10
5.8 Model Output On Completing a Period.....	5-11

6 LINEAR EQUATIONS

6.1 The Basic Equations.....	6- 1
6.2 The Linear Non-adiabatic Hydro-Dynamic Equations.....	6- 2
6.3 Solving The Linear Non-Adiabatic Equations.....	6- 8
6.4 The Stability Coefficient and Work Integral for Linear Pulsation.....	6-11

CONTENTS

RESULTS

7 LINEAR NON-ADIABATIC RESULTS

7.1 Introduction.....	7- 1
7.2 The why and where of the surveys.....	7- 3
7.3 Results of the Survey Using Opacity Table R040	
7.3.1 A Detailed Discussion of One Model.....	7- 8
7.3.2 Fundamental Eigenfunctions of the $1 M_{\odot}$ Models.....	7- 11
7.3.3 Presentation of Results	
7.3.3.1 Survey results for $0.8 M_{\odot}$ models.....	7- 21
7.3.3.2 Survey results for $1.0 M_{\odot}$ models.....	7- 26
7.3.3.3 Survey results for $1.2 M_{\odot}$ models.....	7- 31
7.3.4 A Discussion of The Survey Results.....	7- 36
7.4 Results of the Survey Using Opacity Table R040	
7.4.1 A Detailed Discussion of One Model.....	7- 40
7.4.2 Fundamental Eigenfunctions of the $1 M_{\odot}$ Models.....	7- 44
7.4.3 Presentation of Results	
7.4.3.1 Survey results for $0.8 M_{\odot}$ models.....	7- 54
7.4.3.2 Survey results for $1.0 M_{\odot}$ models.....	7- 59
7.4.3.3 Survey results for $1.2 M_{\odot}$ models.....	7- 64
7.4.4 A Discussion of The Survey Results.....	7- 69
7.5 Results of the Survey Using Opacity Table R040	
7.5.1 A Detailed Discussion of One Model.....	7- 73
7.5.2 Fundamental Eigenfunctions of the $1 M_{\odot}$ Models.....	7- 74
7.5.3 Presentation of Results	
7.5.3.1 Survey results for $0.8 M_{\odot}$ models.....	7- 87
7.5.3.2 Survey results for $1.0 M_{\odot}$ models.....	7- 92
7.5.3.3 Survey results for $1.2 M_{\odot}$ models.....	7- 97
7.5.4 A Discussion of The Survey Results.....	7-102
7.6 Mass-Luminosity Limits For 7 Variable RCB Stars.....	7-105
7.7 Conclusion.....	7-113

CONTENTS

RESULTS

8 NON-LINEAR NON-ADIABATIC RESULTS

8.1 Introduction.....	8- 1
8.2 Preliminary Tests	
8.2.1 Calculation of state variables.....	8- 3
8.2.2 Calculation of opacity.....	8- 9
8.2.3 How viscous should a star be ?	8-16
8.2.4 Boundary conditions and diluted radiation.....	8-18
8.2.5 How much star ?	8-19
8.2.6 Re-zoning a static model envelope.....	8-20
8.2.7 Other considerations.....	8-21
8.3 Choosing the Opacity Table for Non-linear RCB Modelling	
8.3.1 Effects of input parameters on non-linear DXIX model.....	8-23
8.3.2 A brief look at some models of DY Centauri.....	8-28
8.4 Non-linear Models of 7 Variable RCB Stars	
8.4.1 The models of the 5,000 K RCB variables	
8.4.1.1 GU Sagittarii.....	8-46
8.4.1.2 RS telescopii.....	8-58
8.4.1.3 RT Normae and WX Coronae Australis.....	8-63
8.4.1.4 The 6,000 K models of UW Centauri.....	8-64
8.4.2 The models of the 7,000 K RCB variables	
8.4.2.1 RY Sagittarii.....	8-74
8.4.2.2 R Coronae Borealis.....	8-85
8.5 Summary of Results.....	8-96

CONCLUSIONS

9 CONCLUSION

9.1 Overall summary.....	9- 1
9.2 Possible Directions of Future Research.....	9- 5

CONTENTS

REFERENCES

APPENDICES

A ABBREVIATIONS USED IN REFERENCES

B OPACITY TABLES

C EQUILIBRIUM MODEL

- C.1 Calculating The Equilibrium Model.....C- 1
- C.2 Rezoning The Equilibrium Model.....C- 5
- C.3 Relaxation of The Rezoned Equilibrium Model.....C- 7

D MATHEMATICAL NOMENCLATURE

- D.1 A Few Essential Definitions.....D- 1
- D.2 Covariant Derivatives Used in This Work.....D- 2
- D.3 The Covariant Derivatives in Spherical Co-ordinates.....D- 4

E TABLES OF LINEAR RESULTS

- E.1 Linear Results for Opacity Table R040.....E- 1
- E.2 Linear Results for Opacity Table DXIX.....E-19
- E.3 Linear Results for Opacity Table BD9C.....E-37

F TABLES OF LINEAR STABILITY EDGES

- F.1 Linear Stability Edges for Opacity Table R040.....F- 1
- F.2 Linear Stability Edges for Opacity Table DXIX.....F- 2
- F.3 Linear Stability Edges for Opacity Table BD9C.....F- 3

TABLES

CHAPTER 2

2. 1	Location of some RCB stars.....	2-	4
2. 2	Stellar parameters of some RCB stars.....	2-	6
2. 3	Pulsation parameters of variable RCB stars.....	2-	6

CHAPTER 4

4. 1	Opacity tables used in this study.....	4-	14
------	--	----	----

CHAPTER 7

TABLES OF POLYNOMIAL COEFFICIENTS FOR R040 OPACITY TABLE SURVEY

7. 1	For fits to fundamental periods of $0.8M_{\odot}$ models.....	7-	21
7. 2	For fits to first overtone periods of $0.8M_{\odot}$ models.....	7-	22
7. 3	For fits to fundamental periods of $1.0M_{\odot}$ models.....	7-	26
7. 4	For fits to first overtone periods of $1.0M_{\odot}$ models.....	7-	27
7. 5	For fits to fundamental periods of $1.2M_{\odot}$ models.....	7-	31
7. 6	For fits to first overtone periods of $1.2M_{\odot}$ models.....	7-	32

TABLES OF POLYNOMIAL COEFFICIENTS FOR DXIX OPACITY TABLE SURVEY

7. 7	For fits to fundamental periods of $0.8M_{\odot}$ models.....	7-	54
7. 8	For fits to first overtone periods of $0.8M_{\odot}$ models.....	7-	55
7. 9	For fits to fundamental periods of $1.0M_{\odot}$ models.....	7-	59
7.10	For fits to first overtone periods of $1.0M_{\odot}$ models.....	7-	60
7.11	For fits to fundamental periods of $1.2M_{\odot}$ models.....	7-	64
7.12	For fits to first overtone periods of $1.2M_{\odot}$ models.....	7-	65

TABLES OF POLYNOMIAL COEFFICIENTS FOR BD9C OPACITY TABLE SURVEY

7.13	For fits to fundamental periods of $0.8M_{\odot}$ models.....	7-	87
7.14	For fits to first overtone periods of $0.8M_{\odot}$ models.....	7-	88
7.15	For fits to fundamental periods of $1.0M_{\odot}$ models.....	7-	92
7.16	For fits to first overtone periods of $1.0M_{\odot}$ models.....	7-	93
7.17	For fits to fundamental periods of $1.2M_{\odot}$ models.....	7-	97
7.18	For fits to first overtone periods of $1.2M_{\odot}$ models.....	7-	98

TABLES FOR LUMINOSITY LIMITATIONS

7.19	Showing observed T_{eff} and periods of 7 variable RCB stars...	7-	105
7.20	Luminosity limitations of 5 'cool' variable RCB stars.....	7-	109
7.21	Luminosity & mass limitations of 2 'hot' variable RCB stars.....	7-	109

CHAPTER 8

8. 1	Abundances used in non-linear models.....	8-	2
8. 2	Pre-set input parameters for non-linear models.....	8-	2
8. 3	Input parameters from theory and observation for RCB models.....	8-	46

FIGURES

CHAPTER 2

2. 1	HR Diagram showing main groups of stars.....	2- 2
2. 2	Colour diagram for 12 RCB stars (Feast, 1986).....	2-12
2. 3	Light curve of R CrB (Glasby, 1978).....	2-18
2. 4	Model fit to R CrB deep minima (Ashby, 1976).....	2-18
2. 5	Semi-regular variations in R CrB (Glass, 1978).....	2-20
2. 6	Variation in the 3.5 m band for R CrB (Strecker, 1975).....	2-20
2. 7	Light curve of RY Sgr (Alexander et al, 1972).....	2-23
2. 8	Semi-regular variations in RY Sgr (Alexander et al, 1972)...	2-23
2. 9	Light curve of S Aps (Kilkenny, 1983b).....	2-27
2.10	Semi-regular variations in S Aps (Kilkenny, 1983b).....	2-27
2.11	Semi-regular variations in UW Cen (Bateson 1972 - 1978).....	2-29
2.12	Small variations in XX Cam's light curve (Totochava, 1975)..	2-32
2.13	Light curve of WX CrA (Bateson, 1975).....	2-37
2.14	Light curve of RS Tel (Bateson, 1975).....	2-37
2.15	Light curve of RZ Nor (Bateson, 1975).....	2-39
2.16	Light curve of DY Cen (Bateson, 1975).....	2-39
2.17	Light curve of V348 Sgr (Hecht et al, 1981).....	2-41
2.18	Light curve of MV Sgr (Hoffliet, 1958).....	2-41
2.19	HR Diagram showing blue edges of Saio's (1984) models.....	2-45
2.20	A theoretical RCB light curve (Trimble, 1972).....	2-54
2.21	Evolutionary Tracks for extreme Helium stars (Weiss, 1986)..	2-56

CHAPTER 4

4. 1	A diagram showing diatomic molecule and parameters.....	4- 4
4. 2	A diagram showing triatomic molecule and parameters.....	4- 7
4. 3	Surface fit to opacity table R040.....	4-15
4. 4	Surface fit to opacity table R631.....	4-15
4. 5	Surface fit to opacity table R622.....	4-16
4. 6	Surface fit to opacity table R613.....	4-16
4. 7	Surface fit to opacity table K610.....	4-17
4. 8	Surface fit to opacity table BD9C.....	4-17
4. 9	Surface fit to opacity table DXIX.....	4-18

CHAPTER 5

5. 1	Labelling of boundaries and zones in stellar envelope.....	5- 1
------	--	------

FIGURES

CHAPTER 7

- 7. 1 HR diagram showing location of survey models.....7- 2
- 7. 2 Period-Mass diagrams for Carbon opacity models.....7- 6

FIGURES FOR R040 OPACITY TABLE SURVEY

- 7. 3 Amplitude of eigenfunctions for first 6 modes of one model..7- 9
- 7. 4 Phase of eigenfunctions for first 6 modes of one model.....7- 9
- 7. 5 Work functions and integrals for first 6 modes of one model.7-10
- 7. 6 Low luminosity, 1 solar mass ($\delta T/T$) eigenfunctions.....7-13
- 7. 7 High luminosity, 1 solar mass ($\delta T/T$) eigenfunctions.....7-14
- 7. 8 Low luminosity, 1 solar mass ($\delta L/L$) eigenfunctions.....7-15
- 7. 9 High luminosity, 1 solar mass ($\delta L/L$) eigenfunctions.....7-16
- 7.10 Low luminosity, 1 solar mass ($\delta R/R$) eigenfunctions.....7-17
- 7.11 High luminosity, 1 solar mass ($\delta R/R$) eigenfunctions.....7-18
- 7.12 Pulsation parameters for 0.8 solar mass, $L/L_{\odot} = 1,000$7-23
- 7.13 Pulsation parameters for 0.8 solar mass, $L/L_{\odot} = 3,000$7-23
- 7.14 Pulsation parameters for 0.8 solar mass, $L/L_{\odot} = 6,000$7-24
- 7.15 Pulsation parameters for 0.8 solar mass, $L/L_{\odot} = 10,000$7-24
- 7.16 Pulsation parameters for 0.8 solar mass, $L/L_{\odot} = 15,000$7-25
- 7.17 Pulsation parameters for 0.8 solar mass, $L/L_{\odot} = 20,000$7-25
- 7.18 Pulsation parameters for 1.0 solar mass, $L/L_{\odot} = 1,000$7-28
- 7.19 Pulsation parameters for 1.0 solar mass, $L/L_{\odot} = 3,000$7-28
- 7.20 Pulsation parameters for 1.0 solar mass, $L/L_{\odot} = 6,000$7-29
- 7.21 Pulsation parameters for 1.0 solar mass, $L/L_{\odot} = 10,000$7-29
- 7.22 Pulsation parameters for 1.0 solar mass, $L/L_{\odot} = 15,000$7-30
- 7.23 Pulsation parameters for 1.0 solar mass, $L/L_{\odot} = 20,000$7-30
- 7.24 Pulsation parameters for 1.2 solar mass, $L/L_{\odot} = 1,000$7-33
- 7.25 Pulsation parameters for 1.2 solar mass, $L/L_{\odot} = 3,000$7-33
- 7.26 Pulsation parameters for 1.2 solar mass, $L/L_{\odot} = 6,000$7-34
- 7.27 Pulsation parameters for 1.2 solar mass, $L/L_{\odot} = 10,000$7-34
- 7.28 Pulsation parameters for 1.2 solar mass, $L/L_{\odot} = 15,000$7-35
- 7.29 Pulsation parameters for 1.2 solar mass, $L/L_{\odot} = 20,000$7-35
- 7.30 HR diagrams showing stability edges found in survey.....7-39

FIGURES FOR DXIX OPACITY TABLE SURVEY

- 7.31 Amplitude of eigenfunctions for first 6 modes of one model..7-42
- 7.32 Phase of eigenfunctions for first 6 modes of one model.....7-42
- 7.33 Work functions and integrals for first 6 modes of one model.7-43
- 7.34 Low luminosity, 1 solar mass ($\delta T/T$) eigenfunctions.....7-46
- 7.35 High luminosity, 1 solar mass ($\delta T/T$) eigenfunctions.....7-47
- 7.36 Low luminosity, 1 solar mass ($\delta L/L$) eigenfunctions.....7-48
- 7.37 High luminosity, 1 solar mass ($\delta L/L$) eigenfunctions.....7-49
- 7.38 Low luminosity, 1 solar mass ($\delta R/R$) eigenfunctions.....7-50
- 7.39 High luminosity, 1 solar mass ($\delta R/R$) eigenfunctions.....7-51
- 7.40 Pulsation parameters for 0.8 solar mass, $L/L_{\odot} = 1,000$7-56
- 7.41 Pulsation parameters for 0.8 solar mass, $L/L_{\odot} = 3,000$7-56
- 7.42 Pulsation parameters for 0.8 solar mass, $L/L_{\odot} = 6,000$7-57
- 7.43 Pulsation parameters for 0.8 solar mass, $L/L_{\odot} = 10,000$7-57
- 7.44 Pulsation parameters for 0.8 solar mass, $L/L_{\odot} = 15,000$7-58
- 7.45 Pulsation parameters for 0.8 solar mass, $L/L_{\odot} = 20,000$7-58

FIGURES

CHAPTER 7

7.46	Pulsation parameters for 1.0 solar mass, $L/L_{\odot} = 1,000$	7- 61
7.47	Pulsation parameters for 1.0 solar mass, $L/L_{\odot} = 3,000$	7- 61
7.48	Pulsation parameters for 1.0 solar mass, $L/L_{\odot} = 6,000$	7- 62
7.49	Pulsation parameters for 1.0 solar mass, $L/L_{\odot} = 10,000$	7- 62
7.50	Pulsation parameters for 1.0 solar mass, $L/L_{\odot} = 15,000$	7- 63
7.51	Pulsation parameters for 1.0 solar mass, $L/L_{\odot} = 20,000$	7- 63
7.52	Pulsation parameters for 1.2 solar mass, $L/L_{\odot} = 1,000$	7- 66
7.53	Pulsation parameters for 1.2 solar mass, $L/L_{\odot} = 3,000$	7- 66
7.54	Pulsation parameters for 1.2 solar mass, $L/L_{\odot} = 6,000$	7- 67
7.55	Pulsation parameters for 1.2 solar mass, $L/L_{\odot} = 10,000$	7- 67
7.56	Pulsation parameters for 1.2 solar mass, $L/L_{\odot} = 15,000$	7- 68
7.57	Pulsation parameters for 1.2 solar mass, $L/L_{\odot} = 20,000$	7- 68
7.58	HR diagrams showing stability edges found in survey.....	7- 72

FIGURES FOR BD9C OPACITY TABLE SURVEY

7.59	Amplitude of eigenfunctions for first 6 modes of one model..	7- 75
7.60	Phase of eigenfunctions for first 6 modes of one model.....	7- 75
7.61	Work functions and integrals for first 6 modes of one model..	7- 76
7.62	Low luminosity, 1 solar mass ($\delta T/T$) eigenfunctions.....	7- 79
7.63	High luminosity, 1 solar mass ($\delta T/T$) eigenfunctions.....	7- 80
7.64	Low luminosity, 1 solar mass ($\delta L/L$) eigenfunctions.....	7- 81
7.65	High luminosity, 1 solar mass ($\delta L/L$) eigenfunctions.....	7- 82
7.66	Low luminosity, 1 solar mass ($\delta R/R$) eigenfunctions.....	7- 83
7.67	High luminosity, 1 solar mass ($\delta R/R$) eigenfunctions.....	7- 84
7.68	Pulsation parameters for 0.8 solar mass, $L/L_{\odot} = 1,000$	7- 89
7.69	Pulsation parameters for 0.8 solar mass, $L/L_{\odot} = 3,000$	7- 89
7.70	Pulsation parameters for 0.8 solar mass, $L/L_{\odot} = 6,000$	7- 90
7.71	Pulsation parameters for 0.8 solar mass, $L/L_{\odot} = 10,000$	7- 90
7.72	Pulsation parameters for 0.8 solar mass, $L/L_{\odot} = 15,000$	7- 91
7.73	Pulsation parameters for 0.8 solar mass, $L/L_{\odot} = 20,000$	7- 91
7.74	Pulsation parameters for 1.0 solar mass, $L/L_{\odot} = 1,000$	7- 94
7.75	Pulsation parameters for 1.0 solar mass, $L/L_{\odot} = 3,000$	7- 94
7.76	Pulsation parameters for 1.0 solar mass, $L/L_{\odot} = 6,000$	7- 95
7.77	Pulsation parameters for 1.0 solar mass, $L/L_{\odot} = 10,000$	7- 95
7.78	Pulsation parameters for 1.0 solar mass, $L/L_{\odot} = 15,000$	7- 96
7.79	Pulsation parameters for 1.0 solar mass, $L/L_{\odot} = 20,000$	7- 96
7.80	Pulsation parameters for 1.2 solar mass, $L/L_{\odot} = 1,000$	7- 99
7.81	Pulsation parameters for 1.2 solar mass, $L/L_{\odot} = 3,000$	7- 99
7.82	Pulsation parameters for 1.2 solar mass, $L/L_{\odot} = 6,000$	7-100
7.83	Pulsation parameters for 1.2 solar mass, $L/L_{\odot} = 10,000$	7-100
7.84	Pulsation parameters for 1.2 solar mass, $L/L_{\odot} = 15,000$	7-101
7.85	Pulsation parameters for 1.2 solar mass, $L/L_{\odot} = 20,000$	7-101
7.86	HR diagrams showing stability edges found in survey.....	7-104

FIGURES USED TO FIND MASS-LUMINOSITY LIMITS OF 7 VARIABLE RCB STARS

7.87	Period-Luminosity curves for fundamental mode pulsation.....	7-107
7.88	Period-Luminosity curves for first overtone mode pulsation..	7-108
7.89	Mass-Luminosity plots for the 5 'cool' variable RCB stars...	7-110
7.90	Mass-Luminosity plots for the 2 'hot' variable RCB stars...	7-112

FIGURES

CHAPTER 8

FIGURES OF PRELIMINARY NON-LINEAR TEST MODELS

- 8. 1 How molecules effect the luminosity of a low T_{eff} model.....8- 5
- 8. 2 How molecules effect the velocity of a low T_{eff} model.....8- 6
- 8. 3 How molecules effect the radius of a low T_{eff} model.....8- 7
- 8. 4 How molecules effect the work integral.....8- 8
- 8. 5 How the choice of opacity table effects the light curves....8-10
- 8. 6 How the choice of opacity table effects the work integral...8-11
- 8. 7 How the artificial viscosity effects the radius.....8-13
- 8. 8 How the artificial viscosity effects the velocity.....8-14
- 8. 9 How the artificial viscosity effects the luminosity.....8-15
- 8.10 How the artificial viscosity effects the work integral.....8-17
- 8.11 How altering the zone number effects the light curves.....8-22

A CHECK ON THE FINDINGS OF THE LINEAR SURVEYS

- 8.12 Light curves showing effects of varying mass of models.....8-25
- 8.13 Light curves showing effects of varying luminosity of model.8-26
- 8.14 Light curves showing effects of varying T_{eff} of models.....8-27

DY CENTAURI MODELS

- 8.15 Some hot models with parameters characteristic of DY Cen....8-29
- 8.16 A special case of a model envelope that does not pulsate....8-30
- 8.17 Full radial history of model RD1010.....8-33
- 8.18 Full velocity history of model RD1010.....8-34
- 8.19 Full luminosity history of model RD1010.....8-35
- 8.20 Full radial history of model RD3010.....8-36
- 8.21 Full velocity history of model RD3010.....8-37
- 8.22 Full luminosity history of model RD3010.....8-38
- 8.23 Full radial history of model RB2010.....8-39
- 8.24 Full velocity history of model RB2010.....8-40
- 8.25 Full luminosity history of model RB2010.....8-41
- 8.26 Full radial history of model RB2012.....8-42
- 8.27 Full velocity history of model RB2012.....8-43
- 8.28 Full luminosity history of model RB2012.....8-44

NON-LINEAR NON-ADIABATIC RESULTS OF 5,000K AND 6,000K MODELS

- 8.29 Peak kinetic energy curves for the 5,000K and 6,000K models.8-50
- 8.30 Period and amplitude graphs for GU Sgr model.....8-51
- 8.31 Work integral for model GU Sgr.....8-51
- 8.32 Full radial history of model GU Sgr.....8-52
- 8.33 Full velocity history of model GU Sgr.....8-53
- 8.34 Full luminosity history of model GU Sgr.....8-54
- 8.35 Radial 'snapshot' graphs over for GU Sgr model.....8-55
- 8.36 Velocity 'snapshot' graphs over for GU Sgr model.....8-56
- 8.37 Luminosity 'snapshot' graphs over for GU Sgr model.....8-57
- 8.39 Period and amplitude graphs for RS Tel model.....8-59
- 8.40 Work integral for model RS Tel.....8-59
- 8.41 Full radial history of model RS Tel.....8-60
- 8.42 Full velocity history of model RS Tel.....8-61
- 8.43 Full luminosity history of model RS Tel.....8-62

8.44	Period and amplitude graphs for WX CrA & RT Nor model.....	8-65
8.45	Work integral for model WX CrA & RT Nor.....	8-65
8.46	Full radial history of model WX CrA & RT Nor.....	8-66
8.47	Full velocity history of model WX CrA & RT Nor.....	8-67
8.48	Full luminosity history of model WX CrA & RT Nor.....	8-68
8.49	Period and amplitude graphs for UW Cen model.....	8-69
8.50	Work integral for model UW Cen.....	8-69
8.51	Full radial history of model UW Cen.....	8-70
8.52	Full velocity history of model UW Cen.....	8-71
8.53	Full luminosity history of model UW Cen.....	8-72
8.54	Luminosity 'snapshot' graphs over for UW Cen model.....	8-73

NON-LINEAR NON-ADIABATIC RESULTS OF 6,900K MODELS

8.55	Peak kinetic energy curve for RY Sgr model.....	8-78
8.56	Kinetic and potential energy curves for RY Sgr model.....	8-78
8.57	Work integral for model RY Sgr.....	8-79
8.58	Period and amplitude graphs for RY Sgr model.....	8-79
8.59	Comparison of theoretical light curves with observation.....	8-80
8.60	Light curves for RY Sgr model.....	8-81
8.61	Full radial history of model RY Sgr.....	8-82
8.62	Full velocity history of model RY Sgr.....	8-83
8.63	Full luminosity history of model RY Sgr.....	8-84
8.64	Light curves for R CrB model.....	8-89
8.65	Work integral for model R CrB.....	8-89
8.66	Full radial history of model R CrB.....	8-90
8.67	Full velocity history of model R CrB.....	8-91
8.68	Full luminosity history of model R CrB.....	8-92
8.69	Radial 'snapshot' graphs over for R CrB model.....	8-93
8.70	Velocity 'snapshot' graphs over for R CrB model.....	8-94
8.71	Luminosity 'snapshot' graphs over for R CrB model.....	8-95

INTRODUCTION

CHAPTER 1
INTRODUCTION

1.1 WHAT IS A VARIABLE STAR ?

The definition of a variable star is usually cited in the literature as :

A variable star is a star in which some property changes by an appreciable amount, at a rate which is fairly easy to observe i.e., a few milli-seconds to a few decades.

The group of stars which are classified as variable, can be split into two main sub-groups: Intrinsic and Non-intrinsic. The non-intrinsic variables are stars in which their variability depends on external sources, i.e., interaction with the interstellar medium, eclipsing binaries, etc. While the intrinsic variables owe their variability to stellar sources, i.e., pulsation, novae, etc.

The intrinsic variables can be further sub-divided into the following three groups: 'Eruptive variables' (i.e., Supernovae, Novae, T-Tauri stars, etc.), 'Rotational variables' (i.e., Pulsars, X-ray Bursters, Magnetic Variables, etc.), and 'Pulsational variables' (i.e., Cepheids, RR Lyrae stars, ZZ Ceti stars, etc.). Of these three groups we are only interested in the 'Pulsational variables' of which the main properties that vary are Luminosity, Radial Velocity, Colour, Spectral Line Profiles (53 Persei stars), etc.

INTRODUCTION

The first variable of a cyclic type to be discovered was α Ceti (MIRA) by Fabricius in 1596. By the end of the 18th century only sixteen more variables had been discovered, of which five were Novae and two eclipsing binaries. Of those remaining, two were classical Cepheids : Delta Cephei, discovered by J. Goodricke in 1784 and Eta Aquilae, discovered by E. Pigott in 1784. Since then some 25,000 intrinsic variables have been recognised in our galaxy, of which some 90% are of the pulsational type. From these numbers it has been inferred by Kukarkin et. al. (1963) that about 1 in 1,000,000 stars are of the pulsational class in our galaxy. The recent discovery of ZZ Ceti stars (White Dwarf variables) may mean this estimate is one or two orders of magnitudes too small. The rough positions of some of the pulsational variables and eruptive variables on the HR diagram are shown in Figure 2.1 . The elongated dashed region in the centre of the HR diagram is usually termed 'The Instability Region'. The variables in this 'Instability Region' are all believed to be driven by the same mechanism, i.e., the second ionisation of Helium ($\text{He}^+ \rightarrow \text{He}^{++}$) in the envelope.

Historically and observationally, the most important group of variable stars are the the Classical Cepheids. This is because of the famous relation connecting total luminosity to period, which makes them one of the best tools for measuring inter-galactic distances. They are also important theoretically as their variations can be explained very well using the pure radial pulsation theory. To date only about 700 have been found in our own galaxy, most of which lie in the galactic plane and are obscured by dust.

INTRODUCTION

Classical Cepheids are yellow giants or super-giants of extreme population I which have absolute luminosities of $(300 - 26,000)L_{\odot}$ and masses in the range $(3.7 - 14.0)M_{\odot}$. They are periodic in both their light and radial velocity curves, which are non-symmetric in shape and have periods of $(1 - 50)$ days. A common feature of the decreasing luminosity part of the light curves is a small secondary 'bump' that first appears at a period of about 7 days, occurs earlier in phase as the period increases and then disappears at a period of about 16 days. Finally, there is a phase lag of around 0.2 periods between the luminosity and the radial velocity maxima, indicating that maximum luminosity occurs when the star is expanding through its equilibrium radius and not at maximum compression as may be expected.

The long period Cepheids, RV Tauri and W Virginis stars have been explained to a reasonable degree by radial pulsation theory. This then indicates that other high luminosity helium stars may also be explained by radial pulsation theory and this is the prime reason why the following research was undertaken.

To conclude this brief discussion of variable stars, it cannot be overstated that stellar pulsation theory cannot only give great insight into stellar structure but also increases our understanding of phenomena in many other fields of astrophysics and physics, impossible to study in any other way.

INTRODUCTION

1.2 AIMS, HOPES AND ASPIRATIONS

The aim of this thesis is to try and obtain a better understanding of the semi-regular variations seen in some of the R Coronae Borealis group of stars (referred to as the RCB group throughout the rest of this thesis). Questions such as: why are they semi-regular in nature, in contrast to the regular behaviour of the Cepheid variables? Why are the amplitudes of the semi-regular variations in the observed light curves so small ($<0.5^m$) in comparison to those found in other variable stars? Do these semi-regular variations have any bearing on the observed deep minima? It is hoped that not only will these questions be answered but a better estimate of the luminosity and mass of some of the RCB variables will be found.

The thesis is split into five parts plus six appendices. The appendices mainly consist of raw data and useful references, and are not necessary for the understanding of the work presented in this thesis. The five parts split the work into the following sections: Review, Theory, Computational Schemes, Results and Conclusions.

The Review section consists of Chapter 2 and gives a full account of all that is known about the RCB group observationally and theoretically, as well as an indication of the range of stellar parameters a typical RCB star might have.

The Theory section consists of Chapter 3 & 4. Chapter 3 gives a basic derivation of the dynamic stellar equations and their radial formulation as used in this work. Chapter 4 summarises the physics required to solve the dynamic stellar equations derived in Chapter 3.

INTRODUCTION

The Computational Schemes section consists of Chapters 5 & 6. Chapter 5 shows how the dynamic stellar equations of Chapter 3 were differenced for non-linear non-adiabatic pulsation calculations. Chapter 6 shows how the dynamic stellar equations were differenced for the linear non-adiabatic pulsation calculations.

The results section is again split into two chapters: Chapters 7 & 8. Chapter 7 presents the results of a series of surveys carried out using the linear non-adiabatic codes and places some restrictions upon the masses and luminosities of 7 RCB variables. Chapter 8 tests some of the input physics used and attempts to discern whether the findings of the linear results, with regard to the opacity tables, are correct. Finally, the results of the non-linear analyses of the 7 RCB variables discussed in Chapter 7 are presented, discussed and compared with the observations.

Chapter 9 presents the conclusions and gives an overall summary of what has been achieved in this thesis, as well as indicating the areas in which future work should be undertaken.

REVIEW

CHAPTER 2

OBSERVATIONS OF THE RCB GROUP

2.1 INTRODUCTION

This Chapter deals with the observational information available in the literature on the RCB group of stars. Firstly, an overview of the group as a whole are considered, in which estimates of stellar parameters are discussed together with the sources used to obtain individual parameters. After this discussion, a brief 'history' of selected RCB stars is given. There follows a brief review of previous theoretical work and the evolutionary status of the RCB group as a whole. The overall findings and status of these objects are discussed in the summary.

Figure 2.1 below shows the rough location in the HR diagram of the RCB group of stars in comparison with other variables and Table 2.1 lists their location and apparent magnitude where known (by author).

2.2 REVIEW OF THE RCB GROUP

2.2.1 Definition And Distribution

The RCB stars form a very interesting if small group of objects. Kukarkin et al (1969) lists 34 stars as RCB's, though several of these have been wrongly classified i.e., Rho Cas (Payne-Gaposchkin, 1963), Z Cir (Feast, 1975), etc. Table 2.1 gives a list of all stars that have not been definitely removed from the group. Of these, 24 have

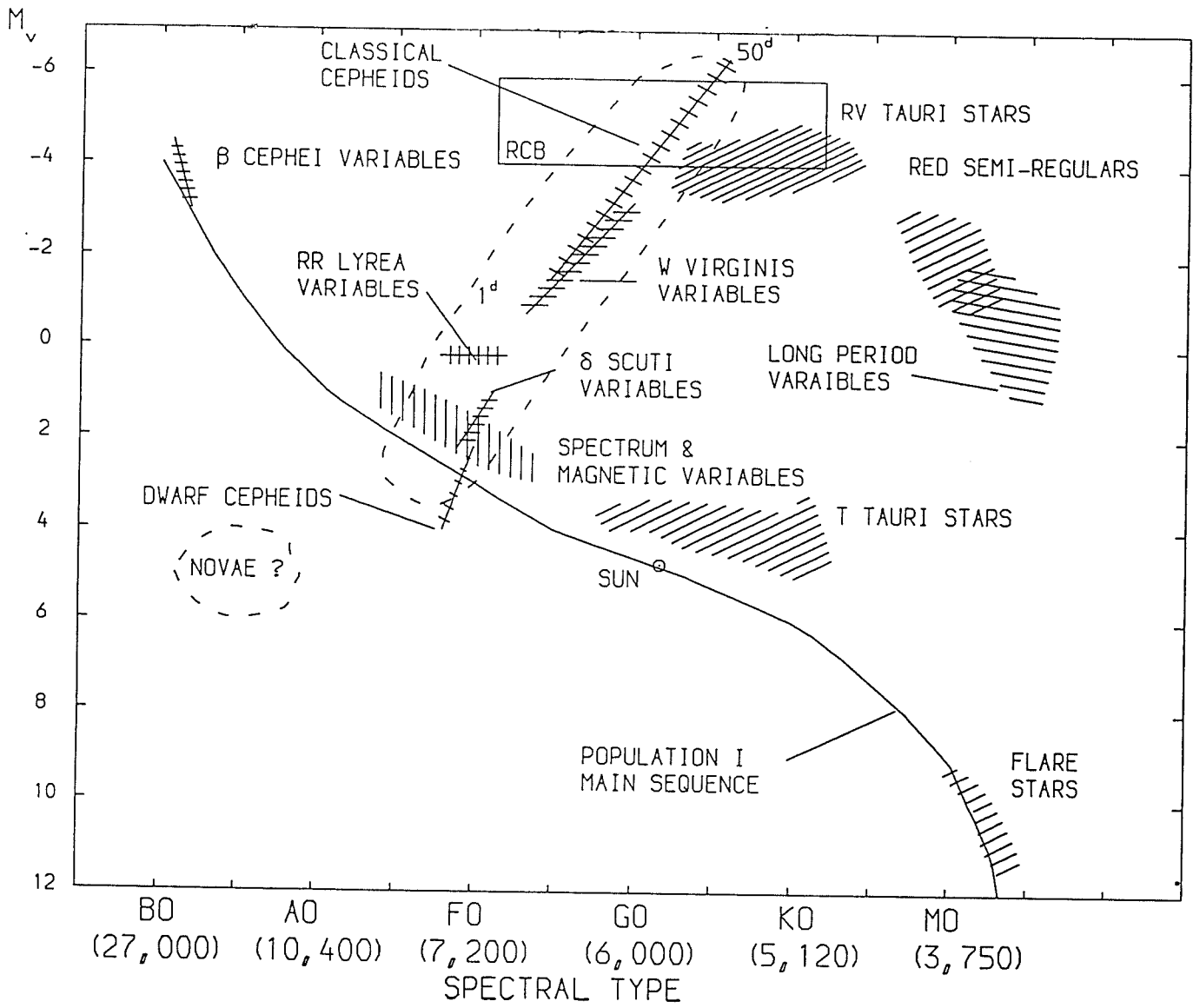


Figure 2.1 : This figure shows the location (BOXED REGION) of the majority of the RCB variables, on an HR diagram in comparison to the main sequence (ms) and other variables.

OBSERVATIONS OF THE RCB GROUP

been spectroscopically verified, though 5 of this 24 are in doubt for various reasons, e.g., too hot or few deep minima.

The class definition has changed many times over the years, the present definition being:

- (i) The stars must be hydrogen deficient ($X < 0.0001$) carbon ($Z_c \sim 0.04$) objects.
- (ii) The stars must undergo deep minima on an irregular basis of at least 2 magnitudes, the minima declining rapidly ($< \text{few months}$) and recovering slowly (a few months to a few years).
- (iii) The stars must have large infrared excesses.
- (iv) The majority of the stars are of spectral class F,G or R.

Case (iv) is not rigorously applied as there are three objects falling well outside this temperature range and case (ii) has been overlooked in the case of LR Sco, whose membership is doubtful.

The stars of this group, though few in number, appear to be concentrated towards the disc of the galaxy, indicating that they may belong to the old disc population. Eggen (1965) has argued from the distribution of their proper motions that some belong to his Wolf 630 group and hence are definitely old disc population objects.

OBSERVATIONS OF THE RCB GROUP

Table 2.1 : location of RCB group stars.

STAR	R.A.	DEC.	l°	b°	m_v (m_{pg})	RCB
DZ And ^b	00 27 17	25 28 06	117.65	-36.66	(10.0 - >14)	?
UX Ant ^b	10 52 30	-36 51 36	279.06	+20.12	(12.2 - 15.8)	?
S Aps ^a	15 04 21	-71 52 18	313.21	-11.99	9.6 - 15.2	Y
U Aqr ^a	21 57 54	-17 06 36	039.15	-49.81	10.5 - 14.4	Y
XX Cam ^a	04 00 55	53 05 36	149.84	+01.12	7.1 - 8.7	?
UV Cas ^a	22 58 04	59 04 24	109.52	-00.38	(11.8 - 16.5)	N
V425 Cas ^b	22 59 15	52 44 00	107.11	-06.25	(14.5 - 18.0)	N
DY Cen ^a	13 22 27	-53 59 11	307.96	+08.29	(12.0 - 16.4)	?
UW Cen ^a	12 40 26	-54 15 15	301.74	+08.32	(9.6 - 16.0)	Y
AE Cir ^b	14 40 23	-69 10 58	312.67	-08.69	(12.2 - 16.0)	Y
V CrA ^a	18 40 42	-38 15 48	357.67	-15.65	(9.4 - >14)	Y
WX CrA ^a	18 05 26	-37 20 17	355.12	-08.32	(11.0 - >16.5)	Y
R CrB ^a	15 44 27	28 27 48	045.05	+50.98	5.8 - >14	Y
V482 Cyg ^a	19 55 54	33 42 00	070.43	+02.49	10.9 - 12.2	?
W Men ^a	05 27 46	-71 16 00	282.09	-32.39	(13.8 - 16.0)	Y
Y Mus ^a	13 02 34	-65 14 44	304.43	-02.68	(10.5 - 12.0)	Y
RT Nor ^a	16 20 03	-59 13 47	327.23	-06.93	(11.3 - 16.3)	Y
RZ Nor ^a	16 28 45	-53 10 48	332.45	-03.57	(11.1 - 12.7)	Y
LR Sco ^a	17 24 17	-43 48 24	345.50	-05.00	(10.9 - 12.3)	?
CL Sge ^b	20 08 18	18 11 42	058.87	-08.55	(13.9 - 15.2)	?
SV Sge ^a	19 03 45	17 28 12	050.52	+04.37	(10.8 - 14.5)	Y
GU Sgr ^a	18 21 12	-24 17 08	008.32	-05.24	(11.0 - 15.0)	Y
MV Sgr ^a	18 41 33	-21 00 23	013.41	-07.93	(12.0 - 15.6)	?
RY Sgr ^a	19 13 17	-33 36 12	004.44	-19.45	6.5 - 14.0	Y
VZ Sgr ^a	18 16 48	-27 28 00	002.51	-05.96	(11.8 - >14)	Y
V348 Sgr ^a	18 37 19	-22 57 24	011.20	-07.92	(11.0 - >16.5)	?
V589 Sgr ^b	17 58 35	-34 45 00	357.05	-06.51	(14.2 - >17.6)	?
V618 Sgr ^b	18 15 20	-24 47 48	355.77	-07.82	(11.0 - >16.5)	Y
V3795 Sgr ^a	18 07 12	-25 48 24	006.00	-04.00	(11.0 - >16.5)	Y
SU Tau ^a	05 43 12	49 02 00	188.87	-04.42	9.5 - 16.0	Y
RS Tel ^a	18 15 07	-46 34 08	347.53	-14.14	(9.3 - >13.0)	Y
CT Vul ^b	19 43 11	18 11 42	057.83	-02.22	(13.9 - 15.6)	N
HV5637 ^a	05 11 32	-67 56 00	LMC	LMC	(15.8 - >16.0)	Y
HV12842 ^a	05 45 03	-64 24 24	LMC	LMC	(13.7 - >16.0)	Y

Notes: 'a' indicates that the tabulated information was taken from Drilling & Hill (1986) and associated references.

'b' indicates that the tabulated information was taken from Kukarkin et al (1969, 1970).

OBSERVATIONS OF THE RCB GROUP

2.2.2 Abundances And Effective Temperatures

Only five objects have undergone detailed spectroscopic study for abundance purposes (R CrB - Bidelman, 1953, Searle, 1961 and Cottrell & Lambert, 1982; RY Sgr - Danziger, 1965 and Searle, 1961; XX Cam - Bidelman (1948), Cottrell & Lambert (1982), Orlov & Rodriguez (1974); U Aqu - Bond et al, 1979; UW Cen - Giridhar & Rao, 1986). All these analyses showed that the stars were hydrogen deficient carbon objects and that the heavier elements have roughly solar abundances, although Y and Sr were very over-abundant in U Aqu and Li was similarly over-abundant in R CrB and RY Sgr (Danziger, 1965 and Keenan & Greenstein, 1963). A good review of recent work on the chemical composition of the RCB group of stars can be found in Lambert (1986).

All the spectroscopy of RCB objects show C_2 bands to some degree. The stronger these bands are the cooler the star appears to be, e.g., S Aps is a cool RCB and has very strong C_2 bands, whereas RY Sgr is quite hot and has weak C_2 bands. Bidelman (1953) has pointed out that isotope ^{13}C is oddly absent from C_2 molecules in RCB's, while it is generally present in other carbon stars. The main constituent of RCB stars seems to be helium. This conclusion is made on the direct evidence of He I lines being seen during obscuration of several RCB's. e.g., see Alexander et al (1972) or Bidelman (1953). The conclusion is valid, as at the effective temperatures of these stars, helium is virtually invisible, with carbon accounting for most of the opacity.

The effective temperatures for about 13 RCB stars have been estimated using broad band photometry by Kilkenny & Whittet (1984) and others. From these, together with estimates based upon the spectral class, the temperature range appears to be about (4000 -7000)K,

OBSERVATIONS OF THE RCB GROUP

Table 2.2 : some stellar parameters

STAR	$a_{T_{\text{eff}}}$	$a_{T_{\text{circ}}}$	$b_{V_{\text{rad}}}$ (km/sec)	$a_{\text{Spec type}}$
S Aps	4,000	750	-	R3
XX Cam	7,000	-	+16	G2
DY Cen	10,000	<800	-	?
UW Cen	6,000	700	-	K?
V CrA	4,000	-	-	?
WX CrA	5,000	900	-	R5
R CrB	6,900	700	+21	G0
Y Mus	7,000	900	-	G2
RT Nor	7,000	900	-	R?
RZ Nor	5,000	700	-	R8
GU Sgr	5,000	700	-	?
MV Sgr	16,000	1500, 500	-91	B?
RY Sgr	6,900	800	-10	G0
SU Tau	6,000	900	+37	G0
RS Tel	5,000	800	-	R8

Table 2.3 : Table of variable RCB stars

STAR	PERIOD (dys)	dm_v	dV (km/s)	k (dys/per)	REMARKS
S Aps ^d	39.8 (138.7)	<0.3	-	+0.019 (-0.184)	Uncertainties in k
XX Cam ^h	40	0.4	-	-	Doubtful RCB
DY Cen ^c	120 (?)	<0.2	-	-	Not verified
UW Cen ^c	42.8	0.2	-	+0.003	Uncertainties in k
AE Cir ^c	100 (?)	<0.1	-	-	Not verified
V CrA ^c	75 (?)	<0.2	-	-	Not verified
WX CrA ^c	60 (?)	<0.1	-	-	Not verified
R CrB ^f	44	0.15	4	-	Spasmodic
RZ Nor ^c	68 (?)	<0.2	-	-	Not verified
RT Nor ^e	59 (175) (?)	<0.2	-	-	Not verified
LR Sco ^g	104.4	1.4	-	-	Doubtful RCB
GU Sgr ^c	38 (?)	<0.1	-	-	Not verified
RY Sgr ^e	38.6	0.45	30	-0.00004	Good cyclic curve
VZ Sgr ^c	47 (?)	<0.25	-	-	Not verified
RS Tel ^c	45.8 (?)	<0.3	-	-	Not verified

Notes: 'a' indicates that data was taken from Kilkenney & Whittet (1984).
 'b' indicates that data was taken from Drilling & Hill (1986).
 'c' indicates that data was taken from Bateson (1975).
 'd' indicates that data was taken from Kilkenney (1983b).
 'e' indicates that data was taken from Kilkenney (1982).
 'f' indicates that data was taken from Fernie et al (1972).
 'g' indicates that data was taken from Shapley & Swope (1974).

OBSERVATIONS OF THE RCB GROUP

(see Table 2.2), MV Sgr (16,000 K), DY Cen (10,000 K) and V348 Sgr (15,000 K) are the only members that fall outside this range. So from the observational data available, we can fix the following stellar parameters:

$$\langle X \rangle < 0.0001$$

$$\langle Y \rangle = 0.9099$$

$$\langle Z \rangle = 0.09$$

$$\langle Z_c \rangle = 0.75 \langle Z \rangle$$

$$T_{\text{eff}} = (4000 - 7000)\text{K}.$$

2.2.3 Luminosity And Mass

The absolute magnitudes of RCB stars are still in doubt, though there have been many attempts to determine them. Eggen (1969) estimated $M_V = -3.1$ for R CrB based upon membership of his Wolf 630 group. Feast (1972) derives $M_V = -4$ for RY Sgr by assuming a star 12" away is a companion star. Feast (1972) also estimates absolute magnitudes of -4 for HV5637 and HV12842, as well as -5 for W Men based upon their being LMC objects. Assuming a theoretical mass of 0.8 solar masses, Wood (1978) finds $\log(L/L_0) = (3.93 \pm 0.15)$ and from theoretical modelling of these objects, Saio et al (1984) finds the following limitations:

$$4.2 < \log(L/L_0) < 4.7$$

$$0.9 < M/M_\odot < 3.0 .$$

OBSERVATIONS OF THE RCB GROUP

The mass is even more uncertain, though from fine spectroscopic analysis by Danziger (1965) and Schonberner (1975), the mass was found to be in the range 1-2 solar masses. Evolution work of Paczynski (1971) and Trimble (1971, 1972) on R CrB places the mass between 0.9 and 2.5 solar masses. Thus in summary, we can place the following limits upon the absolute magnitude and masses of RCB objects:

$$\begin{array}{l} -3 < M_V < -6 \quad \text{probably} < -5 \\ 0.8 < M/M_{\odot} < 3.0 \quad \text{probably} < 2.0 . \end{array}$$

2.2.4 Variability Of Some RCB Stars

Semi-regular variations have been reported in 15 RCB stars of which 9 have not been verified (see Bateson, 1974, 1975 and Bateson & Jones, 1972). In the remaining 6, the variations are periodic in nature and generally have a period of around 40 days and amplitude < 0.5 mag. The exceptions are S Aps which underwent what appears to be a period change (Kilkenny, 1983b) from 120 days to 39.8 days, and LR Sco which has a period of 104.4 days and amplitude 1.4 mag. (The membership of LR Sco star in the RCB group is not certain as it has not undergone any deep minima yet.)

The variations appear to vary in amplitude, sometimes fading out altogether (R CrB - Fernie et al, 1972 and RY Sgr - Mayall, 1972) and at other times increasing in amplitude (UW Cen in recovery from deep minima - Bateson, 1972). Sometimes there also appears to be a very rapid variation superimposed upon the slower one (R CrB - Miskin in Herbig, 1967 and XX Cam - Totochava, 1973)

OBSERVATIONS OF THE RCB GROUP

Two of these stars have sparse radial velocity curves along with light curves that vary with the same periods, thus indicating that the stars are pulsating radially. Furthermore, RY Sgr shows a definite decrease in its period over time of -0.00004 days/period which agrees well with that predicted from evolutionary models of low mass hydrogen deficient stars in Schonberner (1975). UW Cen and S Aps also show changes in their periods, though these values are uncertain, being based upon far less data than that for RY Sgr. If the value for S Aps is correct, it will be hard to explain how these objects evolve or even to model them (for variation parameters see Table 2.3). In contrast to these 'pulsators' SU Tau has been shown by Howarth (1976) to have no semi-regular pulsations above 0^m04 mag in its visual light curves.

2.2.5 Deep Minima

RCB stars are characterised by their irregular deep minima, up to 9 magnitudes in V, while staying fairly constant in the infrared. These deep minima can be quite complex, involving several sub-minima on decline and sometimes on recovery. The following characteristics are common to virtually all deep minima

- (i) The deep minima start with a rapid decline in light (lasting about 5 days), during which the continuum fades rapidly and the absorption spectrum is replaced with an emission spectrum. Also the absorption component of the sodium D lines and calcium H & K lines are displaced by 200 km/sec (Alexander et al, 1972; Querci & Querci, 1978).

OBSERVATIONS OF THE RCB GROUP

- (ii) A slower (lasting about 20 days) decline in light is observed after the above decline. Throughout this phase the chromospheric emission spectrum fades and shows structure similar to that observed with height in the solar chromosphere during an eclipse. The broad bright lines remain roughly constant in intensity throughout this phase.

The He I (3888), calcium H & K and sodium D broad emission lines remain roughly constant in half width (they are roughly constant from deep minima to deep minima and from star to star). Although they show complex structure and 'central wavelength' development in time (see Alexander et al, 1972; Spite & Spite, 1974; Feast, 1979). These broad lines are roughly centred on the stellar velocity.

- (iii) The recovery from deep minima is generally slow (500-1000 days). Throughout this time the spectrum gradually returns to normal and the star returns to its normal colour. During this phase P Cygni profiles have been observed in the He I (10830) line of R CrB (Querci & Querci, 1978); also in sodium D and calcium H & K lines of RY Sgr (Alexander et al, 1982). Zirin (1982) also found that the He I (10830) line was shifted to 10822A, indicating a velocity of about 220 km/sec, after the star had fully recovered to maximum light. Alexander (1972) reports that the calcium H & K

OBSERVATIONS OF THE RCB GROUP

and sodium D lines vanished after recovery to maximum light of RY Sgr (This result was obtained from low dispersion spectra).

Several theories have been put forward to explain the observed light curves of these stars during deep minima. These models range from eclipsing infrared stars (Humphreys & Ney, 1974) to random 'puffs' of soot. The eclipsing models can generally be eliminated as they cannot explain the development in the spectra with time. This leaves some form of ejection model. Forrest et al (1972) showed from energy considerations that any ejection of material must be asymmetric and only partially covers the star. Feast (1975) argues that as no noticeable change in the infrared occurs during deep minima, the amount of material ejected must be small in comparison to what is already in the circumstellar 'shell'. From the structure in broad emission lines noted above, it would seem the 'puff' is small and from wavelength changes that there may be more than one 'puff' at any one time. Feast (1986) argues that the multiple 'puffs' can explain roughly all observations, though, of course, such a rough model cannot explain the detailed behaviour of such complex objects as these stars obviously are.

2.2.6 Infra-red Excesses

The infra-red excesses were discovered about the same time in both R CrB (Stein et al 1969) and RY Sgr (Lee & Feast, 1969). These observations indicated circumstellar 'shell' temperatures of about 900 K. Since then, extensive broad band photometry by Feast & Glass (1973), Glass (1978), Kilkenny & Whittet (1984) and Walker (1985) have shown that infra-red excesses are characteristic of the RCB group, with only XX Cam (a doubtful RCB) not having an infra-red excess

OBSERVATIONS OF THE RCB GROUP

(Rao et al 1980). From these observations, Feast (1986) has shown that the majority of well observed RCB stars fall in a narrow band when plotted on a $(J-H)_0/(H-K)_0$ colour diagram (see Figure 2.2). This suggests a narrow range of colour temperatures for both the central stars (5000-7000 K) and the surrounding circumstellar shells. Though the hotter RCB objects show complex energy distributions indicating that more than one shell is present, it also shows that the shell structure is probably more complex than a simple black body model assumes. The fluxes at L and M have been shown from rough calculations to be due almost entirely to the circumstellar shell and underlying star, respectively. This fact shows that the circumstellar shell is heated directly from the underlying star, as Feast et al (1977) showed that both J and L varied with a period of 38 days. Forrest et al (1972), Glass (1978) and Feast (1979) have all observed that L stays roughly constant throughout the deep minimum in the visual bands, showing that the deep minima are due to obscuration of some kind. From the spectroscopic studies we know that ejection is the most likely cause of these obscurations. This result, taken with the above invariance in L during an obscuration, indicates that the amount of ejected material is small in comparison to the circumstellar material. This leads on to the variations observed in R CrB's L band (Strecker, 1975 and references therein) with a timescale of about 1000 days. Since then, similar variations have been observed in RY Sgr (Menzies, 1985) and 10 other RCB stars (unpublished SAAO observations mentioned in Feast, 1975), all varying on a timescale of (1000-2000) days with amplitudes of between (1-3) magnitudes. Feast (1986) has suggested that this variance maybe linked to the pulsation of the central star, which ejects 'puffs' of dust every period in a random direction. Obscuration then occurs when a 'puff' is ejected along the 'line of sight'.

OBSERVATIONS OF THE RCB GROUP

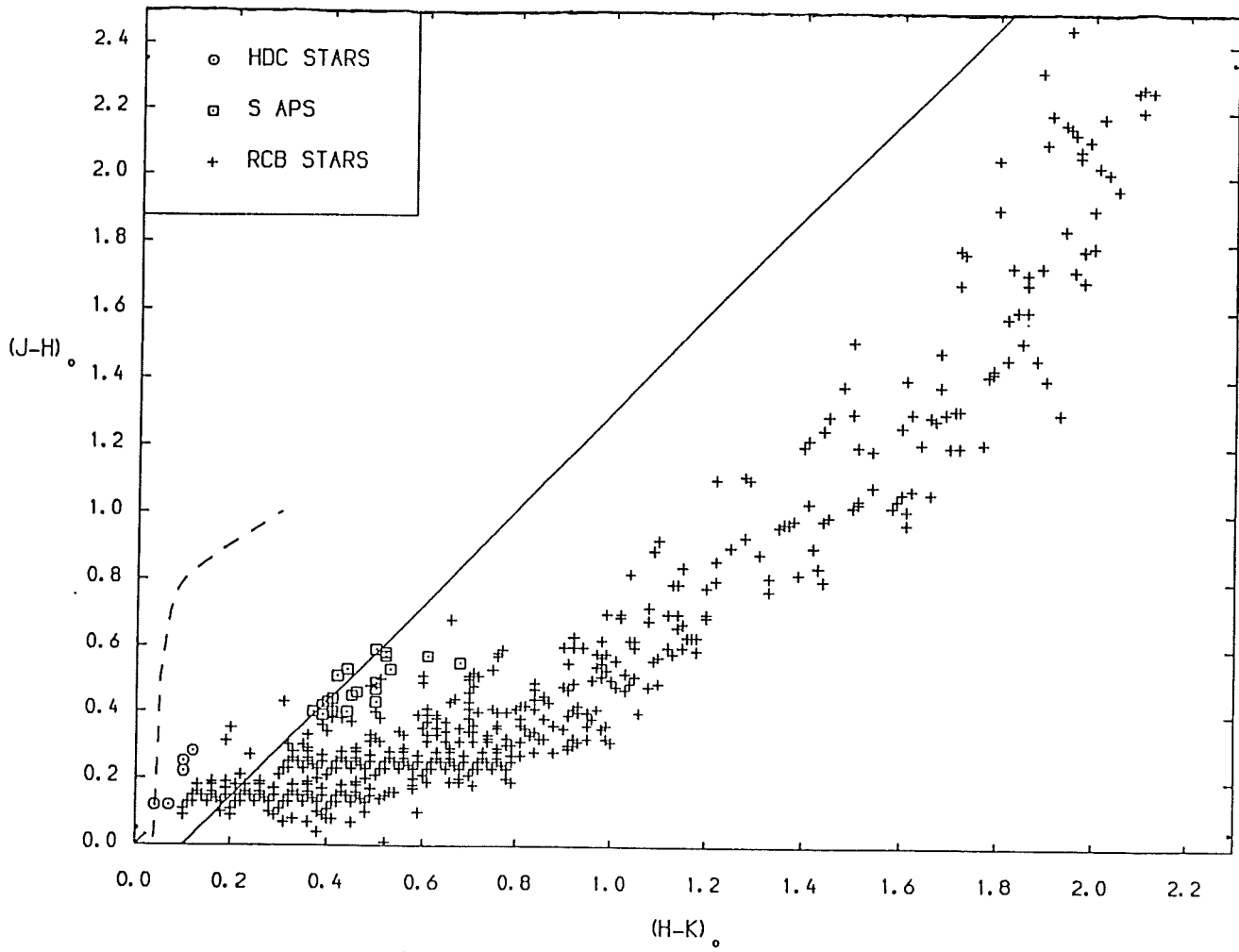


Figure 2.2 : $(J-H) / (H-K)$ diagram for 12 RCB stars (taken from Feast 1986). Open boxes refer to S Aps, open circles to HdC stars. The (straight) black body line is shown. The curve is the locus of normal stars.

OBSERVATIONS OF THE RCB GROUP

The composition of the circumstellar material is thought to be mainly carbon particles mingled with some gas dragged from the central star upon ejection (see Rao et al, 1986, Nandy & Rao, 1986). This hypothesis is supported by the lack of silicon emission in RCB spectra, the peculiar reddening laws observed for these objects, and polarimetric observations. From several models, (e.g., Wickramasinghe, 1973), Borghesi et al 1985, Fadeyev, 1986) it has been shown that the particles are probably small (10-300)nm amorphous carbon grains.

2.3 INDIVIDUAL STARS

2.3.1 Variable RCB Stars

2.3.1.1 R Coronae Borealis - Was discovered in 1795 by Piggot, though it was not observed regularly until 1855. A good list of references for observations at visual wavelengths can be found in Howarth (1977) (See Figure 2.3 for visual light curve of R CrB). In this paper, Howarth confirms the findings of Sterne (1935) that the fadings of R CrB are 'perfectly' irregular in nature, i.e., their distribution in time obeys Poisson statistics with a time constant of (1026 +/- 156) days. Stein et al (1969) were the first to do broad band photometry on this object. Since then many such observations have been made (for further details see Geisel (1970), Gillett et al (1970), Forrest et al (1971, 1972), Fernie (1972, 1982), Feast & Glass (1973), Humphreys & Ney (1974), Glass (1978), Shenavrin et al (1979) and references therein). The first low dispersion spectra were taken by Ludendorff (1906) and Joy & Humason (1923). The detail of these first spectra was limited and it was not until Berman (1935) took the first high dispersion spectrum of R CrB that any real abundance analysis could be done. Since then quite a few high dispersion spectra have been taken.

OBSERVATIONS OF THE RCB GROUP

The following references refer to the more prominent papers in the literature: Herbig (1949), Bidelman (1953), Payne-Gaposchkin (1963), Keenan & Greenstein (1963), Whitford (1967), Coyne & Shawl (1973) and Cottrell & Lambert (1982).

The RCB (R Coronae Borealis) group was first designated in 1855 when it was found that RY Sgr also underwent irregular fading, in a similar manner to that of the group's progenitor. The criterion for membership in this group was that a star must rapidly fade by several magnitudes (up to 7 mag.) and then slowly recover to maximum light (generally over several months to years). The next significant discovery was found by Ludendorf (1906) in his low dispersion spectra, that showed very weak hydrogen Balmer lines. This led to the tentative conclusion that R CrB was extremely hydrogen deficient. Joy & Humason (1923) took several spectra throughout the fading of R CrB and noticed that its spectrum changed radically as the fading progressed. Herbig (1949) gave a detailed account of the spectral changes he observed during his own observations, and this was later summarised by Mayall (1960) and then Payne-Gaposchkin (1963). The overall spectral changes observed were briefly:

- (i) The absorption spectrum was always present. Broad bright lines appear in initial stages of deep minima and remain roughly of constant intensity while the star fades, weakening as the star recovers to maximum light.

- (ii) The sharp emission lines are intense as the star fades, weakening during minima and recovery.

OBSERVATIONS OF THE RCB GROUP

(iii) Throughout the recovery violet displaced absorption lines are present and remain until near maximum light (within 1^m.0).

Bidelman (1953) found clear evidence that R CrB was a carbon star, his results being supported by Berman (1935) and by Herbig (1949). He then classified R CrB as a HdC (hydrogen deficient carbon) star. Both Berman (1935) and Bidelman (1953) noticed a strong line that could only be assigned to He I. Though the presence of this line is still not fully explained this gives a strong indication that the stars main constituent is helium. Searle (1961) carried out a coarse analysis on Berman's spectra, using a model atmosphere, and found the following abundances:

$$\langle X \rangle < 0.0001$$

$$\langle Y \rangle = 0.9099$$

$$\langle Z \rangle = 0.09 \quad (\text{heavier elements having solar abundances})$$

$$\langle Z_c \rangle = 0.75 \langle Z \rangle.$$

Myerscough (1968) obtained similar abundances based on the spectral data of Berman (1935) and Keenan & Greenstein (1963) and gives a value of (5800 +/- 200) K for the effective temperature, based on model atmosphere results rather than spectral type alone. Schonberner (1975) and Cottrell & Lambert (1982) have carried out fine analyses of these spectra using more accurate modelling schemes and both agree (within the error limits) on the following parameters:

$$T_{\text{eff}} = (6900 \pm 500) \text{ K}$$

$$\log(g) = (0.15 \pm 0.2)$$

$$V_{\text{turb}} = (6.5 \pm 1.0) \text{ km/sec.}$$

OBSERVATIONS OF THE RCB GROUP

Whitford (1967) was the first to state the four main features of R CrB (also RY Sgr and XX Cam), which were:

- (i) Strong carbon feature in spectrum
- (ii) Weak or absent hydrogen lines
- (iii) Irregular fading by several magnitudes (>1 mag.)
- (iv) Spectral class generally Supergiant F or G.

This list was soon extended to include large infrared excesses upon the discovery of large infrared excesses in the broad band photometry of R CrB by Stein et al (1969) and soon after in RY Sgr (Lee & Feast, 1969) and SU Tau (Low, 1970). Indeed it was Feast who fixed the criteria for membership in the RCB group based upon the above features for R CrB.

These large excesses fitted in with the theoretical work of Loreta & O'Keefe (1939) in which the star 'ejects' clouds of carbon grains, during deep minima, which after a few months or years join a circumstellar shell around the star. Forrest et al (1971) showed that in the case of R CrB the infra-red and visual wavelengths are uncorrelated and hence that such a circumstellar shell must be irregular and supplied by non-uniform 'ejections' of dust from the star. They put forward the hypothesis that perhaps the star was eclipsed by one or more large dust clouds. The 'ejection' model suffers from the problem that the grains would have to form near the star's photosphere to explain the spectral changes observed, and to date no one has been able to model such grain formation around such a hot star (see Coyne & Shawl, 1973 for further details). The 'dust cloud' model cannot explain the spectral changes at all. Coyne & Shawl (1973) shows that the circumstellar material during deep minima

OBSERVATIONS OF THE RCB GROUP

consists of small graphite particles of size (50-100)nm, that appear to occur in irregular clouds. Whether these clouds are present during maximum light is unknown as the underlying star swamps out the light from the clouds during maximum light, thus preventing polarimetry. Using this grain size Ashby (1976) has shown that a free particle grain model fits the observed visual recovery phase of R CrB light curve (see Figure 2.4).

By fitting Black Body curves and using colour diagrams Shenavrin et al (1979), Glass (1978) and Fernie (1982) have shown that a star with an effective temperature of (6500 +/- 500)K surrounded by an optically thick shell of dust of temperature (700 +/- 50)K fits the observed data quite well.

Fernie et al (1972) observed a sporadic semi-irregular variation at visual wavelengths of period (46 +/- 5)days and amplitude (0.15 +/- 0.1) magnitudes (see Figure 2.5) which appears to be due to radial pulsation, as radial velocities with the same period and amplitude of about 4 km/sec were also observed. This variation was again observed by Glass (1978) and since confirmed by several other authors. Shortly after this discovery, Humphreys & Ney (1974) found that there was significant variation (about 1^m.4) in the infra-red over a period of 1100 days. Strecker (1975) gathered all the infrared observations together and plotted them along with some of their own results (see Figure 2.6) and showed conclusively that the above variation existed. Since then the variation has been proved to be periodic in nature.

OBSERVATIONS OF THE RCB GROUP

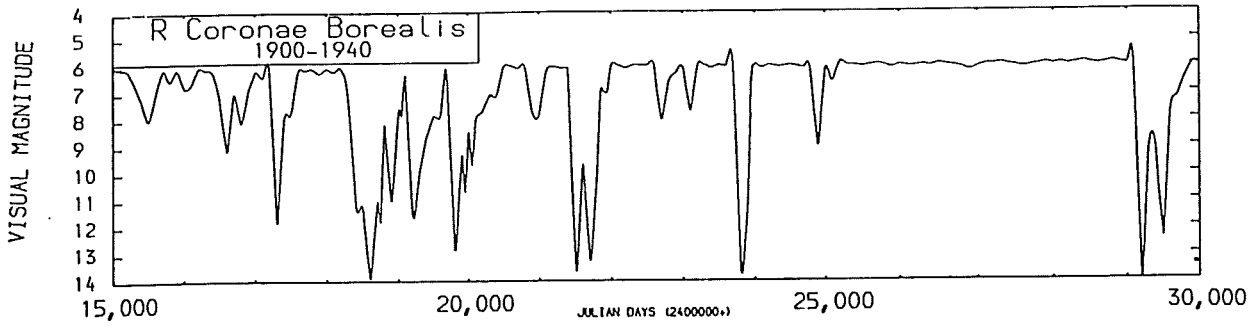


Figure 2.3 : Light curve of the R CrB variable, as shown in Glasby (1978).

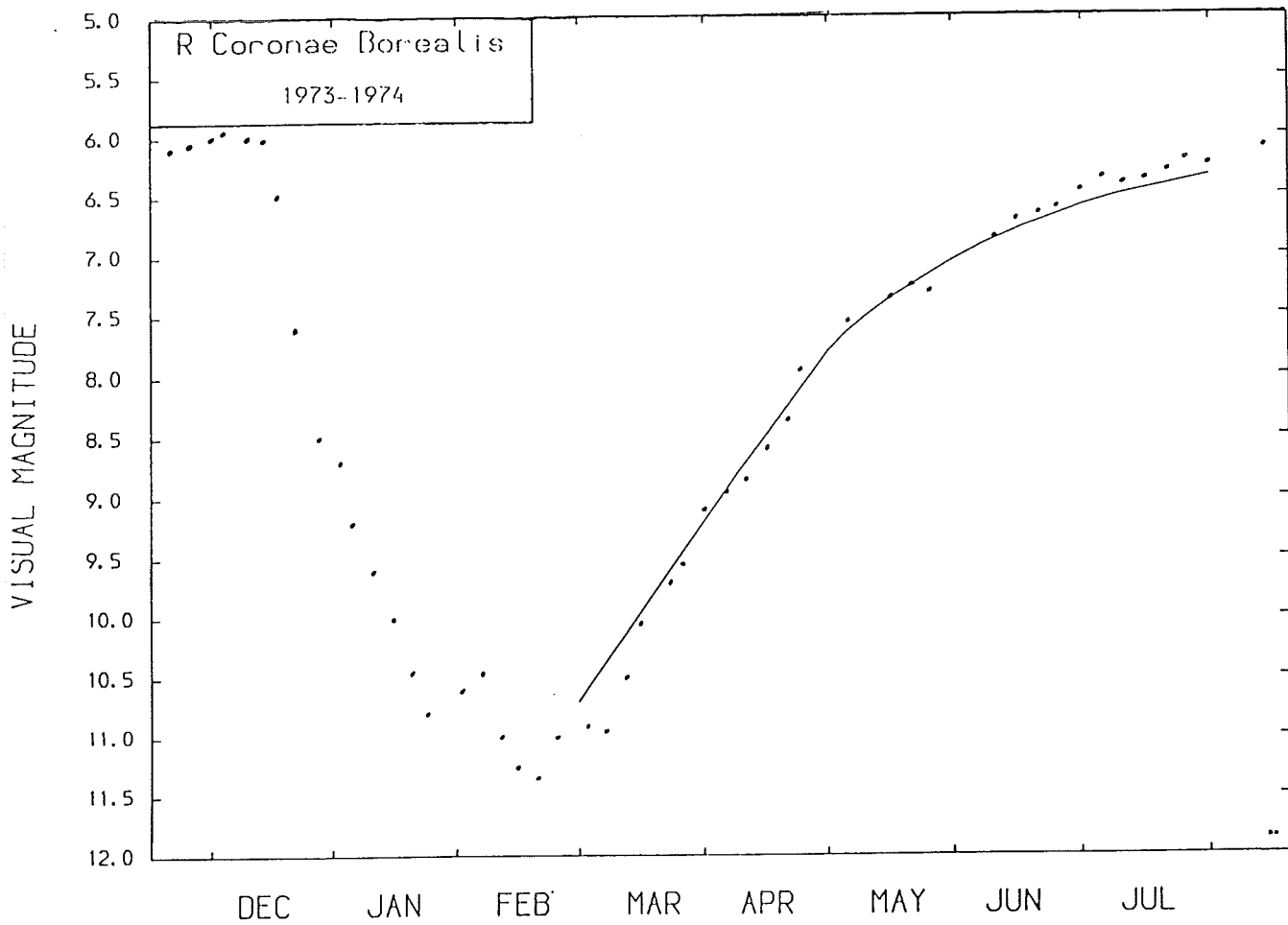


Figure 2.4 : This Figure shows a model fit, taken from Ashby (1976), of the light curve obtained by assuming a free carbon dust cloud moving away from the star in comparison with observed recovery of R CrB from a deep minimum.

OBSERVATIONS OF THE RCB GROUP

Many attempts have been made to estimate the luminosity and mass of R CrB, e.g., Eggen (1969). These have usually been based upon the spatial distribution or spectroscopic analysis which until recently fixed the mass as 'low' and the bolometric magnitude somewhere between -1.0 and -6.0. Wood (1976) was the first to fix the mass at about 1 solar mass from his linear non-adiabatic modelling of the star, from which he obtained a bolometric magnitude of (-5.1 ± 0.4) , which agrees well with what was expected.

Later Saio (1983) found the following theoretical constraints:

$$0.9 < M/M_{\odot} < 3.0$$
$$4.2 < \log (L/L_{\odot}) < 4.7 .$$

From evolution work of Paczynski (1971) and Trimble (1971,1972), it is possible to show that the upper mass limit should be $2.5M_{\odot}$.

The last major issue is the evolution of these objects, which is poorly understood and a subject for speculation. Searle (1961) proposed that R CrB evolved from a 1 or 2 solar mass main sequence star that has obtained a C/O core (with helium shell and hydrogen envelope). Sometime during its evolution after leaving the main sequence, the star either consumes or ejects its hydrogen envelope. The possible ejection of the hydrogen envelope has led to speculation by Searle that R CrB may be the nucleus of a planetary nebula. (This could explain the marked differences in their respective abundances). Wheeler (1978) also expressed this view, connecting it with planetary nebulae via SN I. He pointed out that the spatial distribution of both classes of objects is similar. Schonberner (1975) has shown that stars with the above configuration and low mass, (0.65-1.0) solar

OBSERVATIONS OF THE RCB GROUP

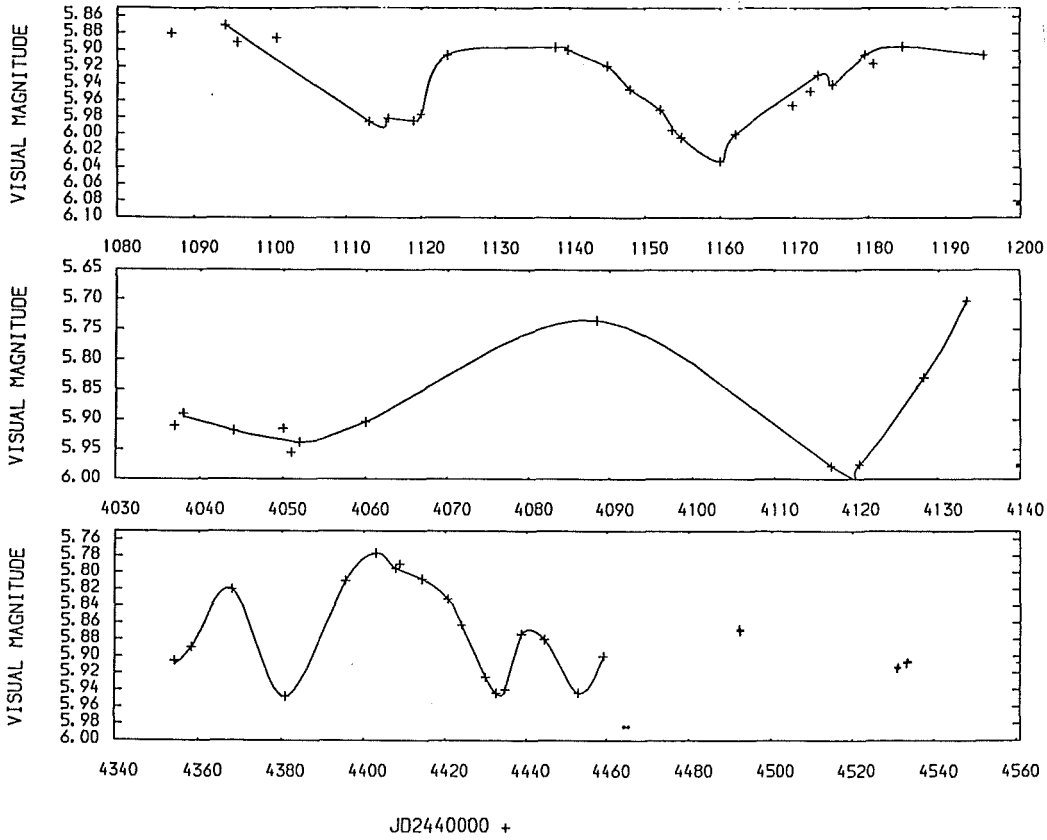


Figure 2.5 : This Figure shows the semi-regular light variations observed in R CrB (taken from Glass, 1978).

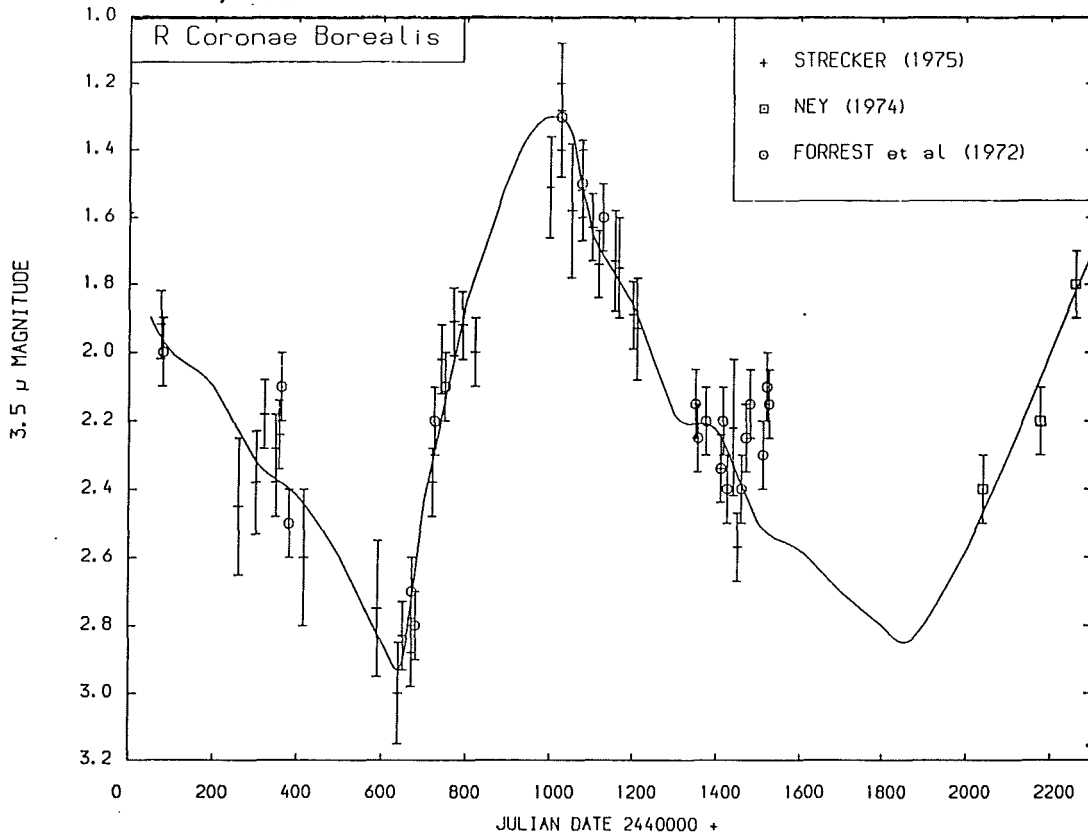


Figure 2.6 : This Figure shows the variation in the 3.5μm band for R Coronae Borealis (taken from Strecker, 1975).

OBSERVATIONS OF THE RCB GROUP

masses, progressed from RCB objects to He B like objects, in about 10000 years and then evolve on to the white dwarf stage. Heber & Schonberner (1981) showed that the galactic distribution of He B stars is consistent with this evolutionary sequence. The work of Kilkenny (1982) on RY Sgr's period change is consistent with this evolutionary sequence, though Hunger (1975) pointed out that He B stars are comparatively poor in CNO compared with RCB objects.

2.3.1.2 RY Sagittarii - RY Sgr has been known since 1751, though only spasmodically observed up until 1897 (i.e., Lacaille, 1847), from which point it was systematically observed by Innes (1903, 1907) until 1902. Since then it has been fairly regularly observed at many observatories around the world. For a detailed list of visual observations from 1897 to 1982 see the references cited in Marraco & Milesi (1982). See Figure 2.7 for light curve of RY Sgr.

RY Sgr was found to be variable in its visual light curve, by Campbell & Jacchia (1946). This variability was confirmed by the intensive photometry and spectrometry of Alexander et al (1972) between 1967 and 1970. Alexander et al (1972) found that RY Sgr was a semi-regular variable in U, B and V with a period of about 38.6 days, and an amplitude of about 0.5 magnitudes in V (see Figure 2.8). From the spectroscopic analysis, a velocity curve was obtained, which varied in about the same period (amplitude of 30 km/sec), showing that the variations are due to small amplitude pulsations. These pulsations were also observed in L, and seem to indicate that the infrared excesses are governed by the star and not by an eclipsing infrared companion star as put forward by Humphreys & Ney (1974). There was little phase-lag between the visual and infrared 'light' curves, which is to be expected if the star is surrounded by small

OBSERVATIONS OF THE RCB GROUP

particles. The amplitude of pulsation seems to decrease with decreasing wavelength, as is found in the classical Cepheids (Wisniewski & Johnson, 1968). There is also a long term variation in the infra-red excess with a period of ~ 1100 days and 1.4 magnitudes (see Humphrey & Ney, 1974, Kilkenny, 1978). Pugach (1977) has shown that the deep minima of RY Sgr always occur around the same phase in the semi-regular pulsations of the star, indicating that the deep minima may depend upon the pulsation in some way. Feast (1986) postulated that the star may eject material during this phase of pulsation, and tentatively shows that if material is ejected at every pulsation maximum in a random direction, then the solid angle of material required for obscuration of the underlying star, divided by four π steradians times the observed pulsation period, is about 1100 days, or the observed long term period of variation seen in L.

Kilkenny (1982) analysed all available visual observations in the literature and found that the period of RY Sgr is changing by about -0.00004 days/day (confirmed by Marraco & Milesi, 1982). In this analysis he also found that the phase of the semi-regular pulsations changed sinusoidally over a 50 year period. There was also a further random 10 day phase change in some periods.

The observed change in period can be explained by either mass loss or evolution. It has been shown that the former explanation would require a mass loss of about 0.001 solar masses a year, which is inconsistent with observation (e.g., Spite & Spite, 1979; Forrest et al, 1972) indicate that small amounts of material are ejected asymmetrically at deep minima. Also, such a large mass loss rate would contradict the estimated lifetime of about 1000 years (based on distribution and numbers). The evolutionary explanation has been shown by Kilkenny (1982) (using Schonberner's (1977) evolutionary

OBSERVATIONS OF THE RCB GROUP

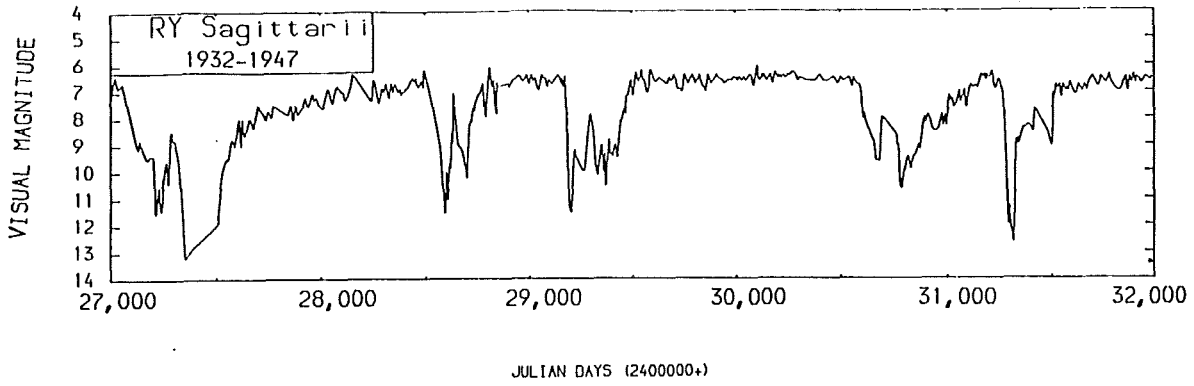


Figure 2.7 : This Figure shows the light curve of RY Sgr over a few deep minima (taken from Alexander et al, 1972)

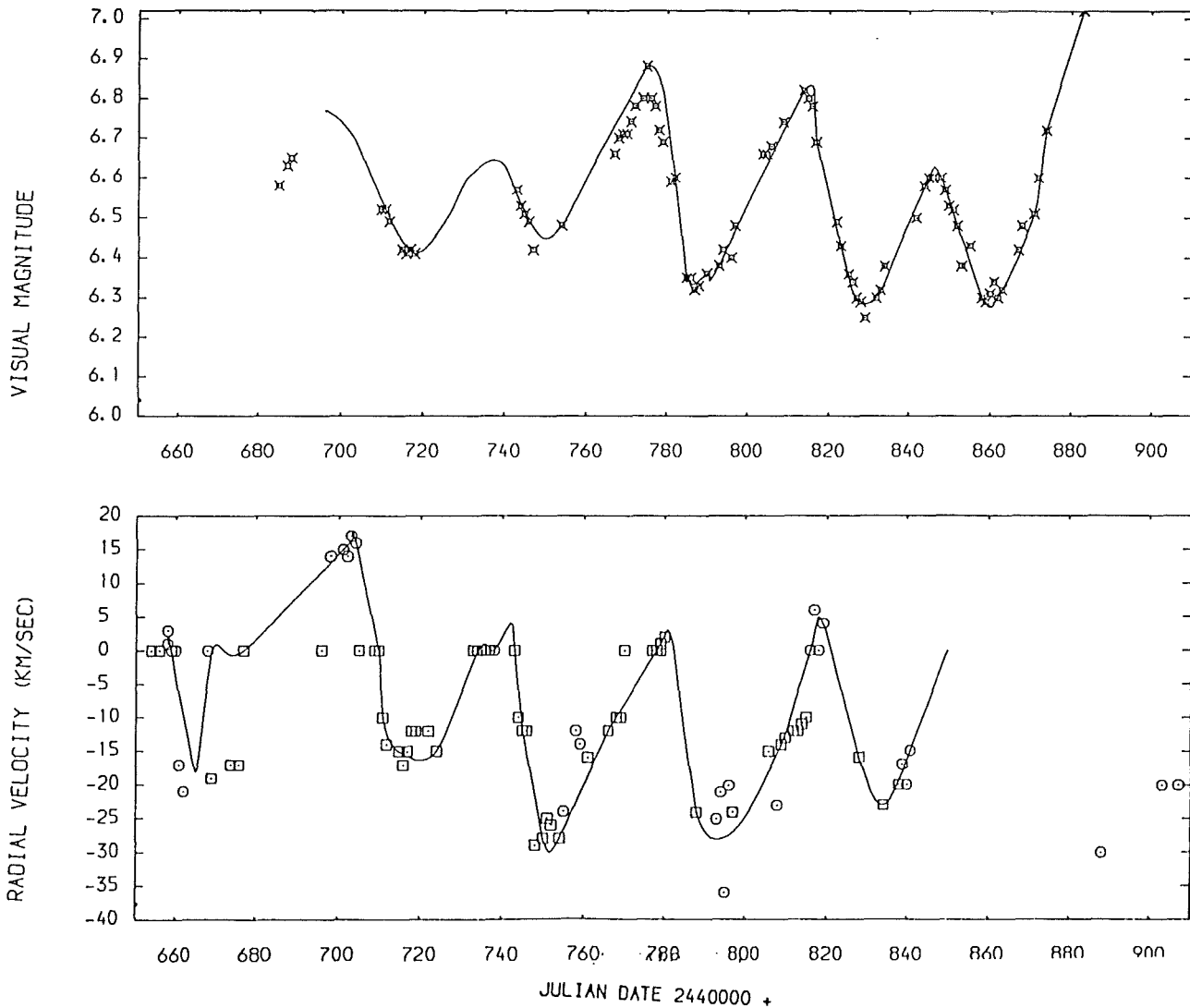


Figure 2.8 : these Figures show the semi-regular variations in RY Sgr's light curve and Velocity curve, as found by Alexander et al (1972).

OBSERVATIONS OF THE RCB GROUP

sequences for a one solar mass hydrogen deficient star of effective temperature 6900 K) to give good agreement with the observed decrease in period.

Ludendorf (1906) noticed that the hydrogen Balmer lines were missing in his low dispersion spectra of RY Sgr. This was later confirmed by Bidelman (1953). Bidelman (1953) also noticed that RY Sgr's spectra also showed strong C I lines, though C₂ bands were weak and the isotope ¹³C was virtually absent (this absence has still to be explained). Danziger (1965) and Searle (1961) obtained similar spectra from their own spectroscopy on RY Sgr. From the spectral analysis found in Bidelman (1953), Searle (1961), Danziger (1965) the following stellar parameters for RY Sgr can be found:

$$\begin{aligned}T_{\text{eff}} &= (6900 \pm 600) \text{ K} \\ \log(g) &= (0.1 \pm 0.5) \\ \langle X \rangle &< 0.0001 && \text{(by number)} \\ \langle Z_{\text{c}} \rangle &= 0.1 && \text{(by number)}\end{aligned}$$

Spectral type = G0 Ib

Alexander (1982) gives a good description of how RY Sgr's spectrum changes during a deep minima. The main features are chromospheric emission lines that decay in about 22 days, while the initial decrease in photospheric radiation is on a time scale of 5 days. During this phase, Ca II lines show displacement velocities of about +250 km/sec, indicating the ejection of matter. This fits in well with Loreta & O'Keefe's (1939) carbon cloud model, as well as satisfying the Forrest et al (1972) and Lee & Feast (1969) theories of asymmetric ejection of matter. The absorption spectrum and colours follow a drop in light on the rising branch, apparently due to filling in of the photospheric absorption lines by chromospheric emission lines. The primary cause

OBSERVATIONS OF THE RCB GROUP

of this phase seems to be due to a decline in photospheric radiation. This may possibly be due to the formation of fresh dust near the photosphere. Displaced absorption lines Ca II and Na I are present throughout this stage.

RY Sgr is heavily reddened. This fact combined with the large infra-red excesses observed by Lee & Feast (1969), Feast & Glass (1973) and Kilkenny & Whittet (1984), strongly supports Loreta & O'Keefe's (1939) dust shell model. From analysis of the broad band photometry of Lee & Feast (1969), Feast & Glass (1973) and Kilkenny & Whittet (1984), it can be shown that RY Sgr has an effective temperature of $(7000 \pm 500)K$ and is surrounded by a circumstellar dust shell of about $(800 \pm 100)K$. This assumes that the cloud is opaque, isothermal and emits radiation as a black body. The shell has been shown by Hecht et al (1984) using IUE data, to consist of small (5 - 70)nm amorphous carbon grain's, though the estimates for the grain sizes range up to a few hundred nanometers. The absolute magnitude of this star is still in doubt. Estimates range from -3.0 (Eggen, 1969) to -4.2 (Kilkenny & Whittet, 1984). Saio & Wheeler (1983) has shown using theoretical models that:

$$0.8 < M/M_{\odot} < 3.0$$

$$4.1 < \log(L/L_{\odot}) < 4.8.$$

This agrees with the results of Hill et al (1981), based on Schonberner's evolution curves for hydrogen deficient objects, which give:

$$M/M_{\odot} = (1.25 \pm 0.25)$$

$$\log(L/L_{\odot}) = (4.2 \pm 0.2).$$

OBSERVATIONS OF THE RCB GROUP

2.3.1.3 S Apodis - S Aps first appears in the Cape Photographic Catalogue of 1894. It was only scantily observed up until about 1960. Since, it has been well observed at visual wavelengths. Kilkenny (1983b) published light curves for the period 1960 - 1982 (See Figure 2.9). Using quadratic fits to this data, he found that S Aps was a semi-regular variable of amplitude <0.2 magnitudes and period (138.7 ± 0.9) days. He also found an astonishing value for k (the growth rate) of (-0.184 ± 0.07) days/period. This value is hard to explain as no model of hydrogen deficient stellar evolution has such a large k . Roser's (1975) values are the largest in the literature and these are a hundred times smaller than the above k . If this k is correct, there are two possibilities according to Kilkenny (1983a):

(i) Schonberner (1975) has shown that for stars with stellar masses < 0.65 solar mass the helium flash does not occur and that it is possible for a star to collapse under gravity in a few hundred years, rising rapidly in effective temperature as it does so.

(ii) Schonberner (1979) has shown that stars on the asymptotic giant branch (AGB) with steady mass loss can undergo helium flashes at low effective temperatures (4000 K), which cause extensive blue loops with time scales of about a 1000 years. The rapid changes in effective temperature give k of about -0.04 days/period. The problem with this mechanism is that the models assume normal main sequence abundances initially ($X = 0.74$). The loss of the hydrogen envelope poses a problem, as no mechanism for this is known.

OBSERVATIONS OF THE RCB GROUP

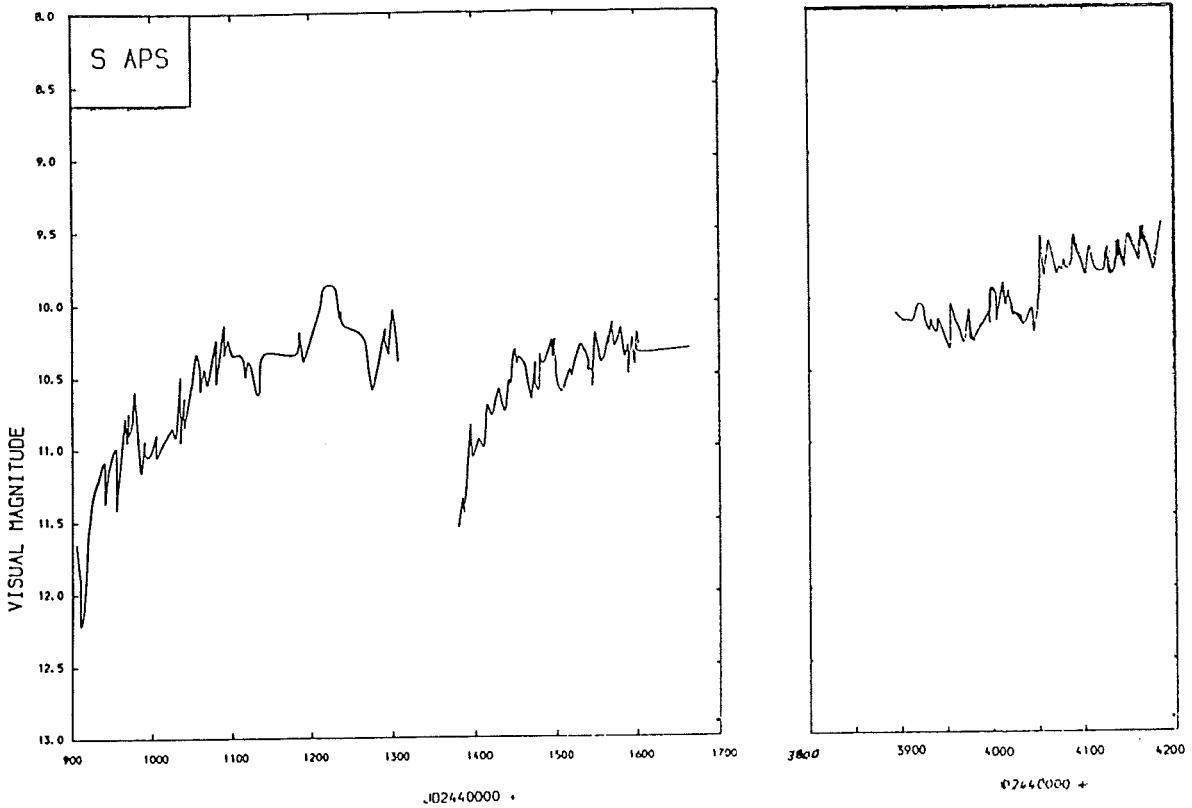


Figure 2.9 : Light curve from Kilkenny (1983b), of S Aps During the period 1960-1982

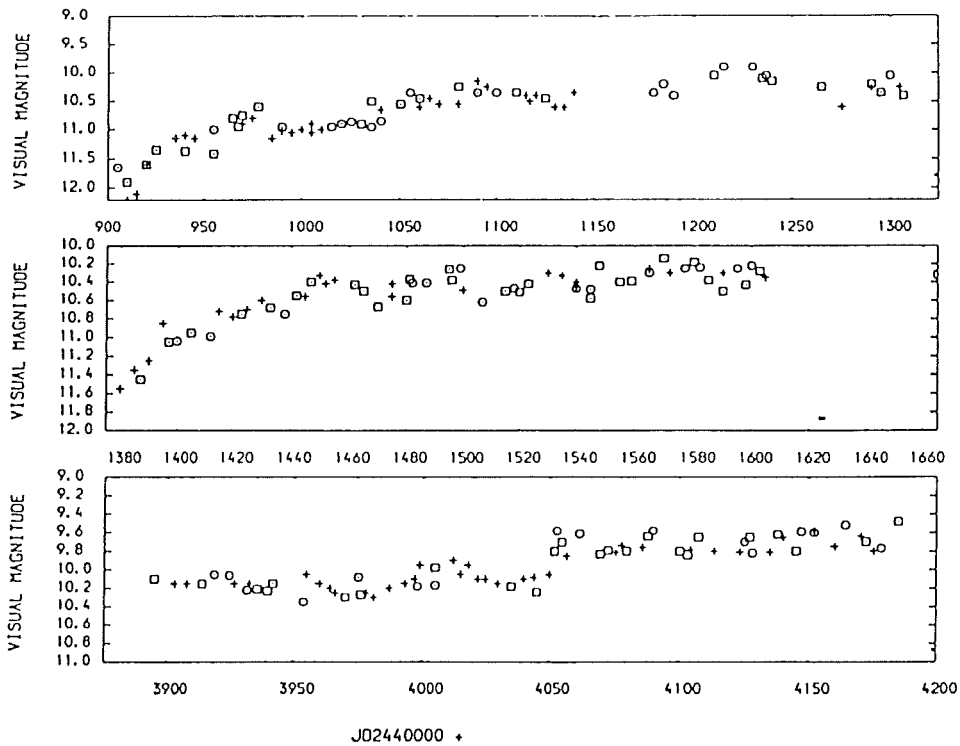


Figure 2.10 : This Figure shows the semi-regular variations in S Aps's visual light curve, before and after the change in its period from 120 to 40 days.

OBSERVATIONS OF THE RCB GROUP

Kilkenny (1983b) shows that there has been a mode change in S Aps sometime between the 1971 deep minima and 1980, the new period being (39.8 ± 0.2) days with a k of (0.019 ± 0.019) days/period (least squares fit). This change can clearly be seen in Figure 2.10. Kilkenny also notices that the amplitude of these small variations seem more prominent during or just after the recovery of the star from a deep minimum.

Glass (1978) observed that the carbon feature is very strong in S Aps, but states that this is probably due to a low effective temperature, rather than high carbon abundance. Payne-Gaposchkin (1963) found an effective temperature of (4200 ± 500) K for S Aps, which was later confirmed by the broad band photometry of Kilkenny & Whittet (1984). Kilkenny & Whittet (1984) also found a circumstellar opaque isothermal shell temperature of (800 ± 50) K which fits the observations well.

2.3.1.4 UW Centauri - Since UW Cen was discovered in 1885 it was infrequently observed beyond classification as an RCB star. The first systematic observing programme on UW Cen was by Bateson (1972, 1974, 1975 and 1978) from 1956 to 1978 and shows clearly that UW Cen undergoes small amplitude (<0.4 mag.) semi-regular variations with a period of about 43 days (see Figure 2.11) in its visual light curve. Kilkenny (1983b) analysed the available visual data and found a period of (42.82 ± 0.09) days with a growth constant (k) of $(+0.003 \pm 0.0004)$ days/period. This disagrees with Schonberner's (1977) evolution of low mass hydrogen deficient stars where k is about -0.0001 .

OBSERVATIONS OF THE RCB GROUP

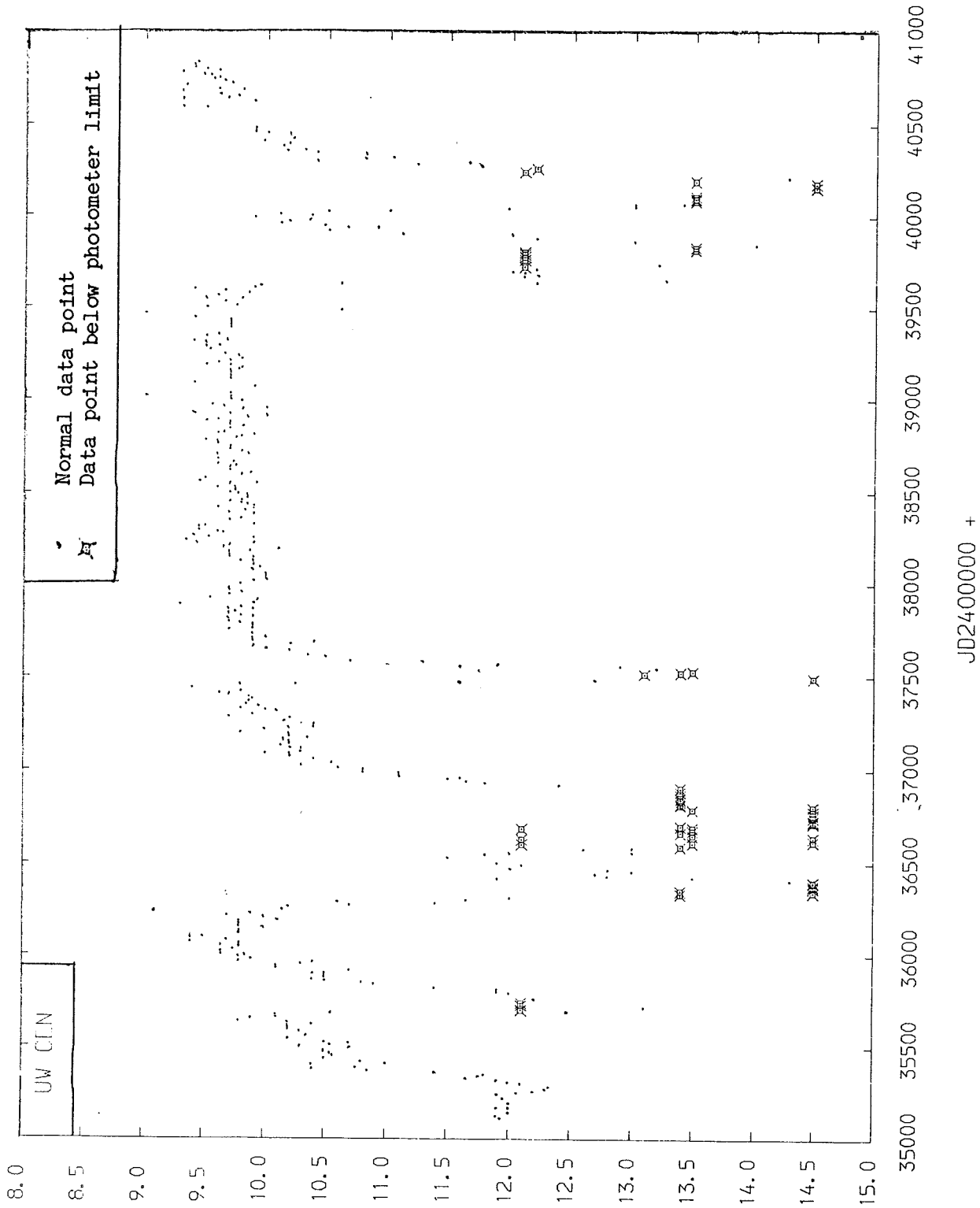


Figure 2.11 : This Figure shows the semi-regular variations of UW Cen using the data given in Bateson (1972, 1974, 1975 and 1978)

OBSERVATIONS OF THE RCB GROUP

Kilkenny & Whittet (1984) estimated the effective temperature of the star to be (6000 ± 500) K from their broad band photometry. They found it hard to fit an opaque isothermal shell to the infra-red observations and concluded that the shell in this case could not be so simplified (the best fit was about 700 K). This agrees with the spectral analysis of Feast & Glass (1973), who found a typical RCB spectra and a spectral type of R_3 .

2.3.1.5 LR Scorpii - LR Sco was classified as an SR variable of period 104.4 days and amplitude 1.4 magnitudes by Shapley & Swope (1934) and later Kukarkin et al (1970). Recently Stephenson (1978) found that its spectrum was typical of the RCB group, i.e., no Balmer lines and a strong carbon feature.

Carter et al (1979) found that the star had a typical RCB infra-red excess and argued that it should be classified as an RCB star. Its spectral class is Fp which at least places it in the right part of the HR diagram. The main problem with this classification is that the star does not appear to have ever faded during all the years it has been observed. If it does prove to be a member, then its long period would help to confirm the mode change detected in S Aps (Kilkenny, 1983b) by showing that long period variations do exist in RCB's.

2.3.1.6 XX Camelopardalis -

XX Cam was discovered in 1948 by Yuin (1948) after its only recorded deep minimum in 1939/40 (JD2429631.573). Bidelman (1948) then showed by spectral analysis that XX Cam belonged to the RCB group, and also that it was a 'hot carbon star'.

OBSERVATIONS OF THE RCB GROUP

Bidelman (1951) gives the following data:

$$m_v = 8.7-10.3$$

$$V_{rm} = +15.9 \text{ KM/SEC (Radial Motion)}$$

Spectral type = F_p .

The classification of this star was later confirmed by Warner (1967). Fernie (1971) shows that XX Cam has no Cepheid-like pulsations in its light curves at U, B and V wavelengths, confirming the findings of Landolt (1968) who found that the visual magnitude at maximum light was 7.32 magnitudes. Since then Totochava (1973, 1975) observed that a 40 day variation was present at UBV wavelengths (See Figure 2.12) during the period 1971-1973. Also, there appeared to be a rapid 2 hour, small amplitude (<0.2 mag.) variation in V, though the observations at UBV wavelengths were too widely spaced to notice such a rapid variation in their light curves. The first high dispersion spectrogram was taken by Bidelman (1948) who found the following atmospheric parameters:

$$V_{turb} = 9 \text{ +/- } 1 \text{ KM/SEC}$$

$$m_v = 7.35$$

$$T_{eff} = 5,800 \text{ +/- } 500 \text{ K}$$

Spectral type = G_2 .

Orlov & Rodriguez (1974) gives abundances that agree with those found by Bidelman (1948). Wallerstein et al (1984) show from their spectral analysis of the surface of XX Cam; that XX Cam and R CrB are the only stars to show the activity of the Ne - Na burning cycle.

OBSERVATIONS OF THE RCB GROUP

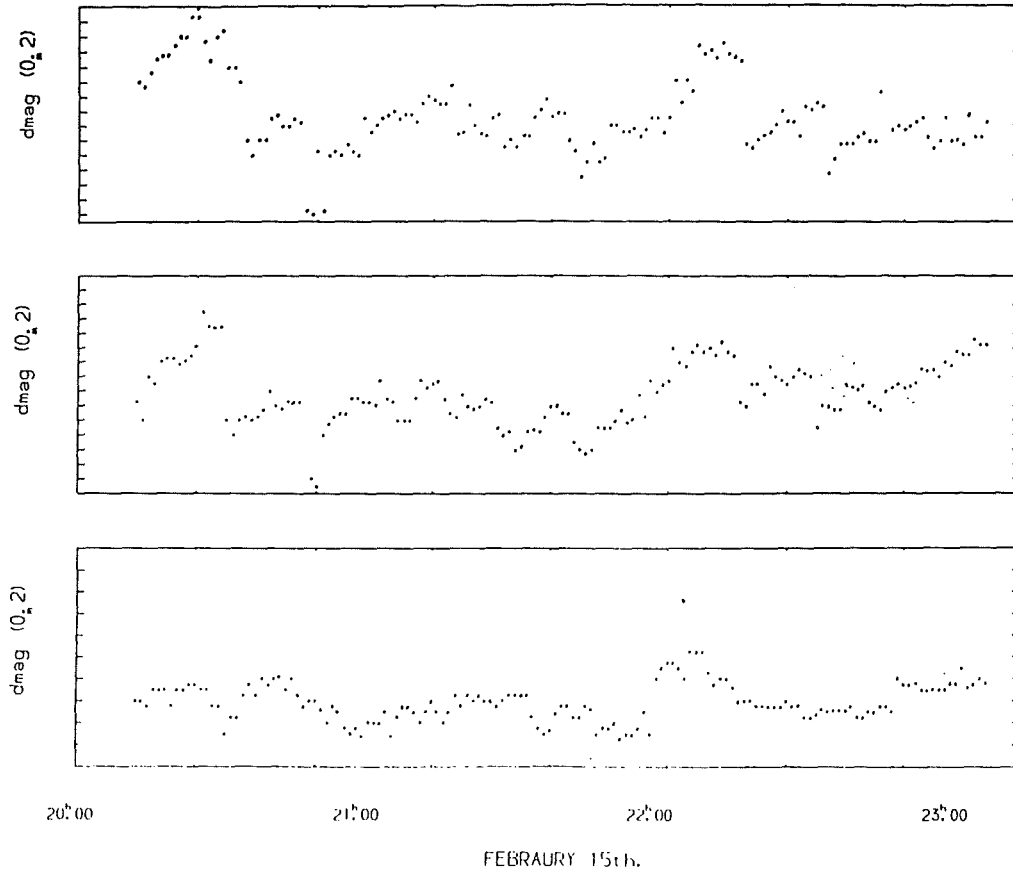


Figure 2.12 : This Figure shows the small variations in XX Cam's light curve seen by Totochava (1975).

OBSERVATIONS OF THE RCB GROUP

Cottrell & Lambert (1982) gives a detailed array of elemental abundances together with some other useful atmospheric parameters:

$$\begin{aligned}\text{Log}(g) &= 0.0 \pm 0.3 \\ T_{\text{eff}} &= 7,000 \pm 250 \text{ K} \\ [\text{C}]/[\text{He}] &= 0.003 \quad (\text{by volume}) \\ [\text{H}]/[\text{He}] &< 0.0001 \quad (\text{by volume}).\end{aligned}$$

Shenavrin et al (1979) cast doubt upon XX Cam belonging to the RCB group, pointing out that it has undergone only one deep minimum since 1895, and that this was a relatively shallow (about $1^{\text{m}}.7$) symmetric one, instead of the usual asymmetric deep minima, characteristic of the RCB class. Also no appreciable infra-red excesses have as yet been found around XX Cam. This indicates that it probably belongs to the hydrogen deficient carbon class of stars rather than the RCB class of stars.

2.3.2 Other RCB Stars

2.3.2.1 UV Cassiopeiae - UV Cas was found to be variable by D'Esterre (1913) and from this minimum Ludendorff (1919) placed it in the RCB group. Payne-Gaposchkin & Gaposchkin (1938) doubted the membership of UV Cas in the RCB group and this seemed to be verified by Weber (1966) in his observations between 1945 and 1965, in which UV CAS does not appear to undergo any more deep minima. Its membership was doubted even more when Zavatti & Burchi (1975) published further observations from 1965 to 1975 in which no deep minima occurred. Finally Rao (1980) observed a deep minimum for this star in the late seventies and also argues that its spectrum shows classic RCB signs, i.e., no Balmer lines and a strong carbon feature. UV Cas also has a large infra-red excess typical of the RCB group.

OBSERVATIONS OF THE RCB GROUP

2.3.2.2 SU Tauri - SU Tau was first visually observed by Miss Cannon in 1906, though it was not classified as an RCB until Pickering (1908), who observed SU Tau during a deep minimum, and confirmed his findings by looking at Harvard patrol plates back to 1885. SU Tau is not circumpolar, making it impossible to get complete light curves. Nonetheless, it is the second best observed Northern hemisphere RCB after R CrB itself.

Bidelman (1953) took a high dispersion spectrum of SU Tau in which though the C_2 bands were weak, the C I lines were strong indicating a spectral class of $G0_{ep}$. The next major discovery was made by Low (1970) and confirmed by Geisel (1970) that SU Tau has an infra-red excess. They gave the circumstellar shell a temperature of 1450 K based on their photometry. Yashmita (1974) finds that SU Tau has a radial velocity of (58 ± 5) km/sec. This along with its galactic co-ordinates (See Table 2.1) indicates that it could be a disc star. Howarth (1976) shows that the minima follow Poisson statistics with a time constant of (1143 ± 220) days. Thus it would appear that SU Tau is perfectly aperiodic in nature. Yashmita's analysis of the light curves dating back to 1885 therefore show that there is no semi-regular behaviour with amplitude greater than 0.04 magnitudes.

Shenavrin et al (1979), from his broad band photometry, has shown that SU Tau is best fitted by a supergiant F8 I ($T_{eff} = 6000$ K) surrounded by an opaque isothermal shell of temperature <900 K.

OBSERVATIONS OF THE RCB GROUP

2.3.2.3 W Mensae -

W Men was discovered in 1927 by Luyten, who noticed it had the deep minima peculiarities of the RCB type variables and so assigned it to the RCB group. W Men was then virtually unobserved until 1956 when Feast (1956) took a high dispersion spectrogram of it. From this spectrogram he derived its absolute magnitude, effective temperature, radial velocity and spectral type along with an estimate of its visual magnitude:

$$M_{\text{abs}} = -5.4$$

$$m_v < 16.0$$

$$V_{\text{rad}} = +260 \text{ KM/SEC}$$

$$T_{\text{eff}} = (6000-7000) \text{ K}$$

$$\text{Spectral type} = \text{S.gt. } F_5-G_0.$$

The next paper of any significance was again by Feast (1970), in which the question of the mass of RCB's is raised (later found by Wheeler (1978) to lie within the range $0.8-2.5 M_{\odot}$). In this paper, a better estimate of -5.2 for the bolometric magnitude at maximum light is given, along with corrected differential magnitudes. Glass (1972) finally fixed W Men's visual magnitude at maximum light to be 13.83 and assigned it a spectral type of $F8:I_p$. Later, Glass (1976) found an effective temperature of $6,500 \pm 500 \text{ K}$ by fitting black body curves to colour diagrams of the star.

2.3.2.4 WX Corona Australis - Other than infrequent observations after it was classified as an RCB, little appears in the literature until Payne-Gaposchkin (1963) made a spectroscopic analysis of the star. She found that WX CrA was of spectral type R_5 and assuming that

OBSERVATIONS OF THE RCB GROUP

it was a 1 solar mass star of absolute magnitude -4 assigned an effective temperature of (3700 ± 500) K. Glass (1978) showed that it has a very strong carbon feature, although he points out that this is probably due to the low effective temperature and not to high carbon abundance (compared with other RCB stars). Kilkenny & Whittet (1984) carried out an analysis on his broad band photometry of this star and found that a star of effective temperature (5000 ± 1000) K surrounded by an opaque isothermal dust shell of temperature (900 ± 50) K fitted the observations quite well. The temperature of the dust shell was later confirmed by Walker (1985) using IRAS data (See Figure 2.13 for WX CrA's light curve).

2.3.2.5 RS Telescopii - RS Tel first appears in The Cape Photographic Catalogue (1905). Other than being classified as RCB in nature it appears infrequently in the literature until 1963, with the exception of a high dispersion spectral analysis by Bidelman (1953). In this analysis, Bidelman (1953) found that the hydrogen lines were very weak and the carbon feature was very prominent, with strong CN bands also. This confirmed its membership of the RCB group. Feast & Glass (1973) also found some He I lines in its spectrum, during a deep minima, as seen in other RCB stars.

Payne-Gaposchkin (1963) fitted a model atmosphere to her spectra, found an effective temperature of 2500 K and assigned the star a spectral type of R_8 . The effective temperature was found to be (5000 ± 500) K by Kilkenny & Whittet (1984) from a black body fit to their broad band photometry. The circumstellar shell was found to be fitted best by an isothermal opaque shell of temperature (800 ± 50) K. This value is supported by IRAS observations in Walker (1985). See Figure 2.14 for RS Tel's light curve.

OBSERVATIONS OF THE RCB GROUP

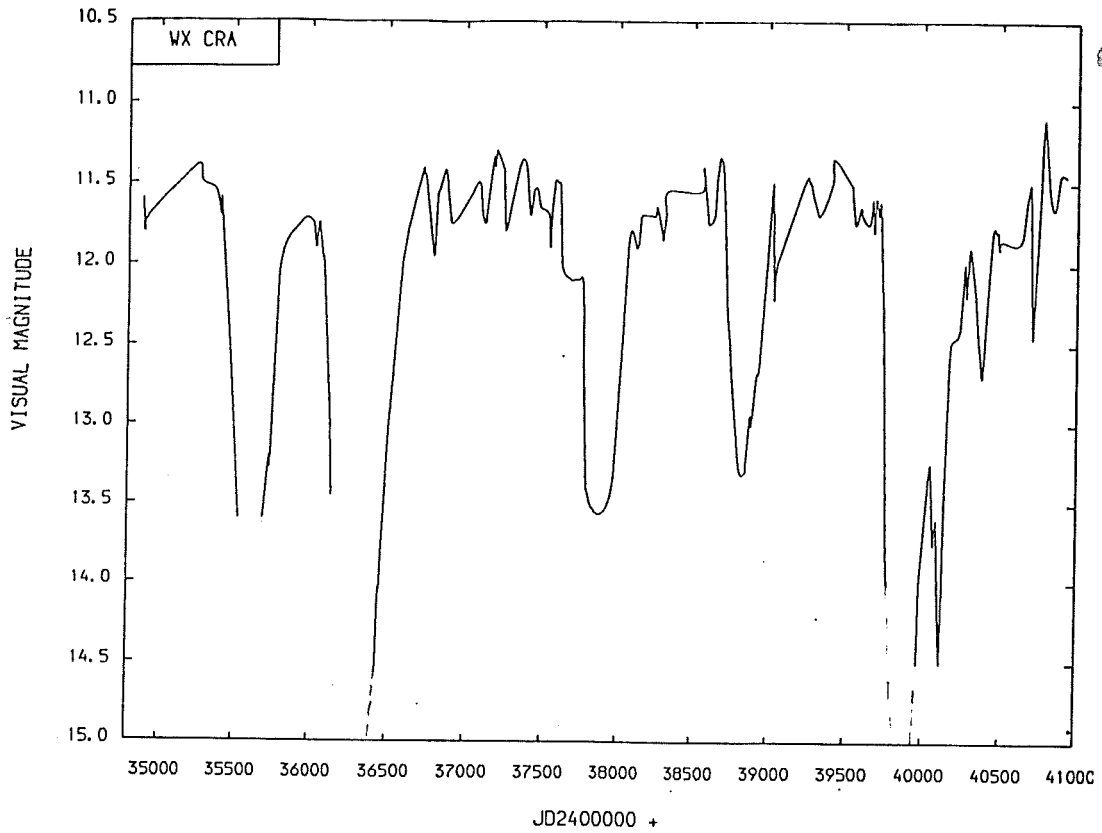


Figure 2.13 : This Figure shows the light curve of WX CrA taken from Bateson (1975).

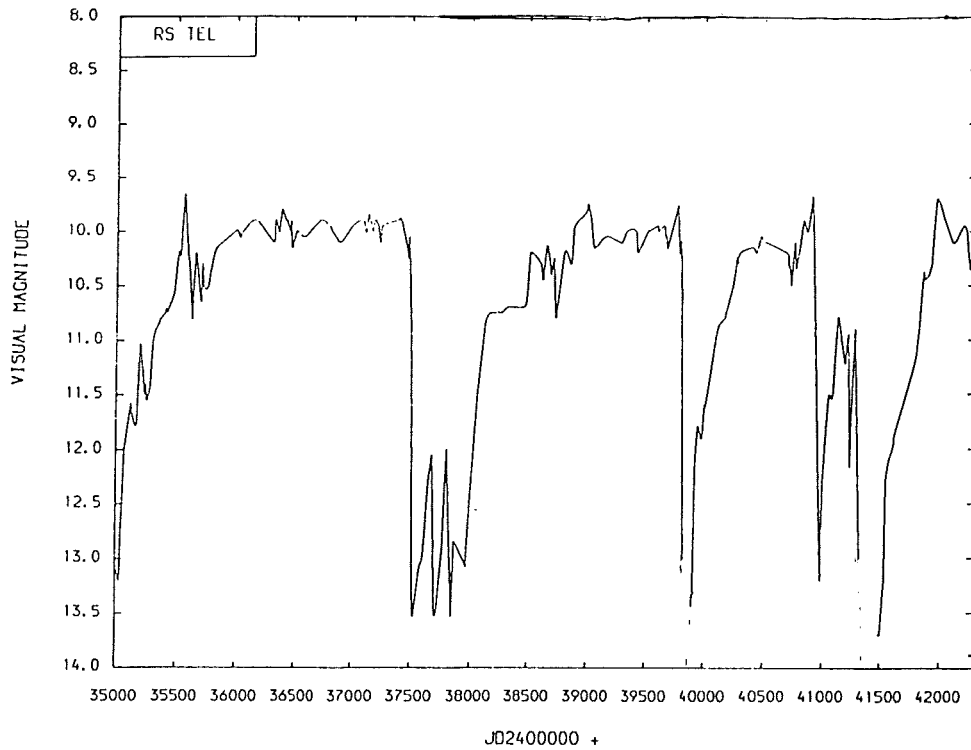


Figure 2.14 : This Figure shows the light curve of RS Tel also taken from Bateson (1975)

OBSERVATIONS OF THE RCB GROUP

2.3.2.6 RZ Normae - RZ Nor seems to have been little observed after it was placed in the RCB group, until Feast & Glass (1973) carried out broad band photometry and found that it did not appear to have any infrared excess. This cast doubt upon its membership of the RCB group, and this view was further compounded by the uncertainty of any C_2 lines in its spectrum. It was not until Glass (1978) observed RZ Nor and found strong infrared excesses, that this doubt was dispelled. The reason for the doubt, on closer examination, was due to observing the wrong star. Kilkenny & Whittet (1984) found that the fluxes from the broad band photometry were best fitted by a star of effective temperature (5000 +/- 500) K surrounded by a circumstellar shell (assumed isothermal and optically thick) of temperature (700 +/- 50) K. The temperature of the circumstellar shell was confirmed by Walker (1985) using IRAS observations. RZ Nor is notably redder than most of the RCB group (excepting RT Nor and GU Sgr). A light curve of RZ Nor is shown in Figure 2.15 .

2.3.2.7 U Aquarii - U Aqr seems to have been first observed in any detail by Feast (1975), who found it to have infrared excesses. U Aqr went through a normal RCB type fading in 1977. The main feature of U Aqr that warranted attention was found in the spectra of Bond et al (1979). As well as the usual strong carbon feature, Y II and Sr II lines were found, making it the first RCB star to show s-process elements in its atmosphere. The evolution and hydrodynamic modelling of this star is presented in Malaney (1985)

OBSERVATIONS OF THE RCB GROUP

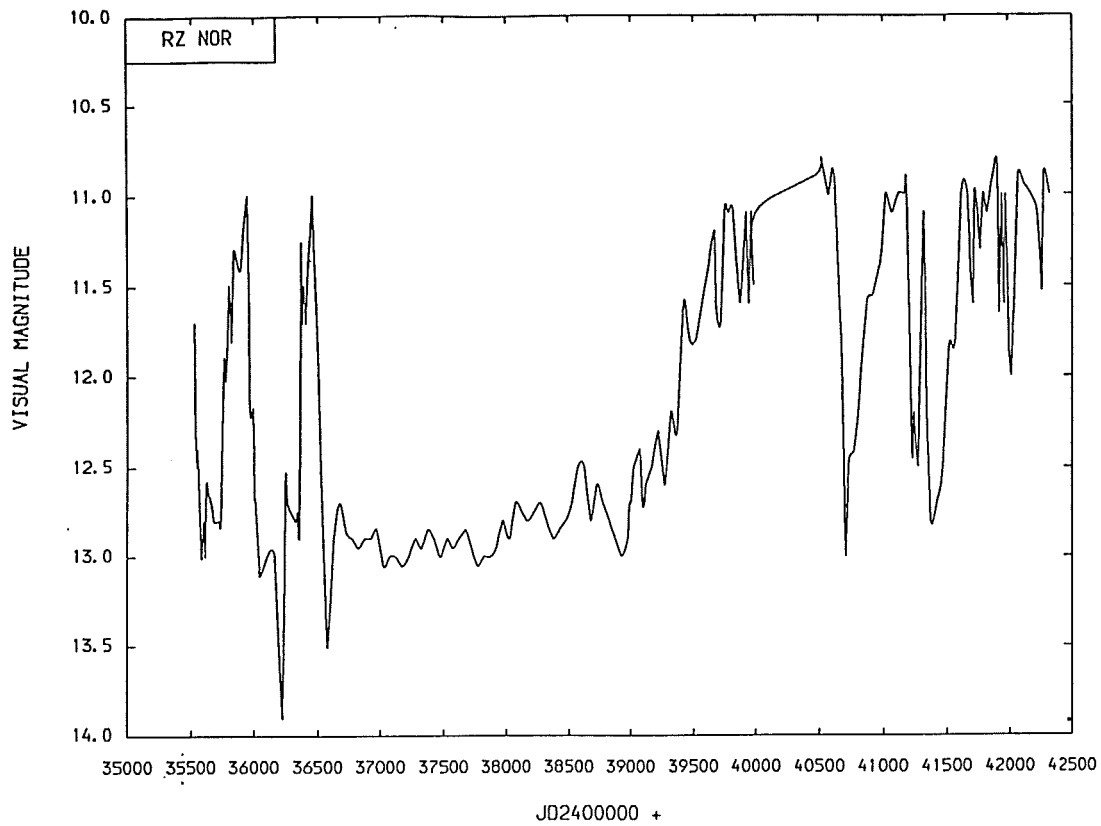


Figure 2.15 : This Figure shows the light curve of RZ Nor, taken from Bateson (1975)

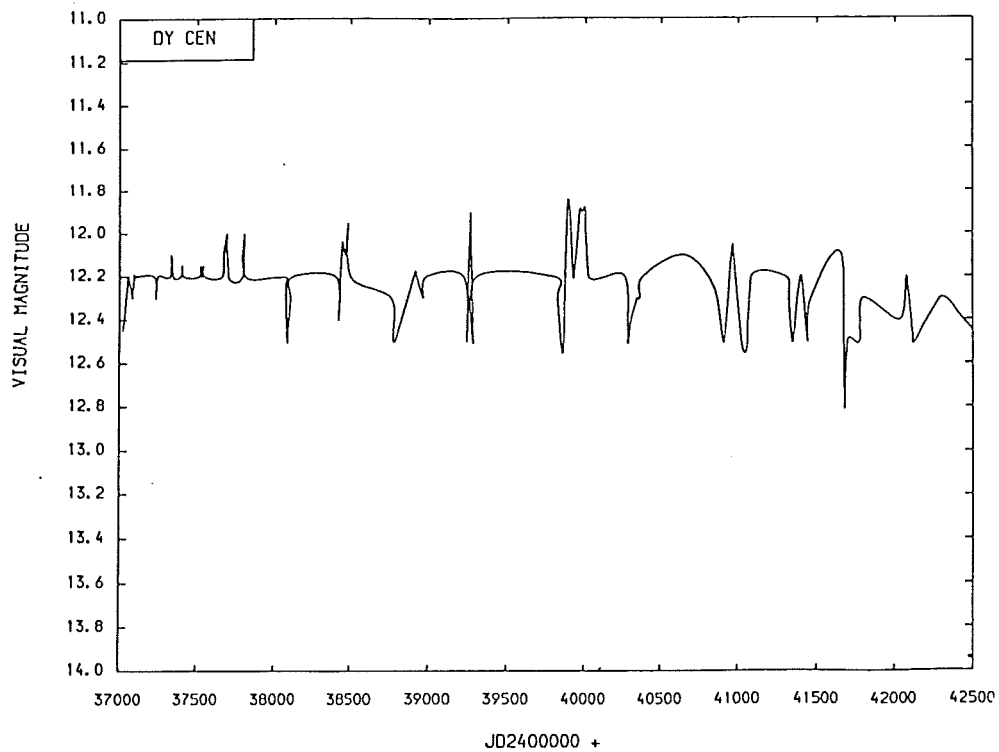


Figure 2.16 : This Figure shows the light curve of DY Cen, taken from Bateson (1975). Note that there are no deep minima in this period of observation.

OBSERVATIONS OF THE RCB GROUP

2.3.3 Hot RCB Stars

2.3.3.1 DY Centauri - DY Cen has undergone few deep minima. In 4000 days of observation by Bateson (1975), DY Cen did not fade once (see Figure 2.16). Further doubt about this star belonging to the RCB group was raised when Feast & Glass (1973) found no infra-red excesses at L wavelengths. Feast & Glass (1973) also found that all the spectral lines, including the calcium H & K lines were weak and that the star was bluer in the UBV region than most other RCB stars. Glass (1978) found similar results.

Kilkenny & Whittet (1984) found infra-red excesses at M though not at L or N and concluded that the star has complex fluxes that may be similar to those seen in MV Sgr. From a rough black body fit to the data, a star of effective temperature 10,000 K surrounded by circumstellar material of temperature <800 K is as good a model as any, short of a detailed model of the star.

2.3.3.2 V348 Sagittarii -

V348 Sgr was discovered to be variable independently by Woods (1926) and Schajn (1929). Parenago (1931), on the basis of the first light curve, classified it as an RCB object. Hoffliet (1958), after re-examining the star for the period 1900-1954, concluded that during the period JD2417500-JD2425000 it did indeed have an RCB type light curve. But since then its light curve has been more like that of a semi-regular variable. V348 Sgr was reported to spend most of its time near either maximum or minimum light, with quite rapid transitions between extremes (30-60 days rise, but decline was somewhat more rapid). The star shows quite frequent changes between extremes (150-250 days). The extremes are generally about 6 magnitudes (see Figure 2.17) in size.

OBSERVATIONS OF THE RCB GROUP

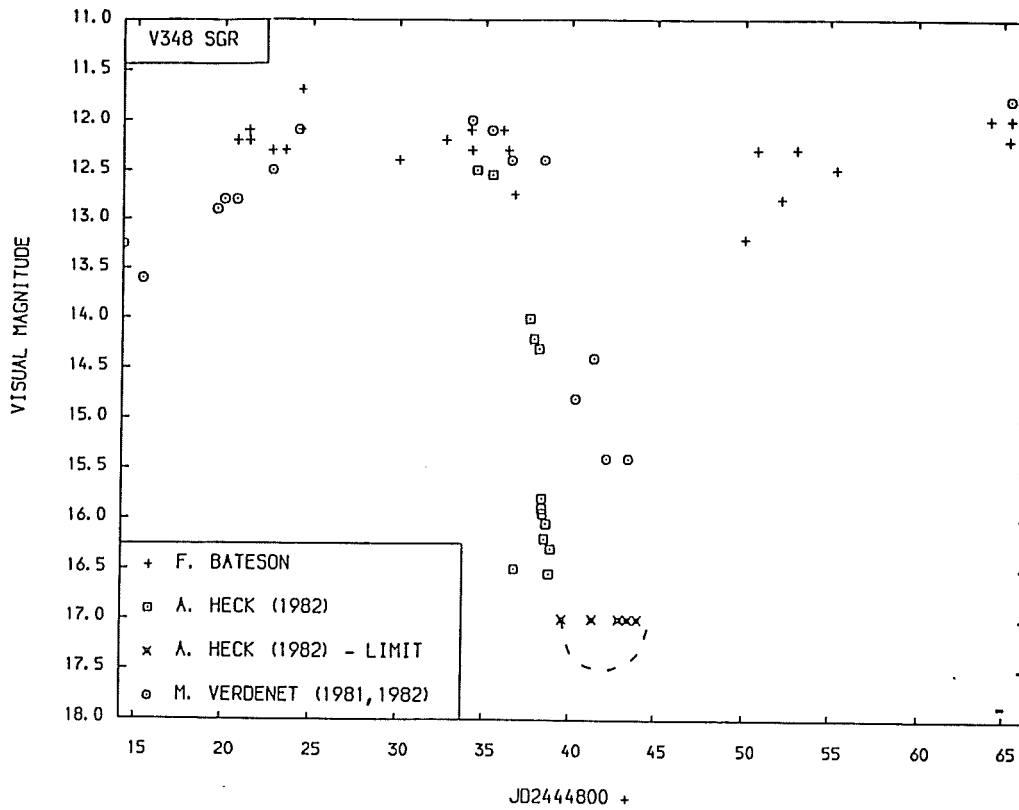


Figure 2.17 : This shows the light curve of V348 Sgr during its 1981 deep minimum as seen in Hecht et al (1981).

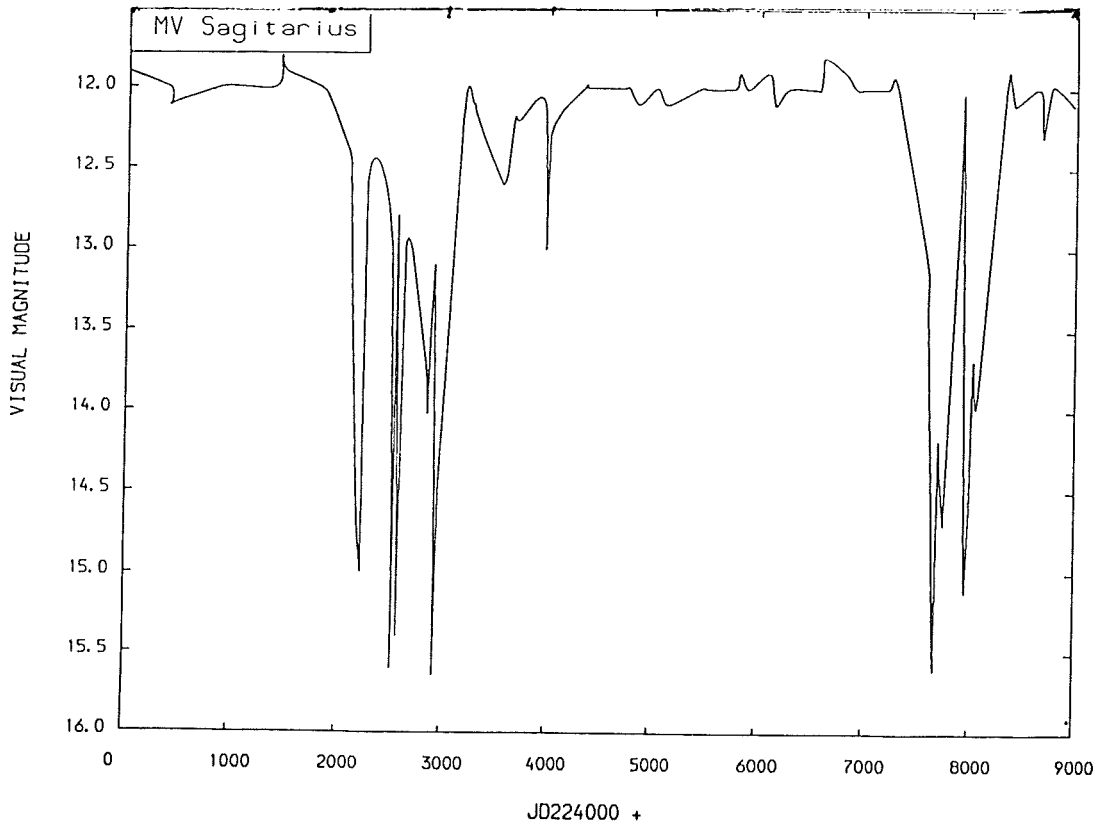


Figure 2.18 : Light curve of MV Sgr taken from Hoffliet (1958).

OBSERVATIONS OF THE RCB GROUP

High dispersion spectroscopy was carried out by Houziaux (1968) who found that it was a hydrogen deficient carbon object with strong C II lines in spectra. The spectra were reported by Houziaux (1968) to be nebula-like during minima and that P Cygni profiles were present at shorter wavelengths. Webster & Glass (1974) attempt to link V348 Sgr with a small group M4-18, He2-113 and CPD-56 8032 which are apparently old disc population stars in a late stage of evolution. These 3 form a natural extension of planetary nebulae with WC nuclei towards slightly cooler temperatures. Allen et al (1982) point out that there may be a connection between MV Sgr and V348 Sgr, both being hot RCB type objects, and with similar spectra.

From Feast & Glass (1973) and Roche & Aitken (1984) V348 Sgr is modelled, using a simple black body fit to broad band photometric data, as a star of effective temperature 10,000 K surrounded by a 'shell' of material at 900 K. Hence, along with MV Sgr, this is a hot RCB object and could indicate a later/earlier stage of evolution than the rest of the RCB group.

2.3.3.3 MV Sagittarii -

Miss Wood first found that MV Sgr was variable in her 1928 paper. Although it was not confirmed to be variable and a possible member of the RCB group until 1958 (Hoffliet, 1958). This membership was later confirmed by Herbig (1963). Using the photometry and spectroscopy of Hoffliet's paper, he found the following stellar parameters near maximum light:

$$T_{\text{eff}} = 20,000 \text{ K}$$

$$V_{\text{rad}} = -68 \pm 3 \text{ km/sec (20 blended lines)}$$

$$m_v = 11.38.$$

OBSERVATIONS OF THE RCB GROUP

Herbig (1963) also noted that He I was the predominant spectrum with a fainter underlying C II spectrum. Indeed the object appeared to resemble BD+10 2179 in most aspects except that MV Sgr also had faint Ne II lines in its spectra. In 1975, Herbig (1975) noticed that MV Sgr has forbidden Ca II lines in its spectra, which are quite rare in stellar objects, there being only a few objects known to have them. Freidjung & Viutti (1976) completed some theoretical work on the observed data using model atmospheres and found, assuming an optically thick circumstellar cloud, that:

$$\begin{array}{ll}
 R_* > 4.6 R_\odot & R_{\text{circ}} = (26-45) R_* \\
 T_{\text{eff}} = (16,000 \pm 5,000) \text{K} & T_{\text{circ}} = (1500-2000) \text{K}.
 \end{array}$$

Freidjung also derives the evolutionary sequence which is attributed to Heber & Schonberner (1981) who produced extreme HdC evolutionary sequences across the RCB region of the HR diagram. From these results, the following relation was shown to exist for these sequences:

$$\text{Log}(T_{\text{eff}}) = 3.7 + 0.25 \text{Log}(g).$$

Freidjung also obtains an over-estimate of the effective temperature of 19,600 K by neglecting all back warming from lines other than those due to He I. He does point out that the majority of RCB's have temperatures below 8,000 K and that:

$$\text{Log}(L/L_\odot) = 4.1 \pm 0.5 .$$

Drilling et al (1984a) place the effective temperature firmly at 16,000 K, by using full back warming in their analysis of IUE data. They note that MV Sgr is very similar to HD124448 in all respects in the ultraviolet, except that HD124448 only has stronger C II lines and no infra-red excess, and pose the question of whether this similarity may indicate some evolutionary connection between extreme He stars and MV Sgr. It seems more probable that extreme He stars come from HdC stars (Drilling et al, 1984b), and MV Sgr evolved from RCB stars on the ground that MV Sgr has an infrared excess while HdC stars do not. A light curve of MV Sgr can be seen in Figure 2.18

2.4 REVIEW OF LINEAR MODELS

This Section is a brief review of linear non-adiabatic models of the RCB stars. There are 6 main papers in the literature : Saio (1982), Saio & Wheeler (1983, 1985), Saio et al (1984), Cox & Stellingwerf (1980) and Wood (1976). The majority of this work has been done for abundances (0.0,0.9,0.1) and (0.0,0.98,0.02) using either the codes in Castor (1971) or the modified Castor (1971) codes in Saio (1983). In these codes, convection is treated using mixing length theory (mixing length = 1.5 x pressure scale height) in the initial equilibrium model. The reason for it not being included in the dynamic stage is that the theory is not very good and for the region of interest, ($T_{\text{eff}} > 6000$ K) convection carries only a small part of the flux. The outer boundary condition of total reflection was brought into doubt by Wood (1976), who thought that a running wave boundary condition would be more appropriate (due to the fact that his models showed running waves in their outer envelope). Saio (1984) showed from theory that the reflective boundary condition was quite acceptable as long as the pulsation frequency remained larger than a

OBSERVATIONS OF THE RCB GROUP

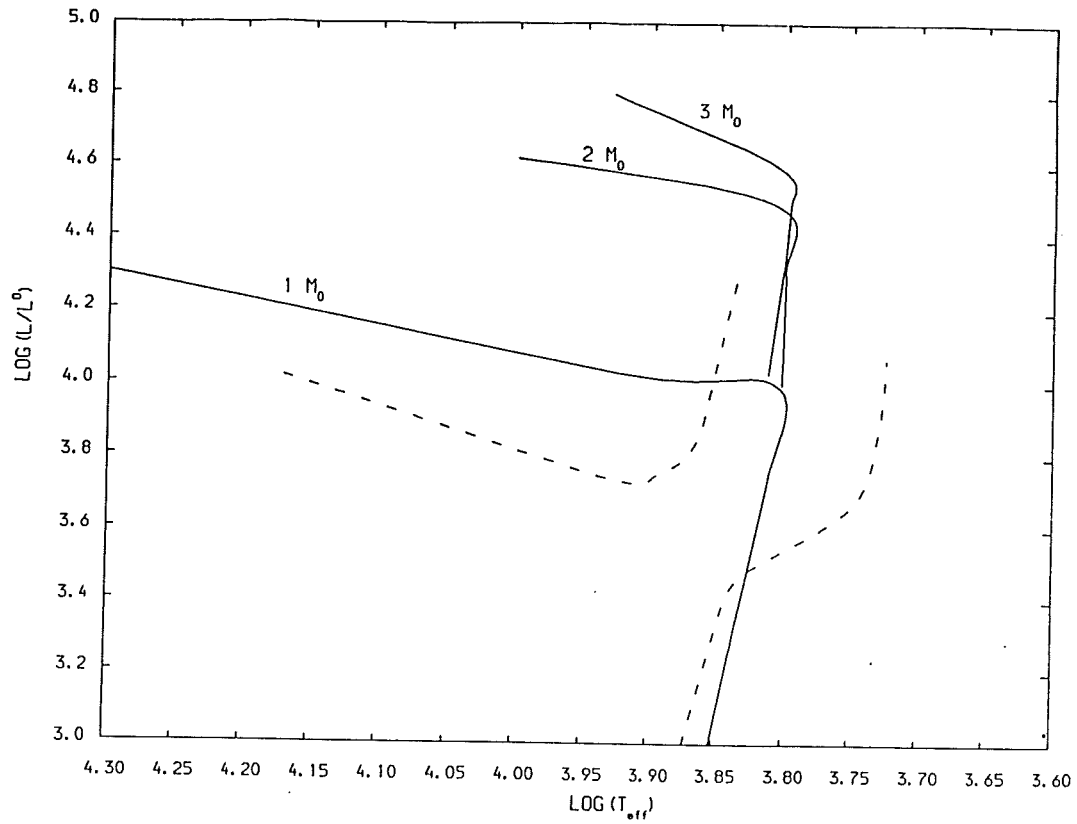


Figure 2.19 : HR diagram showing the fundamental blue edges of Saio (1984), linear non-adiabatic models, for models with masses of 1, 2 and $3 M_{\odot}$

OBSERVATIONS OF THE RCB GROUP

critical frequency (see Saio (1984) appendix B for proof). He also demonstrated that in all his models this criterion was met, though some came quite close to the critical frequency.

Cox & Stellingwerf (1980) found 'strange modes' which they attributed to some envelope ionisation mechanism. Saio (1982) defines them by the He I stabilisation effect they have in contrast to de-stabilisation usually observed for ordinary modes. This can be clearly seen if the work curves of the strange modes (Saio, 1982; Cox & Stellingwerf, 1980), which show damping in ionisation zones, are compared with ordinary mode work curves (Cox, 1974) which do not. This damping type behaviour is also seen in secular modes (Hansen, 1978) and has led Saio (1984) to associate these with the 'strange modes'. He points out that for high T_{eff} ($\log(T_{\text{eff}}) > 4.1$) the He I zone is very near or outside the outer boundary and this makes mode identification difficult.

Wood (1976) and Saio (1984) found the following trends of the periods in their linear analysis (P_k = period of mode k):

- (i) $P_k - P_{k-1}$ increases with increasing (L/M)
- (ii) P_1/P_0 increases rapidly with L for given mass
- (iii) ($P_{\text{nonad}} - P_{\text{ad}}$) increases with increasing L
- (iv) ${}^{\text{nonad}}P_k \rightarrow {}^{\text{ad}}P_k$ for lower T_{eff} ($\log(T_{\text{eff}}) < 3.88$) in many cases
- (v) ${}^{\text{nonad}}P_k \rightarrow {}^{\text{ad}}P_{k+1}$ for higher T_{eff} ($\log(T_{\text{eff}}) > 3.88$) in many cases.

The strange modes behaved in a more complex manner, having sequences of their own in $\log(P)$ - $\log(T_{\text{eff}})$ diagrams (especially at higher luminosities and effective temperatures), or appearing in the middle

of ordinary mode sequences (especially at lower luminosities and effective temperatures). The models of Wood (1976), Cox & Stellingwerf (1980) and Saio (1984) find good agreement between their models' strange modes, though some of those found by Cox & Stellingwerf (1980) are very non-adiabatic ordinary modes. Saio (1984) splits the strange modes into 3 distinct types with the following properties:

- TYPE I : Long periods with relative low T_{eff}
- TYPE II : Short period high harmonic for $T_{\text{eff}} < 3.9$
- TYPE III : Fundamental or low harmonics for $T_{\text{eff}} > 3.9$.

Saio (1984) notes that when a strange mode sequence crosses an ordinary mode sequence in the $\log(P)$ - $\log(T_{\text{eff}})$ diagram, that the ordinary mode is stabilised. Although at relatively high T_{eff} ($\log(T_{\text{eff}}) > 4.1$) it becomes unstable again. This might explain the stable region found for the first overtone in his HR diagram (see Figure 2.19). From Figure 2.19 it can also be seen that the blue edge behaves peculiarly at very high luminosities, in that it shows a marked blueward shift above some critical luminosity. This was also seen by Wood (1976) and Cox & Stellingwerf (1980) in their models. This effect was thought to be due to extreme non-adiabatic effects which somehow cause damping interior to the He II ionisation zone. The following characteristics were found for L_{crit} :

- (i) L_{crit} increases with increasing mass
- (ii) A composition change from $Z_c=0.1$ to 0.02 causes a 30 per cent increase in L_{crit} (This is probably due to the product of opacity and luminosity in the radiative transfer equation)
- (iii) Strange mode periods decrease as T_{eff} decreases ($T_{\text{eff}} < 6000$) below L_{crit}
- (iv) Strange mode periods increase as T_{eff} decreases ($T_{\text{eff}} < 6000$) above L_{crit} .

OBSERVATIONS OF THE RCB GROUP

Saio (1984) thought that the small amount of hydrogen might explain these strange modes and so he constructed models using opacity Tables containing the observed quantity of hydrogen ($X=0.0001$). He found that the inclusion of this small amount of hydrogen did cause quite large changes in opacity for $T_{\text{eff}} < 6000$ K (neglect of convection would probably cause greater deviations than this), but insignificant changes for the region of interest. He also showed that the periods and stability coefficients are insensitive to the opacity gradients throughout the stellar envelope, except in the region just below the He II ionisation zone (most of the pulsation K.E. is locked up in this region).

Saio (1984) shows that the non-adiabaticity of these objects is due to the large L/M ratio and that in objects with slightly lower L/M ratios (i.e., Cepheids or RR Lyrae stars) the non-adiabaticity is confined to, or above, the ionisation regions. Thus the regions in which most of the pulsational K.E. is locked are unaffected; the periods are unchanged and no strange modes are apparent. Non-adiabaticity has been noted to be larger for increasing T_{eff} and L/M ratios; higher modes also tend to be more non-adiabatic than lower modes.

In Saio (1984) the following observations and explanations were made for the observed phase changes in the modes with depth:

ORDINARY MODES : Phase increases from centre to surface with a total phase change $n \text{ PI}$ ($n = \text{mode}$) in the adiabatic limit, or $(n+1) \text{ PI}$ in the non-adiabatic limit. The displacements form a standing wave towards the centre, though the phase changes are not discrete due to

OBSERVATIONS OF THE RCB GROUP

non-adiabaticity in outer layers. The increase in phase can be explained if we assume that they are acoustic waves, i.e.,

$$\text{nonad}_{C_s} = \text{isotherm}_{C_s} < \text{ad}_{C_s} \quad \therefore d(\text{phase}) \text{ increases}$$

STRANGE MODES : Phase decreases from centre to surface with a total phase change approaching 0 for the non-adiabatic limit, or one of two values for the adiabatic limit. That is, TYPE II strange modes appear to approach a finite phase change, while TYPE I strange mode phases tend to increase indefinitely. The TYPE I behaviour is explained if we assume they are thermal waves. i.e.,

$$\begin{array}{lll} \text{nonad}_{C_{\text{therm}}} & \rightarrow \text{infinity} & \therefore d(\text{phase}) \rightarrow 0 \\ \text{ad}_{C_{\text{therm}}} & \rightarrow 0 & \therefore d(\text{phase}) \rightarrow \text{infinity} \end{array}$$

The following explanations and results are based entirely upon Saio (1984) and specifically his 'alpha' experiment in which he altered the non-adiabaticity of a model by multiplying the ratio of the thermal timescale to dynamic timescale by a constant factor, alpha (alpha = 0 for non-adiabaticity and infinity for adiabaticity). For clarity the results and hypotheses will be presented in modular form.

ORDINARY MODES : In the 'alpha' experiment Saio (1984) found that $|w|$ (where $|w|$ is the modulus of the complex frequency) decreased slowly as alpha increased (becomes adiabatic) and that around alpha = 1 the modes change to strange modes, reverting to ordinary modes at high and low

OBSERVATIONS OF THE RCB GROUP

alpha's. These are essentially long wave acoustic modes in which the adiabatic mode (i) changes considerably with increasing non-adiabaticity (α) approaching the period of adiabatic mode ($i+1$) in the extreme non-adiabatic limit. This increase is explained by the fact that the adiabatic sound speed is greater than the non-adiabatic (isothermal) sound speed resulting in a large change in the wave number (K). Why the phase changes by π between the extremes is not known.

STRANGE MODES : The 'alpha' experiments show that the periods of these strange modes are insensitive to the value of α . This leads to the conclusion that the 'strangeness' of these modes is confined to the outer regions, i.e., as the period is set by the region just interior to the He II ionisation zone, the 'strangeness' must occur in or exterior to the He II ionisation region.

TYPE I : In the 'alpha' experiment Saio (1984) found that $|w|$ decreases as α increases (becomes more adiabatic) and that $|w|$ is roughly proportional to $1/\alpha$. These are essentially secular (thermal) modes and have been studied in some depth by Hansen (1978).

TYPE II : In the alpha experiment Saio (1984) found that $|w|$ increases as α increases (becomes more adiabatic) and that $|w|$ is roughly proportional to α . This type of strange mode only appears in the adiabatic to non-adiabatic transition of an ordinary mode. Such a transition requires that $|w \times \alpha|$ approximately equals $|w^2|$ and indicates

OBSERVATIONS OF THE RCB GROUP

that this condition is necessary for the appearance of these modes. This condition is met when $|w| \sim \alpha$ and for such modes the energy involved in accelerating the material is comparable with that of heat exchange. Hence, TYPE II strange modes can be said to be present when strong coupling between acoustic and thermal waves occurs.

The condition $|w| \sim \alpha$ occurs just below the He II zone in RCB objects (the region where most of the pulsational K.E. is locked), resulting in strong dissipation of pulsational K.E. (damping) and stability. This probably explains the appearance of the stability strip in the HR diagram for the first overtone of the 1 solar mass models (see Figure 2.19). It also explains the stabilisation of ordinary modes in $\log(P)$ - $\log(T_{\text{eff}})$ diagram when crossed by a TYPE II strange mode.

TYPE III : In the 'alpha' experiment Saio (1984) found that $|w|$ increases very slowly with α and that these modes only occur during the transitions of TYPE I or TYPE II strange modes to ordinary modes. These modes occupy a broad band of T_{eff} (for $T_{\text{eff}} > 1000$ K) in the $\log(P)$ - $\log(T_{\text{eff}})$ diagram due to their insensitivity to α , and behave in a similar manner to adiabatic ordinary modes with T_{eff} . This probably means that they are due to some kind of weak coupling between thermal and acoustic waves.

Saio (1984) also notes from his 'alpha' experiment that increasing luminosity causes the thermal timescale to dynamic timescale ratio to fall rapidly in and just below the He II region. When α has

fallen enough (extreme non-adiabaticity) in these regions, the luminosity perturbations become 'frozen in' (see Cox (1974) for a description of 'freezing in' effects) which decreases the effects of driving/damping of the region. This ratio falls faster in the radiative damping zone than in the He II ionisation zone, resulting in a greater 'freezing in' of radiative damping zone, compared to that of the He II ionisation zone. Hence increasing luminosity causes less damping and could result in a blueward excursion of the blue-edge. It could even explain the critical luminosity seen in blue edges.

2.5 REVIEW OF NON-LINEAR MODELS

In the literature only four papers mention non-linear models of RCB type objects, these being King et al (1980), Trimble (1972), Wood (1976) and Saio & Wheeler (1985). The latter's paper is primarily concerned with linear non-adiabatic models and only mentions the non-linear models briefly. This review is therefore based mainly on the work done by Trimble (1972).

Trimble (1972) reports that the model with $(M/M_{\odot}, L/L_{\odot}, T_{\text{eff}}) = (1, 10^4, 6000)$ was violently unstable and never produced a repeatable light curve (this is similar to the results that Wood 1976 reports for the P_0 mode in his model with the same parameters.) TRIMBLE's other two non-linear models with parameters $(2, 5 \times 10^3, 6000)$ and $(2, 10^4, 6000)$ settle down to steady pulsations with roughly constant period and irregular amplitudes. (Again Wood, 1976 reports similar results for his $P_{1,2}$ and $P_{2,3}$ modes.) From this limited number of models she draws the following comparisons with Christy's (1966b) work on W Virginis type stars:

OBSERVATIONS OF THE RCB GROUP

- (i) Both RCB and W Virginis models showed violent behaviour in the high L/M limit, with the upper model layers lifting off and falling back every second period, producing alternate maxima and minima in light amplitudes.

- (ii) In both models the light curve had a 'shoulder' (see Figure 2.20) on the decline from maximum light. Trimble (1972) however points out that Christy's (1966b) light curve for W Virginis is much smoother.

- (iii) Both sets of models have large $Q = P(\rho/\rho_0)^{1/2}$ values (0.056) in comparison with Christy's (1966b) models of RR Lyrae which have lower Q values.

These similarities would seem to indicate that the overall characteristics of the star's light curves are governed by the high L/M ratio rather than the exact composition of the star.

Trimble (1972) found that, though her models had roughly correct velocity amplitudes (after dividing by a correction factor of 1.33; see Parsons 1971 for explanation of where this factor comes from), the luminosity and temperature amplitudes were too large and out of phase when compared with the observations. Trimble (1972) puts this down to incorrect opacities in the atmosphere of the models and also the lack of convection, which would be present in real stars.

OBSERVATIONS OF THE RCB GROUP

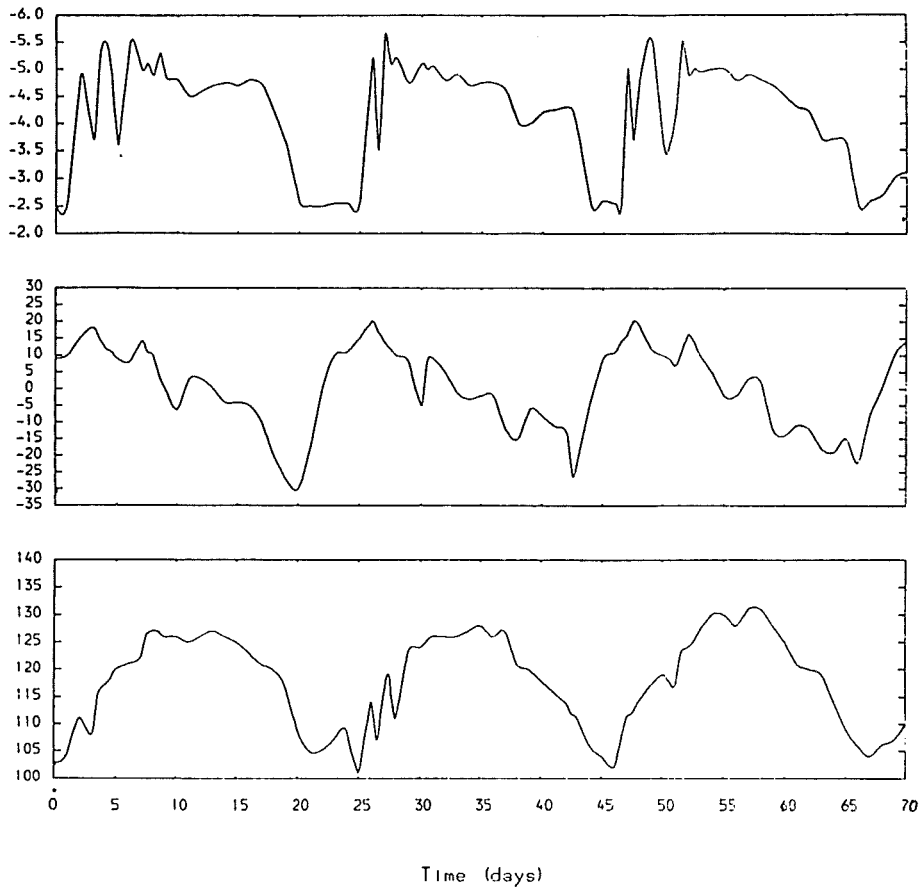


Figure 2.20 : A theoretical light curve of one of Trimble's models published in her 1972 paper (Trimble, 1972).

OBSERVATIONS OF THE RCB GROUP

From her results she concludes that RCB objects probably have L/M ratios $\ll 10^4$. Wood (1976) found for his hotter models ($\log(T_{\text{eff}}) = 4.0$ and 4.08) that at minimum the light curves showed sharp dips due to a shock wave reaching the surface at R_{min} causing a rapid reversal in the velocity.

Since these four papers there have been no further attempts to produce non-linear models of RCB objects (or very high L/M objects).

2.6 EVOLUTION OF THE RCB GROUP

From observations we know that at least three of the RCB group of stars are undergoing a change in their periods; these are RY Sgr, UW Cen and S Aps. The latter of which has a k (change in period/period) of -0.388 , which is far too large for present evolution calculations and hence will be ignored for the majority of this discussion. From the work of Kilkenny (1982) and Marraco & Milesi (1982) we know that RY Sgr has a k of -10^{-3} to -1.5×10^{-3} and UW Cen a value of k between 0.006 and -0.012 with 0.006 having the best fit.

As the periods of the fundamental mode decrease with increasing effective temperature on the upper horizontal branch of the evolutionary track of extreme helium stars (see Figure 2.21 for a sample evolutionary track, or Schonberner, 1977), and as stars modelled in this region by Weiss (1986) with RY Sgr's parameters, are in good agreement with its observed period and k ; it seems likely that RY Sgr is indeed evolving along the upper horizontal branch from the supergiant region to the white dwarf region of the HR diagram. On the other hand, UW Cen would appear to be evolving along the lower

OBSERVATIONS OF THE RCB GROUP

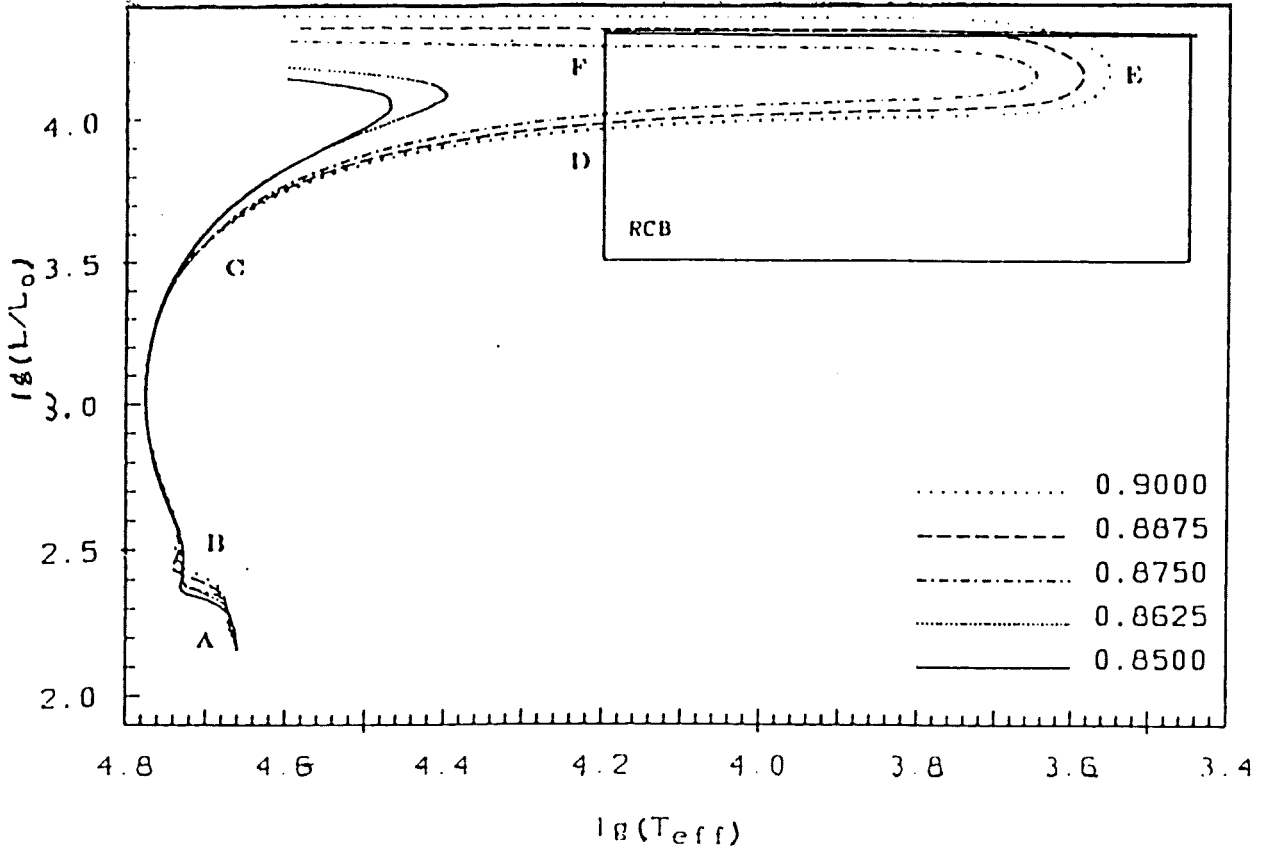


Figure 2.21 : This Figure shows the evolutionary tracks of several helium star models with differing masses. On this Figure, the lower luminosity branch is marked with a D and the upper luminosity branch is marked with a F. The other letters are not used in this discussion (this Figure was taken from Weiss, 1986).

OBSERVATIONS OF THE RCB GROUP

luminosity branch of the evolutionary track, though the value of k is still too uncertain to be sure about this.

Having given a brief outline of the probable evolution of two of the better observed RCB objects, let us now consider evolutionary limitations on the group as a whole. Assuming that all RCB's have a homogeneous composition, we see from Habets' (1985) evolutionary models of extreme helium stars with $M/M_{\odot} > 2.9$ that the effective temperature never drops below 7,000 K and thus excludes the majority of the RCB group. His evolutionary models with $2 < M/M_{\odot} < 2.9$ became too luminous ($> -6.3^m$) for all known RCB objects as well as the stability strip being too "hot" for the cooler RCB objects and too cool for the "hotter" RCB objects. Also the models with masses $> 2.0M_{\odot}$ had positive k values, in contradiction to the k 's found for RY Sgr and S Aps. Thus it seems likely that all RCB objects have masses $< 2M_{\odot}$.

Weiss (1986) has shown that although extreme helium models with masses between $0.9M_{\odot}$ and $2.0M_{\odot}$ can be evolved down to effective temperatures of 4,000 K and have luminosities in the accepted RCB range ($2,000L_{\odot} - 20,000L_{\odot}$). That these models when leaving the red edge of the RCB region have luminosities greater than those observed amongst the RCB objects (the lower mass limit here is dependent upon the maximum luminosity allowed, which in turn is dependent on observation and correction errors). Hence models in this mass range can only describe RCB's if they are on the lower luminosity branch of the evolutionary track (see Weiss, 1987). These models have negative k values and hence probably do not include most of the RCB objects (UW Cen may possibly be described by these models).

OBSERVATIONS OF THE RCB GROUP

Weiss (1986) and Law (1982) have shown that models of $0.9M_{\odot}$ and $1 M_{\odot}$ (respectively) evolving along the lower luminosity branch of the evolutionary track, remain stable to pulsation below $7,000^{\circ}\text{K}$. These models therefore can not account for RY Sgr, R CrB or any of the other RCB stars (with perhaps the exception of UW Cen), as not only are they stable in the RCB region, but also k has the wrong sign. The upper horizontal branch models in this mass range are too luminous for observed RCB stars.

For models with masses between $0.8M_{\odot}$ and $0.9M_{\odot}$, Schonberner (1977) has shown that such models evolve through the RCB region of the HR diagram on the upper horizontal branch. Not only do they occupy the right region of the HR diagram, but they also have the correct periods and k values. The models also extend to high enough effective temperatures to include all but the two hottest RCB objects (whose membership of the RCB group is in doubt, anyway). From these models Weiss (1987) infers that all RCB's, with perhaps the exception of UW Cen, V348 Sgr and MV Sgr, have masses in the range $(0.8-0.9)M_{\odot}$ and are evolving along the upper horizontal branch of the evolutionary track. He also points out that other extreme helium stars with slightly higher effective temperatures do not pulsate and that the instability is probably the cause of the RCB syndrome. This is supported to some extent by the fact that the demarcation between the two groups of objects appears to be about where the blue edge of the instability strip occurs. Finally, he points out that stars on the lower luminosity branch of the evolutionary track will be either stable or have shorter periods than those on the upper horizontal track and hence, given detailed observations, it should be possible to tell which branch of the evolutionary track the stars are evolving along.

OBSERVATIONS OF THE RCB GROUP

Thus the RCB group appear to have masses in the range $(0.8-1.2)M_{\odot}$ and to be evolving along the upper horizontal branch of the evolutionary track, from the red supergiant region to the white dwarf region of the HR diagram. They also appear to be unstable to fundamental, very non-adiabatic, radial pulsations which may be the cause of the RCB syndrome.

2.7 SUMMARY OF RCB OBSERVATIONS

From the above summation of observations in the literature, it can be seen that the average RCB star has a mass between 0.8 and 2.0 solar masses and an absolute magnitude between -4 and -6. This typical RCB star is a hydrogen deficient, carbon object, with an effective temperature in the range (5,000 - 7,000) K. The central star is surrounded by circumstellar clouds of small amorphous carbon grains which are probably maintained by irregular ejection of 'soot' from the star itself. If this average RCB star pulsates, it will be a small amplitude pulsation of <0.5 magnitudes and have a period of between 40 and 60 days (fundamental pulsator ?). The periods will probably change quite rapidly with time ($k \sim -0.00001$ dys/period) due to evolutionary effects upon the star.

The exceptions to this typical star are generally hotter and hence are probably at an evolutionary stage, either before or after the RCB stage of evolution. The fossil shell found around MV Sgr seems to indicate that these hotter objects are post- rather than pre-RCB in their evolution. The recent discovery of hydrogen lines in V348 Sgr's spectrum (Pollacco, 1987), may indicate that these hotter objects are not connected with the RCB group at all.

OBSERVATIONS OF THE RCB GROUP

The other exception whose membership of this group is in doubt is LR Sco, which might perhaps represent a fundamental mode pulsator immediately prior to the RCB star stage of evolution. S Aps, which previously had a period similar to that of LR Sco, appears to have undergone a period change to 40 days and seems to support this pre-RCB view.

THEORY

CHAPTER 3
PULSATION THEORY

3.1 INTRODUCTION

Shapley (1914) created the theoretical foundation of the postulate that the cyclic variability observed in stellar objects was due to free adiabatic radial oscillations. Soon after this paper, Eddington (1918a,b; 1926) put Shapley's (1914) theories into a mathematical form and in so doing established the mathematical theory for the free adiabatic radial oscillations of a gaseous sphere. Eddington found that free oscillations soon decayed, which was contrary to observations. To overcome this problem he postulated the existence of a 'driving' mechanism, that would prevent this rapid decay. Eddington first considered that the nuclear reactions might supply the required 'driving'. This has now been shown to be untenable, as the amplitude of pulsation in the interior is a million times smaller than that at the surface (see Epstein, 1950).

Eddington (1941) also put forward the idea of a 'valve' mechanism, in which some layers in the star would act as a thermodynamic heat engine. If a mass element can absorb energy upon compression and release it upon expansion, then it can 'drive' the pulsations. This is the approach taken by modern theories of pulsation analysis.

PULSATION THEORY

To date, three possible 'valve' mechanisms have been put forward. Baker & Kippenhahn (1962) stated the following possibility: given an opacity law of the form $\kappa = \kappa_0 \rho^n T^{-s}$ ($n, s > 0$), the opacity may increase upon compression if $(\Gamma_3 - 1)$ is small enough, e.g., in an ionisation region. This would lead to 'damming' of the radiation causing more 'driving'. Another mechanism based upon the same opacity law was put forward by Stellingwerf (1978, 1979). This mechanism, called the 'bump' mechanism, relies on 's' in the above opacity law being either large and negative or just less positive, i.e., as in the hydrogen ionisation zone. Under these circumstances radiation can be 'dammed' even for large $(\Gamma_3 - 1)$ and so may cause 'driving' in some stars. The last and most important mechanism is the ν -mechanism put forward by Cox et al (1966) which relies upon the fact that in an ionisation region $(\Gamma_3 - 1)$ becomes small, due to energy causing ionisation rather than increased temperature. This then 'dams' the radiation upon compression. Upon expansion, the gases then de-ionise causing a higher temperature than would otherwise be expected and hence 'driving'.

Whether or not a particular ionisation region will cause driving in a star seems to depend upon whether it lies in or below a transition region. This is the region that separates the quasi-adiabatic interior from the non-adiabatic exterior. This transition region moves outwards in mass for decreasing effective temperature (for given mass, luminosity and composition). Above this region, variations in the luminosity seem to be 'frozen in', maintaining the values they had in the transition region, i.e., despite variations in adiabatic luminosity, the luminosity variations become spatially independent.

When the He II ionisation region coincides with this transition region, the inner part of the ionisation region follows the quasi-adiabatic variations and the outer part is 'frozen' to the small value the luminosity perturbation had at the transition region. This results in less 'damping' and can lead to pulsational instability due to more 'driving'. It appears that this coincidence is responsible for the whole region termed the 'Cepheid Instability Strip' in the HR diagram (the outer hydrogen ionisation region having little effect upon the instability). As the effective temperature decreases, the hydrogen ionisation region coincides with this transition region, giving potentially very strong 'driving'. This driving is, however, heavily damped by convection, which brings the star back to stability and hence forms the 'red-edge' (this coincidence is probably the cause of the red variables, which are only seen at higher luminosities).

The suggestion that the He II ionisation region was the 'seat' of Eddington's 'valve' mechanism was put forth by Cox & Whitney (1958) and Aleshin (1959). Work by Baker & Kippenhahn (1967) and Cox (1963) confirmed the effectiveness of the He II region as a driving mechanism. This mechanism has since been confirmed by many other studies. A history of pulsation theory may be found in Rosseland (1949), Ledoux & Walraven (1958), Zhevakin (1963) and Cox (1980), while a good treatise on stellar structure is given in Cox & Giuli (1969).

The rest of this chapter briefly derives the basic dynamic equations of stellar pulsation and indicates the approximations and assumptions used in each case. The equations derived here will be used in chapters 5 and 6, where computational schemes and linearisation are discussed.

3.2 ASSUMPTIONS AND DEFINITIONS

The following assumptions will be made throughout the remainder of this thesis :

- a) Space is assumed to be Euclidean everywhere inside and outside the stellar models.
- b) Newtonian gravitation is assumed, as it is adequate for all models considered in this thesis.
- c) All velocities are assumed to be much less than the speed of light.

The major part of this thesis is concerned with radial modes only, and so will be presented using the Lagrangian description, though the derivations will require the use of the Eulerian description. For clarity in the brief derivations that follow, a definition of both descriptions and the Stokes derivative follow :

EULERIAN DESCRIPTION : In this view, all physical properties of the fluid, such as fluid velocity (\underline{V}), total pressure (P), temperature (T), etc. are regarded as field quantities, i.e., as functions of the independent variables \underline{r} and t . In this view, \underline{r} is a point of observation and consequently it is meaningless to take a time derivative of \underline{r} unless a qualitative reason is given.

PULSATION THEORY

LAGRANGIAN DESCRIPTION : In this view, the motion of a given fluid element is followed. Now \underline{r} represents the position of the element and is therefore no longer independent. Thus some other variable \underline{a} is defined as independent and this need not be a position variable, i.e., it could be temperature in a [1D] space.

STOKES DERIVATIVE : We are sometimes interested in following the motion of a particular fluid element, and/or observing the rate of change of some physical property, e.g., P, T. Such a derivative taken following the motion of a particular fluid element is the Stokes Derivative and is denoted by d/dt . The Stokes Derivative operator for the above descriptions can be shown to be:

$$\text{EULERIAN DESCRIPTION : } \frac{d}{dt} = \frac{\partial}{\partial t} + \underline{v} \cdot \underline{\nabla}, \quad (3.1)$$

$$\text{LAGRANGIAN DESCRIPTION : } \frac{d}{dt} = \frac{\partial}{\partial t}, \quad (3.2)$$

where:

$$\underline{v}(r, t) = \frac{\partial \underline{r}}{\partial t} = \text{Fluid velocity.}$$

\underline{r} is obviously no longer the Eulerian position vector, but rather a Lagrangian position variable.

3.3 CONSERVATION OF MASS

In the Eulerian description, the conservation of mass principle is synonymous with the continuity equation:

$$\frac{\partial \rho}{\partial t} + \underline{v} \cdot (\rho \underline{v}) = 0, \quad (3.3)$$

where ρ is the fluid density and \underline{v} the fluid velocity. By using $\underline{v} \cdot (\phi \underline{\Lambda}) = \phi \underline{v} \cdot \underline{\Lambda} + \underline{\Lambda} \cdot \underline{v} \phi'$ and the definition given in (3.1) we obtain:

$$\frac{d\rho}{dt} + \rho (\underline{v} \cdot \underline{v}) = 0. \quad (3.4)$$

As we are only concerned with the radial component of this equation, it can be re-written as:

$$\frac{1}{\rho} \frac{d\rho}{dt} = - \frac{1}{r^2} \frac{\partial}{\partial r} (r^2 \underline{v}). \quad (3.5)$$

Upon re-arranging in a more useful way, we can integrate w.r.t. time, to obtain:

$$\ln(\rho) - \ln(C) = - \int \frac{1}{r^2} \frac{dt}{dr} \frac{\partial}{\partial r} \left(r^2 \frac{dr}{dt} \right) \frac{dr}{dt} dt = \ln(r^2 \underline{v}). \quad (3.6)$$

Then at some time t , $r = a$ and $\rho = \rho_0$, which lets us find the constant C :

$$C = \rho_0 a^2 \frac{\partial a}{\partial t}, \quad (3.7)$$

$$\frac{\rho}{\rho_0} = \frac{a^2}{r^2} \frac{\partial a}{\partial r}, \quad (3.8)$$

PULSATION THEORY

This may be written in a more familiar form if it is stated that the mass of a thin concentric shell that moves with the fluid is constant. This statement means that $dm = \rho 4\pi r^2 dr = \rho 4\pi a^2 da$. Thence:

$$\frac{\partial r}{\partial m} = \frac{1}{4\pi\rho r^2}. \quad (3.9)$$

3.4 CONSERVATION OF MOMENTUM

A general form of the conservation of momentum can be written in the Eulerian description as:

$$\frac{\partial}{\partial t} (\rho \underline{v}) + \nabla \cdot (\rho \underline{v} \underline{v} + \underline{P}) = \rho \underline{f}, \quad (3.10)$$

where ρ is the fluid density, \underline{v} the velocity of fluid motion, \underline{P} the pressure tensor. If we assume that the principle of the conservation of mass is valid (as we will for all the theoretical work in this thesis), then (3.10) reduces to Newton's second law as applied to fluids:

$$\rho \frac{d\underline{v}}{dt} = -\nabla \cdot \underline{P} + \rho \underline{f}. \quad (3.11)$$

The 'dot product' is in dyadic notation (for further explanation of this see Appendix D) and \underline{f} is the external body force per unit mass. If the pressure stresses reduce to a pure hydrostatic pressure (as is generally the case), we may write $\underline{P} = P \underline{I}$, where \underline{I} is a unit tensor normal to the surface of the element in question. Thus we now have:

$$\rho \frac{d\underline{v}}{dt} = -\nabla P + \rho \underline{f}. \quad (3.12)$$

The pressure tensor form can be used when turbulence, viscosity or

PULSATION THEORY

large scale magnetic fields are present. Equation (3.12) can be re-written in the Lagrangian description as:

$$\frac{\partial^2 \underline{r}}{\partial t^2} = -\frac{1}{\rho} \sum_{j=1}^3 (\underline{\nabla} a_j) \frac{\partial P}{\partial a_j} + \underline{f}, \quad (3.13)$$

where a_j is an identifying variable component of the Lagrangian description, instead of r_j of the Eulerian description. We may reduce this, for our purposes, to the radial component only and substitute m for a_1 giving:

$$\frac{\partial^2 \underline{r}}{\partial t^2} = -\frac{1}{\rho} \frac{\partial m}{\partial r} \frac{\partial P}{\partial m} + \underline{f}(m, t). \quad (3.14)$$

Then using the form of the continuity equation given in (3.9), we can re-write this as:

$$\frac{\partial^2 \underline{r}}{\partial t^2} = -4\pi r^2 \frac{\partial P}{\partial m} + \underline{f}(m, t). \quad (3.15)$$

From here on, it is assumed that \underline{f} is due to self gravitation only and is thus directly identifiable with \underline{g} , the gravitational acceleration. Then from the Poisson equation for the gravitational potential we can obtain the equation for \underline{g} :

$$\underline{\nabla}^2 \psi = 4\pi G\rho, \quad (3.16)$$

$$\underline{f} = \underline{g} = -\underline{\nabla}\psi, \quad (3.17)$$

$$\underline{\nabla} \cdot \underline{f} = -4\pi G\rho. \quad (3.18)$$

PULSATION THEORY

We can solve equation (3.18) in the radial case using (3.9), the equation for mass conservation, to obtain \underline{f} :

$$f = -\frac{G_m}{r^2} + A. \quad (3.19)$$

Note that, as \underline{f} must vanish for zero mass, the constant (A) must be equal to zero. (3.15) can then be re-stated as follows:

$$\frac{\partial \underline{r}}{\partial t^2} = -4\pi r^2 \frac{\partial P}{\partial m} - \frac{G_m}{r^2}. \quad (3.20)$$

3.5 CONSERVATION OF ENERGY

Firstly, the equation for the conservation of mechanical energy can be found in the Eulerian description by forming a scalar product of the momentum equation (3.11) with \underline{v} :

$$\underline{v} \cdot \frac{d\underline{v}}{dt} = -\frac{1}{\rho} \underline{v} \cdot (\underline{\nabla} \cdot \underline{P}) + \underline{v} \cdot \underline{f}, \quad (3.21)$$

$$\frac{d}{dt} (v^2/2) = -\frac{1}{\rho} \underline{v} \cdot (\underline{\nabla} \cdot \underline{P}) + \underline{v} \cdot \underline{f}. \quad (3.22)$$

For a better understanding of this equation we can use the identity ' $\underline{\nabla} \cdot (\underline{v} \cdot \underline{P}) = \underline{v} \cdot (\underline{\nabla} \cdot \underline{P}) + \underline{P} : (\underline{\nabla} \underline{v})$ ' (the ':' signifies the double dot product of the tensors or their complete contraction; see Appendix D for further explanation) to replace the first term on the R.H.S. and then integrate over the entire volume (V) of the fluid mass (M):

$$\frac{d}{dt} \int_M \frac{v^2}{2} dm = -\int_V \underline{v} \cdot (\underline{\nabla} \cdot \underline{P}) d\tau + \int_V \underline{P} : (\underline{\nabla} \underline{v}) d\tau + \int_M \underline{f} \cdot \underline{v} dm. \quad (3.23)$$

PULSATION THEORY

Using the generalized divergence theorem on the first term on the R.H.S. of this equation, we can obtain equation (3.25) using one of two assumptions : that either the pressure is approximately zero at the surface or that $(\underline{v} \cdot \underline{P})$ is perpendicular to $d\underline{S}$ at the surface (generally the case for uniformly rotating stars). We can obtain the following result:

$$\int_V \underline{v} \cdot (\underline{v} \cdot \underline{P}) d\tau = \oint_S (\underline{v} \cdot \underline{P}) \cdot d\underline{S} \sim 0, \quad (3.24)$$

$$\frac{d}{dt} \int_M \frac{v^2}{2} dm = \int_V \underline{P} : (\underline{\nabla} \underline{v}) d\tau + \int_M \underline{f} \cdot \underline{v} dm. \quad (3.25)$$

If we now invoke mass conservation and reduce the pressure stresses to that of a pure hydrostatic pressure, the first term on the R.H.S. of (3.24) can be further reduced to:

$$\int_V \underline{P} : (\underline{\nabla} \underline{v}) d\tau = \int_M \underline{P} \frac{d}{dt} (1/\rho) dm, \quad (3.26)$$

$$\frac{d}{dt} \int_M \frac{v^2}{2} dm = \int_M \underline{P} \frac{d}{dt} (1/\rho) dm + \int_M \underline{f} \cdot \underline{v} dm. \quad (3.27)$$

We can obtain the equation for conservation of thermal energy (internal energy) by writing the equation for the conservation of mechanical and thermal energy (3.28) and then subtracting (3.22) from it:

$$\frac{d}{dt} (v^2/2 + E) = -\frac{1}{\rho} \underline{v} \cdot (\underline{P} \cdot \underline{v}) + \underline{f} \cdot \underline{v} + \frac{dq}{dt}, \quad (3.28)$$

$$\frac{dE}{dt} = -\frac{1}{\rho} \underline{P} : (\underline{\nabla} \underline{v}) + \frac{dq}{dt}. \quad (3.29)$$

PULSATION THEORY

Here, E represents the internal energy and dq/dt represents the rate of loss/gain of heat following the fluid motion. We can reduce ' $\underline{P}:(\nabla V)$ ' as before, if we assume pure hydrostatic pressure, and obtain:

$$\frac{dq}{dt} = \frac{dE}{dt} + P \frac{d(1/\rho)}{dt} = \frac{dE}{dt} + P \frac{dV}{dt}, \quad (3.30)$$

where $V = 1/\rho$ is the specific volume of the fluid. If it is assumed that there are no composition changes due to nuclear reactions and that P and E are state variables given at every point by two other state variables (for given composition), e.g., ρ , T . Then we can re-write the above equation in the useful form:

$$\frac{d \ln(P)}{dt} = \Gamma_1 \frac{d \ln(\rho)}{dt} + \rho (\Gamma_3 - 1) \frac{dq}{dt}, \quad (3.31)$$

where:

$$\Gamma_1 = \left. \frac{d \ln(P)}{d \ln(\rho)} \right|_{ad}, \quad (3.32)$$

$$(\Gamma_3 - 1) = \left. \frac{d \ln(T)}{d \ln(\rho)} \right|_{ad}. \quad (3.33)$$

As we are only interested in the radial component and a pure hydrostatic pressure is assumed, we may reduce equation (3.28) to:

$$\frac{d}{dt} (v^2/2 + E) - f_{r,v} = - \frac{1}{r^2 \rho} \frac{\partial}{\partial r} (r^2 v P) + \frac{dq}{dt}. \quad (3.34)$$

PULSATION THEORY

Using the continuity equation (3.9) and the expression obtained for \underline{f} in equation (3.19) we can simplify (3.34) to:

$$\frac{d}{dt} (v^2/2 + E - Gm/r) = - \frac{\partial}{\partial m} (4\pi r^2 P v) + \frac{dq}{dt} \quad (3.35)$$

Now we may write the heat flow equation (3.30) in another form:

$$T \frac{\partial s}{\partial t} = \frac{dq}{dt} = - \frac{\partial L}{\partial m} \quad (3.36)$$

where s is the specific entropy. Then, assuming that there is no energy generation, we can re-write (3.35) in the following form:

$$\frac{d}{dt} (v^2/2 + E - Gm/r) + \frac{\partial}{\partial m} (4\pi r^2 P v + L) = 0 \quad (3.37)$$

3.6 TRANSPORT EQUATIONS

In this section the problem of energy transport is dealt with. For our study conduction can be considered negligible, leaving radiative and convective transport as the two most efficient ways of energy transport. In general the heat flow term dq/dt is just the difference between the heat sources and heat sinks. Let ϵ represent the energy generated per unit mass, and let \underline{F} be the total energy flux vector, perpendicular to the surface dS of a mass element, due to all transport mechanisms. We may then write the general equation for energy transport as:

$$\frac{dq}{dt} = \epsilon - \frac{1}{\rho} \nabla \cdot \underline{F} \quad (3.38)$$

PULSATION THEORY

In the stellar interior external to the core, it is generally adequate to compute the integrated radiative flux from a formula based upon the diffusion approximation (no energy generation is assumed):

$$\underline{E} = -\frac{4\pi}{3\kappa_R\rho} \frac{dB(T)}{dT} \cdot \nabla T, \quad (3.39)$$

where T is the temperature, ρ the density, κ_R the mean Rosseland opacity and $B(T)$ the integrated Planck function.

The convective part of (3.38) is either ignored due to the poor understanding of how convection works (usually with no serious effects for $T_{\text{eff}} > 6000\text{K}$) or described by a simple mixing length model.

3.7 BOUNDARY CONDITIONS

For the models considered here, we shall only consider a purely reflective boundary condition. There are two main reasons for this, the first being that in the case of non-linear analysis it would be quite difficult to implement a 'running wave' or transmitting boundary condition. The second reason is that Saio et al (1984) have shown that providing the cyclic frequency remains above some critical frequency (defined in their paper), then the 'standing wave' or total reflective boundary condition is quite adequate (compared with effects like convection and transport approximations made). Christy (1967) defined his outer boundary condition as:

$$P_{\text{TOT}}^{\text{surface}} = 0. \quad (3.40)$$

PULSATION THEORY

A better condition, if the radiation pressure is not insignificant, is:

$$\text{surface } P_g = 0, \quad (3.41)$$

$$\text{surface } P_{TOT} = 1/2 \text{ surface } P_{rad}, \quad (3.42)$$

where P_{tot} is the total pressure, P_{rad} is the radiation pressure and P_g is the gas pressure. The 1/2 in (3.42) allows for the fact that only half the radiation produces a net back pressure upon the surface. Near the surface of the star, the radiation should be described by a time dependent transport equation. This, however, proves to be a much more difficult problem, needing temperature points from several mean free paths. Thus, to reduce complexity and computing time the radiative diffusion approximation is used instead. Although this is not a very good description, it produces a simpler and more rapid solution, requiring only the adjacent temperature points (for models using a dynamic transport equation, see Deupree, 1976). The radiative outer boundary condition is chosen to approximate Christy's (1967) "extrapolated boundary". In the Eddington approximation, this may be expressed as:

$$\left. \frac{\partial (T^4)}{\partial \tau} \right|_{\text{surface}} = \frac{3}{4} T_{\text{eff}}^4. \quad (3.43)$$

The inner boundary conditions are much simpler. In this study, it is assumed that inside some radius $R_{\text{inner}} \cong 0.1 R_*$, the stellar core is adiabatic and non-pulsating, radiating a constant luminosity of L_* . So at the inner boundary of the envelope (in the radial approximation) we have:

$$\left. \frac{dr}{dt} \right|_{R_{\text{inner}}} = 0, \quad (3.44)$$

$$L_{\text{inner}} = L_*. \quad (3.45)$$

3.8 SHOCKS AND VELOCITY PROFILES

During a pulsation, shock waves may appear, causing rapid compression of some regions of the stellar envelope. This is particularly noticeable in outer regions of the stellar envelope. These rapid compressions are a problem, in that the variable mesh used to model the stellar pulsation is quite coarse and hence such shock waves cause discontinuities in the variables. To overcome this problem an artificial viscosity is introduced, based upon the Von Neumann-Richtmyer method. This basically introduces an artificial viscous pressure Q , which spreads the shock across several coarse zones of the model and so removes any discontinuities that may have occurred. The particular form of the artificial viscous pressure used here is that given by Stellingwerf (1975):

$$Q(r) = C_0 P(r) \left[\frac{dU(r)}{C_s(r)} + \alpha_v \right]^2, \quad \text{If } dU(r) < -C_0 C_s(r), \quad (3.46)$$

$$Q(r) = 0, \quad \text{If } dU(r) > -C_0 C_s(r).$$

Here $Q(r)$ and $P(r)$ are the artificial and total pressure at radius r , $C_s(r)$ is the speed of sound at r and $dU(r)$ is the change in velocity over a distance dr at r . α_v is a constant introduced by Stellingwerf to reduce energy dissipation in the lower envelope due to the artificial viscosity. This is important as it affects the limiting amplitude of the pulsation; α_v should have a value between 0.0 and 0.2, with 0.1 being about right. C_0 is a constant, chosen to produce stability without too much loss of accuracy (e.g., about 1.2 is usually adequate).

PULSATION THEORY

Now we have all the equations to solve the dynamics of a stellar model. Given a static stellar envelope, we could find its pulsational stability by allowing computational noise to perturb it. This is a very good way of seeing if a marginally stable envelope (i.e., one that is very close to the edge of a stability region) is unstable to pulsation or not. The major problem with this method is that it can take a long time for an instability to show and grow to its limiting amplitude. To overcome this, a velocity profile can be introduced into the model envelope, so that the star is artificially forced to pulsate. The general form of the profiles used is:

$$U(r) = - A. (r/R_*)^5 - B. (r/R_*)^{10} \text{ Km/sec.} \quad (3.47)$$

Christy used $A = 13$ and $B = 7$, while Stobie (1969) used $A = 18$ and $B = 0$. Stobie (1969) gives several profiles for classical Cepheids, depending upon the mode of pulsation required. For the case of RCB objects mode contamination should not be a problem as the e-folding time is very short and the first overtone is unstable to pulsation in the HR-diagram where the fundamental instability strip occurs (Saio et al, 1984). Due to the short e-folding times of the RCB class of objects, no artificial amplification of the velocities is needed; the pulsations reaching their maximum amplitudes within 8 to 14 periods.

CHAPTER 4

THE PHYSICS

4.1 THE EQUATION OF STATE

4.1.1 General Overview Of The Problem

To complete the set of stellar equations, we need an equation of state. That is, given the abundances of elements, the density, ρ and temperature, T at a given point, we need an equation to find the total pressure P , the total entropy per unit mass S , the internal energy per unit mass E and the mean molecular weight μ . In the majority of stellar objects the alpha elements are probably the most important, along with H and N. So in the equation of state used for this study the following elements were included: H, He, C, N, O, Ne, Mg, Si, S and Fe. It was also thought that for cooler stars some molecules might become important. To allow for this possibility, the 10 most likely diatomic molecules (H_2 , CH, NH, OH, C_2 , CN, CO, N_2 , NO and O_2) and the 5 most likely tri-atomic molecules (H_2O , C_2O , HCN, N_2O , NO_2) were included. For the stars considered in this study, the temperature at the bottom of the pulsation envelope seldom exceeded $1.5 \times 10^6 K$ and hence was not likely to deplete the heavier elements of more than a few electrons. With this in mind and given the speed of computation of the dynamic stellar envelope, only the first four ionisation states were included. The negative ion states of all elements allowed such were also included as the objects under consideration were generally cool enough for such states to be

THE PHYSICS

non-negligible. The gas is assumed to be ideal and in L.T.E., allowing the use of Boltzmann statistics throughout.

Before solving the main equations we note that the equation for converting the abundance by mass β into the abundance by number α and the equation for μ are:

$$\alpha_i = \frac{\beta_i / A_i}{\sum_{i=1}^{\text{all}} (\beta_i / A_i)}, \quad (4.1)$$

$$\mu = \sum_{i=1}^{\text{all}} (\alpha_i A_i), \quad (4.2)$$

where A_i is the atomic mass of element i . To simplify things further, the number density $^{\text{ion}}n_i$ of element i is defined as:

$$^{\text{ion}}n_i = \frac{N_o \rho \alpha_i}{\mu}. \quad (4.3)$$

Using these and defining the number density of element i in ionisation state j to be n_{ij} and the number density of element i tied up in molecules to be $^{\text{mol}}n_i$ ($= D n_i + T n_i$), we can write the following expression for the electron number density, n_e :

$$n_e = \sum_i \sum_j n_{ij} (n_e, T). \quad (4.4)$$

This equation is generally non-linear (only exactly solvable for pure hydrogen) and must be solved by some iterative scheme. A Newton-Raphson scheme is slow and requires a good initial guess of n_e , because $\delta n_e / n_e$ must be small for rapid convergence. Rather than using this method, the equations are solved for n_e by an iterative scheme in

THE PHYSICS

which the geometric mean of converging extremes is used (see equations 4.5 - 4.7) to find n_e in consecutive iterations:

$$n_e(\min) = \max[n_e(\min), \min(n_e^n, n_e^{n+1})], \quad (4.5)$$

$$n_e(\max) = \min[n_e(\max), \max(n_e^n, n_e^{n+1})], \quad (4.6)$$

$$n_e = \sqrt{n_e(\min) \cdot n_e(\max)}. \quad (4.7)$$

The iterations are repeated until both n_e and molecular number densities converge to 6 figures. When convergence has been achieved, the state variables P, S and E can then be found using:

$$P = {}^{\text{ion}}P + {}^{\text{D}}P + {}^{\text{T}}P + n_e kT + 1/3 aT^4, \quad (4.8)$$

$$E = {}^{\text{ion}}E + {}^{\text{D}}E + {}^{\text{T}}E + [3/2 n_e kT + aT^4]/\rho, \quad (4.9)$$

$$S = {}^{\text{ion}}S + {}^{\text{D}}S + {}^{\text{T}}S + [(5/2 - \eta) n_e kT + 4/3 aT^4]/\rho T, \quad (4.10)$$

where the super-scripts 'ion', 'D', 'T' indicate that the variable represents the contributions from free ions, diatomic molecules and triatomic molecules, respectively. The Planck radiation constant is a , η is the electron degeneracy factor and the other variables have their usual meaning.

THE PHYSICS

4.1.2 Diatomic Molecules

The equilibrium abundance for diatomic molecules has to be found, to enable the partial pressure $^D P$, partial entropy per unit mass $^D S$, partial energy density per unit mass $^D E$ and the number density of neutral ions i , $^D n_i$, bound up in diatomic molecules, to be found. Figure 4.1 below defines some of the parameters used in this sub-section. z_{k1} and z_{k2} represent the atomic numbers, and A_{k1} and A_{k2} the atomic masses of the atoms making up diatomic molecule k . The bonding length is given by b_k , and the main vibration frequency by ν_k .

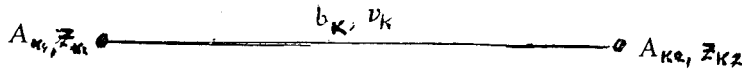


Figure 4.1 : A diagram of the diatomic molecule k and its associated parameters.

The reduced mass μ_k for molecule k is given by:

$$\mu_k = \frac{(A_{k1} \cdot A_{k2})}{(A_{k1} + A_{k2})} \quad (4.11)$$

Using the definition of the equilibrium constant $^D K_k$ for diatomic molecule k , we have:

$$^D K_k = \frac{^{ion} n_{k1} \ ^{ion} n_{k2}}{^D n_k} = \frac{^{ion} Z_{k1} \ ^{ion} Z_{k2}}{^D Z_k} e^{-\chi_v^k / kT} \quad (4.12)$$

where Z_{k1} , Z_{k2} and n_{k1} , n_{k2} are the total partition functions and number densities of the free constituent atoms 1 & 2 of molecule k , before any 'reactions'. Z_k is the total partition function, $^D n_k$ the number density and χ_v^k the dis-association energy of diatomic molecule

THE PHYSICS

k. The total diatomic molecular partition function, D_{Z_k} can be expanded to give:

$$D_{Z_k} = D_{Z_e}^k \cdot D_{Z_{\text{trans}}}^k \cdot D_{Z_{\text{rot}}}^k \cdot D_{Z_{\text{vib}}}^k, \quad (4.13)$$

where $D_{Z_e}^k$ is the electron partition function (multiplicity and symmetry), $D_{Z_{\text{trans}}}^k$ is the translational partition function, $D_{Z_{\text{rot}}}^k$ is the rotational partition function and $D_{Z_{\text{vib}}}^k$ is the vibrational partition function of diatomic molecule k. These individual partition functions are given below:

$$D_{Z_{\text{trans}}}^k = \left(\frac{2\pi\mu_k kT}{h^2} \right)^{3/2}, \quad (4.14)$$

$$D_{Z_{\text{rot}}}^k = \frac{8\pi^2 \mu b_k^2 kT}{h^2}, \quad (4.15)$$

$$D_{Z_{\text{vib}}}^k = \frac{1}{(1 - e^{-h\nu_k/kT})}, \quad (4.16)$$

$$D_{Z_e}^k = M_k S_k, \quad (4.17)$$

in which:

$$\begin{aligned} S_k &= 0.5, & \text{if atom 1} = \text{atom 2 and } \Lambda_k &= 0, \\ S_k &= 2.0, & \text{if atom 1} = \text{atom 2 and } \Lambda_k &= 1, \\ S_k &= 1.0, & \text{otherwise.} \end{aligned}$$

Here M_k is the multiplicity, S_k a symmetry term and Λ_k the quantum number associated with the $C_{+1,d}$ component of the electronic angular momentum. The equilibrium constant is further modified by a pressure dissociation factor $D_{K_{\text{press}}}^k$ given by:

$$D_{K_{\text{press}}}^k = e^{+x_p^k/kT}, \quad (4.18)$$

THE PHYSICS

in which χ_p^k is a pressure dissociation term. χ_p^k can be found approximately by assuming that it is roughly equal to the difference in the molecule's Coulomb repulsion potential, at equilibrium separation and at the actual separation:

$$\chi_p^k = z_{k1} z_{k2} e^2 \left(\frac{1}{b_k} - \frac{1}{r} \right), \quad (4.19)$$

where:

$$r = N^{-1/3} \quad (4.20)$$

The variables z_{k1} , z_{k2} and b_k are as defined in Figure 4.1, N is the number density of free particles in the gas, and e is the charge of an electron. The partition function of a free ion i is just the associated translational partition function multiplied by g_i^k (a degeneracy term). Hence we can now write down the equilibrium constant in terms of known parameters:

$$D_{K_k} = M_k S_k g_1 g_2 \left(\frac{8\pi^2 \mu_k kT}{b_k^2 h^2} \right)^{1/2} (1 - e^{-h\nu_e/kT}) e^{-(\chi_v^k - \chi_p^k)/kT} \quad (4.21)$$

Using the equilibrium constant, the total number density of free ions i (n_i^D) tied up in the diatomic molecules can be found:

$$n_i^D = \sum_k \xi_{ki} \frac{n_{k1}^{ion} n_{k2}^{ion}}{D_{K_k}}, \quad (4.22)$$

where ξ_{ki} is the number of element i atoms in molecule k . The contributions of the diatomic molecules to the state variables P , E and S are now easily found to be:

THE PHYSICS

$${}^0P = \left(\sum_k {}^{00}n_k \right) kT \quad , \quad (4.23)$$

$${}^0E = \sum_k {}^{00}n_k \left[5/2 kT - \chi_V^k + \chi_P^k + h\nu_k / (e^{h\nu_k/kT} - 1) \right] / \rho \quad , \quad (4.24)$$

$${}^0S = {}^0E + [{}^0P + \left(\sum_k {}^{00}n_k {}^0\eta_k \right) kT] / \rho T \quad . \quad (4.25)$$

The degeneracy factor or chemical potential, ${}^0\eta_k$ is defined by:

$$e^{0\eta_k} = \frac{N}{[2\pi (A_{k1} + A_{k2}) kT/h^2]^{1/2}} \quad . \quad (4.26)$$

4.1.3 Triatomic Molecules

In a similar way to the diatomic molecules, we can find the partial pressure ${}^T P$, partial entropy per unit mass ${}^T S$, energy density per unit mass ${}^T E$ and number density of neutral ions i , ${}^T n_i$ bound up in the triatomic molecules. Figure 4.2 below defines some of the parameters used in this sub-section. z_{k1} , z_{k2} & z_{k3} represent the atomic numbers and A_{k1} , A_{k2} & A_{k3} represent the atomic masses of the constituent atoms. Also in each molecule b_k , c_k , d_k represent the bond lengths, θ_k represents the bond angle, and ν_{k1} , ν_{k2} , ν_{k3} represent the main vibration frequencies.

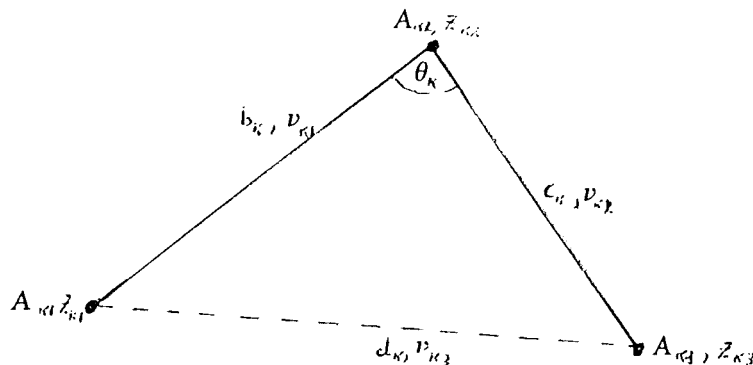


Figure 4.2 : A diagram of triatomic molecule k and its associated parameters.

THE PHYSICS

It is useful to define μ_k , the reduced mass and I_k , the angular momentum of the molecule about an axis passing through the triatomic molecule's centre of mass, perpendicular to its plane. This will simplify the algebra later on:

$$\mu_k = \left[\frac{A_{k1} \cdot A_{k2} \cdot A_{k3}}{(A_{k1} + A_{k2} + A_{k3})} \right]^{1/2} \quad (4.27)$$

$$I_k = \frac{(A_{k1} A_{k2} b_k^2 + A_{k2} A_{k3} c_k^2 + A_{k3} A_{k1} d_k^2)}{(A_{k1} + A_{k2} + A_{k3})} \quad (4.28)$$

Using the definition of the equilibrium constant ${}^T K_k$ for triatomic molecule k, we have:

$${}^T K_k = \frac{{}^{10n} n_{k1} {}^{10n} n_{k2} {}^{10n} n_{k3}}{{}^1 n_k} = \frac{{}^{10n} Z_{k1} {}^{10n} Z_{k2} {}^{10n} Z_{k3}}{{}^1 Z_k} e^{-\chi_v^k/kT} \quad (4.29)$$

where Z_{k1} , Z_{k2} , Z_{k3} and n_{k1} , n_{k2} , n_{k3} are the partition functions and number densities of the free constituent atoms 1, 2 & 3 before any 'reactions'. ${}^T Z_k$ is the total partition function, ${}^1 n_k$ the number density and χ_v^k the dis-association energy of molecule k. The total triatomic molecular partition function, ${}^T Z_k$, can now be expanded as in (4.13). The individual partition functions for the triatomic molecules are given below:

$${}^T Z_{\text{trans}}^k = \left(\frac{8\pi^2}{h^2} (A_{k1} + A_{k2} + A_{k3}) kT \right)^{3/2} \quad (4.30)$$

$$\begin{aligned} {}^T Z_{\text{rot}}^k &= \left(\frac{8\pi^2 kT}{h^2} \right)^{3/2} (\pi I_k)^{1/2} \mu_k b_k c_k s \ln \theta_k, \quad \text{if } \theta_k = 180^\circ, \\ &= \frac{8\pi^2 I_k kT}{h^2}, \quad \text{if } \theta_k \neq 180^\circ, \end{aligned} \quad (4.31)$$

THE PHYSICS

$${}^T Z_{\text{vib}}^k = \prod_{i=1}^3 \frac{(1 + S_k e^{-h\nu_i/kT})}{(1 - e^{-h\nu_i/kT})} \quad (4.32)$$

where:

$$\begin{aligned} S_k &= 0, & \text{if } i = 2 \text{ or } \theta_k \neq 180^\circ, \\ S_k &= 1, & \text{if } i \neq 2 \text{ and } \theta_k = 180^\circ, \end{aligned}$$

$${}^T Z_e^k = M_k L_k, \quad (4.33)$$

where:

$$\begin{aligned} L_k &= 0.5, & \text{if atom 1} = \text{atom 3}, \\ L_k &= 1.0, & \text{if atom 1} \neq \text{atom 3}. \end{aligned}$$

The symbols are the triatomic equivalents of those used in the diatomic equations (4.14) - (4.17). The pressure dis-association factor ${}^T K_{\text{press}}^k$ for triatomic molecules is given by:

$${}^T K_{\text{press}}^k = e^{+\chi_p^k/kT}, \quad (4.34)$$

and the pressure dis-association term χ_p^k is found by a similar approximation as that used in the diatomic case:

$$\chi_p^k = z_{k1} z_{k2} e^2 \left(\frac{1}{b_k^2} - \frac{1}{r} \right) + z_{k2} z_{k3} e^2 \left(\frac{1}{c_k^2} - \frac{1}{r} \right) + z_{k3} z_{k1} e^2 \left(\frac{1}{d_k^2} - \frac{1}{r} \right), \quad (4.35)$$

where:

$$r = N^{-1/3}. \quad (4.36)$$

THE PHYSICS

The total partition function of a free ion is the same as before. Hence we can now write down the equilibrium constant in terms of known parameters:

$${}^T K_k = g_1^k g_2^k g_3^k \frac{(8\pi^2 kT/h^2)^{3/2} (\mu_k/\pi I_k)^{1/2} (1/b_k c_k \sin\theta_k)}{\left[\frac{\pi (1 + S_k e^{-h\nu_1/kT})}{(1 - e^{-h\nu_1/kT})} \right]}, \quad \text{if } \theta_k \neq 180^\circ, \quad (4.37)$$

$$= g_1^k g_2^k g_3^k \frac{(8\pi^2 kT/h^2) (\mu_k^{3/2}/I_k)}{\left[\frac{\pi (1 + S_k e^{-h\nu_1/kT})}{(1 - e^{-h\nu_1/kT})} \right]}, \quad \text{if } \theta_k = 180^\circ.$$

Using this equilibrium constant, we can find the total number density of ion i , ${}^T n_i$ tied up in the triatomic molecules:

$${}^T n_i = \sum_k {}^{\text{all}} \xi_{ik} \frac{{}^{\text{ion}} n_{k1} {}^{\text{ion}} n_{k2} {}^{\text{ion}} n_{k3}}{{}^T K_k}, \quad (4.38)$$

where ξ_{ki} is the number of element i atoms in molecule k . The contributions of triatomic molecules to the state variables P , E and S are now easily found to be:

$${}^T P = \left(\sum_k {}^{\text{all}} n_k \right) kT, \quad (4.39)$$

$${}^T E = \left[\sum_k {}^{\text{all}} n_k \sum_{i=1}^3 \frac{(1+S_k) h\nu_i e^{-h\nu_i/kT}}{(1 - e^{-h\nu_i/kT})} + (1.5+D_k) kT - \chi_V^k + \chi_V^k \right] / \rho, \quad (4.40)$$

where:

$$D_k = 1.0, \quad \text{if } \theta_k = 180^\circ,$$

$$D_k = 1.5, \quad \text{if } \theta_k \neq 180^\circ,$$

$${}^T S = {}^T E + [{}^T P - \sum_{k=1}^{\text{all}} (n_k \eta_k kT)] / \rho T, \quad (4.41)$$

The degeneracy factor or chemical potential, e^{η_k} is given by

$$e^{\eta_k} = \frac{N}{[2\pi (A_{k1} + A_{k2} + A_{k3}) kT/h^2]^{1/2}} \quad (4.42)$$

4.1.4 Free Ions

Having obtained expressions for the number density, n_i^D, n_i^T , of neutral ions i tied up in the molecules, we can now find the number density n_{ij}^{ion} of ion i in ionisation state j and hence the contribution of these free ions to the state variables P, S and E as well as the total number density of free ions n^{ion} . Before finding n_{ij}^{ion} , we have to find the number density of ion i (n_i^{ion}) by subtracting from n_i the number densities of ion i tied up in the molecules:

$$n_i^{ion} = n_i - n_i^T - n_i^D \quad (4.43)$$

We can now use Saha's equation to find the number density, n_{ij}^{ion} of ion i in ionisation state j :

$$\frac{n_{ij}^{ion}}{n_i^{ion}} = \frac{\prod_{l=0}^{j-1} n_e \Phi_{il}(T)}{\sum_{l=0}^{j-1} \prod_{l=0}^{j-1} n_e \Phi_{il}(T)} \quad (4.44)$$

in the above:

$$\Phi_{ij}(T) = \frac{n_{ij}^{ion}}{n_{i,j+1} n_e} = \frac{1}{2} \frac{B_{ij}}{B_{i,j+1}} \left(\frac{h^2}{2\pi m_e kT} \right)^{3/2} e^{x_{ij}/kT} \quad (4.45)$$

where:

$$B_{ij} = \frac{g_i!}{(g_i - P_{ij})! g_i!}$$

THE PHYSICS

J_i is the highest ionisation state (or highest ionisation state considered) of ion i and w_i is zero, unless the atom can have negative ions in which case it is -1 . B_{ij} is the internal partition function (i.e., translational part of partition function is excluded) or the statistical weight of the outer shell configuration of ionisation state j of ion i ; χ_{ij} is the transition energy of ion i between ionisation states j and $j+1$; g_i is the statistical weight of the outer shell of ion i and P_{ij} is the number of electrons left in the outermost shell of ion i . It is now a simple matter to find the total number density of free ions, ${}^{ion}n$, the partial pressure, ${}^{ion}P$, the internal energy per unit mass ${}^{ion}E$ and the partial entropy per unit mass, ${}^{ion}S$:

$${}^{ion}n = \sum_{i=1}^{all} n_i, \quad (4.46)$$

$${}^{ion}P = {}^{ion}n kT, \quad (4.47)$$

$${}^{ion}E = \left[\sum_{i=1}^{all} \sum_{j=1}^{J_i-1} ({}^{ion}n_{ij} \chi_{ij}) + 3/2 {}^{ion}n kT \right] / \rho, \quad (4.48)$$

$${}^{ion}S = {}^{ion}E + [{}^{ion}P - \sum_{i=1}^{all} (n_i {}^{ion}\eta_i kT)] / \rho T, \quad (4.49)$$

The degeneracy factor or chemical potential, ${}^{ion}\eta_i$ is given by:

$$e^{ion\eta_i} = \frac{N}{[2\pi (A_i) kT/h^2]^{1/2}}, \quad (4.50)$$

4.2 STELLAR OPACITIES

A lot of the theoretical work on stellar pulsation has made use of the Cox-Stewart (1965) opacity tables or later modifications, known as the Los Alamos opacities. These opacities are based upon work by Stromgren (1932), etc. The models used in Cox-Stewart (1965) are based on the hydrogenic approximation using an effective nuclear charge to obtain the initial field, which is then perturbed for the specific atomic species. This approach was questioned by Carson & Hollingsworth (1968) who showed, using a numerically exact method for the one electron case, that great care has to be taken in choosing the effective nuclear charge. To overcome this problem, Carson & Hollingsworth (1968) used a non-hydrogenic method and showed in the few results that they obtained that the opacities may be 2-3 times larger than those given in the Cox-Stewart tables.

Carson (1976) went on to calculate a full series of tables using a method that treats hydrogen and helium exactly and all other elements using the Thomas-Fermi statistical model. Negative ions and a few selected diatomic molecules were also included in the calculations (these contributing significantly at lower temperatures). Conduction was treated by codes supplied by Hubbard & Lampe (1968).

This study employs smoothed and unsmoothed cubic interpolations in Z_c of Dr Carson's H_e -C series of tables, and the Demarque XIX table of Cox & Tabor (1976). Details of the tables used in this study can be found in Table 4.1 below, and the actual tables can be found in Appendix A (Figures 4.3 - 4.9 give a graphical representation of these tables). The interpolation used to obtain table K610 was a simple, third order Taylor expansion in Z_c , about $Z_c = 0$. The fit was found to be good enough, though there was no noticeable difference in the

THE PHYSICS

models if a second order fit was used.

TABLE	X	Y	Z _c	REMARKS
R040	0.00	1.00	0.00	Dr Carson's He-C series
R631	0.00	0.75	0.25	Dr Carson's He-C series
R622	0.00	0.50	0.50	Dr Carson's He-C series
R613	0.00	0.25	0.75	Dr Carson's He-C series
K610	0.00	0.90	0.10	Interpolation of He-C tables
BD9C	0.00	0.90	0.10	Interpolation of He-C tables
DXIX	0.00	0.90	0.10	Demarque XIX table

Table 4.1 : A table of all the opacity tables used in this study.

In this study the opacity gradient is found by a numerical method using linear interpolation within the table. This was the method used by Bridger (1983), who found that a quadratic fit was unreliable. From work in in Stothers (1974a, 1974b), Carson & Stothers (1976) and Vemury & Stothers (1977, 1978), etc., it has shown that opacity tables, using the same techniques as used to create tables K610 and BD9C give good and generally better results than the equivalent Cox-Stewart opacity tables. The only problem with these tables is that the CNO bump is too large by a factor of 2 or 3. To overcome this, the CNO bump has been smoothed by Dr Jeffrey in opacity table BD9C. Judging by the good results obtained in Stothers & Vemury (1981), Carson & Stothers (1982) on BL Her variables and Bridger (1983) on bump Cepheids (all using opacity tables generated by the same techniques as the opacity tables used in this study), we may confidently assume that the opacity tables used here will also produce good results.

THE PHYSICS

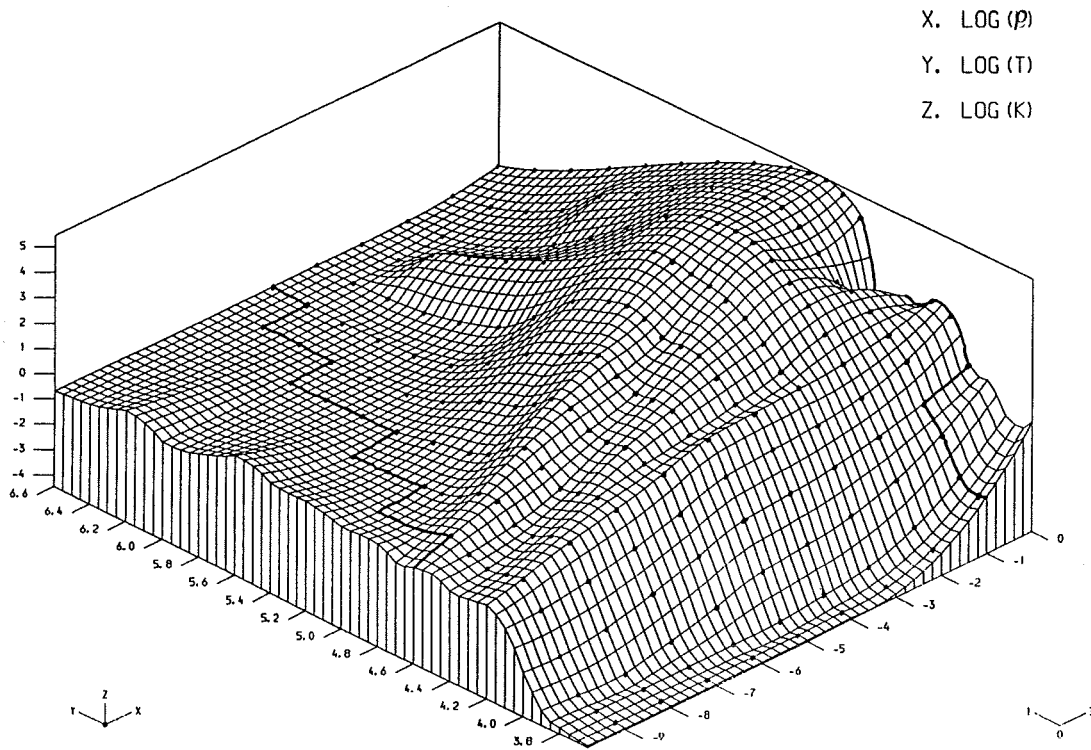


Figure 4.3 : A graph showing a cubic spline surface fitted to opacity table R040 over the region of the table used in this study. The original opacity points, to which the spline was fitted, are shown by the dots.

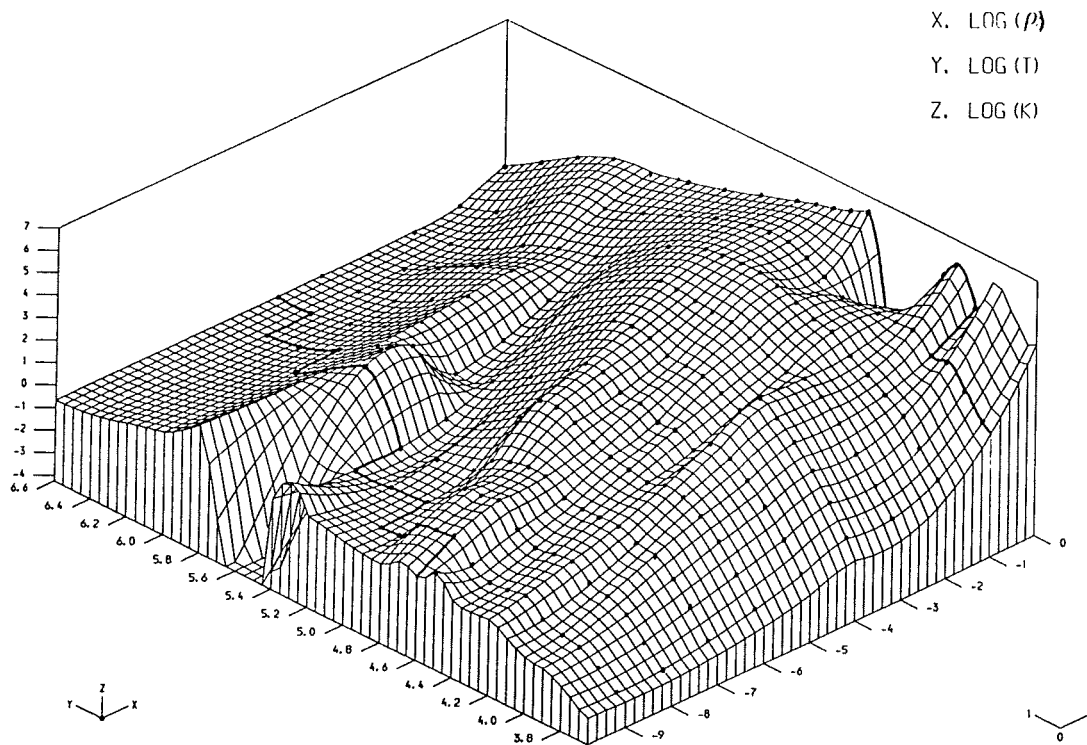


Figure 4.4 : A graph showing a cubic spline surface fitted to opacity table R631 over the region of the table used in this study. The original opacity points, to which the spline was fitted, are shown by the dots.

THE PHYSICS

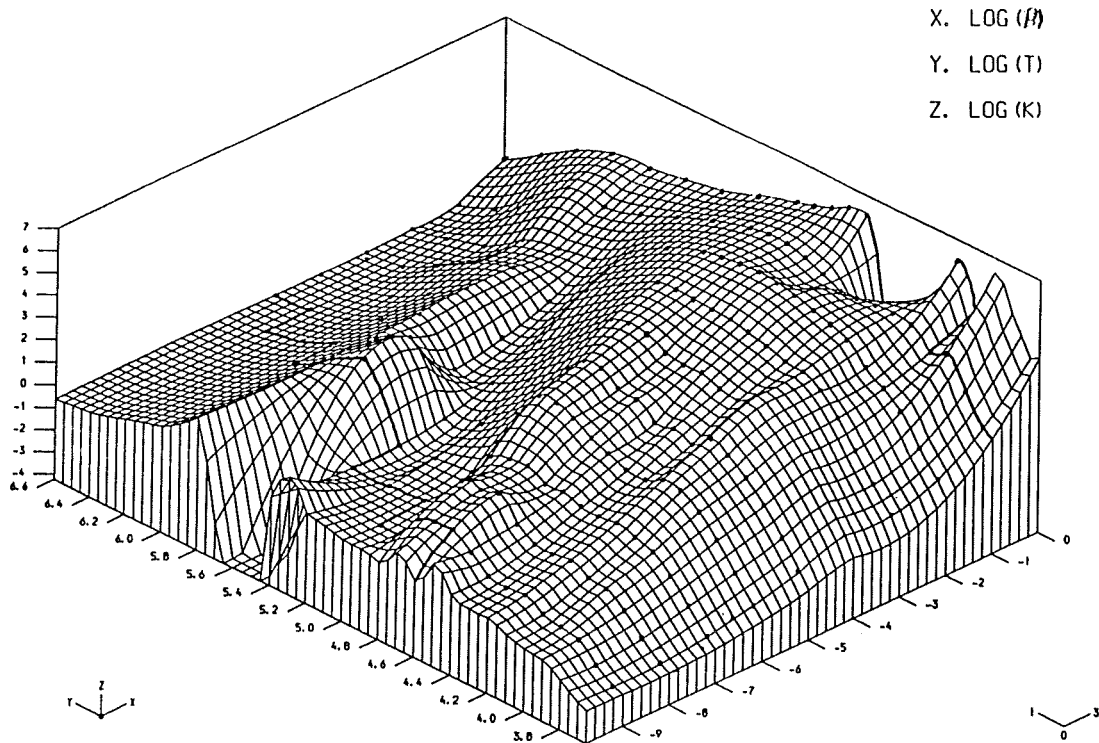


Figure 4.5 : A graph showing a cubic spline surface fitted to opacity table R622 over the region of the table used in this study. The original opacity points, to which the spline was fitted, are shown by the dots.

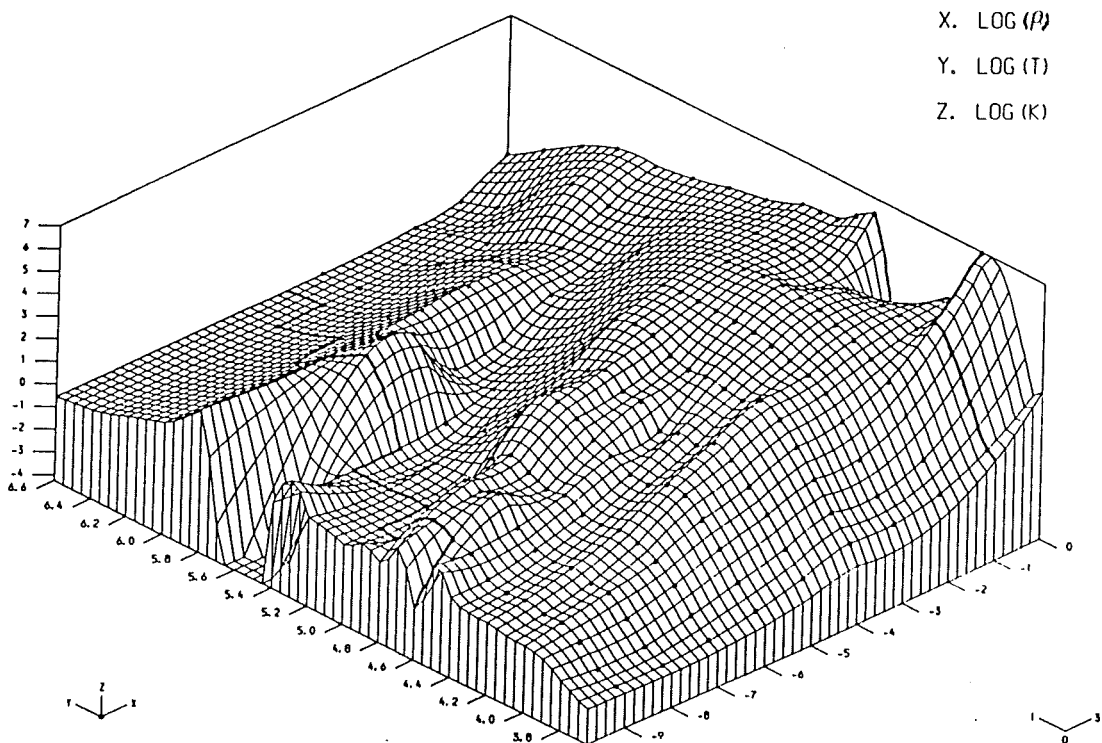


Figure 4.6 : A graph showing a cubic spline surface fitted to opacity table R613 over the region of the table used in this study. The original opacity points, to which the spline was fitted, are shown by the dots.

THE PHYSICS

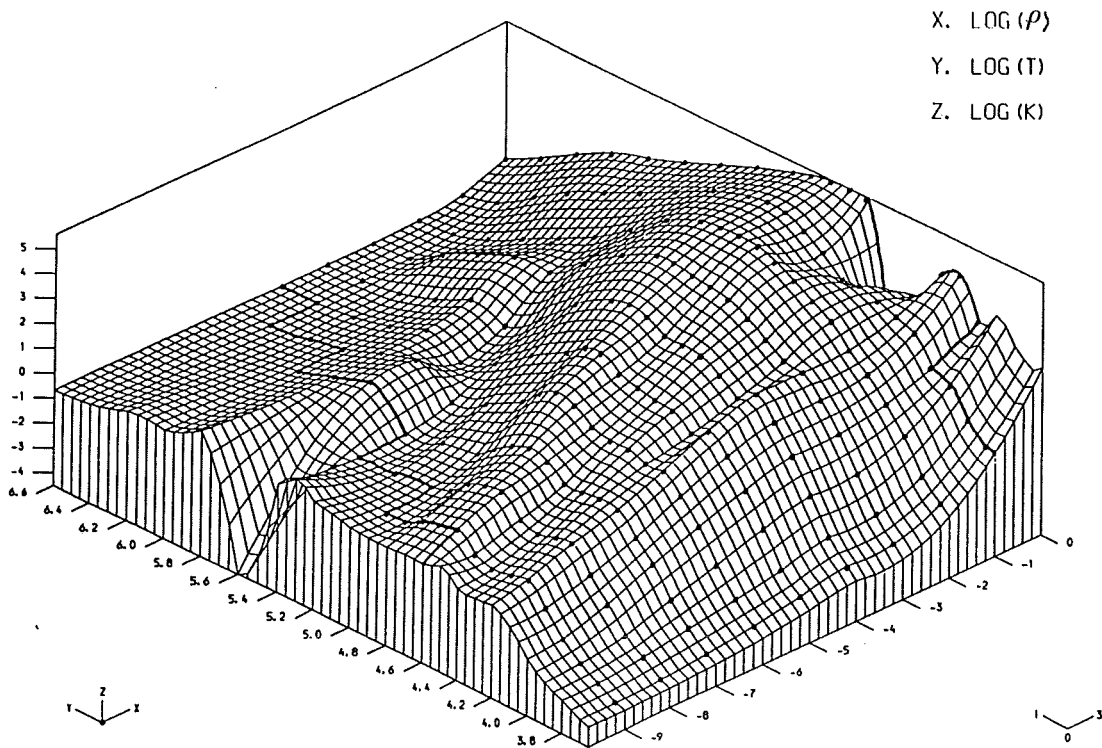


Figure 4.7 : A graph showing a cubic spline surface fitted to opacity table K610 over the region of the table used in this study. The original opacity points, to which the spline was fitted, are shown by the dots.

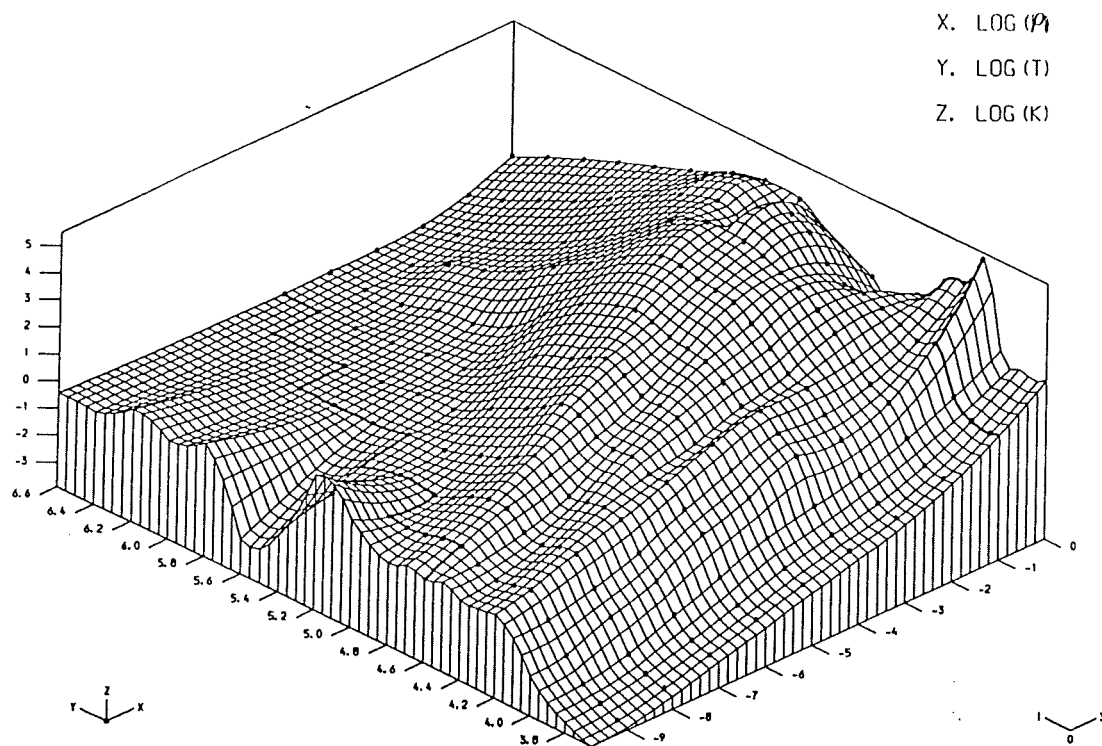


Figure 4.8 : A graph showing a cubic spline surface fitted to opacity table BD9C over the region of the table used in this study. The original opacity points, to which the spline was fitted, are shown by the dots.

THE PHYSICS

X. LOG (P)
Y. LOG (T)
Z. LOG (K)

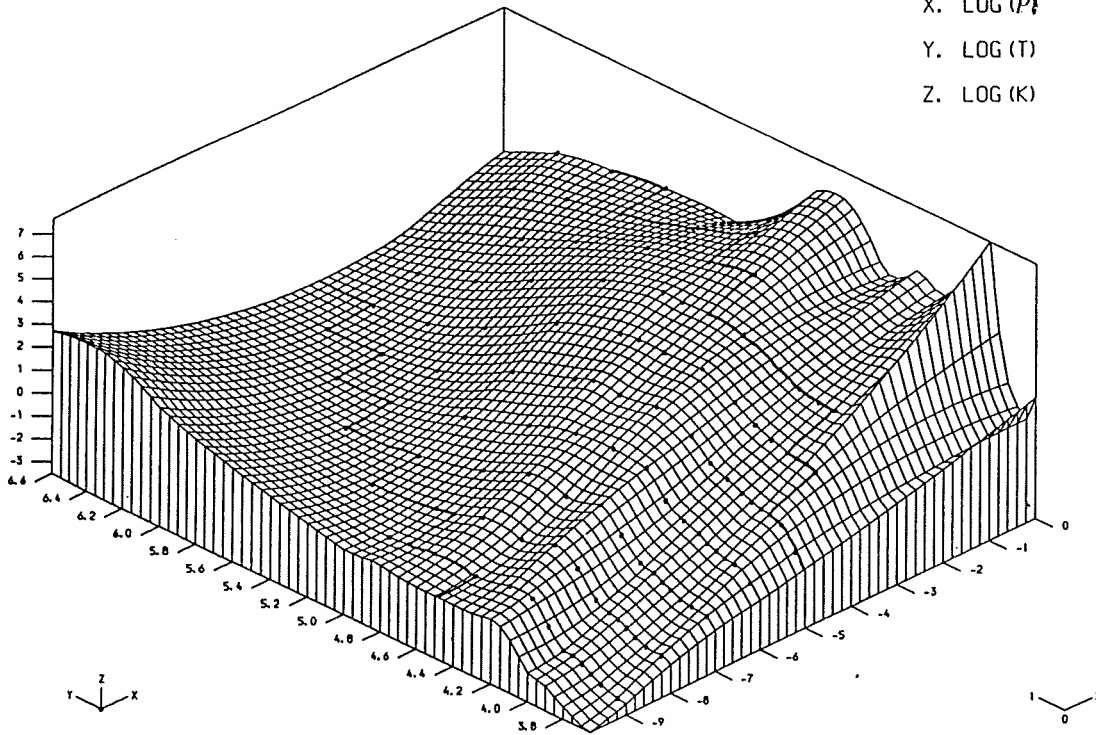


Figure 4.9 : A graph showing a cubic spline surface fitted to opacity table DXIX over the region of the table used in this study. The original opacity points, to which the spline was fitted, are shown by the dots.

COMPUTATIONAL SCHEMES

CHAPTER 5

DIFFERENCING THE NON-LINEAR EQUATIONS

5.1 PRELIMINARIES

The method used here is a semi-implicit one in that the thermodynamic equations are solved implicitly, while the dynamic equations are solved explicitly (following the method in Christy, 1967). Firstly, a static stellar envelope is required (see appendix C), along with the velocity profile to be used, if any (see section 3.8). This envelope is split into N mass zones; the zone boundaries being labelled by i . The innermost boundary has $i = 1$ and the outermost boundary has $i = N$; the zones are represented by half integers: see Figure 5.1 for details. The present time step is denoted by the superscript n .

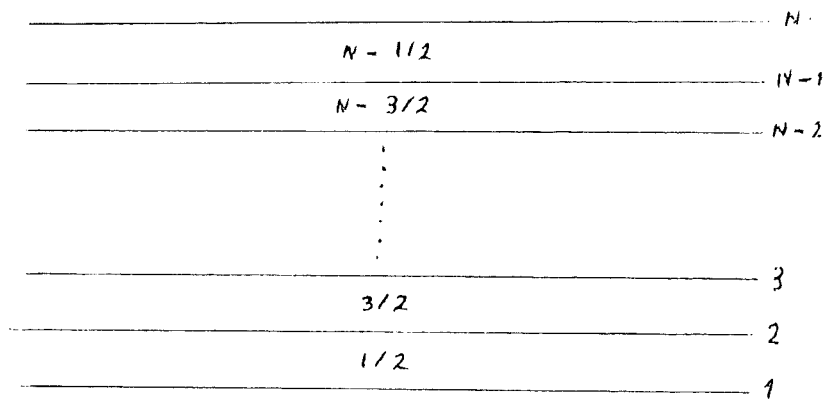


Figure 5.1 : This Figure shows how the boundaries and zones were labelled in the model envelope.

DIFFERENCING THE NON-LINEAR EQUATIONS

Defining the mass contained within boundary i by ΔM_i , the zonal masses defined in zone $i-1/2$ and on boundary i are:

$$\Delta M_{i-1/2} = M_i - M_{i-1} , \quad (5.1)$$

$$\Delta M_i = \frac{1}{2} (\Delta M_{i+1/2} + \Delta M_{i-1/2}) = \frac{1}{2} (M_{i+1} - 2M_i + M_{i-1}) . \quad (5.2)$$

The radius $r(m,t)$ and velocity $U(m,t)$ at time step n of boundary i are R_i^n and U_i^n respectively. For better results and quicker convergence the velocity is usually time-centred (represented by half integers of n). A time-centred variable X is defined, for simplification of the following theory, by:

$$X^{n+1/2} = \frac{1}{2} (X^{n+1} + X^n) . \quad (5.3)$$

Then in time increment $\Delta t^{n+1/2}$ we can write the new radius at time step $n+1$ of boundary i as:

$$R_i^{n+1} = R_i^n + \Delta t^{n+1/2} U_i^{n+1/2} , \quad (5.4)$$

where:

$$\Delta t^{n+1/2} = t^{n+1} - t^n . \quad (5.5)$$

We can also write the acceleration a_i^{n+1} of boundary i as:

$$a_i^{n+1} = \frac{(U_i^{n+1/2} - U_i^{n-1/2})}{\Delta t^n} , \quad (5.6)$$

where:

$$\Delta t^n = t^{n+1/2} - t^{n-1/2} = \frac{1}{2} (t^{n+1} - t^{n-1}) . \quad (5.7)$$

In the following discussion V represents the specific volume. The other symbols have their usual meaning unless otherwise stated.

DIFFERENCING THE NON-LINEAR EQUATIONS

5.2 DIFFERENCING THE CONTINUITY EQUATION

A direct difference of equation (3.9) for zone $i-1/2$ will give:

$$V_{i-1/2}^n = 4\pi (R_{i-1}^n)^2 \frac{(R_i^n - R_{i-1}^n)}{\Delta M_{i-1/2}} \quad (5.8)$$

An exact value for the specific volume of zone $i-1/2$ can be found from:

$$V_{i-1/2}^n = 4\pi \frac{[(R_i^n)^3 - (R_{i-1}^n)^3]}{\Delta M_{i-1/2}} \quad (5.9)$$

In this study the zones were too coarse for (5.8) so the exact expression (5.9) was used.

5.3 DIFFERENCING THE MOMENTUM EQUATION

The acceleration in equation (5.6) is found by differencing (3.20), the momentum equation. To facilitate understanding, the area of boundary i at time step n will be represented by $A_i^n = 4\pi(R_i^n)^2$. The differenced momentum equation is then:

$$U_i^{n+1/2} = U_i^{n-1/2} - \frac{GM_i}{(R_i^n)^2} + \frac{A_i^n}{\Delta M_i} (P_{i+1/2}^n + Q_{i+1/2}^{n-1/2} - P_{i-1/2}^n - Q_{i-1/2}^{n-1/2}) \Delta t^n \quad (5.10)$$

where $Q_{i-1/2}^{n-1/2}$ is the artificial time-centred viscous pressure of zone $i-1/2$. It is time-centred so as to give the best representation of the viscosity in a rapidly accelerating shock wave. The equation of artificial pressure (3.48) is differenced as follows:

$$Q_{i-1/2}^{n-1/2} = C_0 P_{i-1/2}^{n-1/2} \text{MIN} \left[\frac{(U_{i-1/2}^{n-1/2} - U_{i-1/2}^{n-1/2})^2}{(P_{i-1/2}^{n-1/2} V_{i-1/2}^{n-1/2})^{1/2}} + \alpha_v, 0 \right]^2 \quad (5.11)$$

DIFFERENCING THE NON-LINEAR EQUATIONS

So, given $U_1^{n+1/2}$, $P_{N+1/2}^n$ and ΔM_N , we can find the new velocity for every zone for time step $n+1$. From the inner boundary condition (3.46) of a non-pulsating core, we have:

$$U_1^{n+1/2} = 0.0 . \quad (5.12)$$

$P_{N+1/2}^n$ is found from one of the two possible outer boundary conditions given in equations (3.42) and (3.43). If we assume that the atmosphere is nearly isothermal and let $W = T^H$, then:

$$P_{N+1/2}^n = P_{N-1/2}^n, \quad \text{If (3.42),} \quad (5.13)$$

$$P_{N+1/2}^n = 2BaW_{N-1/2}^n + P_{N-1/2}^n, \quad \text{If (3.43),} \quad (5.14)$$

where B is between 0 (no radiative pressure) and $1/3$ (full radiative pressure). If the envelope has been zoned using constant mass ratio a instead of by constant sound speed, it is sometimes useful to include a zone extending out to $\tau = 0.0$ and having mass ΔM_N . (This can be useful in preventing the outer zones of stars with low effective temperature from leaving the stellar surface and wandering off, causing the model to become numerically too large for the computer.) As the atmosphere is approximately isothermal, we can proceed as in Bridger (1983) and make the approximation that $P_{N+1/2} \propto \Delta M_{N-1/2}$, and hence:

$$P_{N+1/2}^n = \frac{1}{\alpha} P_{N-1/2}^n . \quad (5.15)$$

Finally ΔM_N can be found for all the above cases from:

$$\Delta M_N = \frac{1}{2} \left\{ \Delta M_{N-1/2} + C \sum_{j=1}^{\infty} (\Delta M_{N-1/2} / \alpha^j) \right\}, \quad (5.16)$$

$$\Delta M_N = \left[1 + \frac{C}{(\alpha - 1)} \right] \frac{\Delta M_{N-1/2}}{2} . \quad (5.17)$$

DIFFERENCING THE NON-LINEAR EQUATIONS

C is 0 for no direct inclusion of the external mass and 1 if the external mass is to be explicitly included. The required outer boundary condition is selected by the values of B and C.

5.4 DIFFERENCING THE ENERGY EQUATION

For energy conservation, the energy equations must be differenced implicitly. To do this we substitute (3.36) in (3.30) and make the reasonable assumption of constant entropy throughout the pulsation:

$$\left[E_{i+1/2}^{n+1} - E_{i+1/2}^n + (P_{i+1/2}^{n+1/2} + Q_{i+1/2}^{n+1/2}) \cdot (V_{i+1/2}^{n+1} - V_{i+1/2}^n) \right] \Delta M_{i+1/2} = (L_1^{n+1/2} - L_{i+1}^{n+1/2}) \Delta t^{n+1/2}. \quad (5.18)$$

Before an attempt can be made to solve equation (5.18), we need to find L_1^{n+1} and the photospheric radius, R_{phot} . The inner boundary condition (3.47) lets us find L_1^{n+1} :

$$L_1^{n+1} = L_* \quad (5.19)$$

To find the photospheric radius we need the outer boundary condition, which in this case is the Eddington approximation. From the Eddington approximation we know that $T_{eff}^{\downarrow} = 2T_s^{\downarrow}$ where T_s is the temperature at the stellar surface, or roughly the temperature at zone N-1/2. Having found T_{eff} , a rough location can be found by finding in which zone the temperature crosses T_{eff} . Once this zone is known, a simple interpolation (taking care to use the correct space centring) can be performed to locate R_{phot} . Having found R_{phot} , we can now write the outer boundary condition as:

$$\left[E_{N-1/2}^{n+1} - E_{N-1/2}^n + (P_{N-1/2}^{n+1/2} + Q_{N-1/2}^{n+1/2}) \cdot (V_{N-1/2}^{n+1} - V_{N-1/2}^n) \right] \Delta M_{N-1/2} = \quad (5.20)$$

$$\left\{ L_1^{n+1/2} - 2\alpha (\lambda_{phot}^n W_{N-1/2}^n + \lambda_{N-1/2}^{n+1} W_{N-1/2}^{n+1}) \right\} \Delta t^{n+1/2},$$

The luminosity in the above equations is found by differencing the radiative transport equation (3.39):

$$L_1^n = (A_1^n)^2 (W_{1-1/2}^n - W_{1+1/2}^n) 2F_1^n, \quad (5.21)$$

where $2F_1^n$ is an interpolation of $4\sigma/3\chi\Delta M$ which must stay continuous, numerically bound and properly weighted to represent the effective opacity in the limit of coarse zoning.

5.5 THE LUMINOSITY INTERPOLATION

Christy (1964) at first used the following simple interpolation scheme to find F_1^n :

$$F_1^n = \frac{4\sigma}{3} \frac{1}{(\chi_{1+1/2}^n \Delta M_{1+1/2} + \chi_{1-1/2}^n \Delta M_{1-1/2})}, \quad (5.22)$$

where $\chi_{i+1/2}^n$ is the Rosseland mean opacity in zone $i+1/2$. This formula suffers from convergence problems in regions where large changes in opacity occur across a zone. The reason is that too little weight is given to the larger opacity. To overcome this problem, Christy developed the following equation for F_1^n :

$$F_1^n = \frac{4\sigma}{3} \frac{1}{(\Delta M_{1+1/2} + \Delta M_{1-1/2})} \frac{1}{(W_{1+1/2}^n + W_{1-1/2}^n)} \left[\frac{W_{1+1/2}^n}{\chi_{1+1/2}^n} + \frac{W_{1-1/2}^n}{\chi_{1-1/2}^n} \right]. \quad (5.23)$$

Stobie (1969) proved that this was the best overall formula for F_1^n , though Stellingwerf found a more complex formula involving logarithms that gave slightly better results away from the opacity peak. The increase in accuracy of Stellingwerf's equation is offset by the

DIFFERENCING THE NON-LINEAR EQUATIONS

increase in computing time, and so for this study equation (5.23) will be used. In the solution of the energy equations we will need the following partial differentials:

$$\frac{\partial F_i^n}{\partial W_{i-1/2}^n} = F_i^n \left[\frac{1 - \frac{W_{i-1/2}^n}{(X_{i-1/2}^n)^2} \frac{\partial X_{i-1/2}^n}{\partial W_{i-1/2}^n}}{\frac{W_{i+1/2}^n + W_{i-1/2}^n}{X_{i+1/2}^n X_{i-1/2}^n}} - \frac{1}{(W_{i+1/2}^n + W_{i-1/2}^n)} \right], \quad (5.24)$$

$$\frac{\partial F_i^n}{\partial W_{i+1/2}^n} = F_i^n \left[\frac{1 - \frac{W_{i+1/2}^n}{(X_{i+1/2}^n)^2} \frac{\partial X_{i+1/2}^n}{\partial W_{i+1/2}^n}}{\frac{W_{i-1/2}^n + W_{i+1/2}^n}{X_{i+1/2}^n X_{i-1/2}^n}} - \frac{1}{(W_{i+1/2}^n + W_{i-1/2}^n)} \right]. \quad (5.25)$$

5.6 SOLVING THE DIFFERENCED ENERGY EQUATIONS

The differenced energy equation (5.18) was linearized and then solved by a Newton-Raphson type iteration procedure, iterating on $W_{i+1/2}^{n+1}$ until convergence of at least 5 figures is reached. The new temperatures are corrected as follows on each iteration:

$${}^{j+1}W_{i+1/2}^n = {}^jW_{i+1/2}^{n+1} + {}^j\Delta W_{i+1/2}^n, \quad (5.26)$$

where ${}^j\Delta W_{i+1/2}^n$ is the correction to $W_{i+1/2}^{n+1}$ on iteration j . The new values of P, E and F can be found by using the first order terms of a Taylor expansion about $W_{i+1/2}^{n+1}$:

$${}^{j+1}P_{i+1/2}^{n+1} = {}^jP_{i+1/2}^{n+1} + \frac{{}^j\partial P_{i+1/2}^{n+1}}{\partial W_{i+1/2}^{n+1}} {}^j\Delta W_{i+1/2}^{n+1}, \quad (5.27)$$

$${}^{j+1}E_{i+1/2}^{n+1} = {}^jE_{i+1/2}^{n+1} + \frac{{}^j\partial E_{i+1/2}^{n+1}}{\partial W_{i+1/2}^{n+1}} {}^j\Delta W_{i+1/2}^{n+1}, \quad (5.28)$$

$${}^{j+1}F_{i+1/2}^{n+1} = {}^jF_{i+1/2}^{n+1} + \frac{{}^j\partial F_{i+1/2}^{n+1}}{\partial W_{i+1/2}^{n+1}} {}^j\Delta W_{i+1/2}^{n+1} + \frac{{}^j\partial F_{i+1/2}^{n+1}}{\partial W_{i-1/2}^{n+1}} {}^j\Delta W_{i-1/2}^{n+1}. \quad (5.29)$$

DIFFERENCING THE NON-LINEAR EQUATIONS

By placing equations (5.27) - (5.29) in the differenced energy equation (5.18), we can produce a group of linear equations involving the above temperature corrections as the unknowns. So after the above substitutions and much tedious algebra we obtain:

$$- {}^J\alpha_{i+1/2} {}^J e_{i+3/2} + {}^J\beta_{i+1/2} {}^J e_{i+1/2} - {}^J\gamma_{i+1/2} {}^J e_{i-1/2} = {}^J\phi_{i+1/2}, \quad (5.30)$$

in which:

$${}^J\alpha_{i+1/2} = (A_i^{n+1})^2 \cdot \left[{}^J F_{i+1}^{n+1} - \frac{{}^J \partial F^{n+1}}{\partial W_{i+3/2}^{n+1}} ({}^J W_{i+1/2}^{n+1} - {}^J W_{i+3/2}^{n+1}) \right] \cdot \Delta t^{n+1/2}, \quad (5.31)$$

$$\begin{aligned} {}^J\beta_{i+1/2} = & \frac{{}^J \partial E^{n+1}}{\partial W_{i+1/2}^{n+1}} + \frac{\Delta M_{i+1/2}}{2} \frac{{}^J \partial P^{n+1}}{\partial W_{i+1/2}^{n+1}} (V_{i+1/2}^{n+1} - V_{i+1/2}^n) \\ & + (A_{i-1}^{n+1})^2 \cdot \left[{}^J F_i^{n+1} - \frac{{}^J \partial F^{n+1}}{\partial W_{i+1/2}^{n+1}} ({}^J W_{i-1/2}^{n+1} - {}^J W_{i+1/2}^{n+1}) \right] \cdot \Delta t^{n+1/2} \\ & + (A_{i+1}^{n+1})^2 \cdot \left[{}^J F_i^{n+1} - \frac{{}^J \partial F^{n+1}}{\partial W_{i+1/2}^{n+1}} ({}^J W_{i+1/2}^{n+1} - {}^J W_{i+3/2}^{n+1}) \right] \cdot \Delta t^{n+1/2}, \end{aligned} \quad (5.32)$$

$${}^J\gamma_{i+1/2} = (A_i^{n+1})^2 \cdot \left[{}^J F_i^{n+1} - \frac{{}^J \partial F^{n+1}}{\partial W_{i-1/2}^{n+1}} ({}^J W_{i-1/2}^{n+1} - {}^J W_{i+1/2}^{n+1}) \right] \cdot \Delta t^{n+1/2}, \quad (5.33)$$

$${}^J\phi_{i+1/2} = ({}^J L_i^{n+1} + L_i^n - {}^J L_{i+1}^{n+1} - L_{i+1}^n) \Delta t^{n+1/2} - \quad (5.34)$$

$$\left[{}^J E_{i+1/2}^{n+1} - E_{i+1/2}^n + \left\{ \frac{1}{2} (P_{i+1/2}^n + {}^J P_{i+1/2}^{n+1}) + Q_{i+1/2}^{n+1/2} \right\} \cdot (V_{i+1/2}^{n+1} - V_{i+1/2}^n) \right] \Delta M_{i+1/2},$$

$${}^J e_{i+1/2} = {}^J \Delta W_{i+1/2}^{n+1}. \quad (5.35)$$

DIFFERENCING THE NON-LINEAR EQUATIONS

Applying the inner boundary condition (5.19) to equation (5.21), the transport equation, we have:

$${}^J L_1^{n+1} = (A_1^{n+1})^2 ({}^J W_{1/2}^{n+1} - {}^J W_{3/2}^{n+1}) 2 {}^J F_1^{n+1} = L_* . \quad (5.36)$$

Now if we compare the linearised form of (5.36) with equation (5.30), we can obtain the inner boundary values of $\alpha, \beta, \gamma, \phi$. The results of this comparison are given below:

$${}^J \alpha_{1/2} = 2 (A_1^{n+1})^2 \left[{}^J F_1^{n+1} - \frac{\partial E^{n+1}}{\partial W_{3/2}^{n+1}} ({}^J W_{1/2}^{n+1} - {}^J W_{3/2}^{n+1}) \right] \Delta t^{n+1/2}, \quad (5.37)$$

$${}^J \beta_{1/2} = 2 (A_1^{n+1})^2 \left[{}^J F_1^{n+1} - \frac{\partial E^{n+1}}{\partial W_{1/2}^{n+1}} ({}^J W_{1/2}^{n+1} - {}^J W_{3/2}^{n+1}) \right] \Delta t^{n+1/2}, \quad (5.38)$$

$${}^J \gamma_{1/2} = 0, \quad (5.39)$$

$${}^J \phi_{1/2} = [-2 (A_1^{n+1})^2 {}^J F_1^{n+1} ({}^J W_{1/2}^{n+1} - {}^J W_{3/2}^{n+1}) + L_*] \Delta t^{n+1/2}, \quad (5.40)$$

Repeating this process on equation (5.20), we can obtain the outer values of $\alpha, \beta, \gamma, \phi$. The results of this comparison are given below:

$${}^J \alpha_{N-1/2} = 0, \quad (5.41)$$

$${}^J \beta_{N-1/2} = 2 (A_{N-1}^{n+1})^2 \left[{}^J F_{N-1}^{n+1} - \frac{\partial E^{n+1}}{\partial W_{N-3/2}^{n+1}} ({}^J W_{N-3/2}^{n+1} - {}^J W_{N-1/2}^{n+1}) \right] \Delta t^{n+1/2} + O A_{\text{phot}}^{n+1}, \quad (5.42)$$

$${}^J \gamma_{N-1/2} = 2 (A_{N-1}^{n+1})^2 \left[{}^J F_{N-1}^{n+1} - \frac{\partial E^{n+1}}{\partial W_{N-3/2}^{n+1}} ({}^J W_{N-3/2}^{n+1} - {}^J W_{N-1/2}^{n+1}) \right] \Delta t^{n+1/2}, \quad (5.43)$$

$${}^J \phi_{N-1/2} = \frac{1}{2} [L_{N-1}^n + L_{N-1}^{n+1} - 2 O (A_{\text{phot}}^n W_{N-1/2}^n + A_{\text{phot}}^{n+1} {}^J W_{N-1/2}^{n+1})] \Delta t^{n+1/2} - \quad (5.44)$$

$$[{}^J E_{N-1/2}^{n+1} - E_{N-1/2}^n + \left\{ \frac{1}{2} (P_{N-1/2}^n + {}^J P_{N-1/2}^{n+1}) + Q_{N-1/2}^{n+1/2} \right\} (V_{N-1/2}^{n+1} - V_{N-1/2}^n)] \Delta M_{N-1/2} .$$

DIFFERENCING THE NON-LINEAR EQUATIONS

The gradients $\partial P/\partial W$ and $\partial E/\partial W$ are found using numerical means.

Equation (5.30) can be written as a matrix equation:

$$\underline{D} \underline{\epsilon} = \underline{\phi}, \quad (5.45)$$

where:

$${}^j D_{lm} = -{}^j \alpha_{l-1/2} \delta_{l-1,m} + {}^j \beta_{l-1/2} \delta_{l,m} - {}^j \gamma_{l-1/2} \delta_{l+1,m}, \quad \text{for } 1 < m < N, \quad (5.46)$$

$${}^j D_{l1} = {}^j \beta_{1/2} \delta_{l,1} - {}^j \gamma_{1/2} \delta_{l,2}, \quad (5.47)$$

$${}^j D_{lN} = -{}^j \alpha_{N-1/2} \delta_{l,N-1} + {}^j \beta_{N-1/2} \delta_{l,N}. \quad (5.48)$$

$\delta_{l,m}$ is the Kronecker delta symbol. $\underline{\epsilon}$ is now easily found by inverting the tri-diagonal matrix \underline{D} (see Richtmyer and Morton, 1967 for one possible method of inverting \underline{D}). Having found $\underline{\epsilon}$, the temperatures of each zone are corrected using (5.26) and then another temperature iteration is performed, using the new temperature values, until the desired degree of convergence is obtained.

5.7 TIME STEP

At each time integration step $\Delta t^{''''}$ must be found. The size of the time increment $\Delta t^{''''}$ is limited by two main restrictions. Firstly, the time increment must be small enough to prevent any adjacent zone boundaries from crossing. Secondly, no information from one boundary should be able to affect an adjacent boundary during one time increment. This is the same as saying that an event travelling at the sound speed of the zone, should not be able to cross the zone in one

DIFFERENCING THE NON-LINEAR EQUATIONS

time increment. Thus these two conditions can be combined into the following formulation:

$$dt_i^{n+1/2} < \text{MIN} \left[\frac{-(R_i^{n+1} - R_{i-1}^{n+1})}{(U_i^{n+1/2} - U_{i-1}^{n+1/2})}, \frac{(R_i^{n+1} + R_{i-1}^{n+1})}{(\gamma P_{i-1/2}^{n+1/2} V_{i-1/2}^{n+1/2})} \right], \quad (5.49)$$

$$dt_i^{n+1/2} = \text{MIN}(dt_i^{n+1/2}), \quad \text{for all } i, \quad (5.50)$$

where γ is the ratio of specific heats. Usually (5.50) is halved to allow for the fact that the velocities are found explicitly, and hence would not allow for the rapid transit time of a shock front across a zone. Even when the time step has been halved, a check must be made to ensure that no two zones will cross on the following timestep. If two such zones were found to cross, the timestep is repeated with the timestep increment halved.

5.8 MODEL OUTPUT ON COMPLETING A PERIOD

The completion of a period is defined to be the time at which a pre-selected zone or observation point crosses its own equilibrium radius while contracting or expanding. Three possibilities are considered for this point. This point maybe the radius of the 'halfway zone' of the stellar envelope ($N/2$), the photospheric radius, or the radius of any zone under observation. At the end of each period the following quantities are given for the observation point.

$U_{\text{min}}, U_{\text{max}}$ = Minimum and Maximum Velocity,

$$\Delta U = (U_{\text{max}} - U_{\text{min}});$$

$R_{\text{min}}, R_{\text{max}}$ = Minimum and Maximum Radius,

$$\Delta R = (R_{\text{max}} - R_{\text{min}})/R_0;$$

$L_{\text{min}}, L_{\text{max}}$ = Minimum and Maximum Luminosity,

$$\Delta M_{\text{bol}} = 2.5 \log(L_{\text{max}}/L_{\text{min}});$$

Period (days) = The Period of observation point.

DIFFERENCING THE NON-LINEAR EQUATIONS

Along with these observational quantities, the total work (W), kinetic energy (K.E.), potential energy (P.E.) and overall energy (E) for the model envelope are given. The forms used are shown below:

$$P.E. = -\sum_{i=1}^N [GM_i/R_i^{n+1} + \Delta(P.E.)_i^{n+1}], \quad (5.51)$$

$$K.E. = \sum_{i=1}^N [\frac{1}{2}\Delta M_{i-1/2} (U_{i-1/2}^{n+1})^2 + \Delta(K.E.)_i^{n+1}], \quad (5.52)$$

$$W_i = \Delta M_{i-1/2} \cdot \int_{\tau} (P_{i-1/2} + Q_{i-1/2}) dV + \frac{1}{2} (P_{i-1/2}^n - P_{i-1/2}^{n+1}) \cdot (V_{i-1/2}^n - V_{i-1/2}^{n+1}), \quad (5.53)$$

$$W = \sum_{i=1}^N W_i, \quad (5.54)$$

$$E = P.E. + K.E. + W, \quad (5.55)$$

where W_i is the nett work of zone i over one period. $\Delta(X)$ is the relevant cross-over correction to variable X, to allow for the fact that time is discrete and hence the period probably occurs between time steps n and n+1 rather than on time step n+1. A simple linear interpolation of respective quantities between time steps is found to be adequate for our purposes. The overall energy (E) should remain constant in time since energy is conserved (This is a good check on the model). It is sometimes useful also to have a stability coefficient K, defined below:

$$K = \frac{|W^+| - |W^-|}{|W^+| + |W^-|}, \quad (5.56)$$

where:

$$\begin{aligned} W^+ &= \sum_i^{all} W_i, & \text{for } W_i > 0, \\ W^- &= \sum_i^{all} W_i, & \text{for } W_i < 0. \end{aligned} \quad (5.57)$$

DIFFERENCING THE NON-LINEAR EQUATIONS

This stability coefficient indicates whether the pulsations are growing ($K > 0$) or decaying ($K < 0$) and usually approaches 0 when the pulsations are approaching the limit cycle.

At the completion of a period a graph showing the work integral with depth is given along with a graphical history of the Radial, Velocity and Luminosity variations of the observation point. There is also an option for producing the complete history of Luminosity and Velocity over one period for the whole stellar envelope. This last option should be used with care, as it requires a lot of disk space (2.0 - 2.5 Mbytes).

CHAPTER 6

THE LINEAR EQUATIONS

6.1 THE BASIC EQUATIONS

In this chapter a brief derivation of the linear equations and a description of how they can be solved will be given for completeness. Along with these equations the growth rate coefficient and work integral will also be derived. The derivation will be along similar lines to that found in Castor (1971) and Cox & Stellingwerf (1980). In this derivation, the radiative approximation will be used and convection completely ignored (for a complete discussion on the effects of convection and how to include it in the linear equations, see Worrell, 1985). To simplify the algebra further, radiative diffusion will be assumed to be the only mechanism of energy transport. To further aid the derivation, the required hydrodynamic equations (derived in chapter 3) are re-written below:

$$\frac{1}{\rho} = \frac{4\pi}{3} \frac{dr^3}{dm}, \quad (6.1)$$

$$\frac{d^2 r}{dt^2} = -\frac{Gm}{r^2} - 4\pi r^2 \frac{dP}{dm}, \quad (6.2)$$

$$\frac{dL}{dm} = T \frac{dS}{dt}, \quad (6.3)$$

$$L = \frac{4\sigma}{3} \cdot \frac{(4\pi r^2)^2}{\chi} \cdot \frac{dT^4}{dm}, \quad (6.4)$$

THE LINEAR EQUATIONS

where χ is the Rosseland mean opacity and the other variables have their usual meaning.

6.2 THE LINEAR NON-ADIABATIC HYDRODYNAMIC EQUATIONS

Following the method of Castor (1971), equations (6.1) - (6.4) are differenced as follows:

$$\frac{1}{\rho} = \frac{4\pi}{3} \cdot \frac{(r_{i+1}^3 - r_i^3)}{\Delta m_i}, \quad (6.5)$$

$$\frac{d^2 r_i}{dt^2} = \frac{-Gm_i}{r_i^2} - \frac{4\pi r_i^2 (P_i - P_{i-1})}{\Delta m_i}, \quad (6.6)$$

$$T_i \frac{dS_i}{dt} = \frac{(L_i - L_{i-1})}{\Delta m_i}, \quad (6.7)$$

$$L_i = \frac{8\sigma}{3} \cdot (4\pi r_i^2)^2 \cdot \frac{(T_{i-1}^4 - T_i^4)}{\langle \chi dm \rangle} \quad (6.8)$$

in these, ΔM_i , Δm_i and $\langle \chi dm \rangle$ are defined as:

$$\Delta m_i = (m_{i+1} - m_i), \quad (6.9)$$

$$\Delta M_i = (m_{i+1} - m_{i-1}) / 2, \quad (6.10)$$

$$\langle \chi dm \rangle = \chi_i \Delta m_i + \chi_{i-1} \Delta m_{i-1}. \quad (6.11)$$

Equations (6.5) - (6.8) can now be perturbed, keeping only the linear (first order) terms; the perturbation of variable X being represented

THE LINEAR EQUATIONS

by δX . It is assumed that all the perturbations have a time dependence of the form $e^{i\omega t}$ where ω is a complex frequency, so that we can write the following linear equations:

$$\left(\frac{\delta\rho}{\rho}\right)_i = \frac{4\pi}{dm_i} \cdot (r_{i+1}^2 \delta r_{i+1} - r_i^2 \delta r_i), \quad (6.12)$$

$$-\omega^2 \delta r_i = 4Gm_i \cdot \frac{\delta r_i}{r_i^3} - \frac{4\pi r_i^2}{\Delta m_i} \cdot (\delta\rho_i - \delta\rho_{i-1}), \quad (6.13)$$

$$i\omega T_i \delta S_i = \frac{(\delta L_i - \delta L_{i-1})}{dm_{i-1}}, \quad (6.14)$$

$$\begin{aligned} \left(\frac{\delta L}{L}\right)_i &= 4\left(\frac{\delta r}{r}\right)_i + \left[\frac{4T_{i-1}^4}{(T_{i-1}^4 - T_i^4)} - \frac{\chi_{i-1} dm_{i-1} (\chi_T)_{i-1}}{\langle \chi dm \rangle} \right] \cdot \left(\frac{\delta T}{T}\right)_{i-1} \\ &+ \left[\frac{4T_i^4}{(T_i^4 - T_{i-1}^4)} - \frac{\chi_i dm_i (\chi_T)_i}{\langle \chi dm \rangle} \right] \cdot \left(\frac{\delta T}{T}\right)_i \\ &- \frac{\chi_{i-1} dM_{i-1} (\chi_\rho)_{i-1}}{\langle \chi dm \rangle} \left(\frac{\delta\rho}{\rho}\right)_{i-1} - \frac{\chi_i dM_i (\chi_\rho)_i}{\langle \chi dm \rangle} \left(\frac{\delta\rho}{\rho}\right)_i, \end{aligned} \quad (6.15)$$

where χ_ρ and χ_T are the derivatives of the opacity w.r.t. ρ and T . We also need to linearise the equation of state to get $\delta P/P$ and $\delta T/T$, thus:

$$\left(\frac{\delta P}{P}\right)_i = \frac{\partial \log_e P}{\partial \log_e T} \Big|_{\rho,i} \cdot \frac{\delta S}{C_v} \Big|_i + \frac{\partial \log_e P}{\partial \log_e \rho} \Big|_{s,i} \cdot \left(\frac{\delta\rho}{\rho}\right)_i, \quad (6.16)$$

$$\left(\frac{\delta T}{T}\right)_i = \frac{\delta S}{C_v} \Big|_i + \frac{\partial \log_e T}{\partial \log_e \rho} \Big|_{s,i} \cdot \left(\frac{\delta\rho}{\rho}\right)_i, \quad (6.17)$$

THE LINEAR EQUATIONS

Before continuing, it is useful to define the following variables, which will simplify the algebra greatly:

$$A_i = 4\pi r_i^2, \quad (6.18)$$

$$D_i = \frac{4T_{i-1}^4}{(T_{i-1}^4 - T_i^4)} - \frac{\chi_{i-1} dm_{i-1} (\chi_{T_{i-1}})}{\langle \chi dm \rangle}, \quad (6.19)$$

$$E_i = \frac{4T_i^4}{(T_i^4 - T_{i-1}^4)} - \frac{\chi_i dm_i (\chi_{T_i})}{\langle \chi dm \rangle}, \quad (6.20)$$

$$F_i = \frac{\chi_i dm_i (\chi_{p_i})}{\langle \chi dm \rangle}. \quad (6.21)$$

We now define two dependent vectors \underline{X} and \underline{Y} such that $Y_i \rightarrow 0$ in the adiabatic limit and \underline{X} satisfies:

$$\int_M \left(\frac{\delta r}{r} \right)_j^* \left(\frac{\delta r}{r} \right)_k r^2 dm = \delta_{jk} \left[\int_M \left| \frac{\delta r}{r} \right|_j^2 r^2 dm \right]^{1/2} \left[\int_M \left| \frac{\delta r}{r} \right|_k^2 r^2 dm \right]^{1/2} \quad (6.22)$$

or,

$$\sum_{i=1}^N (X_j)_i^* (X_k)_i = \delta_{jk} \left(\sqrt{\sum_{i=1}^N |X_j|_i^2} \right) \left(\sqrt{\sum_{i=1}^N |X_k|_i^2} \right), \quad (6.23)$$

where δ_{jk} is the Kronecker delta function. Comparing (6.22) with (6.23) and noting that δS_i goes to zero in the adiabatic limit, lets us write the components of vectors \underline{X} and \underline{Y} :

$$X_i = \sqrt{\Delta m_i} \delta r_i, \quad (6.24)$$

$$Y_i = T_i \delta S_i.$$

THE LINEAR EQUATIONS

We can now eliminate $\delta P/P$, $\delta \rho/\rho$ and $\delta T/T$ from equations (6.12), (6.16) and (6.17) and re-write (6.15) in terms of the components of the vectors \underline{X} and \underline{Y} :

$$\begin{pmatrix} \delta L \\ L \end{pmatrix}_i = B1(1)_i X_{i-1} + B1(2)_i X_i + B1(3)_i X_{i+1} + B2(1)_i Y_{i-1} + B2(2)_i Y_i, \quad (6.25)$$

where:

$$B1(1)_i = D_i \left. \frac{\partial \log_e T}{\partial \log_e \rho} \right|_{s, i-1} - \frac{F_{i-1} \Lambda_{i-1}}{dm_{i-1}} \frac{1}{\sqrt{\Delta m_{i-1}}}, \quad (6.26)$$

$$B1(2)_i = \frac{1}{\sqrt{\Delta m_i}} \frac{4}{r_i} - D_i \left. \frac{\partial \log_e T}{\partial \log_e \rho} \right|_{s, i-1} - \frac{F_{i-1} \Lambda_{i-1}}{dm_{i-1}} \frac{1}{\sqrt{\Delta m_i}} \quad (6.27)$$

$$+ E_i \left. \frac{\partial \log_e T}{\partial \log_e \rho} \right|_{s, i} - \frac{F_i \Lambda_{i+1}}{dm_i} \frac{1}{\sqrt{\Delta m_i}},$$

$$B1(3)_i = -E_i \left. \frac{\partial \log_e T}{\partial \log_e \rho} \right|_{s, i} - \frac{F_i \Lambda_{i+1}}{dm_i} \frac{1}{\sqrt{\Delta m_{i+1}}}, \quad (6.28)$$

$$B2(1)_i = E_i \left. \frac{1}{C_v} \right|_{i-1}, \quad (6.29)$$

$$B2(2)_i = D_i \left. \frac{1}{C_v} \right|_i. \quad (6.30)$$

It is now a simple matter to substitute (6.25) into (6.14), to give:

$$\begin{aligned} i \omega Y_i = & K1(1)_i X_{i-1} + K1(2)_i X_i + K1(3)_i X_{i+1} + K1(4)_i X_{i+2} \\ & + K2(1)_i Y_{i-1} + K2(2)_i Y_i + K2(3)_i Y_{i+1}, \end{aligned} \quad (6.31)$$

THE LINEAR EQUATIONS

where:

$$\begin{aligned}
 K1(1)_i &= B1(1)_i L_i / dm_i, & (6.32) \\
 K1(2)_i &= (B1(2)_i - B1(1)_{i+1}) L_i / dm_i, \\
 K1(3)_i &= (B1(3)_i - B1(2)_{i+1}) L_i / dm_i, \\
 K1(4)_i &= -B1(3)_{i+1} L_i / dm_i, \\
 K2(1)_i &= B2(1)_i L_i / dm_i, \\
 K2(2)_i &= (B2(2)_i - B2(1)_i) L_i / dm_i, \\
 K2(3)_i &= -B2(2)_i L_i / dm_i.
 \end{aligned}$$

A similar sequence of substitutions and eliminations can be done on equation (6.13) to give:

$$w^2 = G1(1)_i X_{i-1} + G1(2)_i X_i + G1(3)_i X_{i+1} + G2(1)_i Y_{i-1} + G2(2)_i Y_i, \quad (6.33)$$

where:

$$G1(1)_i = \frac{\Lambda_i}{(\Delta m_i)^{3/2}} \cdot \frac{\partial \log_e P}{\partial \log_e \rho} \Big|_{s, i-1} \cdot \frac{\Lambda_{i-1}}{dm_{i-1}} \cdot \frac{1}{(\Delta m_{i-1})^{1/2}}, \quad (6.34)$$

$$G1(2)_i = \frac{4Gm_i}{r_i^2} + \frac{\Lambda_i}{(\Delta m_i)^2} \cdot \frac{\partial \log_e P}{\partial \log_e \rho} \Big|_{s, i} \cdot \frac{\Lambda_i}{dm_i} + \frac{\Lambda_i}{(\Delta m_i)^2} \cdot \frac{\partial \log_e P}{\partial \log_e \rho} \Big|_{s, i-1} \cdot \frac{\Lambda_{i-1}}{dm_{i-1}}, \quad (6.35)$$

$$G1(3)_i = \frac{\Lambda_{i+1}}{(\Delta m_{i+1})^{3/2}} \cdot \frac{\partial \log_e P}{\partial \log_e \rho} \Big|_{s, i} \cdot \frac{\Lambda_i}{dm_i} \cdot \frac{1}{(\Delta m_i)^{1/2}}, \quad (6.36)$$

$$G2(1)_i = \frac{\Lambda_i}{(\Delta m_i)^{3/2}} P_{i-1} \cdot \frac{\partial \log_e P}{\partial \log_e T} \Big|_{p, i-1} \cdot \frac{1}{(C_V T)_{i-1}}, \quad (6.37)$$

$$G2(2)_i = \frac{\Lambda_i}{(\Delta m_i)^{3/2}} P_i \cdot \frac{\partial \log_e P}{\partial \log_e T} \Big|_{p, i} \cdot \frac{1}{(C_V T)_i}. \quad (6.38)$$

THE LINEAR EQUATIONS

It is now obvious that (6.25) and (6.33) can be re-written as two matrix equations:

$$w^2 \underline{X} = \underline{G1} \underline{X} + \underline{G2} \underline{Y}, \quad (6.39)$$

$$i w \underline{Y} = \underline{K1} \underline{X} + \underline{K2} \underline{Y}, \quad (6.40)$$

where \underline{X} and \underline{Y} are vectors of $N-1$ elements and the matrices are square $(N-1) \times (N-1)$ matrices. To complete this section the boundary conditions must be found. The inner boundary condition is simply:

$$X_1 = 0, \quad (6.41)$$

$$\delta L_1 = 0. \quad (6.42)$$

The outer boundary conditions for the radiative diffusion approximation, assuming perfect reflection of the momentum at the stellar surface boundary, are:

$$\left(\frac{\delta L}{L} \right)_N = 2 \left(\frac{\delta r}{r} \right)_N + \left(\frac{\delta T^4}{T^4} \right)_N, \quad (6.43)$$

$$\left(\frac{\delta P}{P} \right)_N = \left(4 - \frac{w^2 r_N^3}{G m_N} \right) \left(\frac{\delta r}{r} \right)_N. \quad (6.44)$$

This last equation is from Castor (1971) and not particularly good if the stellar atmosphere is extended or the radiation pressure in the atmosphere is not negligible. For a full discussion on this and other more useful boundary conditions see Worrell (1985).

6.3 SOLVING THE LINEAR NON-ADIABATIC EQUATIONS

Having now found the differenced linear non-adiabatic equations, we must consider ways of solving them to give the vectors \underline{X} and \underline{Y} as well as the complex frequency w . We first note that:

$$G1(1)_{i,j} = G1(3)_{j,i} \quad (6.45)$$

This tells us that $\underline{G1}$ is a symmetric tri-diagonal square matrix. This is useful as in the adiabatic limit of $Y_{\perp} \rightarrow 0$ equation (6.39) becomes:

$$w_{ad}^2 \underline{X}_{ad} = \underline{G1} \underline{X}_{ad} \quad (6.46)$$

and so w_{ad}^2 is real. Now in most stars the non-adiabatic effects will be small, and w_{ad} and \underline{X} should be good approximations for w and \underline{X} for each particular eigenmode. The adiabatic problem is easily solved as the zeroes of the characteristic polynomial of (6.46) can be found using Sturm's Theorem (as used by Castor, 1971). A sequence of m polynomials $f_m(x)$ is a Sturm sequence in the interval $x=a$ to $x=b$ if:

- i) $f_m(x)$ does not vanish in interval $x=a$ to $x=b$;
- ii) when $f_k(x) = 0$, then $f_{k-1}(x) \cdot f_{k+1}(x) < 0$;
- iii) no consecutive polynomials are zero.

Sturm's theorem states that for a given value of x , if we count the number of sign changes as k varies from 0 to m this number equals the number of zeroes on the range $x=a$ to ' x '. This then allows us to find the location of the roots of the equations. From this a good estimate of w_{ad} can be made and some iterative scheme can then be used to find the exact value.

THE LINEAR EQUATIONS

Having found w_{ad} and X_{ad} for a mode, we can then use the quasi-adiabatic approximation of Castor (1971) to obtain an estimate for w , by first of all finding Y_{qa} from (6.40):

$$Y_{qa} = (i w_{ad} \underline{1} - \underline{K2})^{-1} \underline{K1} X_{ad}, \quad (6.47)$$

where $\underline{1}$ is the unit matrix. Then placing this approximation to Y in (6.39), thus:

$$w^2 X_{ad} = \underline{G1} X_{ad} + \underline{G2} (i w_{ad} \underline{1} - \underline{K2})^{-1} \underline{K1} X_{ad}, \quad (6.48)$$

which upon transposing vector X and substituting in (6.46) gives us the following estimate of w :

$$w^2 = w_{ad}^2 + X_{ad}^* \underline{G2} (i w_{ad} \underline{1} - \underline{K2})^{-1} \underline{K1} X_{ad}, \quad (6.49)$$

This is a very good approximation to w when the non-adiabaticity is small ($\text{Im}(w)/\text{Re}(w) \ll 1$). It is not such a good approximation if this condition is not met, but generally gives the right sign for $\text{Im}(w)$ and can be used for the initial estimate of w .

To solve the full non-adiabatic problem we first re-write equations (6.39) and (6.40) as one eigenequation:

$$\underline{A} \cdot Z = R, \quad (6.50)$$

THE LINEAR EQUATIONS

in which A , Z and R are defined by:

$$\begin{aligned} \underline{A}_{2i-1} &= \underline{G2}_i \text{ and } (\underline{G1} - w^2\underline{1})_i, & \text{for } i = 1 \text{ to } N-1, \\ \underline{A}_{2i} &= (\underline{K2} - iw\underline{1})_i \text{ and } \underline{K1}_i, & \text{for } i = 1 \text{ to } N-1, \end{aligned} \quad (6.51)$$

$$\begin{aligned} Z_{2i-1} &= Y_i, & \text{for } i = 1 \text{ to } N-1, \\ Z_{2i} &= X_i, & \text{for } i = 1 \text{ to } N-1, \end{aligned} \quad (6.52)$$

$$\begin{aligned} R_i &= 0, & \text{for } i = 1 \text{ to } 2N-6, \\ R_{2N-5} &= K1 (4)_{N-2} X_N, \\ R_{2N-4} &= -G1 (3)_{N-1} X_N, \\ R_{2N-3} &= -K1 (3)_{N-1} X_N. \end{aligned} \quad (6.53)$$

Since the system of equations is homogeneous we are allowed to specify X_N in such a way as to fix the normalisation of the eigenvectors. X_N is chosen so that:

$$\left(\frac{\delta r}{r} \right)_N = 1. \quad (6.54)$$

Using the above estimate of w the system can now be solved using some form of Gaussian elimination and back substitution to find Z . This solution for Z is then placed in the momentum boundary condition:

$$G1 (1)_N X_{N-1} + G2 (1)_N Y_{N-1} + G1 (3)_N X_N = 0. \quad (6.55)$$

However, the R.H.S. of (6.55) is not zero but a function of w because w was only an estimate and not the real value. Thus our task is to solve the equation $f(w)=0$, to find the next estimate of w . This can be done using the secant method. For a discussion of this method and the accuracy of the final result see Castor (1971) and Worrell (1985).

6.4 THE STABILITY COEFFICIENT AND WORK INTEGRAL FOR LINEAR PULSATION

The stability coefficient η is defined as the logarithm of the factor by which the pulsation energy increases/decreases over one period. This can be found in two ways, the first being quick but dependant on knowing w :

$$\eta = \log_e (|e^{i\omega\tau}|^2) = -2\tau \text{Im}(w), \quad (6.56)$$

where τ is $2\pi/\text{Re}(w)$; the period. The other method requires us to find the total pulsational energy E_{pul} and the change in E_{pul} over one period which are then substituted into the following equation:

$$\eta = \frac{d(\log_e E_{\text{pul}})}{dt} \tau = \frac{\langle \Delta E_{\text{pul}} \rangle}{\langle E_{\text{pul}} \rangle}. \quad (6.57)$$

The angular brackets $\langle \dots \rangle$ represent a time average over one period. To find the pulsational energy and the change in it over one period we have to substitute (3.17) into (3.27) and re-arrange as follows:

$$\frac{dE_{\text{pul}}}{dt} = \frac{d}{dt} \int_M \left(\frac{1}{2} v^2 \right) dm = - \int_M P \frac{d}{dt} (1/\rho) dm - \oint P_v \cdot dS, \quad (6.58)$$

The surface integral in (6.58) is easily evaluated for the radial case if we assume that the velocity at the bottom of the envelope is zero. Representing the stellar radius by R , the surface integral then becomes:

$$\oint_s P_v \cdot dS = 4\pi R^2 P_R \frac{dR}{dt}, \quad (6.59)$$

THE LINEAR EQUATIONS

Using the above formulae we can find η and the contribution of each zone to the driving of the pulsations.

The work integral can be found by multiplying the momentum equation (6.40) by $i\omega X^+$, to give:

$$i\omega^3 X^2 - i\omega X^+ G_1 X = X^+ G_2 (i\omega Y), \quad (6.66)$$

which, following Cox & Stellingwerf (1980), can be re-written as:

$$i\omega^3 J - i\omega J \Sigma^2 = C, \quad (6.67)$$

where:

$$J = \int_M |\delta r|^2 dm, \quad (6.68)$$

$$J \Sigma^2 = \int_M \left(4 \left| \frac{\delta r}{r} \right|^2 \frac{G_m}{r} - \Gamma_1 \left| \frac{\delta \rho}{\rho} \right|^2 \right) dm, \quad (6.69)$$

$$C = \int_M (\Gamma_3 - 1) \left(\frac{\delta \rho}{\rho} \right)_{space}^* (i\omega TSS)_{space} dm. \quad (6.70)$$

Sometimes J is called the oscillatory moment of inertia and Σ the oscillatory radius of gyration. The real part of C in the above equations is the required work integral.

RESULTS

CHAPTER 7

LINEAR NON-ADIABATIC RESULTS

7.1 INTRODUCTION

This Chapter is split into four main Sections. The first three Sections give the results of three linear surveys of the HR diagram using different opacity tables. The fourth Section deals with the limitations the above surveys place on the mass and luminosity of γ variable RCB stars.

The surveys were carried out using Dr Worrell's linear codes, which he graciously allowed me to use. The three surveys were carried out using Dr Carson's pure helium opacity table R040, the smoothed carbon opacity table BD9C produced by Dr Jeffery from Dr Carson's He-C sequence of tables, and the Demarque XIX mix opacity table of Cox & Tabor (1976). Each survey was carried out for masses of $0.8M_{\odot}$, $1.0M_{\odot}$ and $1.2M_{\odot}$ between temperatures 5,000 K - 30,000 K and luminosities $1,000L_{\odot}$ - $20,000L_{\odot}$ (see Figure 7.1 for actual models attempted). In all the surveys, convection was only treated in the static models using Saio's version of the mixing length theory, with non turbulent viscosity (a mixing length of 1.2 pressure scale heights was chosen).

For each model in the surveys, the program was asked to stop after finding 6 eigenmodes, as generally the fundamental and first overtone modes will be amongst these. This is especially needed for very

LINEAR NON-ADIABATIC RESULTS

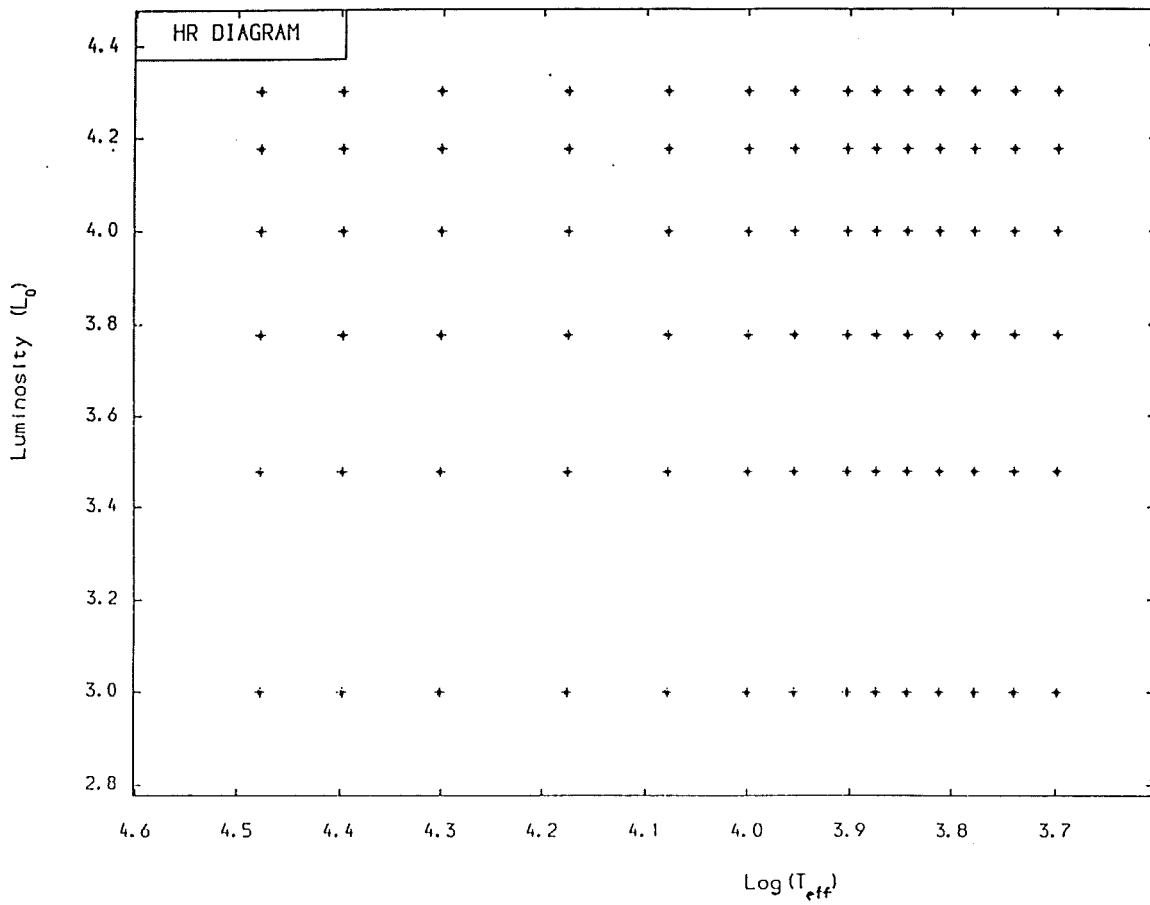


Figure 7.1 : This figure shows the location on the HR diagram of the models produced in each of the surveys presented in this chapter.

LINEAR NON-ADIABATIC RESULTS

non-adiabatic models in which the eigenmodes can occur in any order. For each model the program outputs the adiabatic period, non-adiabatic period, non-adiabatic growth rate and the change in phase of $\Phi(\delta R/R)$ between the inner and outer boundaries of the model's envelope. There is also the option of having the eigenfunction and work integral of each mode found and output in graphical form. This latter option was only selected for the fundamental mode (where found) of the $1.0M_{\odot}$ models in each survey, to get an idea of how the eigenfunctions changed with temperature and luminosity.

The results of the surveys will be presented in four parts. The first part is a detailed discussion of one model's eigenfunctions and work integrals for each mode found. The second part will give a brief description of how the eigenfunctions vary with luminosity and temperature and of the effects on the stability of the models. The third part will present and discuss the dynamical parameters of the models and how these vary with $\log(T_{\text{eff}})$, $\log(L/L_{\odot})$ and M/M_{\odot} . The last part will present the instability edges for each mass in the survey and compare these with previous work in the field.

The last main Section will apply the results of the linear surveys to 7 of the pulsating RCB stars, in the hope of finding limitations upon their luminosities and masses.

7.2 THE WHY AND WHERE OF THE SURVEYS

The first thing to consider is why have a survey at all? The primary reasons were to find out where in the HR diagram the stability edges occur for hydrogen deficient models based on mixes that are similar to those found in RCB stars. It is also desirable to place limits upon the masses and luminosities, to reduce the range of

LINEAR NON-ADIABATIC RESULTS

parameters over which non-linear models have to be made, in order to model some of the variable stars in the RCB group. A secondary reason was that this presented a good opportunity to compare the results of the two methods of opacity table generation over a wide range of densities and temperatures. From the surveys it was hoped that the major differences between the hydrogenic model of opacity generation used by Cox & Tabor (opacity table DXIX) and the hot Thomas-Fermi model of opacity generation used by Dr Carson (opacity table BD9C) would be seen in the survey results. Another useful by-product of the surveys is the production of simple polynomials linking $\log(P_0)$ and $\log(P_1)$ with stellar parameters $\log(L/L_\odot)$ and $\log(T_{\text{eff}})$.

Having decided upon two surveys, one for each opacity generation model, it was thought that a third survey using a pure helium mix (opacity table R040) would be useful, in that we could then see the underlying effects of helium on the model envelopes. This then lets us see how the introduction of carbon affected the models in the two earlier surveys.

The next consideration was to decide upon the range of stellar parameters over which the survey was to be carried out. The temperature proved to be the easiest to decide as the lower limit was set by the lack of convection theory for efficient convection, i.e., 5,000 K. As the majority of the RCB group of stars seem to have effective temperatures of between 5,000 K and 7,500 K with errors of about 500 K, it was decided that the survey should have models with effective temperatures starting at 5,000 K and increasing by a step of 500 K, up to 8,000 K. Now, as DY Cen has a reputed effective temperature of 10,000 K \pm 1,000 K, it was decided that models with effective temperatures of 9,000 K, 10,000 K and 12,000 K would also be useful. Finally, the hotter members of the RCB group have

LINEAR NON-ADIABATIC RESULTS

temperatures ranging up to 20,000 K \pm 5,000 K (depending upon which paper you read). Therefore to make sure that these were also encompassed, the survey was extended in effective temperature from 10,000 K in 5,000 K steps up to 30,000 K.

The luminosities at which stellar models were to be made were even more of a problem as the observational literature only gives the probable range of luminosities as (3,000-20,000) L_{\odot} with 10,000 L_{\odot} being preferred. So in an attempt to split this range up evenly in a logarithmic sense, it was decided that luminosities of 6,000 L_{\odot} and 15,000 L_{\odot} would also be included. The upper limit was about as high as anyone had predicted for the RCB group of stars, but some papers amongst the literature had mentioned a possible lower limit of 1,000 L_{\odot} and so this value of luminosity was also included. The location of the survey models on a HR diagram are shown in Figure 7.1 .

The final consideration was that of the masses at which the models were to be made. It was decided that no more than 3 different masses should be included in the survey as the work would soon become prohibitive. The only major work in the literature at the time of these surveys was by Saio & Wheeler (1985) and this seemed to indicate that the RCB group of stars must have masses in the range (0.8-2.0) M_{\odot} , with 1.0 M_{\odot} being favoured by Saio. Not being too sure whether to favour the low end of this range or to split it evenly, a range of linear models at 0.1 M_{\odot} steps over the whole mass range, for effective temperatures of 5,000 K, 6,000 K and 7,000 K at the most favoured luminosity of 10,000 L_{\odot} , were produced. This was done for both carbon opacity tables. The results of this brief sequence of models can be seen in Figure 7.2, opacity table DXIX is at the top of the page and opacity table BD9C is at the bottom. For each table mass sequence, the L.H.S. graphs are for the fundamental modes and the R.H.S.

LINEAR NON-ADIABATIC RESULTS

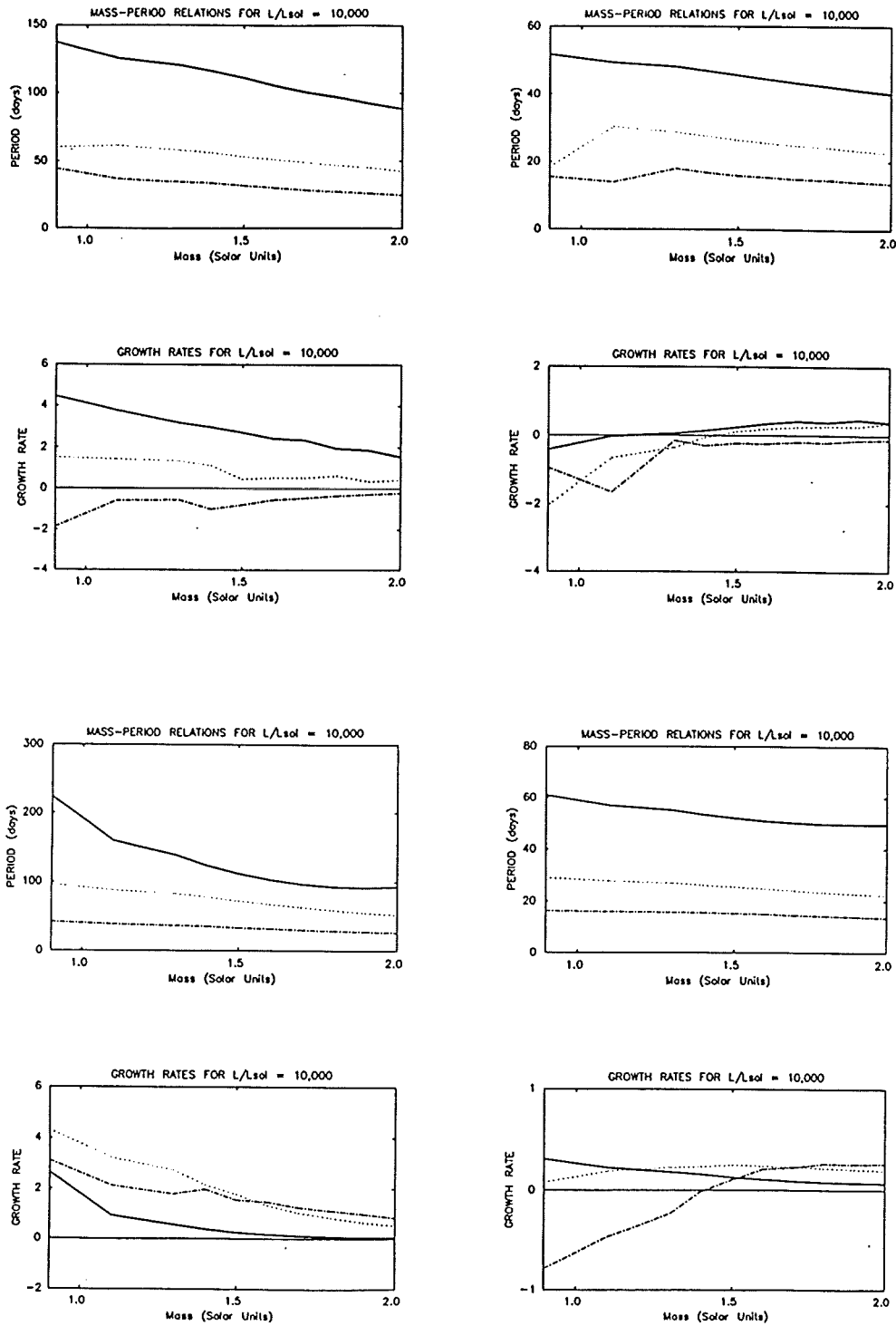


Figure 7.2 : This figure gives the results of the mass sequence for opacity tables DXIX (top) and BD9C (bottom). The graphs show plots for three effective temperatures: 7000 K (chain line), 6000 K (light solid line) and 5000 K (heavy solid line). For other details see text.

LINEAR NON-ADIABATIC RESULTS

graphs are for the first overtone modes. From the 7000 K plots on the fundamental graphs it can be seen that the lower mass limit would be preferred. The different opacities are already showing marked differences, as the DXIX models predict stability for all 7000 K models at this luminosity, while the BD9C models predict instability. The lower effective temperature models are more of a problem, indicating that they are probably of lower luminosities. Though it is worth noting that at around $1.0M_{\odot}$ the first overtones have about the right periods. Again we find a contradiction in the stability of the models between opacity tables. Taking this brief survey in mass into account, it was decided that the models of the surveys should be made with masses of $0.8M_{\odot}$, $1.0M_{\odot}$ and $1.2M_{\odot}$.

To sum up, each opacity table survey was made at 3 masses each consisted of a grid of 78 models. The grids consisting of an array of 13 effective temperatures by 6 luminosities.

7.3 RESULTS OF THE SURVEY USING OPACITY TABLE R040

In the following sub-sections, the results of the pure helium table survey described in the previous Section will be presented. As stated in the last Section, the main reason for this survey is to understand how the helium affects the pulsation parameters and the eigenfunctions in the survey models. It will also be useful to see if non-adiabaticity is present in these models or if it is a consequence of adding carbon. Similarly, the occurrence of 'strange' modes requires investigation.

7.3.1 A Detailed Discussion of One Model

The model chosen for this detailed description has a mass of $1M_{\odot}$, luminosity of $10,000L_{\odot}$ and an effective temperature of 7,500 K. The mass was chosen because it is in the middle of the surveyed range, and the other stellar parameters were chosen because they are the nearest the survey models came to the optimum specification of RY Sgr.

The first thing that is noticed about this model is that the nodes in $|\delta R/R|$ are well defined and are accompanied by a phase change $\Phi(\delta R/R)$ of Π (see Figures 7.3 - 7.4) which indicates that the star is close to the adiabatic limit. This can be further seen from the similarity in the non-adiabatic period and adiabatic period, i.e., 37.44 days and 37.56 days, respectively (see R040 results tables in Appendix E). The next feature of interest is the sharp drop in $|\delta L/L|$ as we go into the star and the lack of features after this drop. This decrease in $|\delta L/L|$ is caused by the rapid increase in helium opacity at this point, which is mainly due to the ionisation of neutral helium to He^+ . This drop in $|\delta L/L|$ is accompanied by a large narrow peak in $|\delta T/T|$ and an integral Π change in $\Phi(\delta L/L)$ of roughly the same width as the $|\delta T/T|$ peak, due to the 'damming up' of the radiation in the He^+ ionisation region mentioned above. It is this 'damming up' that causes the driving peaks seen in the work diagrams of Figure 7.5. This model is quite unusual, in that it does not have the He^{++} damping region which is usually present in these model envelopes. A detailed look at the equilibrium model seems to show that the cause of this anomaly is the presence of strong convection throughout the entire inner envelope below the $|\delta T/T|$ peak. Finally, the 'freezing in' of the luminosity perturbations (as discussed in Cox, 1980) can clearly be seen in the outer part of the model envelope.

LINEAR NON-ADIABATIC RESULTS

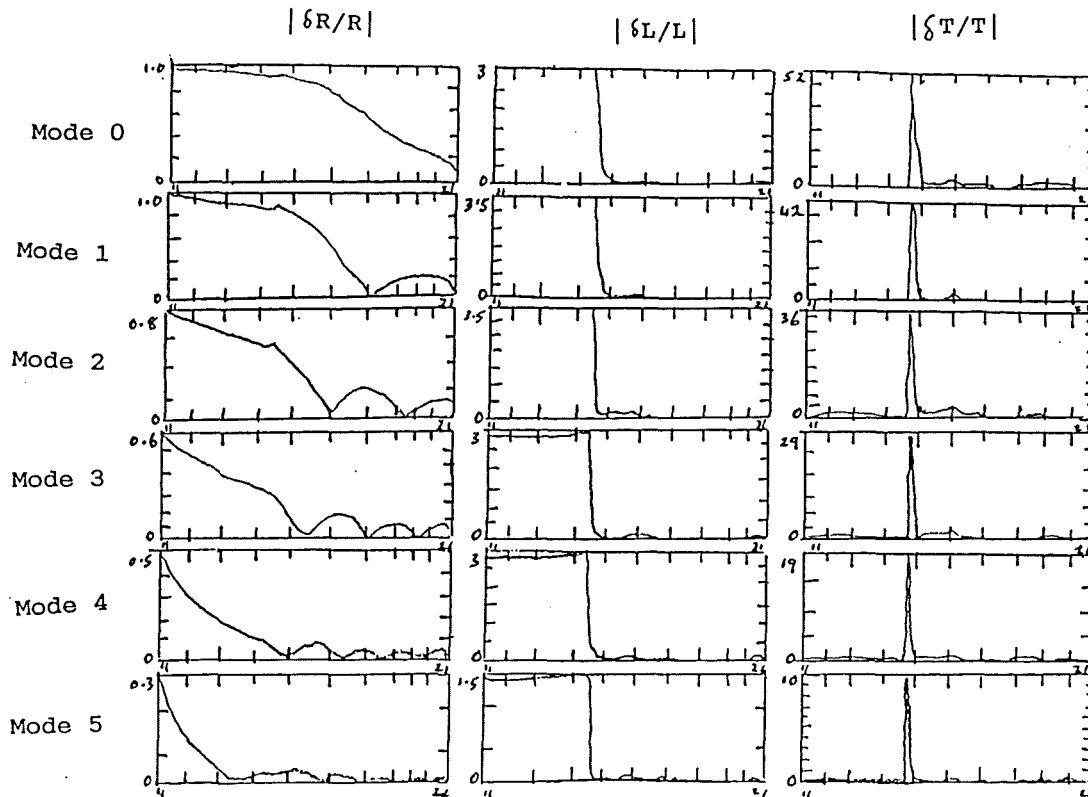


Figure 7.3 : This figure shows $|\delta R/R|$, $|\delta L/L|$ and $|\delta T/T|$ versus $\log(M-m_r) - 24$ for the first 6 eigenmodes of the $1M_{\odot}$ pure Helium model with $L/L_{\odot} = 10,000$ and $T_{\text{eff}} = 7,500$ K.

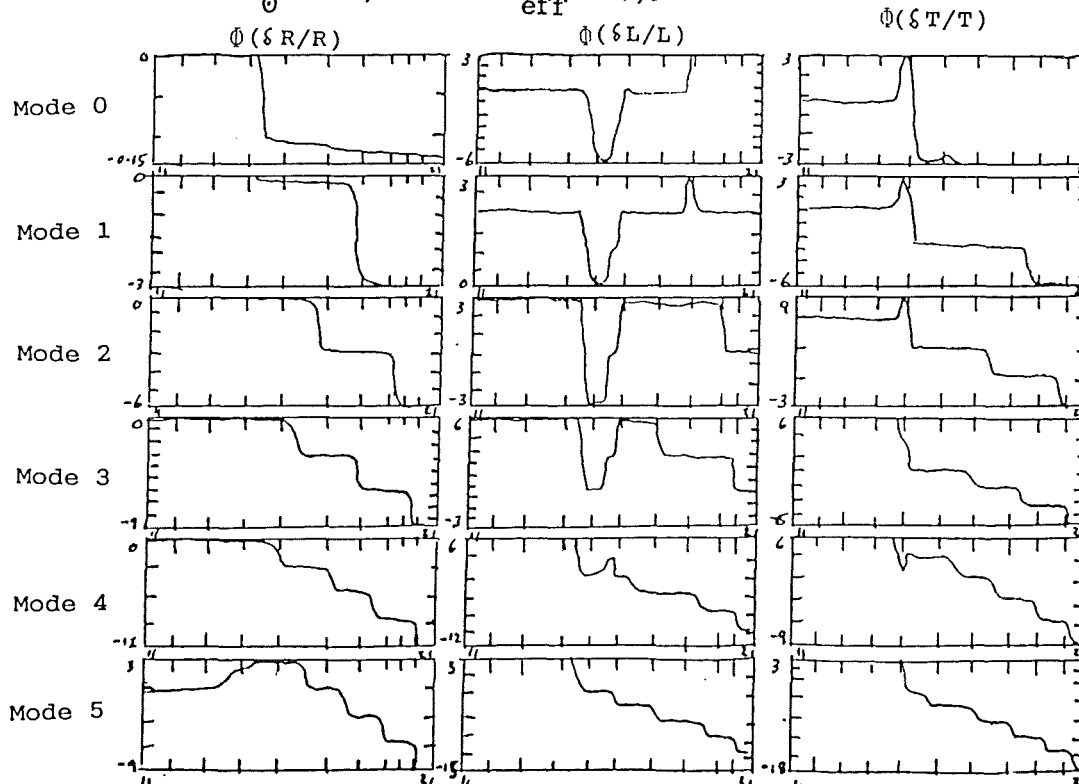


Figure 7.4 : This figure shows $\Phi(\delta R/R)$, $\Phi(\delta L/L)$ and $\Phi(\delta T/T)$ versus $\log(M-m_r) - 24$ for the first 6 eigenmodes of the $1M_{\odot}$ pure Helium model with $L/L_{\odot} = 10,000$ and $T_{\text{eff}} = 7,500$ K.

LINEAR NON-ADIABATIC RESULTS

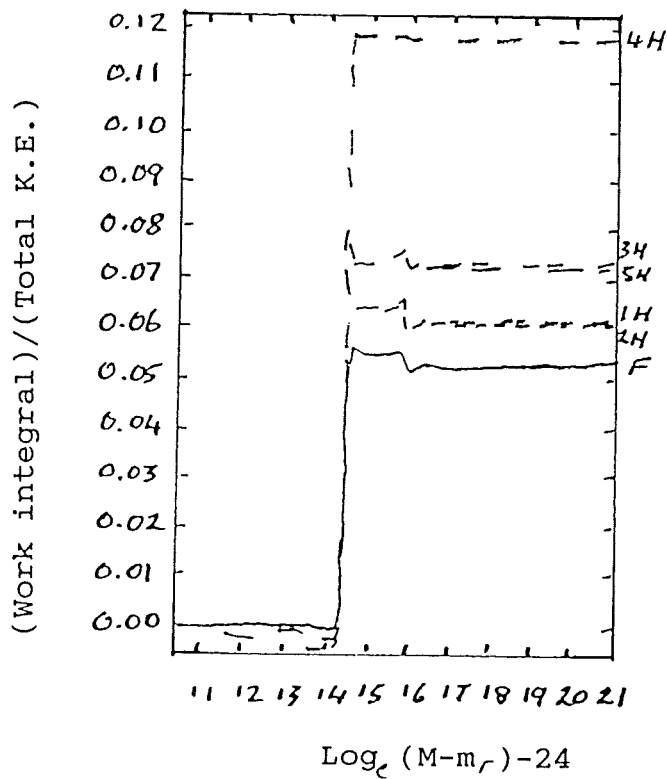
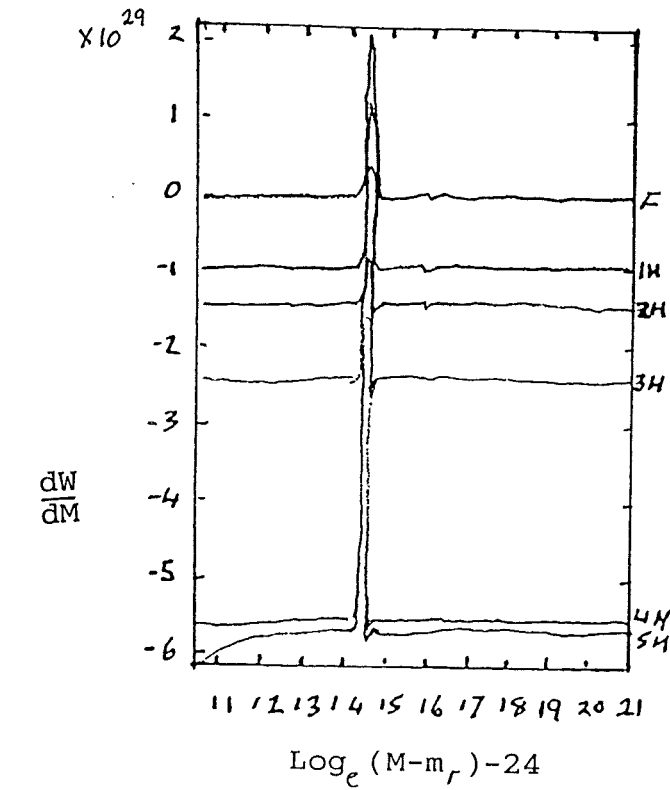


Figure 7.5 : This figure shows the work function and work integral versus $\log(M-m_r) - 24$ for the first 6 eigen modes of the $1M_{\odot}$ pure^r Helium model with $L/L_{\odot} = 10,000$ and $T_{\text{eff}} = 7,500$ K.

7.3.2 Fundamental Eigenfunctions of the $1 M_{\odot}$ Models

The first thing noticed in Figures 7.6 - 7.7 is the marked difference in $|\delta T/T|$ for effective temperatures above and below 15,000 K. This is due to the fact that below 15,000 K the opacity is rising rapidly with temperature (see Figure 4.3), while above 15,000 K the opacity levels off, and even starts to decrease slightly with temperature. For effective temperatures below 15,000 K, the envelope temperature rises very rapidly with mass, and the first helium ionisation zone occurs just below this large temperature change causing the radiation to be 'dammed up' by the resultant opacity bump. This 'damming' up of radiation is what causes the large peak in $|\delta T/T|$ and the sharp rise in $|\delta L/L|$ seen in Figures 7.8 - 7.9. $|\delta T/T|$ has a peak rather than a step, as the opacity drops away very rapidly below 15,000 K. Also $|\delta L/L|$ remains roughly constant for temperatures below 15,000 K as it becomes 'frozen in'. The $|\delta T/T|$ peak narrows and gets larger with both increasing effective temperature of models (up to 10,000 K) and increasing luminosity. This is mainly due to the increase in the opacity gradients of the opacity bump and thus the 'damming' up of the radiation in a smaller area. It is generally this region that produces any 'driving' present in the model.

The small peak in $|\delta L/L|$ (Figures 7.8 - 7.9) to the right of the steep rise is due to the $\text{He}^+ - \text{He}^{++}$ ionisation region of the model, and is the main cause of 'damping' in the model envelope. The size of this bump in $|\delta L/L|$ increases as it moves out in mass with rises in effective temperature. Some of the other smaller bumps towards the centre of the model envelopes are due to convection and have little effect upon the pulsation properties of the model envelopes. For effective temperatures above 10,000 K, we see that the peaks in $|\delta T/T|$

LINEAR NON-ADIABATIC RESULTS

are much broader and smaller in size. This is mainly due to the lack of rapid changes in opacity, so the opacity bump is well spread out, in mass. In the case of $T_{\text{eff}} = 15,000$ K we can see the two peaks in $|\delta T/T|$ due to the opacity bumps caused by the He-He⁺ and He⁺-He⁺⁺ ionisation zones. As the effective temperature increases the model envelopes become diffuse and the He⁺-He⁺⁺ ionisation peak in $|\delta T/T|$ vanishes. Bumps in $|\delta L/L|$ vanish and the size of the $|\delta L/L|$ step increases with rising effective temperatures or falls in luminosity, as more radiation can seep out due to a drop in opacity of the outer envelope.

Figures 7.10 - 7.11 give $|\delta R/R|$ for this set of models and add little to the above discussion, but have been included for completeness. The missing graphs are those of models that would not converge. After a close look at the equilibrium models of these models, it was decided that convection was the probable cause. This conclusion was drawn from the fact that in all the non-converging models convection had replaced radiative transfer as the major form of energy transport in the envelopes below the 15,000 K opacity drop. As the convection is modelled using the mixing length theory, which is only valid in regions of inefficient convection, it is reasonable to assume that this is the most likely cause of the non-convergence seen in the lower effective temperature models.

To summarise, the major features found above are that the models increase in non-adiabaticity with increasing effective temperature and luminosity. Above $T_{\text{eff}} = 10,000$ K they become diffuse and for the larger luminosities very non-adiabatic. This is mainly due to the outward movement of the helium ionisation zones. Below about 8,000 K convection becomes significant and results in the diminution or loss of He⁺⁺ 'damping' in the envelope extending the red edge to lower effective temperatures. For lower effective temperatures, convection becomes dominant and the models no longer converge.

LINEAR NON-ADIABATIC RESULTS

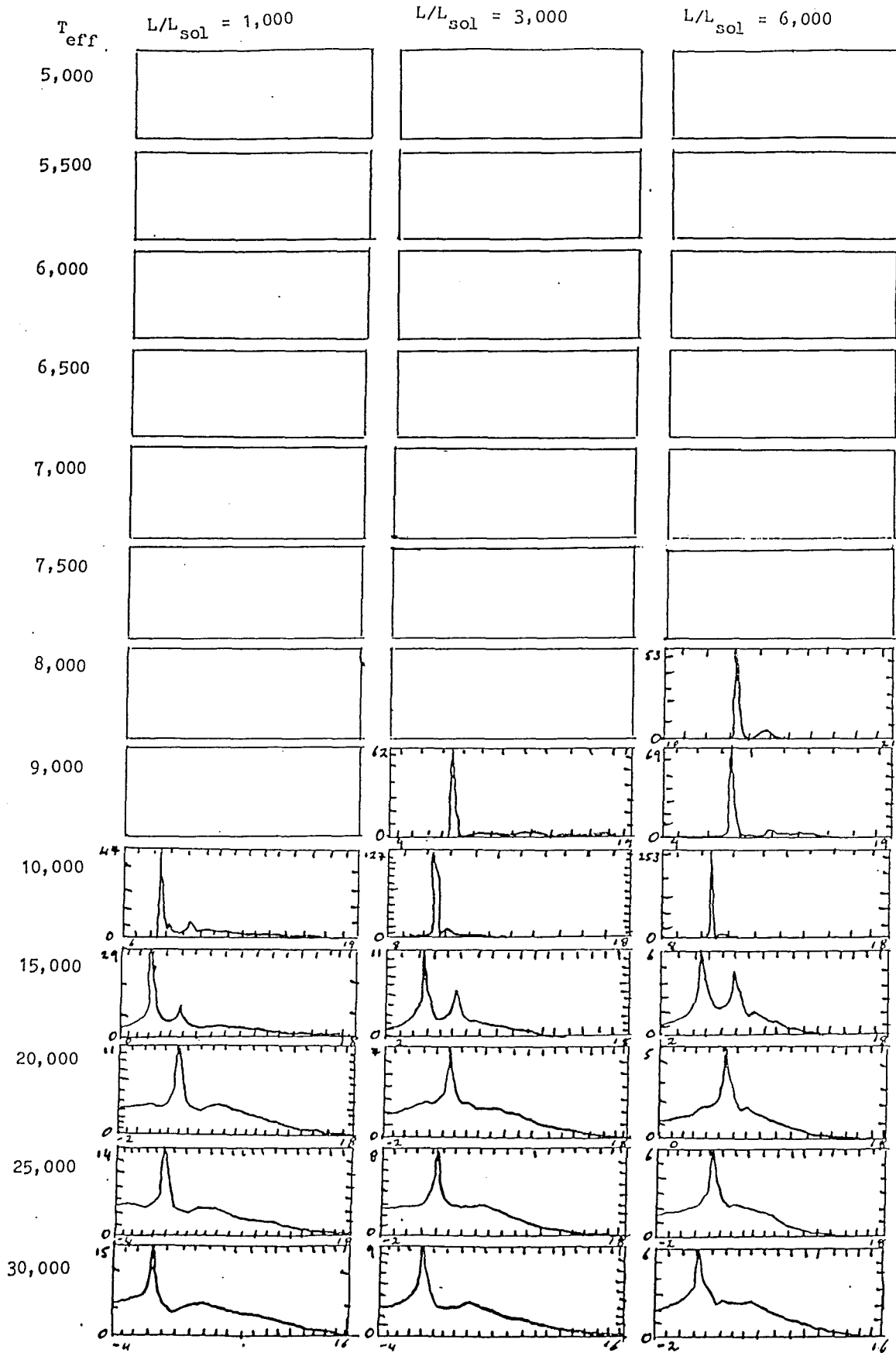


Figure 7.6 : This figure shows plots of γ_1 versus $\log(M-m_p) - 24$ for the Low luminosity fundamental modes of the $1M_{\odot}$ models of the survey using opacity table R040.

LINEAR NON-ADIABATIC RESULTS

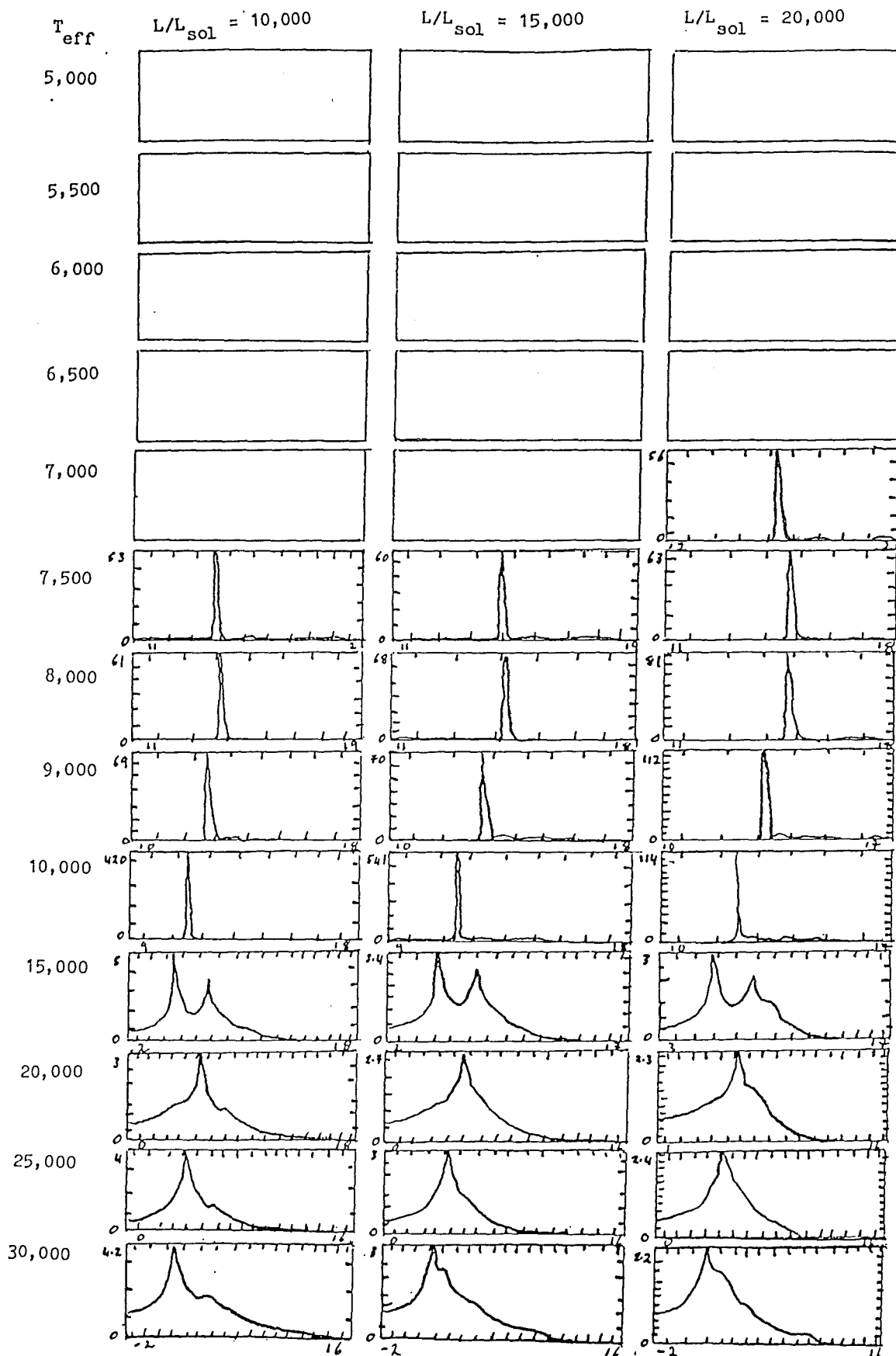


Figure 7.7 : This figure shows plots of γ_1 versus $\log(M-m_r)-24$ for the High luminosity fundamental modes of the $1M_{\odot}$ models of the survey using opacity table R040.

LINEAR NON-ADIABATIC RESULTS

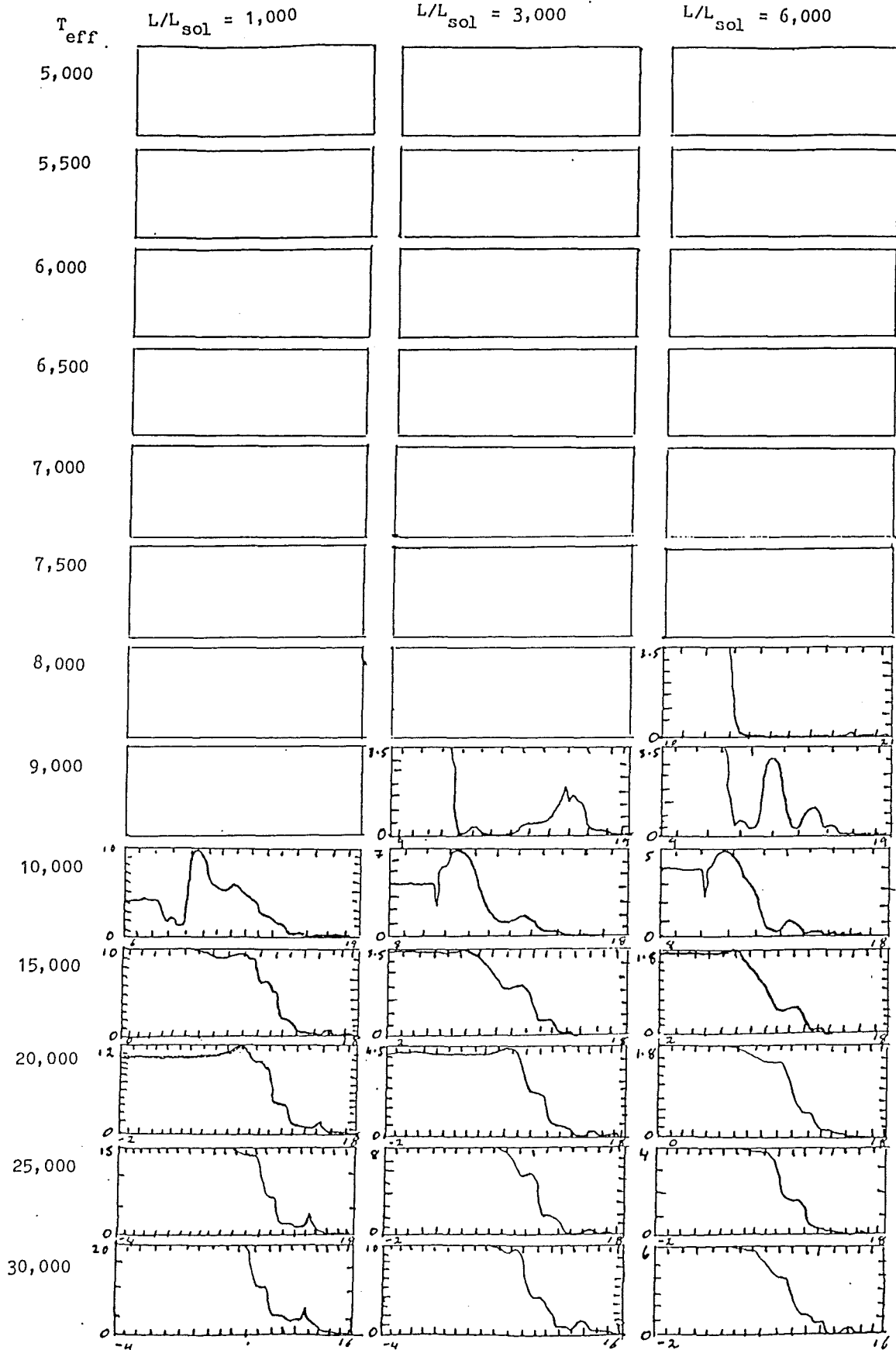


Figure 7.8 : This figure shows plots of $\log(L/L)$ versus $\log(M-m_r)-24$ for the Low luminosity fundamental modes of the $1M_{\odot}$ models of the survey using opacity table R040.

LINEAR NON-ADIABATIC RESULTS

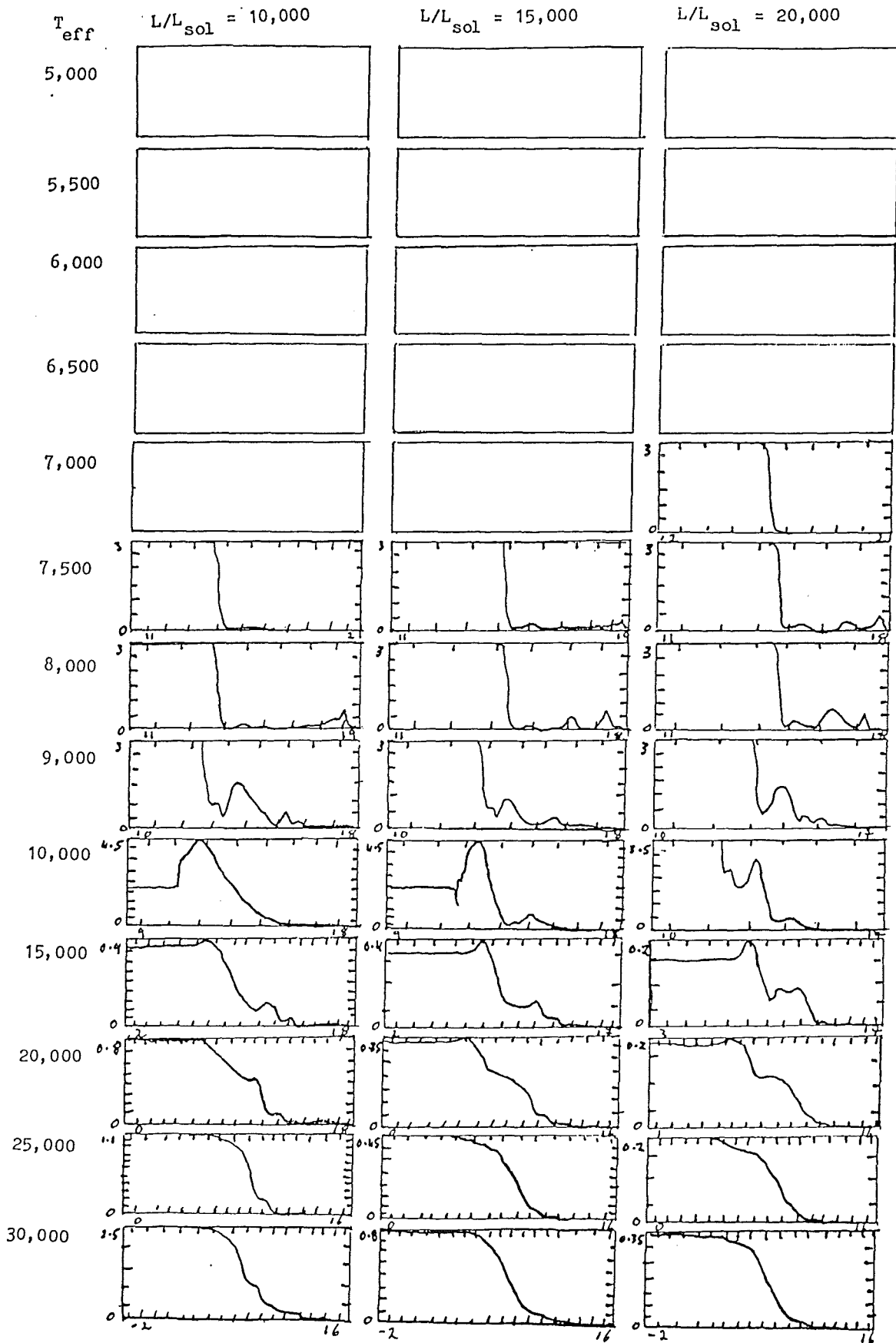


Figure 7.9 : This figure shows plots of $\delta L/L$ versus $\log(M-m_r)-24$ for the High luminosity fundamental modes of the $1M_{\odot}$ models of the survey using opacity table R040.

LINEAR NON-ADIABATIC RESULTS

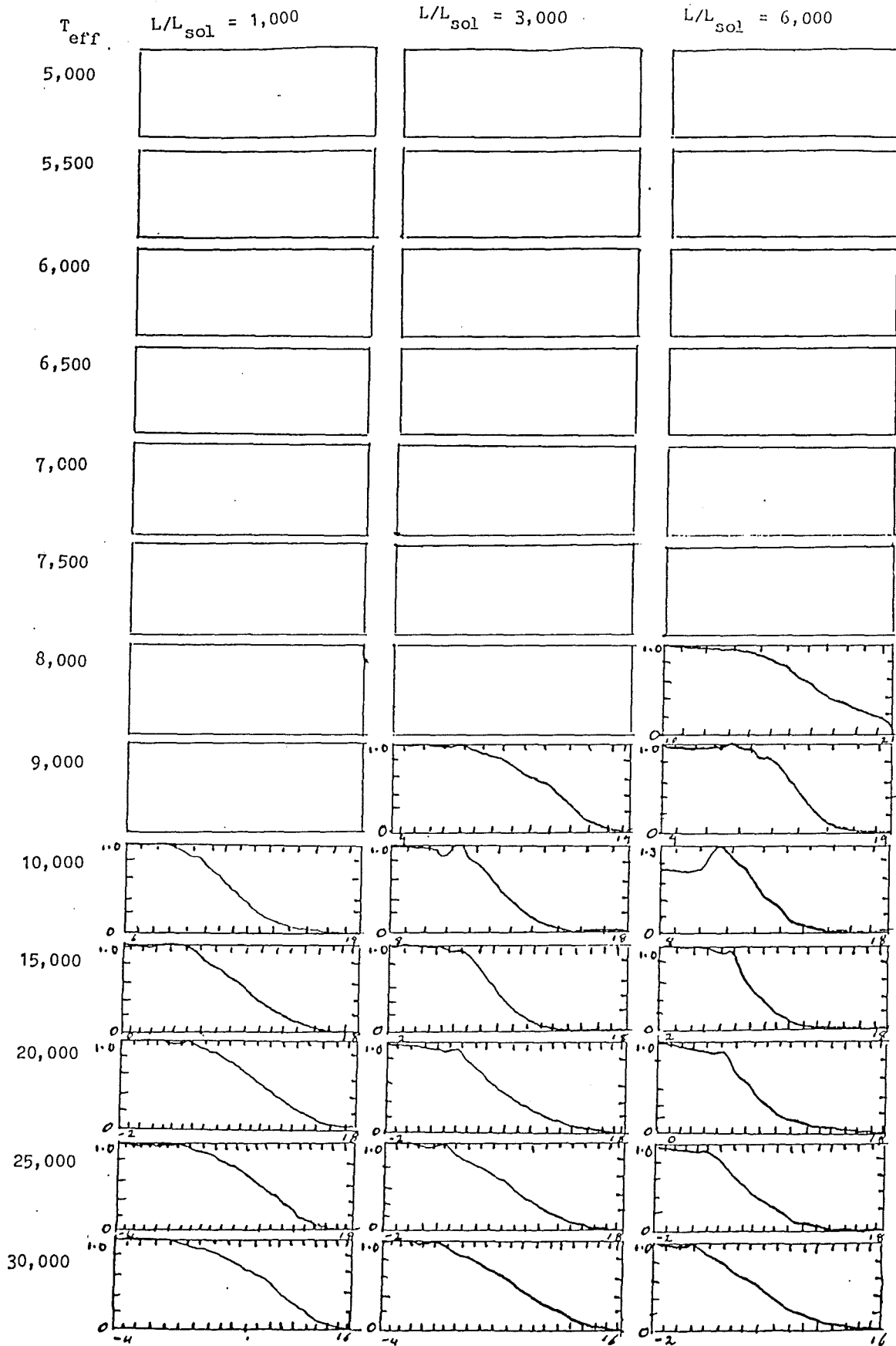


Figure 7.10 : This figure shows plots of $\log(R/R_1)$ versus $\log(M-m)-24$ for the Low luminosity fundamental modes of the $1M_{\odot}$ models of the survey using opacity table R040.

LINEAR NON-ADIABATIC RESULTS

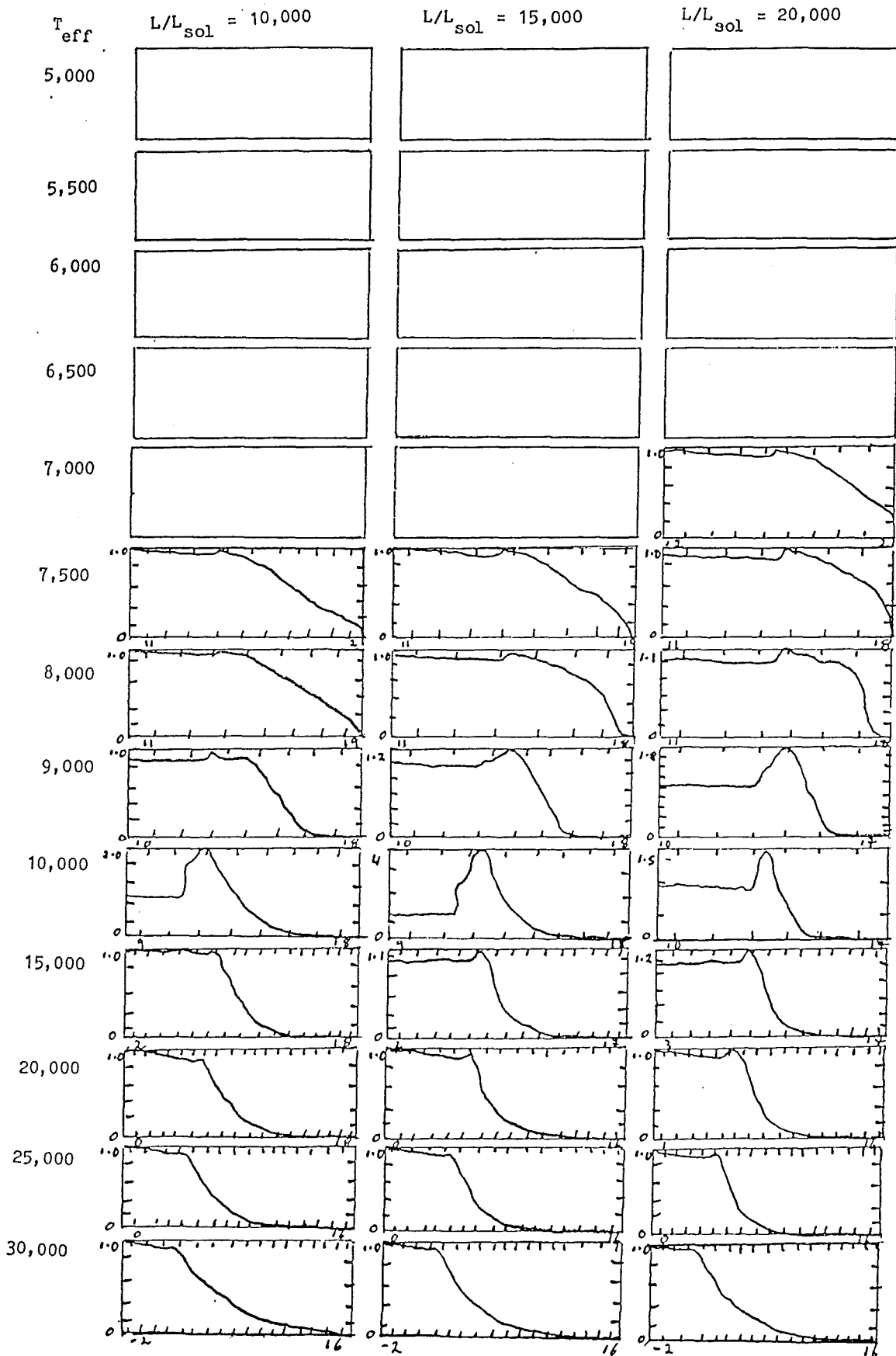


Figure 7.11 : This figure shows plots of $\log(R/R_0)$ versus $\log(M-m_c)-24$ for the High luminosity fundamental modes of the $1M_{\odot}$ models of the survey using opacity table R040.

7.3.3 Presentation of Results

In the following sub-sections, the results of the R040 opacity table survey will be given in graphical form, along with several polynomial fits to the fundamental and first overtone data. The raw data has been tabulated for the fundamental and first overtone modes and can be found in the R040 Section of Appendix E (pages E-1 to E-18).

The graphs are in groups of 4 showing from top left to bottom right:

- TOP LEFT : adiabatic and non-adiabatic Log (period) vs Log (T_{eff})
- TOP RIGHT : adiabatic and non-adiabatic Log (Q) vs Log (T_{eff})
- BOTTOM LEFT : non-adiabatic Growth Rate vs Log (T_{eff})
- BOTTOM RIGHT : Nonadiabatic II^c vs Log (T_{eff}).

where II^c is the phase change in degree of $\Phi(\delta R/R)$ between the inner and outer boundaries of the model envelope in question. The symbols and lines used in the graphs are given below to maximise the size of the graphs and reduce repetition:

- DOTTED SOLID LINE - Shows the adiabatic fundamental modes
- LIGHT SOLID LINE - Shows the adiabatic first overtone modes
- CHAINED LINE - Shows the adiabatic second overtone modes
- DOTTED LINE - Shows the adiabatic third overtone modes

- + PLUS - Shows the non-adiabatic fundamental modes
- * ASTERISK - Shows the non-adiabatic first overtone modes
- O CIRCLE - Shows the non-adiabatic second overtone modes
- X CROSS - Shows the non-adiabatic third overtone modes.

LINEAR NON-ADIABATIC RESULTS

For each mass in the survey three polynomial fits have been made to the data. The first of these will fit the following polynomial to non-adiabatic Log (Period), with $\text{Log}(T_{\text{eff}})$ as the independent variable at each luminosity.

$$\text{Log (Period)} = a_0 + a_1 \cdot \text{Log}(T_{\text{eff}}) + a_2 \cdot [\text{Log}(T_{\text{eff}})]^2$$

A table of the coefficients at each luminosity, together with the mean residual, M.R., of fits and range in effective temperature, over which fits were made, will be given for each mass and mode considered.

The second and third fits will fit a [2D] polynomial of the form:

$$X = \sum_{i=0}^2 \sum_{j=0}^2 B_{ij} [\text{Log}(T_{\text{eff}})]^i [\text{Log}(L/L_0)]^j, \quad \forall i+j = 1, 2,$$

where X is the non-adiabatic Log (Period) in the second fit, and non-adiabatic Log (Q) in the third fit. For each mass, for the modes considered, the range in T_{eff} at each luminosity over which the fit was made is the same as that used in the first fits. For each fit the root mean of the residual squares divided by the range of X used in the fit is given as a percentage (X_i) alongside the polynomial coefficients.

LINEAR NON-ADIABATIC RESULTS

7.3.3.1 Survey Results for $0.8 M_{\odot}$ Models - Table 7.1, below gives the coefficients of fits to the non-adiabatic fundamental mode Log (periods) at constant luminosities.

L/L_{\odot}	a_0	a_1	a_2	M.R	$\text{Log}(T_{\text{eff}})$
1,000	55.577	-23.634	2.450	0.00717	3.954 - 4.301
3,000	34.987	-13.221	1.162	0.00381	3.954 - 4.477
6,000	8.559	-3.563	-0.384	0.01712	3.903 - 4.477
10,000	-5.803	6.778	-1.253	0.02400	3.875 - 4.477
15,000	17.057	-4.428	0.133	0.03295	3.845 - 4.477
20,000	5.379	1.343	-0.571	0.02157	3.845 - 4.477

TABLE 7.1 : Table of coefficients of first fit for fundamental mode.

The coefficients for the [2D] fit to the non-adiabatic fundamental mode Log (periods) are:

$$b_{00} = 10.958 \quad b_{01} = 1.066 \quad X_1 = 2.29\% \quad i+j = 1$$

$$b_{10} = -3.490$$

$$b_{00} = 9.608 \quad b_{10} = -1.270 \quad X_1 = 1.93\% \quad i+j = 2$$

$$b_{01} = -0.746 \quad b_{11} = 0.050$$

$$b_{02} = 0.218 \quad b_{20} = -0.287$$

The coefficients for the [2D] fit to the non-adiabatic fundamental mode Log (Q's) are:

$$b_{00} = -0.675 \quad b_{01} = 0.126 \quad X_1 = 20.60\% \quad i+j = 1$$

$$b_{10} = -0.230$$

$$b_{00} = -6.514 \quad b_{10} = 0.719 \quad X_1 = 14.71\% \quad i+j = 2$$

$$b_{01} = 1.806 \quad b_{11} = -1.256$$

$$b_{02} = 0.483 \quad b_{20} = 0.477$$

LINEAR NON-ADIABATIC RESULTS

Table 7.2, below gives the coefficients of fits to the non-adiabatic first overtone mode Log (periods) at constant luminosities.

L/L_0	a_0	a_1	a_2	M.R	$\text{Log}(T_{\text{eff}})$
1,000	16.739	-5.068	0.226	0.00437	3.954 - 4.301
3,000	132.623	-61.100	7.014	0.14904	3.954 - 4.477
6,000	5.067	0.786	-0.468	0.01090	3.903 - 4.477
10,000	16.739	-5.068	0.226	0.03904	3.875 - 4.477
15,000	43.656	-17.946	1.819	0.03290	3.845 - 4.477
20,000	30.200	-11.315	1.011	0.04615	3.854 - 4.477

TABLE 7.2 : Table of coefficients of first fit for first overtone mode.

The coefficients for the [2D] fit to the non-adiabatic first overtone mode Log (periods) are:

$$b_{00} = 8.923 \quad b_{01} = 0.798 \quad X_1 = 5.62\% \quad i+j = 1$$

$$b_{10} = -2.810$$

$$b_{00} = 36.156 \quad b_{10} = -17.089 \quad X_1 = 4.99\% \quad i+j = 2$$

$$b_{01} = 2.112 \quad b_{11} = -0.273$$

$$b_{02} = -0.032 \quad b_{20} = 1.842$$

The coefficients for the [2D] fit to the non-adiabatic first overtone mode Log (Q's) are:

$$b_{00} = -2.234 \quad b_{01} = 0.252 \quad X_1 = 17.35\% \quad i+j = 1$$

$$b_{10} = -0.061$$

$$b_{00} = 16.581 \quad b_{10} = -10.536 \quad X_1 = 13.21\% \quad i+j = 2$$

$$b_{01} = 1.673 \quad b_{11} = -0.821$$

$$b_{02} = 0.226 \quad b_{20} = 1.679$$

The results presented here will be discussed in Section 7.3.4 .

LINEAR NON-ADIABATIC RESULTS

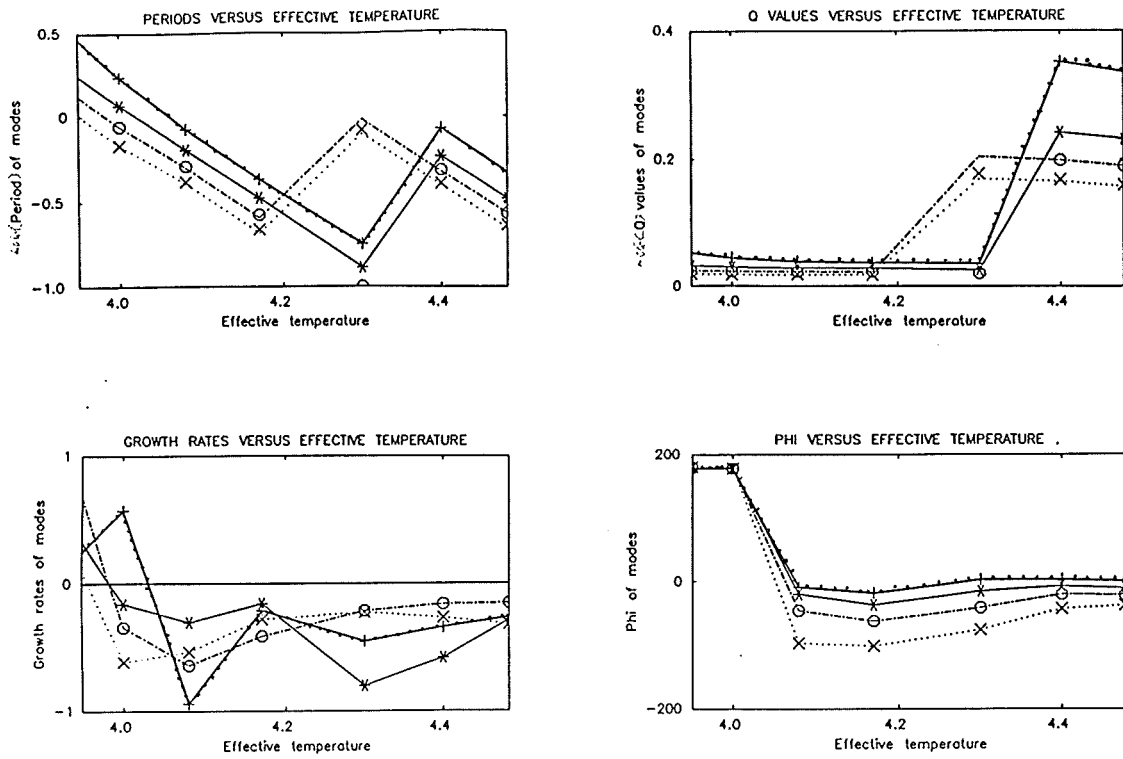


Figure 7.12 : Pulsation parameters for $L/L_{\odot} = 1,000$ and $M/M_{\odot} = 0.8$ (R040 opacity table).

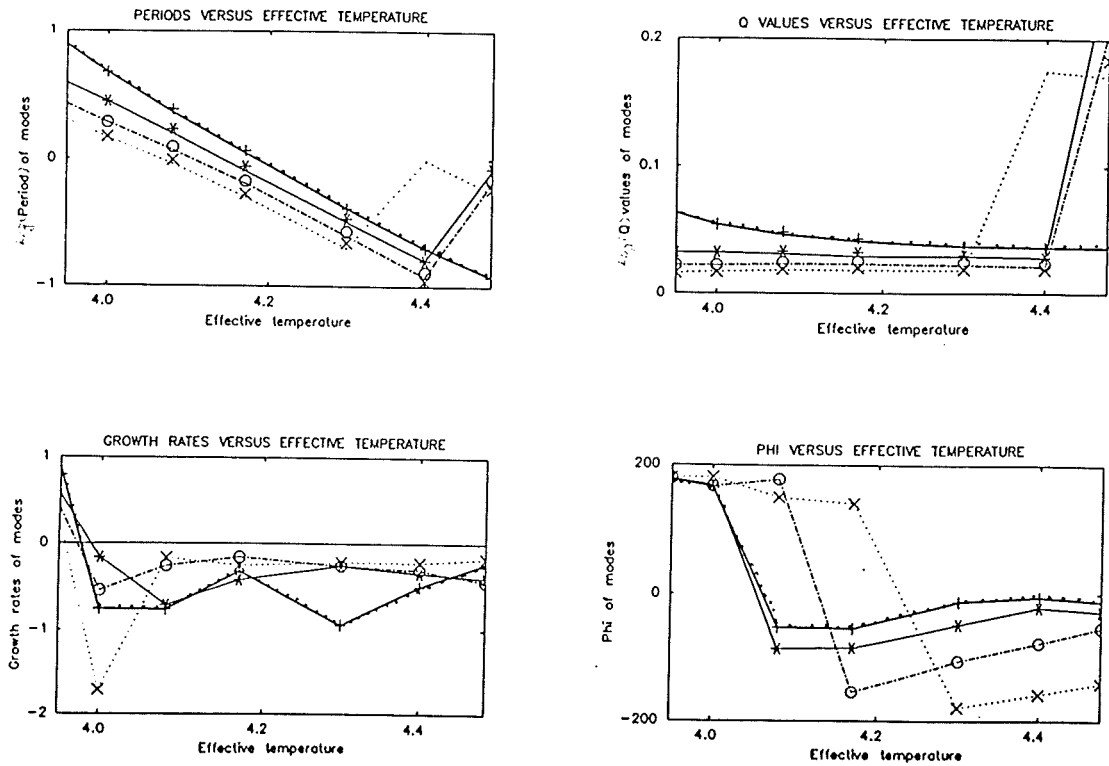


Figure 7.13 : Pulsation parameters for $L/L_{\odot} = 3,000$ and $M/M_{\odot} = 0.8$ (R040 opacity table).

LINEAR NON-ADIABATIC RESULTS

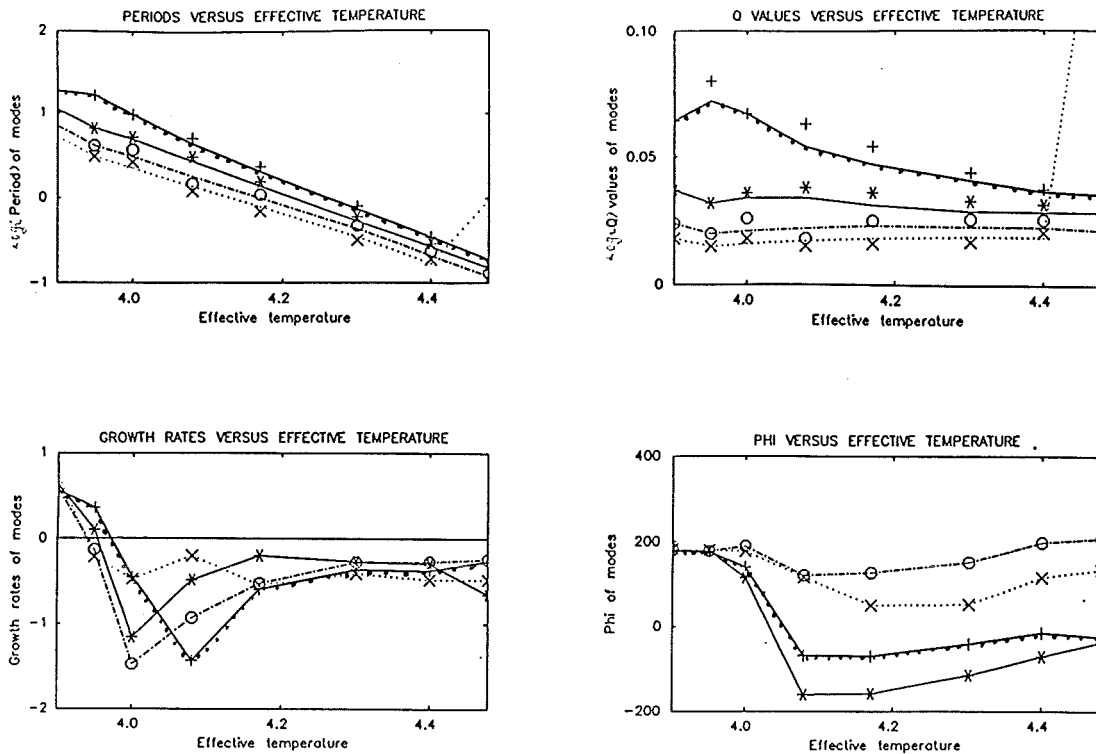


Figure 7.14 : Pulsation parameters for $L/L_{\odot} = 6,000$ and $M/M_{\odot} = 0.8$ (R040 opacity table).

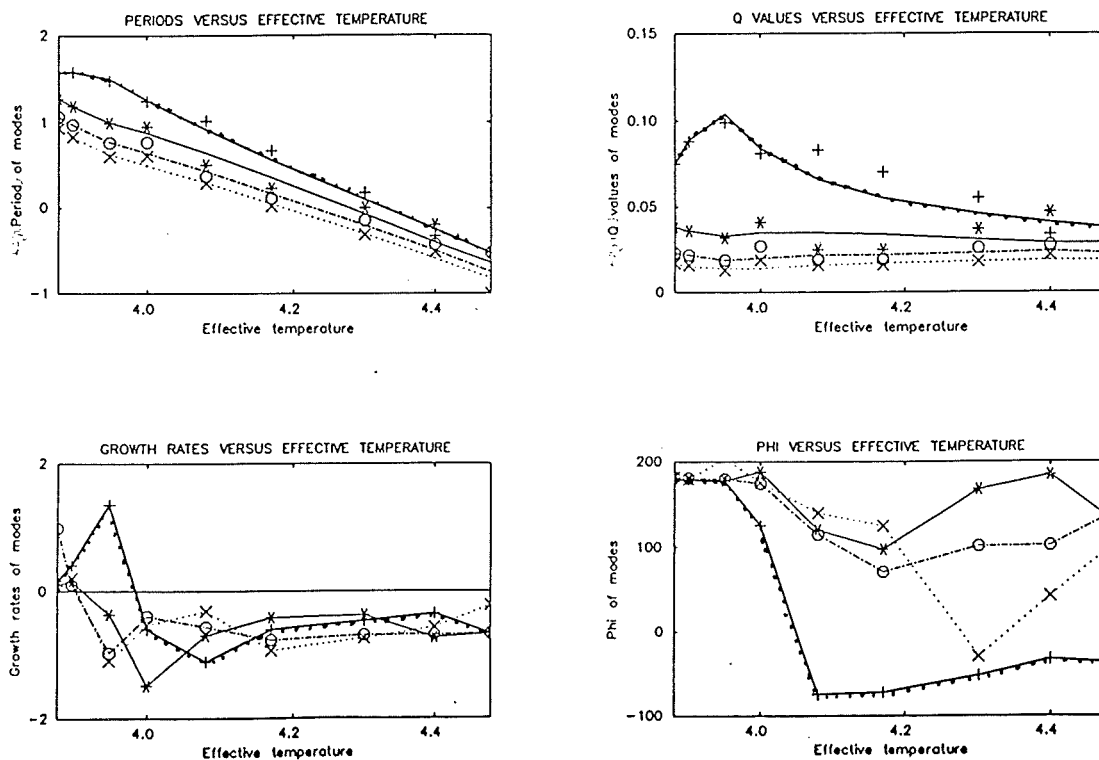


Figure 7.15 : Pulsation parameters for $L/L_{\odot} = 10,000$ and $M/M_{\odot} = 0.8$ (R040 opacity table).

LINEAR NON-ADIABATIC RESULTS

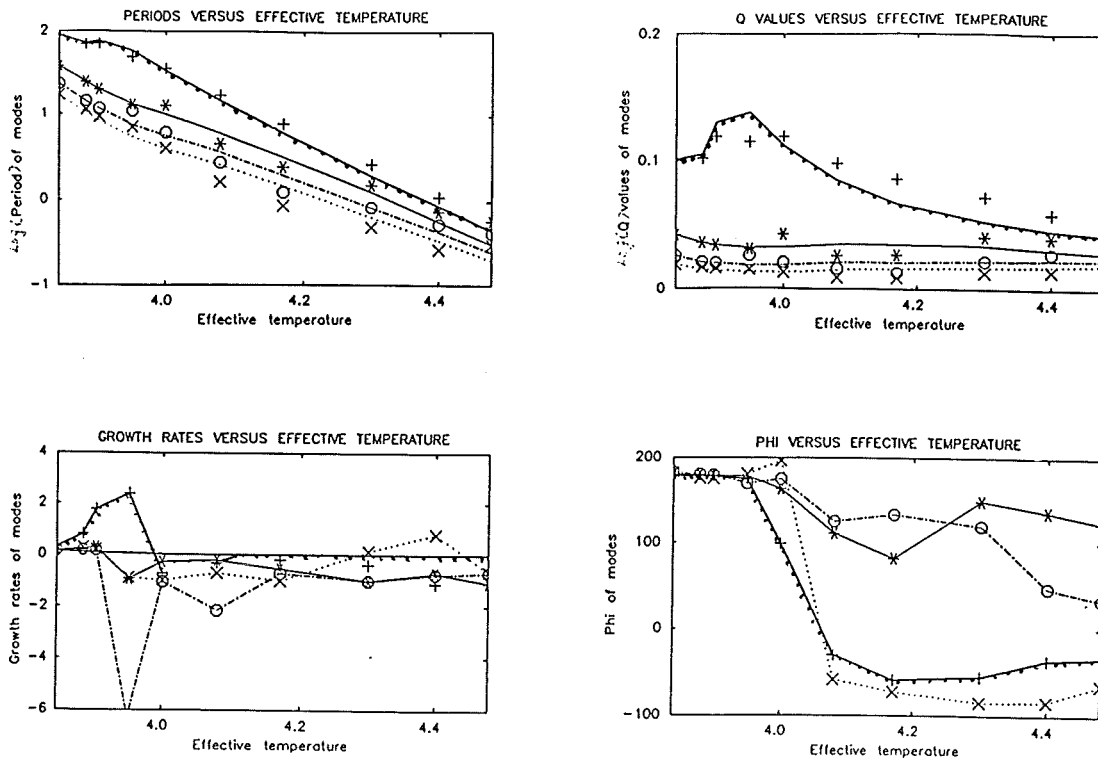


Figure 7.16 : Pulsation parameters for $L/L_{\odot} = 15,000$ and $M/M_{\odot} = 0.8$ (R040 opacity table).

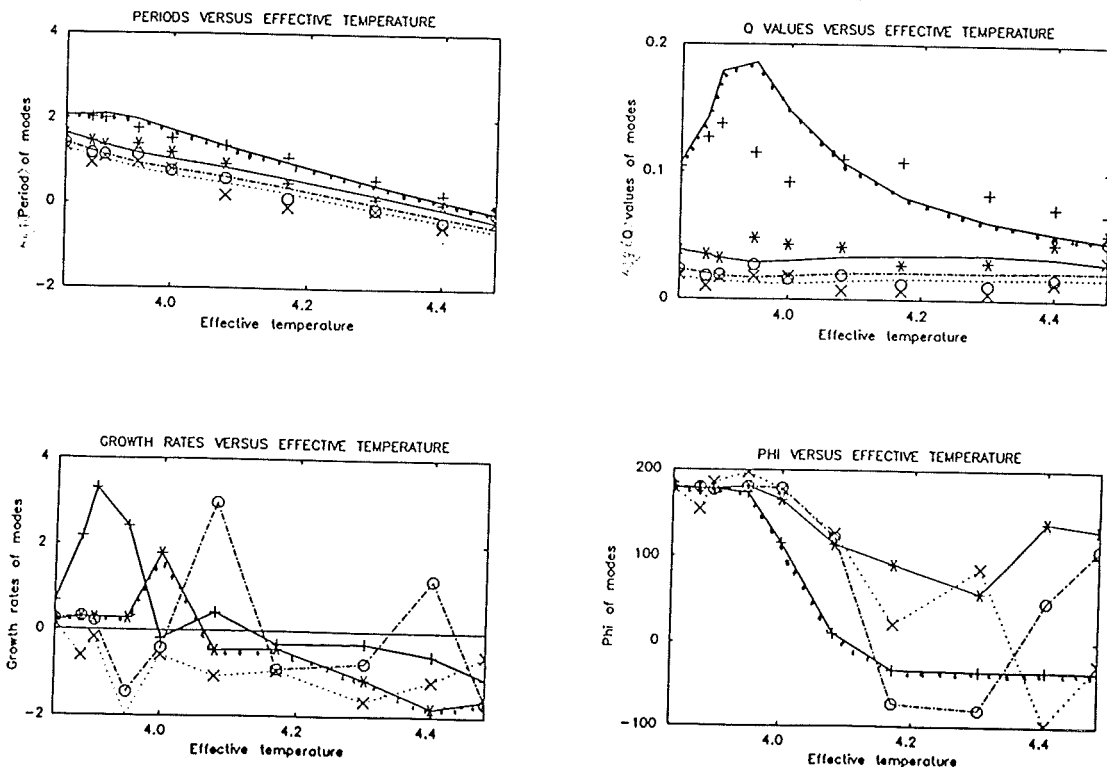


Figure 7.17 : Pulsation parameters for $L/L_{\odot} = 20,000$ and $M/M_{\odot} = 0.8$ (R040 opacity table).

LINEAR NON-ADIABATIC RESULTS

7.3.3.2 Survey Results for $1.0 M_{\odot}$ Models - Table 7.3, below gives the coefficients of fits to the non-adiabatic fundamental mode Log (periods) at constant luminosities.

L/L_{\odot}	a_0	a_1	a_2	M.R	$\text{Log}(T_{\text{eff}})$
1,000	25.360	-9.094	0.699	0.00000	4.000 - 4.301
3,000	165.580	-76.506	8.814	0.12007	3.954 - 4.477
6,000	20.562	-6.221	0.326	0.01494	3.903 - 4.477
10,000	7.193	0.328	-0.461	0.01696	3.875 - 4.477
15,000	2.710	2.634	-0.742	0.01548	3.875 - 4.477
20,000	21.518	-6.580	0.394	0.03357	3.845 - 4.477

TABLE 7.3 : Table of coefficients of first fit for fundamental mode.

The coefficients for the [2D] fit to the non-adiabatic fundamental mode Log (periods) are:

$$b_{00} = 10.388 \quad b_{01} = 1.066 \quad X_1 = 6.01\% \quad i+j = 1$$

$$b_{10} = -3.490$$

$$b_{00} = 20.163 \quad b_{10} = -10.020 \quad X_1 = 5.40\% \quad i+j = 2$$

$$b_{01} = 3.036 \quad b_{11} = -0.799$$

$$b_{02} = 0.166 \quad b_{20} = 1.188$$

The coefficients for the [2D] fit to the non-adiabatic fundamental mode Log (Q's) are:

$$b_{00} = -0.056 \quad b_{01} = 0.017 \quad X_1 = 21.86\% \quad i+j = 1$$

$$b_{10} = -0.288$$

$$b_{00} = -9.015 \quad b_{10} = 1.154 \quad X_1 = 14.16\% \quad i+j = 2$$

$$b_{01} = 2.679 \quad b_{11} = -1.448$$

$$b_{02} = 0.466 \quad b_{20} = 0.511$$

LINEAR NON-ADIABATIC RESULTS

Table 7.4, below gives the coefficients of fits to the non-adiabatic first overtone mode Log (periods) at constant luminosities.

L/L_{\odot}	a_0	a_1	a_2	M.R	$\text{Log}(T_{\text{eff}})$
1,000	14.636	-4.014	0.090	0.03357	4.000 - 4.301
3,000	139.104	-64.177	7.373	0.13641	3.954 - 4.477
6,000	11.776	-2.447	-0.083	0.01202	3.903 - 4.477
10,000	14.636	-4.014	0.090	0.01280	3.875 - 4.477
15,000	19.392	-6.046	0.360	0.03214	3.875 - 4.477
20,000	33.521	-12.982	1.216	0.03069	3.845 - 4.477

TABLE 7.4 : Table of coefficients of first fit for first overtone mode.

The coefficients for the [2D] fit to the non-adiabatic first overtone mode Log (periods) are:

$$b_{00} = 8.923 \quad b_{01} = 0.800 \quad X_1 = 5.64\% \quad i+j = 1$$

$$b_{10} = -2.890$$

$$b_{00} = 27.387 \quad b_{10} = -13.471 \quad X_1 = 5.13\% \quad i+j = 2$$

$$b_{01} = 2.112 \quad b_{11} = -0.273$$

$$b_{02} = -0.049 \quad b_{20} = 1.842$$

The coefficients for the [2D] fit to the non-adiabatic first overtone mode Log (Q's) are:

$$b_{00} = -1.517 \quad b_{01} = -0.108 \quad X_1 = 18.28\% \quad i+j = 1$$

$$b_{10} = 0.121$$

$$b_{00} = -0.570 \quad b_{10} = -2.641 \quad X_1 = 13.95\% \quad i+j = 2$$

$$b_{01} = 2.122 \quad b_{11} = -1.005$$

$$b_{02} = 0.271 \quad b_{20} = 0.805$$

The results presented here will be discussed in Section 7.3.4 .

LINEAR NON-ADIABATIC RESULTS

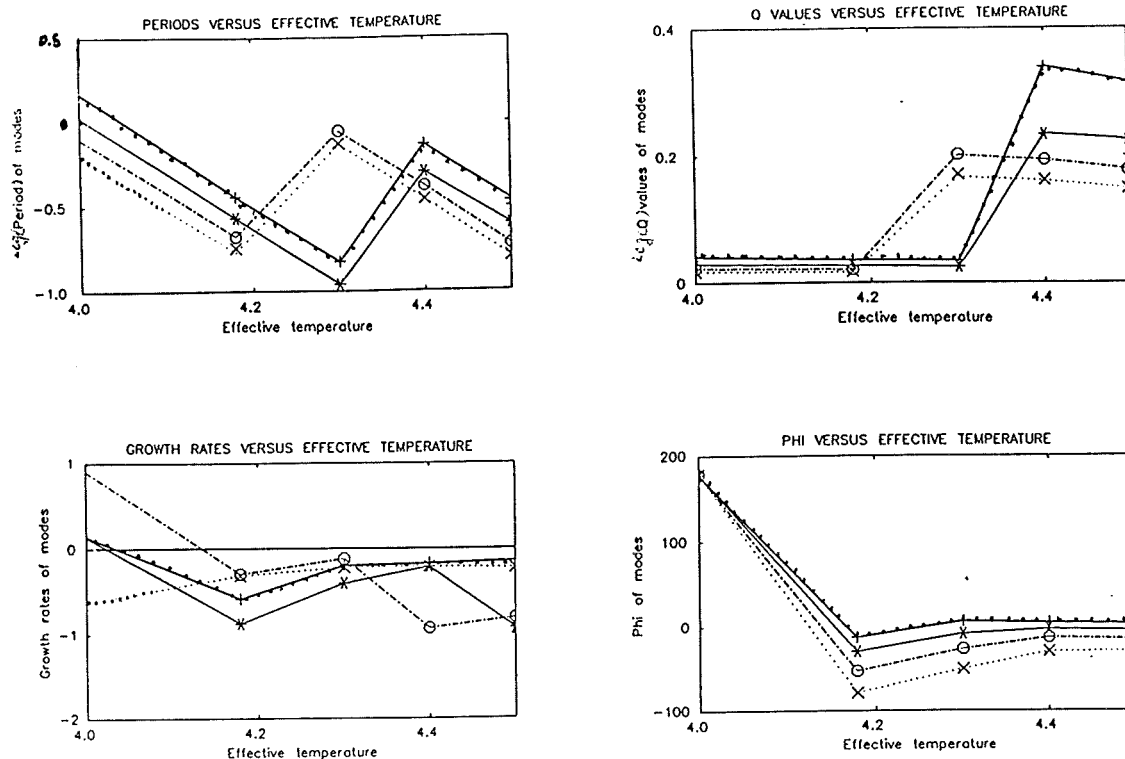


Figure 7.18 : Pulsation parameters for $L/L_0 = 1,000$ and $M/M_0 = 1.0$ (R040 opacity table).

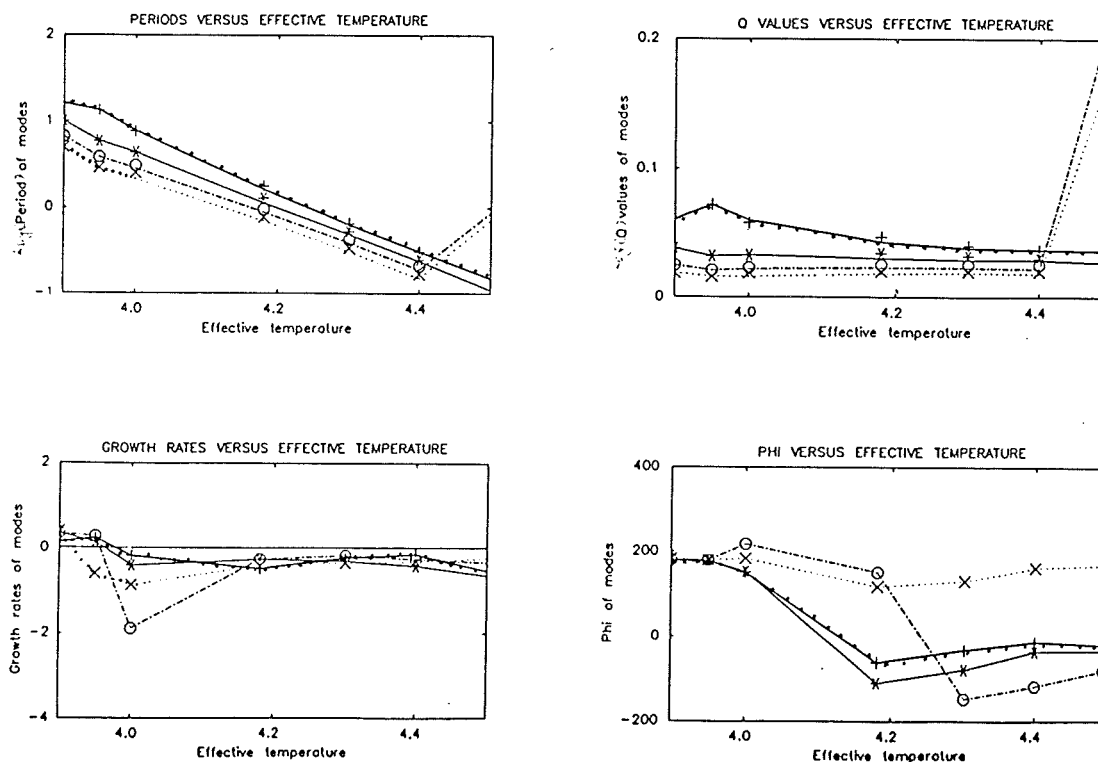


Figure 7.19 : Pulsation parameters for $L/L_0 = 3,000$ and $M/M_0 = 1.0$ (R040 opacity table).

LINEAR NON-ADIABATIC RESULTS

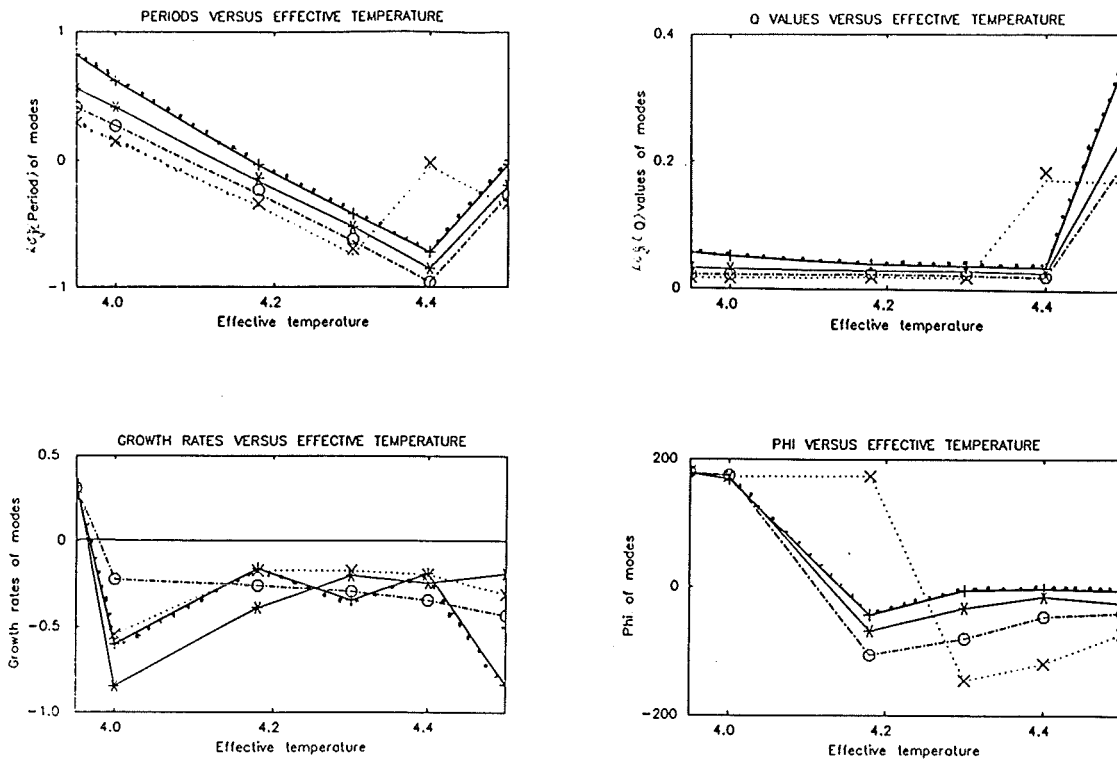


Figure 7.20 : Pulsation parameters for $L/L_{\odot} = 6,000$ and $M/M_{\odot} = 1.0$ (R040 opacity table).

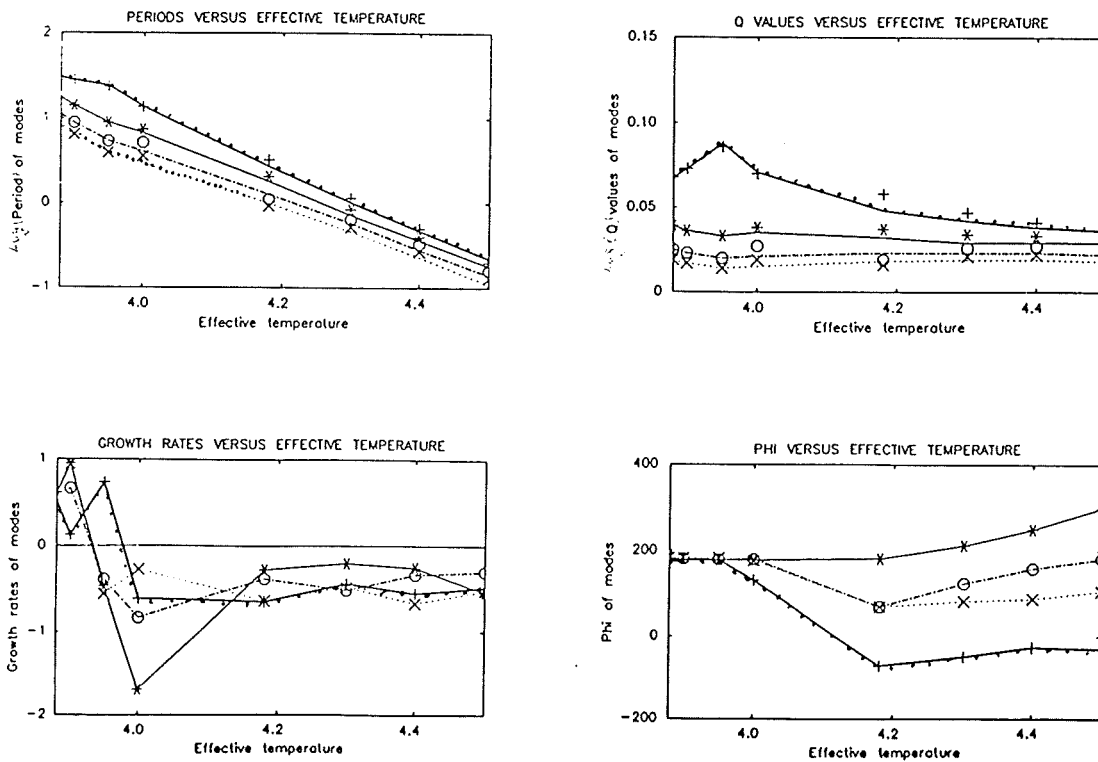


Figure 7.21 : Pulsation parameters for $L/L_{\odot} = 10,000$ and $M/M_{\odot} = 1.0$ (R040 opacity table).

LINEAR NON-ADIABATIC RESULTS

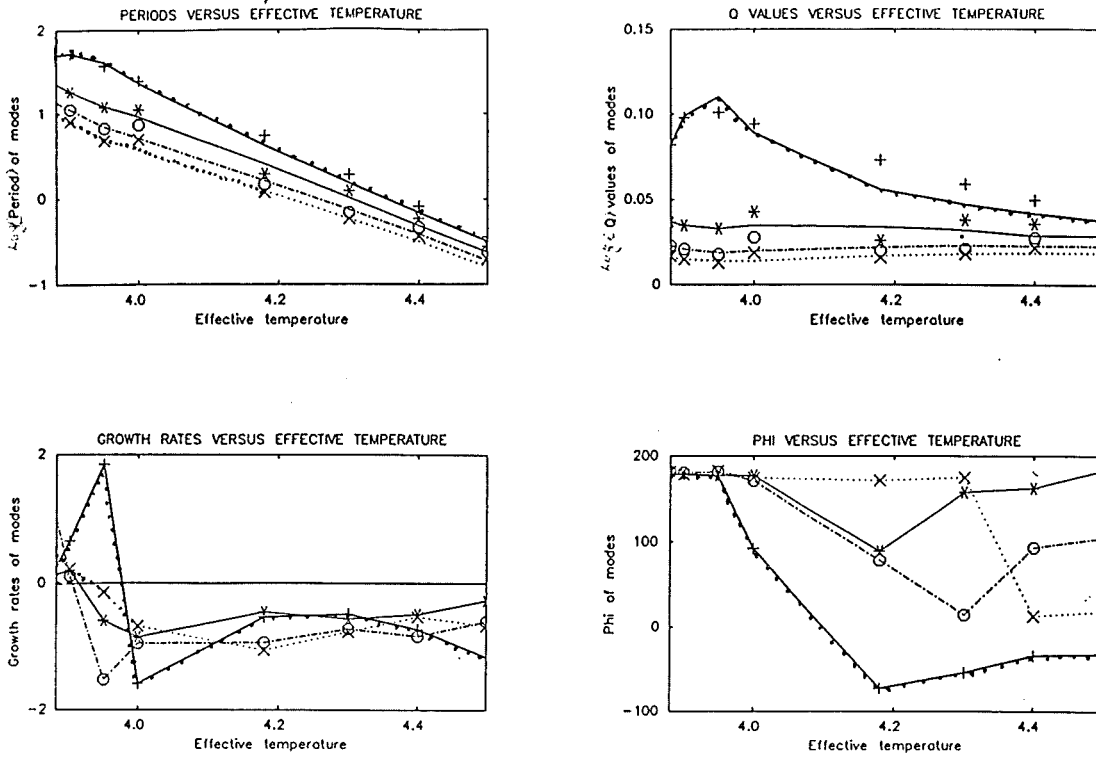


Figure 7.22 : Pulsation parameters for $L/L_{\odot} = 15,000$ and $M/M_{\odot} = 1.0$ (R040 opacity table).

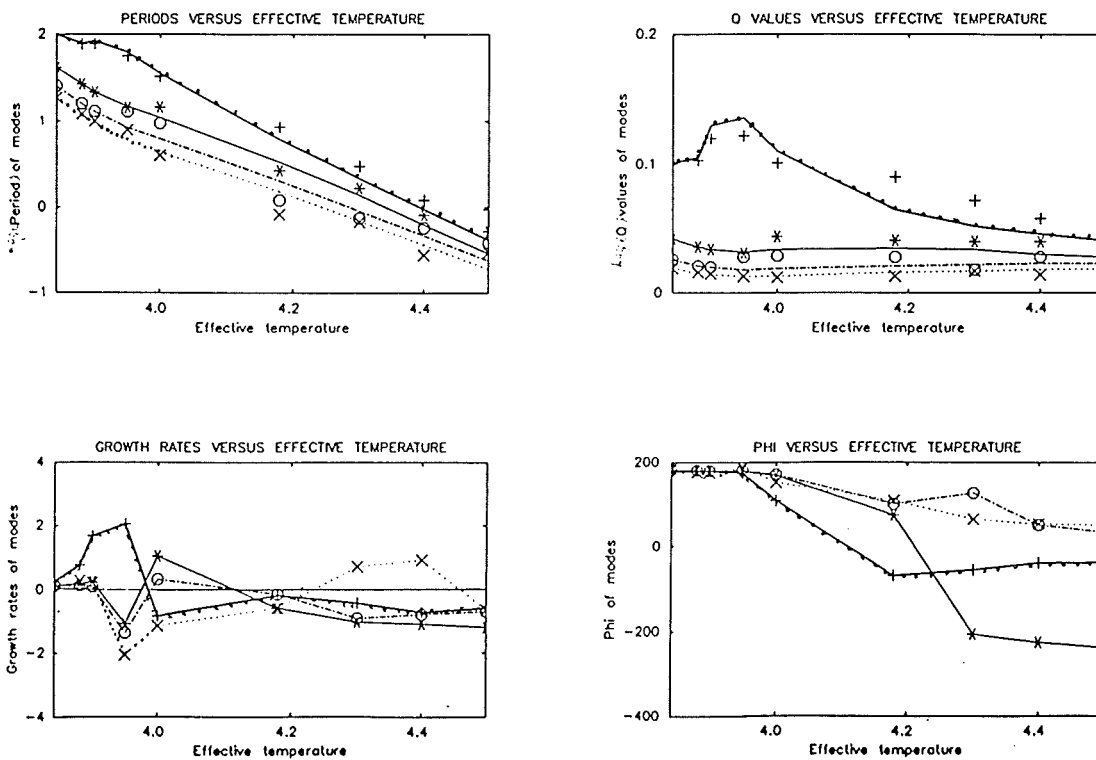


Figure 7.23 : Pulsation parameters for $L/L_{\odot} = 20,000$ and $M/M_{\odot} = 1.0$ (R040 opacity table).

LINEAR NON-ADIABATIC RESULTS

7.3.3.3 Survey Results for $1.2 M_{\odot}$ Models - Table 7.5, below gives the coefficients of fits to the non-adiabatic fundamental mode Log (periods) at constant luminosities.

L/L_{\odot}	a_0	a_1	a_2	M.R	$\text{Log}(T_{\text{eff}})$
1,000	128.825	-59.978	6.948	0.24469	4.000 - 4.477
3,000	35.438	-13.631	1.228	0.00317	3.954 - 4.398
6,000	36.057	-13.650	1.211	0.00725	3.954 - 4.398
10,000	16.082	-3.957	4.982	0.01556	3.903 - 4.477
15,000	4.906	1.519	-0.607	0.01648	3.875 - 4.477
20,000	1.673	3.191	-0.812	0.02105	3.875 - 4.477

TABLE 7.5 : Table of coefficients of first fit for fundamental mode.

The coefficients for the [2D] fit to the non-adiabatic fundamental mode Log (periods) are:

$$b_{00} = 11.222 \quad b_{01} = 0.718 \quad X_i = 8.31\% \quad i+j = 1$$

$$b_{10} = -3.292$$

$$b_{00} = 8.369 \quad b_{10} = -5.389 \quad X_i = 5.12\% \quad i+j = 2$$

$$b_{01} = 4.093 \quad b_{11} = -1.545$$

$$b_{02} = 0.427 \quad b_{20} = 0.982$$

The coefficients for the [2D] fit to the non-adiabatic fundamental mode Log (Q's) are:

$$b_{00} = -0.013 \quad b_{01} = -0.033 \quad X_i = 22.60\% \quad i+j = 1$$

$$b_{10} = -0.261$$

$$b_{00} = -2.553 \quad b_{10} = -2.566 \quad X_i = 13.97\% \quad i+j = 2$$

$$b_{01} = 3.371 \quad b_{11} = -1.546$$

$$b_{02} = 0.423 \quad b_{20} = 1.003$$

LINEAR NON-ADIABATIC RESULTS

Table 7.6, below gives the coefficients of fits to the non-adiabatic first overtone mode Log (periods) at constant luminosities.

L/L_{\odot}	a_0	a_1	a_2	M.R	$\text{Log}(T_{\text{eff}})$
1,000	-8.716	4.796	-0.662	0.41234	4.000 - 4.477
3,000	4.296	1.060	-0.510	0.00296	3.954 - 4.398
6,000	3.035	1.672	-0.571	0.00254	3.954 - 4.398
10,000	-8.716	4.796	-0.662	0.00918	3.903 - 4.477
15,000	6.406	0.206	-0.392	0.01328	3.875 - 4.477
20,000	16.757	-4.754	0.205	0.03254	3.875 - 4.477

TABLE 7.6 : Table of coefficients of first fit for first overtone mode.

The coefficients for the [2D] fit to the non-adiabatic first overtone mode Log (periods) are:

$$b_{00} = 10.053 \quad b_{01} = 0.504 \quad X_1 = 8.66\% \quad i+j = 1$$

$$b_{10} = -2.824$$

$$b_{00} = 11.445 \quad b_{10} = -0.787 \quad X_1 = 5.66\% \quad i+j = 2$$

$$b_{01} = 2.519 \quad b_{11} = -1.303$$

$$b_{02} = 0.474 \quad b_{20} = 0.369$$

The coefficients for the [2D] fit to the non-adiabatic first overtone mode Log (Q's) are:

$$b_{00} = -1.225 \quad b_{01} = -0.244 \quad X_1 = 20.83\% \quad i+j = 1$$

$$b_{10} = 0.181$$

$$b_{00} = -10.484 \quad b_{10} = 2.266 \quad X_1 = 13.59\% \quad i+j = 2$$

$$b_{01} = 1.903 \quad b_{11} = -1.491$$

$$b_{02} = 0.464 \quad b_{20} = 0.370$$

The results presented here will be discussed in Section 7.3.4 .

LINEAR NON-ADIABATIC RESULTS

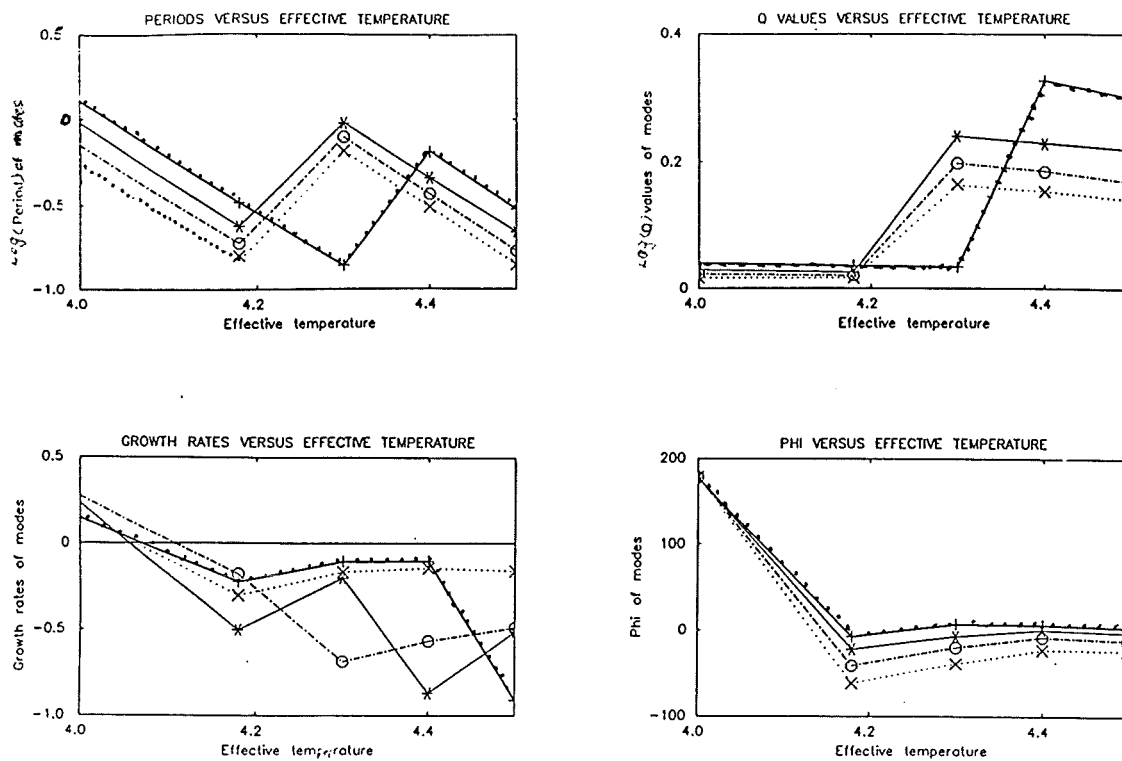


Figure 7.24 : Pulsation parameters for $L/L_0 = 1,000$ and $M/M_0 = 1.2$ (R040 opacity table).

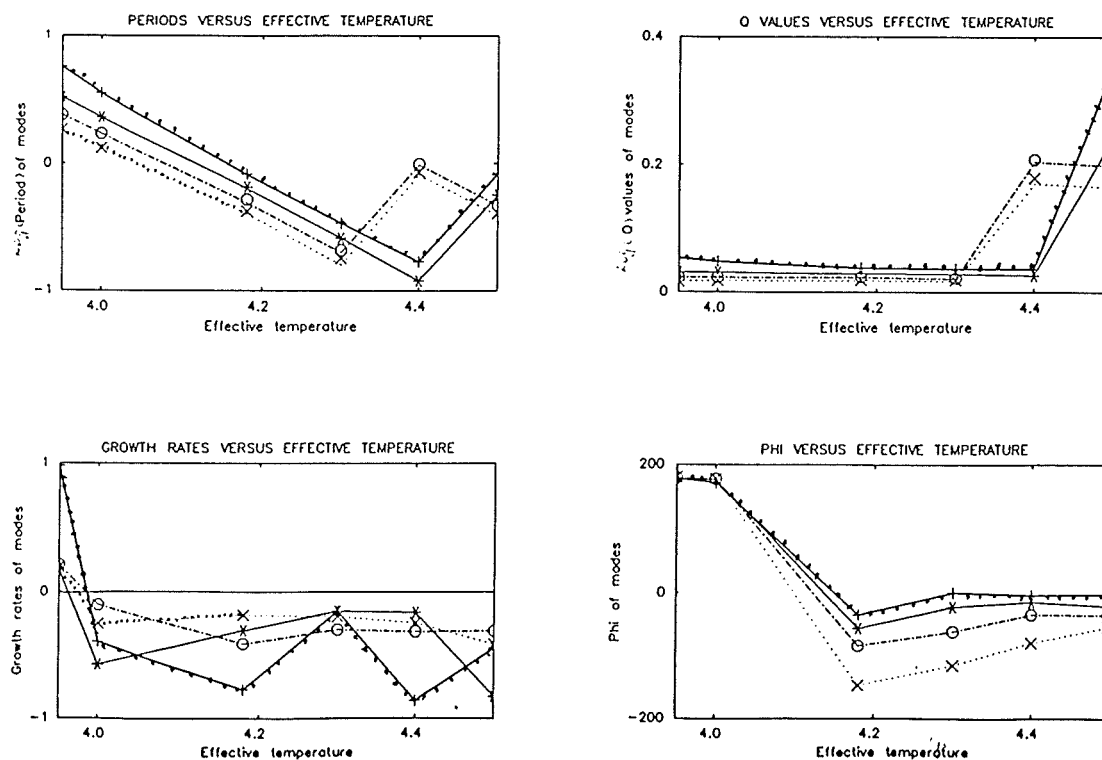


Figure 7.25 : Pulsation parameters for $L/L_0 = 3,000$ and $M/M_0 = 1.2$ (R040 opacity table).

LINEAR NON-ADIABATIC RESULTS

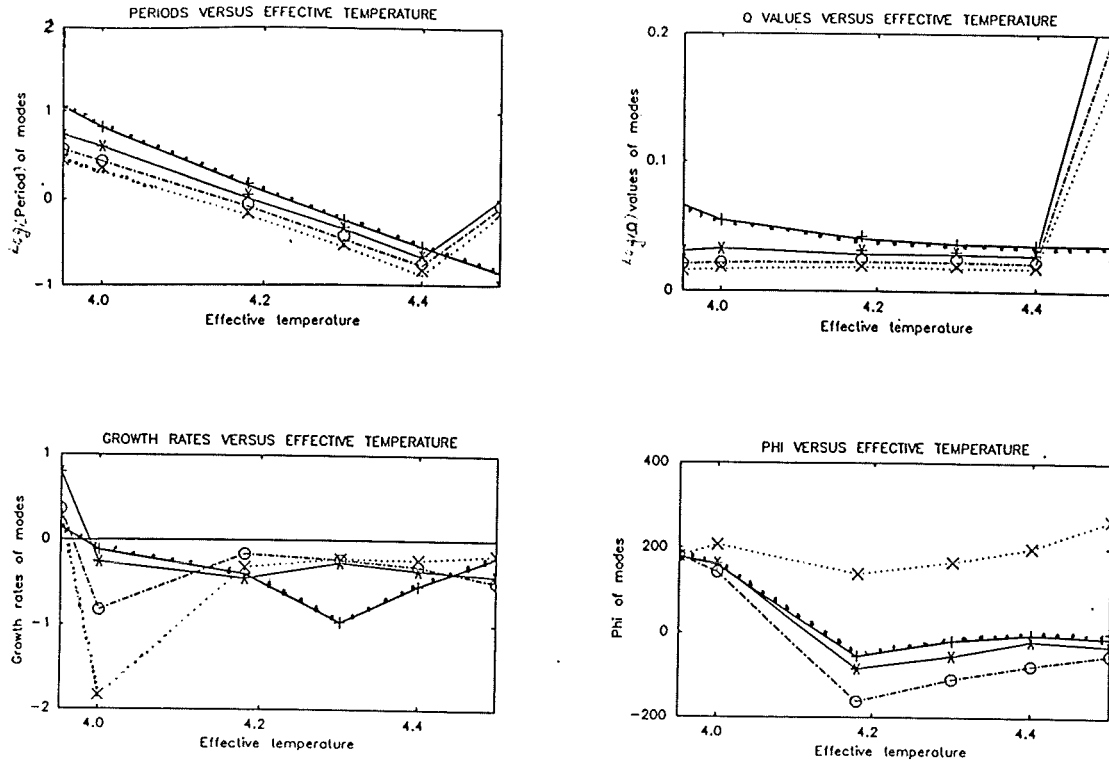


Figure 7.26 : Pulsation parameters for $L/L_{\odot} = 6,000$ and $M/M_{\odot} = 1.2$ (R040 opacity table).

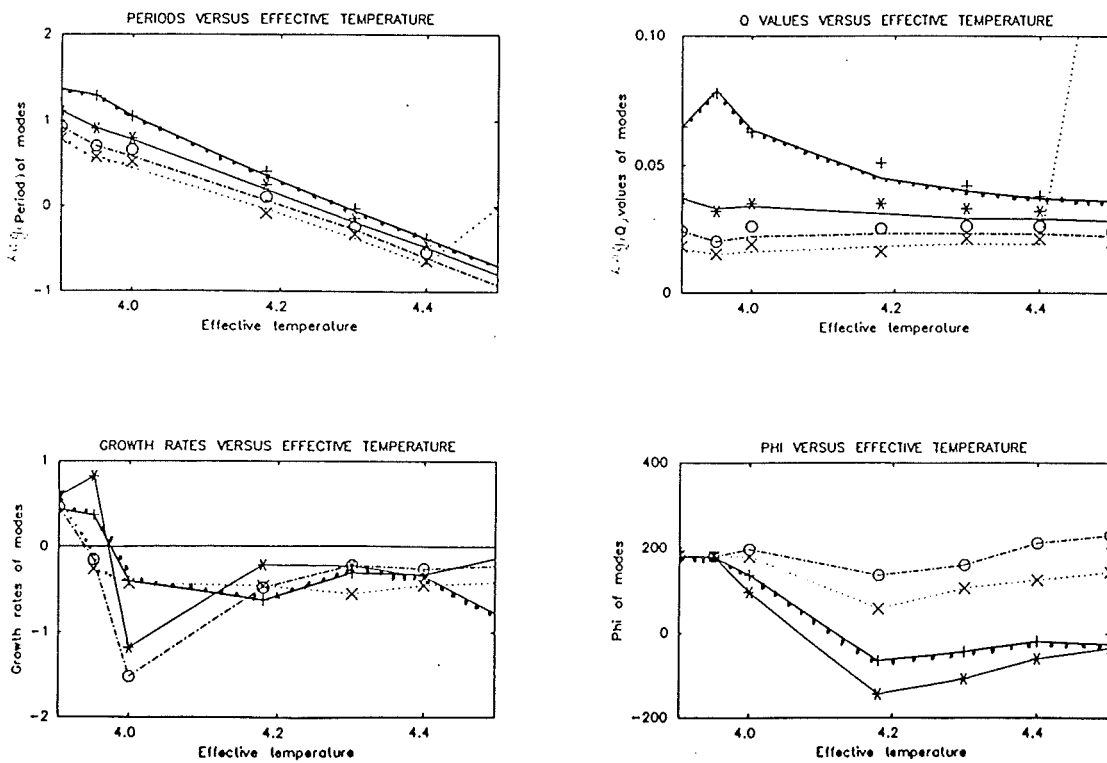


Figure 7.27 : Pulsation parameters for $L/L_{\odot} = 10,000$ and $M/M_{\odot} = 1.2$ (R040 opacity table).

LINEAR NON-ADIABATIC RESULTS

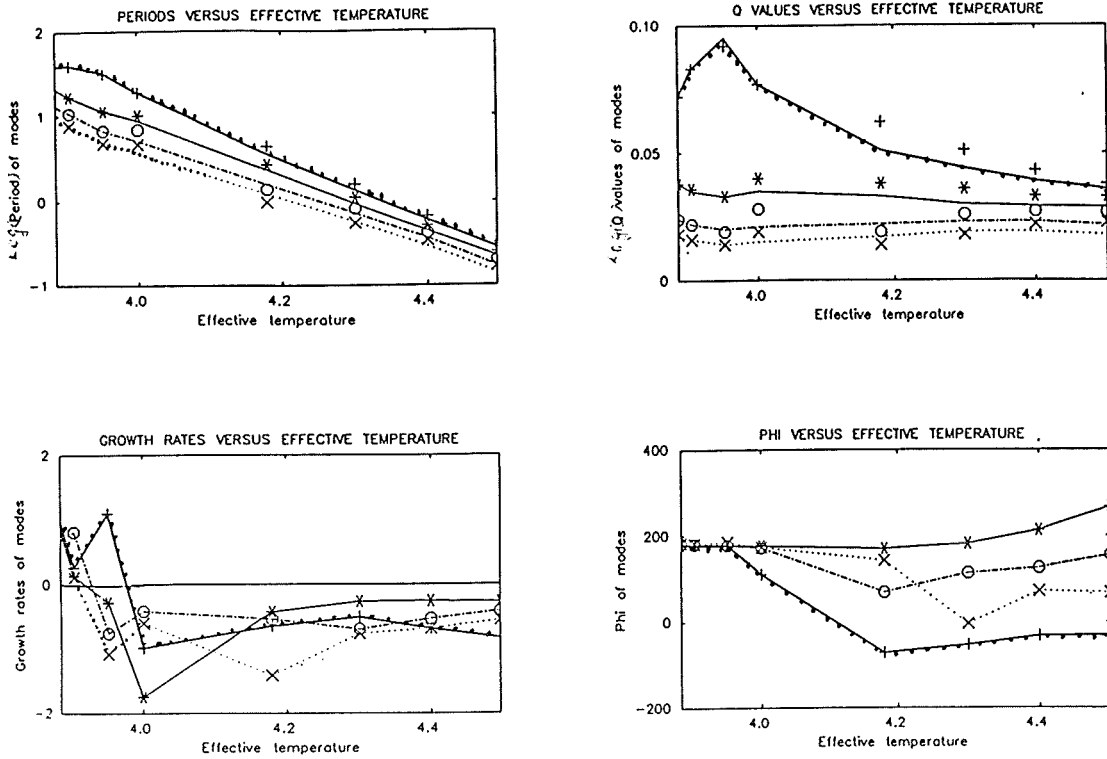


Figure 7.28 : Pulsation parameters for $L/L_{\odot} = 15,000$ and $M/M_{\odot} = 1.2$ (R040 opacity table).

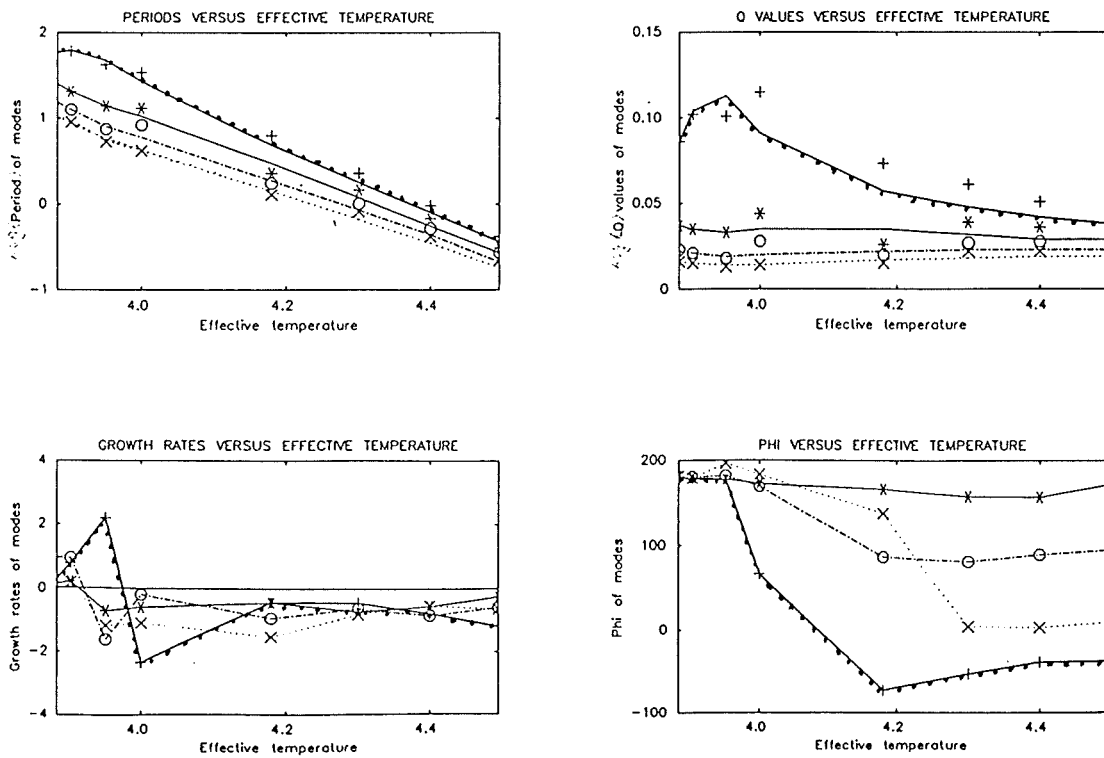


Figure 7.29 : Pulsation parameters for $L/L_{\odot} = 20,000$ and $M/M_{\odot} = 1.2$ (R040 opacity table).

7.3.4 A Discussion of the Survey Results

In Figures 7.12 - 7.29 we can see the pulsation parameters for the pure helium survey models. In these graphs it can be seen that all models that did not converge are excluded, leaving only the high effective temperature models. We first of all consider the upper two graphs of each quartet showing $\text{Log}(\text{Period})$ and $\text{Log}(Q)$ versus effective temperature. From these graphs it was clear that something was happening in the low luminosity high effective temperature models, i.e., there was an unexpected step. This did not appear to be connected with the mean envelope density which could cause such an effect or the non-adiabaticity of models as both adiabatic and non-adiabatic periods show the same step. The only other things that could have affected the period are the pressure and γ , of which the latter is the more likely cause. No time was available to check this conclusion; hence no firm cause can be given.

In the results sections, [2D] fits using first and second order polynomials were made to all $\text{Log}(\text{Period})$ and $\text{Log}(Q)$ data in given $\text{Log}(T_{\text{eff}})$ ranges, at each mass. From this we see that a better fit can be made to the period data: for periods only, a [1D] second order polynomial was fitted to the data of each mass and luminosity sequence. Below are given the fits to fundamental periods at each mass (this mode was chosen as it is the mode that RCB stars are thought to pulsate in) :

$$\begin{array}{ll}
 P_0 = 9.1 \times 10^{10} (T_{\text{eff}})^{-3.49} (L/L_0)^{1.066} & (3\%) \quad M/M_0 = 0.8 \\
 P_0 = 2.4 \times 10^{10} (T_{\text{eff}})^{-3.49} (L/L_0)^{1.066} & (6\%) \quad M/M_0 = 1.0 \\
 P_0 = 1.7 \times 10^{11} (T_{\text{eff}})^{-3.29} (L/L_0)^{0.718} & (8\%) \quad M/M_0 = 1.2
 \end{array}$$

LINEAR NON-ADIABATIC RESULTS

From the above we see that as the mass increases, the dependence upon T_{eff} and L/L_0 decreases, as is to be expected, due to the decrease in the non-adiabaticity of models. As there are so few mass points it was decided not to try and fit a [3D] polynomial to the whole of the data, as the fit would be dubious and not very accurate. Finally, it can be seen that at the lower effective temperature end of the higher luminosity graphs the periods 'turn-over' with decreasing T_{eff} and start diminishing. This is due to the increased efficiency of convection in the lower temperature models, which causes a slight decrease in mean density and hence period.

We then consider briefly the lower two graphs of the quartets, which show growth rates and phase change of $\Phi(\delta R/R)$ between inner and outer boundaries of envelope. The phase graphs are quite useful in locating the instability edges, as the phase either changes down or up when the growth rate drops or increases sharply. This is mainly due to large increases/decreases in 'damming' of radiation and hence 'driving'. These phase graphs are also a useful indication as to whether you have found the right modes or not, as they are reasonably continuous at lower luminosities. The growth rate graphs are only really used to find the instability region, as there are not enough points to map these complex curves properly. From fits to the fundamental and first overtone growth rates at each mass, the blue edges have been found and are displayed in Figure 7.30. These edges are blue-wards of the usual Cepheid edges, due to the reduction in available electrons and hence decrease in 'damping'. This may help to explain why some extreme helium stars with effective temperatures around 8,000 K pulsate (see Morrison & Willingale, 1987) where normally you would expect stability. The 'dog-leg' discussed in Saio & Wheeler (1985) is evident at the lower masses in both modes shown,

LINEAR NON-ADIABATIC RESULTS

but vanishes as the model mass is increased. The reason for this is not obvious, but may have something to do with the increase in non-adiabaticity as the L/M ratio increases which results in less 'driving' than would otherwise be the case. The values of $\text{Log}(T_{\text{eff}})$ along the blue edges are given in Appendix F.1. It is seen that in the case of these pure helium models the first overtone and fundamental mode are unstable in the same region of the HR diagram. Hence when both modes have similar growth rates bi-periodicity could occur. Generally one would expect the fundamental mode to be the dominant pulsating mode as it has the larger growth rate for any given effective temperature in the instability region.

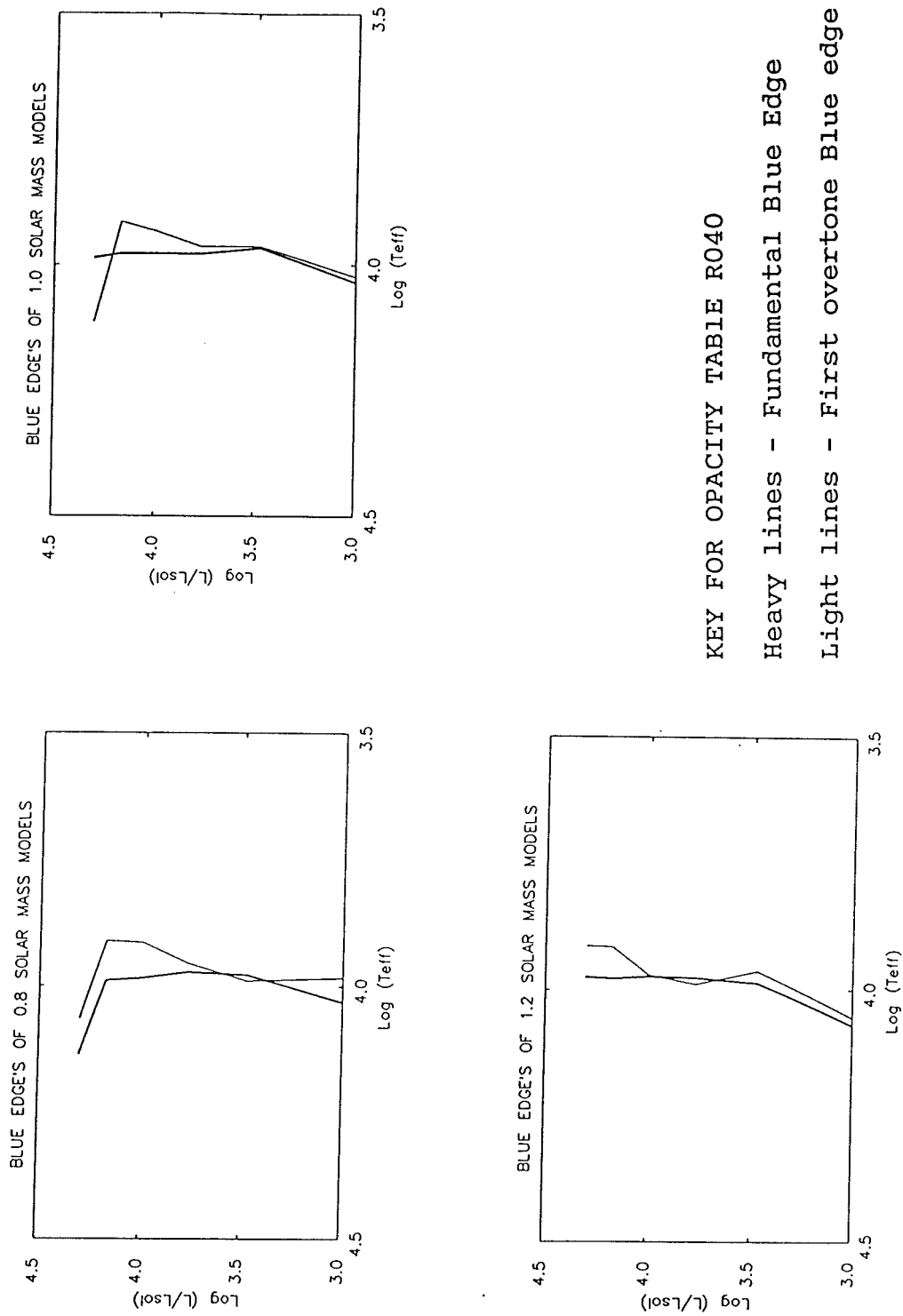


Figure 7.30 : This figure shows the position of the blue edges of pure Helium opacity table survey, on HR diagrams. The heavy solid lines represent the Fundamental blue edges and the light solid lines the first overtone blue edges.

7.4 RESULTS OF THE SURVEY USING OPACITY TABLE DXIX

In the following sub-Sections, the results for the hydrogenic opacity table DXIX of Cox & Tabor (1976), will be presented and compared with the results found in the pure helium survey of Section 7.3. The main purpose of this survey is given in Section 7.2 together with the reasons as to why these particular models were chosen. As no 'strange' modes were found in the models created for the pure helium survey, in Section 7.3, it was decided to see if any could be found amongst the models in this survey.

7.4.1 A Detailed Discussion of One Model

The model chosen for this detailed description has the same mass and luminosity as that used in Section 7.3.1 for the pure helium description. However, in this case, an effective temperature of 7,000 K has been chosen, as this is the value the two best known RCB stars are thought to have, i.e., RY Sgr and R Cr B. This change of effective temperature has no major effect upon the shape of the perturbation curves and work diagrams in Figures 7.31 - 7.33, and can still be compared with that of the pure helium description in 7.3.1.

The first thing to notice in Figure 7.31, is that $|\delta R/R|$ no longer extends all the way down to the inner boundary (R.H.S. of graphs), and, with the exception of the first overtone, the nodes of higher overtones are no longer well defined. Also, that $|\delta R/R|$ in the higher modes has a lot more structure than in the pure helium case. It can be seen, from Figure 7.31, that $|\delta/L|$ also has structure in the same mass regions, which is due to the ionisation of the carbon atoms. The changes in $\Phi(\delta R/R)$ are not well defined; the step-wise change seen in the pure helium model being smoothed out. In the

LINEAR NON-ADIABATIC RESULTS

higher non-pulsating modes, $\Phi(\delta R/R)$ increases by Π towards the inner envelope boundary, while in the low pulsating modes, it does not. Even though the nodes of $|\delta R/R|$ are not well defined we see by comparing the adiabatic period with the non-adiabatic periods (Appendix E, DXIX results Section), that the model's envelope is again quite close to adiabaticity.

From Figure 7.31 we see that the drop in $|\delta L/L|$ (as we go inwards) seen in the pure helium case is still present, and coincident with the peak in $|\delta T/T|$ although now it is less steep and contains a lot of structure due to the ionisation of carbon. The peak in $|\delta T/T|$ is smaller and broader, as the first few ionisation states of carbon have raised the opacity below the 15,000 K edge, above that seen in the pure helium opacity (see Figures 4.3 and 4.9). The peak in $|\delta L/L|$ at mode 0 can be seen to break up into 3 peaks as we go to higher overtones. These peaks are due to the effects of $C^{++}-C^{+++}$, He^+-He^{++} and $C^{+++}-C^{IV}$ ionisation as the envelope temperature increases.

The change in phase $\Phi(\delta L/L)$ is still an integral multiple of Π in the ionisation region. In Figure 7.32, it can be seen, however, that for the unstable low modes, the phase does not return to its inner value, but remains at the ionisation value. This could mean that $|\delta L/L|$ is 'frozen in' or, more likely, that it is being 'dammed' all the way up to the outer boundary. This view is supported by the drop in $\Phi(\delta T/T)$ seen in the lower modes as we approach the outer boundary.

Finally, Figure 7.33 shows the work integral and work function with mass of the model envelope. From these diagrams, the effects that the introduction of carbon has had on the model envelope can clearly be seen, namely, the elimination of efficient convection seen in the pure

LINEAR NON-ADIABATIC RESULTS

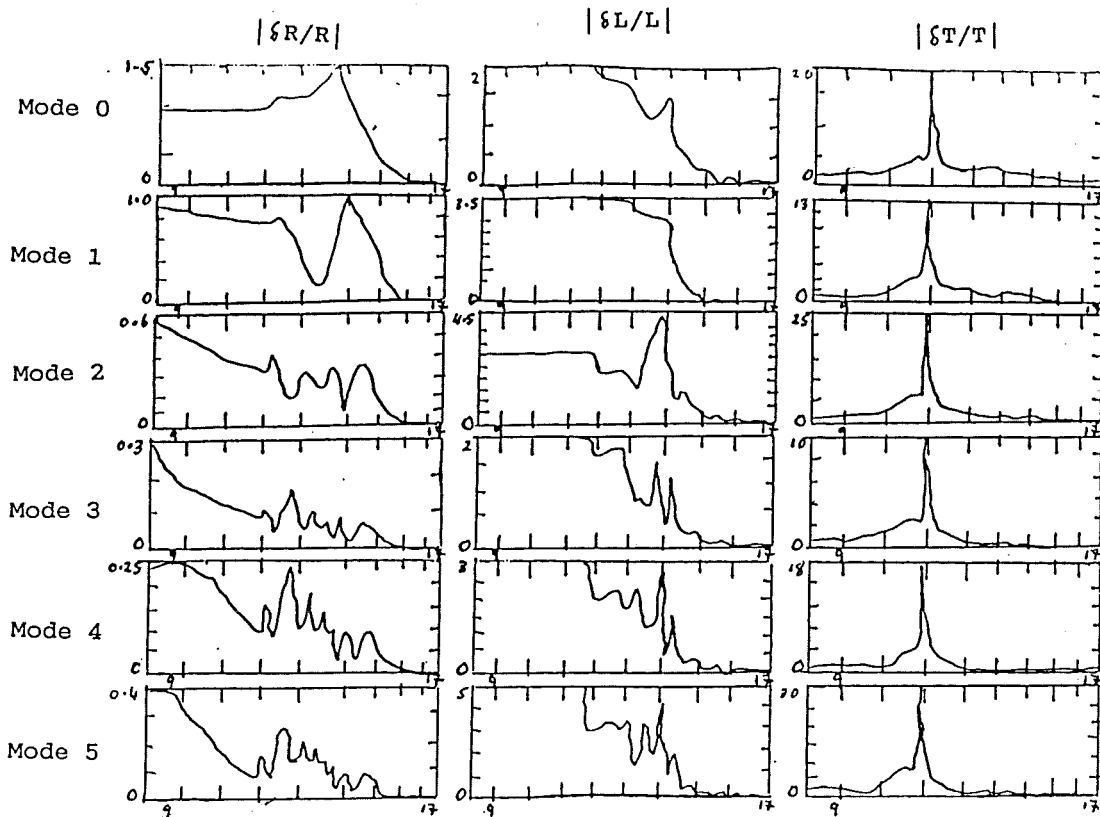


Figure 7.31 : This figure shows $|\delta R/R|$, $|\delta L/L|$ and $|\delta T/T|$ versus $\log(M-m) - 24$ for the first 6 eigenmodes of the $1M_{\odot}$ DXIX model with $L/L_{\odot} = 10,000$ and $T_{\text{eff}} = 7,000$ K.

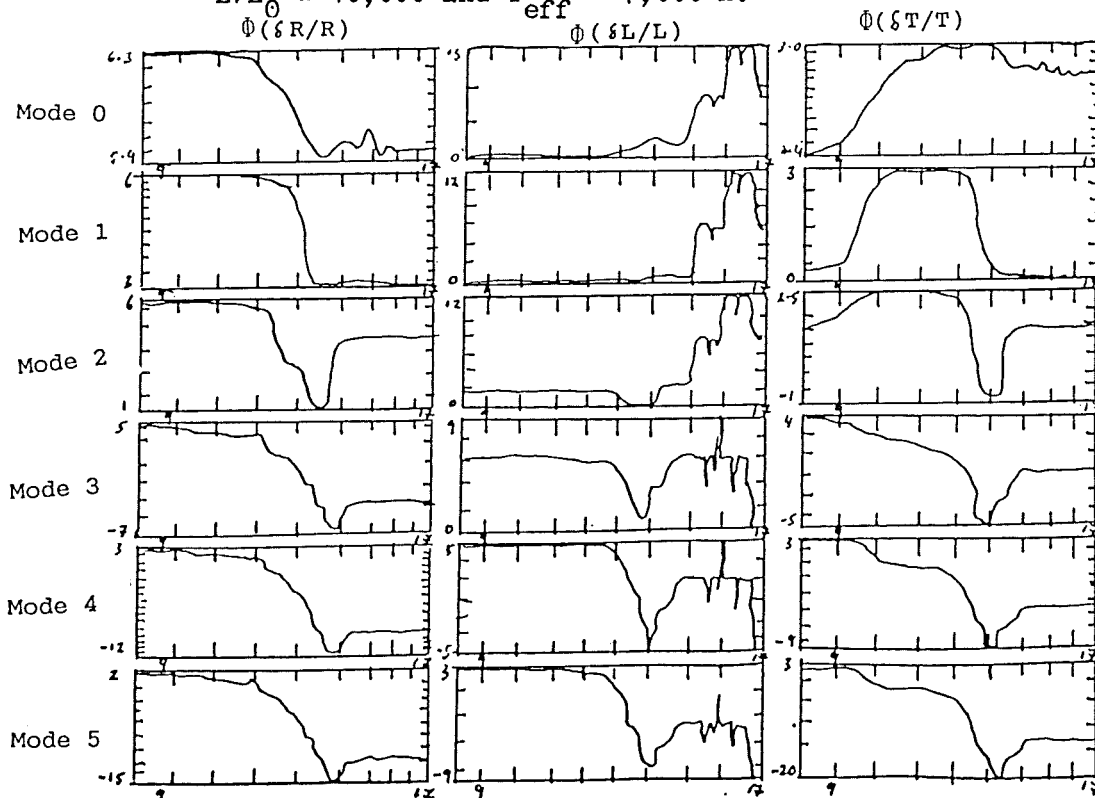


Figure 7.32 : This figure shows $\Phi(\delta R/R)$, $\Phi(\delta L/L)$ and $\Phi(\delta T/T)$ versus $\log(M-m) - 24$ for the first 6 eigenmodes of the $1M_{\odot}$ DXIX model with $L/L_{\odot} = 10,000$ and $T_{\text{eff}} = 7,000$ K.

LINEAR NON-ADIABATIC RESULTS

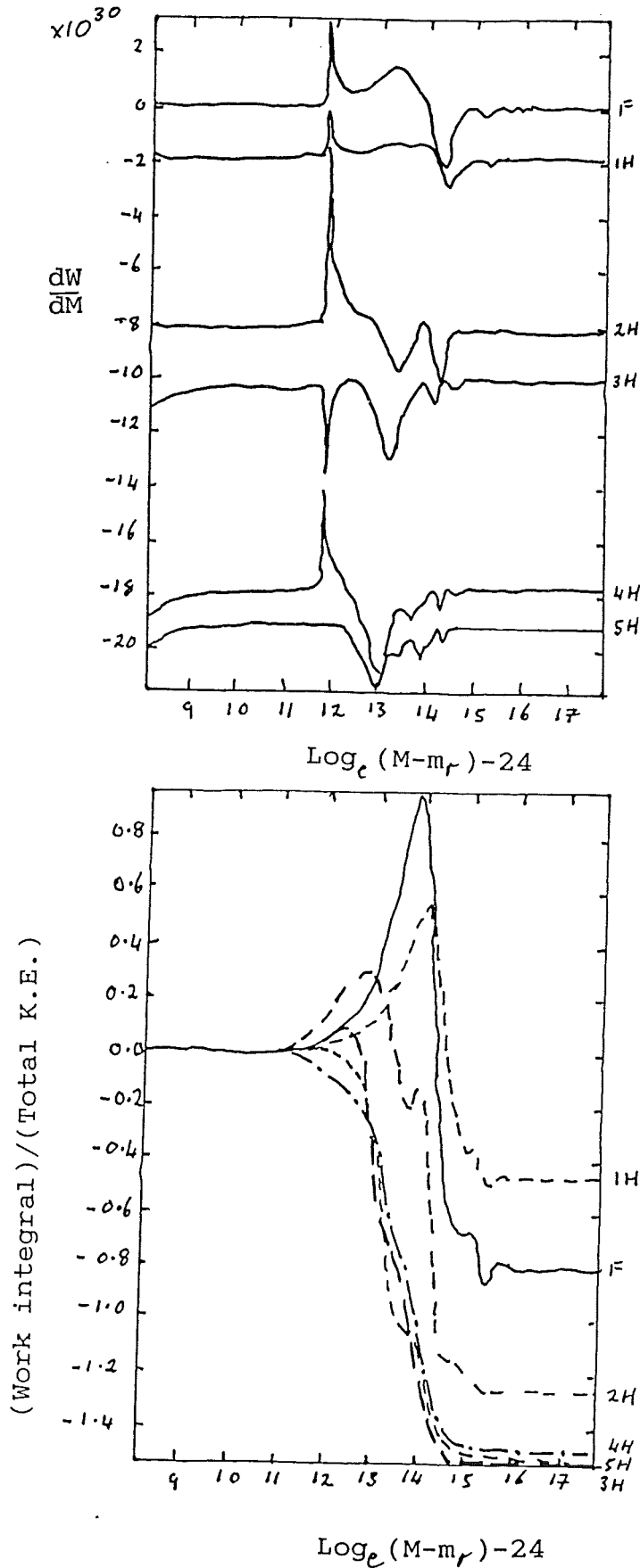


Figure 7.33 : This figure shows the work function and work integral versus $\log(M-m_r) - 24$ for the first 6 eigen modes of the $1M_{\odot}$ DXIX model with $L/L_{\odot} = 10,000$ and $T_{\text{eff}} = 7,000$ K.

helium model, which resulted in the loss of the $\text{He}^+ - \text{He}^{++}$ 'damping', and the increase of the 'driving' in the fundamental and first overtone modes.

7.4.2 Fundamental Eigenfunctions of the $1 M_{\odot}$ Models

In Figures 7.34 - 7.35 it can again be seen that there is a definite change in $|\delta T/T|$ between those models with effective temperatures below and above 15,000 K. Again this is due to the steep drop in opacity at 15,000 K (see Figure 4.9) caused by the $\text{He} - \text{He}^+$ ionisation region. The gradient of this drop is now far less than it is in the pure helium opacity due to the presence of $\text{C} - \text{C}^+$ and $\text{C}^+ - \text{C}^{++}$ ionisation regions below this drop. The reduction in the opacity gradient of this drop has caused the marked decrease in the size and the broadening of the peaks in $|\delta T/T|$ below $T_{\text{eff}} = 15,000$ K. In these models $|\delta T/T|$ is also significant throughout the majority of their envelopes, in contrast to what was found in the the pure helium model survey. This is entirely due to the various degrees of ionisation in the carbon atoms. Above $T_{\text{eff}} = 10,000$ K the $|\delta T/T|$ peaks are similar to those of the equivalent pure helium models with the exception that $\text{C}^{++} - \text{C}^{+++}$ ionisation has filled in the valley between the helium ionisation peaks, visible in pure helium models (see Figures 7.6 - 7.7).

In Figures 7.36 - 7.37, for models below $T_{\text{eff}} = 9,000$ K, the beginnings of the drop in $|\delta L/L|$, which was so pronounced in the pure helium models, can be seen. In the model with $(T_{\text{eff}}, L/L_{\odot}) = (5,000 \text{ K}, 1,000)$ two bumps can be seen in $|\delta L/L|$, due to $\text{C}^{++} - \text{C}^{+++}$ and $\text{He}^+ - \text{He}^{++}$ ionisation regions (as we go into the model envelope from left to right) which, as the effective temperature or luminosity increases, 'merge' with the 'frozen in' part of $|\delta L/L|$. At the luminosities below $L/L_{\odot} = 15,000$ it is this 'merging' that is the apparent cause of the hotter models being stable, i.e., the loss of 'driving' from the helium ionisation zones. This means that the He^{++} damping is large

LINEAR NON-ADIABATIC RESULTS

enough to stabilise the hotter models. The reason for the movement of the stability edge of the $L/L_{\odot} = 20,000$ is not obvious from these models but could possibly be due to the increase in the size of the helium ionisation opacity bumps as we go to lower densities. (See Figure 4.9 .) The other bumps seen in high luminosity and high effective temperature models are due to the higher levels of ionisation of the carbon atoms.

Figures 7.38 - 7.39 give $|\delta R/R|$ for this set of models, which have been included for completeness. The missing graphs are those for which the linear codes did not find a fundamental mode. This was due to the linear codes converging to a higher overtone mode or a secular mode instead. As can be seen from the graphs this only occurred in the high luminosity limit where the model envelopes have become very non-adiabatic. In the Figures presented here, the eigenfunctions of model $(T_{\text{eff}}, L/L_{\odot}) = (5,500 \text{ K}, 15,000)$ have been drawn in the wrong place and those of model $(T_{\text{eff}}, L/L_{\odot}) = (15,000 \text{ K}, 20,000)$ have been mis-identified as belonging to the fundamental mode.

To summarise: the major features found above are that the models increase in non-adiabaticity with effective temperature and luminosity; this is enhanced over that seen in the pure helium case, due to the increase in opacity caused by the introduction of carbon, and the subsequent drop in envelope densities. This drop in density appears to be the cause of the dramatic shift in the blue edge of the instability strip, seen for these models. The models of this survey did not suffer from convection, as did those in the previous pure helium survey. This may be due to the decrease in density of the inner envelope coupled with the lowering of the temperature gradients in this region due to the increase in 'damping' produced by the highly ionised carbon ions.

LINEAR NON-ADIABATIC RESULTS

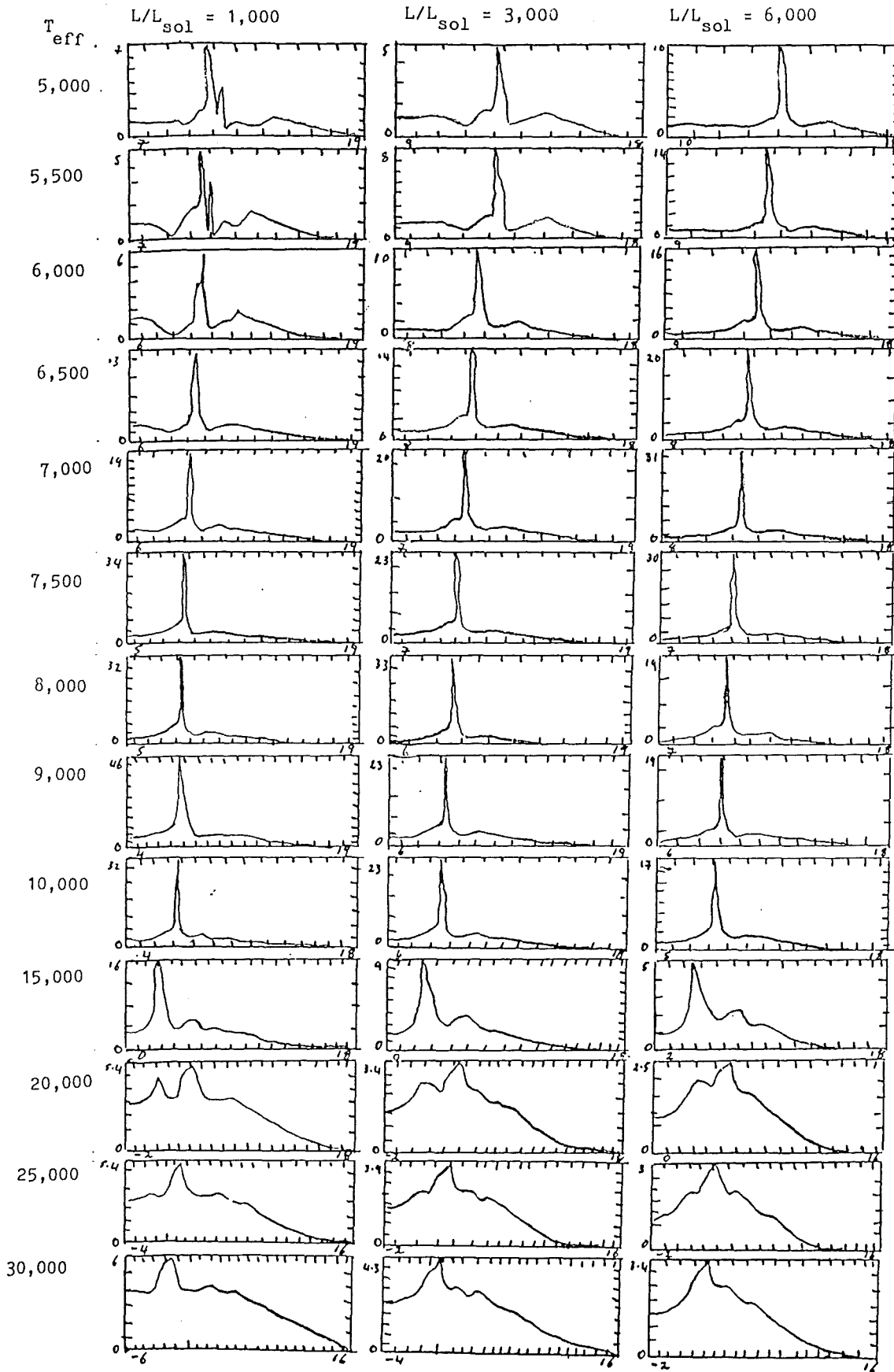


Figure 7.34 : This figure shows plots of $\delta T/T$ versus $\log(M - m_r) - 24$ for the Low luminosity fundamental modes of the $1M_{\odot}$ models of the survey using opacity table DXIX.

LINEAR NON-ADIABATIC RESULTS

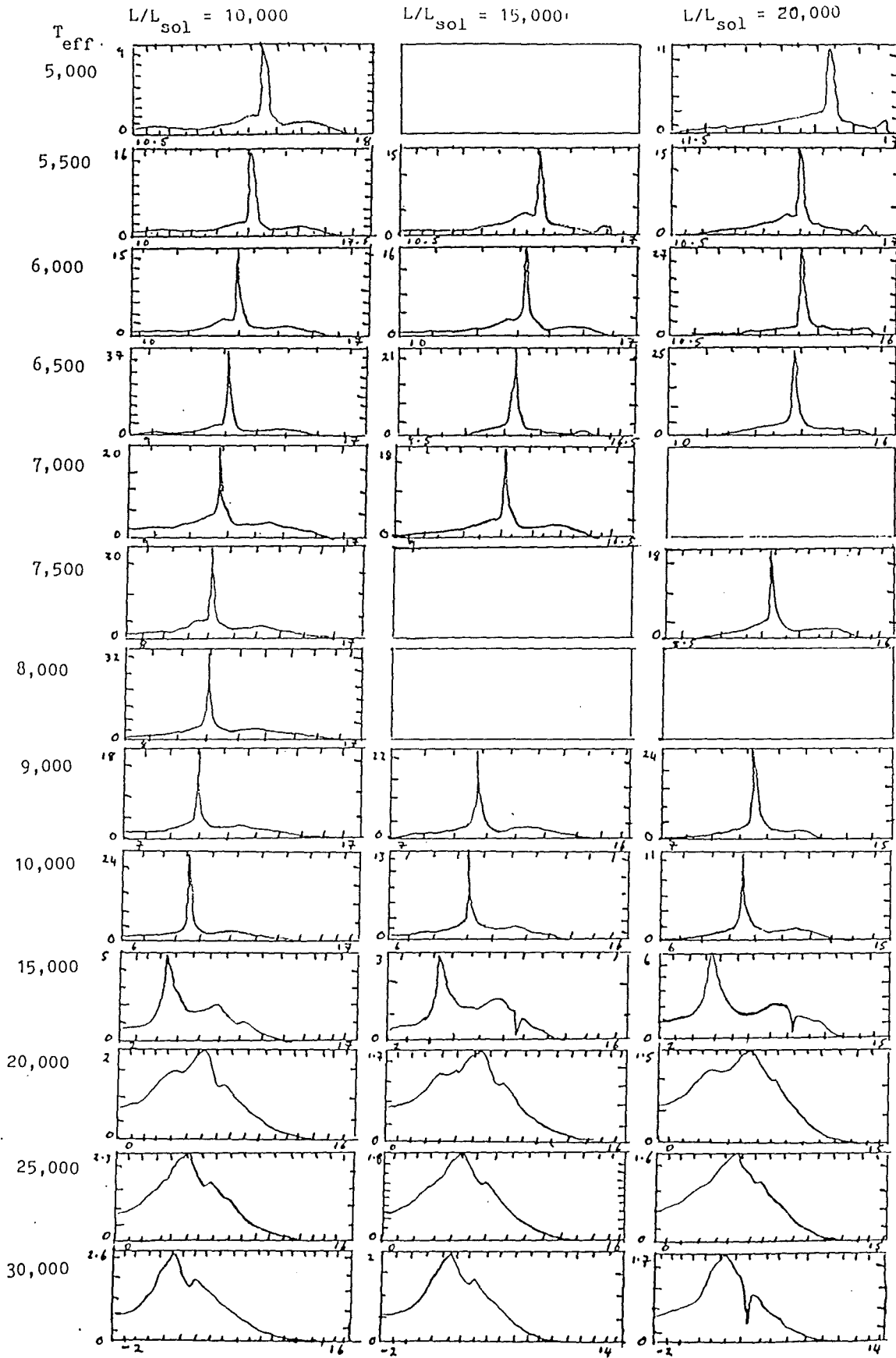


Figure 7.35 : This figure shows plots of $|\delta T/T|$ versus $\log(M - m_r) - 24$ for the High luminosity fundamental modes of the $1M_{\odot}$ models of the survey using opacity table DXIX.

LINEAR NON-ADIABATIC RESULTS

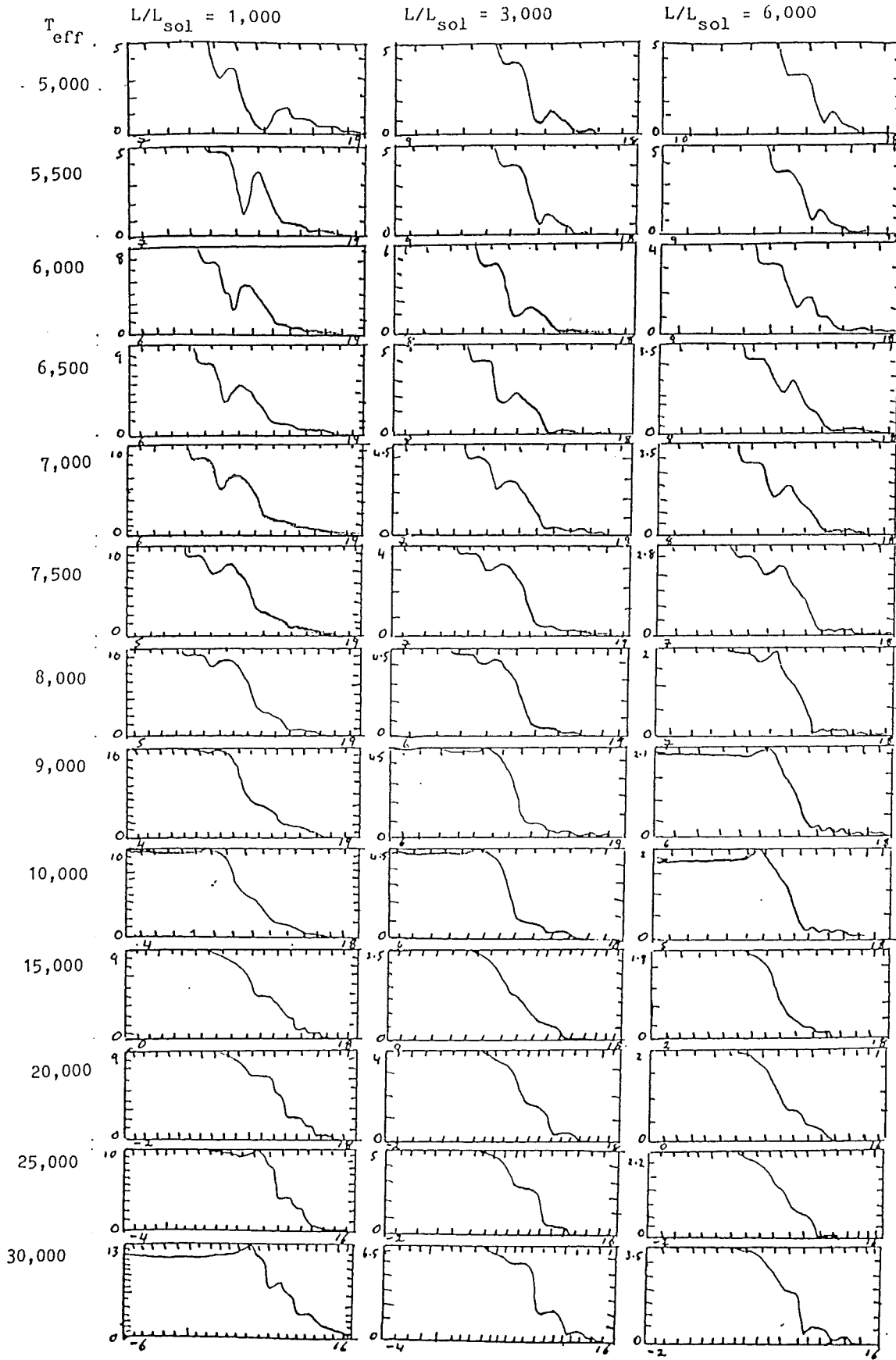


Figure 7.36 : This figure shows plots of $16L/L_1$ versus $\log(M-m)-24$ for the Low luminosity fundamental modes of the $1M_{\odot}$ models of the survey using opacity table DXIX.

LINEAR NON-ADIABATIC RESULTS

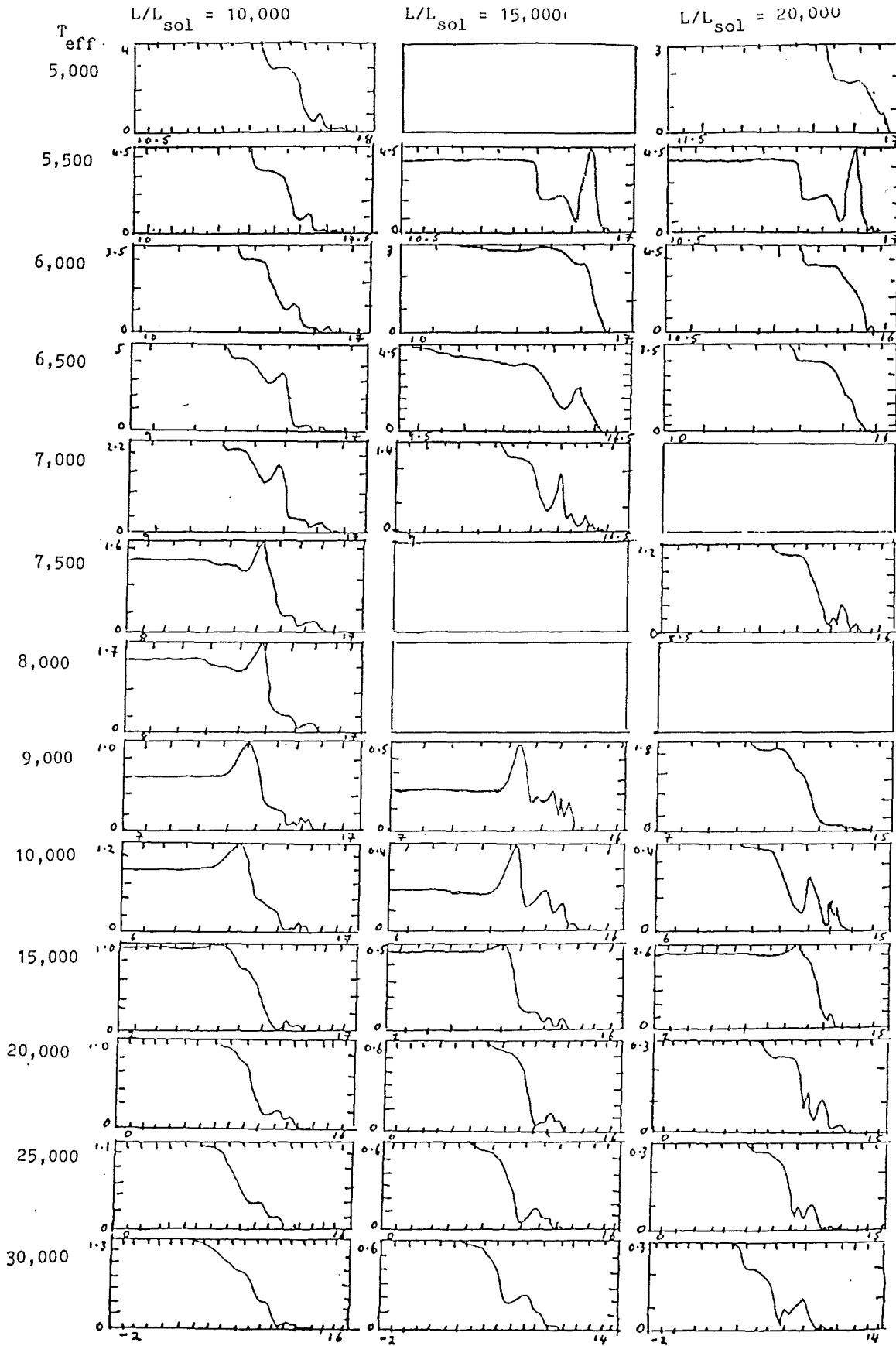


Figure 7.37 : This figure shows plots of $|\delta L/L|$ versus $\log(M-m)-24$ for the High luminosity fundamental modes of the $1M_{\odot}$ models of the survey using opacity table DXIX.

LINEAR NON-ADIABATIC RESULTS

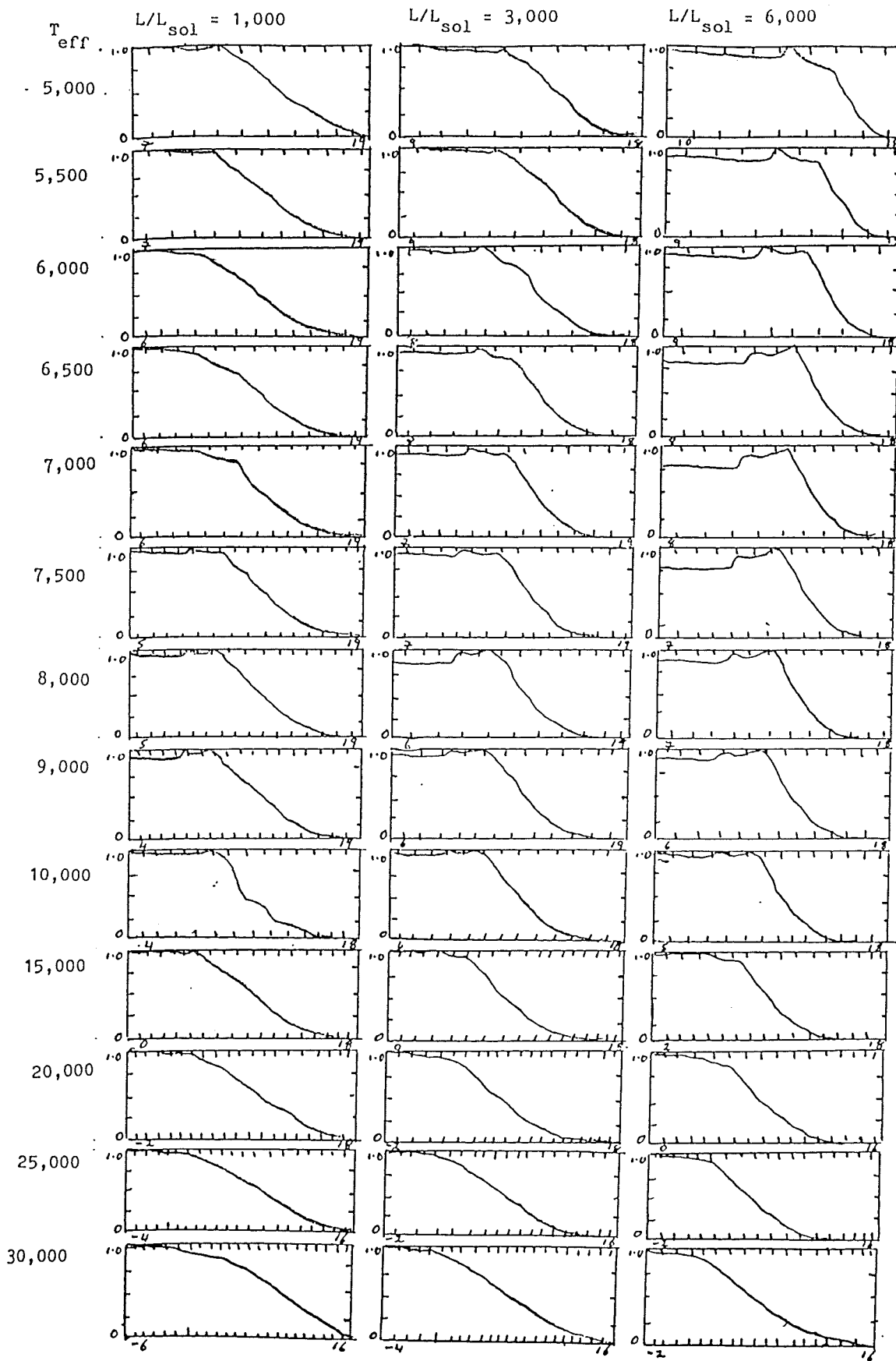


Figure 7.38 : This figure shows plots of $|\delta R/R|$ versus $\log(M - m_r) - 24$ for the Low luminosity fundamental modes of the $1M_{\odot}$ models of the survey using opacity table DXIX.

LINEAR NON-ADIABATIC RESULTS

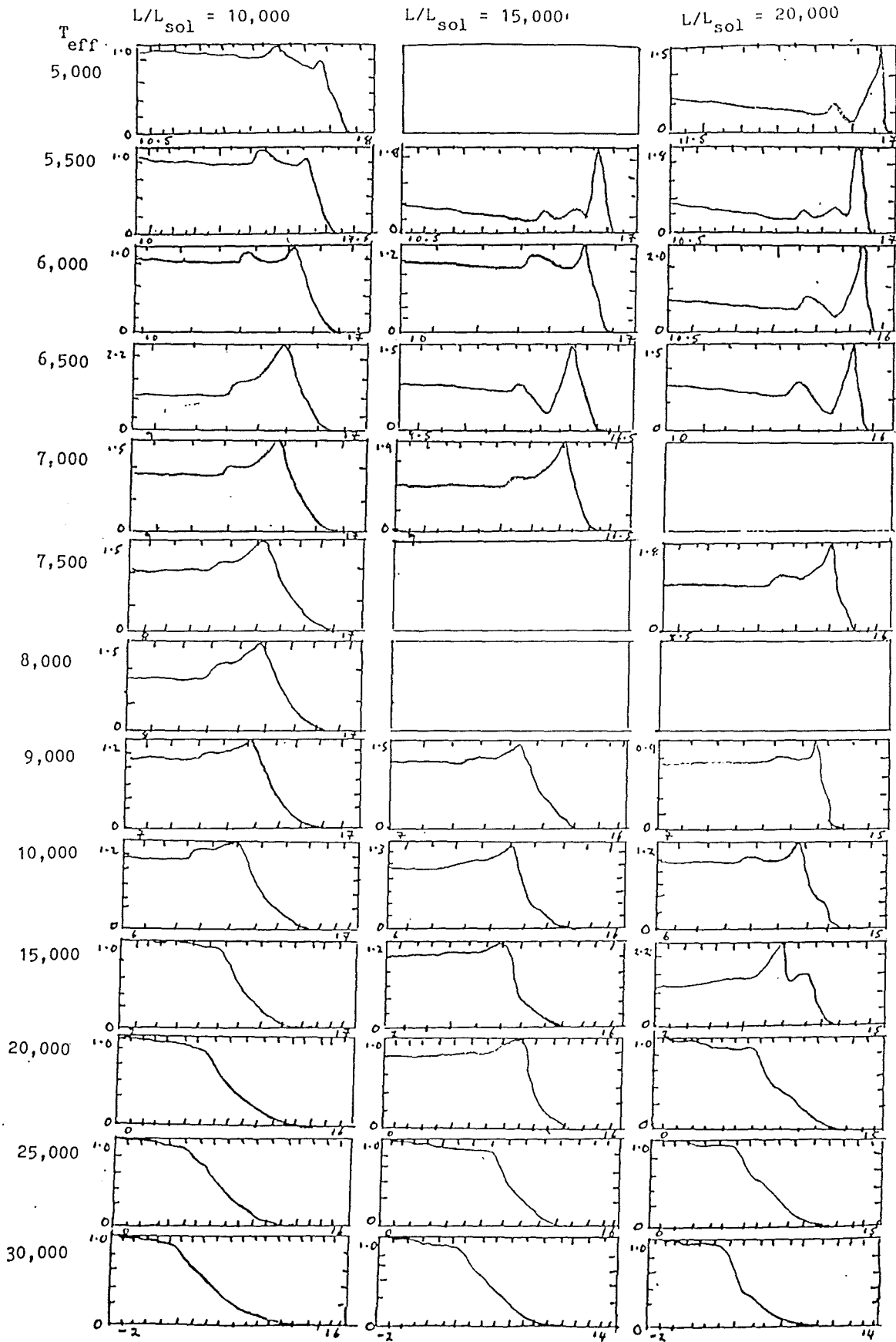


Figure 7.39 : This figure shows plots of $\log(R/R)$ versus $\log(M - m_r) - 24$ for the High luminosity fundamental modes of the $1M_{\odot}$ models of the survey using opacity table DXIX.

LINEAR NON-ADIABATIC RESULTS

7.4.3 Presentation of Results

In the following sub-sections, the results of the DXIX opacity table survey will be given in graphical form, together with several polynomial fits to the fundamental and first overtone data. The raw data has been tabulated for the fundamental and first overtone modes and can be found in the DXIX Section of Appendix E (pages E-19 to E-36).

The graphs are in groups of 4 showing from top left to bottom right:

- TOP LEFT : adiabatic and non-adiabatic Log (period) vs Log (T_{eff})
- TOP RIGHT : adiabatic and non-adiabatic Log (Q) vs Log (T_{eff})
- BOTTOM LEFT : non-adiabatic Growth Rate vs Log (T_{eff})
- BOTTOM RIGHT : Nonadiabatic Π^c vs Log (T_{eff}).

where Π^c is the phase change in degree of $\Phi(\delta R/R)$ between the inner and outer boundaries of the model envelope in question. The symbols and lines used in the graphs are given below to maximise the size of the graphs and reduce repetition:

- DOTTED SOLID LINE - Shows the adiabatic fundamental modes
- LIGHT SOLID LINE - Shows the adiabatic first overtone modes
- CHAINED LINE - Shows the adiabatic second overtone modes
- DOTTED LINE - Shows the adiabatic third overtone modes

- + PLUS - Shows the non-adiabatic fundamental modes
- * ASTERISK - Shows the non-adiabatic first overtone modes
- O CIRCLE - Shows the non-adiabatic second overtone modes
- X CROSS - Shows the non-adiabatic third overtone modes.

LINEAR NON-ADIABATIC RESULTS

For each mass in the survey three polynomial fits have been made to the data. The first of these will fit the following polynomial to non-adiabatic $\text{Log}(\text{Period})$, with $\text{Log}(T_{\text{eff}})$ as the independent variable at each luminosity.

$$\text{Log}(\text{Period}) = a_0 + a_1 \cdot \text{Log}(T_{\text{eff}}) + a_2 \cdot [\text{Log}(T_{\text{eff}})]^2$$

A table of the coefficients at each luminosity, together with the mean residual, M.R., of fits and range in effective temperature, over which fits were made, will be given for each mass and mode considered.

The second and third fits will fit a [2D] polynomial of the form:

$$X = \sum_{i=0}^2 \sum_{j=0}^2 B_{ij} [\text{Log}(T_{\text{eff}})]^i [\text{Log}(L/L_0)]^j, \quad \forall i+j = 1, 2,$$

where X is the non-adiabatic $\text{Log}(\text{Period})$ in the second fit, and non-adiabatic $\text{Log}(Q)$ in the third fit. For each mass, for the modes considered, the range in T_{eff} at each luminosity over which the fit was made is the same as that used in the first fits. For each fit the root mean of the residual squares divided by the range of X used in the fit is given as a percentage (X_i) alongside the polynomial coefficients.

LINEAR NON-ADIABATIC RESULTS

7.4.3.1 Survey Results for $0.8 M_{\odot}$ Models - Table 7.7, below gives the coefficients of fits to the non-adiabatic Fundamental mode Log (periods) at constant luminosities.

L/L_{\odot}	a_0	a_1	a_2	M.R	$\text{Log}(T_{\text{eff}})$
1,000	23.956	-8.498	0.641	0.00343	3.669 - 4.301
3,000	20.392	-6.398	0.366	0.00613	3.669 - 4.398
6,000	9.539	-0.940	-0.299	0.00763	3.669 - 4.477
10,000	-2.230	4.737	-0.968	0.01182	3.778 - 4.477
15,000	92.974	-40.584	4.420	0.00890	3.669 - 4.477
20,000	233.391	-108.671	12.656	0.25972	3.669 - 4.477

TABLE 7.7 : Table of coefficients of first fit for Fundamental mode.

The coefficients for the [2D] fit to the non-adiabatic Fundamental mode Log (periods) are:

$$b_{00} = 12.074 \quad b_{01} = 1.236 \quad X_i = 13.91\% \quad i+j = 1$$

$$b_{10} = -3.921$$

$$b_{00} = 5.896 \quad b_{10} = -29.377 \quad X_i = 12.97\% \quad i+j = 2$$

$$b_{01} = 3.541 \quad b_{11} = -1.855$$

$$b_{02} = 0.682 \quad b_{20} = 4.013$$

The coefficients for the [2D] fit to the non-adiabatic Fundamental mode Log (Q's) are:

$$b_{00} = 0.755 \quad b_{01} = 0.660 \quad X_i = 13.64\% \quad i+j = 1$$

$$b_{10} = -1.074$$

$$b_{00} = 37.305 \quad b_{10} = -19.749 \quad X_i = 11.48\% \quad i+j = 2$$

$$b_{01} = 1.000 \quad b_{11} = -2.074$$

$$b_{02} = 1.070 \quad b_{20} = 3.286$$

LINEAR NON-ADIABATIC RESULTS

Table 7.8, below gives the coefficients of fits to the non-adiabatic first overtone mode Log (periods) at constant luminosities.

L/L_{\odot}	a_0	a_1	a_2	M.R	$\text{Log}(T_{\text{eff}})$
1,000	15.331	-4.455	0.159	0.00261	3.669 - 4.301
3,000	9.459	-1.414	-0.208	0.00336	3.669 - 4.398
6,000	7.241	-0.337	-0.324	0.02084	3.669 - 4.477
10,000	15.331	-4.455	0.159	0.09508	3.778 - 4.477
15,000	28.144	-10.585	0.952	0.08271	3.669 - 4.477
20,000	39.093	-16.096	1.641	0.05717	3.669 - 4.477

TABLE 7.8 : Table of coefficients of first fit for first overtone mode.

The coefficients for the [2D] fit to the non-adiabatic first overtone mode Log (periods) are:

$$b_{00} = 9.224 \quad b_{01} = 0.849 \quad X_1 = 6.22\% \quad i+j = 1$$

$$b_{10} = -2.927$$

$$b_{00} = 11.965 \quad b_{10} = -2.329 \quad X_1 = 5.64\% \quad i+j = 2$$

$$b_{01} = -1.274 \quad b_{11} = 0.397$$

$$b_{02} = 7.583 \quad b_{20} = -0.262$$

The coefficients for the [2D] fit to the non-adiabatic first overtone mode Log (Q's) are:

$$b_{00} = -2.137 \quad b_{01} = 0.115 \quad X_1 = 11.50\% \quad i+j = 1$$

$$b_{10} = 0.066$$

$$b_{00} = -0.943 \quad b_{10} = 1.748 \quad X_1 = 11.26\% \quad i+j = 2$$

$$b_{01} = -2.374 \quad b_{11} = 0.402$$

$$b_{02} = 0.123 \quad b_{20} = -0.397$$

The results presented here will be discussed in Section 7.4.4 .

LINEAR NON-ADIABATIC RESULTS

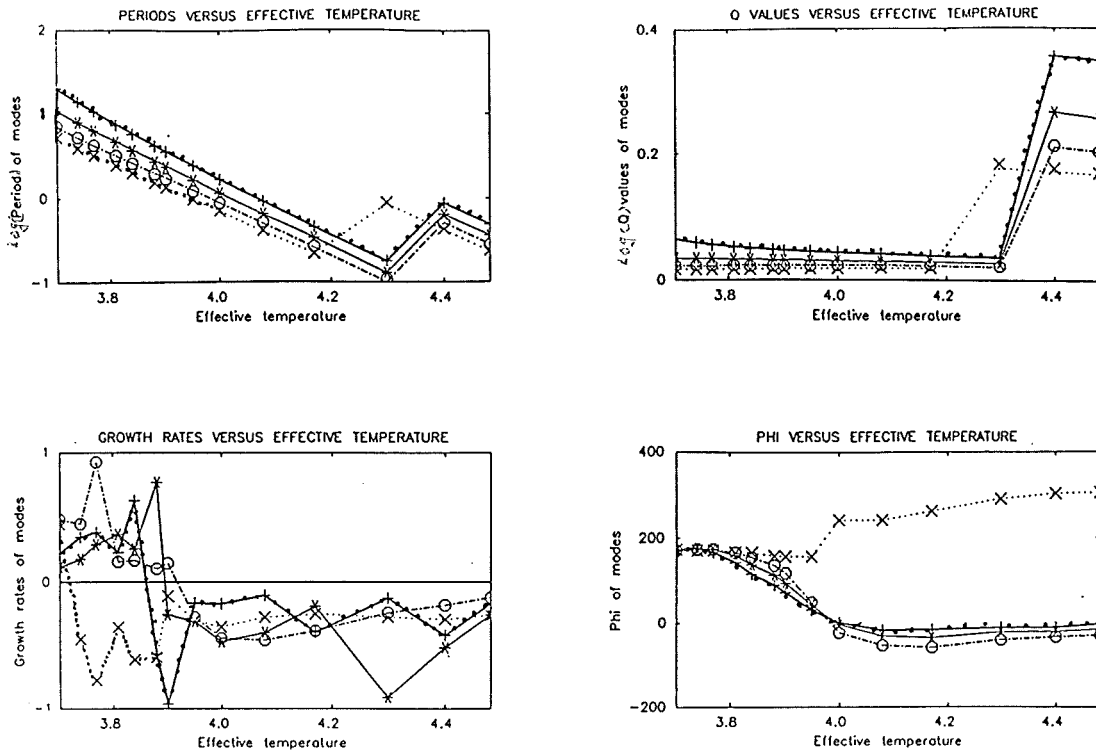


Figure 7.40 : Pulsation parameters for $L/L_{\odot} = 1,000$ and $M/M_{\odot} = 0.8$ (DXIX opacity table).

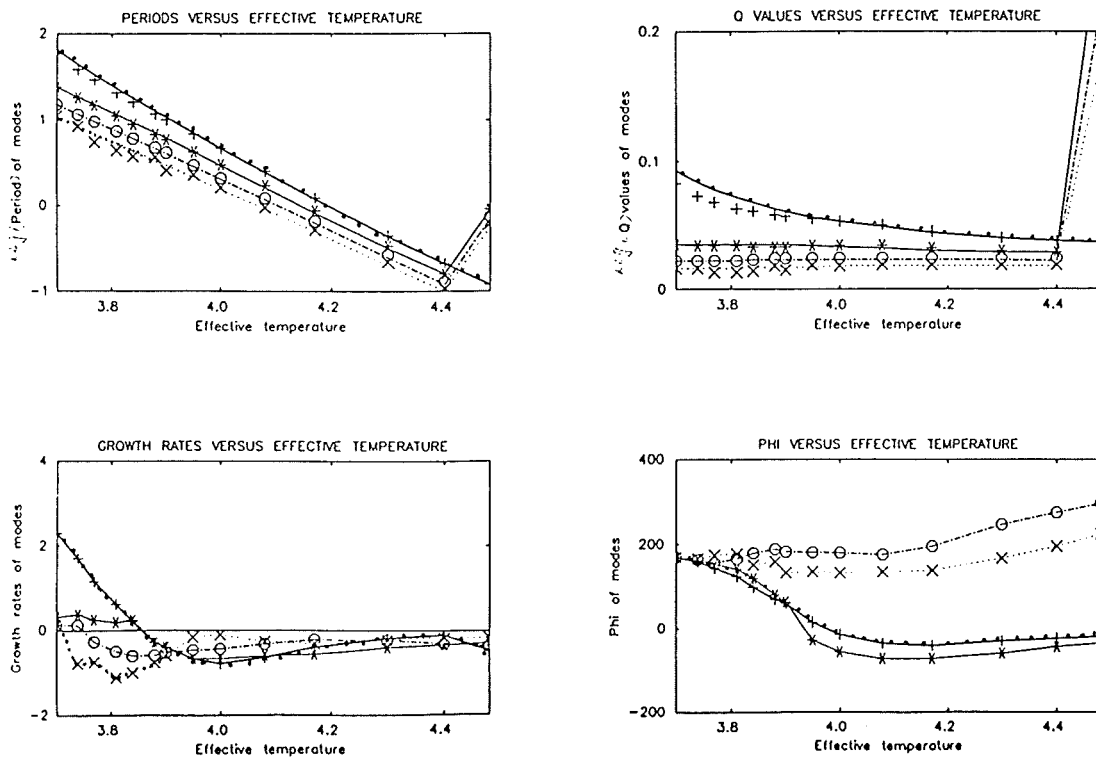


Figure 7.41 : Pulsation parameters for $L/L_{\odot} = 3,000$ and $M/M_{\odot} = 0.8$ (DXIX opacity table).

LINEAR NON-ADIABATIC RESULTS

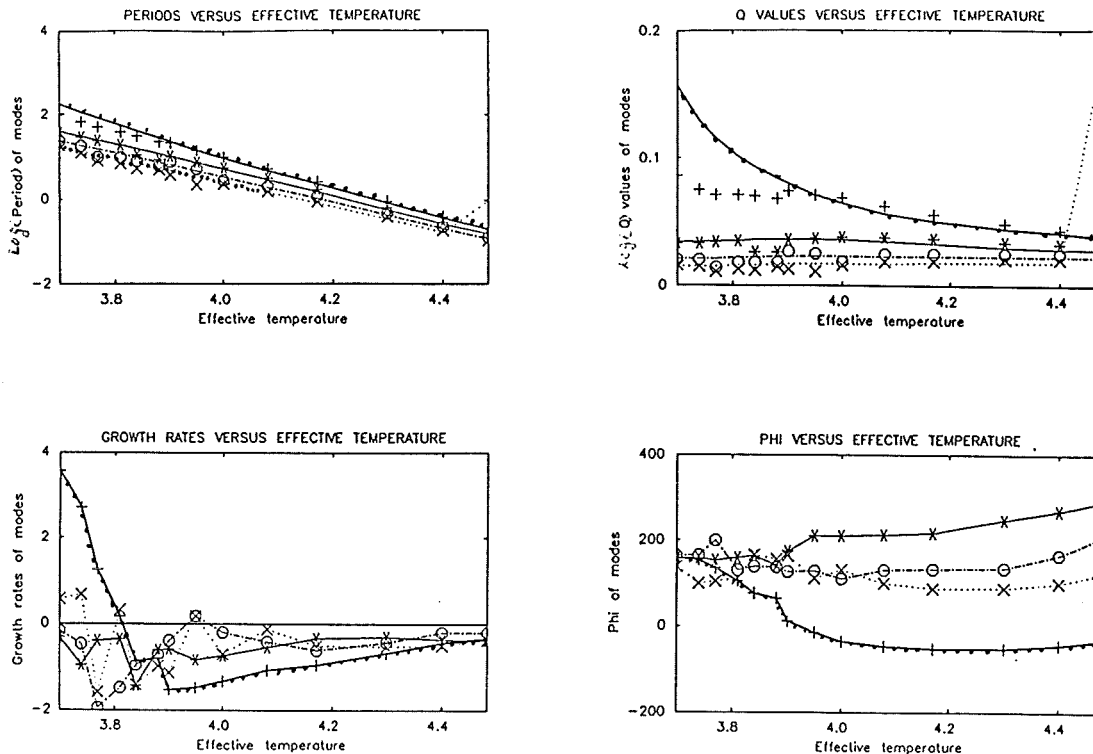


Figure 7.42 : Pulsation parameters for $L/L_{\odot} = 6,000$ and $M/M_{\odot} = 0.8$ (DXIX opacity table).

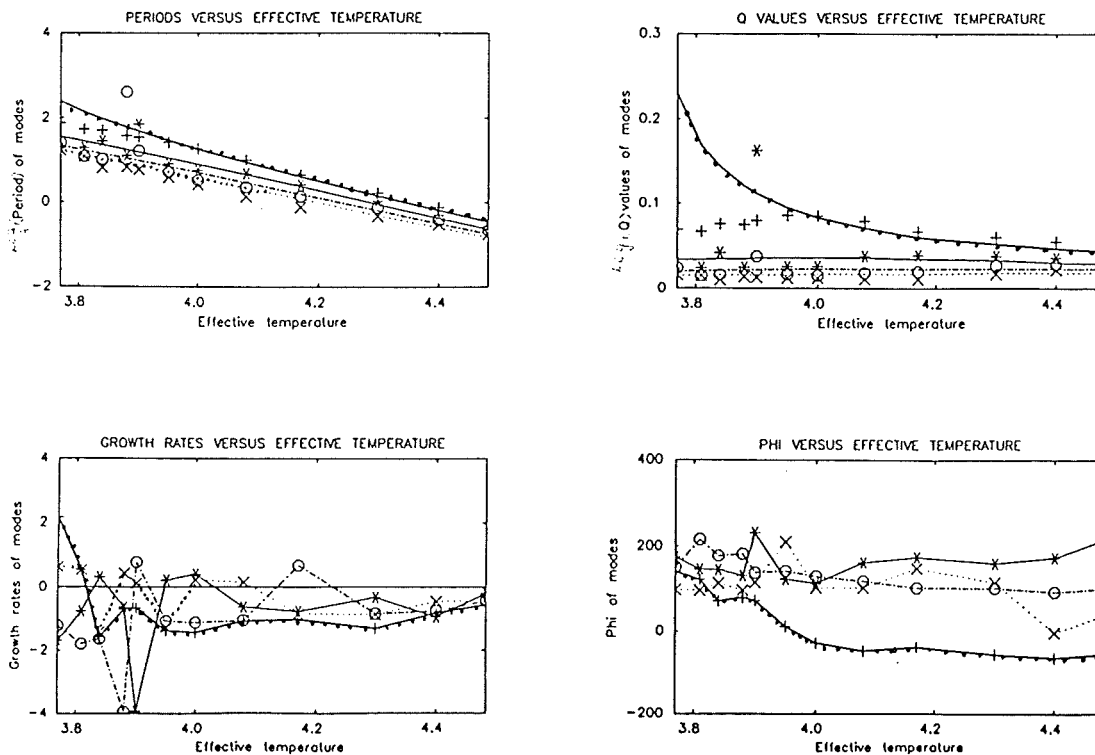


Figure 7.43 : Pulsation parameters for $L/L_{\odot} = 10,000$ and $M/M_{\odot} = 0.8$ (DXIX opacity table).

LINEAR NON-ADIABATIC RESULTS

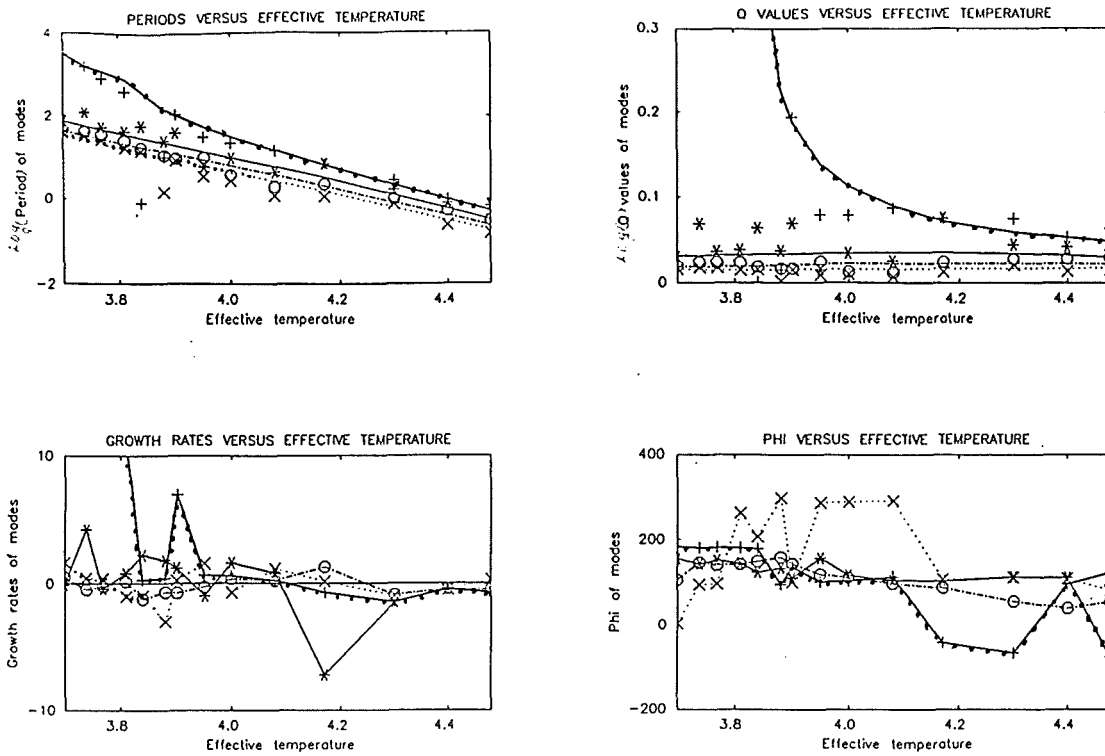


Figure 7.44 : Pulsation parameters for $L/L_{\odot} = 15,000$ and $M/M_{\odot} = 0.8$ (DXIX opacity table).

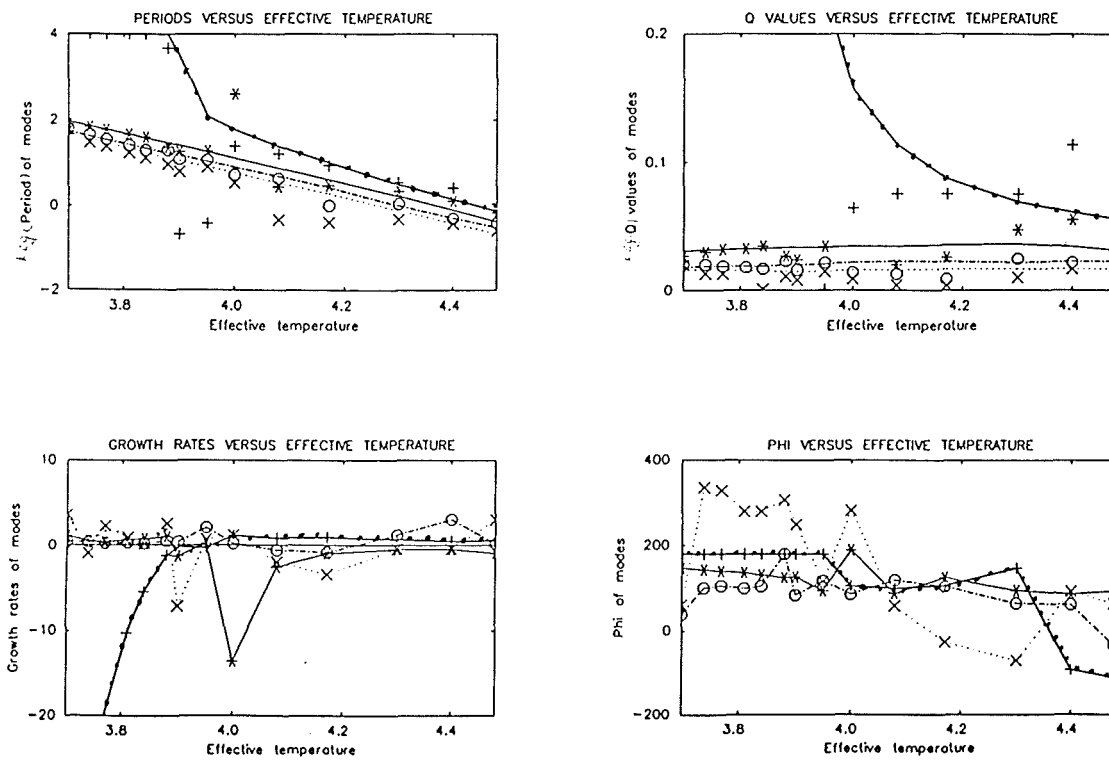


Figure 7.45 : Pulsation parameters for $L/L_{\odot} = 20,000$ and $M/M_{\odot} = 0.8$ (DXIX opacity table).

LINEAR NON-ADIABATIC RESULTS

7.4.3.2 Survey Results for $1.0 M_{\odot}$ Models - Table 7.9, below gives the coefficients of fits to the non-adiabatic fundamental mode Log (periods) at constant luminosities.

L/L_{\odot}	a_0	a_1	a_2	M.R	$\text{Log}(T_{\text{eff}})$
1,000	23.483	-8.343	0.627	0.00219	3.699 - 4.301
3,000	21.101	-6.805	0.419	0.00557	3.699 - 4.398
6,000	18.227	-5.253	0.229	0.00662	3.699 - 4.301
10,000	5.501	1.053	-0.536	0.01839	3.699 - 4.477
15,000	-40.763	23.246	-3.177	0.05427	3.699 - 4.477
20,000	-22.169	13.922	-2.007	0.07035	3.699 - 4.477

TABLE 7.9 : Table of coefficients of first fit for fundamental mode.

The coefficients for the [2D] fit to the non-adiabatic fundamental mode Log (periods) are:

$$b_{00} = 9.798 \quad b_{01} = 0.861 \quad X_i = 4.93\% \quad i+j = 1$$

$$b_{10} = -3.041$$

$$b_{00} = 2.201 \quad b_{10} = 2.868 \quad X_i = 3.92\% \quad i+j = 2$$

$$b_{01} = -1.380 \quad b_{11} = 0.903$$

$$b_{02} = -0.180 \quad b_{20} = -1.161$$

The coefficients for the [2D] fit to the non-adiabatic fundamental mode Log (Q's) are:

$$b_{00} = -1.491 \quad b_{01} = -1.105 \quad X_i = 14.33\% \quad i+j = 1$$

$$b_{10} = -0.004$$

$$b_{00} = -8.709 \quad b_{10} = 5.657 \quad X_i = 11.38\% \quad i+j = 2$$

$$b_{01} = -2.102 \quad b_{11} = 0.908$$

$$b_{02} = -0.186 \quad b_{20} = -1.137$$

LINEAR NON-ADIABATIC RESULTS

Table 7.10, below gives the coefficients of fits to the non-adiabatic first overtone mode Log (periods) at constant luminosities.

L/L ₀	a ₀	a ₁	a ₂	M.R	Log(T _{eff})
1,000	17.499	-5.596	0.305	0.00181	3.699 - 4.301
3,000	12.111	-2.730	-0.005	0.00312	3.699 - 4.398
6,000	8.508	-0.901	-0.265	0.00562	3.699 - 4.301
10,000	17.500	-5.596	0.305	0.03049	3.699 - 4.477
15,000	15.093	-4.216	0.168	0.03279	3.699 - 4.477
20,000	16.786	-5.387	0.358	0.03141	3.699 - 4.477

TABLE 7.10 : Table of coefficients of first fit for first overtone mode.

The coefficients for the [2D] fit to the non-adiabatic first overtone mode Log (periods) are:

$$b_{00} = 9.248 \quad b_{01} = 0.741 \quad X_1 = 2.81\% \quad i+j = 1$$

$$b_{10} = -2.855$$

$$b_{00} = 14.066 \quad b_{10} = -4.091 \quad X_1 = 2.18\% \quad i+j = 2$$

$$b_{01} = -0.432 \quad b_{11} = 0.521$$

$$b_{02} = -0.122 \quad b_{20} = -0.098$$

The coefficients for the [2D] fit to the non-adiabatic first overtone mode Log (Q's) are:

$$b_{00} = -2.001 \quad b_{01} = -0.008 \quad X_1 = 16.33\% \quad i+j = 1$$

$$b_{10} = 0.134$$

$$b_{00} = 1.777 \quad b_{10} = -0.692 \quad X_1 = 13.65\% \quad i+j = 2$$

$$b_{01} = -1.068 \quad b_{11} = 0.506$$

$$b_{02} = -0.129 \quad b_{20} = -0.141$$

The results presented here will be discussed in Section 7.4.4 .

LINEAR NON-ADIABATIC RESULTS

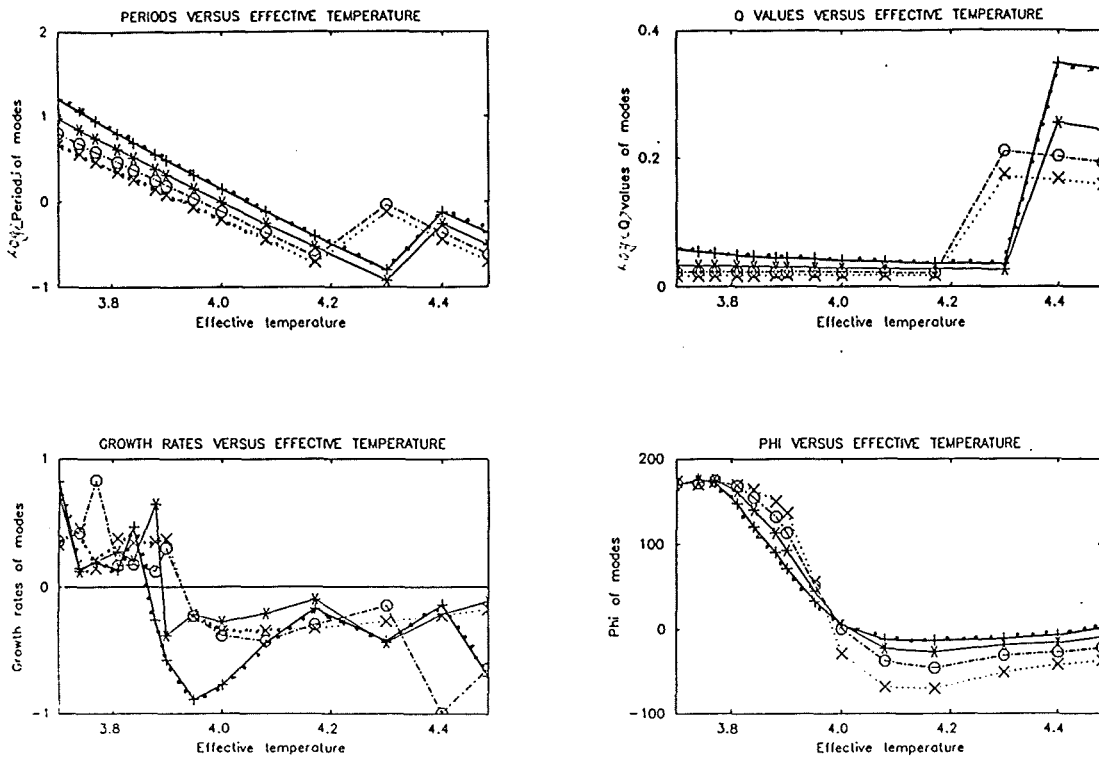


Figure 7.46 : Pulsation parameters for $L/L_{\odot} = 1,000$ and $M/M_{\odot} = 1.0$ (DXIX opacity table).

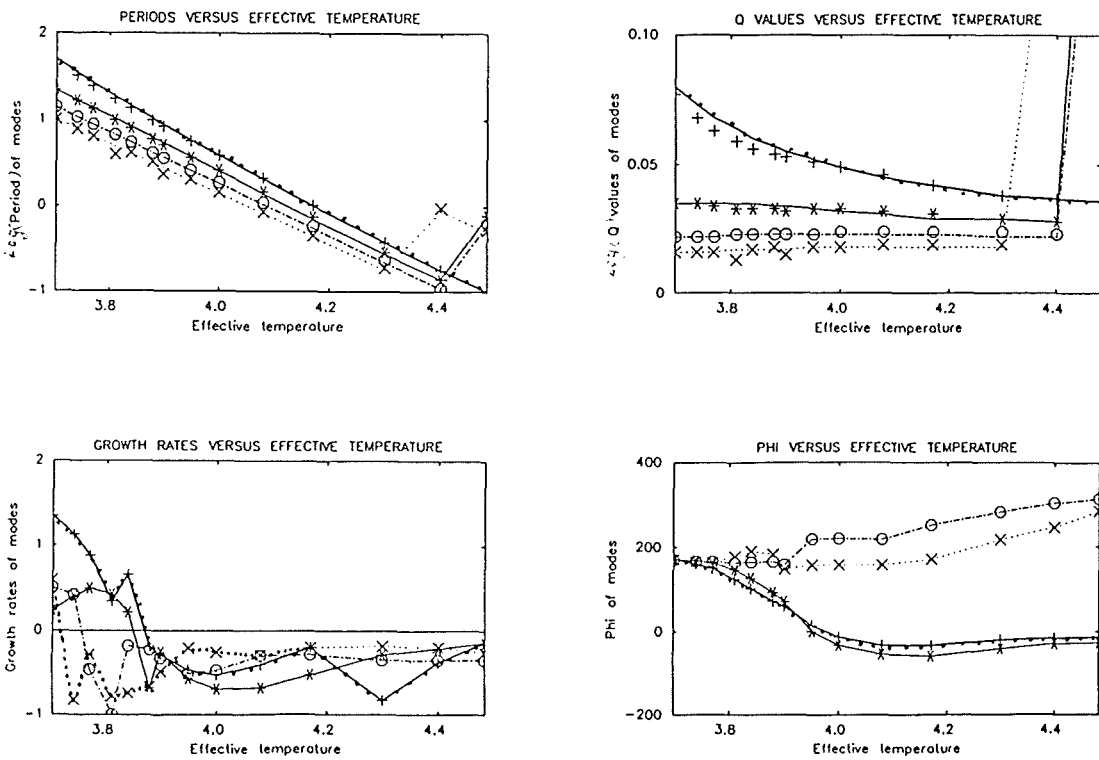


Figure 7.47 : Pulsation parameters for $L/L_{\odot} = 3,000$ and $M/M_{\odot} = 1.0$ (DXIX opacity table).

LINEAR NON-ADIABATIC RESULTS

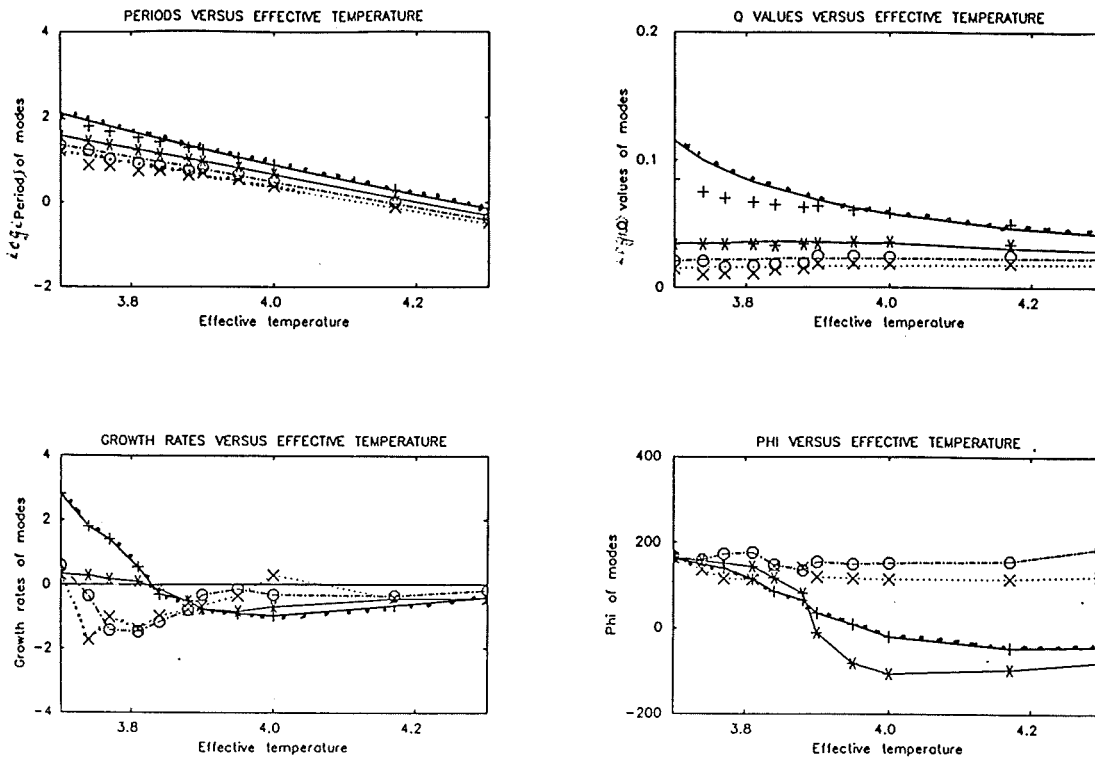


Figure 7.48 : Pulsation parameters for $L/L_{\odot} = 6,000$ and $M/M_{\odot} = 1.0$ (DXIX opacity table).

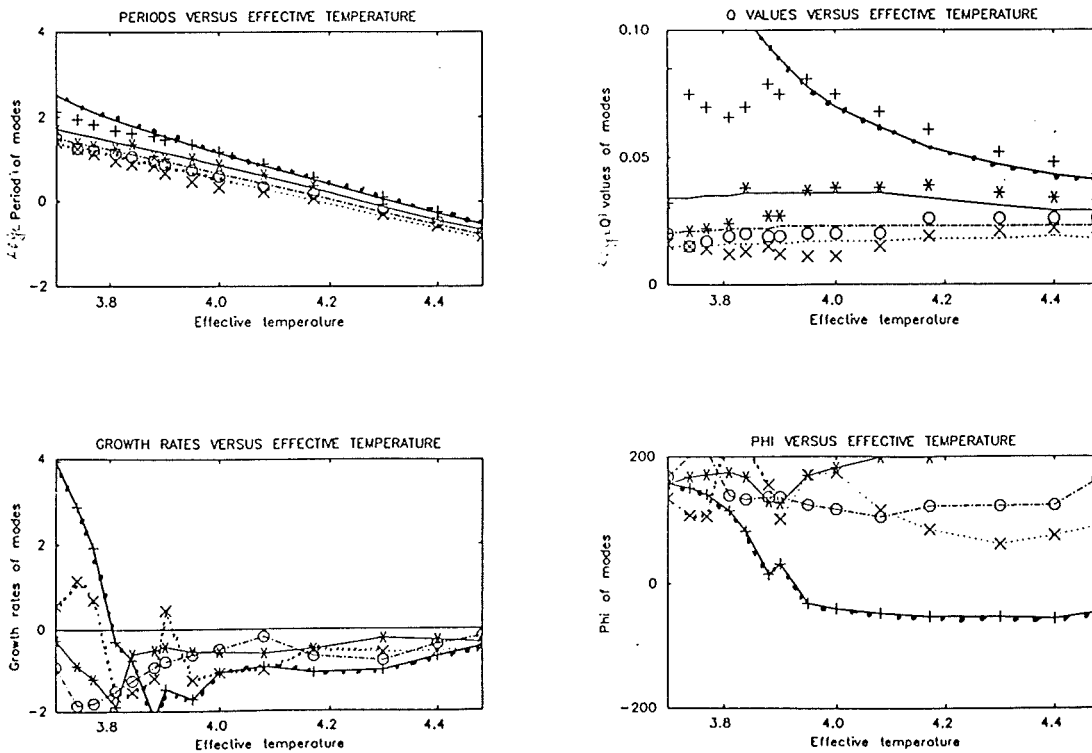


Figure 7.49 : Pulsation parameters for $L/L_{\odot} = 10,000$ and $M/M_{\odot} = 1.0$ (DXIX opacity table).

LINEAR NON-ADIABATIC RESULTS

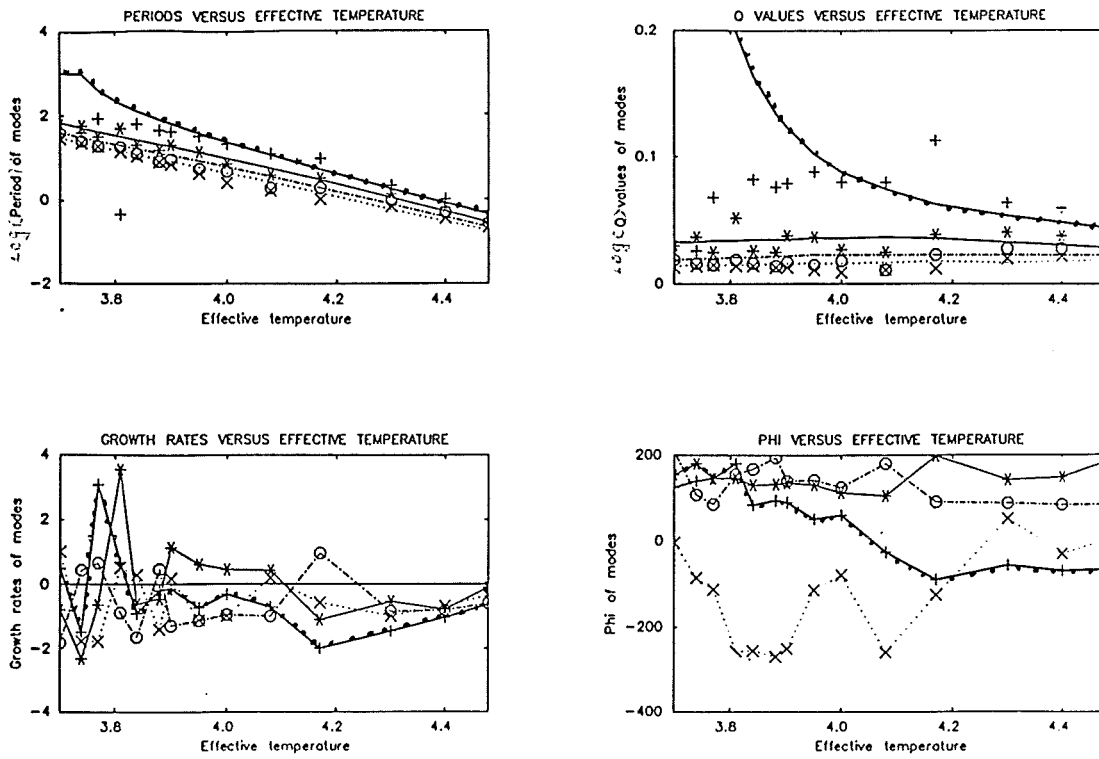


Figure 7.50 : Pulsation parameters for $L/L_{\odot} = 15,000$ and $M/M_{\odot} = 1.0$ (DXIX opacity table).

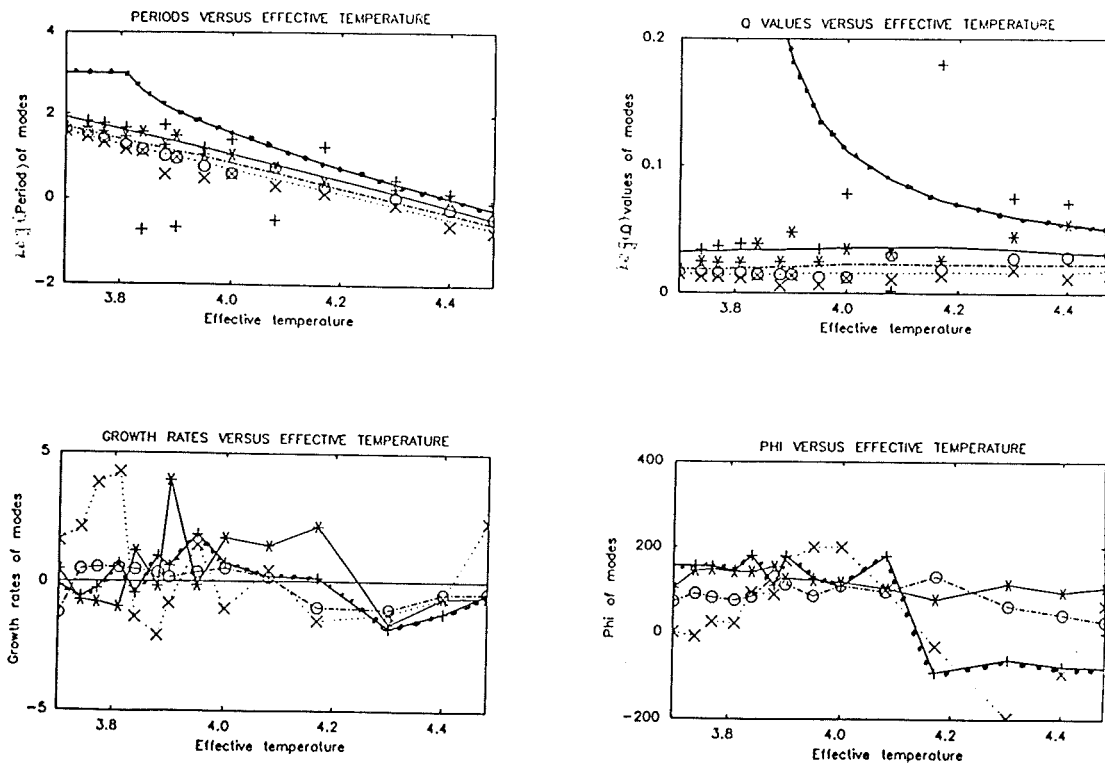


Figure 7.51 : Pulsation parameters for $L/L_{\odot} = 20,000$ and $M/M_{\odot} = 1.0$ (DXIX opacity table).

LINEAR NON-ADIABATIC RESULTS

7.4.3.3 Survey Results for 1.2 M_{\odot} Models - Table 7.11, below gives the coefficients of fits to the non-adiabatic fundamental mode Log (periods) at constant luminosities.

L/L_{\odot}	a_0	a_1	a_2	M.R	$\text{Log}(T_{\text{eff}})$
1,000	21.974	-7.633	0.541	0.00239	3.699 - 4.301
3,000	22.762	-7.703	0.535	0.00440	3.699 - 4.398
6,000	18.844	-5.556	0.262	0.00405	3.699 - 4.477
10,000	11.454	-1.860	-0.185	0.00749	3.699 - 4.477
15,000	2.354	2.630	-0.725	0.01851	3.699 - 4.477
20,000	14.321	-3.412	0.039	0.03729	3.699 - 4.477

TABLE 7.11 : Table of coefficients of first fit for fundamental mode.

The coefficients for the [2D] fit to the non-adiabatic fundamental mode Log (periods) are:

$$\begin{aligned}
 b_{00} &= 10.542 & b_{01} &= 0.929 & X_i &= 1.81\% & i+j &= 1 \\
 b_{10} &= -3.305 & & & & & & \\
 \\
 b_{00} &= 12.060 & b_{10} &= -3.456 & X_i &= 1.75\% & i+j &= 2 \\
 b_{01} &= 0.290 & b_{11} &= 0.171 & & & & \\
 b_{02} &= -0.005 & b_{20} &= -0.063 & & & &
 \end{aligned}$$

The coefficients for the [2D] fit to the non-adiabatic fundamental mode Log (Q's) are:

$$\begin{aligned}
 b_{00} &= -0.707 & b_{01} &= 0.181 & X_i &= 11.63\% & i+j &= 1 \\
 b_{10} &= -0.307 & & & & & & \\
 \\
 b_{00} &= 0.822 & b_{10} &= -0.420 & X_i &= 11.18\% & i+j &= 2 \\
 b_{01} &= -0.504 & b_{11} &= 0.182 & & & & \\
 b_{02} &= -0.005 & b_{20} &= -0.073 & & & &
 \end{aligned}$$

LINEAR NON-ADIABATIC RESULTS

Table 7.12, below gives the coefficients of fits to the non-adiabatic first overtone mode Log (periods) at constant luminosities.

L/L_{\odot}	a_0	a_1	a_2	M.R	$\text{Log}(T_{\text{eff}})$
1,000	14.803	-4.240	0.132	0.00375	3.699 - 4.301
3,000	15.000	-4.183	0.130	0.00190	3.699 - 4.398
6,000	10.056	-1.655	-0.176	0.00419	3.699 - 4.477
10,000	14.803	-4.240	0.132	0.01453	3.699 - 4.477
15,000	4.044	1.134	-0.480	0.03948	3.699 - 4.477
20,000	14.053	-3.784	0.127	0.05105	3.699 - 4.477

TABLE 7.12 : Table of coefficients of first fit for first overtone mode.

The coefficients for the [2D] fit to the non-adiabatic first overtone mode Log (periods) are:

$$b_{00} = 9.566 \quad b_{01} = 0.756 \quad X_1 = 2.66\% \quad i+j = 1$$

$$b_{10} = -2.960$$

$$b_{00} = 11.009 \quad b_{10} = -3.051 \quad X_1 = 2.29\% \quad i+j = 2$$

$$b_{01} = 0.142 \quad b_{11} = 0.407$$

$$b_{02} = -0.135 \quad b_{20} = -0.183$$

The coefficients for the [2D] fit to the non-adiabatic first overtone mode Log (Q's) are:

$$b_{00} = -1.687 \quad b_{01} = 0.009 \quad X_1 = 16.41\% \quad i+j = 1$$

$$b_{10} = 0.036$$

$$b_{00} = -0.529 \quad b_{10} = 0.052 \quad X_1 = 2.29\% \quad i+j = 2$$

$$b_{01} = -0.563 \quad b_{11} = 0.398$$

$$b_{02} = -0.136 \quad b_{20} = -0.193$$

The results presented here will be discussed in Section 7.4.4 .

LINEAR NON-ADIABATIC RESULTS

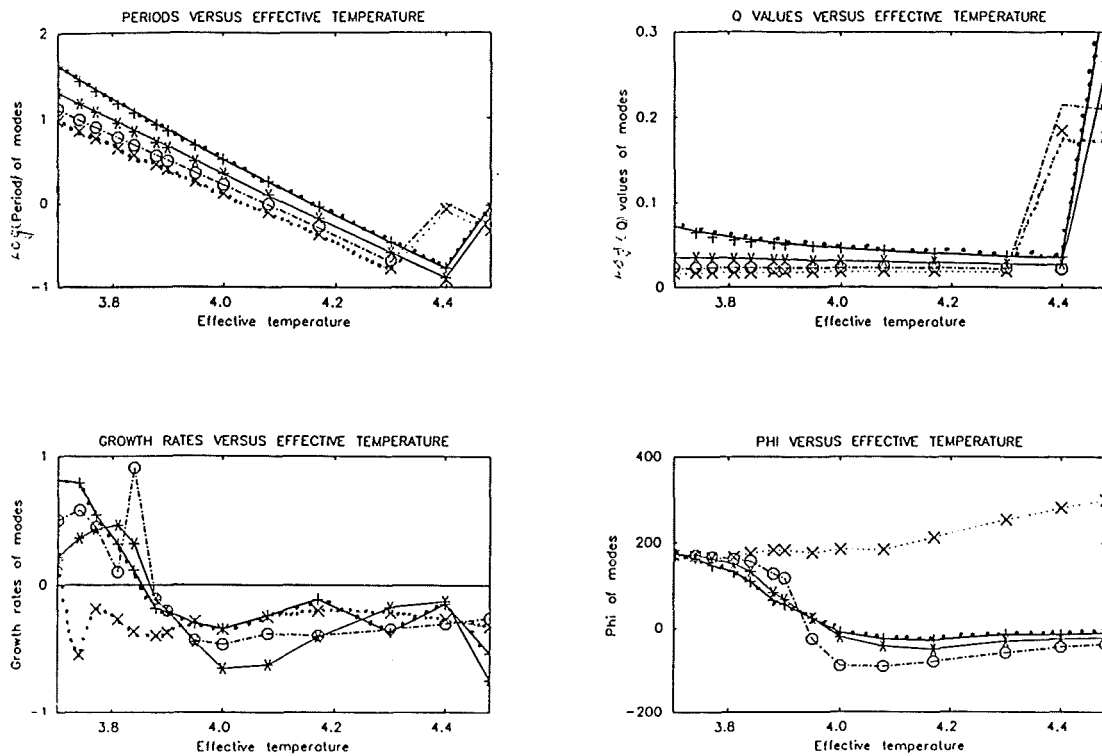


Figure 7.52 : Pulsation parameters for $L/L_{\odot} = 1,000$ and $M/M_{\odot} = 1.2$ (DXIX opacity table).

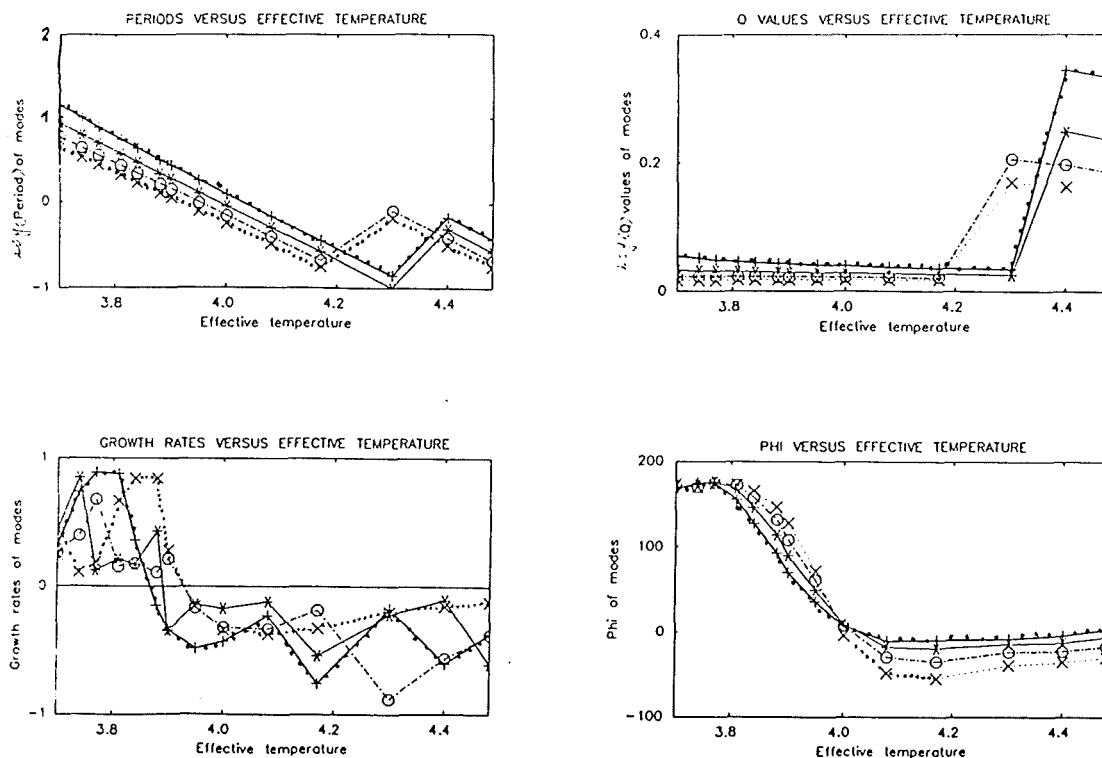


Figure 7.53 : Pulsation parameters for $L/L_{\odot} = 3,000$ and $M/M_{\odot} = 1.2$ (DXIX opacity table).

LINEAR NON-ADIABATIC RESULTS

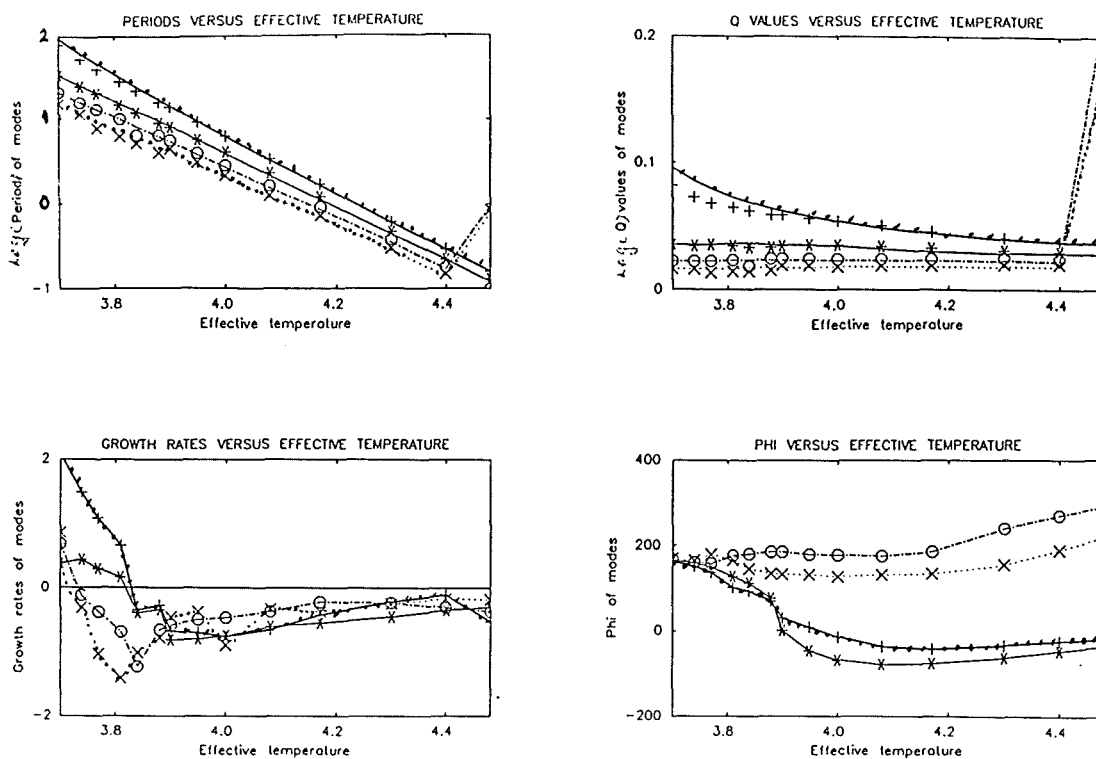


Figure 7.54 : Pulsation parameters for $L/L_{\odot} = 6,000$ and $M/M_{\odot} = 1.2$ (DXIX opacity table).

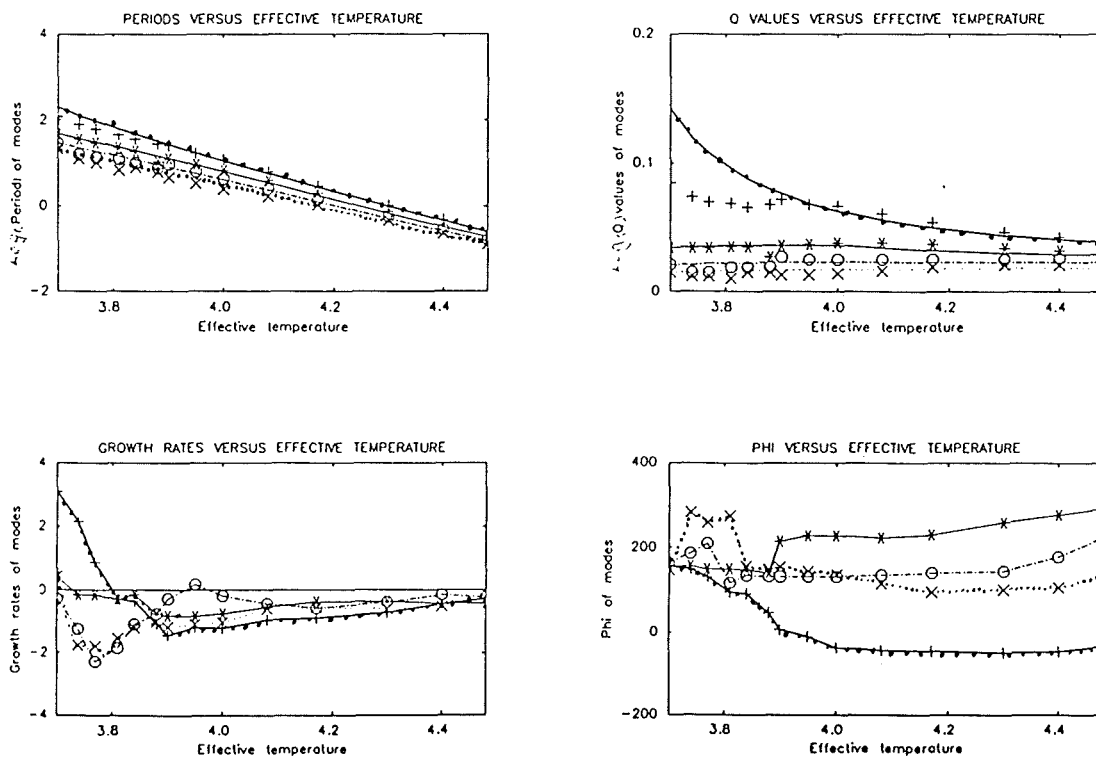


Figure 7.55 : Pulsation parameters for $L/L_{\odot} = 10,000$ and $M/M_{\odot} = 1.2$ (DXIX opacity table).

LINEAR NON-ADIABATIC RESULTS

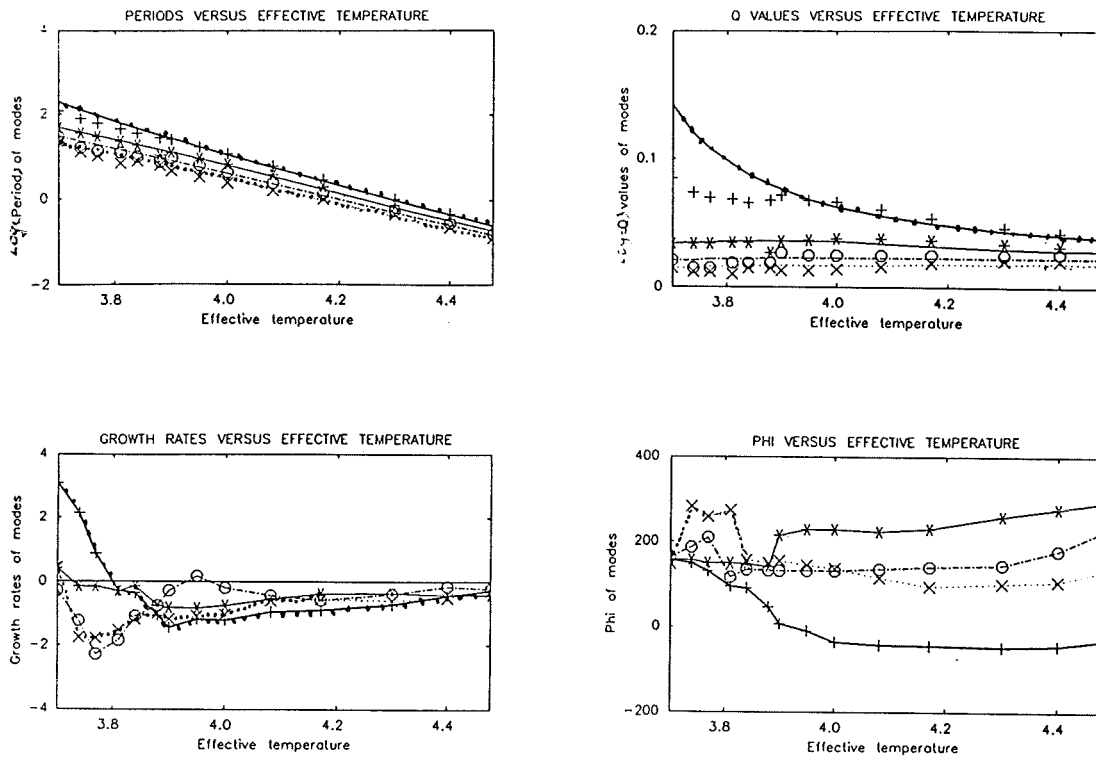


Figure 7.56 : Pulsation parameters for $L/L_{\odot} = 15,000$ and $M/M_{\odot} = 1.2$ (DXIX opacity table).

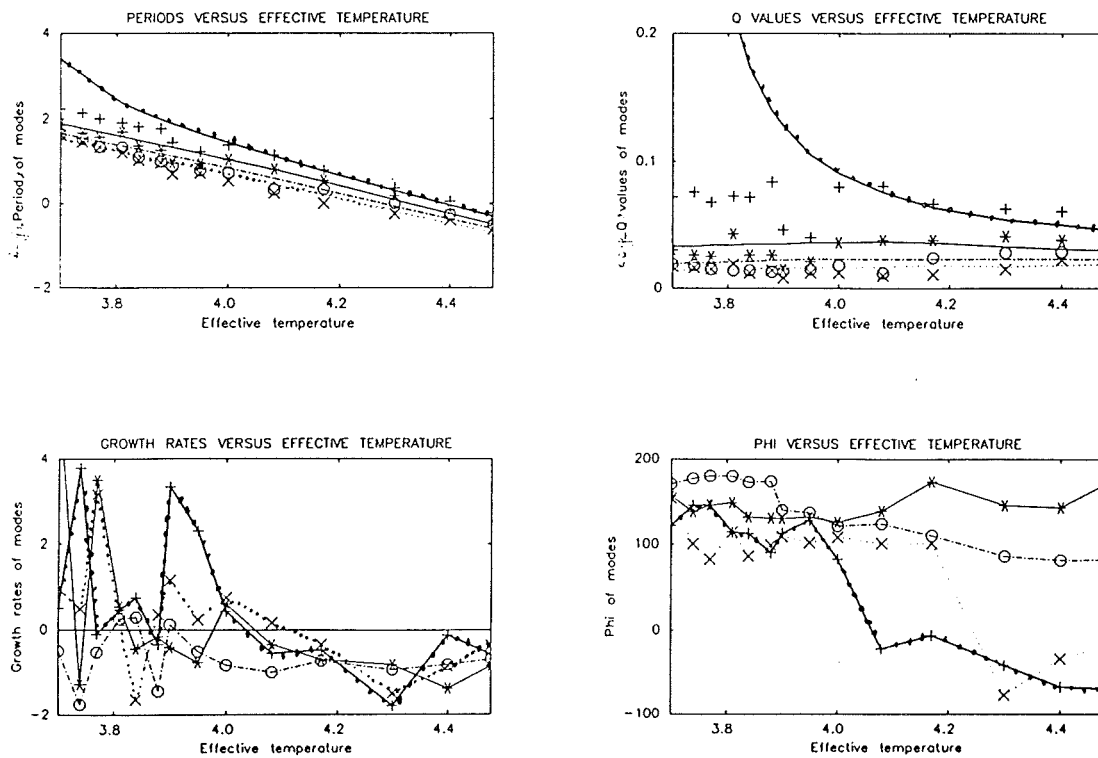


Figure 7.57 : Pulsation parameters for $L/L_{\odot} = 20,000$ and $M/M_{\odot} = 1.2$ (DXIX opacity table).

7.4.4 A Discussion of the Survey Results

The Figures that the following discussion is based upon are Figures 7.40 - 7.57 . First let us take the upper two graphs of each quartet in which we again see the 'step' in both Q and periods which were present in pure helium results. It is again only present in low luminosity, high effective temperature models, and is probably an intrinsic feature of such hot helium models. Here we can see one use of the Q -value graphs, as the divergence of non-adiabatic and adiabatic values with increasing luminosity at lower effective temperatures is far more evident. The flattening out of the non-adiabatic Q -values and periods with decreasing T_{eff} is due to the increasing loss of heat or the growth of non-adiabaticity in the models. We can see that this 'flattening' is very pronounced at high luminosities, where the adiabatic values soar off to infinity. This could indicate that the adiabatic pulsation is swapping from 'acoustic' to 'thermal' standing waves, while the non-adiabatic remains 'acoustic' in nature (see Saio & Wheeler, 1985).

Amongst the results there are some 'odd' points that have periods either too low, or high for their modes. These are not high order overtones as first thought, but appear upon investigating their phase diagrams, to be 'strange modes'. In this study little more was done, beyond recognising and eliminating them from the data set (this was due to lack of time, and the fact that they did not appear to be numerous enough to have a serious influence upon survey results). It is worth noting that a distinct drop in Q is visible at the rough location of the stability edges and may be a good way of locating these edges for such models.

It can be seen that the higher overtones are not affected nearly as much as the fundamental mode, though they do show signs of shortening

LINEAR NON-ADIABATIC RESULTS

their periods to that of the next mode, as was seen by Saio & Wheeler (1985) in his models. Looking at the [2D] fits for the fundamental mode:

$$\begin{aligned}
 P_0 &= 1.2 \times 10^{12} (T_{\text{eff}})^{-3.92} (L/L_{\odot})^{1.236} \quad (13\%) & M/M_{\odot} &= 0.8 \\
 P_0 &= 6.3 \times 10^9 (T_{\text{eff}})^{-3.04} (L/L_{\odot})^{0.861} \quad (5\%) & M/M_{\odot} &= 1.0 \\
 P_0 &= 3.5 \times 10^{10} (T_{\text{eff}})^{-3.31} (L/L_{\odot})^{0.929} \quad (2\%) & M/M_{\odot} &= 1.2
 \end{aligned}$$

from which it can be seen that, with the exception of $0.8M_{\odot}$ fit, the powers are roughly the same as those found for the pure helium survey. This discrepancy could be due to the poor nature of the fit (although it is good enough for our purposes). Again we see that as the mass increases the fits are more accurate, as the models are less non-adiabatic and better behaved. Indeed most of the problems occur at $20,000L_{\odot}$ where the scatter in the fundamental data is quite large due to non-adiabaticity.

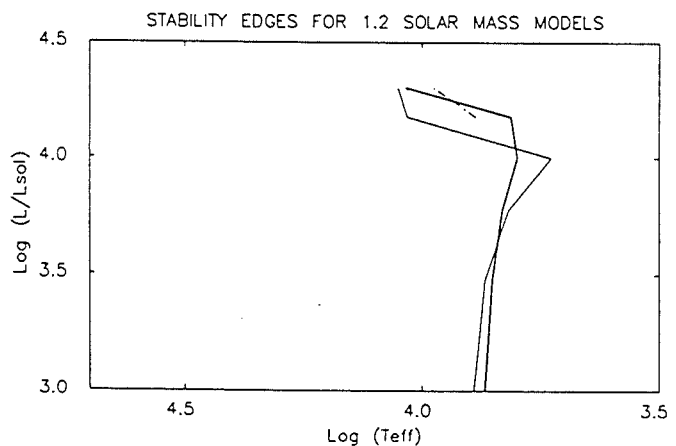
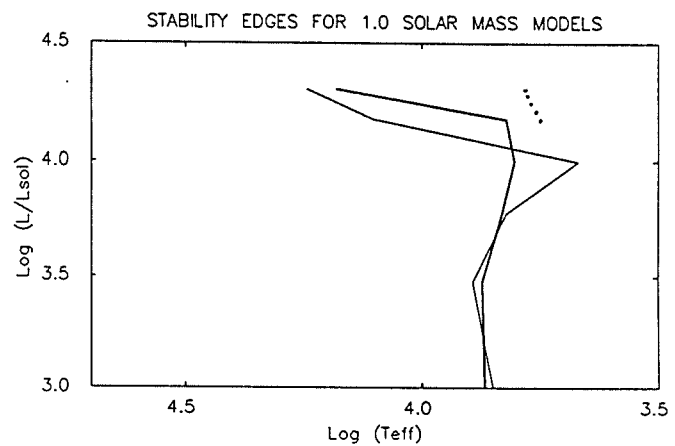
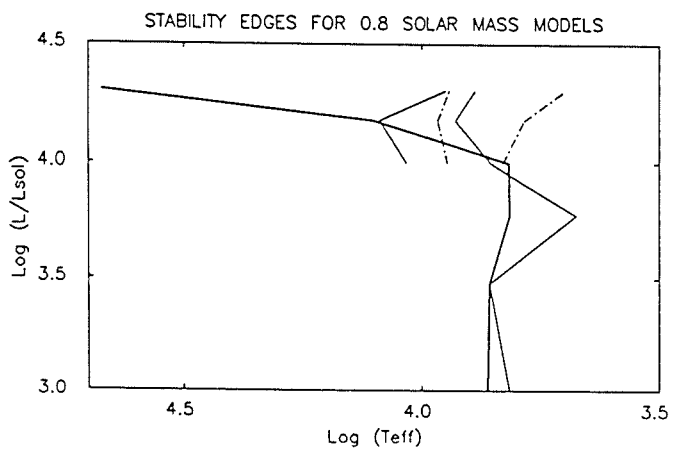
The bottom two graphs in each quartet behave in a similar way to those in the pure helium case and need no further description here. In obtaining the instability edges, shown in Figure 7.58, it was necessary, at the higher luminosities, to take only values that were more than marginally unstable, i.e., in some cases, where the growth rate curves just pop above/below zero at one point, the point was ignored. The instability edges of fundamental and first overtone modes found in this survey are given in Appendix F.2 .

From the graphs in Figure 7.58 we can see that the 'dog-leg' in both fundamental and first overtone blue edges is very pronounced for all masses of the survey, instead of only the lowest mass as found in the pure helium survey. However in this case the first overtone

LINEAR NON-ADIABATIC RESULTS

instability region breaks up into narrow strip-like regions for the $0.8M_{\odot}$ survey. This is due to the ionisation levels of carbon and their increased contribution to the 'driving' at higher luminosities and effective temperatures. This 'dog-leg' effect is apparently only present in helium models, and may be due to the sudden increase in electrons at higher luminosities due to increased ionisation of helium and in this case carbon. This effect could be very useful in explaining why some extreme helium stars pulsate and some do not, as the luminosities of these objects are very close to the onset of the 'dog-leg' effect. We did not find, however, as in Saio & Wheeler (1985), that the first overtone is stable over the instability region of the fundamental mode. This could lead to contamination problems, although for most of the range we find that the fundamental mode has a far larger growth rate than that for the first overtone mode and should swamp the contamination for the first 50 or so periods of a non-linear calculation. The red edge found for $1M_{\odot}$ fundamental modes is not necessarily correctly placed as the graphs of the growth rates used are scattered for the low effective temperature, high luminosity models. There is always the problem that red edges below about $T_{\text{eff}} = 5,500 \text{ K}$ could be moved redward by increased convection (i.e., if a proper convection model was available).

We can see that the introduction of carbon has had a significant effect upon the instability and associated periods of the models, especially at high luminosities ($>10,000L_{\odot}$). Indeed, the opacity at these high luminosities could significantly alter the outcome of any stability analysis. We can see that if opacity table DXIX is correct, the major effect is to move the instability strip redward and to lower the 'dog-leg' onset luminosity. The overall shape of the blue edge remains the same, if more pronounced.



KEY FOR OPACITY TABLE DXIX

- Heavy lines - Fundamental Blue Edge
- Dotted lines - Fundamental Red Edge
- Light lines - First overtone Blue Edge
- Chained lines - First overtone Red Edge

Figure 7.58 : This figure shows the position of the blue edges of DXIX opacity table survey, on HR diagrams. The heavy solid lines represent the Fundamental blue edges and the light solid lines the first overtone blue edges.

7.5 RESULTS OF THE SURVEY USING OPACITY TABLE BD9C

In the following sub-sections the results for the smoothed 'hot' Thomas-Fermi opacity table BD9C, produced by Dr Jeffery from Dr Carson's He-C opacity table sequence, will be presented and compared with the results of previous surveys. This survey was mainly carried out to find limitations upon mass and luminosity for variable RCB objects, and how these compared with the limitations found using opacity table DXIX. It will be interesting to see if the 'strange' modes found in the survey on DXIX are also found in this survey, especially as all previous 'strange' modes have been found for models using the hydrogenic method of opacity generation.

7.5.1 A Detailed Discussion of One Model

This discussion will be based on a model with the same parameters as the model used in the 'one model' discussion of the DXIX opacity table survey (see section 7.4.1) which will be called the DXIX model in this sub-section for simplicity.

In Figure 7.59 we see that a lot of the structure of $|\delta R/R|$ and $|\delta L/L|$ that was present in the DXIX model's eigenfunctions, is no longer present. This has led to the low overtone nodes becoming more distinct and to the merging of the higher overtone anti-nodes, making it more difficult to differentiate between them.

$\Phi(\delta R/R)$ for the eigen modes (see Figure 7.60), with the exception of mode 3, are similar to those of the pure helium model (see Figure 7.4) with the 'steps' smoothed out, as was the case in the DXIX model. In this case, however, there is no increase in $\Phi(\delta R/R)$ towards the envelope's inner boundary (R.H.S.). The loss of phase in $\Phi(\delta R/R)$ in the outer part of envelope for mode 3 appears to be due to the loss of 'driving' from the He-He⁺ ionisation region (see Figure 7.61).

In Figure 7.59, it can be seen that $|\delta L/L|$ has a distinct drop at the 15,000 K He-He⁺ opacity edge (see Figure 4.7), as was the case for the pure helium models. Although this time the drop is not so sharp or deep, due to the presence of carbon (C⁺⁺-C⁺⁺⁺ transition). The left peak in $|\delta L/L|$ is due to He⁺-He⁺⁺ as it was in the DXIX models, which with the C⁺⁺-C⁺⁺⁺ region make up the dual 'driving' peak seen in the work function for the fundamental mode (see Figure 7.61). In this model, the highly ionised carbon atoms have little effect, only appearing as minor spikes in Figures 7.59 and 7.60 .

The only change in $|\delta T/T|$ is that it returns to zero in the inner part of the envelope, in contrast to that found in the DXIX model. The changes in $\Phi(\delta L/L)$ and $\Phi(\delta T/T)$ are similar in nature to those seen in the DXIX model and so will not be discussed again here. Finally, it is worth comparing the work functions of this model with that of the DXIX model (see Figure 7.33) as this shows how the difference in opacity can alter the fundamental behaviour of the envelope, i.e., this model's 'driving' zones are much clearer than those of the DXIX model. Again, convection was negligible throughout the envelope and is probably attributable to the presence of carbon, as the same was found in the DXIX model.

7.5.2 Fundamental Eigenfunctions of the 1 M₀ Models

Comparing Figures 7.62 - 7.63 with those for the pure helium models (Figures 7.6 - 7.7) we can see that for effective temperatures below 15,000 K and luminosities below 15,000L₀ the $|\delta T/T|$ graphs are very similar in shape. The major differences are in amplitude and a small value of $|\delta T/T|$ in the inner regions of the envelope due to the presence of carbon. This is quite different to that seen in opacity table DXIX models (Figures 7.34 - 7.35) where $|\delta T/T|$ is quite

LINEAR NON-ADIABATIC RESULTS

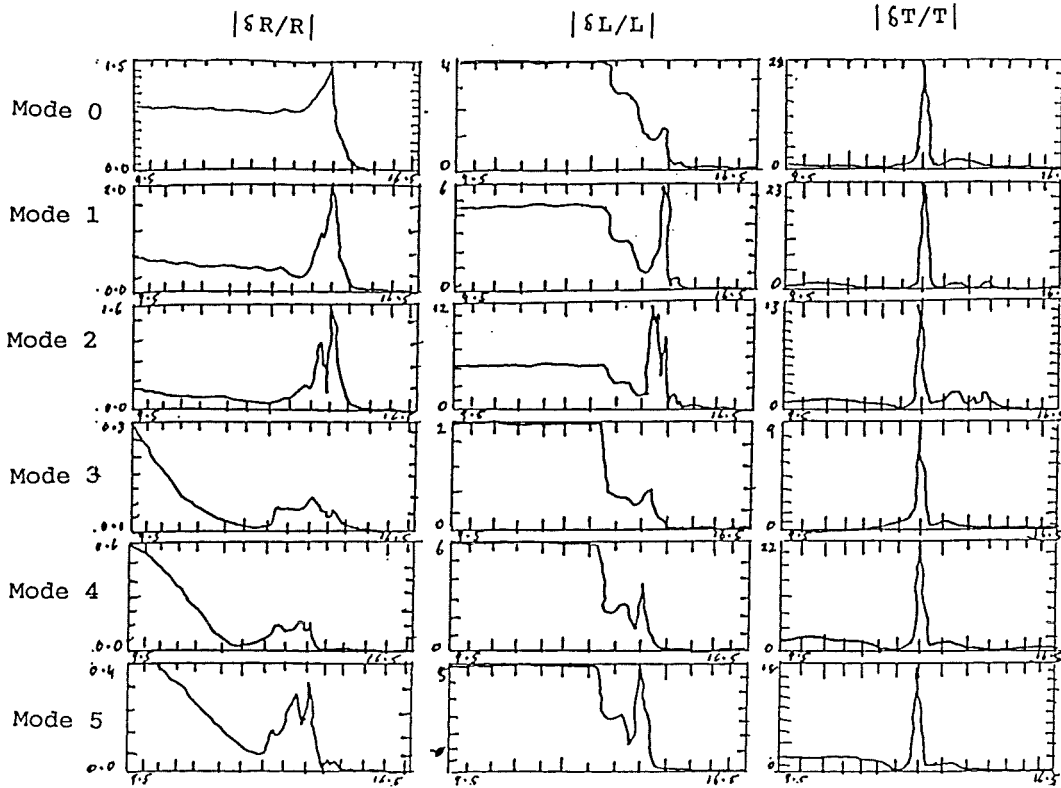


Figure 7.59 : This figure shows $|\delta R/R|$, $|\delta L/L|$ and $|\delta T/T|$ versus $\log(M-m) - 24$ for the first 6 eigen modes of the $1M_{\odot}$ BD9C model with $L/L_{\odot} = 10,000$ and $T_{\text{eff}} = 7,000$ K.

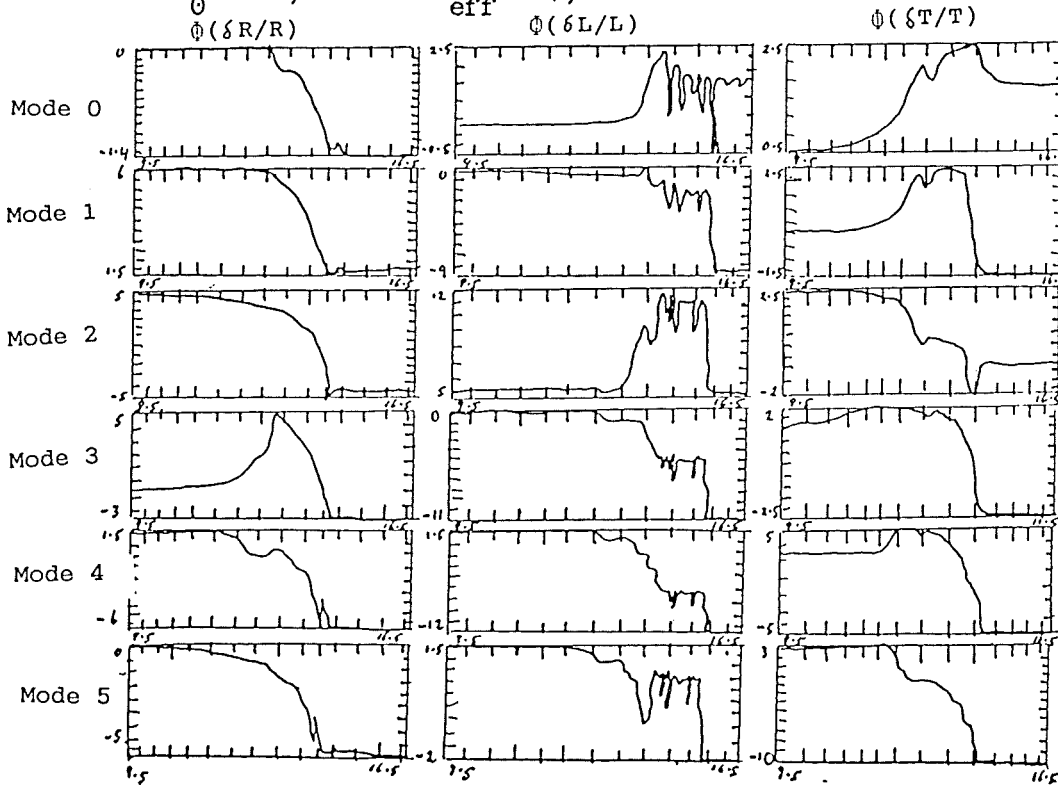


Figure 7.60 : This figure shows $\phi(\delta R/R)$, $\phi(\delta L/L)$ and $\phi(\delta T/T)$ versus $\log(M-m) - 24$ for the first 6 eigen modes of the $1M_{\odot}$ BD9C model with $L/L_{\odot} = 10,000$ and $T_{\text{eff}} = 7,000$ K.

LINEAR NON-ADIABATIC RESULTS

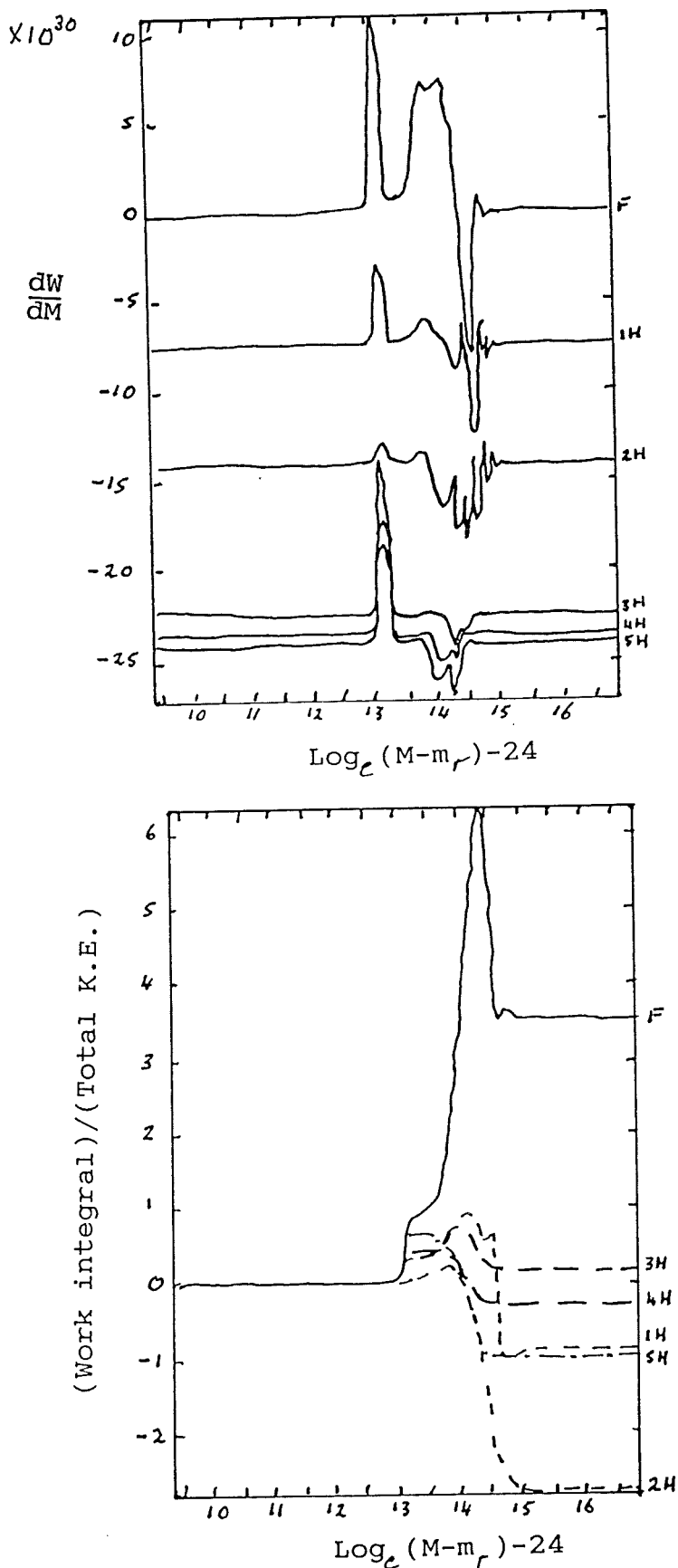


Figure 7.61 : This figure shows the work function and work integral versus $\log(M-m_r) - 24$ for the first 6 eigen modes of the $1M_{\odot}$ BD9C model with $L/L_{\odot} = 10,000$ and $T_{\text{eff}} = 7,000$ K.

LINEAR NON-ADIABATIC RESULTS

prominent throughout the envelope. Above the above limits, we can see an additional peak in $|\delta T/T|$, due to $C^{++}-C^{+++}$ ionisation. Thus the temperature perturbations, $|\delta T/T|$ are not greatly affected by the presence of carbon in the envelope, as they were for the DXIX opacity table models. In $|\delta T/T|$ we can also see that the peaks are nearer the inner boundaries of the envelopes, which is probably due to the smaller envelope masses.

On comparing Figures 7.64 - 7.65 with those for the pure helium models (Figures 7.8 - 7.9) it can be seen that a lot of the valleys in $|\delta L/L|$ have been filled in by the carbon features, and the shapes are similar to those found for opacity table DXIX models (Figures 7.36 - 7.37). In this case however, the bumps due to various levels of carbon ionisation are less prominent or absent altogether. This reduction in the size of these bumps for the BD9C models can be attributed to the decrease in envelope density compared to that of the DXIX opacity models and to a corresponding decrease in opacity. The differences in $|\delta L/L|$ are especially noticeable for effective temperatures below 15,000 K as then the outer envelope opacities are much smaller in the BD9C opacity table models than in the equivalent DXIX opacity table models.

Again, comparing Figures 7.66 - 7.67 for $|\delta R/R|$ with those of the DXIX opacity table models (Figures 7.38 - 7.39) we see a similarity in shape, although the amplitude of perturbation is less in the BD9C opacity table models, as well as the anti-nodes are more compressed with respect to mass. This can be attributed to the narrower $|\delta T/T|$ peak and the corresponding large drop in opacity at 15,000 K.

LINEAR NON-ADIABATIC RESULTS

Convection in these models was inefficient for $T_{\text{eff}} < 5,500$ K, and confined to a small region near the inner boundary. In models below $T_{\text{eff}} = 5,500$ K, convection sometimes grew very efficient throughout the inner envelope and in the models with blank graphs prevented convergence. The other blank graphs are due to codes not finding the fundamental mode or finding a secular mode instead. None of the models considered here had any 'strange' fundamental modes, although many were very non-adiabatic.

In summary, these models are similar to DXIX opacity table models in $|\delta R/R|$ and $|\delta L/L|$, though the effect of carbon is muted somewhat. Carbon is still the main cause of the structure seen in $|\delta L/L|$. On the other hand, helium plays the main role in the temperature perturbations, $|\delta T/T|$, of these models with carbon only causing a slight increase in $|\delta T/T|$ towards the inner boundary of envelope, or when effective temperature and luminosity become large. Even then, helium is the main contributor to $|\delta T/T|$. In this discussion the graphs of models in which the fundamental mode was unstable have been drawn using a broken line.

LINEAR NON-ADIABATIC RESULTS

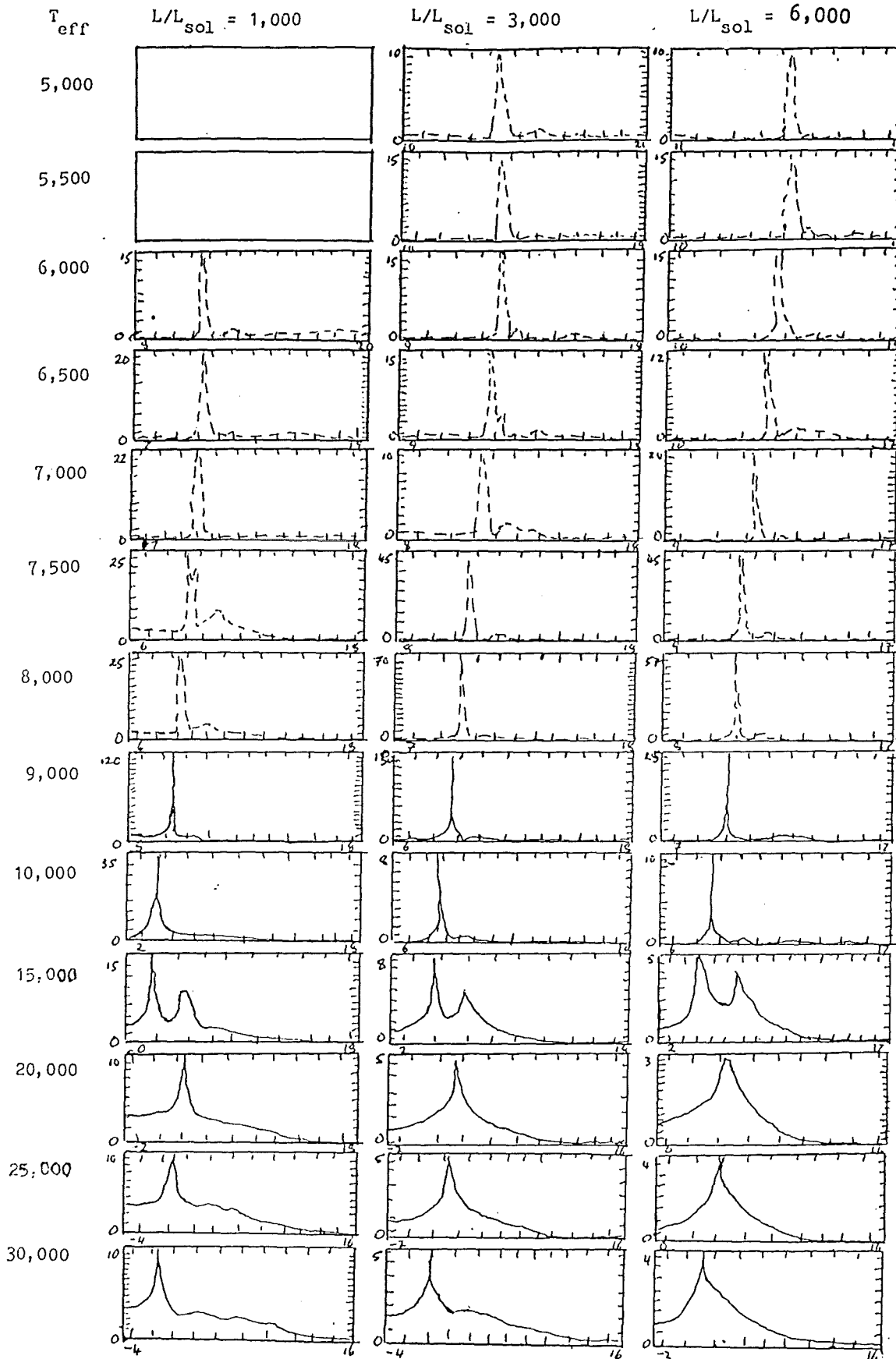


Figure 7.62 : This figure shows plots of $|\delta T/T|$ versus $\log(M-m) - 24$ for the Low luminosity fundamental modes of the $1M_{\odot}$ models of the survey using opacity table BD9C.

LINEAR NON-ADIABATIC RESULTS

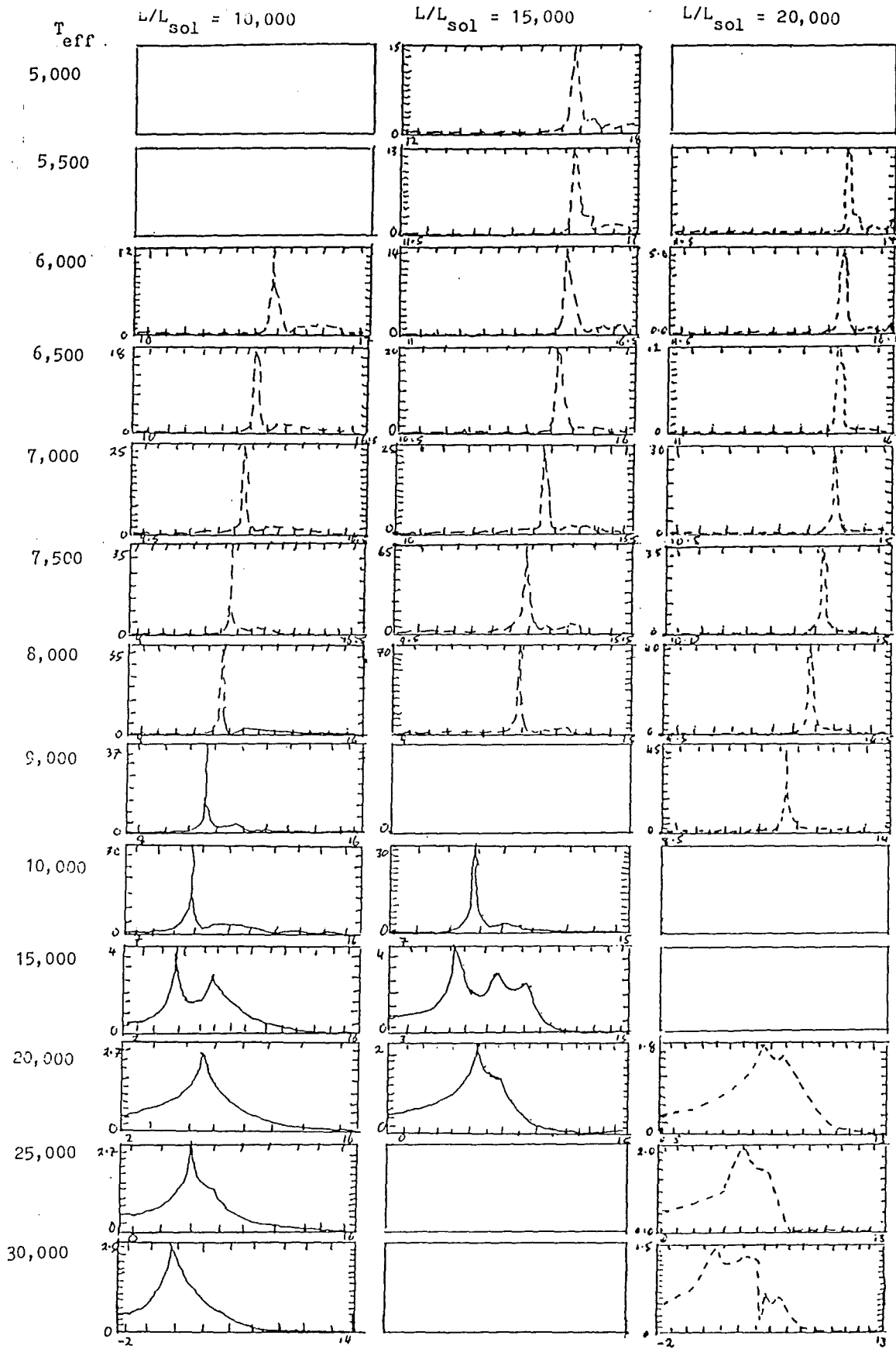


Figure 7.63 : This figure shows plots of $\log(T/T_1)$ versus $\log(M-m_r) - 24$ for the High luminosity fundamental modes of the $1M_{\odot}$ models of the survey using opacity table BD9C.

LINEAR NON-ADIABATIC RESULTS

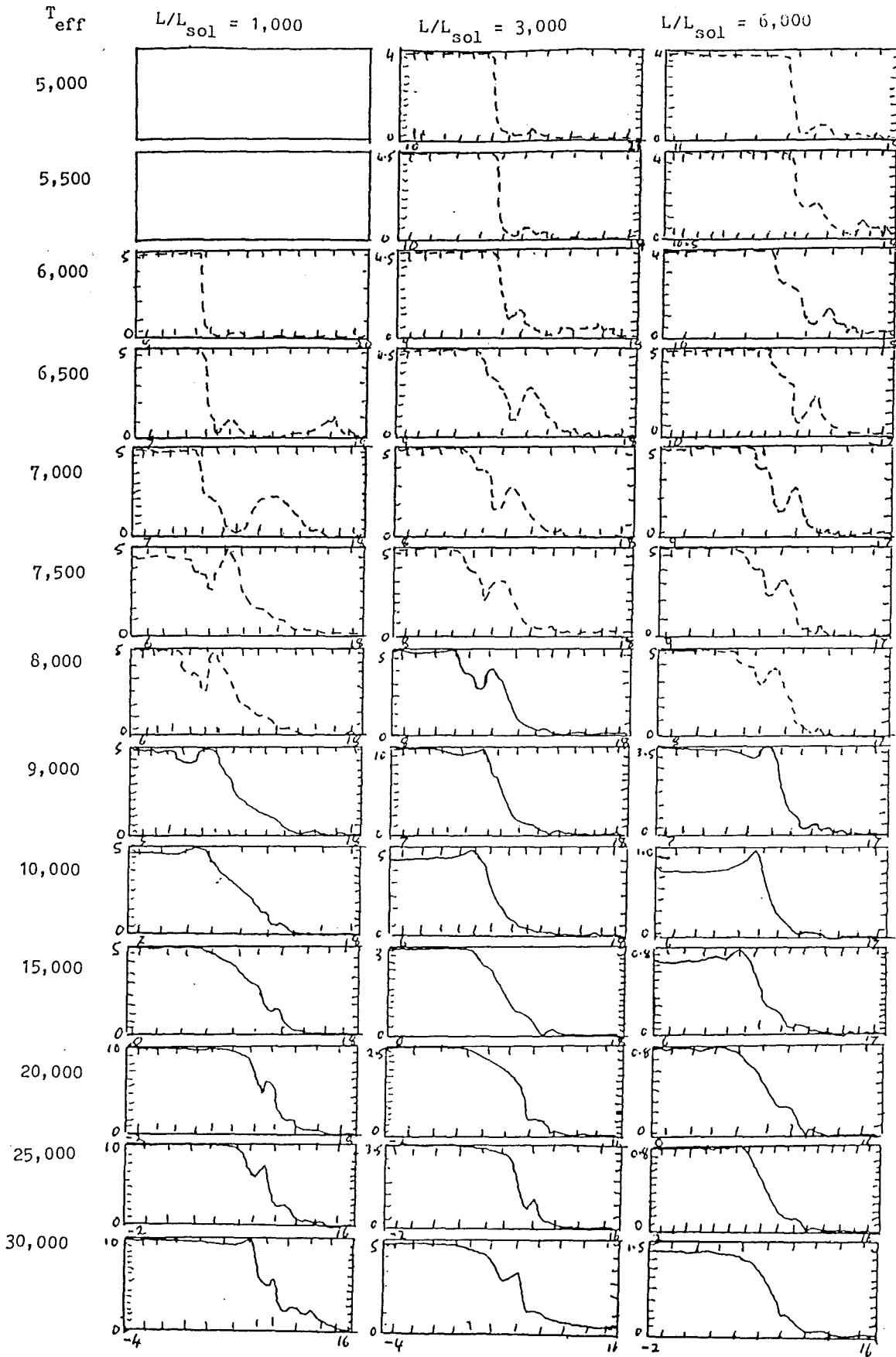


Figure 7.64 : This figure shows plots of $\log(L/L_{sol})$ versus $\log(M - m_r) - 24$ for the Low luminosity fundamental modes of the $1M_{\odot}$ models of the survey using opacity table BD9C.

LINEAR NON-ADIABATIC RESULTS

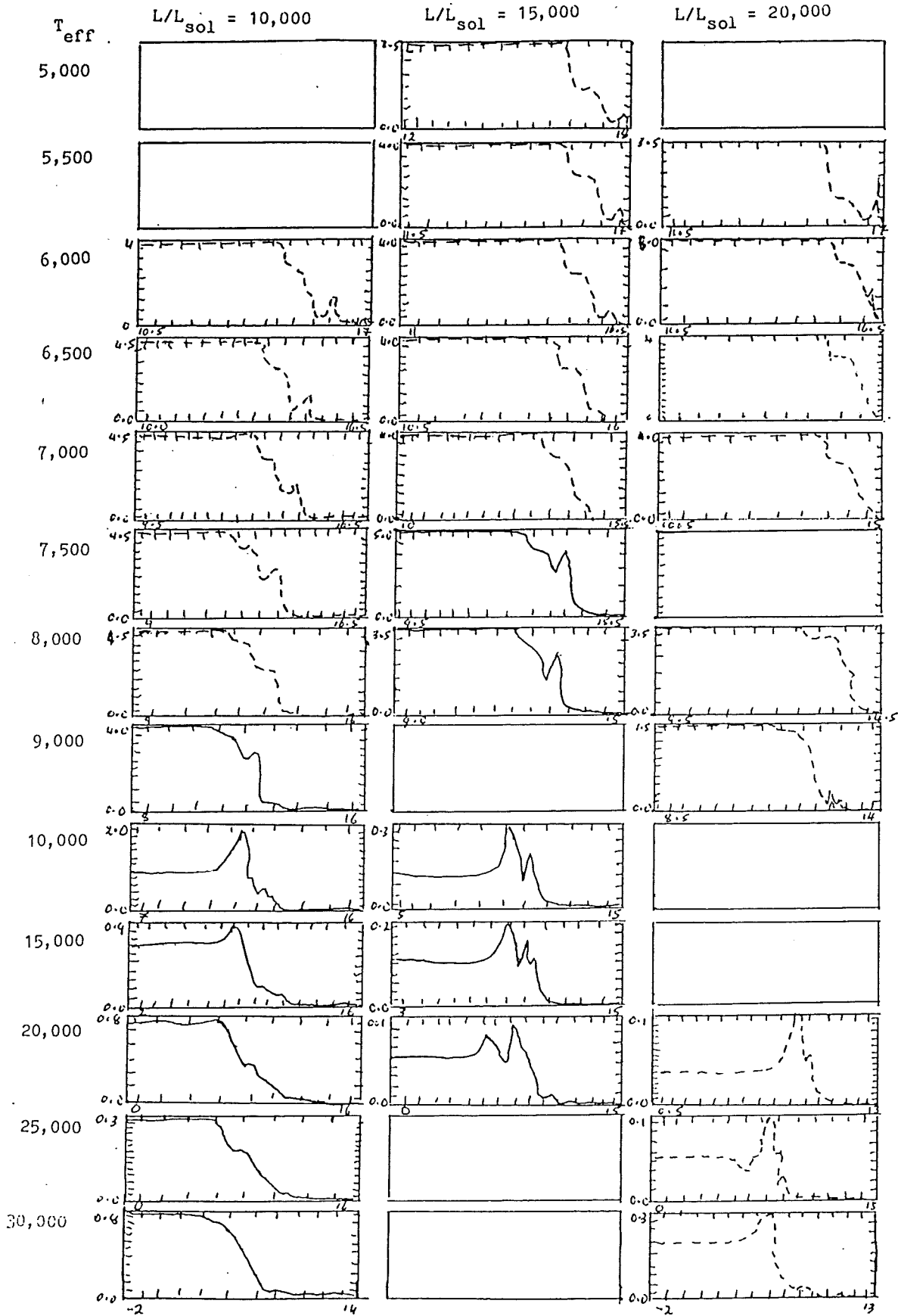


Figure 7.65 : This figure shows plots of $\log(L/L_{sol})$ versus $\log(M-m_r) - 24$ for the High luminosity fundamental modes of the $1M_{\odot}$ models of the survey using opacity table BD9C.

LINEAR NON-ADIABATIC RESULTS

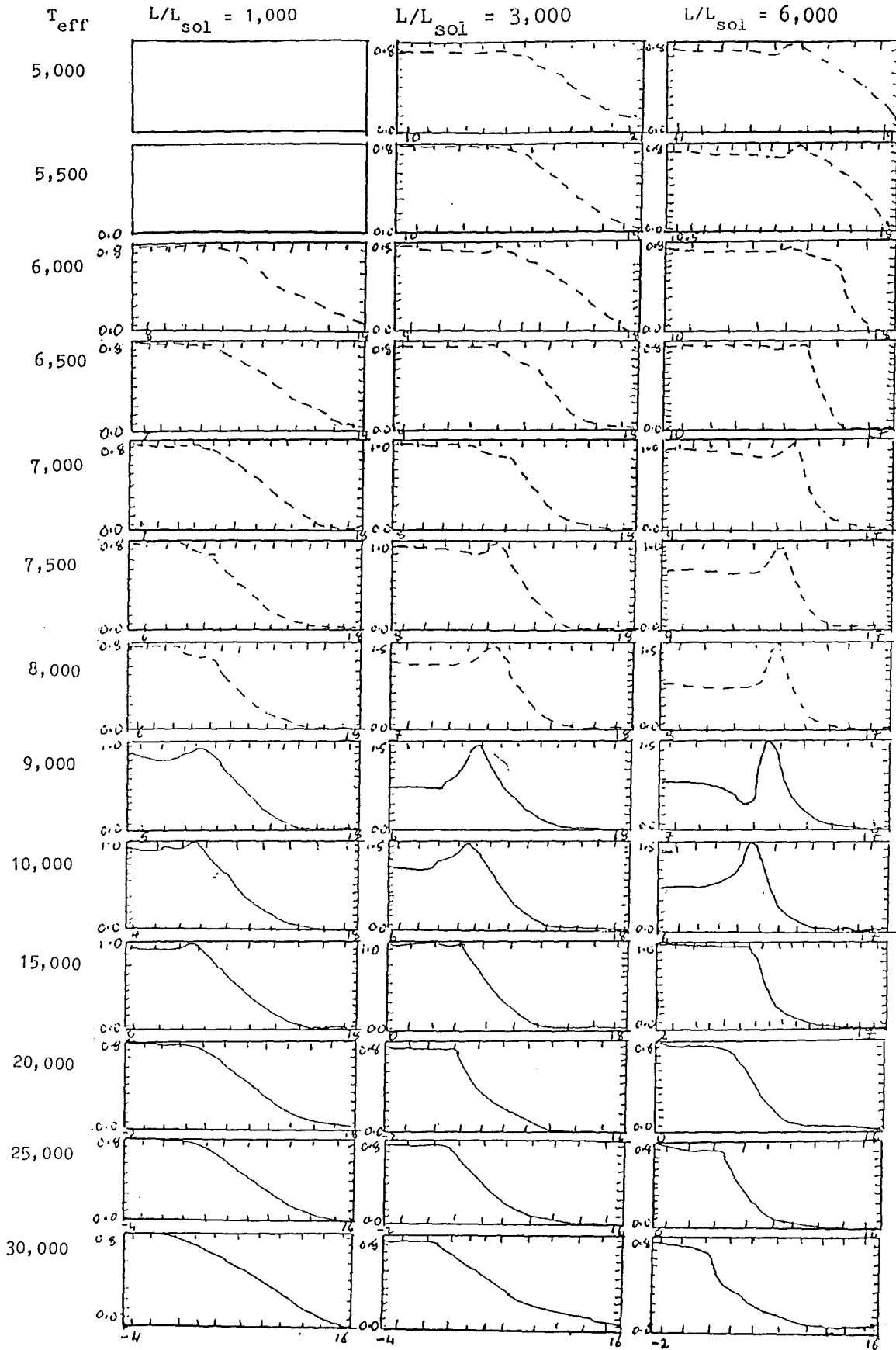


Figure 7.66 : This figure shows plots of $\log(R/R_1)$ versus $\log(M-m)-24$ for the Low luminosity fundamental modes of the $1M_{\odot}$ models of the survey using opacity table BD9C.

LINEAR NON-ADIABATIC RESULTS

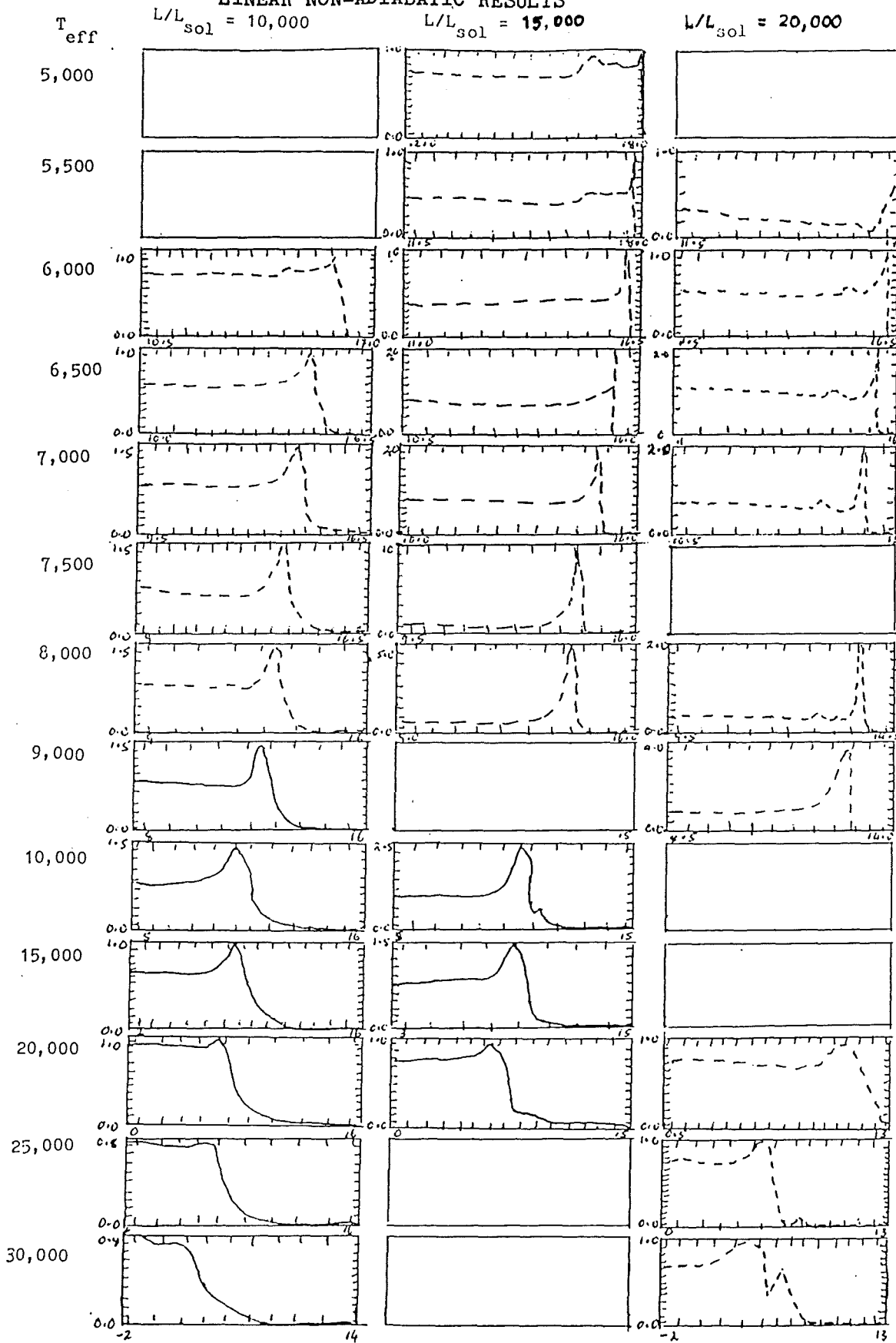


Figure 7.67 : This figure shows plots of $\text{Re}(R)/\text{Im}(R)$ versus $\log(M - m_r) - 24$ for the High luminosity fundamental modes of the $1M_{\odot}$ models of the survey using opacity table BD9C.

7.5.3 Presentation of Results

In the following sub-sections, the results of the BD9C opacity table survey will be given in graphical form, together with several polynomial fits to the fundamental and first overtone data. The raw data has been tabulated for the fundamental and first overtone modes and can be found in the BD9C section of Appendix E (pages E-37 to E-54).

The graphs are in groups of 4 showing from top left to bottom right:

- TOP LEFT : adiabatic and non-adiabatic Log (period) vs Log (T_{eff})
- TOP RIGHT : adiabatic and non-adiabatic Log (Q) vs Log (T_{eff})
- BOTTOM LEFT : non-adiabatic Growth Rate vs Log (T_{eff})
- BOTTOM RIGHT : Nonadiabatic Π^c vs Log (T_{eff}).

where Π^c is the phase change in degree of $\Phi(\delta R/R)$ between the inner and outer boundaries of the model envelope in question. The symbols and lines used in the graphs are given below to maximise the size of the graphs and reduce repetition:

- DOTTED SOLID LINE - Shows the adiabatic fundamental modes
- LIGHT SOLID LINE - Shows the adiabatic first overtone modes
- CHAINED LINE - Shows the adiabatic second overtone modes
- DOTTED LINE - Shows the adiabatic third overtone modes
- + PLUS - Shows the non-adiabatic fundamental modes
- * ASTERISK - Shows the non-adiabatic first overtone modes
- O CIRCLE - Shows the non-adiabatic second overtone modes
- X CROSS - Shows the non-adiabatic third overtone modes.

LINEAR NON-ADIABATIC RESULTS

For each mass in the survey three polynomial fits have been made to the data. The first of these will fit the following polynomial to non-adiabatic $\text{Log}(\text{Period})$, with $\text{Log}(T_{\text{eff}})$ as the independent variable at each luminosity.

$$\text{Log}(\text{Period}) = a_0 + a_1 \cdot \text{Log}(T_{\text{eff}}) + a_2 \cdot [\text{Log}(T_{\text{eff}})]^2$$

A table of the coefficients at each luminosity, together with the mean residual, M.R., of fits and range in effective temperature, over which fits were made, will be given for each mass and mode considered.

The second and third fits will fit a [2D] polynomial of the form:

$$X = \sum_{i=0}^2 \sum_{j=0}^2 B_{ij} [\text{Log}(T_{\text{eff}})]^i [\text{Log}(L/L_0)]^j, \quad \forall i+j = 1, 2,$$

where X is the non-adiabatic $\text{Log}(\text{Period})$ in the second fit, and non-adiabatic $\text{Log}(Q)$ in the third fit. For each mass, for the modes considered, the range in T_{eff} at each luminosity over which the fit was made is the same as that used in the first fits. For each fit the root mean of the residual squares divided by the range of X used in the fit is given as a percentage (X_1) alongside the polynomial coefficients.

LINEAR NON-ADIABATIC RESULTS

7.5.3.1 Survey Results for 0.8 M_{\odot} Models - Table 7.13, below gives the coefficients of fits to the non-adiabatic fundamental mode Log (periods) at constant luminosities.

L/L_{\odot}	a_0	a_1	a_2	M.R	$\text{Log}(T_{\text{eff}})$
1,000	21.588	-7.239	0.474	0.00910	3.778 - 4.301
3,000	19.105	-5.653	0.267	0.09095	3.699 - 4.398
6,000	48.904	-2.064	2.162	0.01235	3.699 - 4.477
10,000	35.000	-1.404	1.333	0.03627	3.699 - 4.477
15,000	-12.657	9.920	-1.423	0.05320	3.699 - 4.477
20,000	18.653	-6.277	0.483	0.07129	3.699 - 4.477

TABLE 7.13 : Table of coefficients of first fit for fundamental mode.

The coefficients for the [2D] fit to the non-adiabatic fundamental mode Log (periods) are:

$$b_{00} = 9.345 \quad b_{01} = 0.873 \quad X_1 = 5.32\% \quad i+j = 1$$

$$b_{10} = -2.913$$

$$b_{00} = 29.305 \quad b_{10} = -11.807 \quad X_1 = 4.21\% \quad i+j = 2$$

$$b_{01} = 0.049 \quad b_{11} = 0.900$$

$$b_{02} = -0.380 \quad b_{20} = 0.661$$

The coefficients for the [2D] fit to the non-adiabatic fundamental mode Log (Q's) are:

$$b_{00} = -1.896 \quad b_{01} = 0.117 \quad X_1 = 20.41\% \quad i+j = 1$$

$$b_{10} = 0.068$$

$$b_{00} = 13.561 \quad b_{10} = -6.454 \quad X_1 = 17.19\% \quad i+j = 2$$

$$b_{01} = -0.894 \quad b_{11} = 0.913$$

$$b_{02} = -0.359 \quad b_{20} = 0.363$$

LINEAR NON-ADIABATIC RESULTS

Table 7.14, below gives the coefficients of fits to the non-adiabatic first overtone mode Log (periods) at constant luminosities.

L/L_0	a_0	a_1	a_2	M.R	$\text{Log}(T_{\text{eff}})$
1,000	18.068	-5.788	0.321	0.00755	3.778 - 4.301
3,000	18.017	-5.642	0.314	0.01382	3.699 - 4.398
6,000	45.587	-19.640	2.100	0.04094	3.699 - 4.477
10,000	18.068	-5.788	3.214	0.01235	3.699 - 4.477
15,000	24.506	-8.931	0.759	0.10737	3.699 - 4.477
20,000	56.031	-2.436	2.640	0.05094	3.699 - 4.477

TABLE 7.14 : Table of coefficients of first fit for first overtone mode.

The coefficients for the [2D] fit to the non-adiabatic first overtone mode Log (periods) are:

$$b_{00} = 9.104 \quad b_{01} = 0.701 \quad X_1 = 5.08\% \quad i+j = 1$$

$$b_{10} = -2.769$$

$$b_{00} = 34.187 \quad b_{10} = -15.783 \quad X_1 = 4.04\% \quad i+j = 2$$

$$b_{01} = 1.532 \quad b_{11} = 0.154$$

$$b_{02} = -0.202 \quad b_{20} = 1.521$$

The coefficients for the [2D] fit to the non-adiabatic first overtone mode Log (Q's) are:

$$b_{00} = -2.240 \quad b_{01} = -0.833 \quad X_1 = 12.57\% \quad i+j = 1$$

$$b_{10} = 0.262$$

$$b_{00} = 24.043 \quad b_{10} = -13.178 \quad X_1 = 9.03\% \quad i+j = 2$$

$$b_{01} = 0.578 \quad b_{11} = 0.251$$

$$b_{02} = -0.230 \quad b_{20} = 1.526$$

The results presented here will be discussed in Section 7.5.4 .

LINEAR NON-ADIABATIC RESULTS

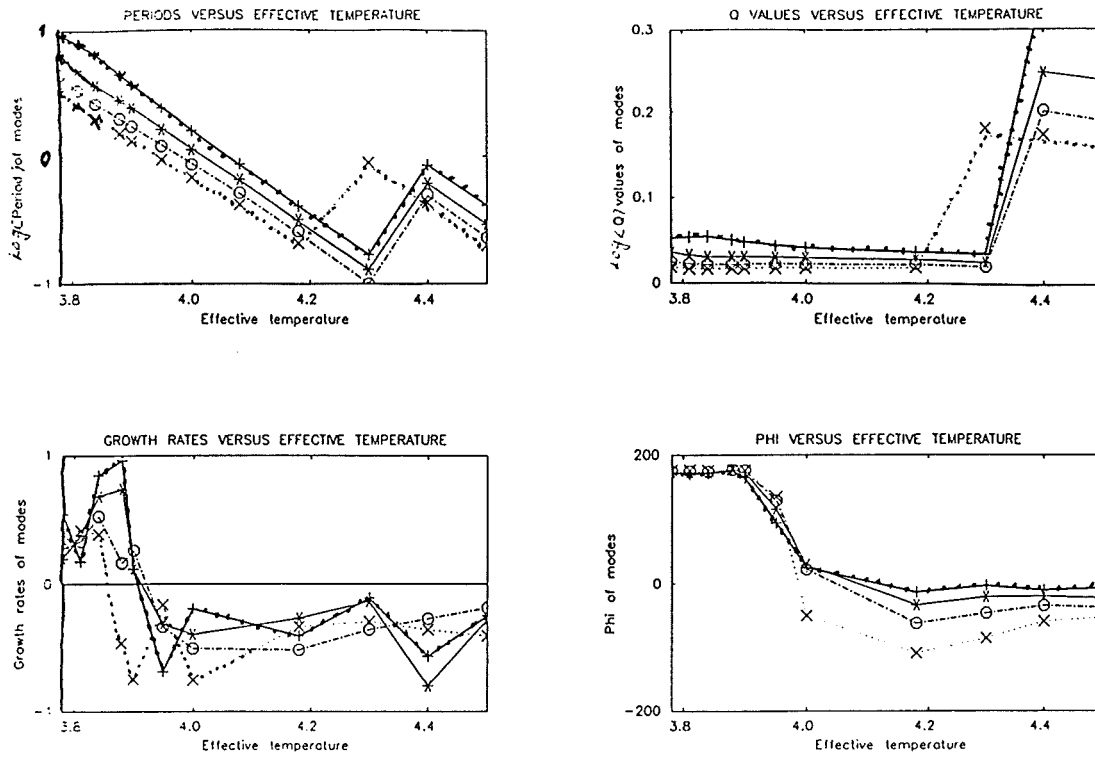


Figure 7.68 : Pulsation parameters for $L/L_{\odot} = 1,000$ and $M/M_{\odot} = 0.8$ (BD9C opacity table).

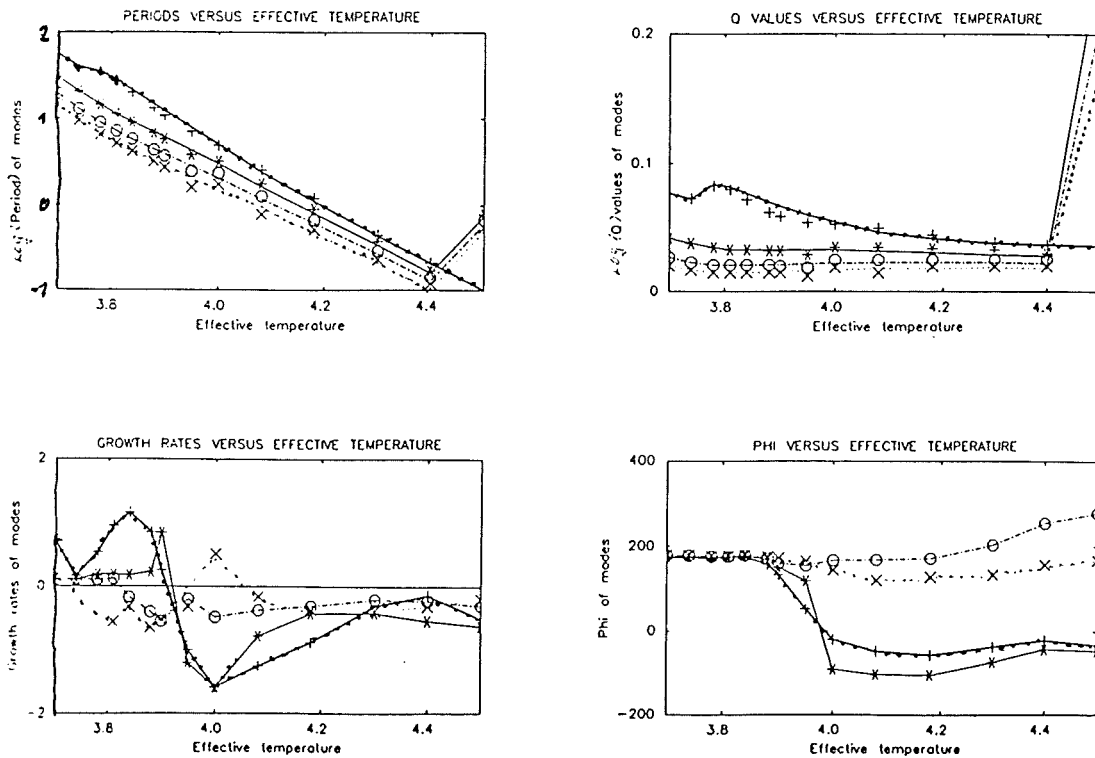


Figure 7.69 : Pulsation parameters for $L/L_{\odot} = 3,000$ and $M/M_{\odot} = 0.8$ (BD9C opacity table).

LINEAR NON-ADIABATIC RESULTS

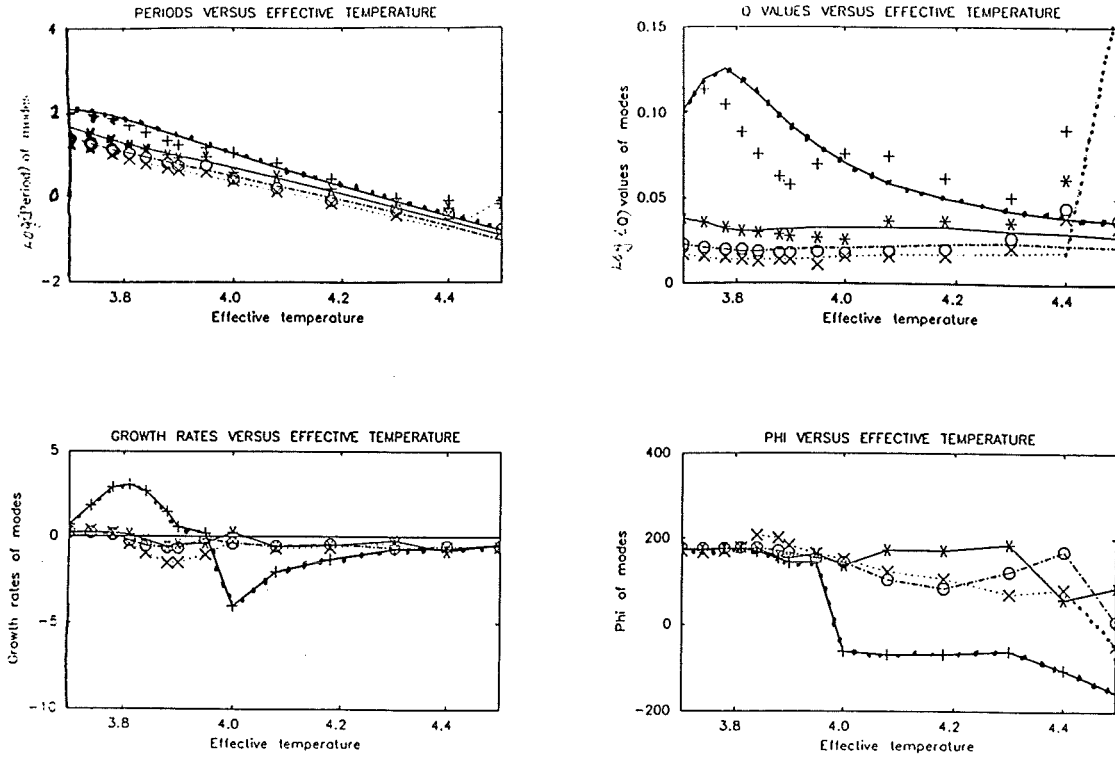


Figure 7.70 : Pulsation parameters for $L/L_{\odot} = 6,000$ and $M/M_{\odot} = 0.8$ (BD9C opacity table).

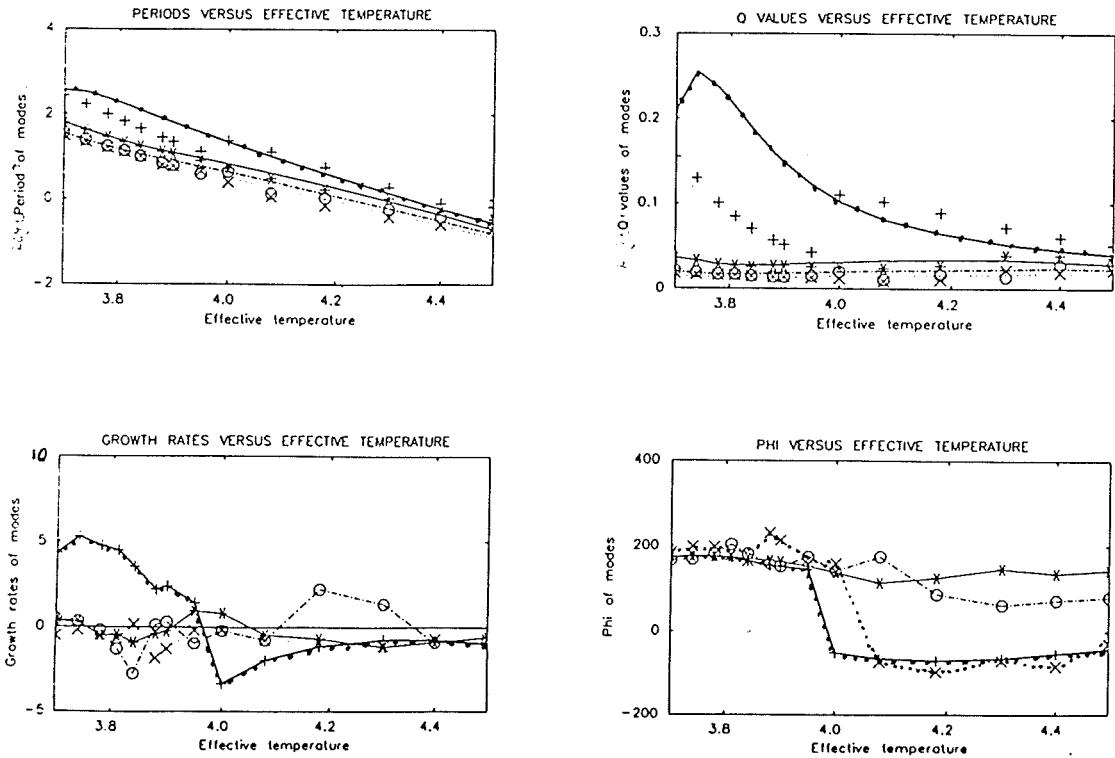


Figure 7.71 : Pulsation parameters for $L/L_{\odot} = 10,000$ and $M/M_{\odot} = 0.8$ (BD9C opacity table).

LINEAR NON-ADIABATIC RESULTS

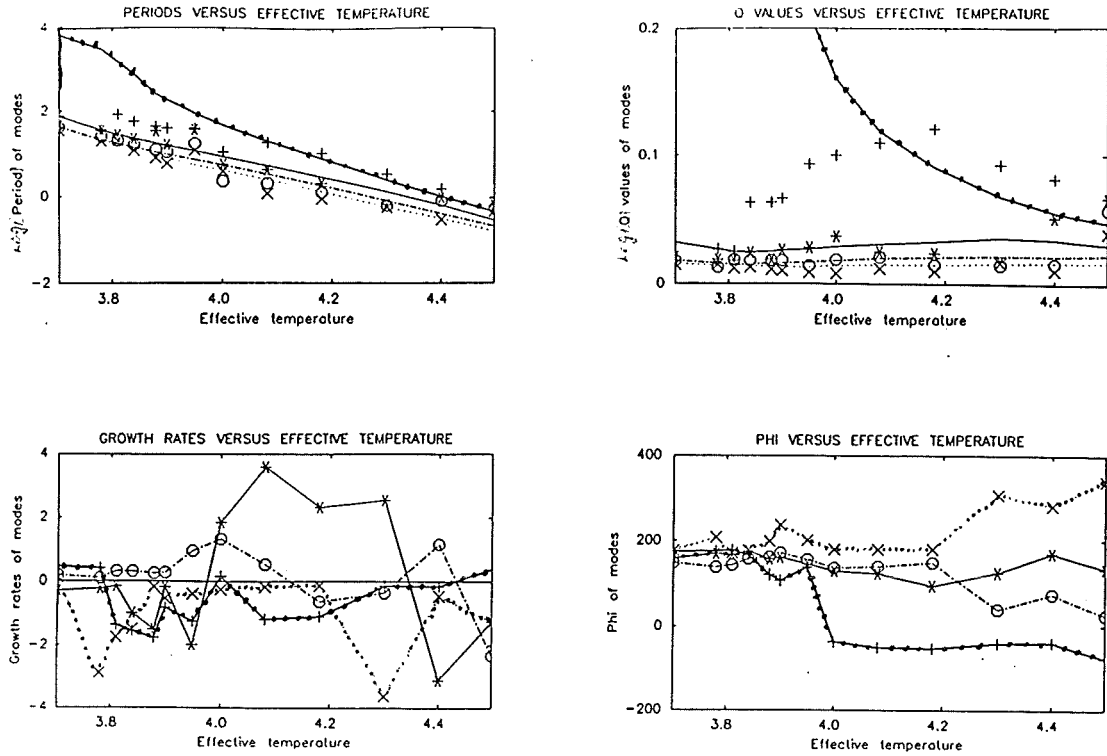


Figure 7.72 : Pulsation parameters for $L/L_{\odot} = 15,000$ and $M/M_{\odot} = 0.8$ (BD9C opacity table).

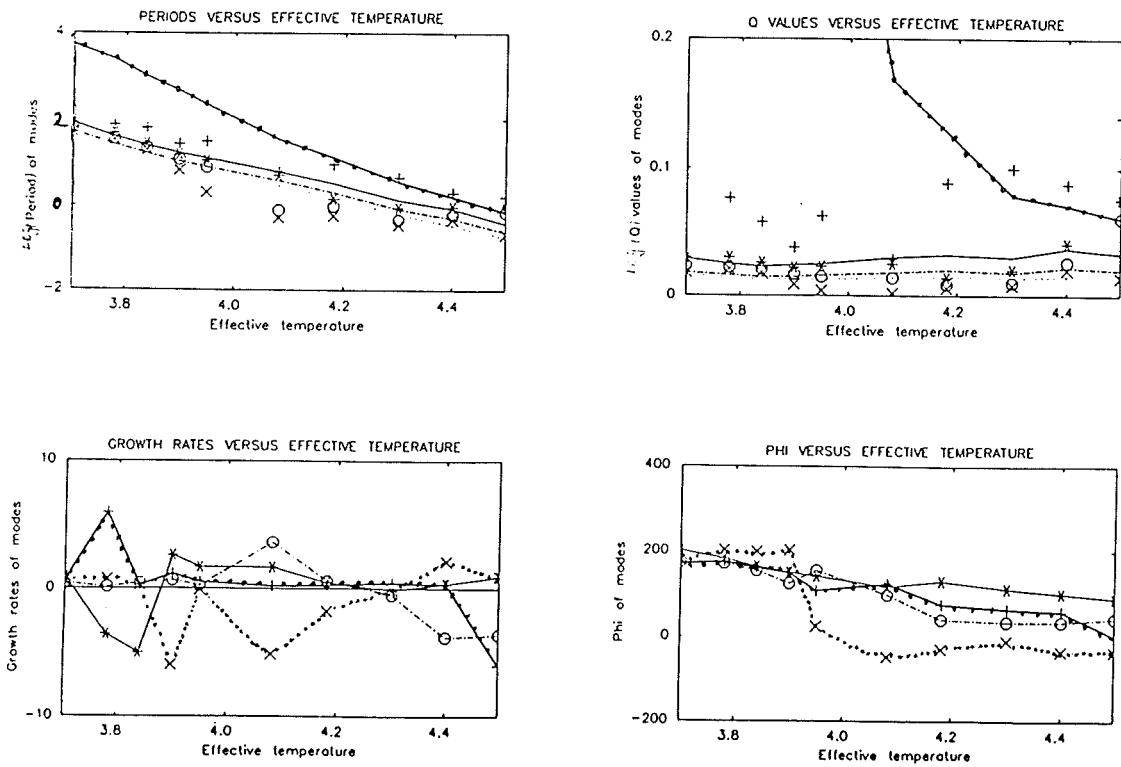


Figure 7.73 : Pulsation parameters for $L/L_{\odot} = 20,000$ and $M/M_{\odot} = 0.8$ (BD9C opacity table).

LINEAR NON-ADIABATIC RESULTS

7.5.3.2 Survey Results for 1.0 M_{\odot} Models - Table 7.15, below gives the coefficients of fits to the non-adiabatic fundamental mode Log (periods) at constant luminosities.

L/L_{\odot}	a_0	a_1	a_2	M.R	$\text{Log}(T_{\text{eff}})$
1,000	26.845	-9.899	0.806	0.00499	3.813 - 4.301
3,000	21.013	-6.711	0.401	0.01139	3.740 - 4.398
6,000	17.525	-4.763	0.152	0.01603	3.699 - 4.477
10,000	22.883	-7.356	0.479	0.03881	3.699 - 4.477
15,000	23.634	-7.846	0.566	0.05511	3.699 - 4.477
20,000	-26.172	1.597	-2.266	0.05058	3.699 - 4.477

TABLE 7.15 : Table of coefficients of first fit for fundamental mode.

The coefficients for the [2D] fit to the non-adiabatic fundamental mode Log (periods) are:

$$b_{00} = 10.411 \quad b_{01} = 0.939 \quad X_i = 3.96\% \quad i+j = 1$$

$$b_{10} = -3.263$$

$$b_{00} = 17.117 \quad b_{10} = -5.167 \quad X_i = 3.69\% \quad i+j = 2$$

$$b_{01} = -0.488 \quad b_{11} = 0.565$$

$$b_{02} = -0.113 \quad b_{20} = -0.038$$

The coefficients for the [2D] fit to the non-adiabatic fundamental mode Log (Q's) are:

$$b_{00} = -0.830 \quad b_{01} = 0.178 \quad X_i = 17.74\% \quad i+j = 1$$

$$b_{10} = -0.266$$

$$b_{00} = 7.258 \quad b_{10} = -3.171 \quad X_i = 16.45\% \quad i+j = 2$$

$$b_{01} = -0.889 \quad b_{11} = 0.533$$

$$b_{02} = -0.145 \quad b_{20} = 0.304$$

LINEAR NON-ADIABATIC RESULTS

Table 7.16, below gives the coefficients of fits to the non-adiabatic first overtone mode Log (periods) at constant luminosities.

L/L_{\odot}	a_0	a_1	a_2	M.R	$\text{Log}(T_{\text{eff}})$
1,000	12.382	-2.996	-0.024	0.00575	3.813 - 4.301
3,000	15.604	-4.454	0.163	0.00981	3.740 - 4.398
6,000	13.063	-3.155	0.013	0.01725	3.699 - 4.477
10,000	12.382	-2.996	-0.024	0.02351	3.699 - 4.477
15,000	31.885	-1.249	1.186	0.01808	3.699 - 4.477
20,000	-20.130	1.278	-1.863	0.04620	3.699 - 4.477

TABLE 7.16 : Table of coefficients of first fit for first overtone mode.

The coefficients for the [2D] fit to the non-adiabatic first overtone mode Log (periods) are:

$$b_{00} = 9.365 \quad b_{01} = 0.764 \quad X_1 = 2.95\% \quad i+j = 1$$

$$b_{10} = -2.907$$

$$b_{00} = 20.850 \quad b_{10} = -7.009 \quad X_1 = 2.53\% \quad i+j = 2$$

$$b_{01} = -0.842 \quad b_{11} = 0.495$$

$$b_{02} = -0.038 \quad b_{20} = 0.265$$

The coefficients for the [2D] fit to the non-adiabatic first overtone mode Log (Q's) are:

$$b_{00} = -1.903 \quad b_{01} = 0.009 \quad X_1 = 16.26\% \quad i+j = 1$$

$$b_{10} = 0.089$$

$$b_{00} = 9.437 \quad b_{10} = -3.930 \quad X_1 = 13.89\% \quad i+j = 2$$

$$b_{01} = -1.605 \quad b_{11} = 0.501$$

$$b_{02} = -0.053 \quad b_{20} = 0.251$$

The results presented here will be discussed in Section 7.5.4 .

LINEAR NON-ADIABATIC RESULTS

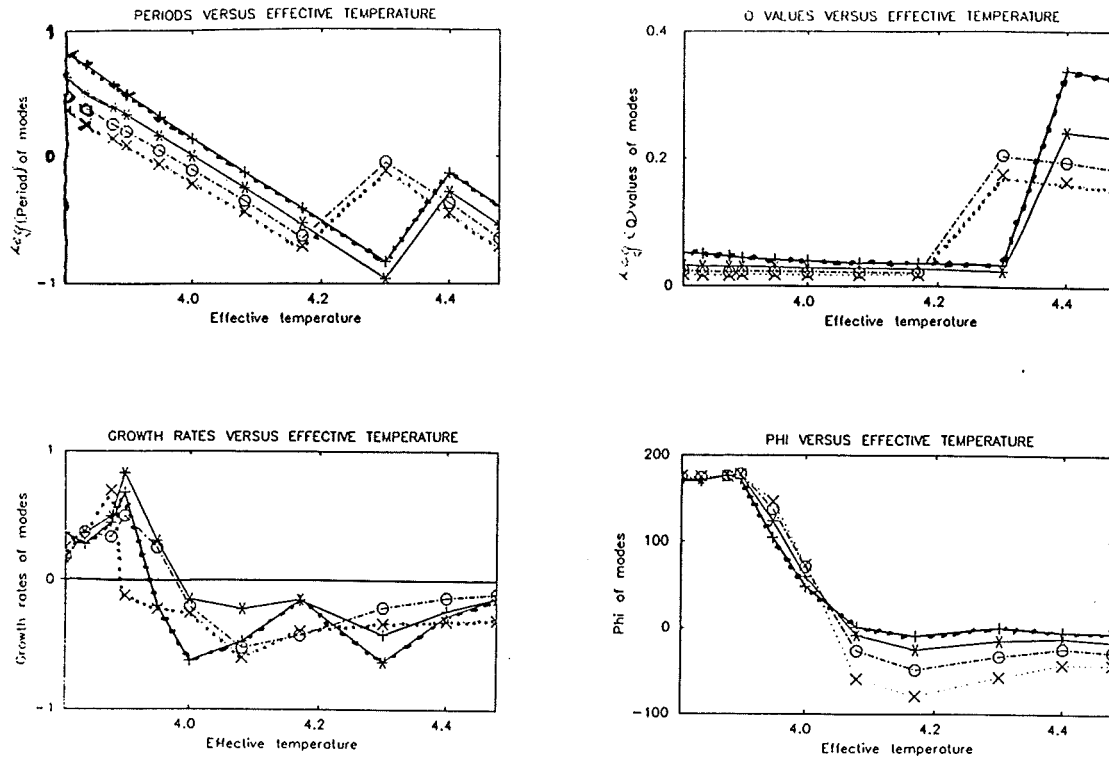


Figure 7.74 : Pulsation parameters for $L/L_{\odot} = 1,000$ and $M/M_{\odot} = 1.0$ (BD9C opacity table).

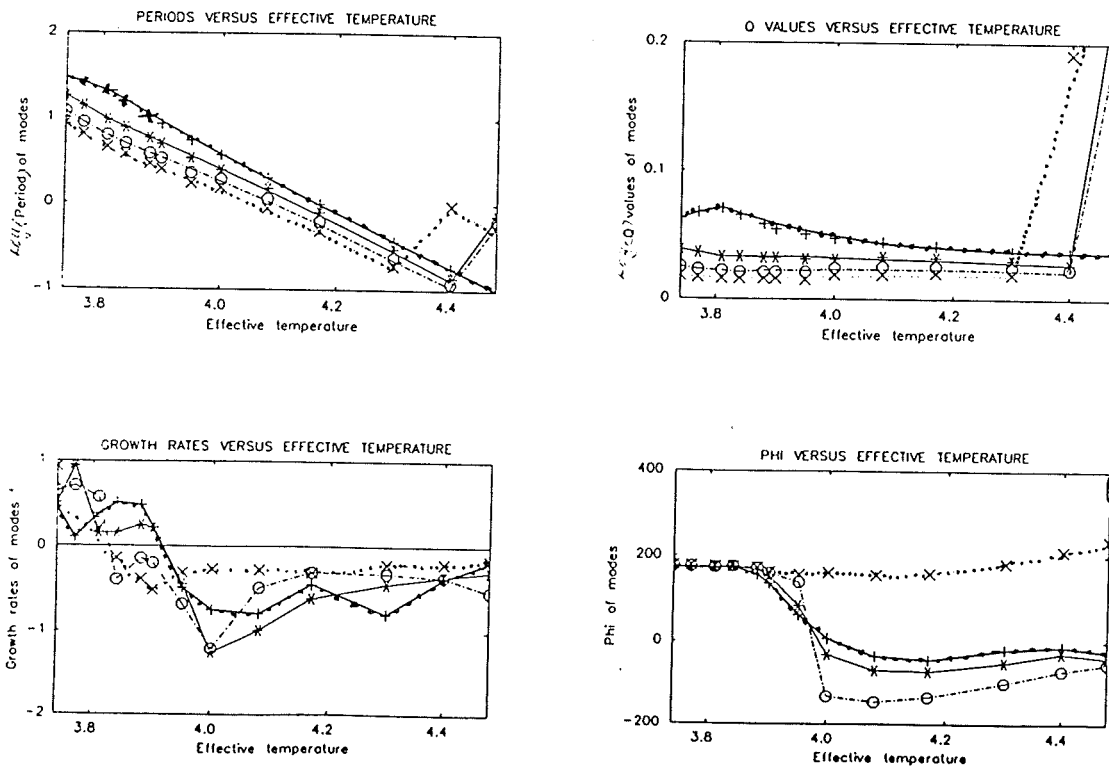


Figure 7.75 : Pulsation parameters for $L/L_{\odot} = 3,000$ and $M/M_{\odot} = 1.0$ (BD9C opacity table).

LINEAR NON-ADIABATIC RESULTS

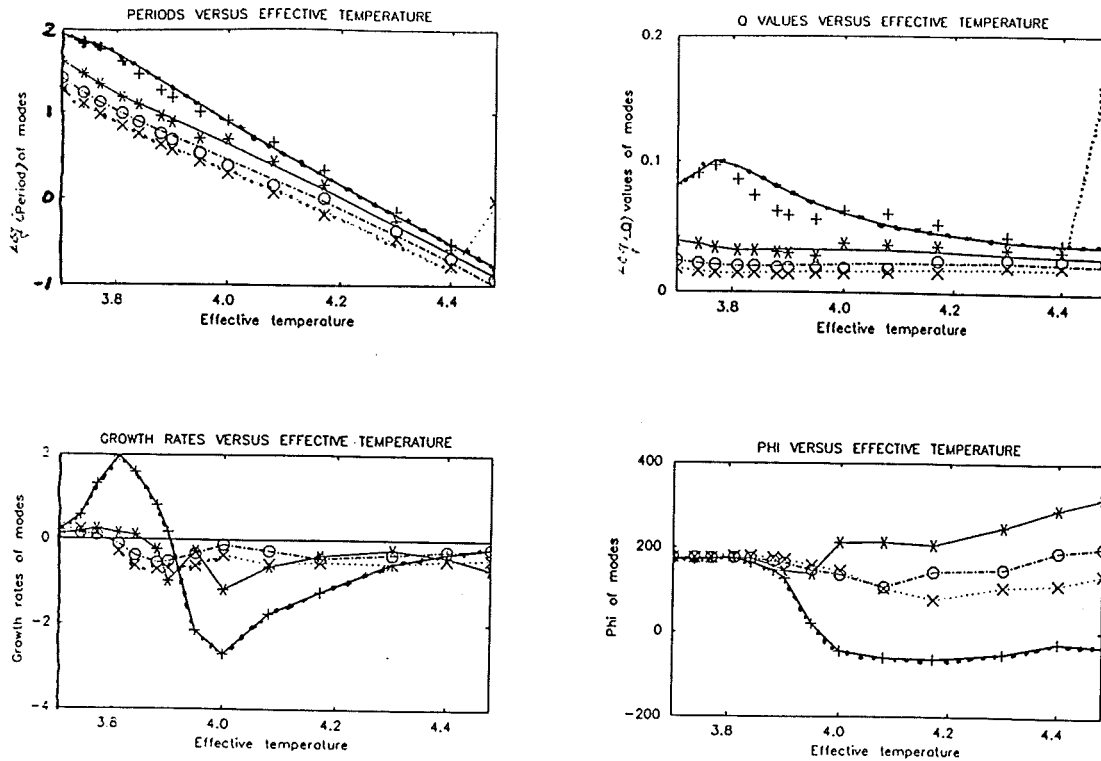


Figure 7.76 : Pulsation parameters for $L/L_{\odot} = 6,000$ and $M/M_{\odot} = 1.0$ (BD9C opacity table).

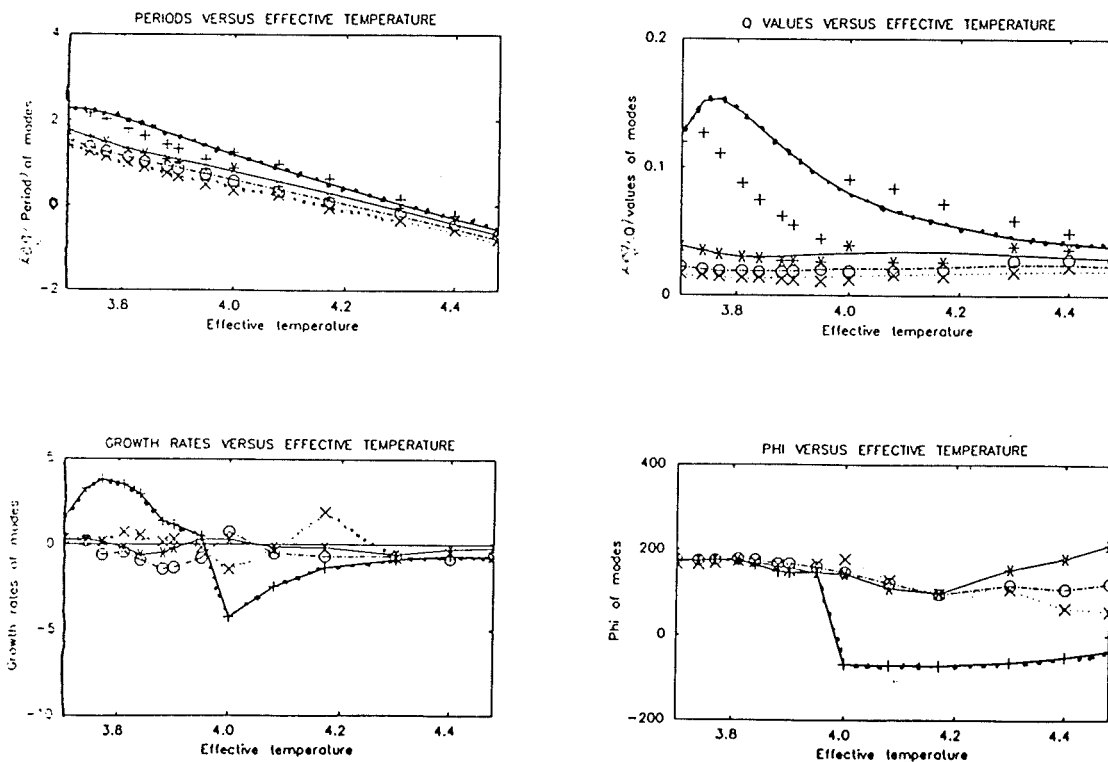


Figure 7.77 : Pulsation parameters for $L/L_{\odot} = 10,000$ and $M/M_{\odot} = 1.0$ (BD9C opacity table).

LINEAR NON-ADIABATIC RESULTS

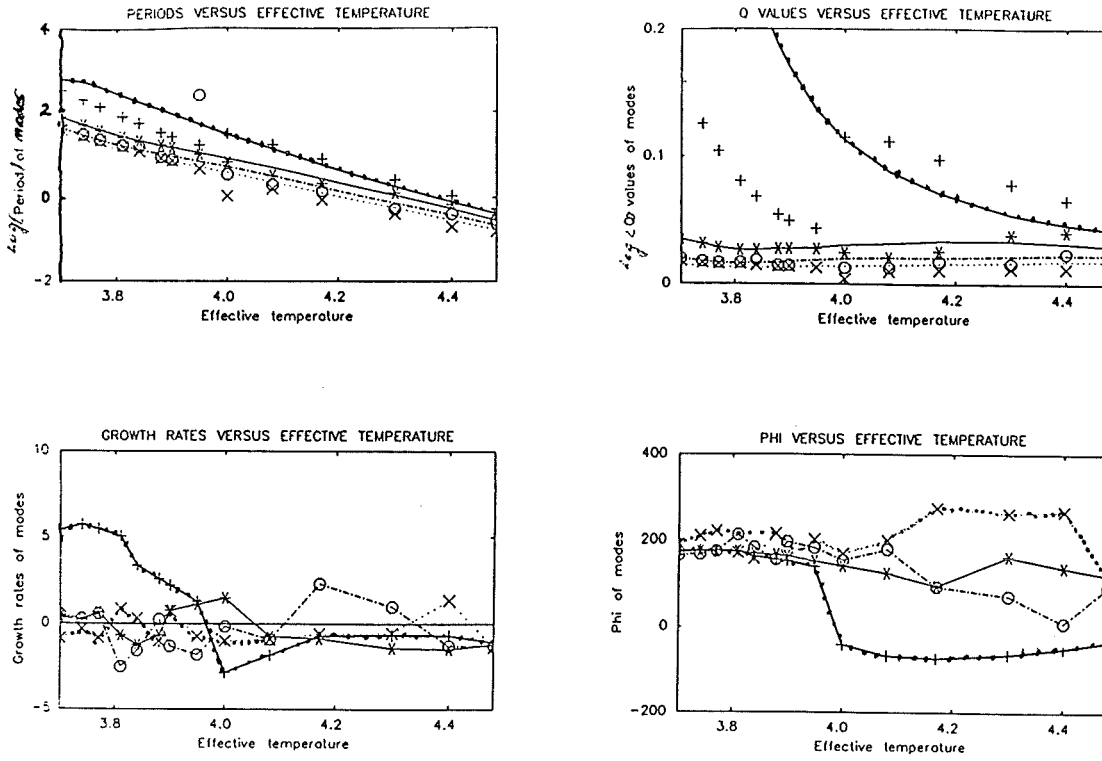


Figure 7.78 : Pulsation parameters for $L/L_{\odot} = 15,000$ and $M/M_{\odot} = 1.0$ (BD9C opacity table).

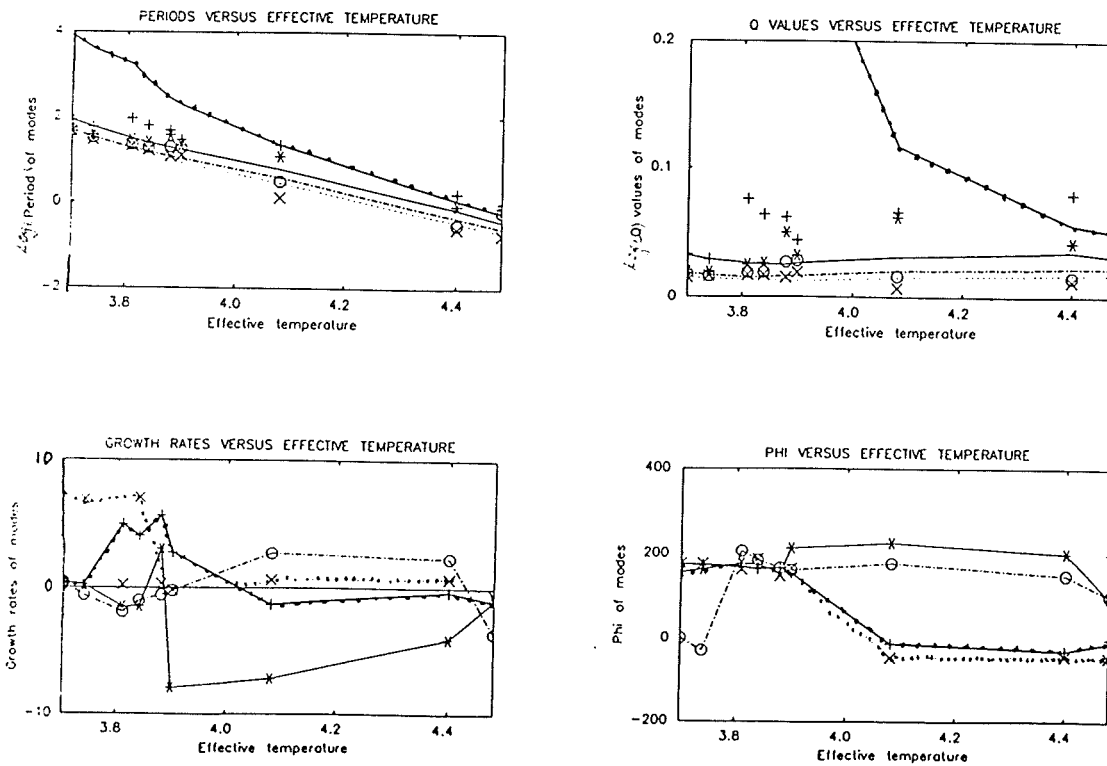


Figure 7.79 : Pulsation parameters for $L/L_{\odot} = 20,000$ and $M/M_{\odot} = 1.0$ (BD9C opacity table).

LINEAR NON-ADIABATIC RESULTS

7.5.3.3 Survey Results for 1.2 M_{\odot} Models - Table 7.17, below gives the coefficients of fits to the non-adiabatic fundamental mode Log (periods) at constant luminosities.

L/L_{\odot}	a_0	a_1	a_2	M.R	$\text{Log}(T_{\text{eff}})$
1,000	45.504	-19.364	2.002	0.00171	3.813 - 4.301
3,000	22.461	-7.480	0.499	0.00819	3.740 - 4.398
6,000	20.840	-6.462	0.364	0.01096	3.699 - 4.477
10,000	16.341	-4.117	0.076	0.02229	3.699 - 4.477
15,000	22.243	-7.053	0.451	0.04612	3.699 - 4.477
20,000	31.379	-11.748	1.059	0.05568	3.699 - 4.477

TABLE 7.17 : Table of coefficients of first fit for fundamental mode.

The coefficients for the [2D] fit to the non-adiabatic fundamental mode Log (periods) are:

$$b_{00} = 10.550 \quad b_{01} = 1.011 \quad X_1 = 2.91\% \quad i+j = 1$$

$$b_{10} = -3.377$$

$$b_{00} = 24.130 \quad b_{10} = -8.358 \quad X_1 = 2.72\% \quad i+j = 2$$

$$b_{01} = -0.803 \quad b_{11} = 0.313$$

$$b_{02} = 0.076 \quad b_{20} = 0.459$$

The coefficients for the [2D] fit to the non-adiabatic fundamental mode Log (Q's) are:

$$b_{00} = -0.686 \quad b_{01} = 0.260 \quad X_1 = 15.26\% \quad i+j = 1$$

$$b_{10} = -0.380$$

$$b_{00} = 12.474 \quad b_{10} = -5.199 \quad X_1 = 14.33\% \quad i+j = 2$$

$$b_{01} = -1.506 \quad b_{11} = 0.304$$

$$b_{02} = 0.074 \quad b_{20} = 0.443$$

LINEAR NON-ADIABATIC RESULTS

Table 7.18, below gives the coefficients of fits to the non-adiabatic first overtone mode Log (periods) at constant luminosities.

L/L_{\odot}	a_0	a_1	a_2	M.R	$\text{Log}(T_{\text{eff}})$
1,000	21.903	-7.831	0.586	0.00791	3.813 - 4.301
3,000	17.264	-5.242	0.253	0.00995	3.740 - 4.398
6,000	13.767	-3.460	0.042	0.01492	3.699 - 4.477
10,000	21.903	-7.831	0.586	0.02358	3.699 - 4.477
15,000	26.015	-9.535	0.811	0.05016	3.699 - 4.477
20,000	42.145	-17.759	1.816	0.02828	3.699 - 4.477

TABLE 7.18 : Table of coefficients of first fit for first overtone mode.

The coefficients for the [2D] fit to the non-adiabatic first overtone mode Log (periods) are:

$$b_{00} = 9.633 \quad b_{01} = 0.751 \quad X_i = 3.01\% \quad i+j = 1$$

$$b_{10} = -2.971$$

$$b_{00} = 25.191 \quad b_{10} = -9.839 \quad X_i = 2.53\% \quad i+j = 2$$

$$b_{01} = -0.008 \quad b_{11} = 0.430$$

$$b_{02} = -0.128 \quad b_{20} = 0.632$$

The coefficients for the [2D] fit to the non-adiabatic first overtone mode Log (Q's) are:

$$b_{00} = -1.657 \quad b_{01} = -0.003 \quad X_i = 15.91\% \quad i+j = 1$$

$$b_{10} = 0.004$$

$$b_{00} = 14.311 \quad b_{10} = -6.863 \quad X_i = 11.93\% \quad i+j = 2$$

$$b_{01} = -0.935 \quad b_{11} = 0.475$$

$$b_{02} = -0.130 \quad b_{20} = 0.615$$

The results presented here will be discussed in Section 7.5.4 .

LINEAR NON-ADIABATIC RESULTS

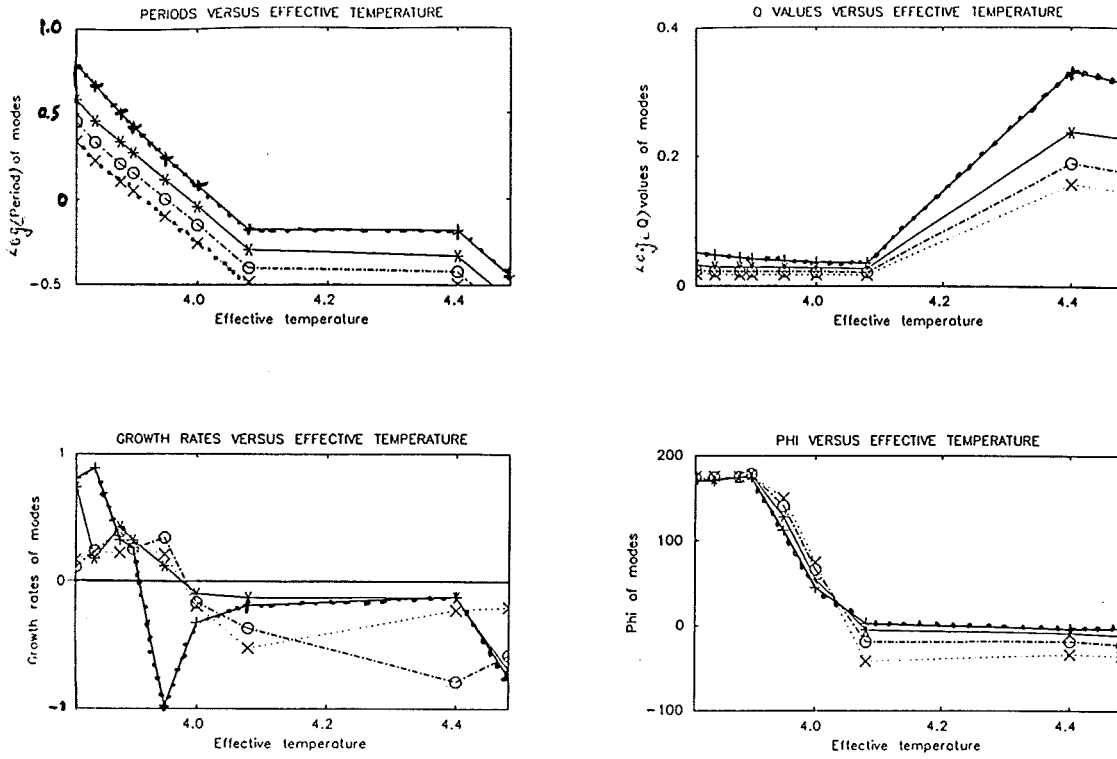


Figure 7.80 : Pulsation parameters for $L/L_{\odot} = 1,000$ and $M/M_{\odot} = 1.2$ (BD9C opacity table).

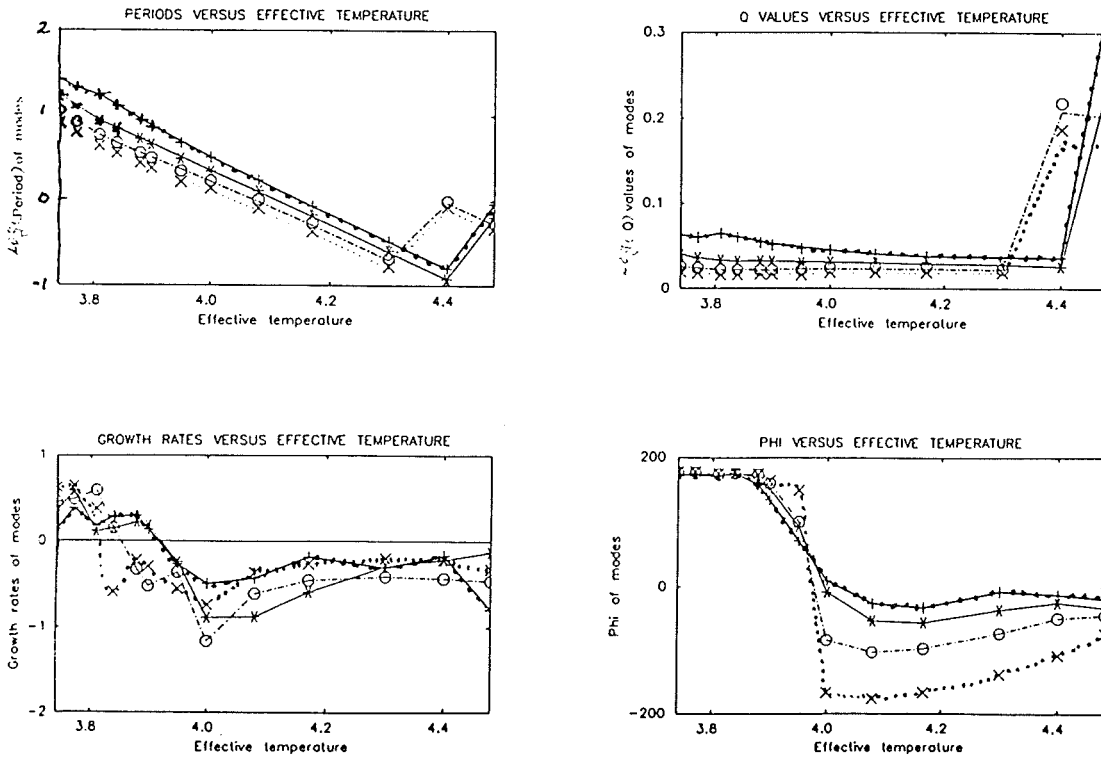


Figure 7.81 : Pulsation parameters for $L/L_{\odot} = 3,000$ and $M/M_{\odot} = 1.2$ (BD9C opacity table).

LINEAR NON-ADIABATIC RESULTS

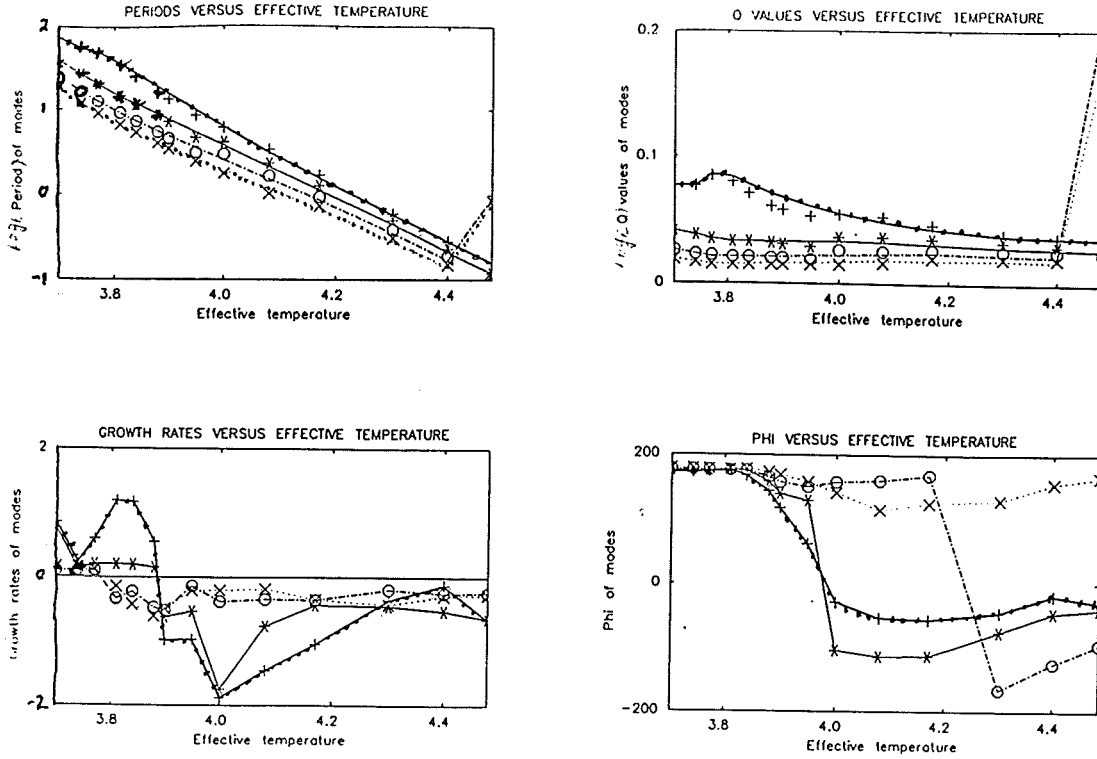


Figure 7.82 : Pulsation parameters for $L/L_{\odot} = 6,000$ and $M/M_{\odot} = 1.2$ (BD9C opacity table).

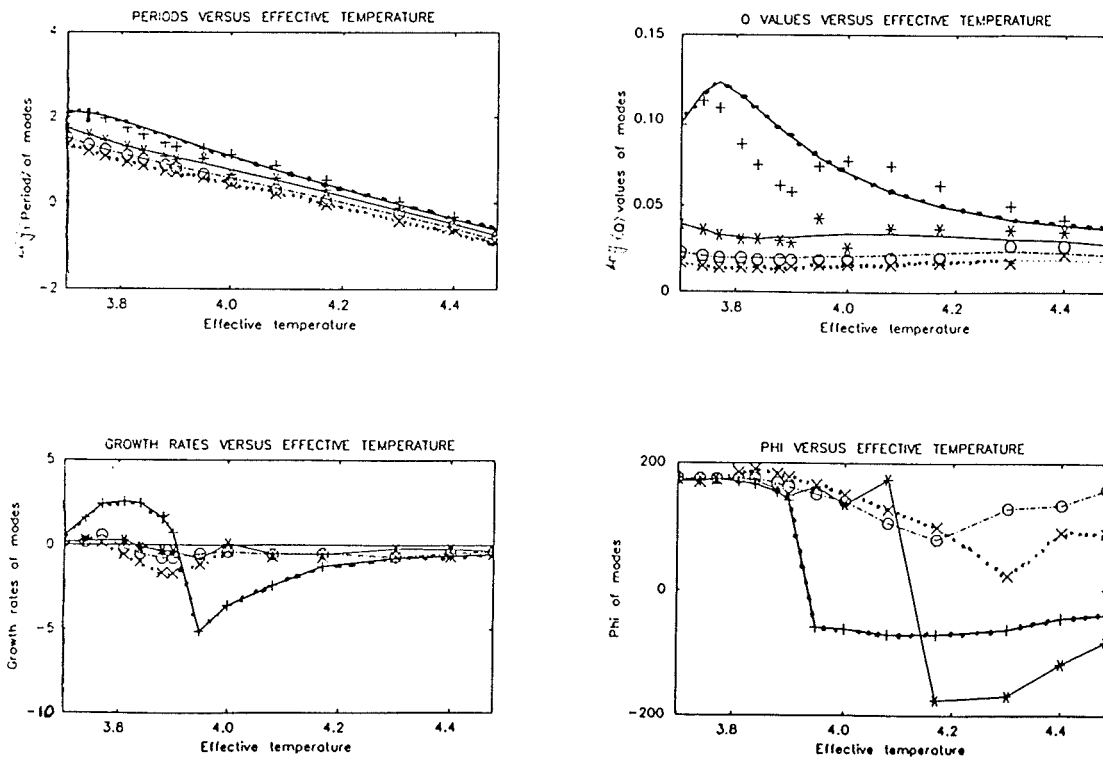


Figure 7.83 : Pulsation parameters for $L/L_{\odot} = 10,000$ and $M/M_{\odot} = 1.2$ (BD9C opacity table).

LINEAR NON-ADIABATIC RESULTS

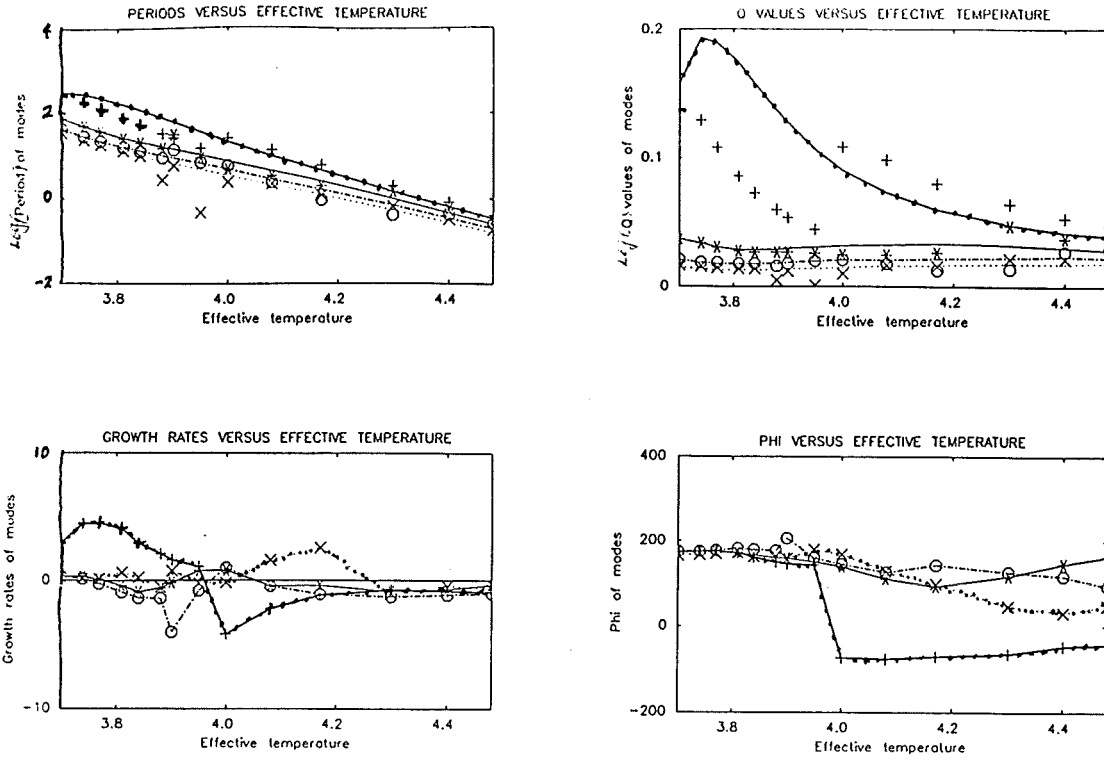


Figure 7.84 : Pulsation parameters for $L/L_{\odot} = 15,000$ and $M/M_{\odot} = 1.2$ (BD9C opacity table).

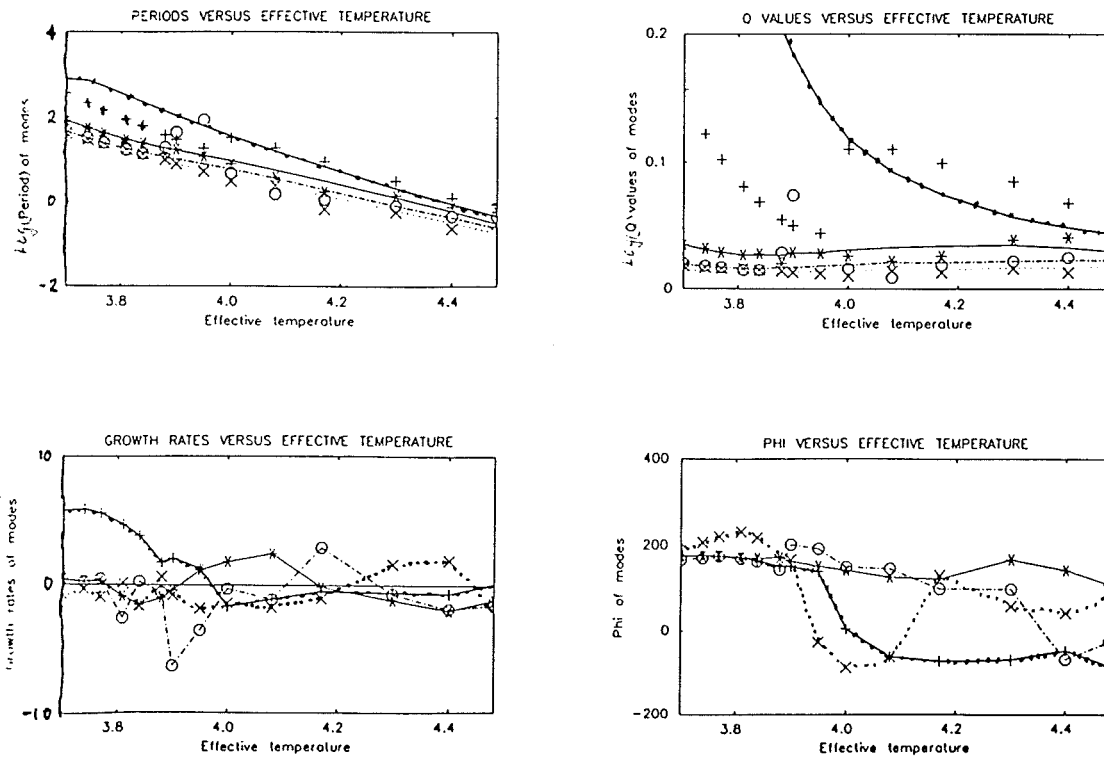


Figure 7.85 : Pulsation parameters for $L/L_{\odot} = 20,000$ and $M/M_{\odot} = 1.2$ (BD9C opacity table).

7.5.4 A Discussion Of The Survey Results

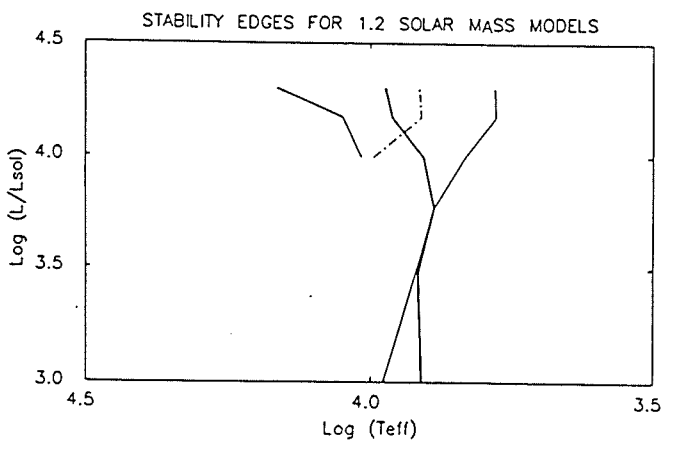
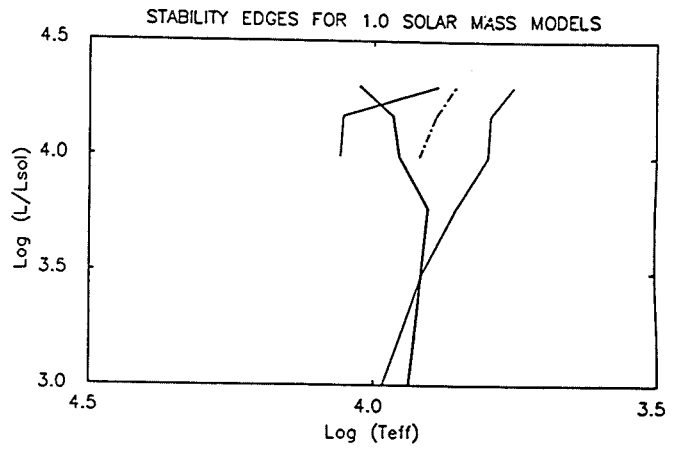
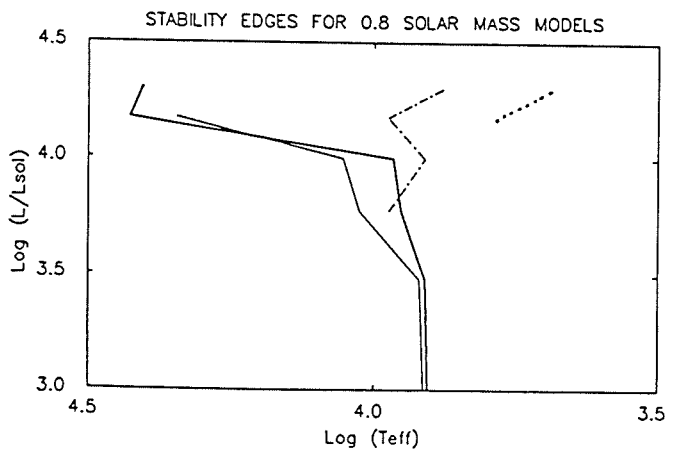
The results are shown graphically in Figures 7.68 - 7.85 . The overall features are the same as found in the DXIX opacity table survey, with the following exceptions. In the adiabatic Q-value (top left) graphs there is a noticeable turnover at the lower effective temperatures of the low luminosity models, which was also seen, to a lesser extent, in the pure helium models. This seems to indicate that carbon is less pronounced in its effects in opacity table BD9C than in opacity table DXIX. From these figures it can be seen that the dip in non-adiabatic Q-values and periods seen in DXIX opacity table survey below $10,000L_{\odot}$ have become far more pronounced at the blue edge of the instability region. Indeed, as the mass of the models increases, the dip becomes very sharp and approaches a discontinuity. This, with the change in phase of $\Phi(\delta R/R)$, is very useful in fixing the exact location of the instability blue edges for the lower luminosity survey sequences. We can see in the graphs that there is quite a large amount of wandering in the higher overtone periods, but little that cannot be explained by non-adiabatic effects. Although in the $1.2M_{\odot}$, $20,000L_{\odot}$ models at 7,500 K, 8,000 K and 9,000 K, a strange mode sequence appears in the second overtone modes. This sequence is characteristic of those found by Saio & Wheeler (1985) and Worrell (1985), and its probable cause and effects are discussed therein. As with the previous survey discussions, the best [2D] fit to the fundamental period data is given below:

$$\begin{array}{ll}
 P_0 = 2.2 \times 10^9 (T_{\text{eff}})^{-2.91} (L/L_{\odot})^{0.873} (5\%) & M/M_{\odot} = 0.8 \\
 P_0 = 2.6 \times 10^{10} (T_{\text{eff}})^{-3.26} (L/L_{\odot})^{0.939} (3\%) & M/M_{\odot} = 1.0 \\
 P_0 = 3.5 \times 10^{10} (T_{\text{eff}})^{-3.38} (L/L_{\odot})^{1.011} (3\%) & M/M_{\odot} = 1.2
 \end{array}$$

LINEAR NON-ADIABATIC RESULTS

Unlike the previous surveys, the above fits are very good and there is no loss of accuracy for the lower mass models. For this opacity table we can see that the periods slowly increase with mass and are roughly proportional to $(R_*/R_\odot)^{1.4}$. Although this is slightly lower than that found for Cepheids, $(R_*/R_\odot)^{1.7}$, it is consistent in mass. Indicating that this opacity table may be better for modelling helium-carbon mix envelopes than the DXIX opacity table, which was less consistent in mass.

If we now consider the instability diagrams shown in Figure 7.86, we see that the 'dog-leg' effect is only present in the lower mass models as was the case for the pure helium survey. The blue edge of the fundamental mode occurs at about the same effective temperature as that of the DXIX opacity table survey. This indicates that the blue edge position in the HR diagram is defined by the carbon while the 'dog-leg' effect is more dependent upon the helium. In this survey, we can see that the first overtone blue edge slopes backward with increasing luminosity at higher masses, due to an increase in 'damping' for low luminosity models. In this case, we can see that the mass of the stellar model could play a crucial role in its stability at higher luminosities. This alone could explain why two similar stars have different pulsational properties. The main cause of the 'dog-leg' effect appears to be in the movement of the He^{++} damping region out in mass, where the density is lower and $|\delta L/L|$ is 'frozen in'. The vertical 'turn up' in the $0.8M_\odot$ fundamental blue edge seems to be real, and apparently is connected with the loss of the 'driving' regions into the atmosphere of the envelope, thus causing stabilisation of the envelope for higher effective temperatures. The fundamental red edge is only indicative and could be quite a long way redward of this position, if convection were treated properly. The values of the instability strip edges of the fundamental and first overtone modes can be found in Appendix F.3 .



KEY FOR OPACITY TABLE BD9C

- Heavy lines - Fundamental Blue Edge
- Dotted lines - Fundamental Red Edge
- Light lines - First overtone Blue Edge
- Chained lines - First overtone Red Edge

Figure 7.86 : This figure shows the position of the blue edges of BD9C opacity table survey, on HR diagrams. The heavy solid lines represent the Fundamental blue edges and the light solid lines the first overtone blue edges.

7.6 MASS-LUMINOSITY LIMITS FOR 7 VARIABLE RCB STARS

In this section, the results of the previous surveys will be used to find limitations on the luminosities of several variable RCB stars. In deciding which of the variable RCB stars are to be considered, the first criterion must be that they have both effective temperatures and periods within the range of the survey. Taking this criterion, we find that there are only ten observed RCB stars that fall within this category, of which XX Cam and LR Sco are doubtful and so were dropped from this analysis. Of the remaining eight DY Cen belongs to the 'hot' RCB sub-group, of which, the members are doubtful RCB type variables (Pollacco, 1988) and so was also eliminated from this analysis. This then leaves the seven RCB variable stars listed in Table 7.19 below.

STAR	T_{eff} (+/-500k)	PERIOD (days)
UW Cen	6,000	42.8
WX CrA	5,000	60
R CrB	6,900	44
RT Nor	5,000	59
GU Sgr	5,000	38
RY Sgr	6,900	38.6
RS Tel	5,000	45.8

TABLE 7.19 : Table of the 7 RCB variables, for which luminosity limitations will be found.

Within the observational errors, the periods of RT Nor and WX CrA are the same and hence were treated together in the following analysis.

To find the luminosity limitations all we have to do is plot graphs of luminosity versus period for $T_{\text{eff}} = (4,500, 5,000, 5,500, 6,000, 6,500, 7,000, 7,500)\text{K}$ for each mass of the DXIX and BD9C opacity table surveys. This is done by using the [2D] fit coefficients of the results Sections, and finding the luminosity for given periods while T_{eff} is held constant. This has been done in Figures 7.87 - 7.88 ,

LINEAR NON-ADIABATIC RESULTS

for the fundamental and first overtone modes. In Figures 7.87 - 7.88, the graphs on the R.H.S. refer to the DXIX opacity table survey and those on the L.H.S. to the BD9C opacity table survey. As we go from top to bottom, the graphs are for 0.8, 1.0 and 1.2 solar mass models and the lines in the graph represent the following effective temperatures:

- - $T_{\text{eff}} = 4,500$ K (BOTTOM)
- - $T_{\text{eff}} = 5,000$ K (BOTTOM)
- - $T_{\text{eff}} = 5,500$ K
- - - - - - - - $T_{\text{eff}} = 6,000$ K
- - - - - - - - $T_{\text{eff}} = 6,500$ K
- - $T_{\text{eff}} = 7,000$ K (TOP)
- - $T_{\text{eff}} = 7,500$ K (TOP)

The following analysis is split into two parts. The first part deals with the low effective temperature RCB variables (UW Cen, WX CrA, RT Nor, GU Sgr, RS Tel) and the second deals with the high effective temperature variables (R CrB, RY Sgr) in Table 7.19. (Throughout this analysis we assume that the given periods are correct.)

For the low effective temperature variables listed above it is a simple matter to read the luminosities from the luminosity-period plots for both modes under consideration. This was done, and the results can be seen in Figure 7.89 which shows the luminosity limitations versus mass that the observed period imposes on the RCB star in question. For both opacity tables, the horizontal lines in graphs of Figure 7.89 are from top to bottom : $T_{\text{eff}} + 500$, T_{eff} , $T_{\text{eff}} - 500$, respectively (where T_{eff} is the effective temperature of the RCB star in question). In Figure 7.98, the BD9C opacity table models were unstable to fundamental and first overtone mode pulsation at all masses considered; while the DXIX opacity table models were only unstable to fundamental mode pulsation. From this figure the following two tables of probable luminosity at given masses (assuming fundamental mode pulsation) were obtained:

LINEAR NON-ADIABATIC RESULTS

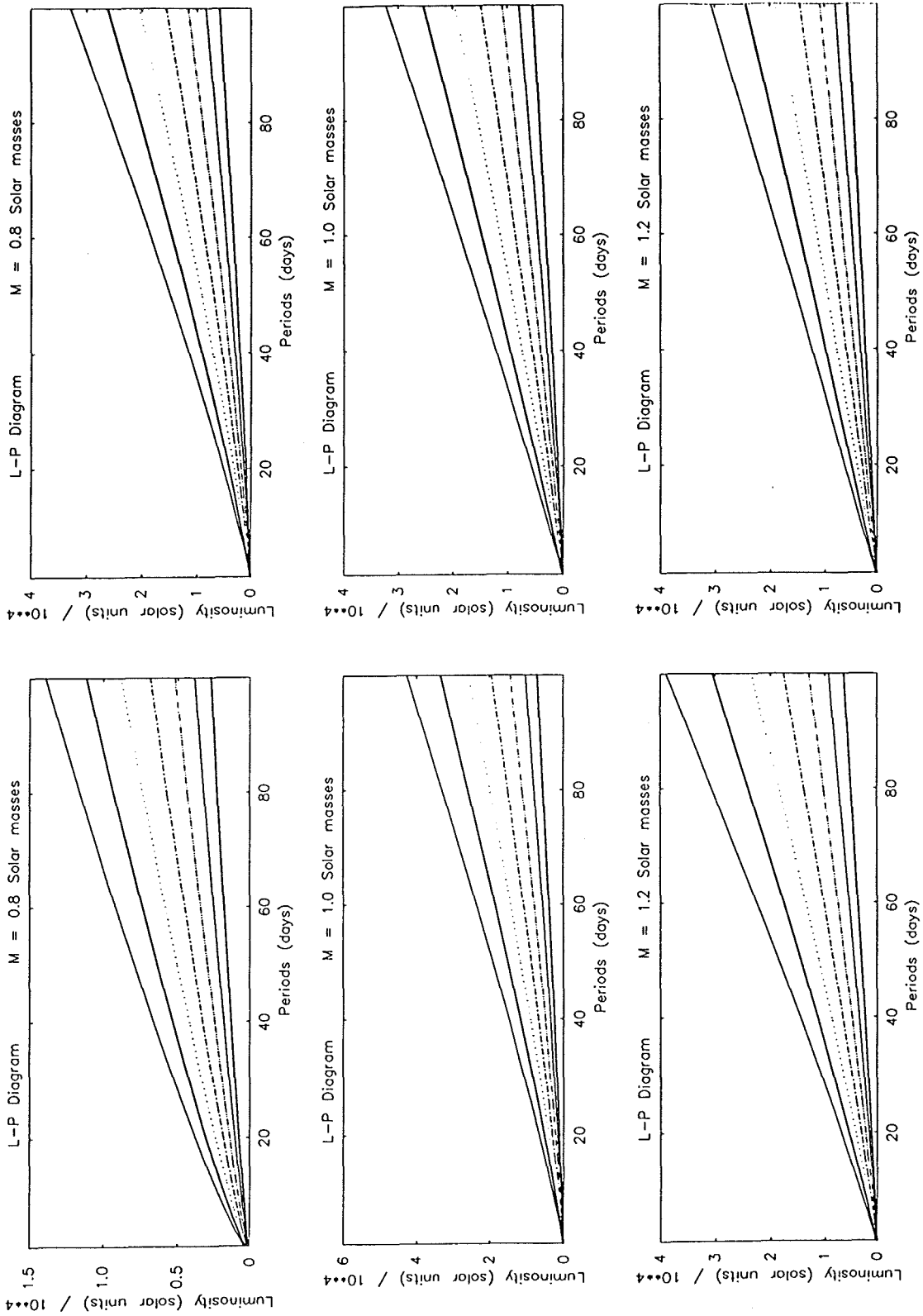


Figure 7.87 : This figure shows Fundamental mode Period - Luminosity graphs for DXIX (L.H.S.) and BD9C (R.H.S.) opacity table surveys.

LINEAR NON-ADIABATIC RESULTS

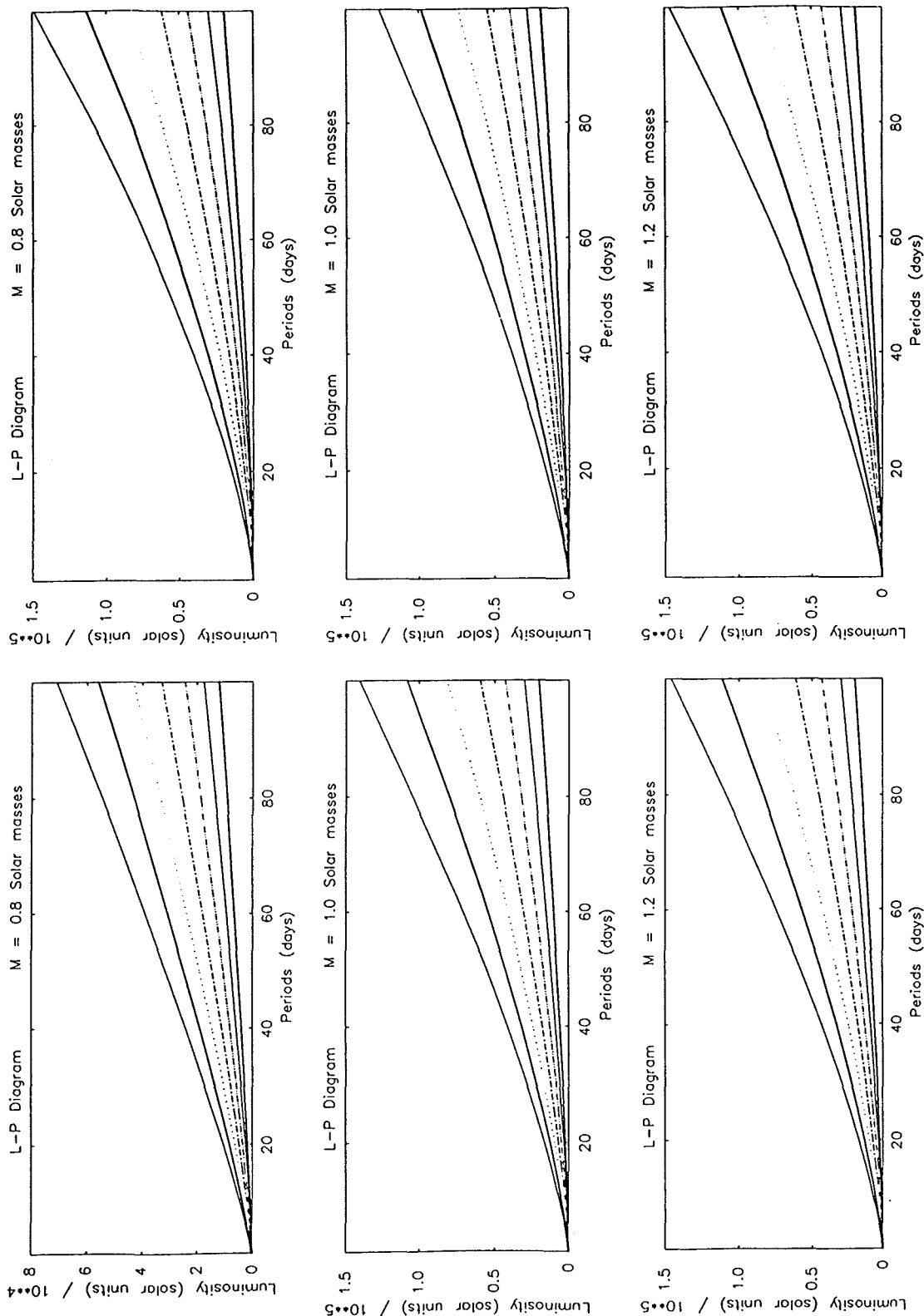


Figure 7.88 : This figure shows First overtone mode Period - Luminosity graphs for DXIX (L.H.S.) and BD9C (R.H.S.) opacity table surveys.

LINEAR NON-ADIABATIC RESULTS

LUMINOSITY LIMITATIONS FOR TABLE DXIX

STAR	0.8M _⊙	1.0M _⊙	1.2M _⊙
UW Cen	7100 + 200 -3700	9400 + 200 -5000	12200 + 200 -6600
WX CrA	5300 + 300 -3000	7400 + 400 -4400	10000 + 600 -5500
RT Nor	5300 + 300 -3000	7400 + 400 -4400	10000 + 600 -5500
GU Sgr	3200 + 100 -1500	4600 + 100 -2200	6200 + 100 -3100
RS Tel	4000 + 100 -2000	5600 + 200 -2800	7600 + 200 -4200

TABLE 7.20 : Table showing Probable luminosity (solar units) of RCB stars, (using DXIX opacity table survey) at each mass of the survey, assuming fundamental mode pulsation.

LUMINOSITY LIMITATIONS FOR TABLE BD9C

STAR	0.8M _⊙	1.0M _⊙	1.2M _⊙
UW Cen	6010 +280 -110	7940 +270 -230	10270 +250 -400
WX CrA	4690 + 50 -160	6440 + 80 -130	8610 +100 - 70
RT Nor	4690 + 50 -160	6440 + 80 -130	8610 +100 - 70
GU Sgr	2810 +230 - 10	3920 +260 - 60	5300 +290 -150
RS Tel	3470 +190 - 40	4780 +260 - 10	6460 +260 - 80

TABLE 7.21 : Table showing Probable luminosity (solar units) of RCB stars, (using BD9C opacity table survey) at each mass of the survey, assuming fundamental mode pulsation.

LINEAR NON-ADIABATIC RESULTS

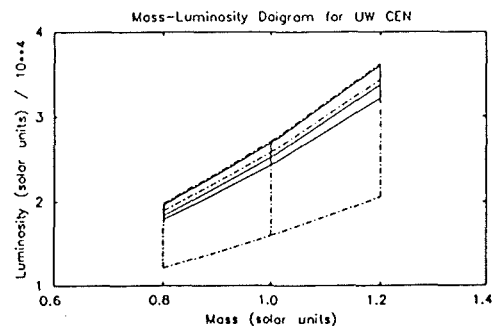
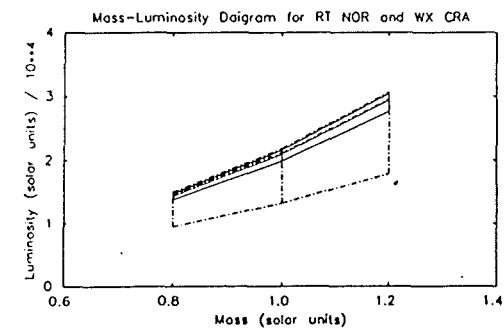
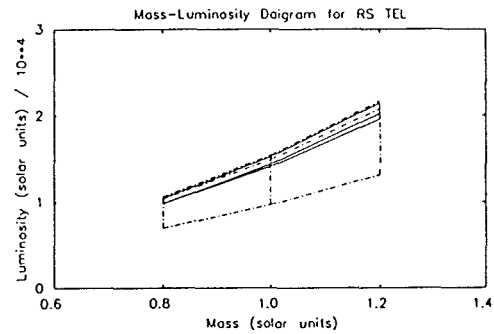
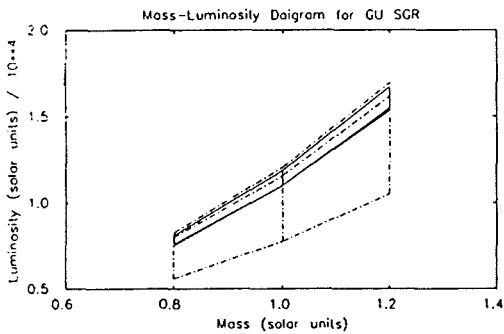
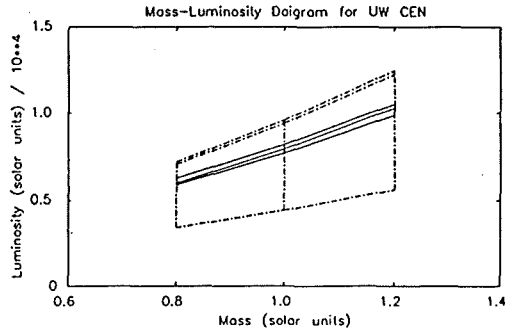
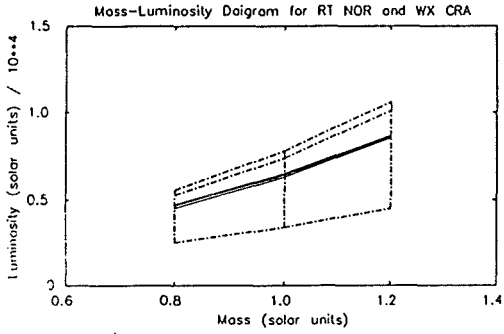
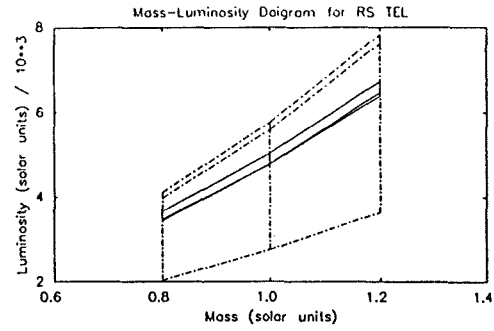
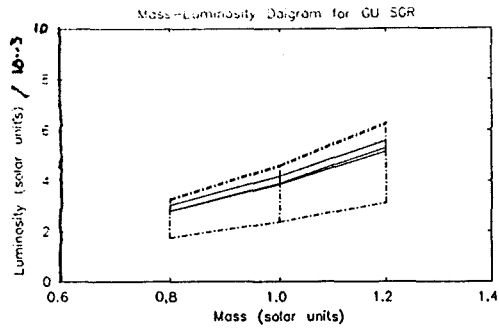


Figure 7.89 : This Figure shows the fundamental mode (top 4 graphs) and first Overtone mode (bottom 4 graphs) Luminosity-Mass graphs, for GU Sgr, RS Tel, RT Nor & WX CrA and UW Cen.

LINEAR NON-ADIABATIC RESULTS

Tables 7.20 and 7.21 indicate that the 5000 K RCB variables are fundamental pulsators near the lower limit of the observed luminosity range. The BD9C opacity table survey however, also allows them to pulsate in the first overtone mode, which would then give them luminosities close to the 'best value' quoted throughout the literature.

For the high effective temperature RCB variables mentioned above, the same procedure was followed, to find limitations on the luminosity at each mass point of the surveys (solid line curves in Figure 7.90). This time, however, we also used the surface gravity given in the literature for these stars to find a second limitation on the luminosity at each mass point of the surveys (chained lines in Figure 7.90). The area of overlap is then where the RCB star in question must lie and where the central line of each 'grid' crosses is the most probable location of the star. As can be seen from the graphs in Figure 7.90, the RCB stars in question are very probably fundamental mode pulsators. This is further confirmed in the DXIX survey models, as they are stable to first overtone mode pulsation in the range of masses considered here. From Figure 7.90, assuming fundamental mode pulsation, the following mass and luminosity limitations were obtained:

STAR	PERIOD	T_{eff}	$\text{Log}(g)$	L/L_{\odot}	M/M_{\odot}	TABLE
R CrB	44 ^d	6900+/-500	0.15+/-0.2	12000 ⁺⁵⁰⁰ ₋₆₅₀₀	0.93 ^{+0.07} _{-0.04}	DXIX
				15500 ⁺¹⁰⁰⁰ ₋₁₀₀₀	0.95 ^{+0.02} _{-0.03}	BD9C
RY Sgr	38 ^d	6900+/-500	0.1 +/-0.5	12000 ⁺¹⁵⁰⁰ ₋₆₅₀₀	0.96 ^{+0.03} _{-0.06}	DXIX
				10500 ⁺¹⁰⁰⁰ ₋₁₀₀₀	0.99 ^{+0.06} _{-0.06}	BD9C

LINEAR NON-ADIABATIC RESULTS

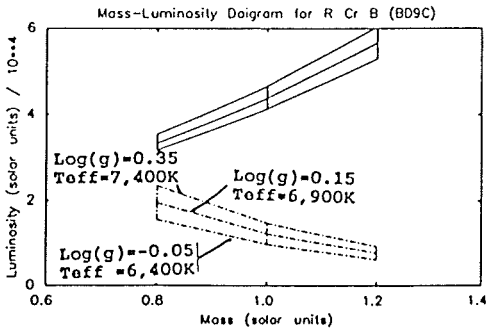
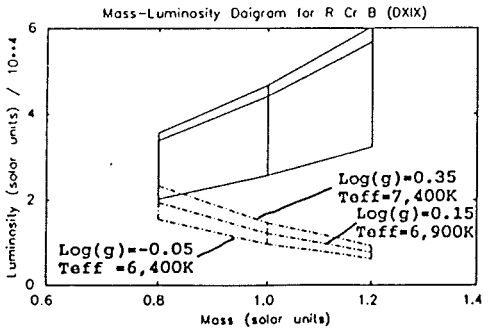
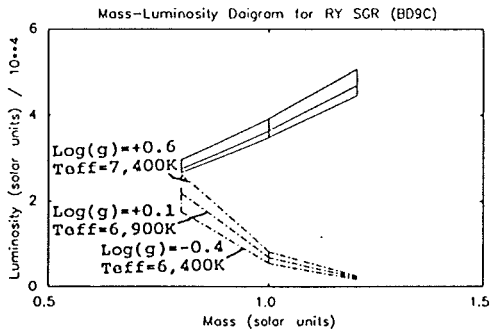
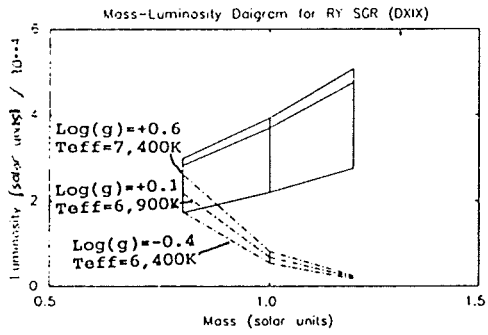
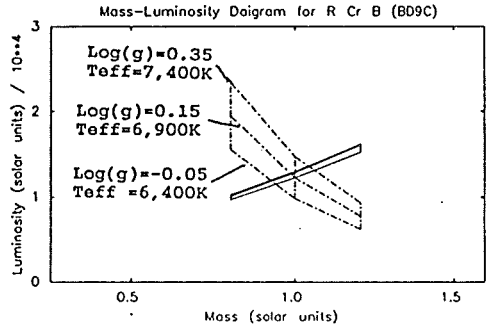
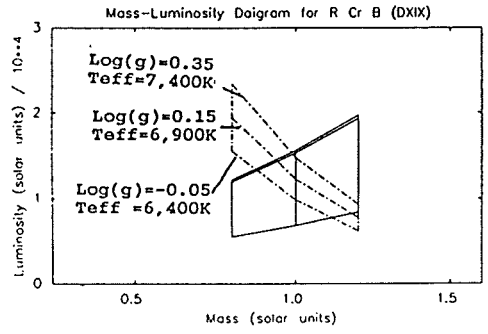
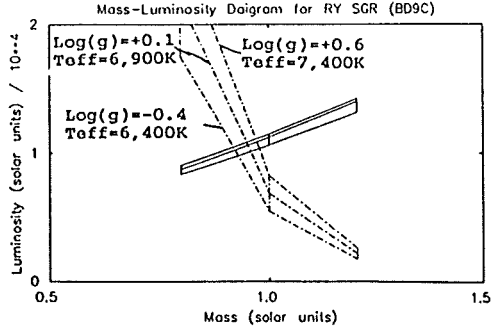
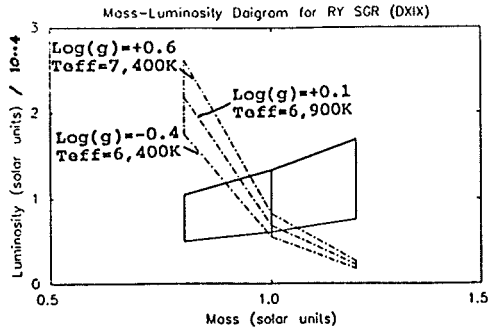


Figure 7.90 : This Figure shows the fundamental mode (top 4 graphs) and first Overtone mode (bottom 4 graphs) Luminosity-Mass graphs, for RY Sgr and R CrB.

LINEAR NON-ADIABATIC RESULTS

In both the stars the DXIX opacity table survey models were stable in the range of masses considered. From this it was concluded that the BD9C opacity table is probably the best table to use when modelling such He-C objects.

7.7 CONCLUSION

From the surveys carried out in this chapter and their application to some of the RCB group of stars, we can see that opacity table BD9C gives better and more consistent results than opacity table DXIX and therefore will be used to produce the non-linear models of the RCB stars discussed in this chapter.

The main reason for the surveys has been fulfilled, in that a limit has been placed on the luminosities of the 'lower' effective temperature models considered in this chapter. But more importantly, R CrB and RY Sgr have been found to have masses of $(0.95 \pm 0.03)M_{\odot}$ and $(0.99 \pm 0.06)M_{\odot}$ and luminosities of $(15,500 \pm 1,000)L_{\odot}$ and $(10,500 \pm 1,000)L_{\odot}$ respectively (from opacity table BD9C results, as opacity table DXIX results were stable to pulsation). These figures agree very well with the recent evolutionary work of Weiss (1987), in which he indicates that the 'hotter' RCB variables (of the type considered in this chapter) should have masses in the range $(0.9-1.0)M_{\odot}$. The masses have recently been confirmed (within errors) by Saio & Jeffery (1988), who used a similar spectroscopic method. Their work was not published until after this work was completed.

The blue edges of the models are interesting, and could show why two hydrogen deficient carbon stars (HdC stars), having similar masses and effective temperatures, have different properties, i.e., why one pulsates and the other does not. The difference in pulsational

LINEAR NON-ADIABATIC RESULTS

stability indicates that the pulsating HdC star has a luminosity above the 'dog-leg' critical luminosity, and the other has a luminosity below it.

Finally, the surveys have shown that 'strange modes' are not opacity table dependent and seem to occur in any model with high abundances of helium and carbon and very little hydrogen. As no 'strange modes' were found in the pure helium opacity table survey, this may indicate that the presence of carbon or some similar element is needed before they manifest themselves.

CHAPTER 8

NON-LINEAR NON-ADIABATIC RESULTS

8.1 INTRODUCTION

In this Chapter some of the results obtained from a modified (the modifications being due to Dr Bridger, Dr Worrell and myself) version of Dr Carson's non-linear codes are presented and discussed. For this Chapter the majority of the models were made using Dr Jeffery's modified version of Dr Carson's He-C Opacity tables, namely the BD9C opacity table. Some of the test models, however, also use Cox & Tabor's (1976) Demarque XIX opacity table: DXIX.

The following presentation of results is split into 3 main sections: tests; check of linear results, and non-linear models of 7 RCB variable stars. The first section attempts to fix some of the input physics and also to find what approximations can be made without altering the results; the approximations are required as the amount of memory is finite and cpu-time is also limited.

The second Section attempts to ascertain whether the results found in the linear analysis for the Demarque XIX opacity table are valid in the non-linear limit. Specifically, it is desirable to know whether the models made using the DXIX opacity table are unstable to pulsation for the values of stellar parameters the RCB variable stars are thought to have. The third and final section will present 7 models which give the best theoretical representation of the 7 RCB stars described in Section 7.6 of the linear results Chapter.

NON-LINEAR NON-ADIABATIC RESULTS

X	= 0.00001	Z _{Ne}	= 0.00000
Y	= 0.95999	Z _{Mg}	= 0.00000
Z _C	= 0.04000	Z _{Si}	= 0.00000
Z _N	= 0.00000	Z _S	= 0.00000
Z _O	= 0.00000	Z _{Fe}	= 0.00000

TABLE 8.1 : Abundances (by mass) of elements used in the non-linear models of this thesis.

Convergence	:	To 6 sig. figs.
States calculations	:	Using exact equations
Number of elements	:	3
Molecules included	:	No
Opacity calculations	:	Using tables
Opacity interpolation	:	Linear
Opacity table	:	BD9C
Outer momentum B.C.	:	B=1/3, C=0 (See 5.13 & 5.17)
Radiation dilution	:	Included
Depth of static model	:	Excluding central core
Zones in static model	:	>500
Re-zoning method	:	By sound travel times
Zones in coarse model	:	>50
Viscosity parameter	:	C _Q = 4.2

TABLE 8.2 : List of parameter values used in the majority of the non-linear analyses carried out in this thesis.

NON-LINEAR NON-ADIABATIC RESULTS

Throughout this work, the homogeneous abundances (by mass) given in Table 8.1 were used, unless otherwise stated. The following molecules were sometimes included: C_2 , N_2 , O_2 , CN, CO, NO, C_2O , N_2O and NO_2 (but only where specifically stated in the text). Other parameters that are pre-set, unless otherwise stated, are given in Table 8.2. This then only leaves the effective temperature, luminosity and mass as free parameters which can be found from linear theory and observations.

8.2 PRELIMINARY TESTS

This Section tries to justify the choice of parameters in Table 8.2, bearing in mind the memory and cpu-time limitations, i.e., keeping both these quantities to a minimum while still maintaining the accuracy of the final results. In some cases, Figures will be used to help show that the compromises made did not alter the dynamic parameters appreciably or affect the basic shape of the photospheric light curves.

8.2.1 CALCULATION OF STATE VARIABLES

One of the first and most important questions to ask is how are the state variables to be found and should molecule formation be included in the state equations? As far as the first question is concerned, we have one of three possibilities:

- (i) an empirical formula
- (ii) exact calculations using an iterative process
- (iii) pre-calculated tables

NON-LINEAR NON-ADIABATIC RESULTS

Option (i) can be ruled out immediately, as no accurate empirical formula exists for the abundances in question, and would be only a rough approximation if it did. Of the remaining two options, (ii) gives the most accurate results if slightly slower to use (a lot slower if molecules are included) while (iii) is far quicker when molecules are included but is too coarse when it comes to evolving the static models in time. Option (iii) has the added problem that 3 very large tables must have been pre-generated for Pressure (P), Internal Energy (U) and Specific Entropy (S); even then it is usually necessary to fit spline surfaces to the tables in order to meet the convergence conditions imposed by the non-linear codes (the convergence conditions are discussed briefly, later on). The saving in cpu-time option (iii) gives is offset by the greatly increased working space and preparation time required to include it. Thus, it was decided that for most non-linear models, option (ii) would be used (the exceptions are all models which include molecules).

The lowest effective temperature considered in this survey was 5,000 K, because at lower effective temperatures the convection becomes efficient, resulting in incorrect and uncertain results. To see what effect the inclusion of molecules has at low effective temperatures, two models were made at 5,000 K with luminosities of $3,000L_{\odot}$ (the bottom end of the RCB range) and masses of $1.0M_{\odot}$, one model including, and the other excluding, molecules. From Figures 8.1 - 8.4, we can see that the effects on the luminosity and velocity curves at each zone are negligible, and that the work integral is not affected greatly by the exclusion of the molecules. This then confirms the belief that the molecules have virtually no effect on the results of models with effective temperatures above 5,000 K and may be safely excluded from all models considered in this thesis.

NON-LINEAR NON-ADIABATIC RESULTS

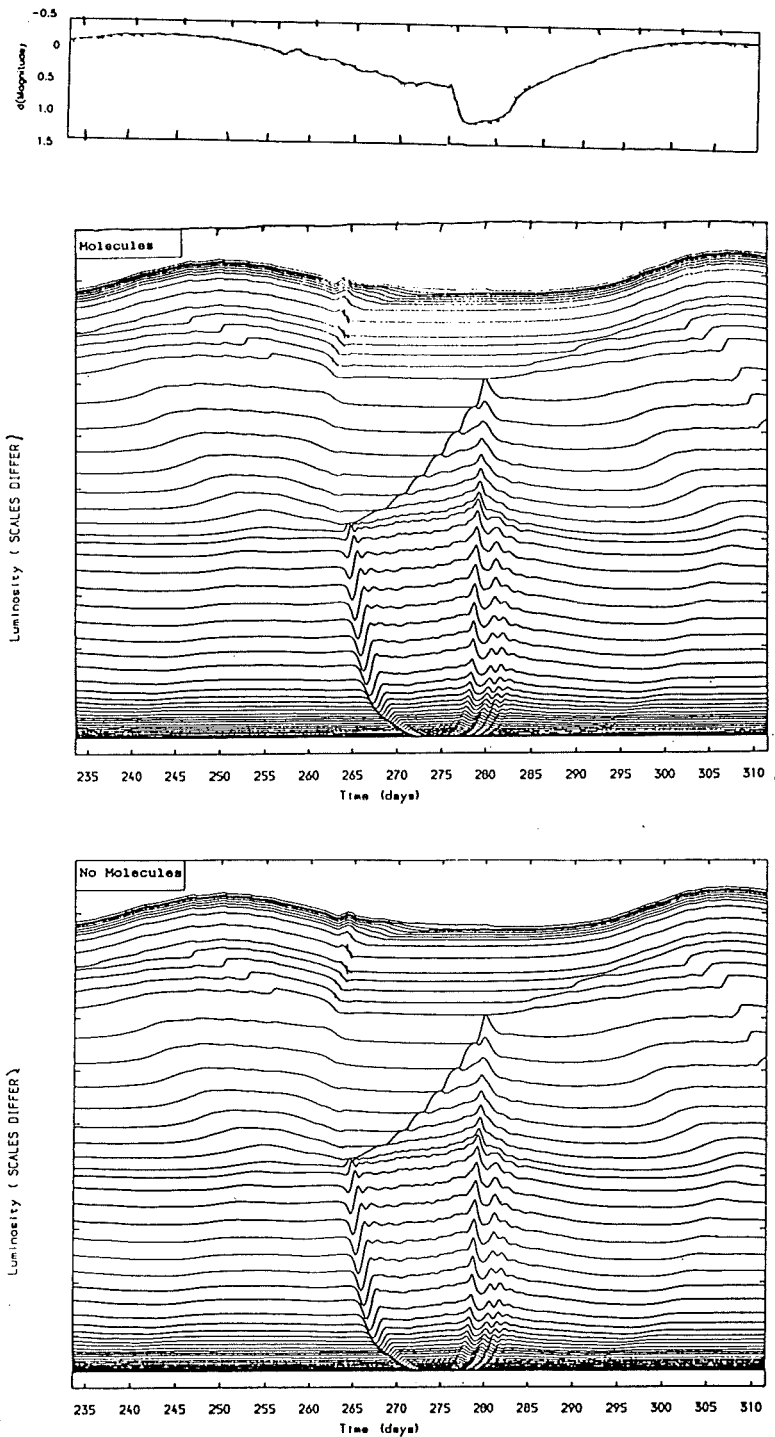


Figure 8.1 : The top graph shows photospheric luminosities of model with molecules (solid line) overlaid on model without molecules (chained line). The middle and bottom graphs, show the luminosity histories over the same time interval of the model, including molecules (top) and the model excluding molecules (bottom), respectively.

NON-LINEAR NON-ADIABATIC RESULTS

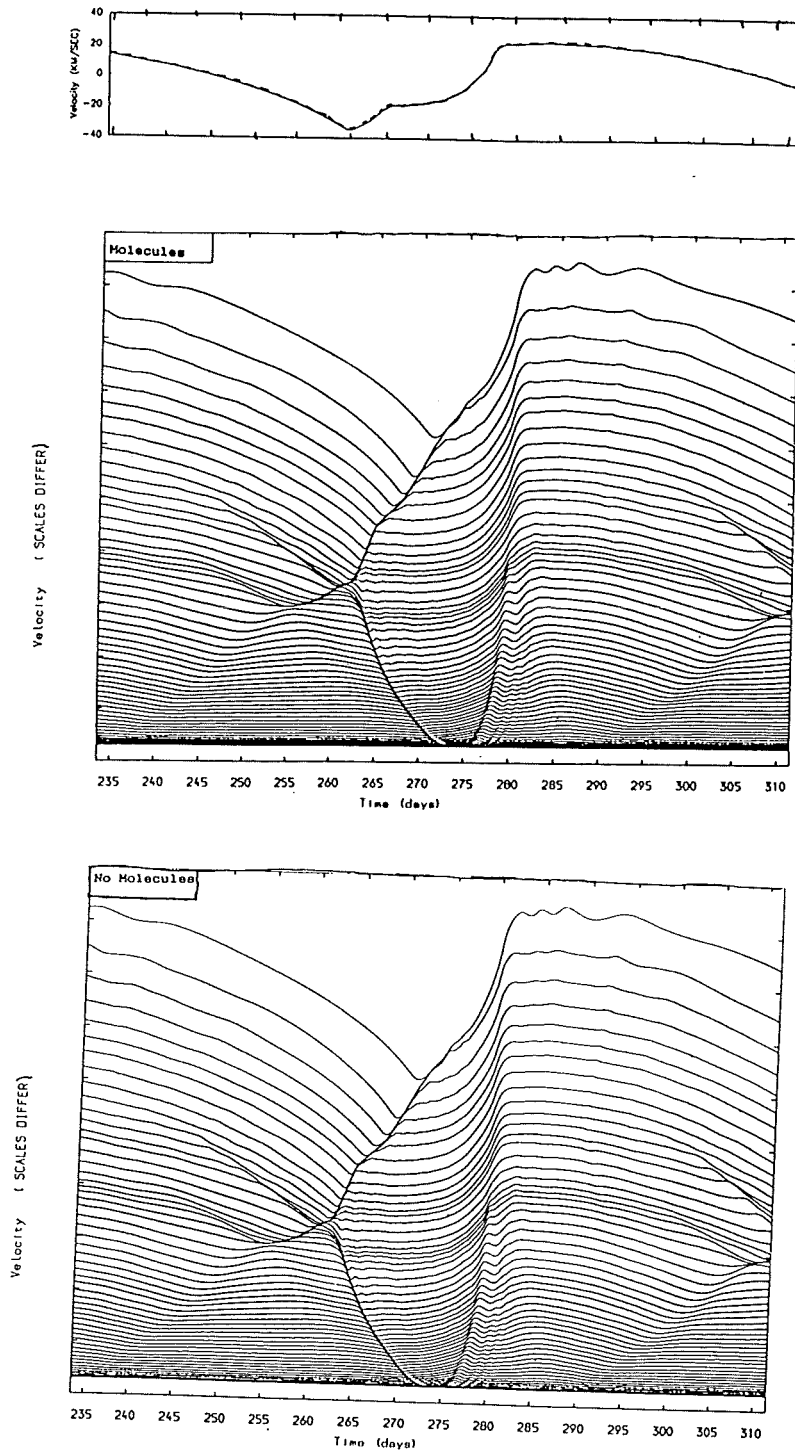


Figure 8.2 : The top graph shows photospheric velocities of model with molecules (solid line) overlaid on model without molecules (chained line). The middle and bottom graphs, show the velocity histories over the same time interval of the model, including molecules (top) and the model excluding molecules (bottom), respectively.

NON-LINEAR NON-ADIABATIC RESULTS

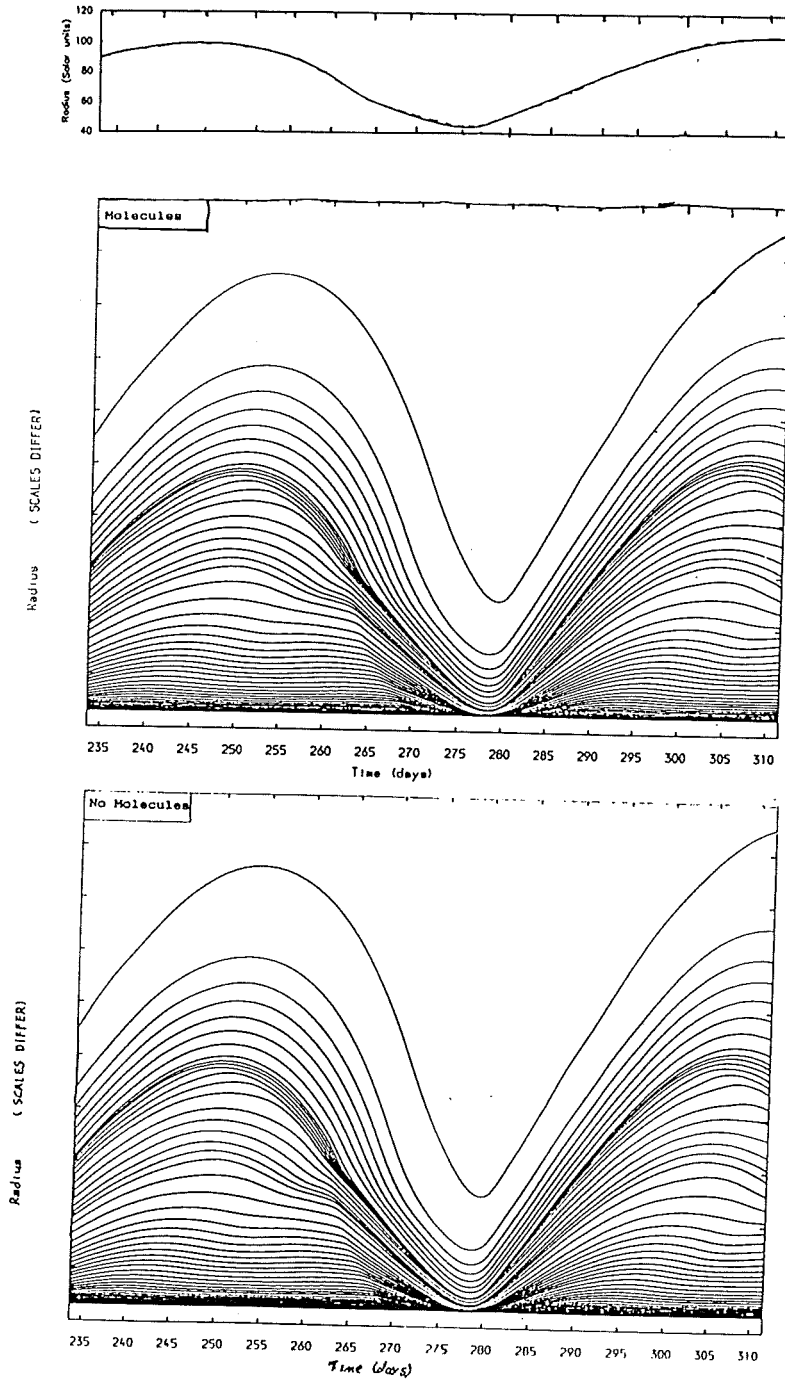


Figure 8.3 : The top graph shows photospheric radii of model with molecules (solid line) overlaid on model without molecules (chained line). The middle and bottom graphs, show the radii histories over the same time interval of the model, including molecules (top) and the model excluding molecules (bottom), respectively.

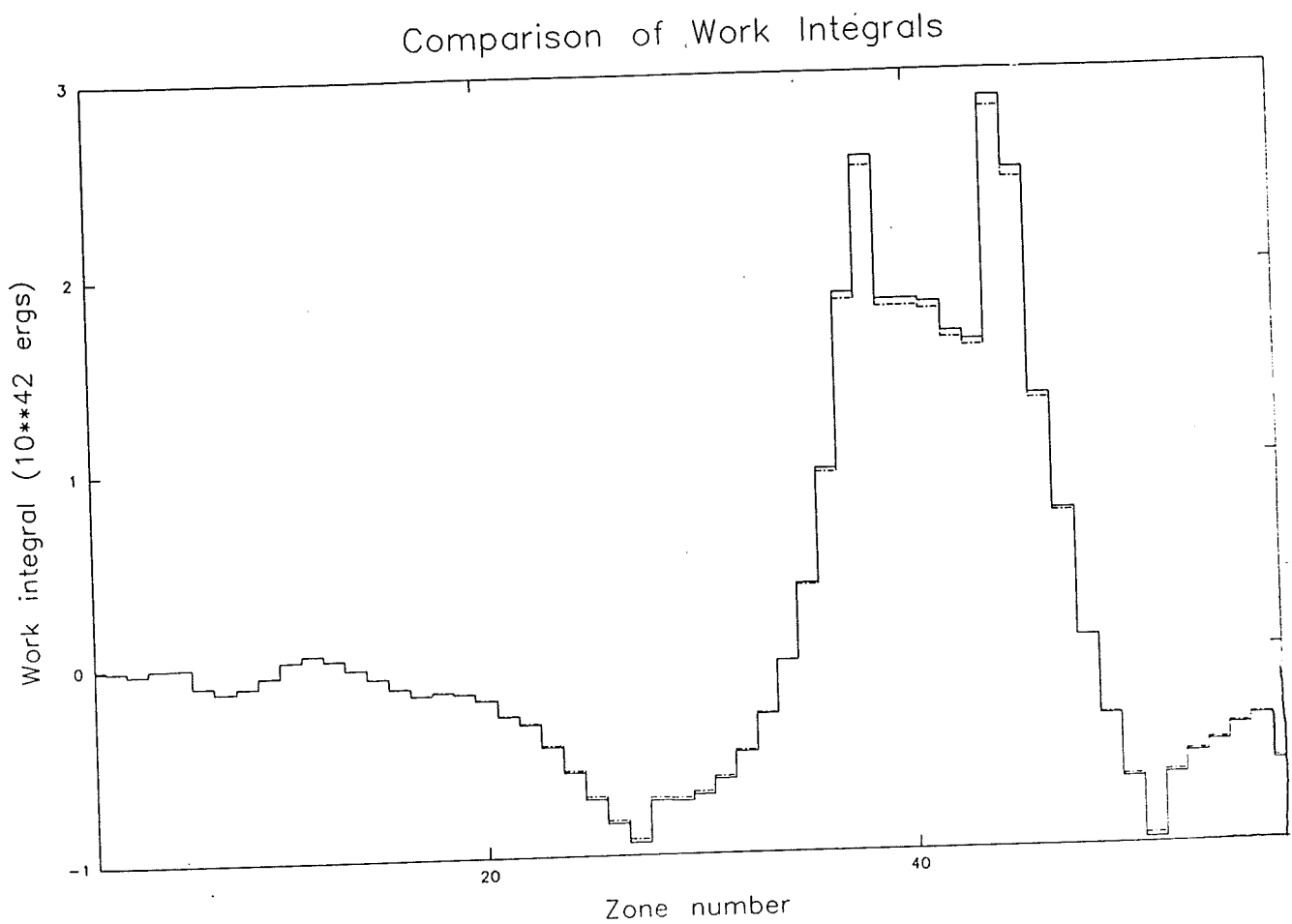


Figure 8.4 : This shows the work integrals with zone number of the model with molecules (solid line) overlayed on the model without molecules (chained line).

8.2.2 CALCULATION OF OPACITY

Let us now consider how the opacity is to be treated in the non-linear calculations. We again have several options available:

- (i) Kramers' polytropic opacity formula
- (ii) empirical formula (Stellingwerf's polynomial)
- (iii) full on-line computation
- (iv) using pre-calculated tables.

Option (i) is really only used for de-bugging purposes and can be eliminated immediately. Option (iii) would take a very long time, especially at the lower temperatures and hence is not viable. This leaves options (ii) and (iv).

Option (ii) was derived for stars containing an appreciable amount of hydrogen, and not the hydrogen deficient carbon objects under consideration here. In any case, the use of such an empirical formula would be a needless introduction of error, when it is just as easy and sometimes quicker to use pre-calculated opacity tables designed specifically for this sort of task.

Having decided to use tables, some form of interpolation procedure within them was needed. We followed the results found in both Dr Worrell's and Dr Bridger's theses, regarding such interpolation in Carson tables; linear interpolation was not only adequate, but desirable.

This then led to the all important question: which opacity table should be used for the non-linear analysis of the RCB variable stars, Carson's or Cox & Tabor's? From the linear results, Carson's BD9C opacity table would appear to be the better choice. However,

NON-LINEAR NON-ADIABATIC RESULTS

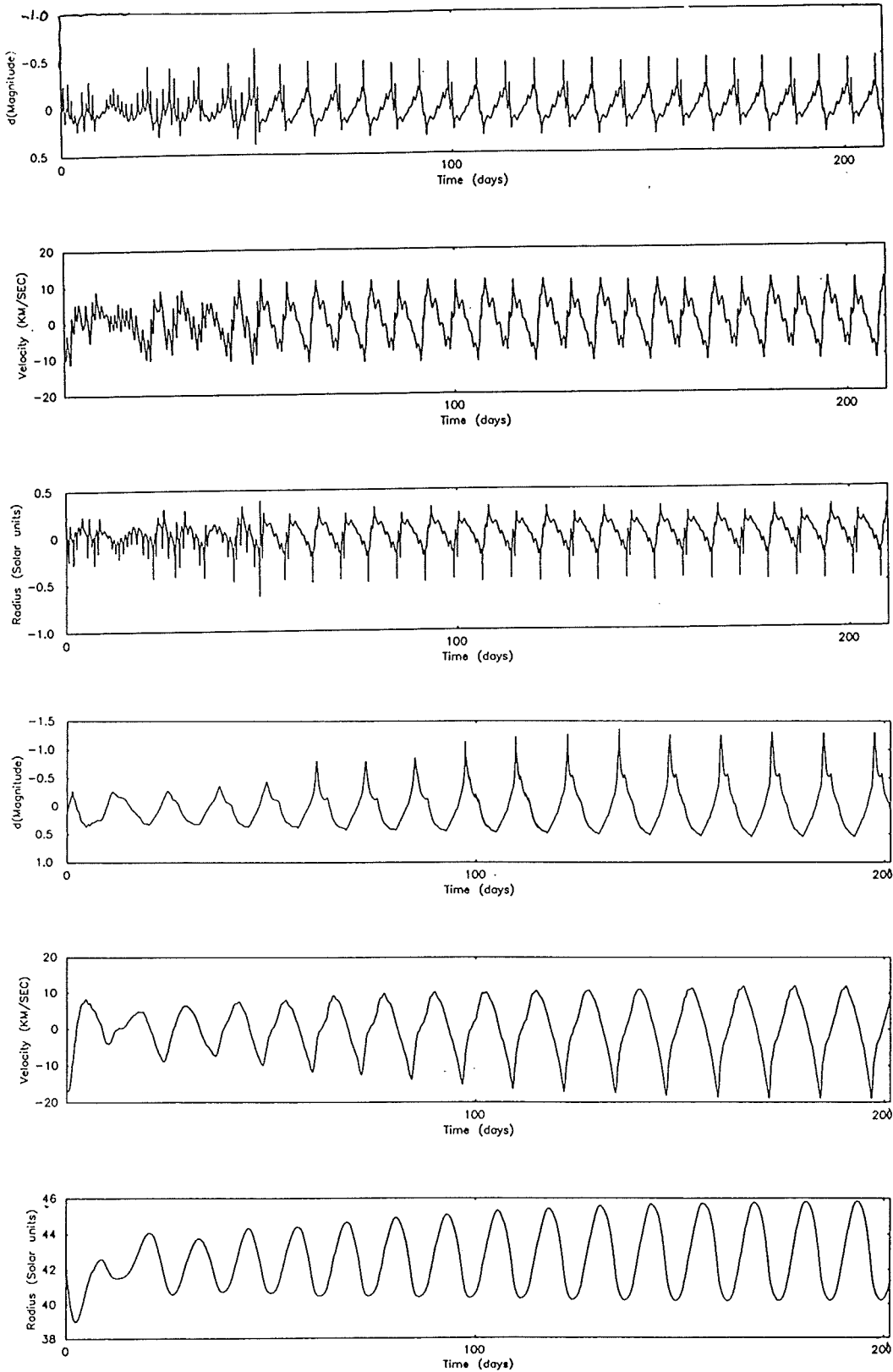


Figure 8.5 : This shows the radius in solar units (top), velocity (middle) and magnitudal variations (bottom) for each opacity table model. The top 3 graphs are the curves for the DXIX opacity table model and the bottom 3 graphs the curves for the BD9C opacity table model.

Comparison of Work Integrals

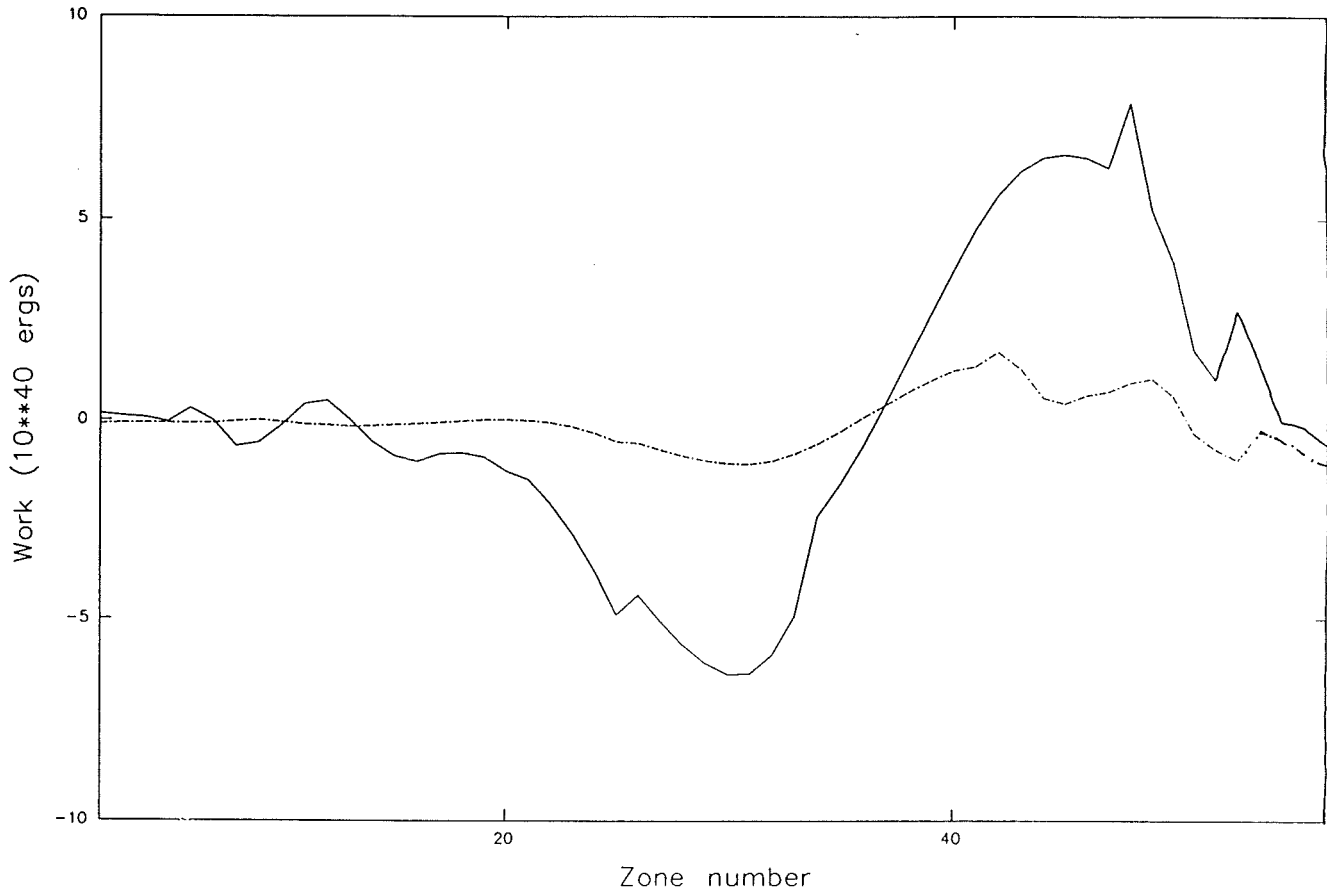


Figure 8.6 : This figure shows work integrals versus zone number for the BD9C opacity table model (solid line) overlaying the DXIX opacity table models work integral (chained line).

this may not be the case in the non-linear arena. To try and see if the linear results were correct, two models were made using both opacities. The models had the following stellar parameters (M/M_{\odot} , L/L_{\odot} , T_{eff}) = (1.0, 10^4 , 9,000) and were allowed to run until the curve shape became reasonably constant. Such a high effective temperature was chosen so that the periods would be short and hence the 'limit cycle' reached quickly. The light curves for both models can be seen in Figure 8.5 and the work integrals in Figure 8.6. We can see that there is a marked difference in the pulsation curves, the BD9C model curves being smooth and even while the DXIX model curves are 'wobbly' and uneven. The 'wobbles' in the DXIX model curves is due to small shock waves in the outer zones of the stellar envelope. An effect of these shock fronts is to produce luminosity spikes, due to the resulting increase in zone temperature and opacity. The absence of this 'wobble' from the BD9C model curves may indicate that these are a spurious effect of the DXIX opacity tables. Also when the work integrals are compared (see Figure 8.6) we see that the 'driving' and 'damping' in the BD9C model are far more prominent than those of the DXIX model.

If we now look in more detail at the two models above (Figures 8.7 - 8.9) we can see that not only does the DXIX opacity table model (RD2090) have half the period of the BD9C opacity table model (RB2090), but model RD2090 has far larger shock waves passing through the outer zones and large luminosity spikes preceding minima on every second period. The luminosity spikes appear to be due to the rarefaction following every second shock, caused by the larger acceleration of matter in every second shock. Thus, the luminosity spikes are caused by fast moving shocks travelling up through the outer zones, heating and expanding the gases of the outer zones as

NON-LINEAR NON-ADIABATIC RESULTS

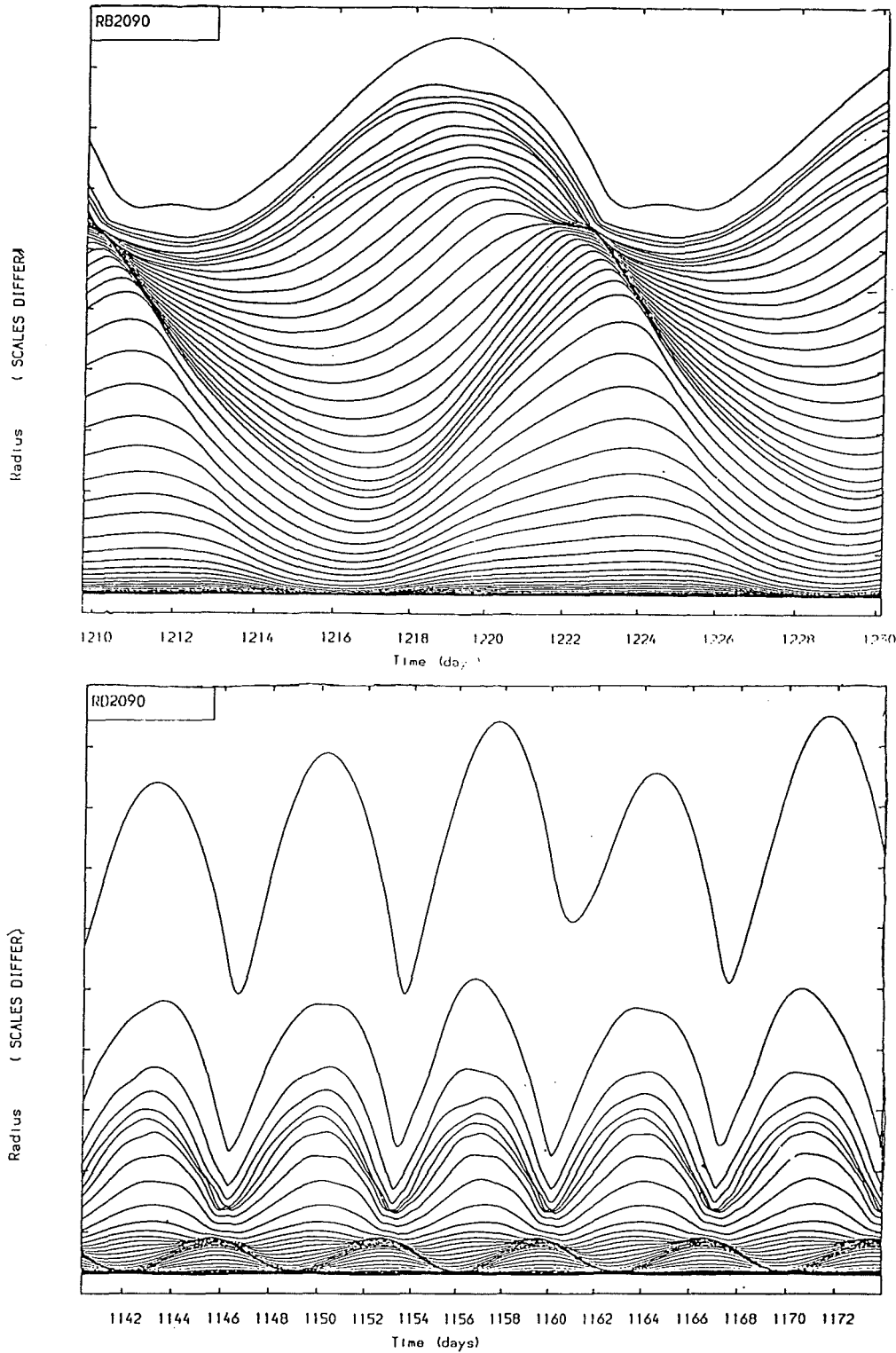


Figure 8.7 : This figure shows partial radial histories of a stellar model with the following input parameters: $(T_{\text{eff}}, L/L_{\odot}, M/M_{\odot}) = (9,000\text{K}, 10,000, 1.0)$. The top graph shows radial history of opacity table BD9C model (RB2090) and the bottom the histories for the DXIX opacity table model (RD2090).

NON-LINEAR NON-ADIABATIC RESULTS

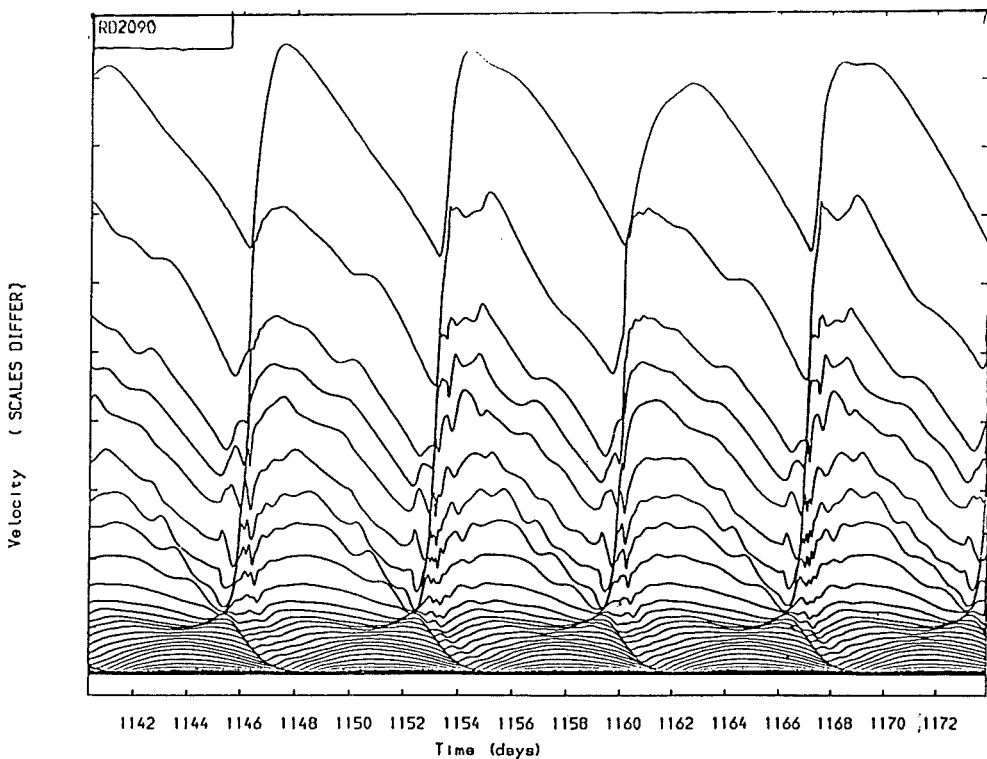
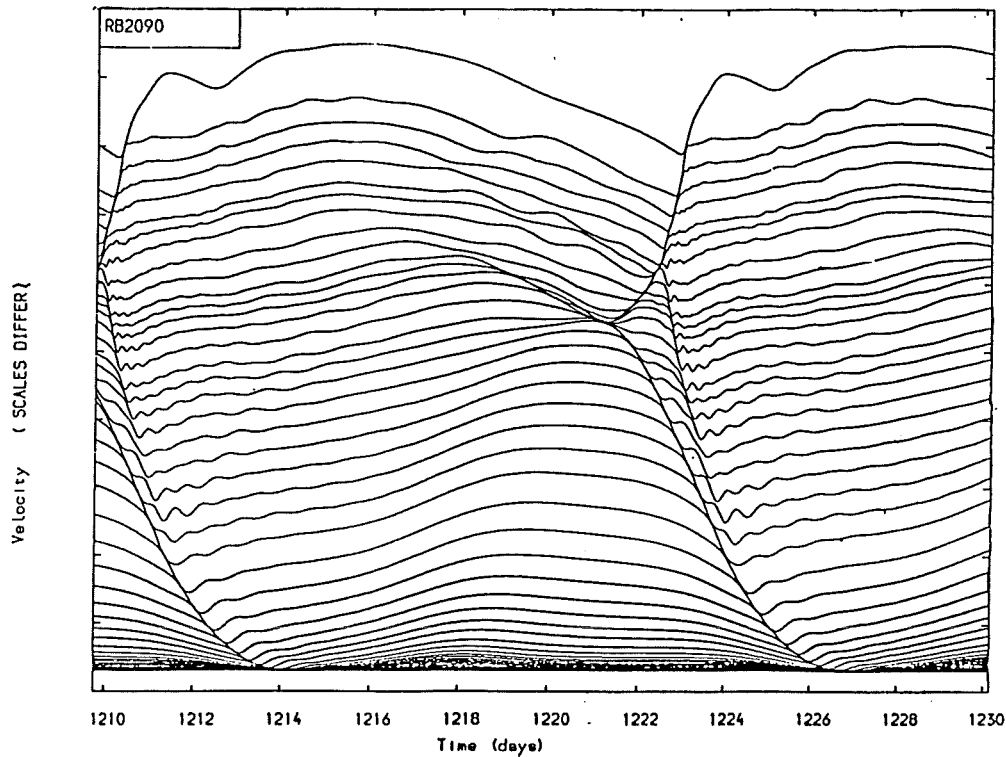


Figure 8.8 : This figure shows partial velocity histories of a stellar model with the following input parameters: $(T_{\text{eff}}, L/L_{\odot}, M/M_{\odot}) = (9,000\text{K}, 10,000, 1.0)$. The top graph shows velocity history of opacity table BD9C model (RB2090) and the bottom the histories for the DXIX opacity table model (RD2090).

NON-LINEAR NON-ADIABATIC RESULTS

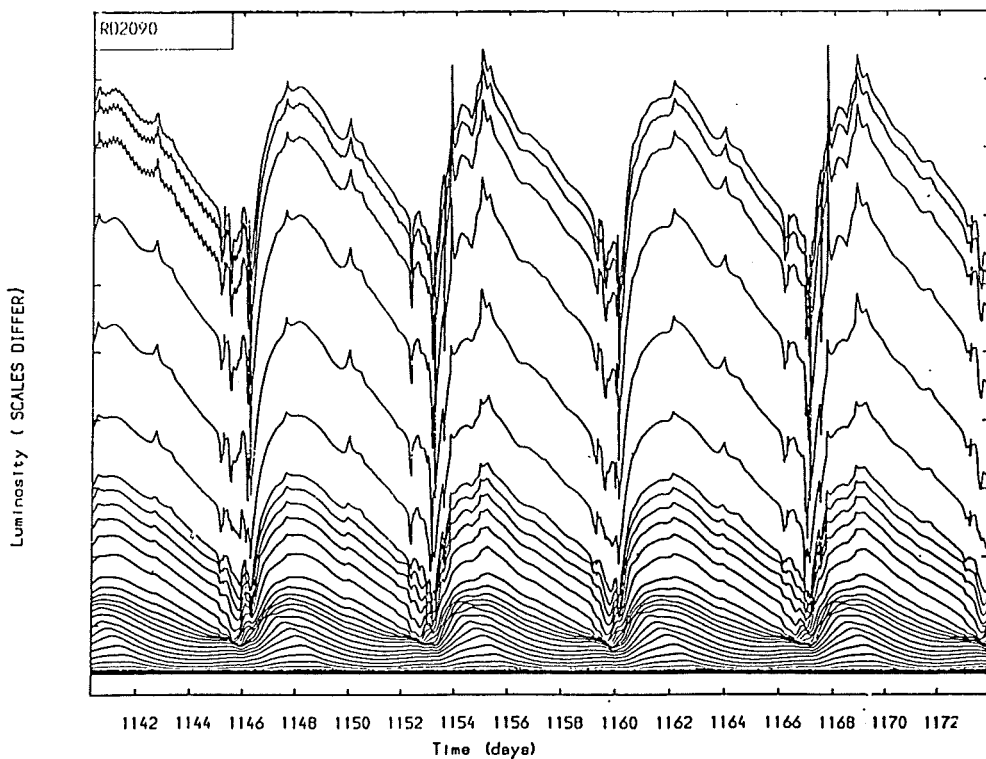
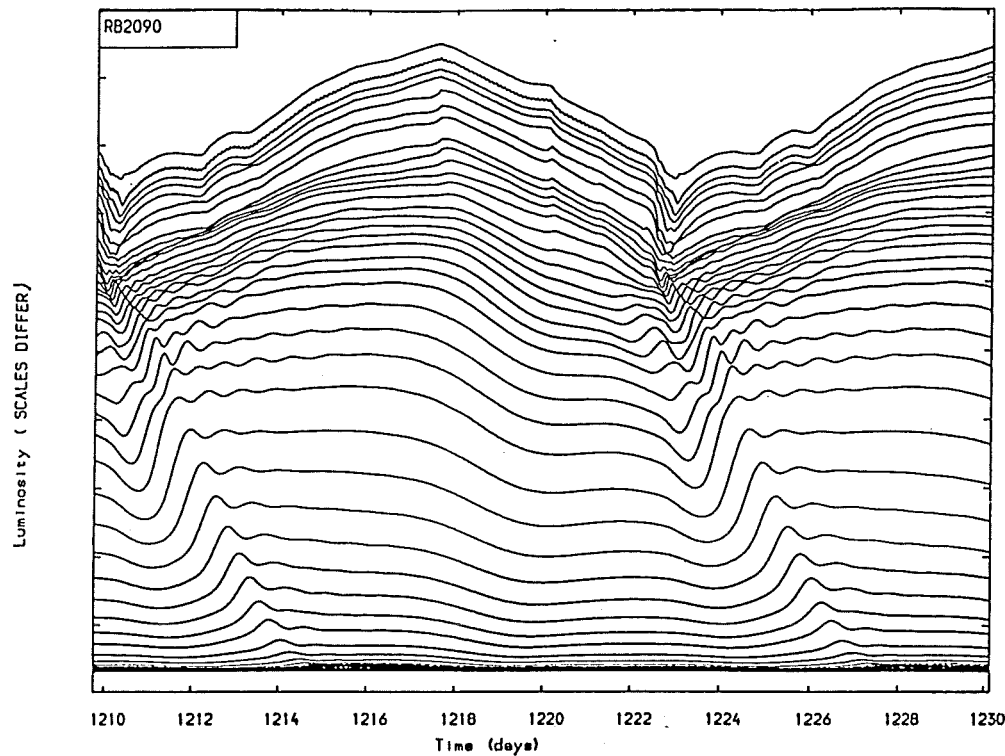


Figure 8.9 : This figure shows partial luminosity histories of a stellar model with the following input parameters: $(T_{\text{eff}}, L/L_{\odot}, M/M_{\odot}) = (9,000\text{K}, 10,000, 1.0)$. The top graph shows luminosity history of opacity table BD9C model (RB2090) and the bottom the histories for the DXIX opacity table model (RD2090).

they pass. Due to the low heat capacities of these outer zones, the shock heating is rapidly radiated away, causing the luminosity spike seen. The spikes are perhaps more prominent in the RD2090 model as the inner zone expansion seems to 'collide' with the outer zone infall around the bottom of the $\text{He}^+ - \text{He}^{++}$ ionisation region, whereas in the RB2090 model the 'collisions' occur approximately halfway through this ionisation region. Also, the shallower opacity gradient of the RD2090 model in these outer zones could also contribute to the presence of the luminosity spikes. In the RB2090 model we can see that a second inward shock is formed, at the top of the helium ionisation zone, that is more powerful than the first and soon merges with the first in the inner regions of the star, though in this case there is no 'Christy echo' of the shock from the adiabatic core. This second shock may also help to prevent the formation of unwanted luminosity spikes, as it is not present in the RD2090 model. Since the luminosity spikes are not observed in real objects it seems that the BD9C opacity table should be used in preference to the DXIX opacity table. To see if these undesirable luminosity spikes are present at other stellar input parameters, several models were made using the DXIX opacity table; the results can be found in Section 8.3 .

8.2.3 HOW VISCOUS SHOULD A STAR BE ?

A problem that occurs when the static models are evolved in time is that shock waves form in the outer envelope which have high accelerations and cause the time steps to become small and the computations processor intensive. To overcome this problem it is usual to introduce an artificial viscosity (see Chapter 3, for details). The problem is, how large should the viscosity parameter, C_Q be? A basic rule of thumb is that a shock wave is spread over $\sqrt{C_Q}$

NON-LINEAR NON-ADIABATIC RESULTS

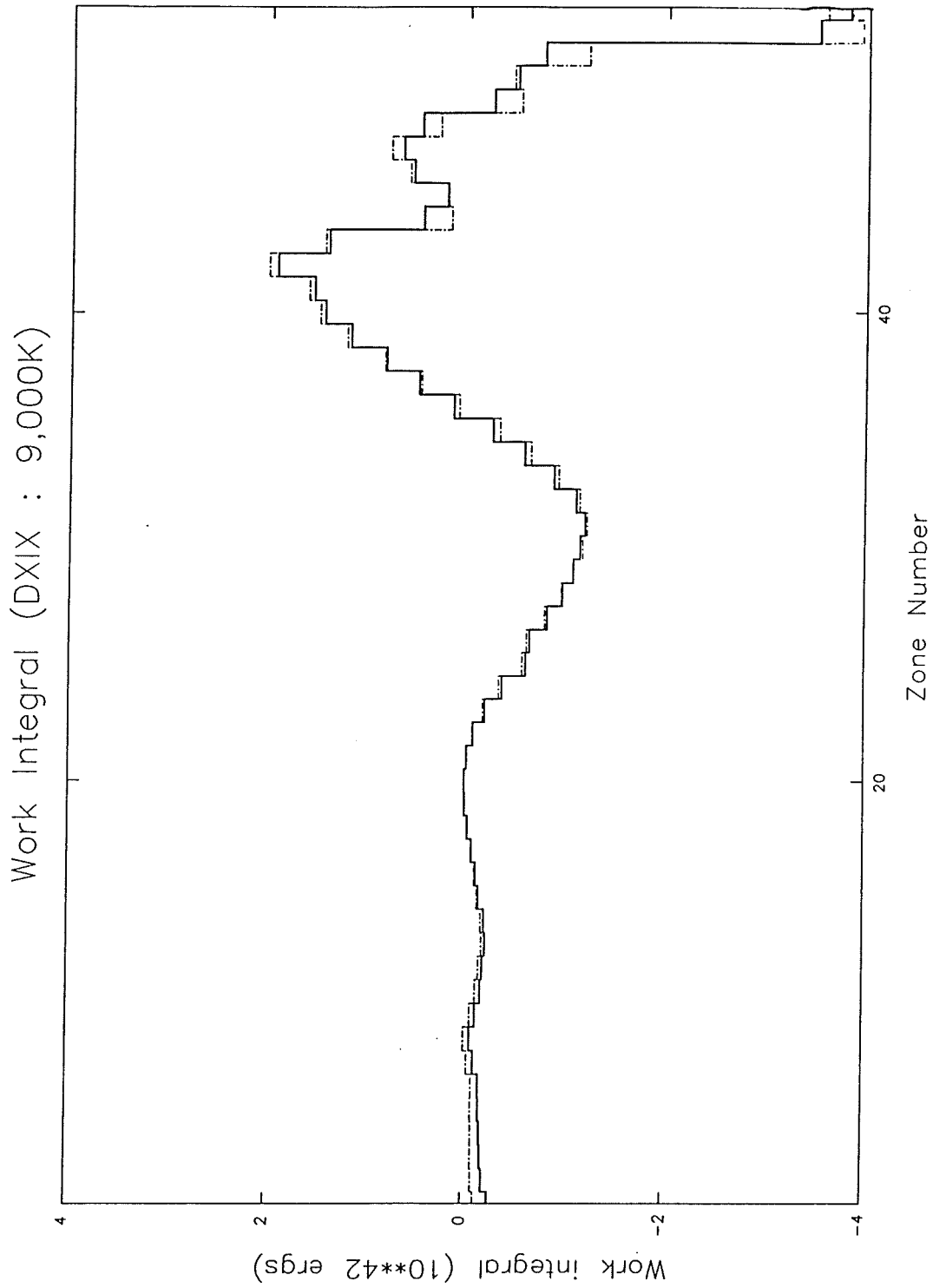


Figure 8.10 : This figure shows the work integral of model RD2090 (see figures 8.7 - 8.9) before (chained line) and after (solid line) C_Q was changed.

zones by the artificial viscosity so C_Q must be kept as low as possible to maintain energy conservation and to keep the models as accurate as possible, while being large enough to prevent the disastrous reduction in the time increment.

This problem was solved by producing several models with varying C_Q values and observing the value at which the time increment remained unaffected by further increases in C_Q . Once this point was found, the next step was to reduce C_Q until the total energy was again conserved, without reducing the time increment too much. In Figure 8.9 the effect of changing C_Q from 1.2 to 4.2 can be seen in the outer 3 zones, as the small oscillations seen in the luminosity on the L.H.S. are 'smoothed' out within a few periods.

Figure 8.10 shows the work integral before and after C_Q was changed. From this figure it can be seen that the work integral is unaffected by this change which spreads the shocks over several zones, and hence eliminates these undesirable fluctuations in luminosity. In all succeeding models $C_Q = 4.2$ was adopted as this greatly improved the calculability of the models, and perhaps gives a better representation of the viscous fluids found in real stars?

8.2.4 BOUNDARY CONDITIONS AND DILUTED RADIATION

It was decided not to include a 'radiation dilution' term in the outer atmosphere of the model as there are no opacity tables that reach to low enough temperatures (the temperatures being too low for accurate extrapolation). Also, if 'radiation dilution' were to be included, then one would also have to treat the radiation transfer equations differently, at the bare minimum introducing some geometric term (see Fadeev & Tutukov, 1981). Indeed, as the radiation diffusion

term is incorrect for such conditions, one would either have to treat the atmosphere using NLTE methods or some form of variable Eddington factor (Mihalas, 1978), which would greatly add to the cpu-time required to run the routines.

The next question was which outer boundary momentum condition should be adopted in the majority of the models? As most of the models were to be made using constant sound travel times (see Section 8.2.6), the external mass outer momentum boundary condition was rejected, i.e., $C = 0$. Now, as the radiation pressure of such luminous stars as the RCB group is not a negligible percentage of the total surface pressure, it was decided to use the full radiative outer boundary momentum condition. As the degree of radiative back pressure on the model surface was not obvious, several models were made with B ranging from 0 to $1/3$, in order to see the effects this had on the pulsation of the model. It was found that the outer boundary momentum condition only altered the amplitude of the photospheric light curve slightly and had a negligible effect on the period of pulsation. (This boundary condition could be important if the model atmosphere were modelled using NLTE or Eddington factor methods.) It was felt that there was no need to complicate things, as the basic results were not dependent on this boundary condition, so $B = 1/3$ was taken for all the models presented in this thesis.

8.2.5 HOW MUCH STAR ?

Having dealt with most of the dynamic problems and considerations, we must decide how much of the star is to be included in the initial static model and how many zones should be used in its creation. The first part of this question is answered in Appendix C, which shows that only the outer envelope and atmosphere need be made as this is

all the dynamic codes model, i.e., the core is considered static.

The second part of the question was a little more complicated and to answer it required the production of several static models. Basically it depended on how consistently the static models could be re-zoned and relaxed onto the dynamic difference equations. It was found that if the static model had more than about 450 zones, then the relaxed models were similar to 1 part in 10^6 , the order of convergence used in the dynamic codes. The consistency was found by finding the mean residual of squares of T^4 , between the relaxed model under consideration and a relaxed static model initially having a 1,000 zones. To err on the side of safety, all initial static models created in this study had at least 500 zones.

8.2.6 RE-ZONING A STATIC MODEL ENVELOPE

A very important consideration was how to re-zone the initial static model to a far coarser static model, and still maintain enough zones to show the gross details and return accurate results. For computation to remain viable the number of zones had to be minimised, while still keeping results as accurate as possible. Linked with this question is the choice of method used to create the coarse zones, i.e., constant mass ratio, or constant sound travel times (see Appendix C part 2 for computational details). Experience soon showed that although the constant mass ratio method allowed choice of the external mass boundary condition, it had the disadvantage of shortening the time increments with which the model could be evolved. This could partially be offset by altering the inner zone mass ratio to increase the sound speed travel time in these zones. Generally, however, it was found that the outer layers were well behaved, and the constant sound travel time method of zoning could be used. This

simplified things a lot, as the time increment was then independent of the inner zone size. However, care must be taken to ensure that the inner zones do not become too heavy, and thus distort the results. This is usually controllable, by increasing the number of zones in the coarse model. An indication of the effect of the number of zones on the photospheric light curves can be seen in Figure 8.11. It was generally found from the models used in this work that about 55 zones in the coarse model gives the best compromise between speed and accuracy.

8.2.7 OTHER CONSIDERATIONS

This only leaves us with two considerations, the convergence and the initial velocity profile. The convergence was set to 6 significant figures, as this was the best accuracy that could be obtained on the computer used. If a greater accuracy was imposed, the grand iteration in temperature at each time step failed to converge, causing the time increment to be continually halved until an underflow occurred. If this problem was relieved, then the iteration in the 'states' routine failed to converge and indefinitely oscillated between two values for the electron number density. Thus, there is an accuracy of about 1 part in 10^7 for each zone, and the results are probably reasonably accurate for the first few hundred thousand time steps (see Worrell (1985) for a full discussion on propagation of errors in hydrodynamic calculations of stellar models).

It was found that, in most cases, the empirical formula that Stobie used for his Classical Cepheids (equation 3.47 with $A = 10$ km/sec and $B = 0$ km/sec) started the models pulsating in their fundamental modes.

NON-LINEAR NON-ADIABATIC RESULTS

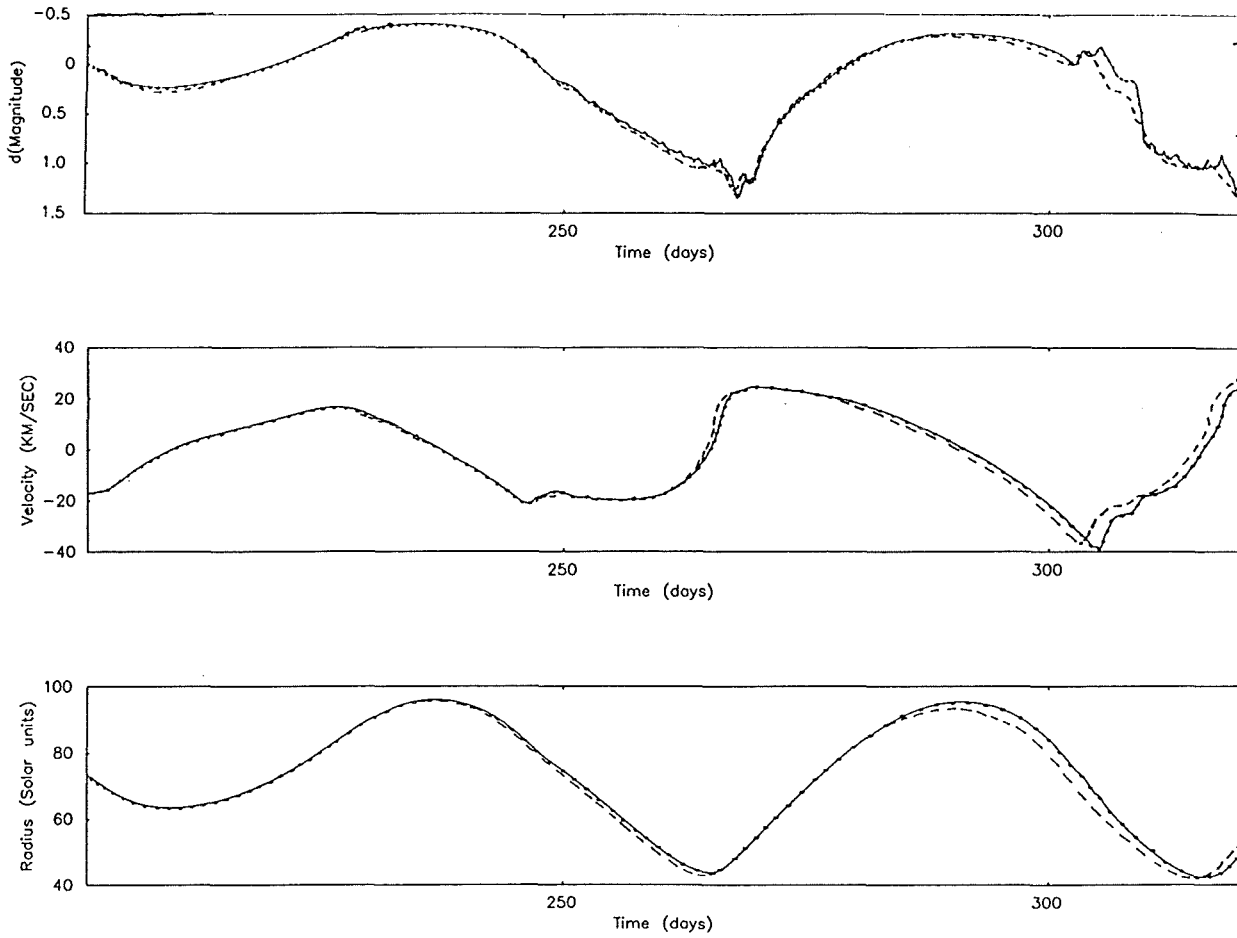


Figure 8.11 : Shows the radius in solar units (top), velocity (middle) and variation in magnitude (bottom) for $(M/M_{\odot}, L/L_{\odot}, T_{\text{eff}}) = (1.0, 3,000, 5,000)$ model. The dashed lines show the 48 zone model, the solid lines shows the 56 zone model and the dotted line shows the 68 zone model.

As these models have low e-folding times, reaching their limit cycles within a few periods (unless stable to pulsation, in which case the light curve variations rapidly decayed) and contamination due to higher overtones was generally damped out within a few periods, or was not present at all.

8.3 CHOOSING THE OPACITY TABLE FOR NON-LINEAR RCB MODELING

8.3.1 How Stellar Parameters Affect The Non-linear DXIX Opacity Table Models

In Figure 8.12, the luminosity and velocity curves of a sequence of models at $L = 10,000L_{\odot}$ and $T_{\text{eff}} = 7,000 \text{ K}$, and having masses of 1.0, 1.2, 1.6, 2.0 M_{\odot} are shown. For the 1.6 M_{\odot} and 2.0 M_{\odot} models it is clear that they do not pulsate in the fundamental mode, which is in agreement with the linear results for higher masses (see Figure 7.2). The small cyclic variation in the velocity curve, and to a lesser extent in the luminosity curve, are due to small shock waves in the outer zones of the model envelopes. As the mass is reduced the shocks become more pronounced and begin to dominate the light curves, becoming erratic in nature and penetrating deep into the stellar envelope. This effect is not found in models using the BD9C opacity table, and may be a spurious effect of the DXIX opacity table. To check that this effect is present at other luminosities and effective temperatures, another two sequences can be seen in Figures 8.13 and 8.14, in which luminosity and effective temperature are the variable parameters, respectively.

From Figure 8.13 again we see that the amplitude of the variations is decaying; this observation is borne out by a Fourier analysis of the light curves which shows a negative growth constant. These models

also show pronounced shock-wave features, that grow in amplitude with increasing luminosity, and also become spike-like. The reason for this correlation between shock induced luminosity spikes and luminosity appears to be the reduction in the envelope density of the outer zones caused by the increased luminosity. This has the effect of reducing the shock front size and hence the time for which the opacity is reduced. The shock-wave spikes in luminosity could be reduced by increasing C_Q (see Section 8.2.3 above), but care has to be taken not to spread the shocks out too much, as above $C_Q = 5$, the total energy is no longer conserved. Again, these shock waves were not present in the equivalent BD9C models.

In Figure 8.14, the models for which the effective temperature was varied, shock-wave luminosity spikes are very evident and, with the exception of the 6,000 K model, dominate the light curves. In the higher effective temperature models, the shock wave effects were found to penetrate up to 50% of the way into the model envelopes, and could no longer be considered surface effects. As the BD9C opacity table models of identical input parameters only had minor shocks present in the outer 2 or 3 zones, it is hard to decide whether these shocks are real or a spurious effect of the DXIX opacity table. For this reason and the fact that the shocks cause the incremental times to become alarming small (from about 6,000 seconds down to about 200 seconds), opacity table BD9C was chosen for most of the non-linear modelling in the next section. This has the other useful effect of making the underlying fundamental mode pulsation easier to see, and to describe. These shock waves are probably real effects, though perhaps not so pronounced, and could explain why the luminosity amplitudes seen in the majority of variable RCB stars are so small (compared with other variable stars in adjacent regions of the HR diagram).

NON-LINEAR NON-ADIABATIC RESULTS

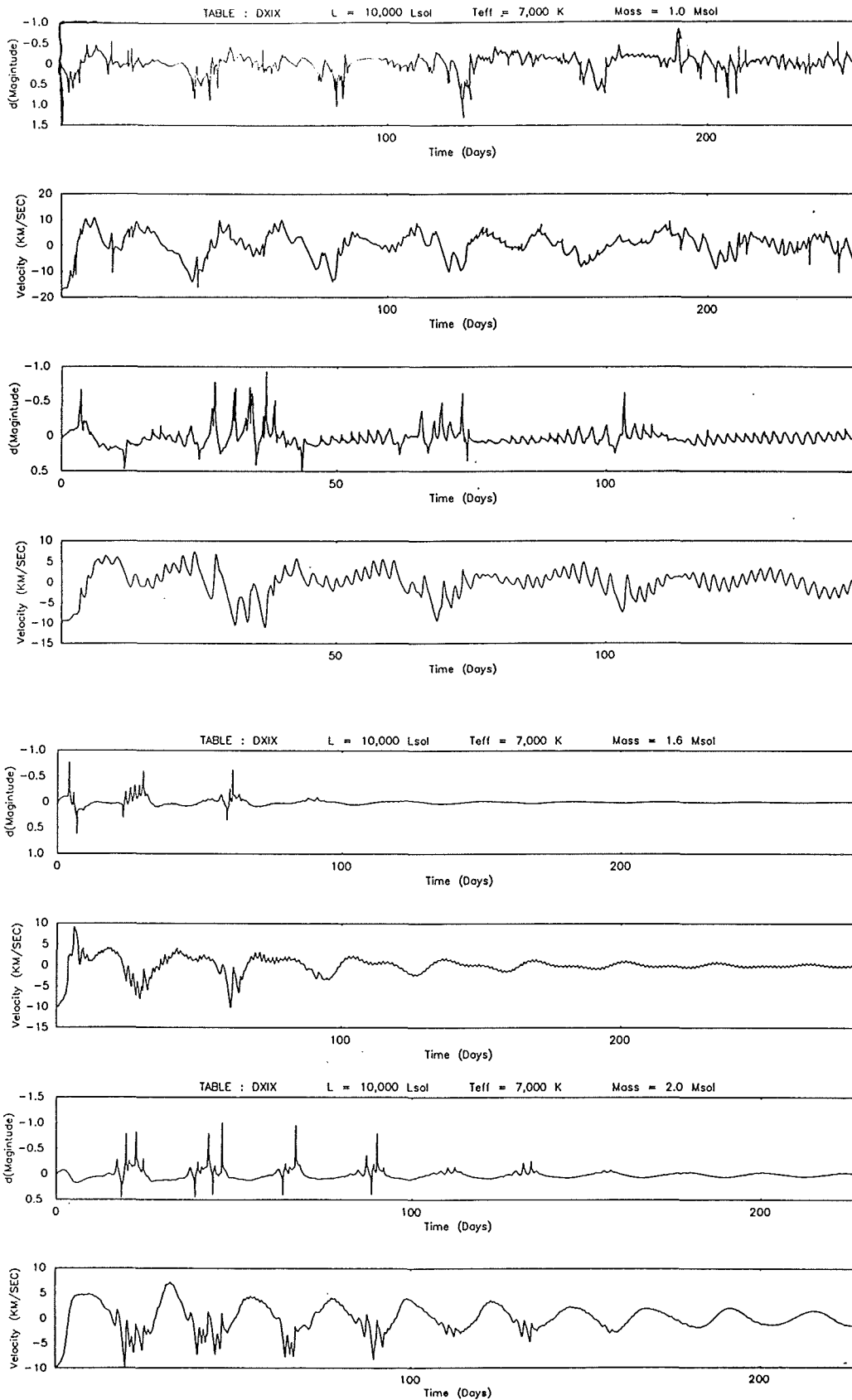


FIGURE 8.12 : In this figure, luminosity and velocity curves are shown for 4 models with differing masses ($1.0M_{\odot}$, $1.2M_{\odot}$, $1.6M_{\odot}$, $2.0M_{\odot}$) All the models have luminosities of $10,000L_{\odot}$ and effective temperatures of 7,000 K.

NON-LINEAR NON-ADIABATIC RESULTS

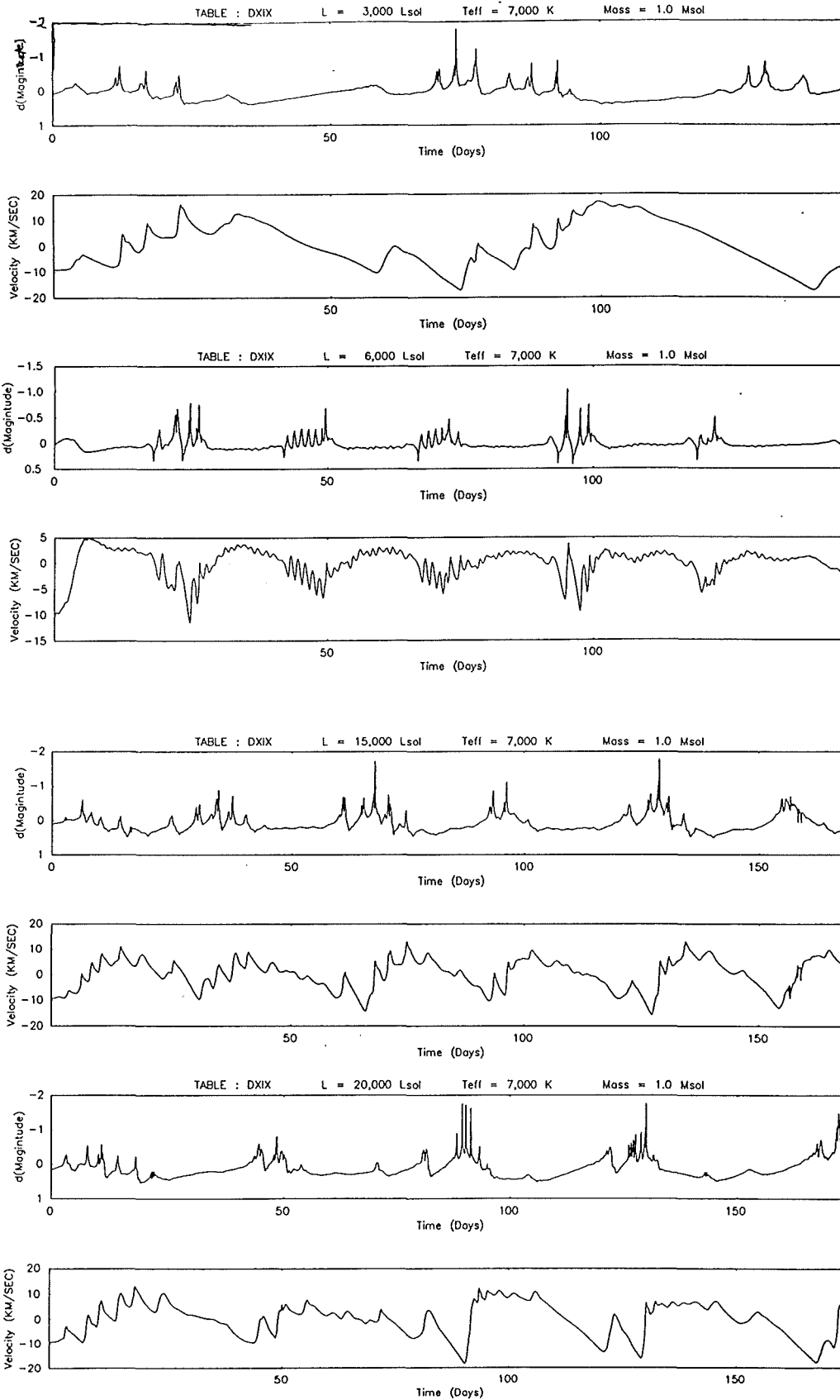


FIGURE 8.13 : In this figure, luminosity and velocity curves are shown for 4 models with differing luminosities ($3,000L_{\odot}$, $6,000L_{\odot}$, $15,000L_{\odot}$, $20,000L_{\odot}$). All the models have masses of $1M_{\odot}$ and effective temperatures of $7,000 \text{ K}$.

NON-LINEAR NON-ADIABATIC RESULTS

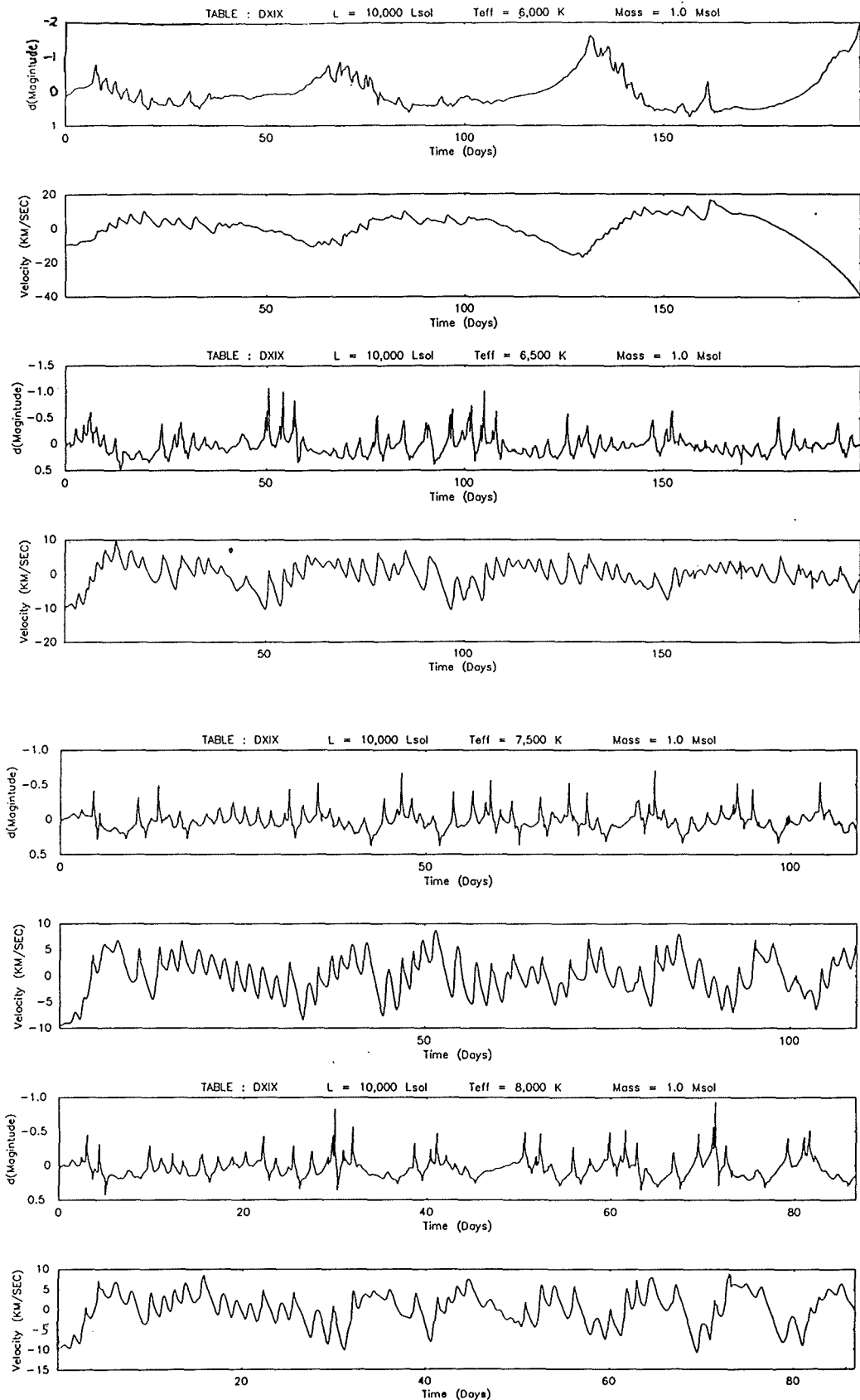


FIGURE 8.14 : In this figure, luminosity and velocity curves are shown for 4 models with differing effective temperatures (6,000K, 6,500k, 7,500k, 8,000K). All the models have masses of $1M_{\odot}$ and luminosities of $10,000L_{\odot}$.

8.3.2 A Brief Look At Some Models Of DY Centauri

As DY Cen is thought to pulsate with a period of 120 days and is the only 'hot' member of the RCB group whose membership of the RCB group has not, as yet, been brought into to doubt, it was decided to make several models, using both opacity tables, to see whether either of them produced a period of the right magnitude. Also, this was used as another check on our preference of opacity table BD9C over DXIX.

From Figure 8.15 we again see that the two attempts at modelling the star using opacity table DXIX are dominated by the 'wobbles' caused by the small shock waves in the outer envelope, this effect is far worse in the higher mass model, where the underlying periodicity of the model envelope is obscured.

If we now look at the two BD9C models on the bottom half of Figure 8.15, we see that the shock waves are small in the 10,000K model, and are quite well behaved when they appear in the 12,000K model. From all the curves for both opacity tables, it is apparent that none of the models have a 120 day period, although the 12,000K BD9C model does have an amplitude of about 0.4^m , which is consistent with the observed amplitude of variation in DY Cen's visual light curve (allowing for the fact that the model's output is in bolometric magnitude and not visual magnitude). Also, the 12,000K BD9C model is semi-regular in nature with no luminosity spikes, unlike the best DXIX models which are full of shock wave luminosity spikes. Again the results seem to favour the BD9C opacity table (although still not conclusively). Figure 8.16 shows a 40,000K model that is a classic case of stability, as is to be expected in such a 'hot' model.

NON-LINEAR NON-ADIABATIC RESULTS

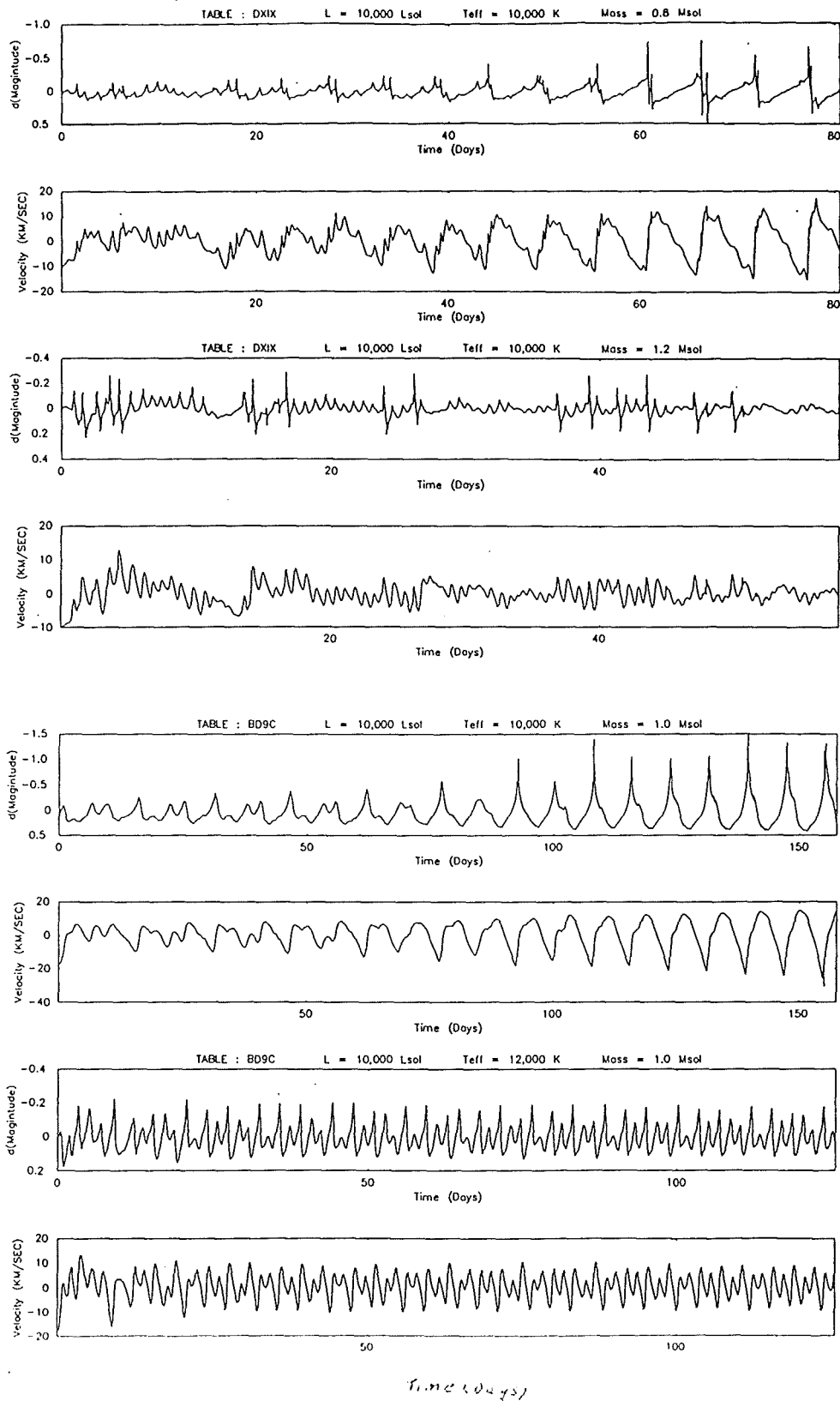


FIGURE 8.15 : This figure shows two 10,000K models with different masses made using opacity table DXIX and two models with effective temperatures of 10,000K and 12,000K, made using opacity table BD9C.

NON-LINEAR NON-ADIABATIC RESULTS

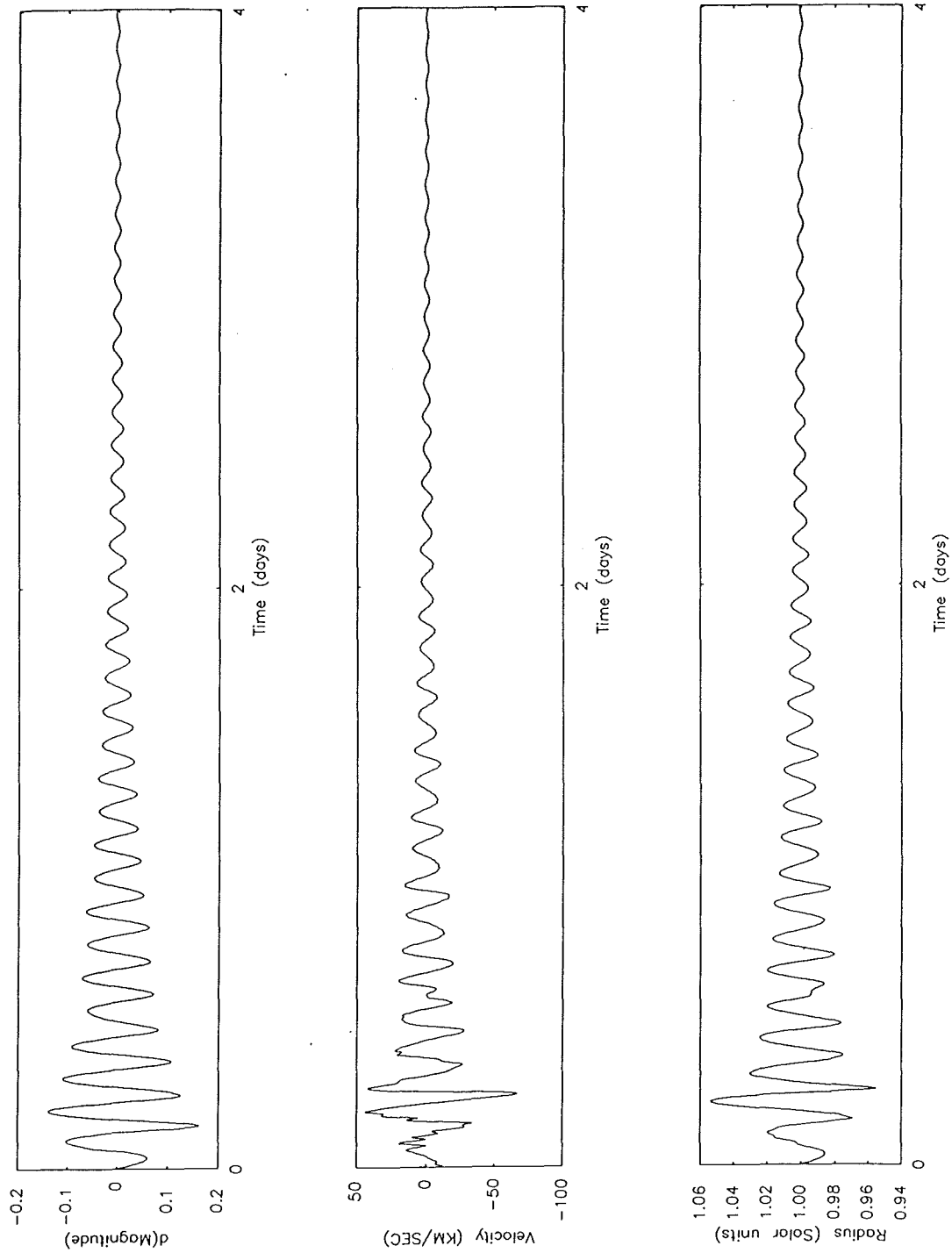


FIGURE 8.16 : A special case, showing what happens when a stable model envelope perturbed; showing clearly a rapid decay back to the stable state.

NON-LINEAR NON-ADIABATIC RESULTS

A more detailed understanding of these models, as well as an understanding of why the two opacity tables produce such remarkably different behaviour in the light curves, can be obtained if we have a closer look at the history of the envelopes over one or more periods. Figures 8.17 - 8.28 show Radial, Velocity and Luminosity histories for all the outer zones of the models discussed above.

From these figures it is apparent that luminosity spikes are a definite feature of models created using the DXIX opacity table. It is also apparent that they are not eliminated by reducing the star's mass or increasing its effective temperature. The luminosity spikes only appear when steep shocks sweep through the outer zones, as can be seen in Figures 8.17 - 8.18 and Figures 8.20 - 8.21. We can see that even a shallow shock (i.e., the secondary shock following the first) can cause large changes in the luminosity, approaching that of a spike. They appear to be caused by the heating the gases undergo as the shock front passes, which not only causes a drop in the opacity of the gases behind the shock front, but also causes shock generated radiation. This radiation is emitted as soon as the shock front has passed, as the gases have little heat capacity and, due to the rarefaction after the shock, low opacity as well. This helps us understand why the spikes only occur in the DXIX models. The reason appears to be the steep 15,000K opacity drop seen in the BD9C opacity table, which is far shallower in the DXIX opacity table. This then leads to the DXIX models having 'thinner' or less dense zones in the outer regions and a corresponding drop in heat capacity. At the same time, the opacity gradient in the outer zones is larger and more dependent upon the temperature and density. These two differences combine to allow a luminosity spike where the denser and shallower opacity gradient of the BD9C models suppresses such rapid changes in

luminosity, i.e., where the luminosity variations are 'frozen in'.

The pulsation in all four models seems to be driven by a sort of shock κ -mechanism, in which subsequent pulsations are driven by the shock produced when the infalling outer zones meet the expanding inner zones. This leads, to a large increase in the ionisation of helium and hence a large increase in pressure, which rapidly develops two shock waves. One of these drives the outer zones rapidly out, and the other re-compresses the inner zones for the next period. The inward shock only seems to build up once the helium ionisation region is truly met, and the top of the opacity bump is reached. After this point the 'dammed' radiation is released allowing zones to decelerate until the opacity bump peak is reached again and a second shock is formed. This second shock is usually steeper than the first and hence merges with the first somewhere in the inner regions (this can be seen in most of the histories). This accounts for the periodicity of the majority of the models, although model RD3010 seems to go through cycles of periodic behaviour followed by semi-erratic cycles of roughly the same period but with greatly reduced amplitudes. These cycles appear to be connected with fluctuations of up to 100K in the outer zone temperatures, and occur when the zones are cooler.

The bi-periodicity seen in the light curves of model RB2012 (Figures 8.26 - 8.28) seems to be explained by the fact that the second inward shock does not merge with the first inward shock, and hence causes the inner zones to be driven out further. This then causes the second inward shock to vanish and the first inward shock to be much weaker on the next compression. Hence the next outward shock is correspondingly weaker. This means that the next infall of the outer zones is longer and thus has more momentum for the following period, leading to the larger amplitude variation seen.

NON-LINEAR NON-ADIABATIC RESULTS

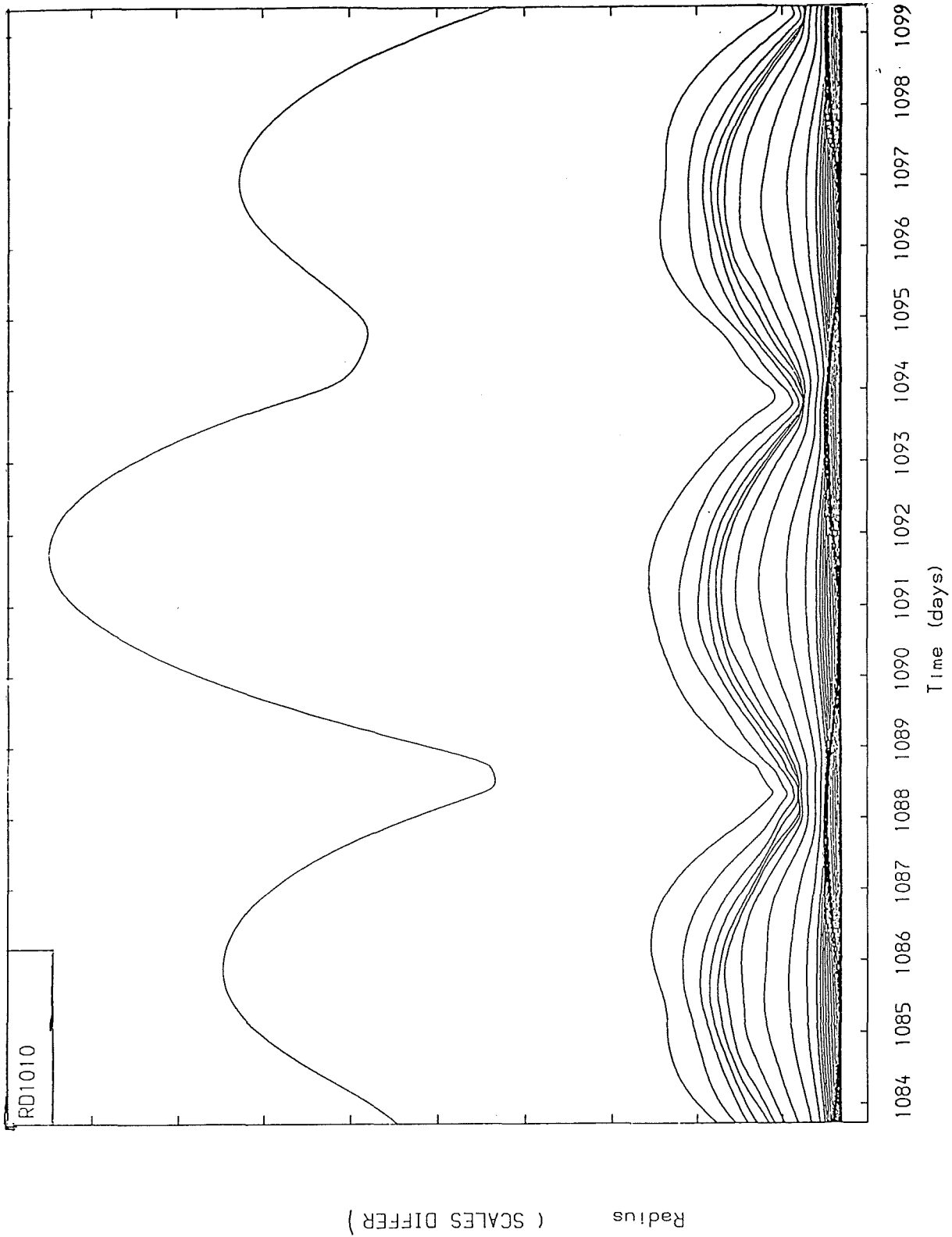
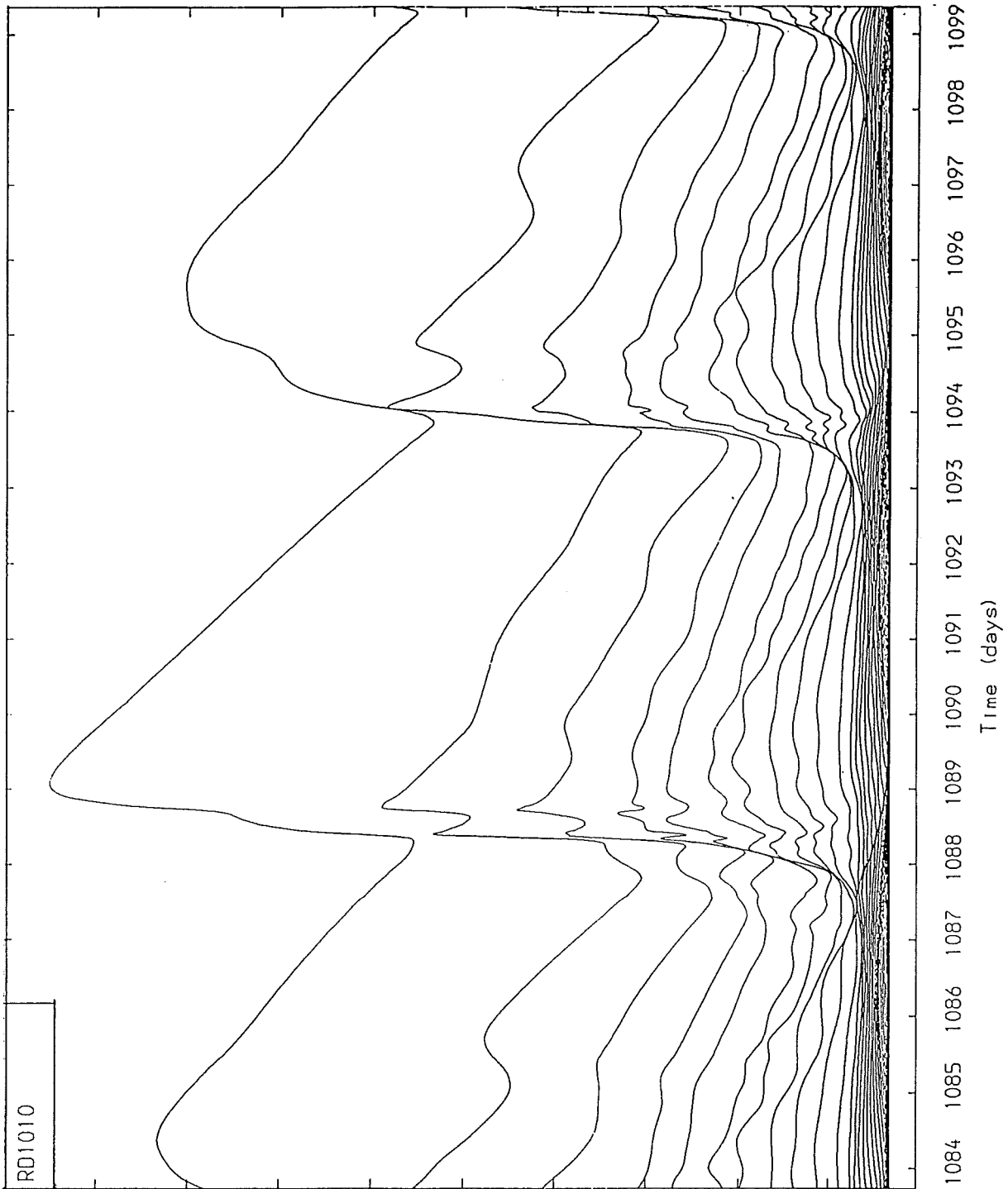


Figure 8.17 : This figure shows the radial (dR/R) history for all zones of the DXIX opacity table model, which as a mass of $0.8M_{\odot}$, a luminosity of $10,000L_{\odot}$ and a effective temperature of $10,000K$ (RD1010).



Velocity (SCALES DIFFER)

Figure 8.18 : This figure shows the velocity history for all zones of the DXIX opacity table model, which as a mass of $0.8M_{\odot}$, a luminosity of $10,000L_{\odot}$ and a effective temperature of $10,000K$ (RD1010).

NON-LINEAR NON-ADIABATIC RESULTS

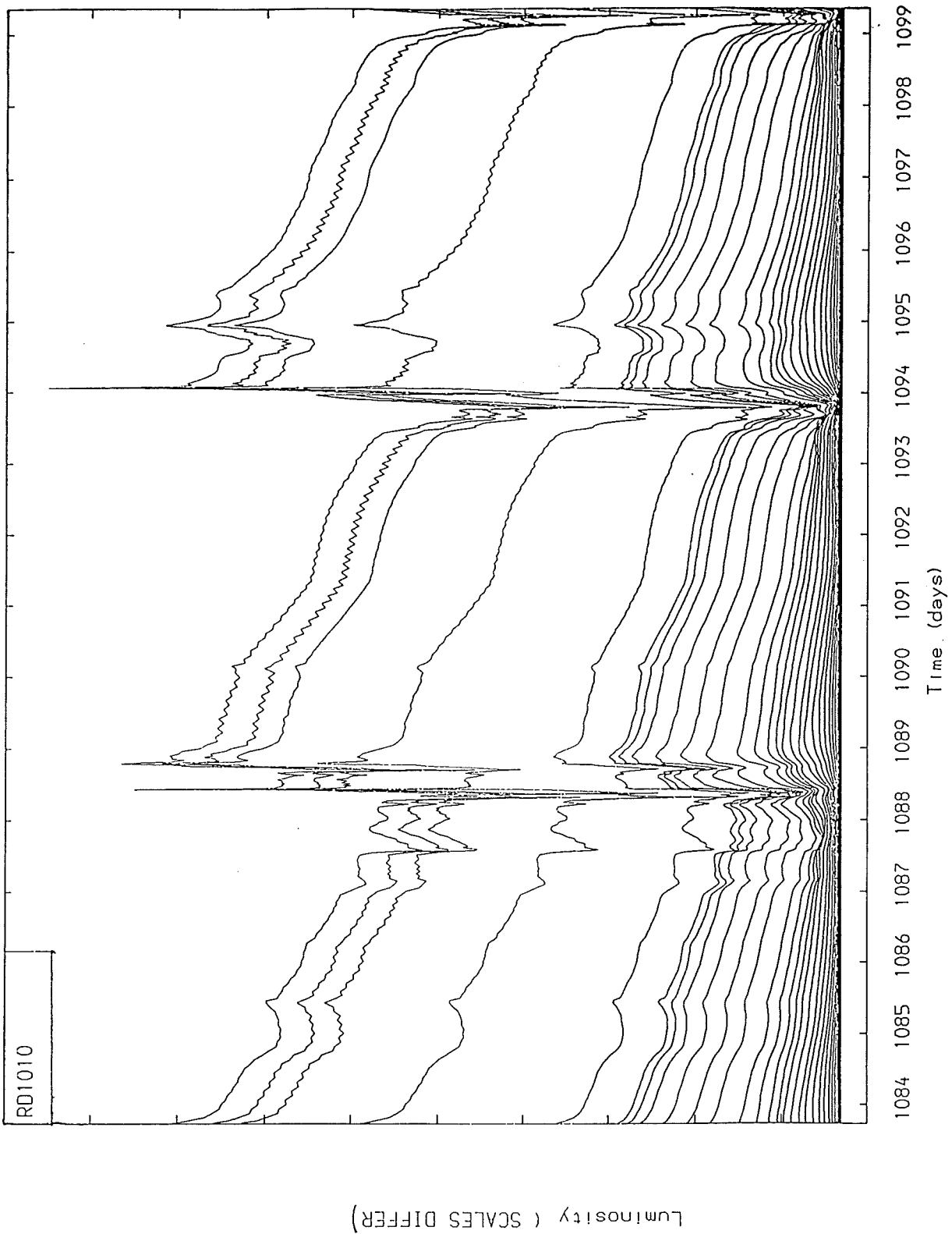


Figure 8.19 : This figure shows the luminosity (dL/L) history for all zones of the DXIX opacity table model, which as a mass of $0.8M_{\odot}$, a luminosity of $10,000L_{\odot}$ and a effective temperature of $10,000K$ (RD1010).

NON-LINEAR NON-ADIABATIC RESULTS

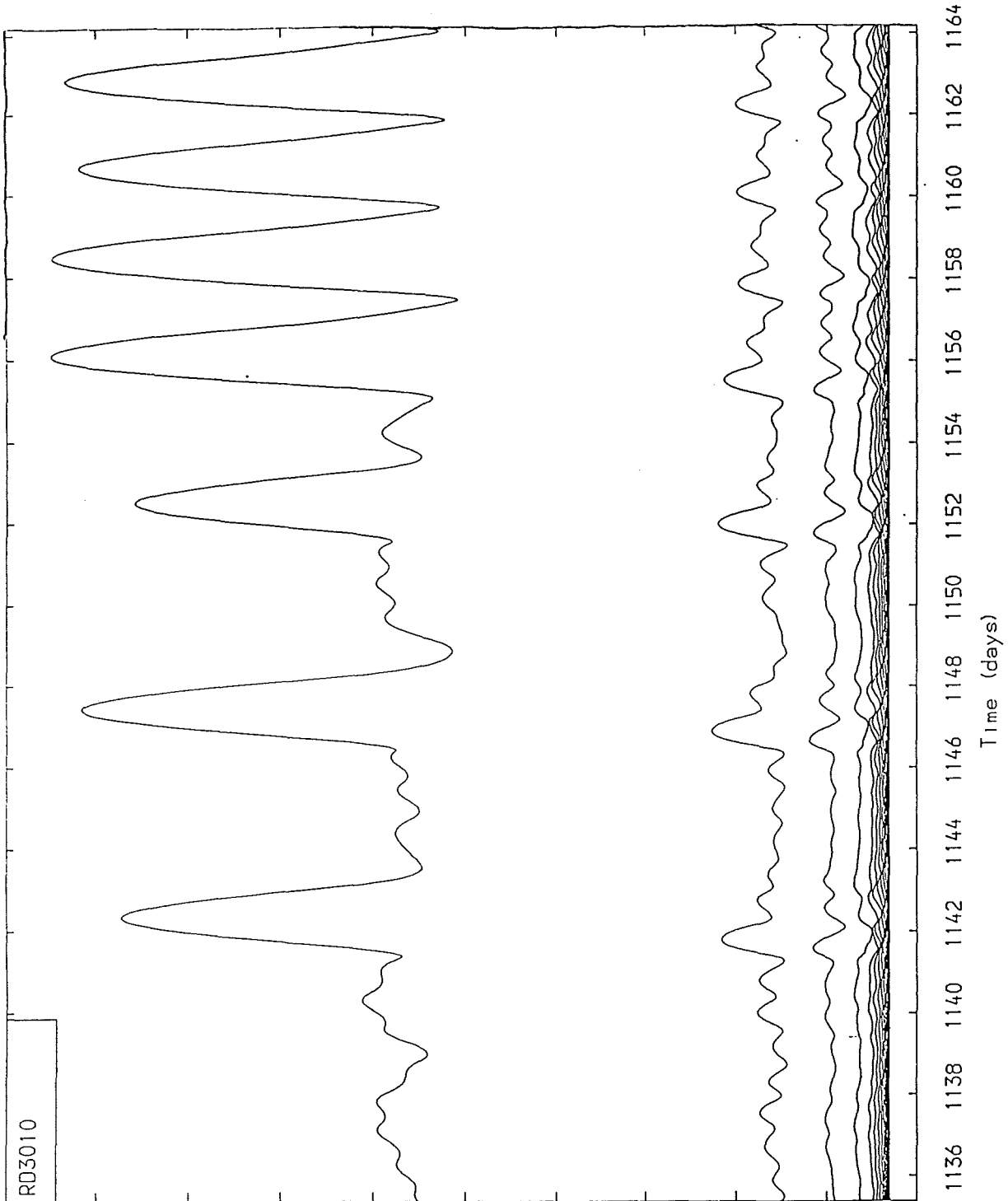


Figure 8.20 : This figure shows the radial (dR/R) history for all zones of the DXIX opacity table model, which as a mass of $1.2M_{\odot}$, a luminosity of $10,000L_{\odot}$ and a effective temperature of $10,000K$ (RD3010).

NON-LINEAR NON-ADIABATIC RESULTS

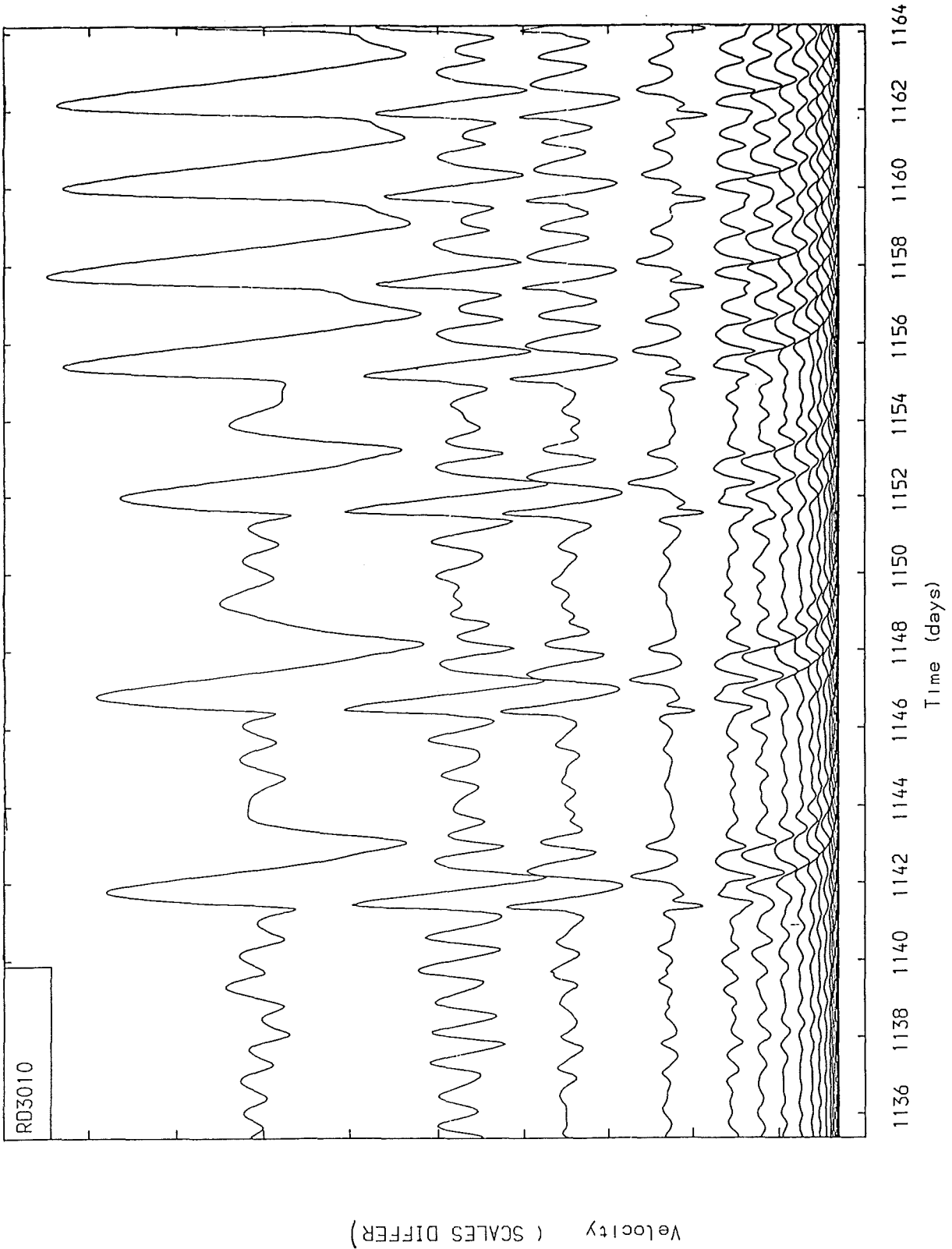
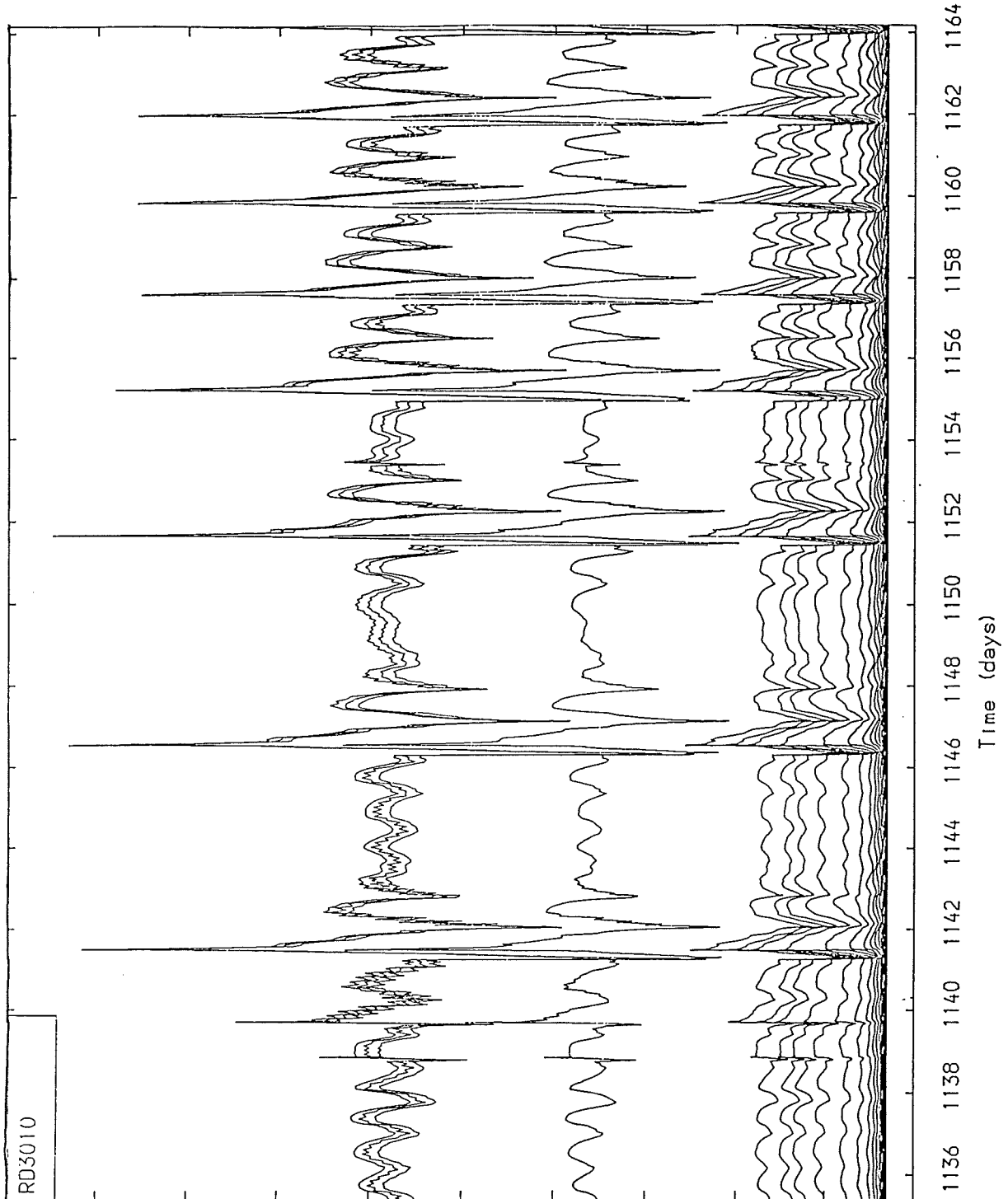


Figure 8.21 : This figure shows the velocity history for all zones of the DXIX opacity table model, which as a mass of $1.2M_{\odot}$, a luminosity of $10,000L_{\odot}$ and a effective temperature of $10,000K$ (RD3010).

NON-LINEAR NON-ADIABATIC RESULTS



Luminosity (SCALES DIFFER)

Figure 8.22 : This figure shows the luminosity (dL/L) history for all zones of the DXIX opacity table model, which as a mass of $1.2M_{\odot}$, a luminosity of $10,000L_{\odot}$ and a effective temperature of $10,000K$ (RD3010).

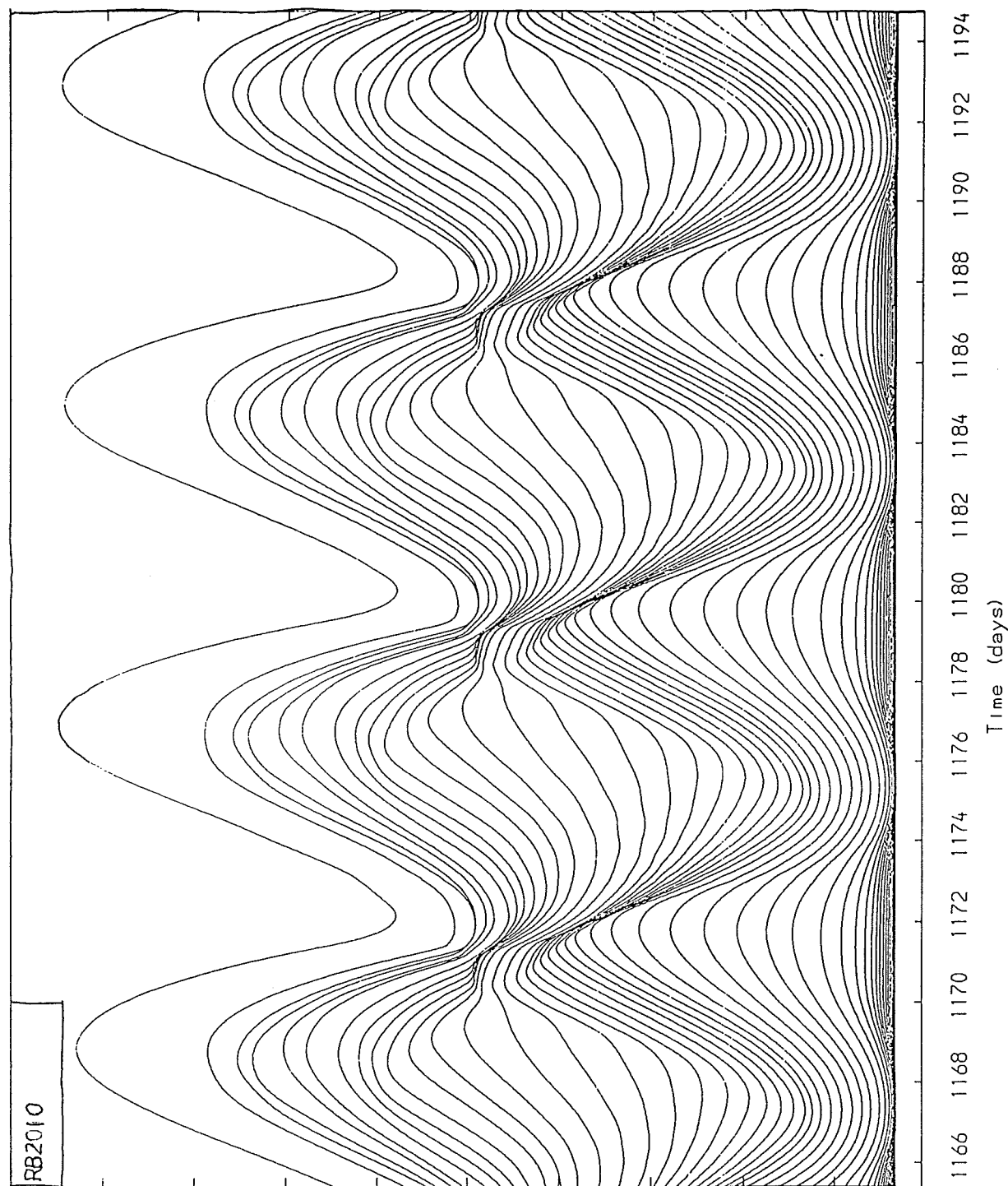
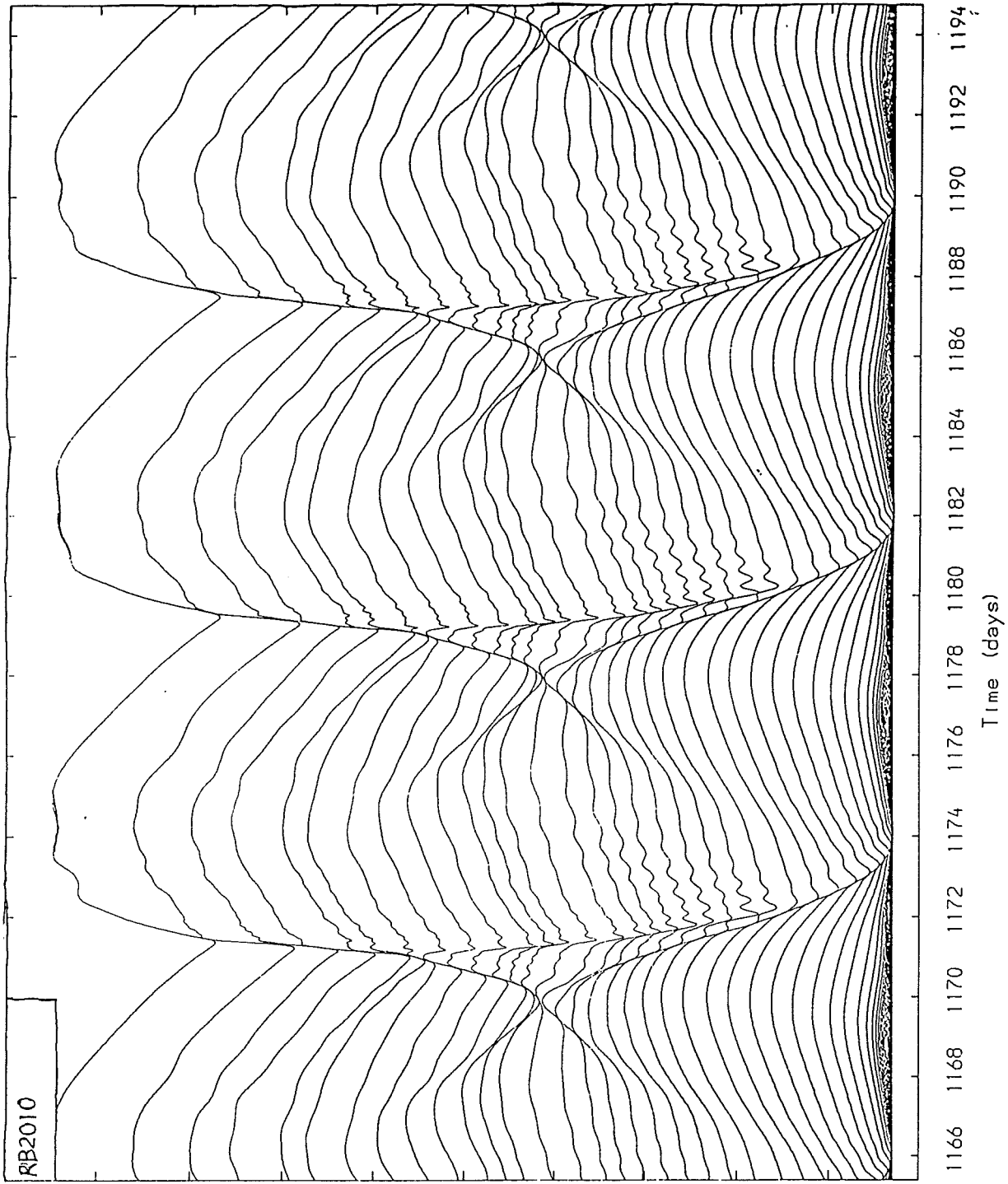
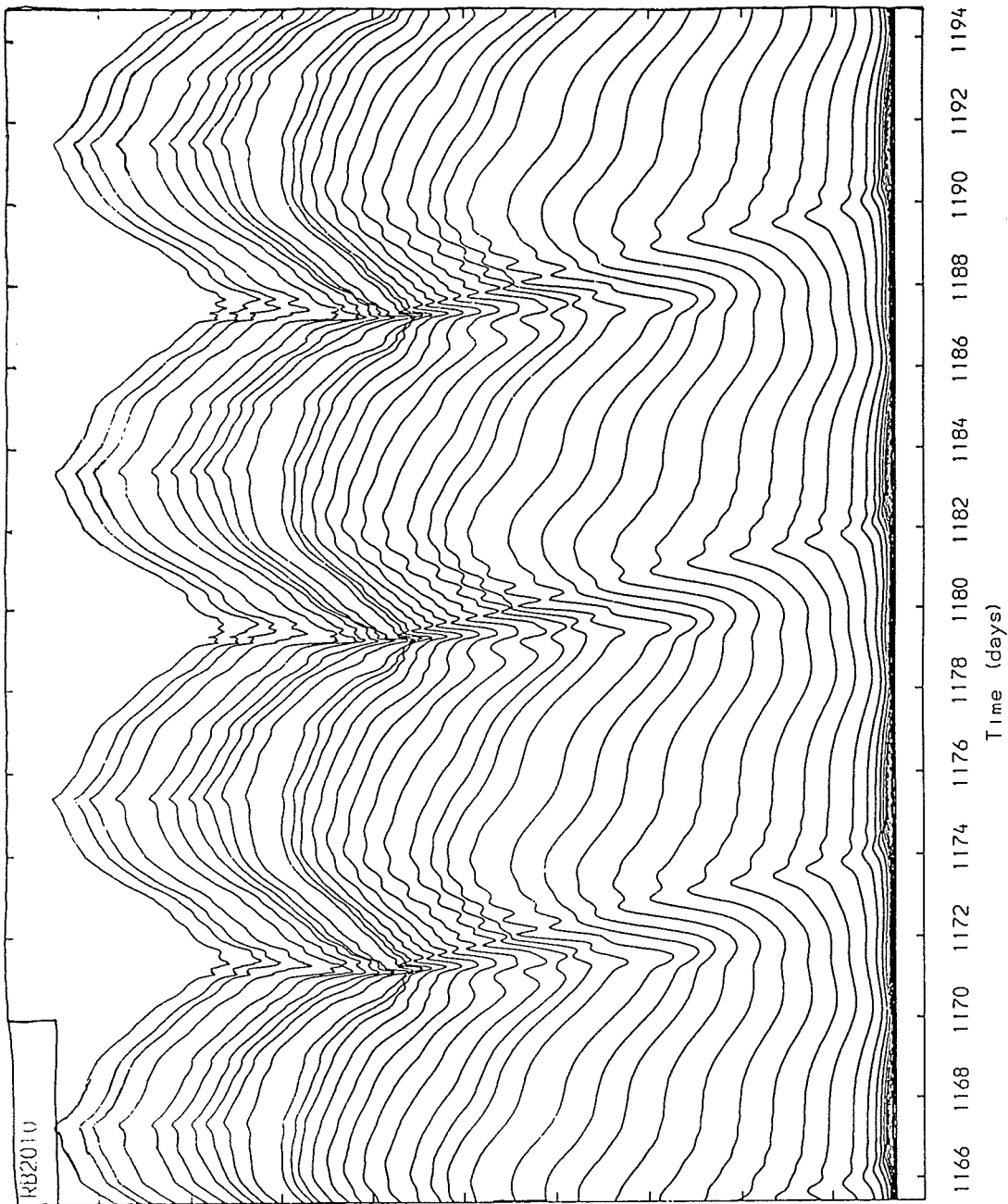


Figure 8.23 : This figure shows the radial (dR/R) history for all zones of the BD9C opacity table model, which as a mass of $1.0M_{\odot}$, a luminosity of $10,000L_{\odot}$ and a effective temperature of $10,000K$ (RB2010).



Velocity (SCALES DIFFER)

Figure 8.24 : This figure shows the velocity history for all zones of the BD9C opacity table model, which as a mass of $1.0M_{\odot}$, a luminosity of $10,000L_{\odot}$ and a effective temperature of $10,000K$ (RB2010).



Luminosity (SCALES DIFFER)

Figure 8.25 : This figure shows the luminosity (dL/L) history for all zones of the BD9C opacity table model, which as a mass of $1.0M_{\odot}$, a luminosity of $10,000L_{\odot}$ and a effective temperature of $10,000K$ (RB2010).

NON-LINEAR NON-ADIABATIC RESULTS

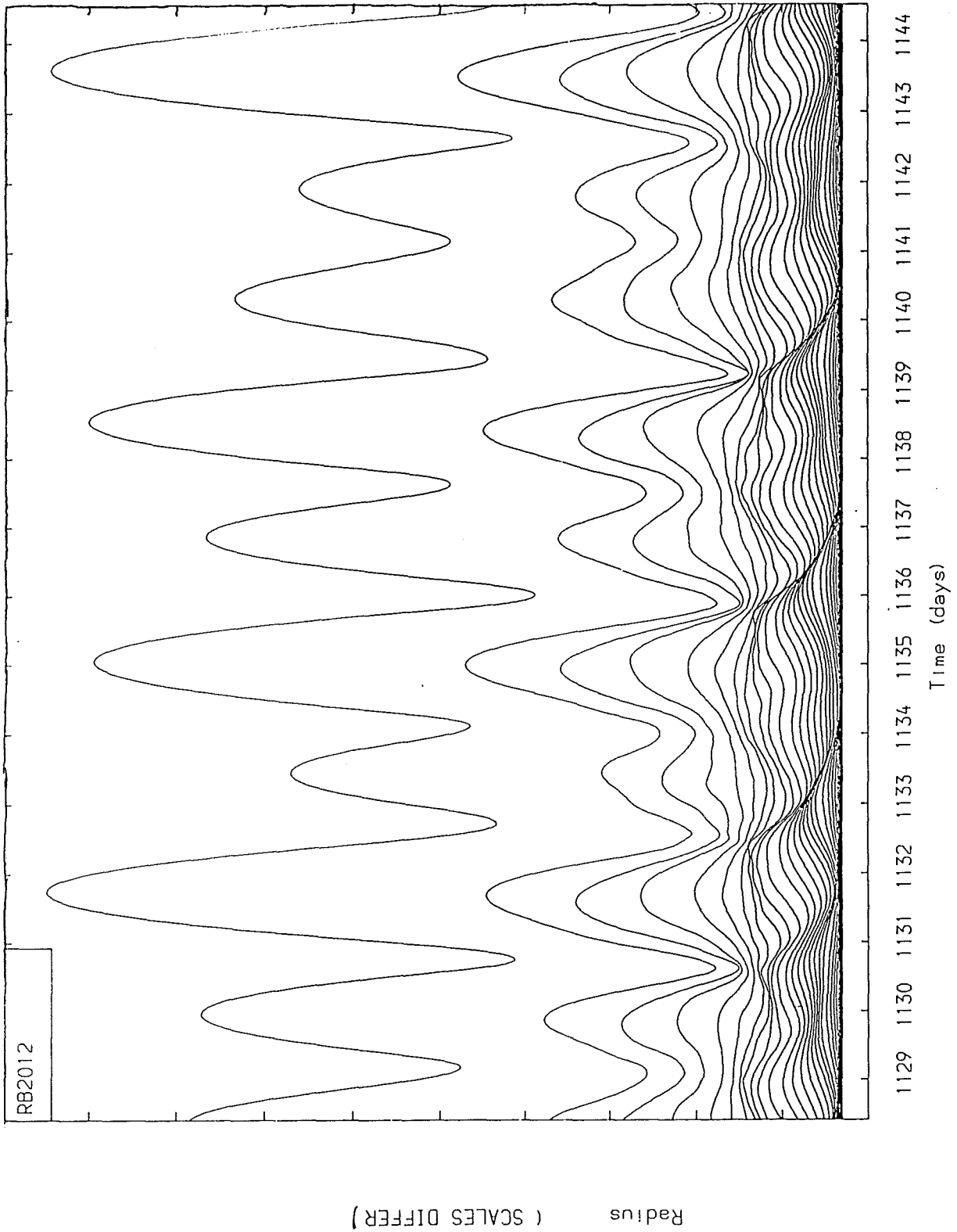
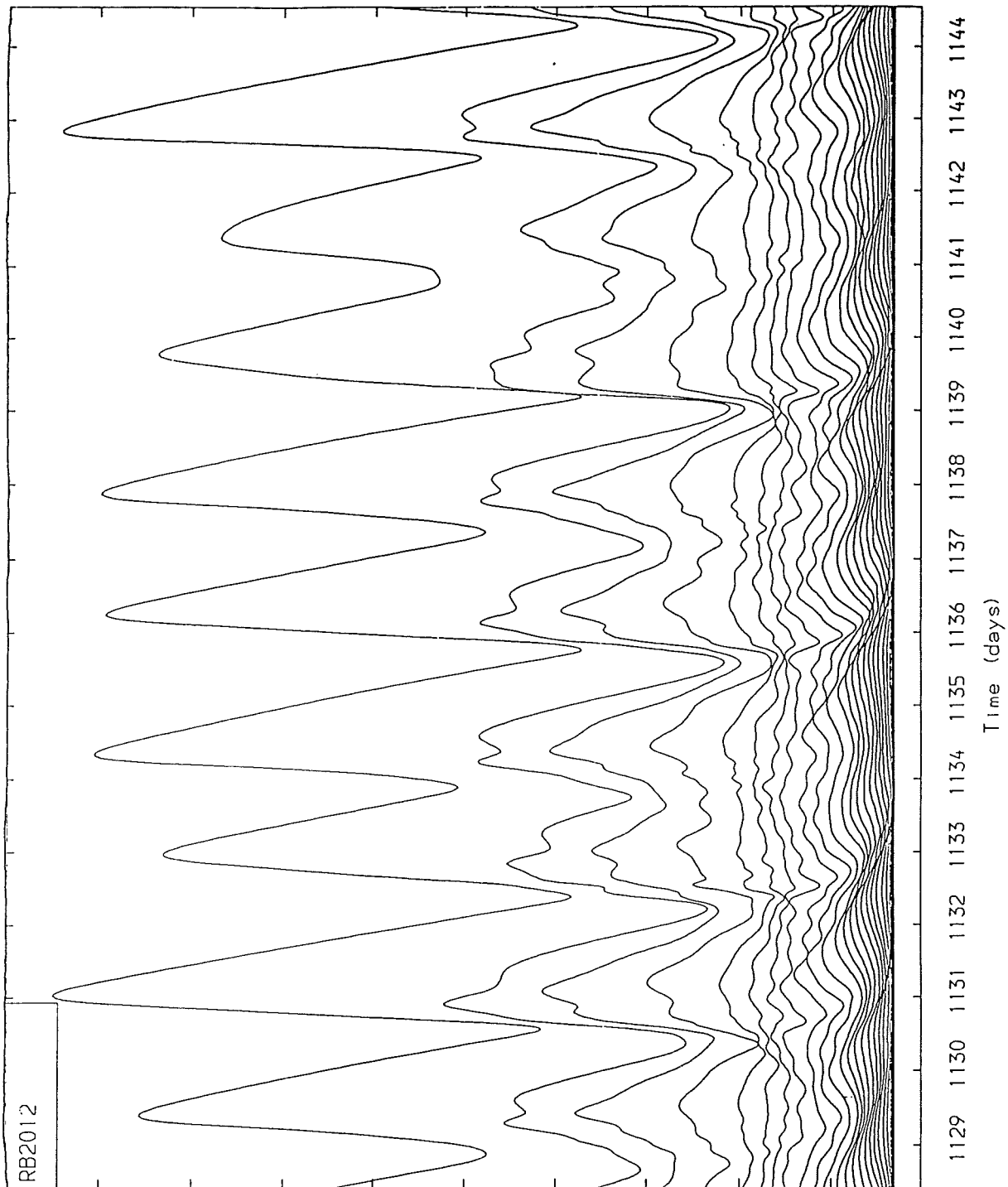


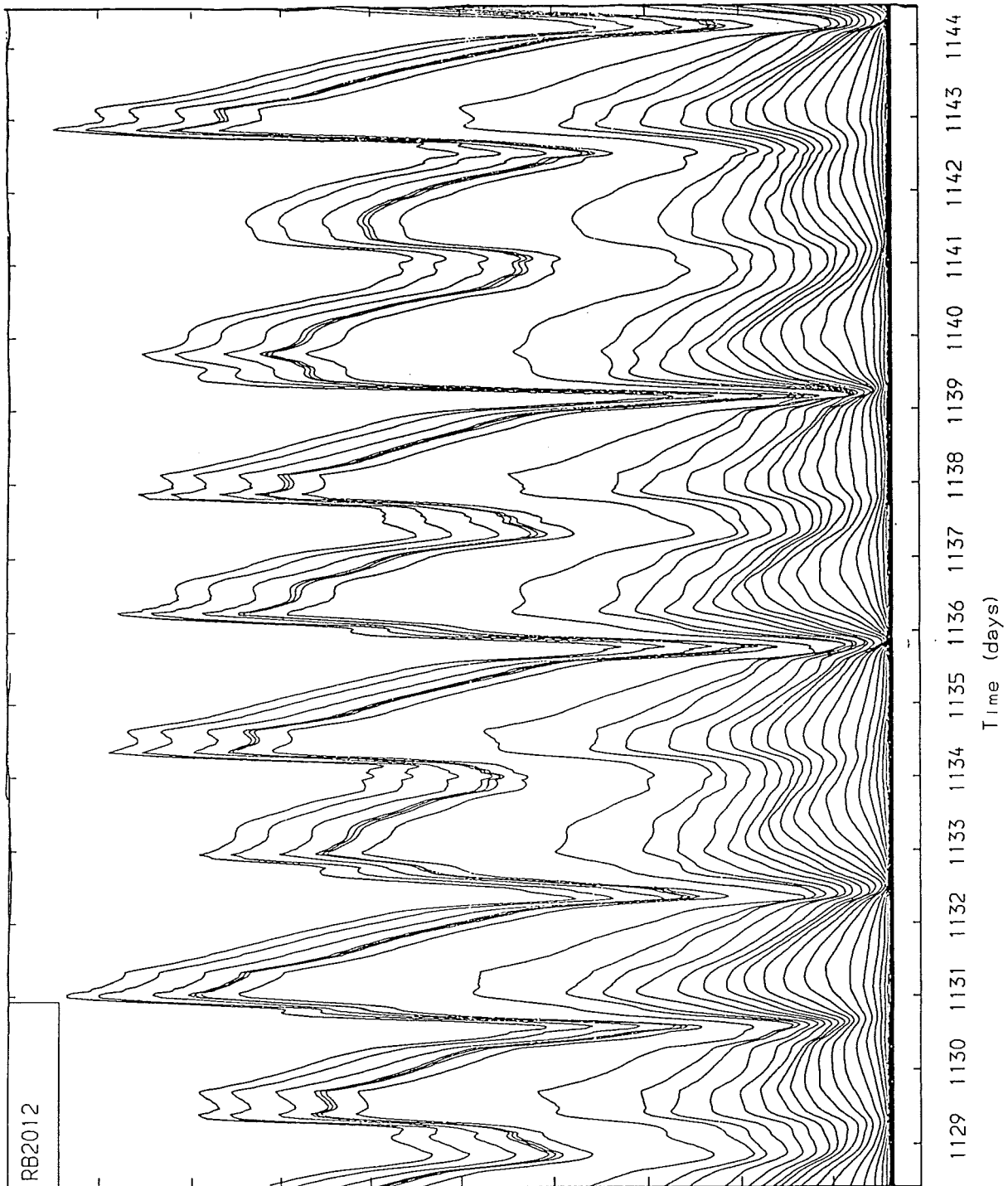
Figure 8.26 : This figure shows the radial (dR/R) history for all zones of the BD9C opacity table model, which as a mass of $1.0M_{\odot}$, a luminosity of $10,000L_{\odot}$ and a effective temperature of $12,000K$ (RB2012).



Velocity (SCALES DIFFER)

Figure 8.27 : This figure shows the velocity history for all zones of the BD9C opacity table model, which as a mass of $1.0M_{\odot}$, a luminosity of $10,000L_{\odot}$ and a effective temperature of $12,000K$ (RB2012).

NON-LINEAR NON-ADIABATIC RESULTS



Luminosity (SCALES DIFFER)

Figure 8.28 : This figure shows the luminosity (dL/L) history for all zones of the BD9C opacity table model, which as a mass of $1.0M_{\odot}$, a luminosity of $10,000L_{\odot}$ and a effective temperature of $12,000K$ (RB2012).

We can see from these figures that the periods and shapes of the light curves are governed by the power of the outward shock and the natural frequency of the inner envelope. The rising part of the curves are defined by the outward shock, and the falling part of the curves by the time taken for gravity to bring the outer zones back for the star's next cycle.

8.4 NON-LINEAR NON-ADIABATIC MODELS OF 7 RCB STARS

In the following section the best 6 models that approach some of the observed parameters of the RCB stars discussed in the previous chapter will be presented and discussed. As before, the discussion will be split into two main parts: the models with effective temperatures of 5,000 K and 6,000 K, and the models with effective temperatures of 6,900 K. As was the case in the linear analysis, WX CrA and RT Nor are grouped together and for the rest of the thesis will be treated as having identical stellar parameters.

Table 8.3 below, shows the adopted masses and luminosities of the 7 selected RCB stars as found from the linear theory. Table 8.3, also shows the observed effective temperatures, periods, amplitudes (in m_v) and radial velocities for the stars as well. Only in the case of RY Sgr are the observations extensive enough for us to be sure that the star is pulsationally unstable and that the given amplitudes of luminosity and radial velocity are probably the real maxima. In all other cases, the observations are far too few and dispersed to be sure of the limitations given or even that the periods quoted are correct. This is why the 5,000K and 6,000K models have been treated in a separate section to the 6,900K models.

NON-LINEAR NON-ADIABATIC RESULTS

STAR	M/M_{\odot}	L/L_{\odot}	T_{eff}	Period	dm_v	dV_r
UW Cen -	1.00	9,400	6,000	- 42.8	<0.2	--
WX CrA -	1.00	7,400	5,000	- 60	0.1	--
R CrB -	0.95	15,500	6,900	- 44	0.15	4
RT Nor -	1.00	7,400	5,000	- 59	<0.2	--
GU Sgr -	1.00	4,600	5,000	- 38	<0.1	--
RY Sgr -	0.99	10,500	6,900	- 38.6	0.45	30
RS Tel -	0.80	4,000	5,000	- 45.8	<0.3	--

TABLE 8.3 : Table showing calculated parameters (M/M_{\odot} , L/L_{\odot}) for models and observed parameters (T_{eff} , Period, dm_v , dV_r) for RCB stars.

8.4.1 The 5,000K And 6,000K RCB Models

8.4.1.1 The GU Sagittarii Model -

The model was run until the radius, velocity, and luminosity curves maintained a roughly constant amplitude and the peak kinetic energy also remained constant (this is generally a good indicator of whether a model has reached its limit cycle). As can be seen from Figure 8.29, the kinetic energy flattened out after about 6 or 7 periods. However, in Figure 8.30, we can see that the period never really settled down to any one value, but wandered about by +/- 3 days. Still, towards the end of the run it maintained a reasonably consistent mean of about 38 days, which is in agreement with the observations. We can also see from Figure 8.30 that the luminosity amplitude is around 2^m5 which is far too high for this group of stars. This may perhaps be due to the fact that this amplitude was measured at the (N-1)th zone instead of at the photosphere.

The model (after an initial contraction of about 1%) settled down to a steady, if semi-regular, pulsation with no extreme behaviour as has been seen in other similar high luminosity helium stars by other authors. If we look at the work integral in Figure 8.31, we can see that there is a lot of damping in the zones above the helium driving region. Also from this figure it is just possible to see a small radiative damping region below the large He^{++} damping region (about zone 10) which appears to be due to the higher ionisation states of carbon. Such heavy damping in the outer zones confirms the belief that convection would have a insignificant effect upon the period and stability of the model, though perhaps playing a crucial role in limiting the amplitude of the pulsation.

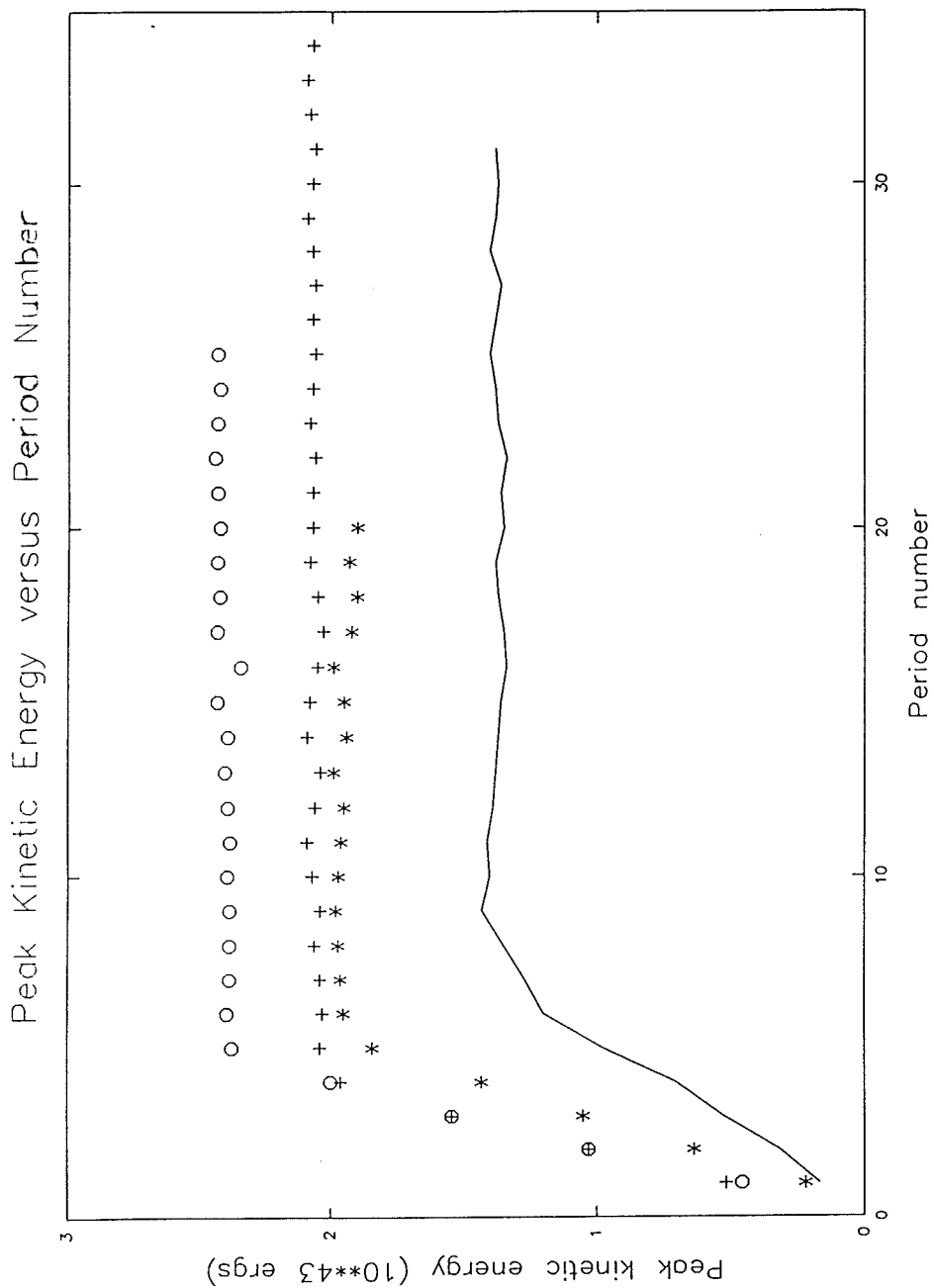
Figures 8.32 - 8.34 show the zonal history of the model over one period. The figures show the fractional change in radius, the fractional change in luminosity, and the velocity of each zone, versus phase. Above each history graph is a plot versus phase of the photospheric quantity in question; the photospheric velocity is multiplied by $17/24$ to allow for limb darkening. (However, in this case there is no radial velocity curve to compare it with.) The light curves were repetitive in shape with the exception that the small luminosity bumps seen around minimum light (phase 0.0 and 1.0) were transitory in nature and were sometimes absent for 2 or 3 periods before returning.

If we look closely at the histories, we can see that the outer zone is greatly expanded due to the nature of the outer boundary condition which holds the temperature of this zone constant and thus as its heat content builds, it has no choice but to expand. The same effect was seen in both Bridger (1983) and Worrell (1985) and did not seem to have any major effect upon the pulsation parameters. This is why the

(N-1)th zone was chosen to measure parameters rather than the Nth zone, as has also been done by many other authors in the field. In Figures 8.32 - 8.34 we can see that zones 8-21 (counting down from outer zone) become highly compressed due to the meeting of the infalling outer envelope with the expanding inner zones. As in the 10,000K models, this has the effect of causing two shocks to form, one travelling inwards and the other outwards. The production of these shocks causes a sharp increase in temperature which, due to the sensitivity of the opacity in this region, pushes the opacity down (over bump) causing the luminosity bump that can be seen in zones 14-19 (from surface) of Figure 8.33 to travel slowly outward. Also in Figure 8.33 we can see the classic up-down 'groove' in luminosity caused by the passing of a shock wave. In this particular history the 'Christy echo' is very evident, as both the velocity and luminosity curves clearly show the shock being reflected at the inner adiabatic core. However, in this case the reflection is not perfect, as several echoes of the shock are also produced due to 'ringing' of the inner boundary. It is the creation of this shock that causes the initial high acceleration of the outer zones, and the echo that causes the infall by over-expanding the already 'thin' gases and allowing gravity to pull them back. It is also this reflected shock that, on passing through the helium ionisation region, causes a far weaker inward travelling pressure wave that is eventually reflected at the adiabatic core and leading to the next large shock-waves. Thus the two distinct eras in the light curves are governed by the travel times of pressure waves - the short steep rise between phase -0.2 and 0.1 by the steep shock wave that reflects off the adiabatic core, and the slow descent between phase 0.1 and 0.8 by the slow moving secondary pressure wave described above, which again reflects off the adiabatic core. Figures 8.35 - 8.37 show snapshots of dL/L , dR/R and velocity versus

fractional radius at 1/16 phase intervals. They start at phase 0.0625 at top L.H.S. and finish at phase 1.0 at bottom R.H.S. In Figures 8.35 & 8.36 showing the velocity and dR/R profiles it is easy to follow the development of the shocks and the corresponding expansion and contraction of the zones. The increase in luminosity can be seen to lead the shock front and is mainly caused by the radiation following the sharp increase in temperature caused by the passage of the shock wave. As the heat capacity and opacity of the outer zones are low, the variation in luminosity is not held long and the shock wave effects soon die out.

From this model it can be seen that a shock driven κ -mechanism is the main driving force behind the pulsation, the period depending upon travel times of pressure and shock waves in the model's interior. These shock waves govern the acceleration of the outer zones and hence the amplitude of the velocity and luminosity variations. To limit the amplitude one only needs to reduce the shock power, which to some extent can be controlled by C_Q and the opacity table chosen. The problem is that the period is related to the speed of travel of the shock through the inner zones, which in turn is related to the power of the shock, so care must be taken not to distort the physics in any way. This generally meant that the shock strength and hence amplitudes of the photospheric variations could not be reduced by much.



NON-LINEAR NON-ADIABATIC RESULTS

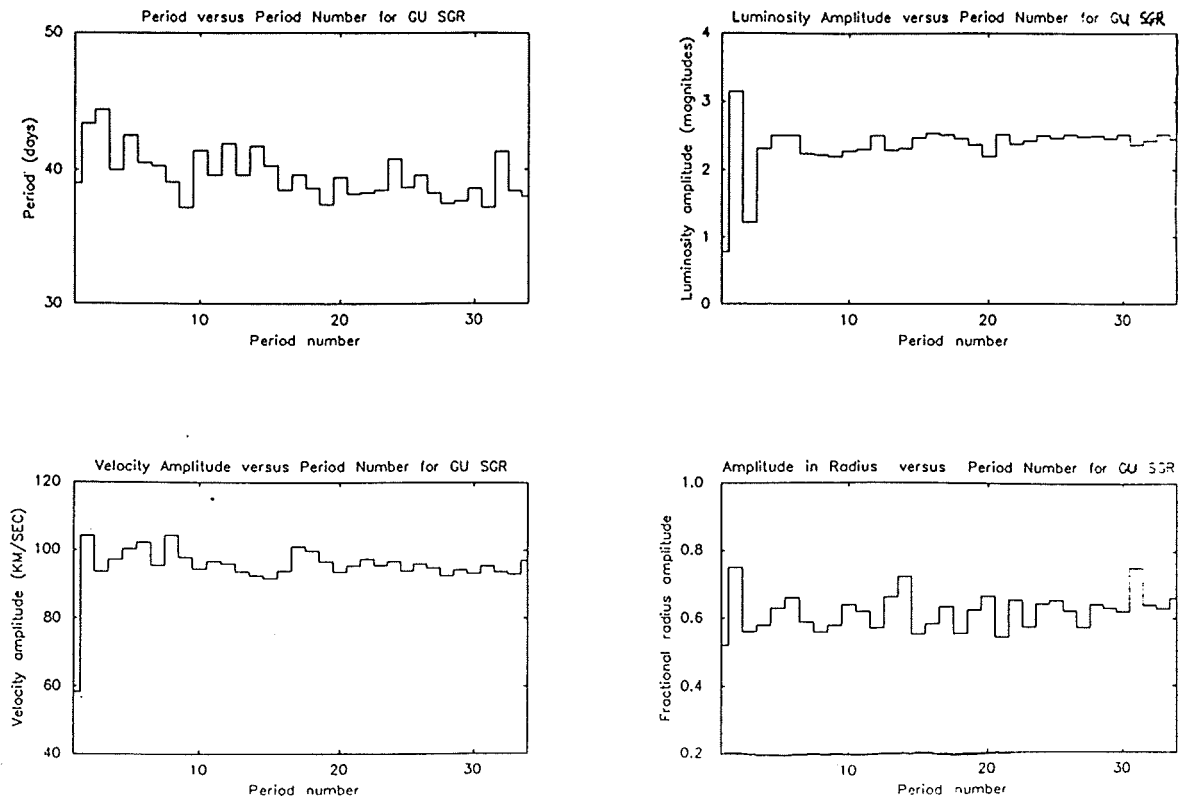


Figure 8.30 : This Figure shows graphs of the period in days and the amplitudes of luminosity in magnitudes, velocity in km/sec and fractional radius versus period number for the GU Sgr model.

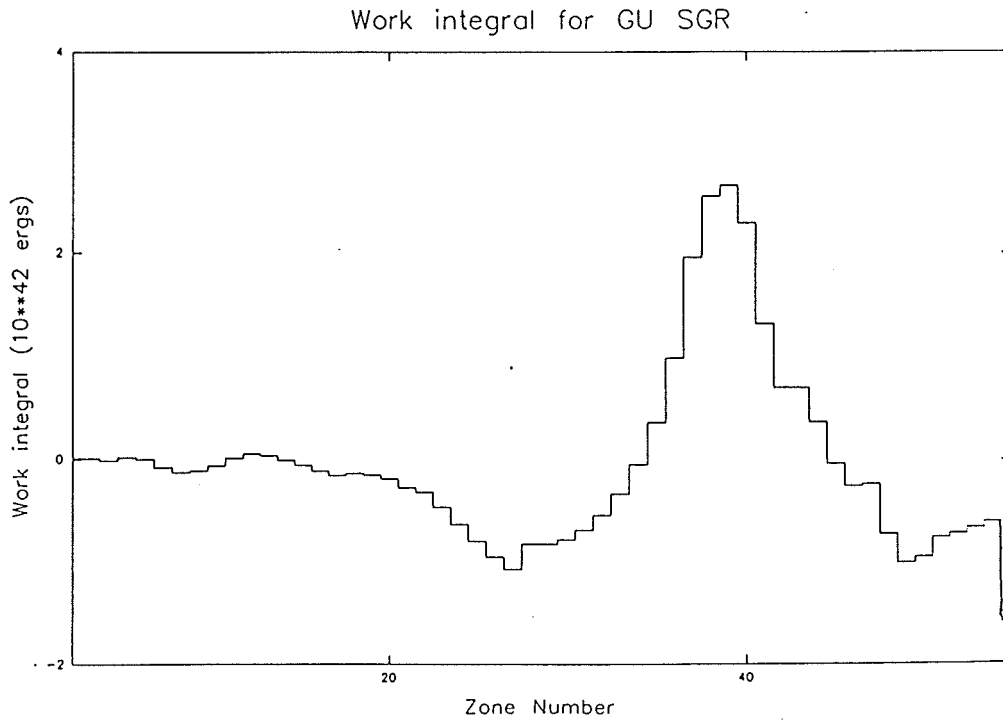


Figure 8.31 : This Figure shows the work integral of GU Sgr model, for period 19, versus zone number (zone 1 = innermost zone).

NON-LINEAR NON-ADIABATIC RESULTS

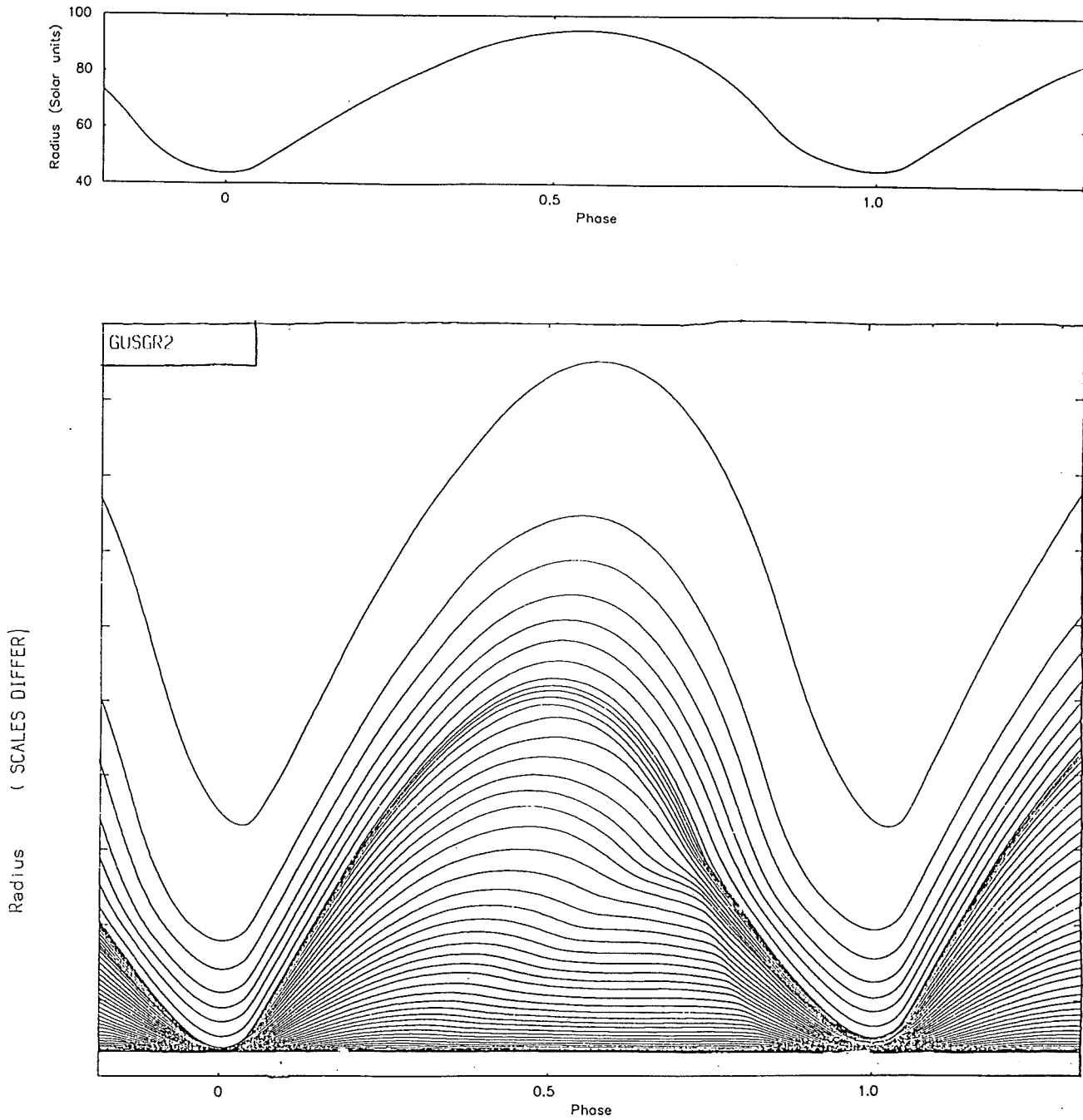


Figure 8.32 : This Figure shows the radial (dR/R) history for all zones of the RCB star model: GU Sgr.

NON-LINEAR NON-ADIABATIC RESULTS

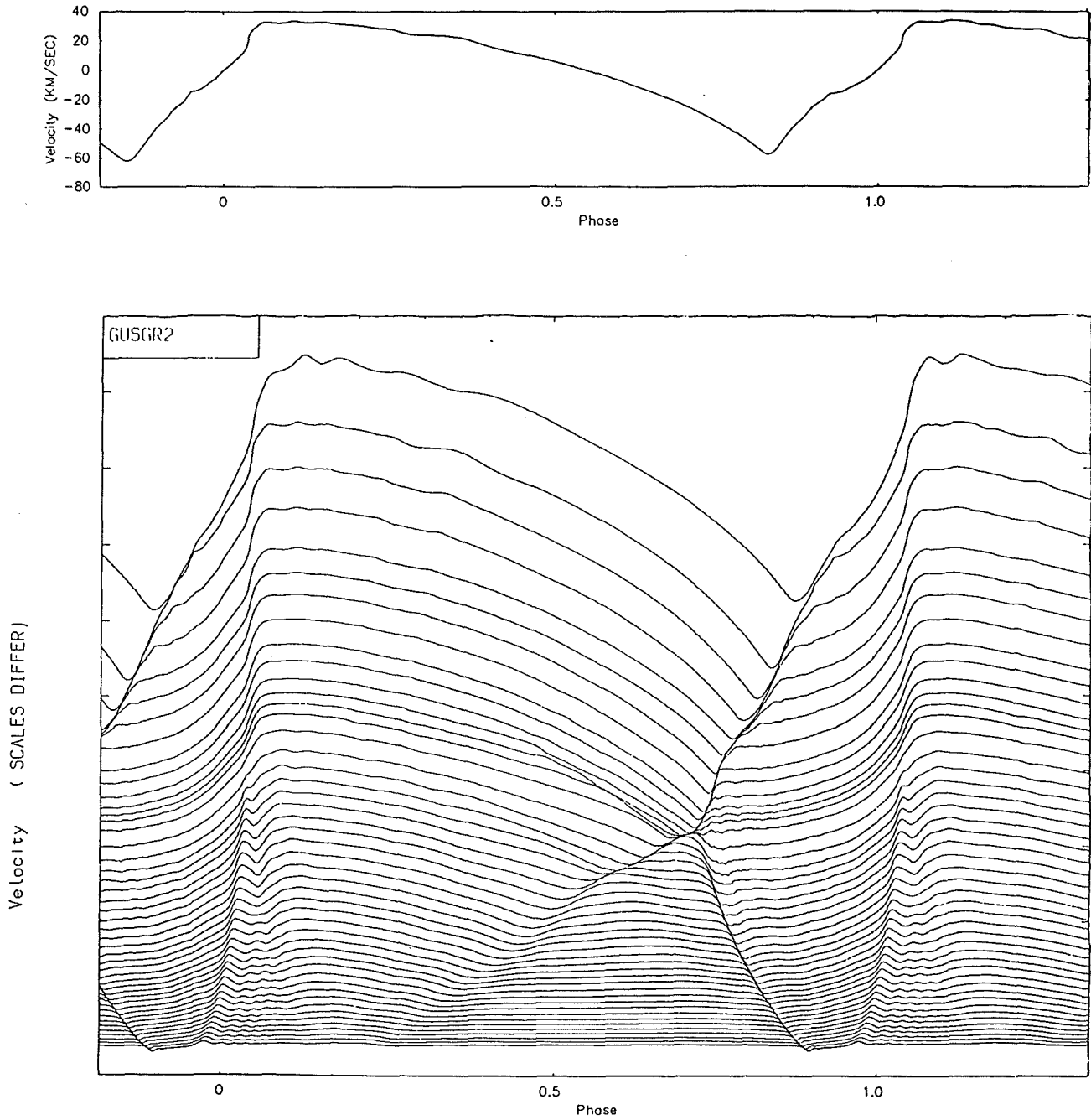


Figure 8.33 : This Figure shows the velocity history for all zones of the RCB star model: GU Sgr.

NON-LINEAR NON-ADIABATIC RESULTS

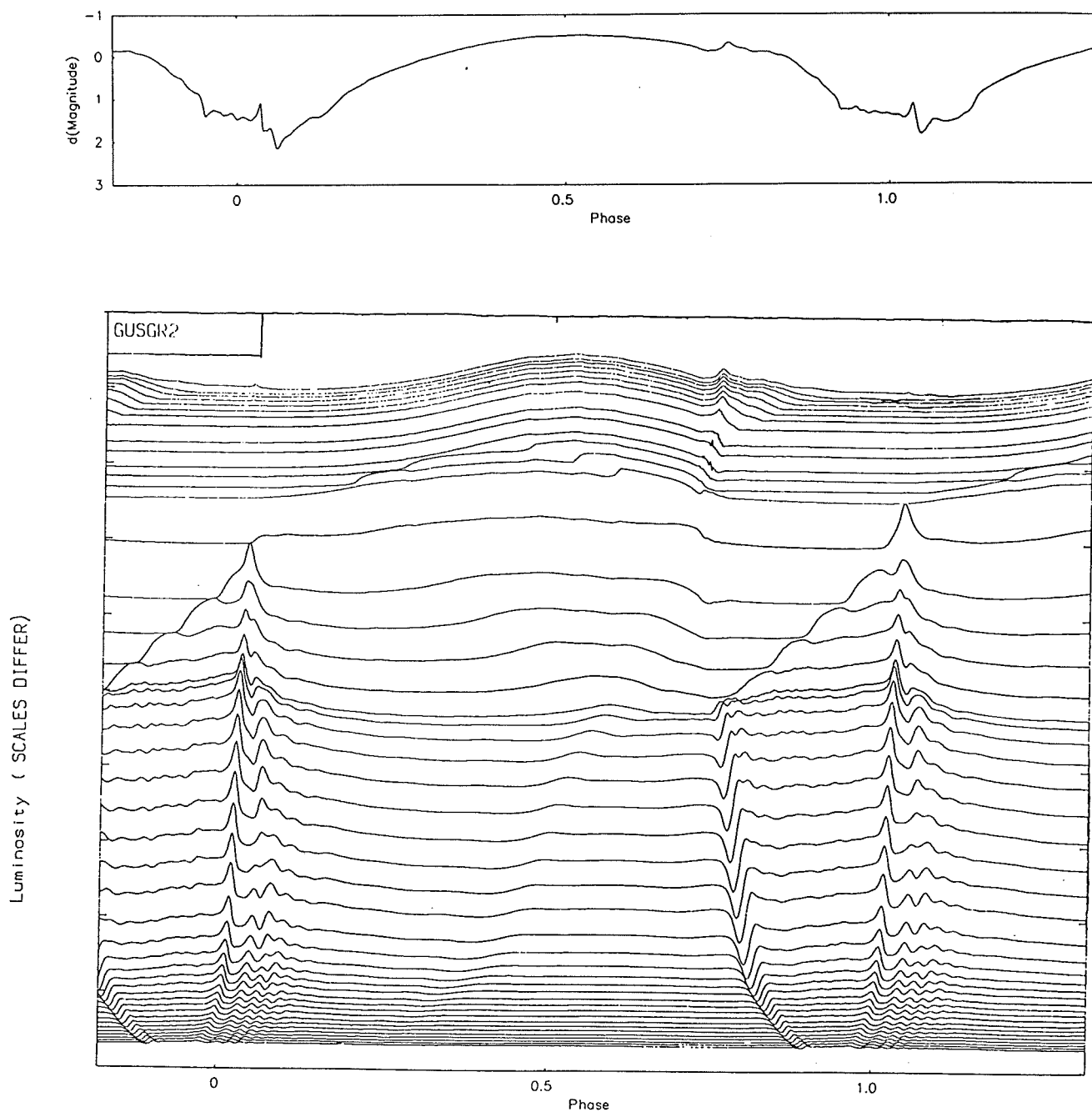


Figure 8.34 : This Figure shows the luminosity (dL/L) history for all zones of the RCB star model: GU Sgr.

NON-LINEAR NON-ADIABATIC RESULTS

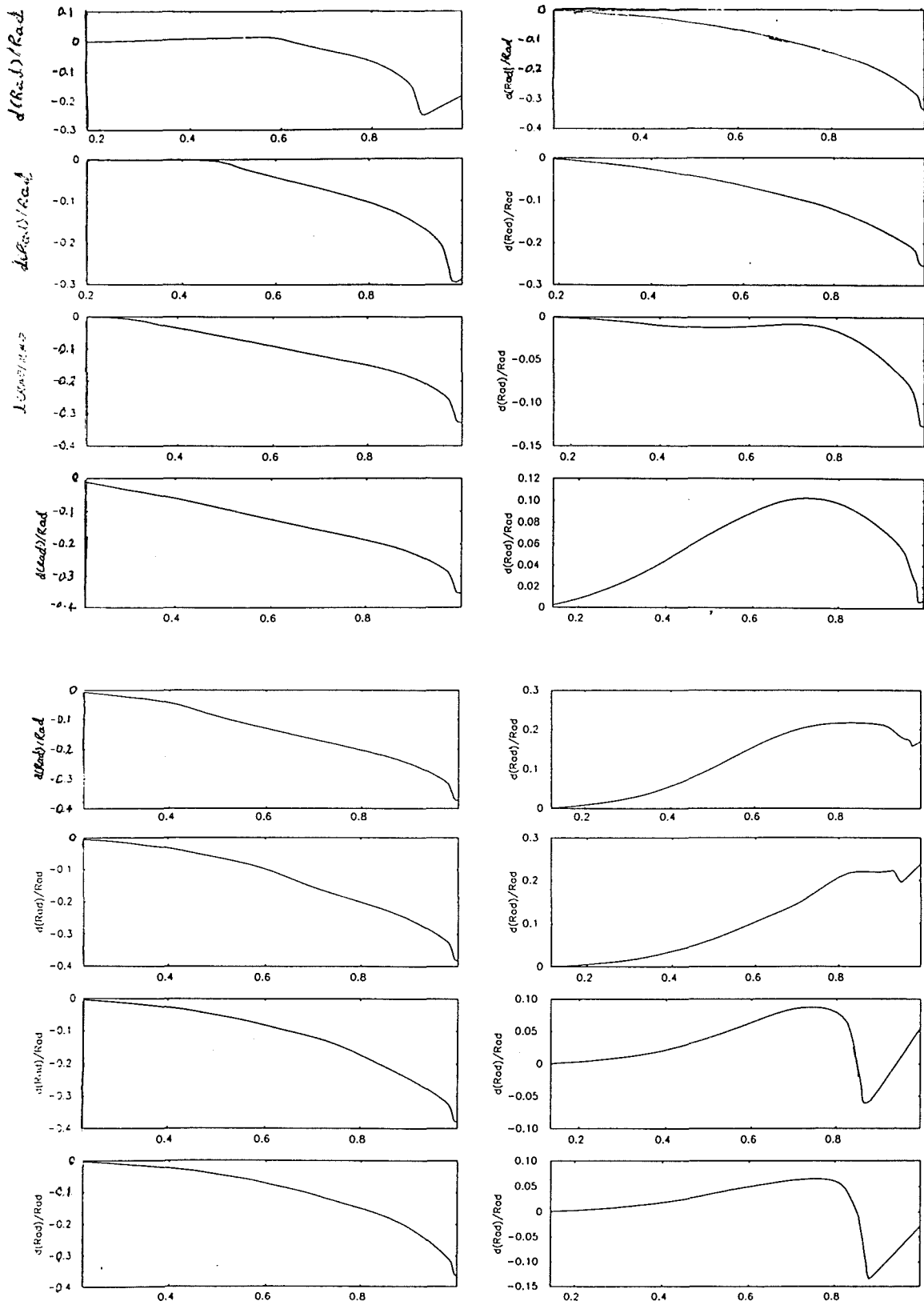


Figure 8.35 : Shows 'snapshots' of dR/R versus fractional radius for model GU Sgr, with the phase between 'snapshots' being 0.0625 . The sequence starts at top L.H.S (phase 0.0625) working down the page and then continues at the top R.H.S., ending at the bottom of the page at phase 1.0 .

NON-LINEAR NON-ADIABATIC RESULTS

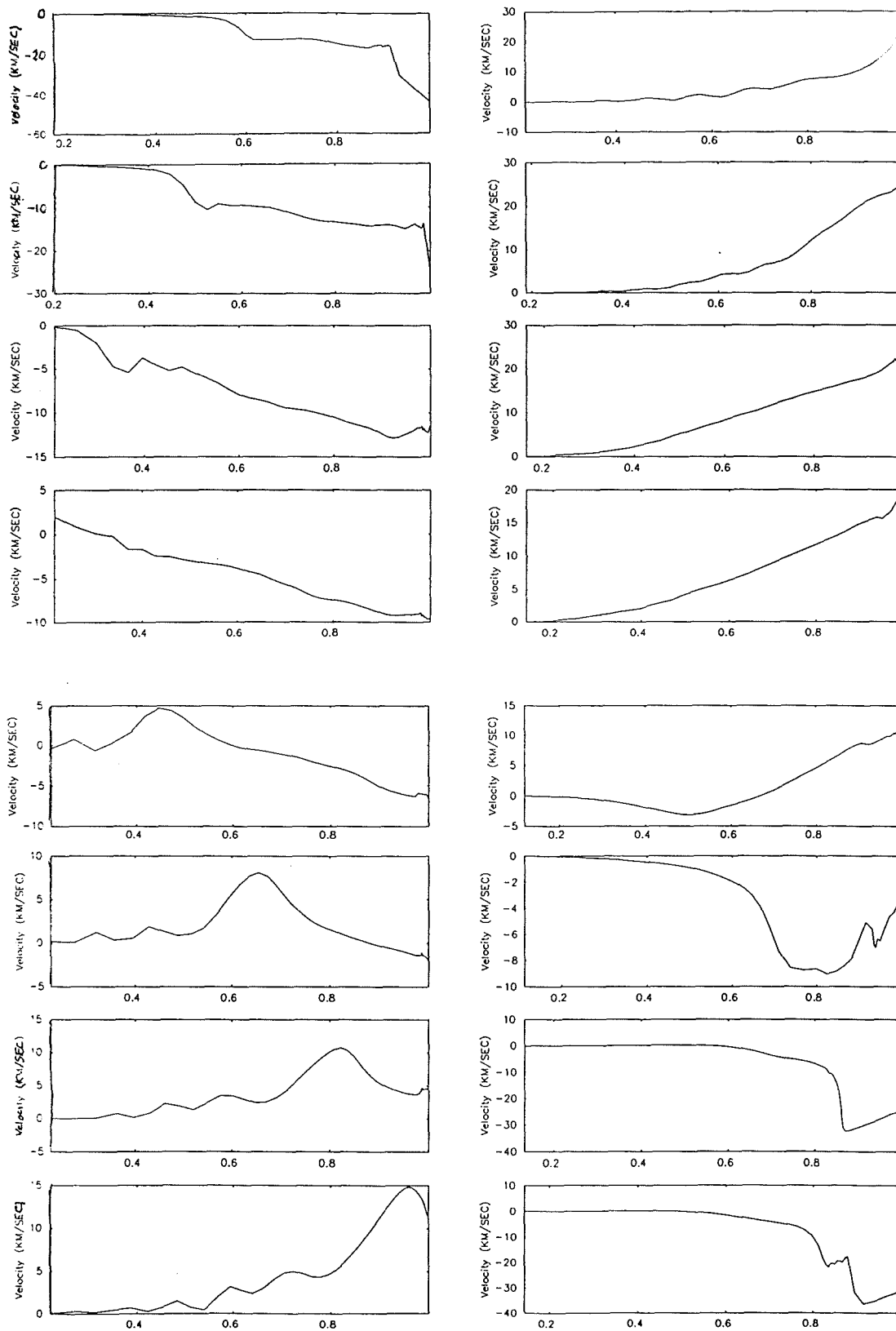


Figure 8.36 : Shows 'snapshots' of velocity versus fractional radius for model GU Sgr, with the phase between 'snapshots' being 0.0625 . The sequence starts at top L.H.S (phase 0.0625) working down the page and then continues at the top R.H.S., ending at the bottom of the page at phase 1.0 .

NON-LINEAR NON-ADIABATIC RESULTS

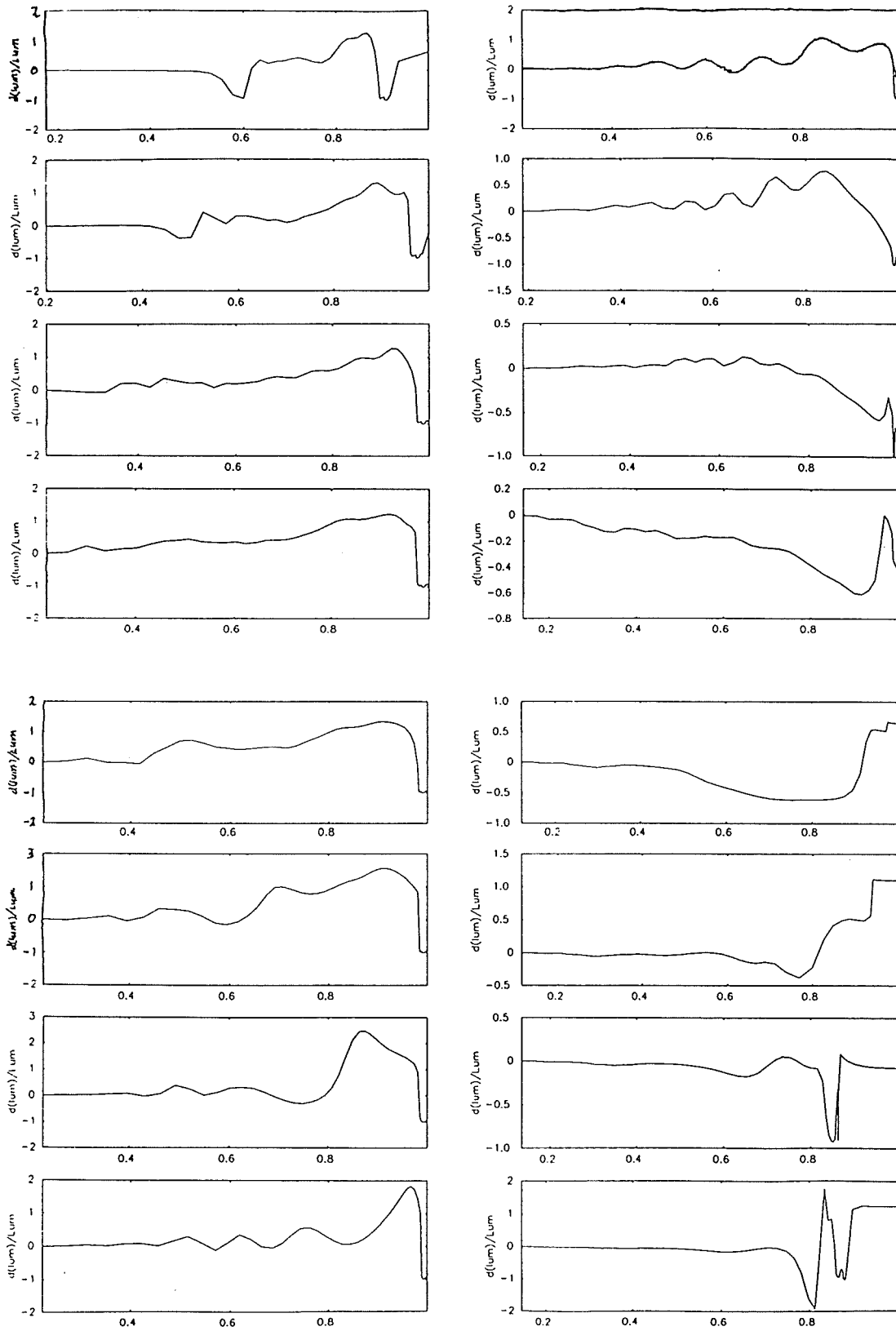


Figure 8.37 : Shows 'snapshots' of dL/L versus fractional radius for model GU Sgr, with the phase between 'snapshots' being 0.0625 . The sequence starts at top L.H.S (phase 0.0625) working down the page and then continues at the top R.H.S., ending at the bottom of the page at phase 1.0 .

As this model is shock driven to a certain extent, it was felt that perhaps the initial kick was the cause of the large amplitude seen in the light curves, so a model was made with $B = -1$ km/sec instead of the usual 10 km/sec. The sole result of this reduction in kick was to extend the time taken for the model to reach its limit cycle; otherwise, it was virtually identical to this model in its features.

8.4.1.2 The RS Telescopii Model -

This model is quite similar to that for GU Sgr. If we compare Figures 8.33 - 8.35 (the zonal histories of GU Sgr) with Figures 8.41 - 8.43, we see that the decrease in mass has had very little effect upon the gross features of the curve, and that the period has only changed marginally to about 42 days \pm 1 day, which is again of the right order. As with the GU Sgr model, we can see that a lot of shock damping occurs in the atmosphere (see Figure 8.40) indicating again that in comparison any effect of convection would be small.

From Figure 8.39 we can see that none of the amplitudes have become steady, even though the the peak kinetic energy in Figure 8.29 shows that the model has reached its limit cycle. It is hard to say for certain, but the trend in the velocity amplitudes seems to indicate that the pulsation is decaying, though this is not supported by the consistency of the peak kinetic energy. Also, we can see from the fractional radius that the model is developing some form of bi-periodicity, with large and small amplitudes alternating. The velocity amplitude is now nearer that seen in RY Sgr though the luminosity amplitude is again far too large. This could perhaps be due to the star having a higher effective temperature and luminosity than is stated in the literature. Otherwise, the model is very similar in characteristics to that found for GU Sgr.

NON-LINEAR NON-ADIABATIC RESULTS

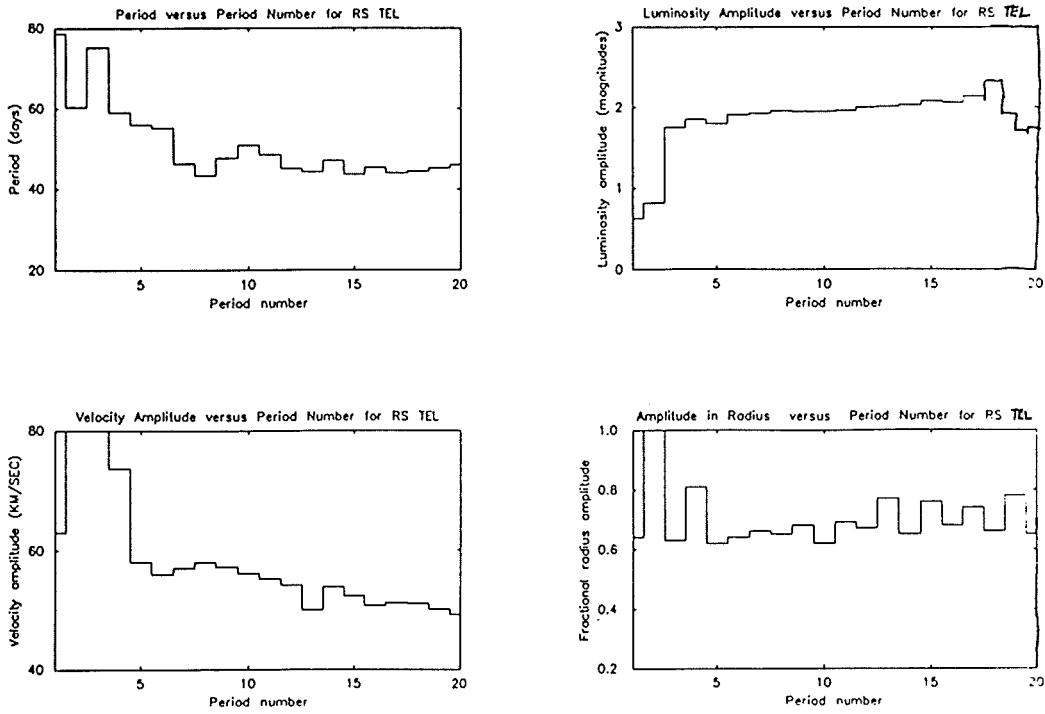


Figure 8.39 : This figure shows graphs of the period in days and the amplitudes of luminosity in magnitudes, velocity in km/sec and fractional radius versus period number for the RS Tel model.

Work integral for *RS TEL*

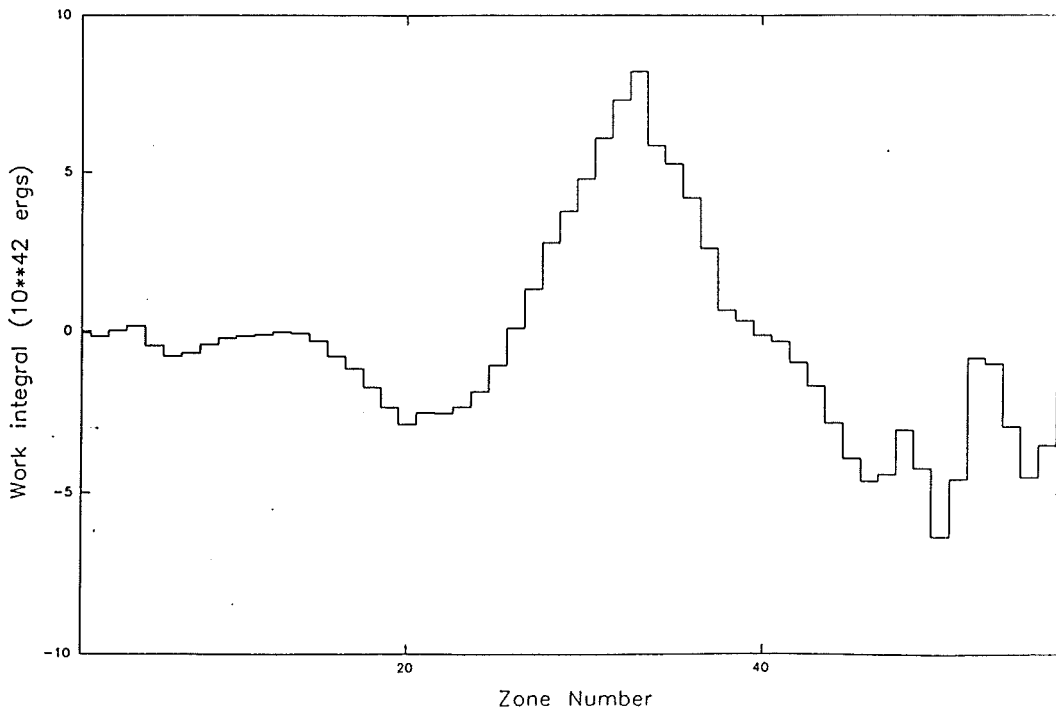


Figure 8.40 : This figure shows the work integral of RS Tel model, for period 19, versus zone number (zone 1 = innermost zone).

NON-LINEAR NON-ADIABATIC RESULTS

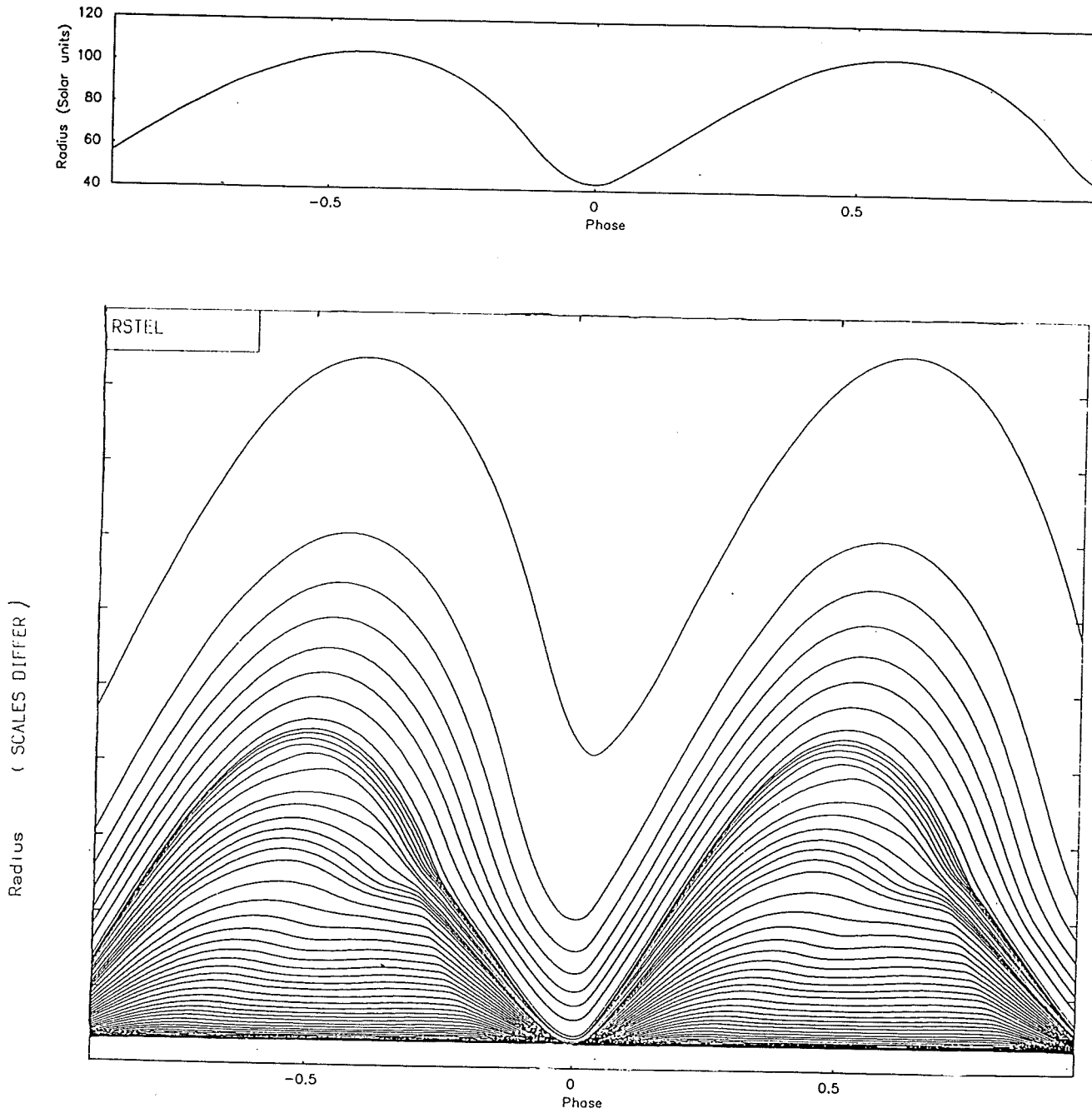


Figure 8.41 : This figure shows the radial (dR/R) history for all zones of the RCB star model: RS Tel.

NON-LINEAR NON-ADIABATIC RESULTS

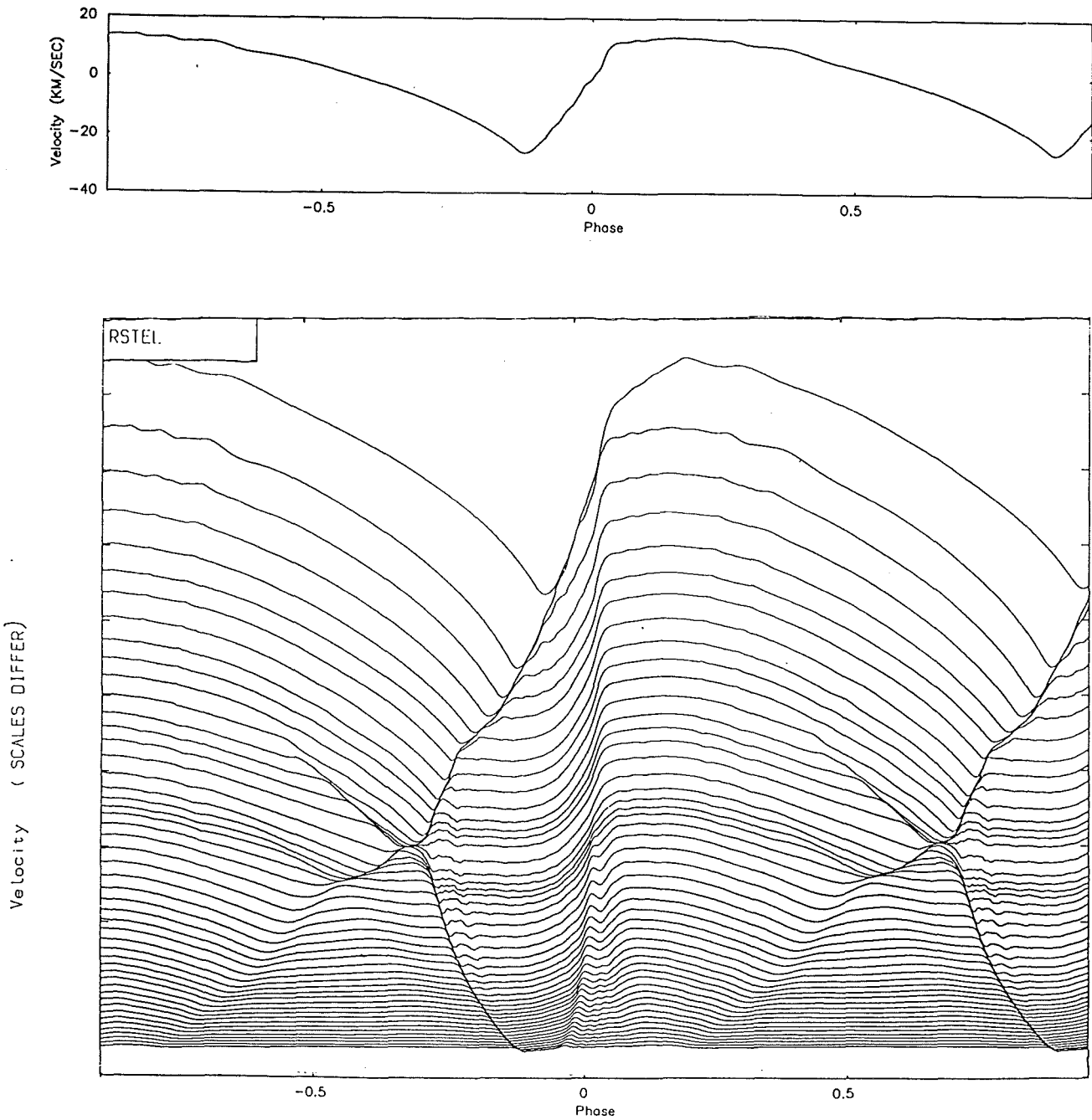


Figure 8.42 : This figure shows the velocity history for all zones of the RCB star model: RS Tel.

NON-LINEAR NON-ADIABATIC RESULTS

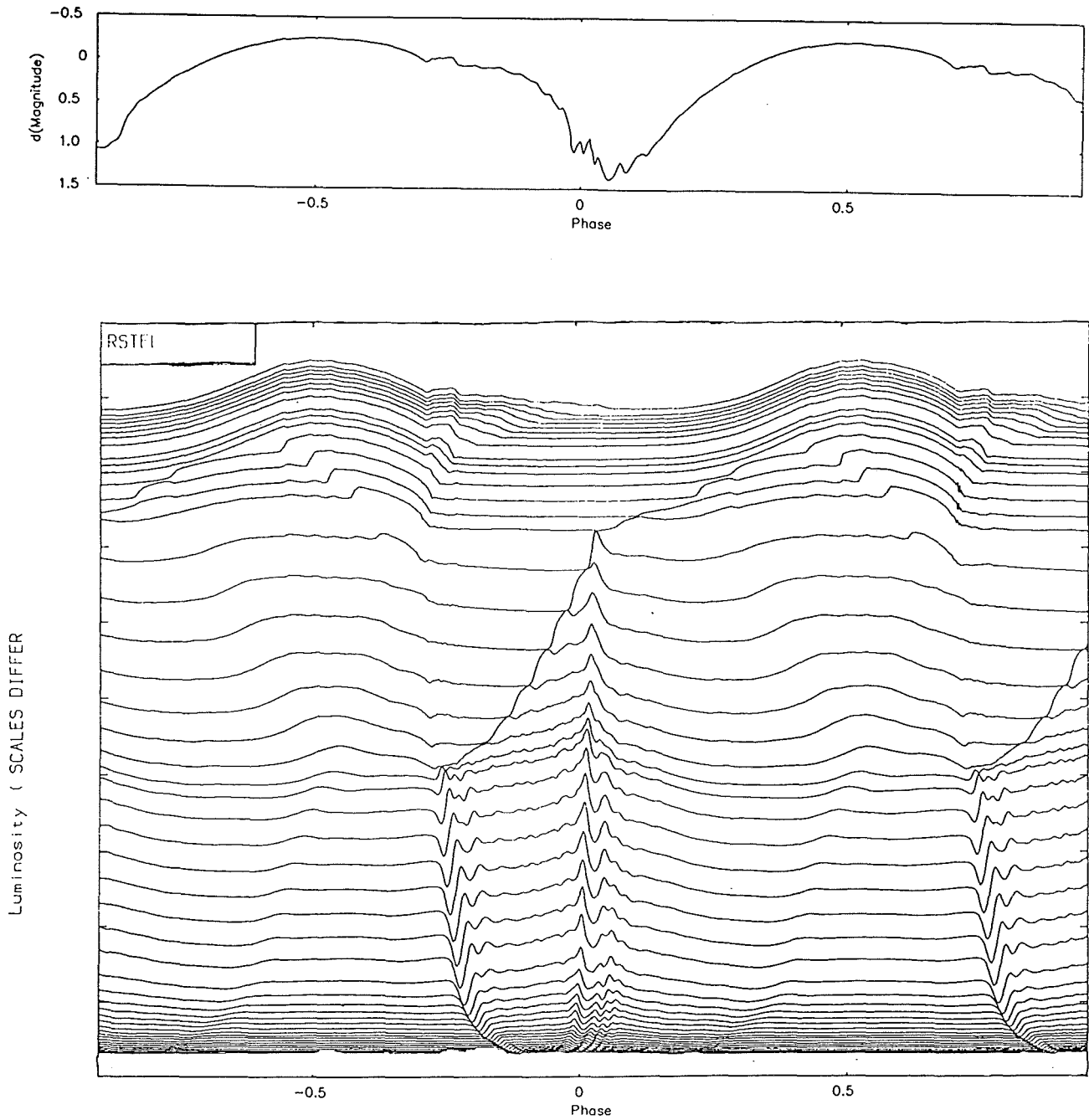


Figure 8.43 : This figure shows the luminosity (dL/L) history for all zones of the RCB star model: RS Tel.

8.4.1.3 The RT Normae & WX Coronae Australis Model -

As in previous models, we can see from Figure 8.44 that the period is unsettled at first but after about 10 or 12 periods settles down to about 60 days, which again agrees with the linear results. We can also see that although the amplitudes are not constant, they vary about fixed means rather than showing any signs of decreasing or growing. Along with the flattening out of the peak kinetic energy curve in Figure 8.29, this indicates that the model has reached its limit cycle. The work integral for period 24, shown in Figure 8.45, is very much the same as those of GU Sgr and RS Tel and indicates that the model is probably driven and damped by the same mechanisms as these previous models. This is confirmed by looking at the histories in Figures 8.46 - 8.48, although we can see that the initial and secondary shocks are far weaker, leading to a more 'rounded top' to the velocity curves of each zone, and also that the outer zones are less sensitive to variations in the underlying zones. The outer zone is still attached to the star, although it now extends out to about $400R_{\odot}$ and moves through large distances over one period.

The reduction in the shock strength appears to be due to the concentration of the mass towards the centre of the model, resulting in the outer zones having very low densities (10^{-8} gm/cm³) which do not have the mass to support such a large shock as the previous models did. This also means that the opacity in the helium ionisation zones is more sensitive to variations in temperature and density, hence the increased structure seen in the luminosity variations (Figure 8.48), which follows the passing of pressure waves and shocks far more closely than the previous less luminous models did. We can see that the luminosity variation in the outer zones is 'frozen in' and the large variation in the helium ionisation zones is 'ironed' out to some

extent. However, the variation is still big enough to produce a 1.8^m variation in the photospheric luminosity curve, which is obviously too large, considering the observed limit of 0.1^m . Again it seems likely that the effective temperature given in the literature may be wrong, or failing that, that convection may play some important role in limiting the amplitude of the luminosity variations.

8.4.1.4 The UW Centaurii Model -

Increasing the temperature by 1,000K means that the luminosity has had to approach the values more often quoted for these stars. This however has not affected the density of the outer zones which remains similar to that found in models GU Sgr and RS Tel. The main effect has been the increase in the amount of variation the period and amplitudes (Figure 8.49) undergo from period to period, and hence an increase in the number of periods modelled to ensure that the model has reached the limit cycle (though we can see from Figure 8.29 that the peak kinetic energy curve flattened out fairly early on, and that these later variations have very little effect upon it). Though the model is not purely cyclic, it is not really irregular either, as the curve shape remains roughly the same after about the sixth period and repeats itself quite regularly.

The work integral shown in Figure 8.50 shows a broader and stronger driving region than was found for the 5,000K models and the helium damping region has become quite negligible in comparison to the shock damping in the outer zones. This is as expected, as the increase in effective temperature has caused the density of the helium ionisation region, the seat of the driving, to be increased and hence have more inertia when expanding.

NON-LINEAR NON-ADIABATIC RESULTS

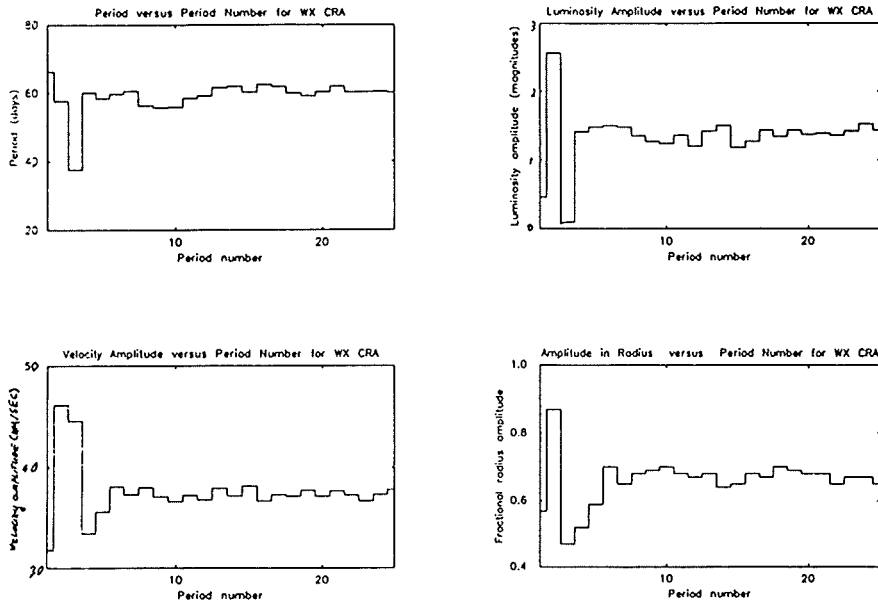


Figure 8.44 : This figure shows graphs of the period in days and the amplitudes of luminosity in magnitudes, velocity in km/sec and fractional radius versus period number for the WX CrA & RT Nor model.

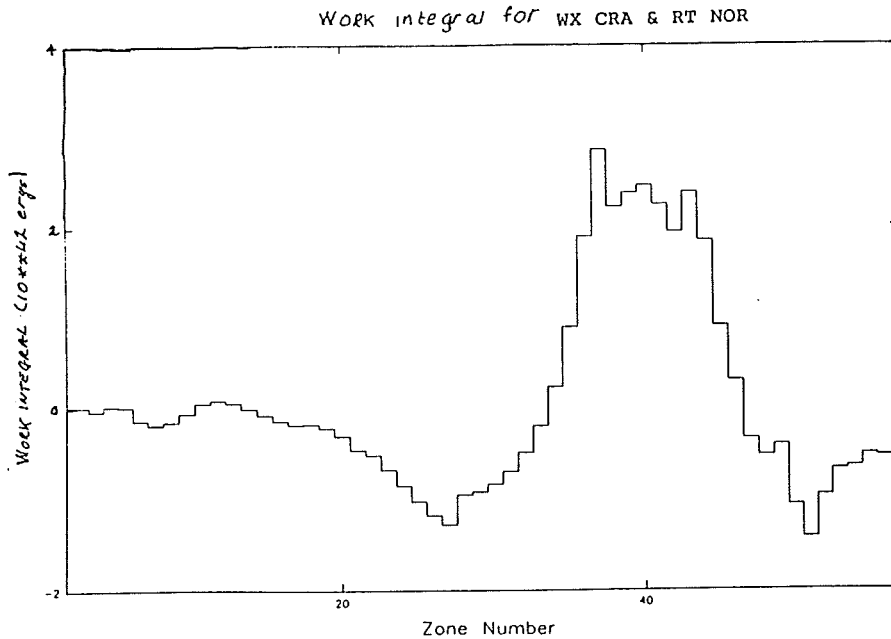


Figure 8.45 : This figure shows the work integral of WX CrA & RT Nor model, for period 24, versus zone number (zone 1 = innermost zone).

NON-LINEAR NON-ADIABATIC RESULTS

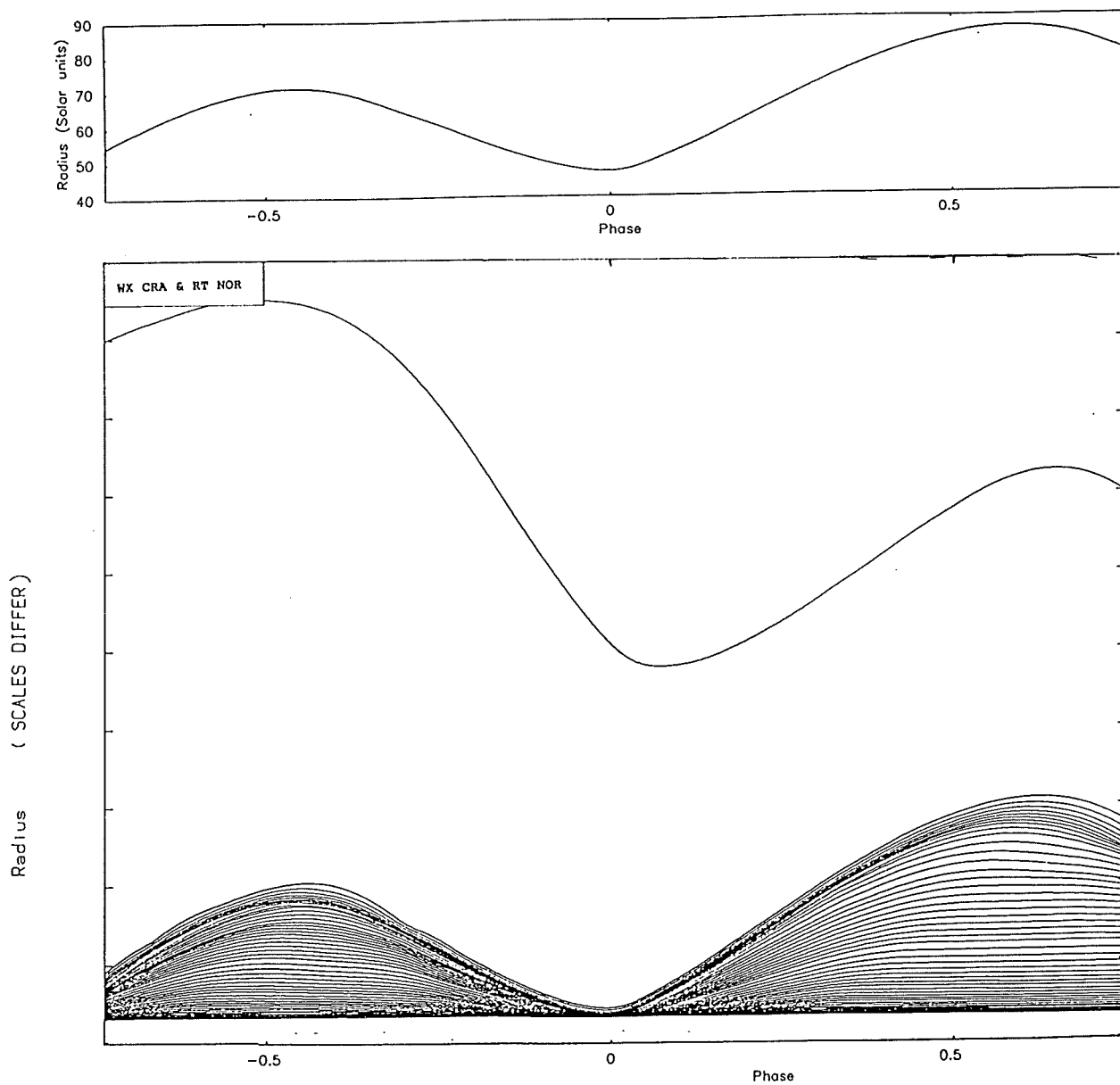


Figure 8.46 : This figure shows the radial (dR/R) history for all zones of the RCB star model: WX CrA & RT Nor.

NON-LINEAR NON-ADIABATIC RESULTS

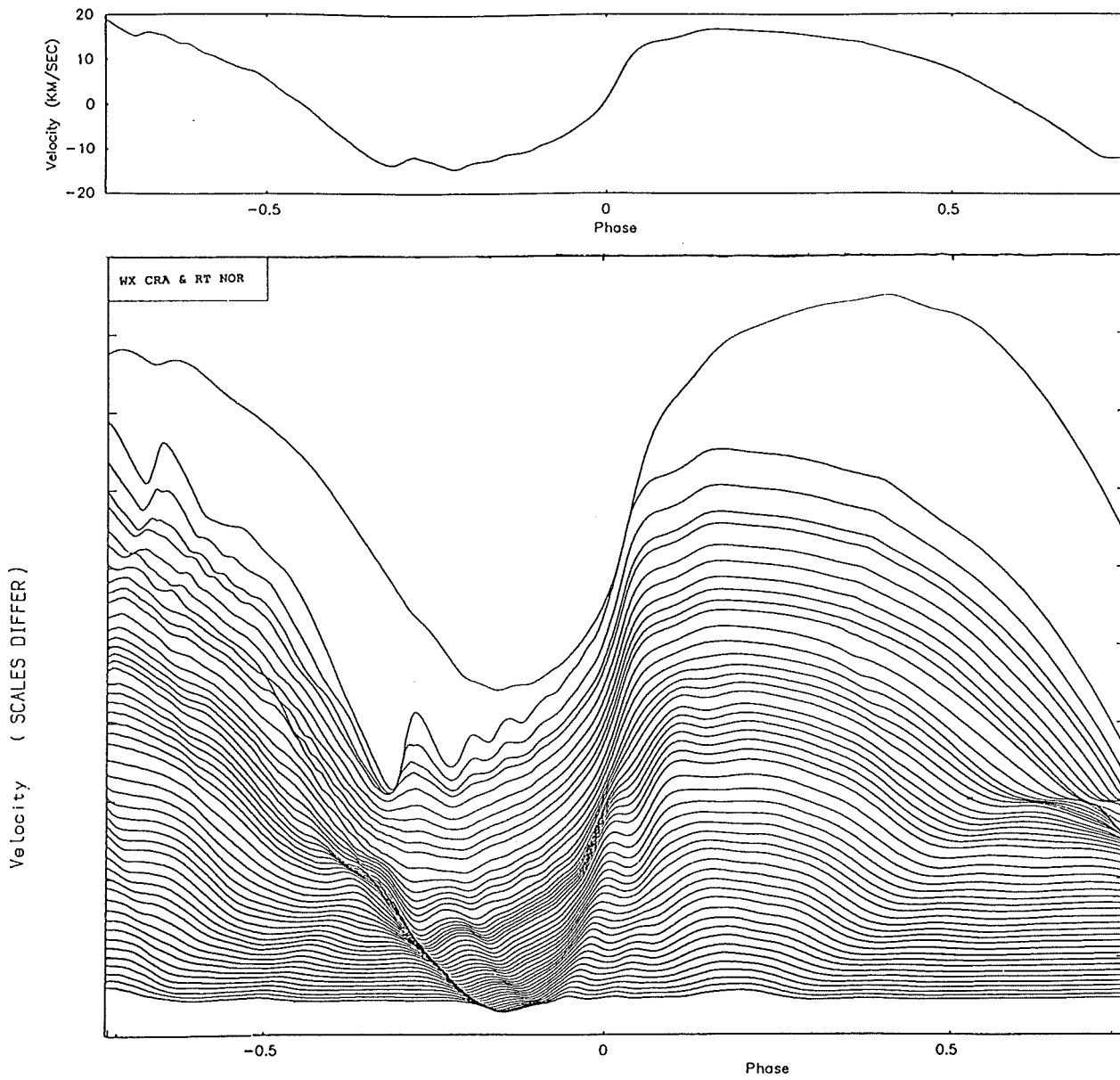


Figure 8.47 : This figure shows the velocity history for all zones of the RCB star model: WX CrA & RT Nor.

NON-LINEAR NON-ADIABATIC RESULTS

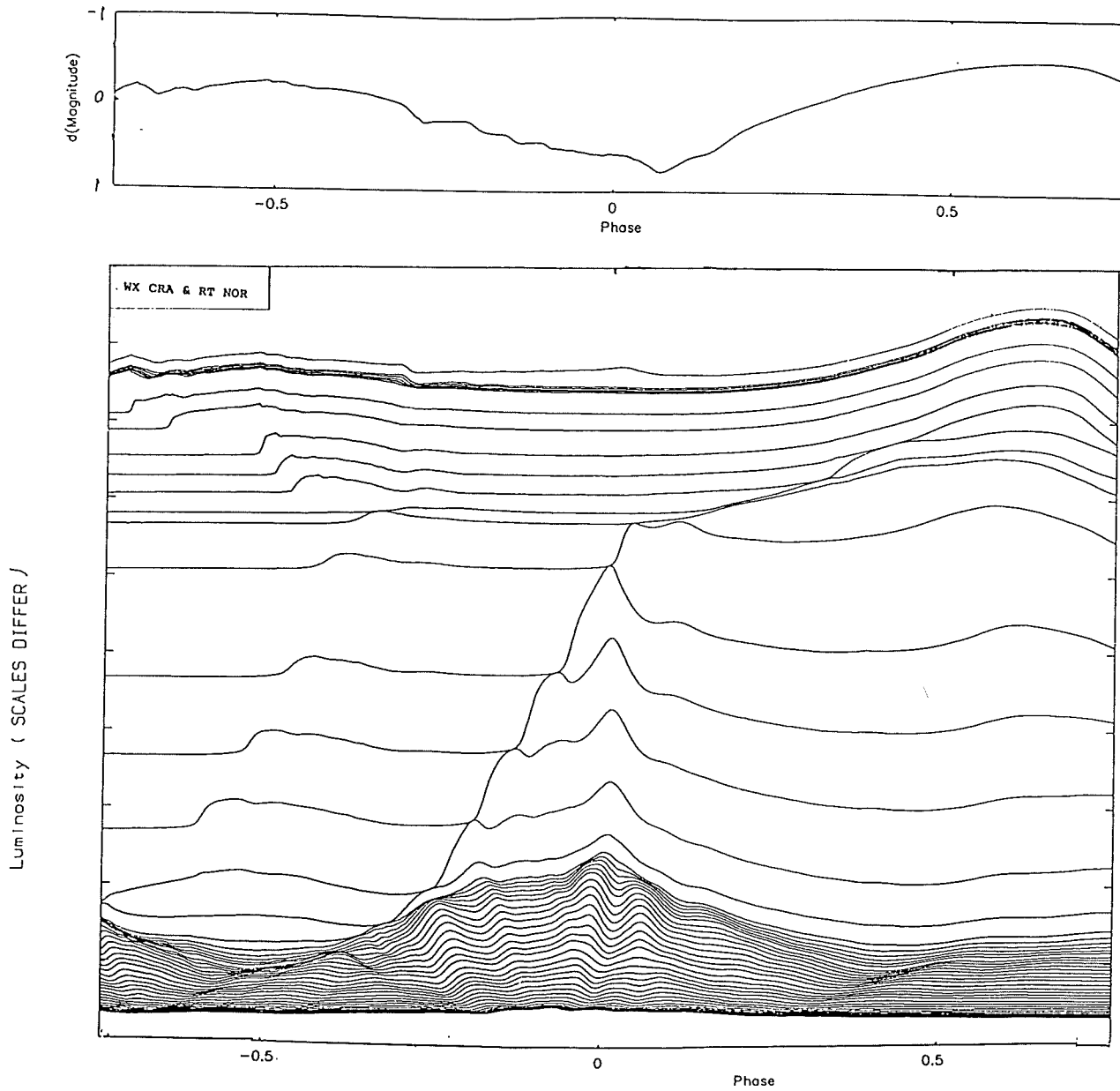


Figure 8.48 : This figure shows the luminosity (dL/L) history for all zones of the RCB star model: WX CrA & RT Nor.

NON-LINEAR NON-ADIABATIC RESULTS

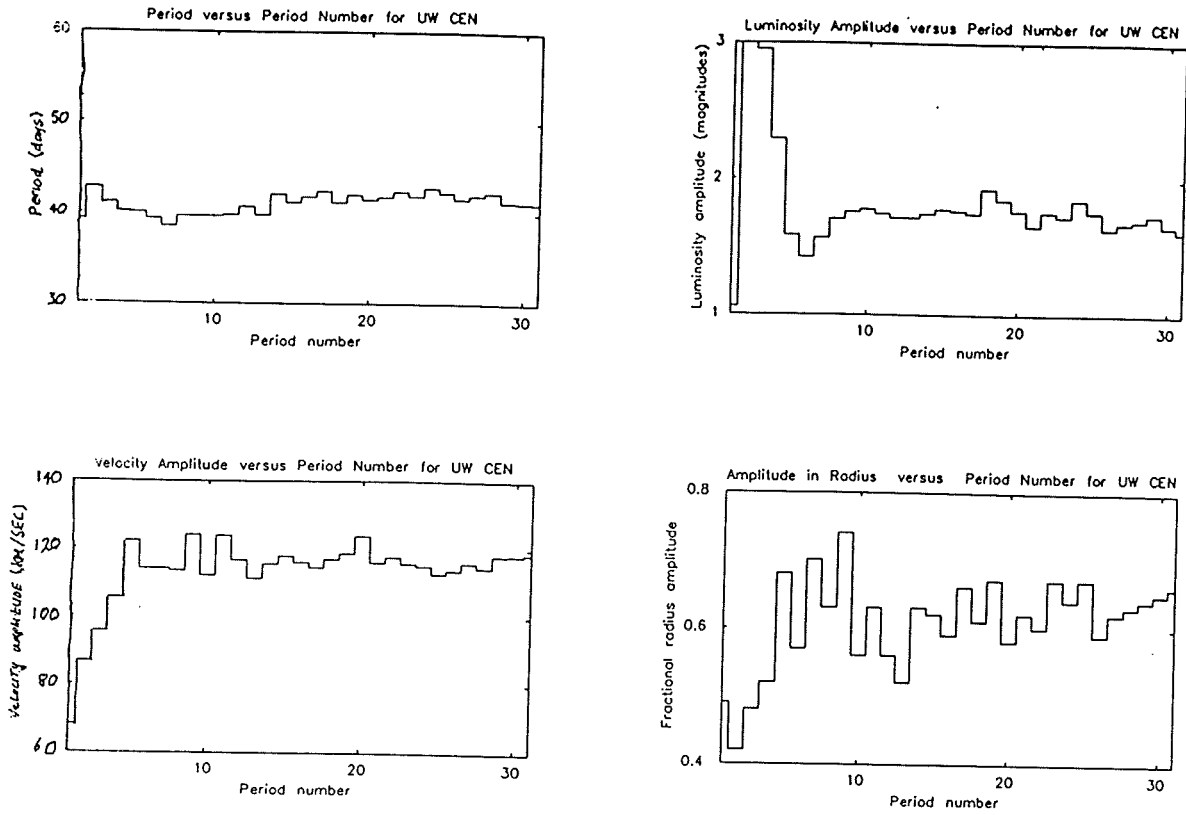


Figure 8.49 : This figure shows graphs of the period in days and the amplitudes of luminosity in magnitudes, velocity in km/sec and fractional radius versus period number for the UW Cen model.

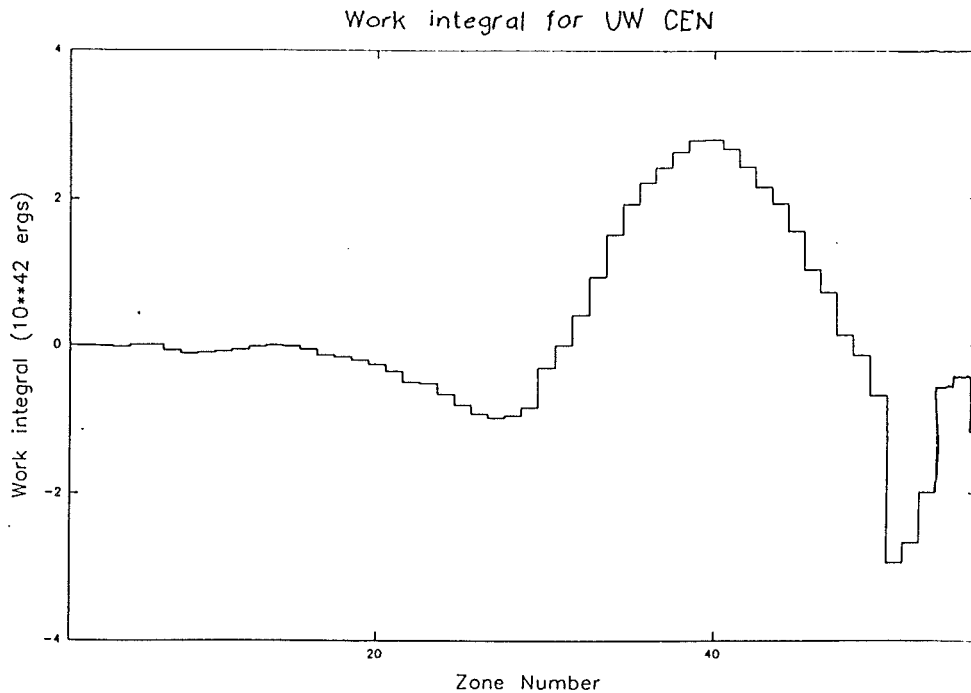


Figure 8.50 : This figure shows the work integral of UW Cen model, for period 31, versus zone number (zone 1 = innermost zone).

NON-LINEAR NON-ADIABATIC RESULTS

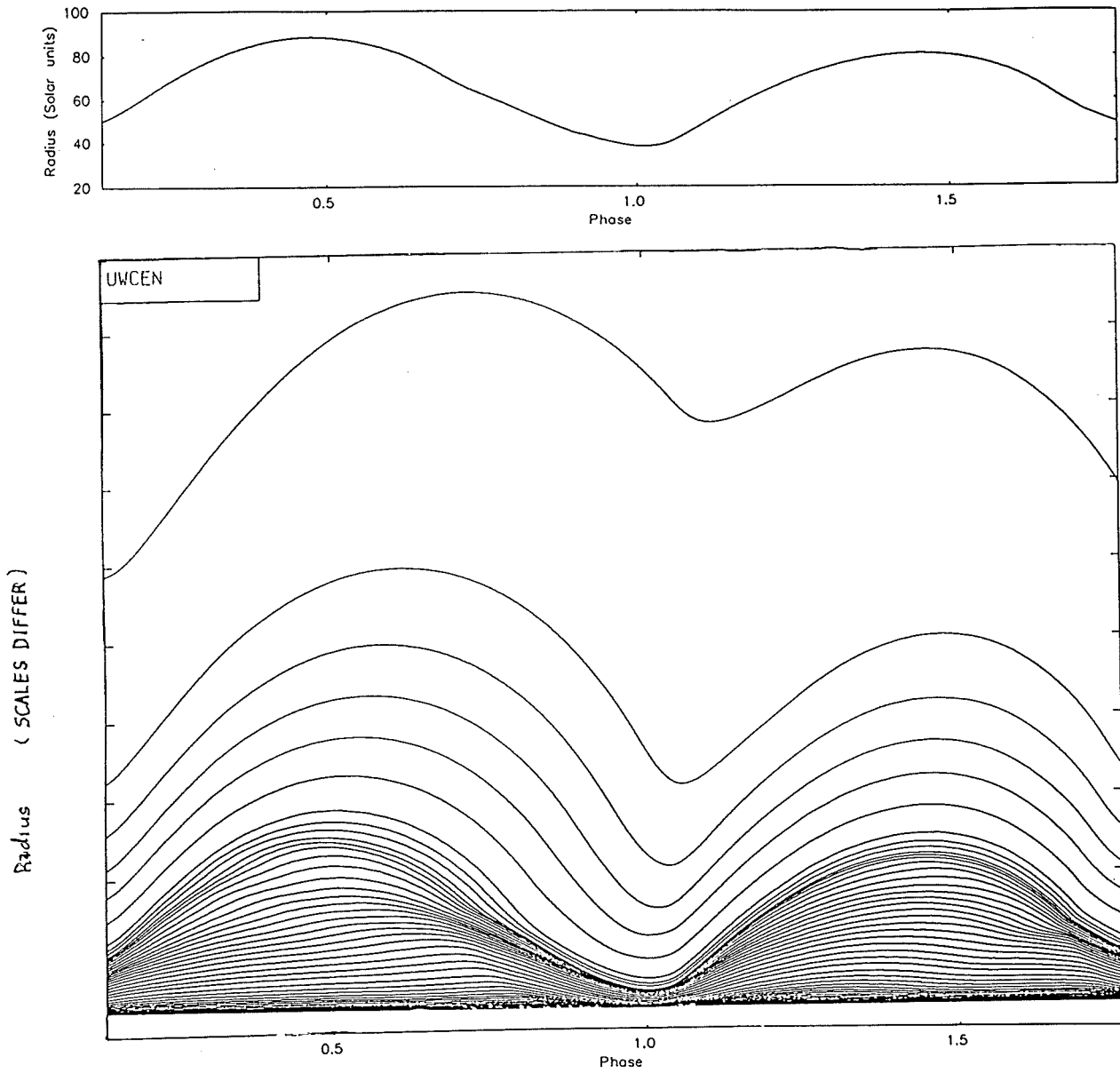


Figure 8.51 : This figure shows the radial (dR/R) history for all zones of the RCB star model: UW Cen.

NON-LINEAR NON-ADIABATIC RESULTS

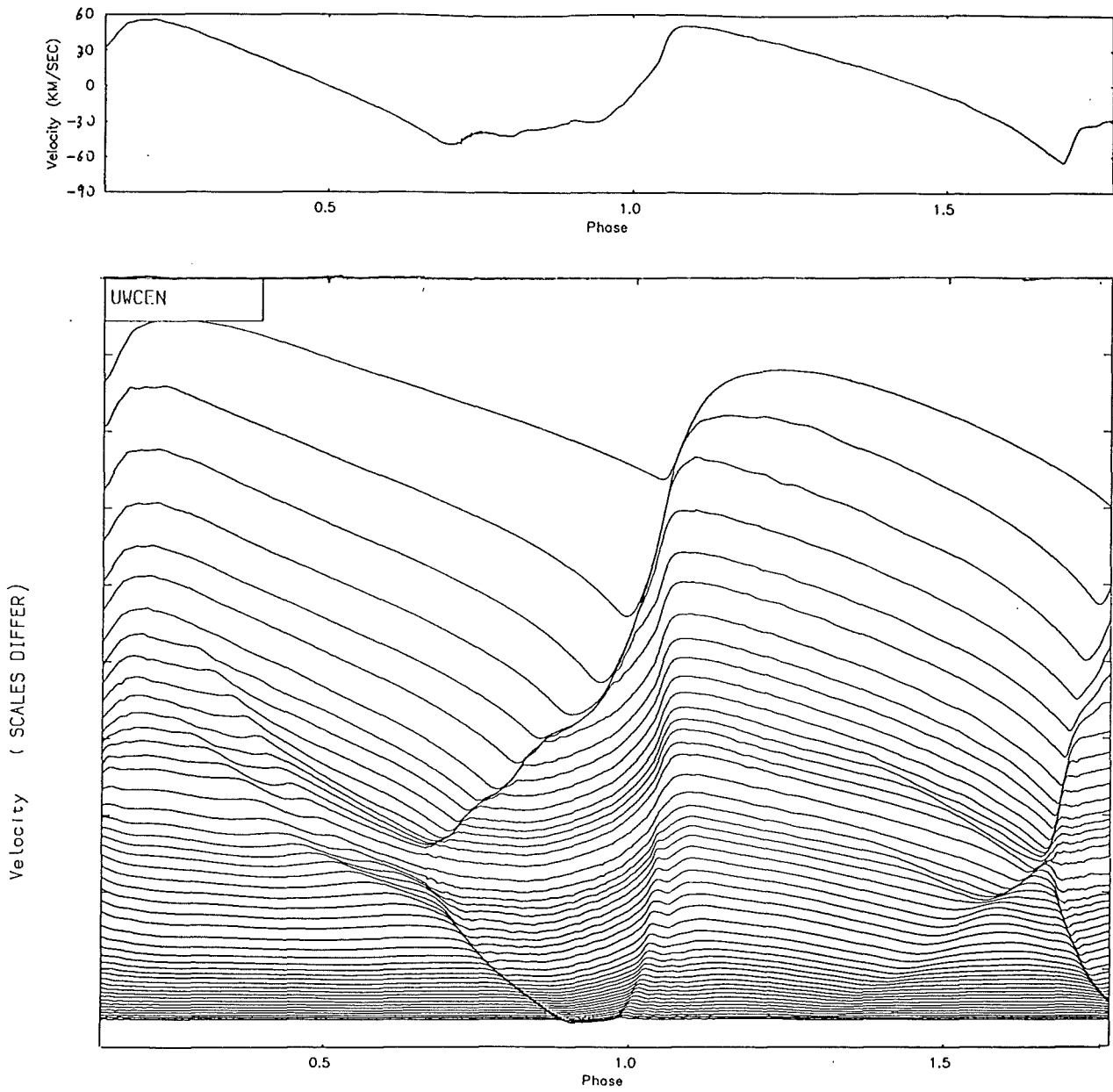


Figure 8.52 : This figure shows the velocity history for all zones of the RCB star model: UW Cen.

NON-LINEAR NON-ADIABATIC RESULTS

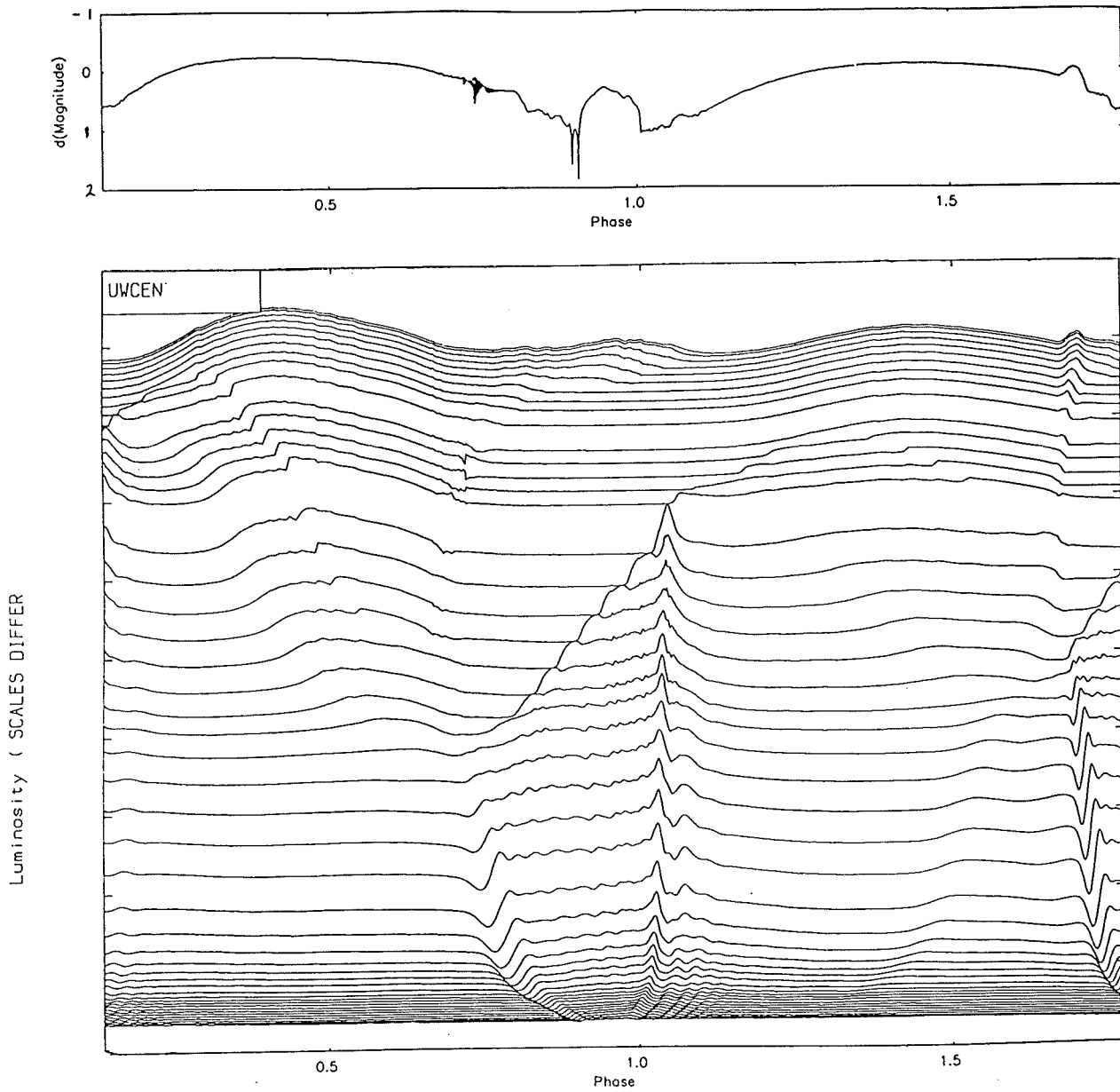


Figure 8.53 : This figure shows the luminosity (dL/L) history for all zones of the RCB star model: UW Cen.

NON-LINEAR NON-ADIABATIC RESULTS

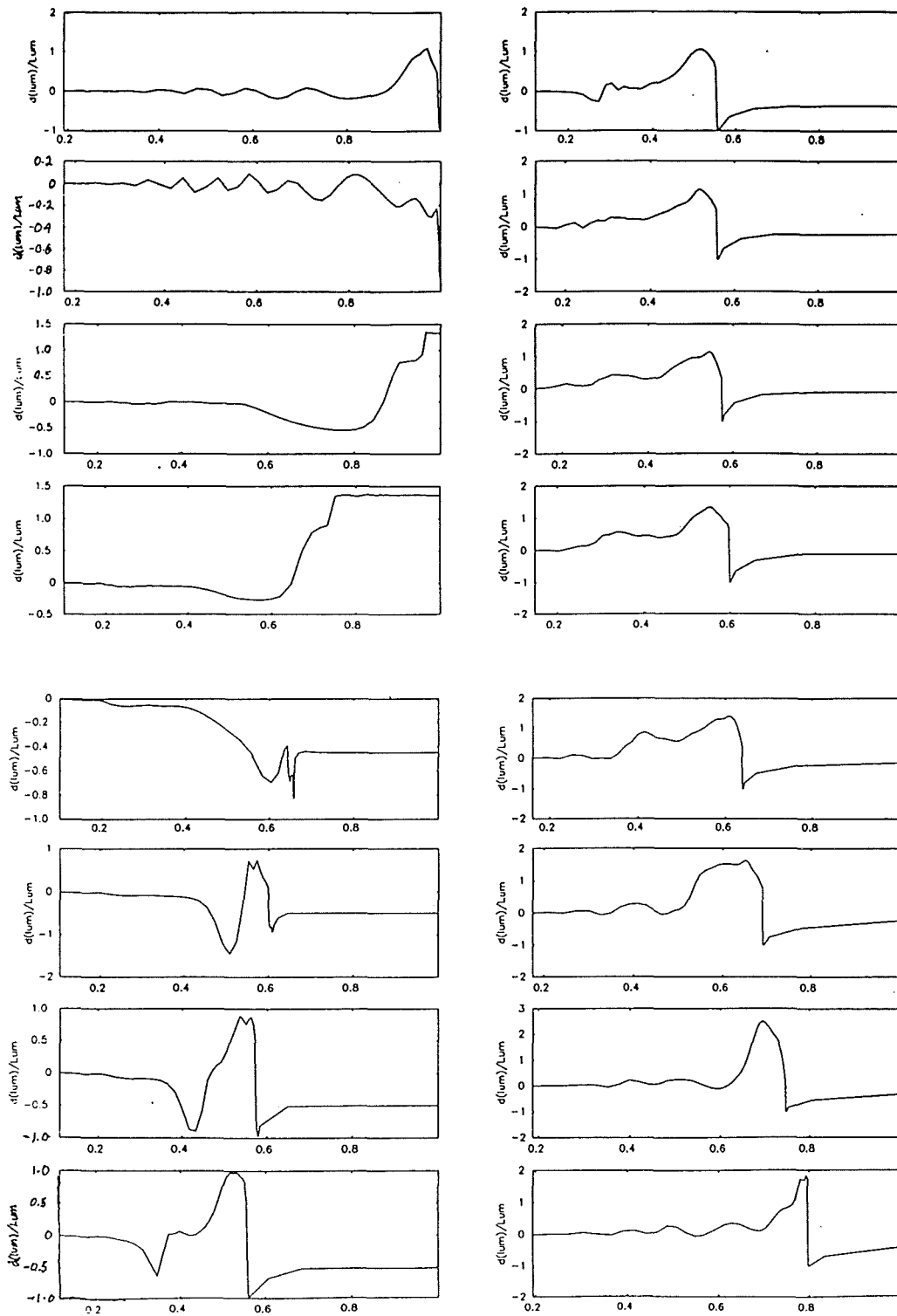


Figure 8.54 : Shows 'snapshots' of dL/L versus fractional radius for model UW Cen, with the phase between 'snapshots' being 0.0625 . The sequence starts at top L.H.S (phase 0.0625) working down the page and then continues at the top R.H.S., ending at the bottom of the page at phase 1.0 .

The history curves for the whole model, shown in Figures 8.51 - 8.53, are very similar to those found for the GU Sgr and RS Tel models, and probably will prove to be the underlying structure of all models having a period of around 40 days. Figure 8.54, a 'snapshot' history of the variation in luminosity ($\delta L/L$), has been included as it shows very well the increase in luminosity as the shock passes, and how the luminosity grows in amplitude, spreads out in mass and finally diminishes after the shock has passed. From this figure we can clearly see that there is a cut-off between the outer and inner zones, and that the 'freezing in' of luminosity prevents the initial shock travelling directly into the outer regions. When it does penetrate however, the whole outer region behaves as one and the luminosity bump, that can be seen in Figure 8.53, is obtained around phase 0.9 .

8.4.2 The Models Of The 6,900K RCB Variables

8.4.2.1 The RY Sagittarii Model -

In Figure 8.55 we can see that the peak kinetic energy, after an initial climb that is common to all the models created in this thesis, has levelled off and remains reasonably constant for the great majority of the model's history. As this model was made with the hope of comparing it with the comparatively few observations given in Alexander et al (1972), the kinetic energy and potential energy were also saved for each time step in the hope that this would perhaps shed some light on the final results. These curves can be seen in Figure 8.56 . Two things are worth noting in these energy curves. Firstly, the potential energy is nearly perfectly sinusoidal and has a period of (39 +/- 1) days, which is in agreement with the pulsational period of the star, and perhaps would be a better and more dependable way of finding the period of future models. Secondly, the kinetic energy

curve alternates between large and small peaks in its amplitude, the small peaks corresponding with contraction of the model. The latter point indicates that a good percentage (~20%) of the kinetic energy is lost in the contraction phase. From Figure 8.57, showing the work integral of the 64th period, we can see that this loss of energy is due to dissipation of the shock waves in the outer zones. The work integral is a little strange in that the $\text{He}^+ - \text{He}^{++}$ and $\text{He} - \text{He}^+$ ionisation zones are quite separated, and the helium 'damping' zone is very shallow. The majority of the 'damping' is due to the dissipation of the shock wave energy in the outer zones, instead of the usual radiative 'damping'. Also there appears to be a third small driving peak just above the inner boundary which may be due to the higher ionisation levels of carbon, as this element is very rich in these models, and the CIV ionisation peak occurs around this region.

If we now look at Figure 8.58, we first of all note that the period seems to oscillate between two diminishing extremes. The cycle repeats about every 16 periods. The reason for this is unknown, but is probably due to some resonance within the model envelope. The luminosity amplitude at first glance looks large, but once we have taken into account that the amplitude is due to very rapid dips in the luminosity curve (for the majority of the time the amplitude is around 0.6^{m}), it is not too far from the observed amplitude given in Alexander et al (1972). The velocity amplitude also has this problem in that it initially looks too large, but after multiplying by $17/24$ (limb darkening and projection correction) we get an average amplitude of about $(27 \pm 5)\text{km/sec}$. This value is slightly less than the radial velocity amplitude observed by Alexander et al (1972). To compare the theoretical model with observation, the observed and theoretical light curves were reduced to phase diagrams, using 38.6 days as the mean

NON-LINEAR NON-ADIABATIC RESULTS

period and an arbitrary zero was taken. The stars maximum visual magnitude was subtracted from the observational magnitude so that it could be easily overlaid on the theoretical M_{Bol} curve. This helps show that the amplitude is roughly right and also that the phase is nearly correct, though of course, with such semi-irregular behaviour, there can be little hope that the curves will in any other way be similar (see Figure 8.59). A similar overlaying was also done for the velocity after adding 10 km/sec (star's radial velocity) to the observed velocity, which allowed for a better comparison to be made. We again see that the amplitude and phase of the curves are not too incorrect, though there was little hope of the curves being more than grossly similar. To give some idea of how irregular the curves can be, a portion of the model's history is shown in Figure 8.60 .

To see why the curves are so irregular in shape, though semi-regular in period, the full zonal histories of dR/R , Velocity and dL/L can be seen for periods 63 and 64 in Figures 8.61 - 8.63, along with the associated photometric curves. From Figure 8.61, we can see that the outer zones, with the exception of the outer boundary, experience regular outward accelerations on top of the periodic outward movement. The inner zones undergo nearly sinusoidal motion with periods varying slightly about the characteristic frequency of the model envelope. We can also see that in the transitional or middle zones, 2 or 3 distinct changes in the inward acceleration of these zones occur about 0.1 in phase before the contraction of the inner zones. The smallness and number of these changes in acceleration is in contrast to the single sharp acceleration seen in the cooler 5,000 K and 6,000 K models.

NON-LINEAR NON-ADIABATIC RESULTS

A look at Figure 8.62, which shows the velocity variations throughout the envelope, gives us some idea of why the curves are so different from those of the cooler models referred to above. Instead of the single sharp shock followed by the secondary shock seen in most of the cooler models, we have a series of small successive shocks. Thus instead of driving the outer zones out to large distances with one powerful shock where the gravitational force is slow to bring them back, the shocks only push them out a little way before gravitational acceleration exceeds the initial outward acceleration and brings the outer zones back. Hence the shocks repeat with a frequency that is dependent upon the time it takes for the helium ionisation zone to respond to compression and cause the next expansion shock, due to opacity and pressure changes due to the increased ionisation. Underlying all this outer zonal activity is the oscillation of the inner zones, which are only slightly affected by the multiple shocks present in the outer regions of the envelope. Thus, in the case of these hotter models, the period of the inner zones dictates the mean period of the observed fundamental pulsation, and the outer zones cause the slight variations seen in the period. This to some extent explains the changes seen in the velocity and luminosity amplitudes, as large velocity amplitudes occur when maximum compression occurs in the helium ionisation region, i.e., when the outer and inner zones have large opposite velocities causing large compression in the ionised helium zones.

The deep minima seen in Figure 8.63 and the light curves in Figure 8.60 appear to be due to the rapid increase in temperature and density of the helium ionisation region resulting in an increase in the opacity, which is quite sensitive to such changes in this region of the envelope. This increase in opacity acts in a similar way to the

NON-LINEAR NON-ADIABATIC RESULTS

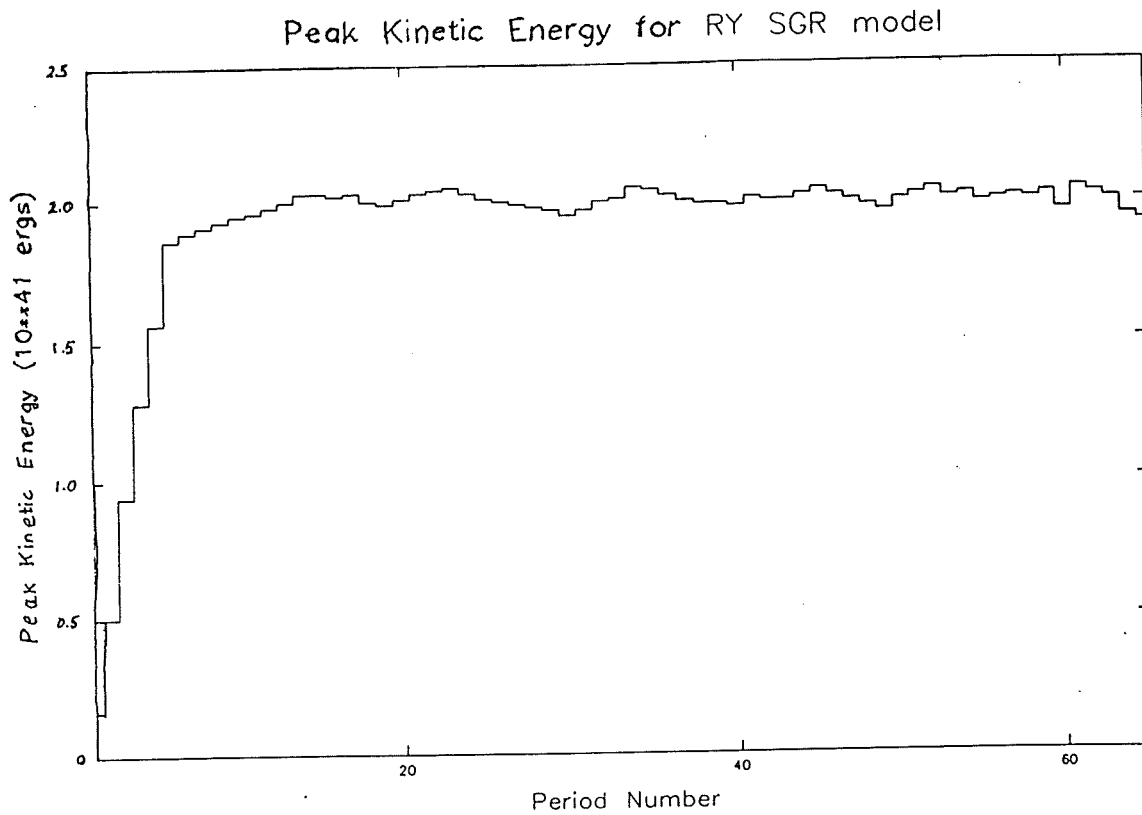


Figure 8.55 : Shows the peak kinetic energy versus period number for the RY Sgr model.

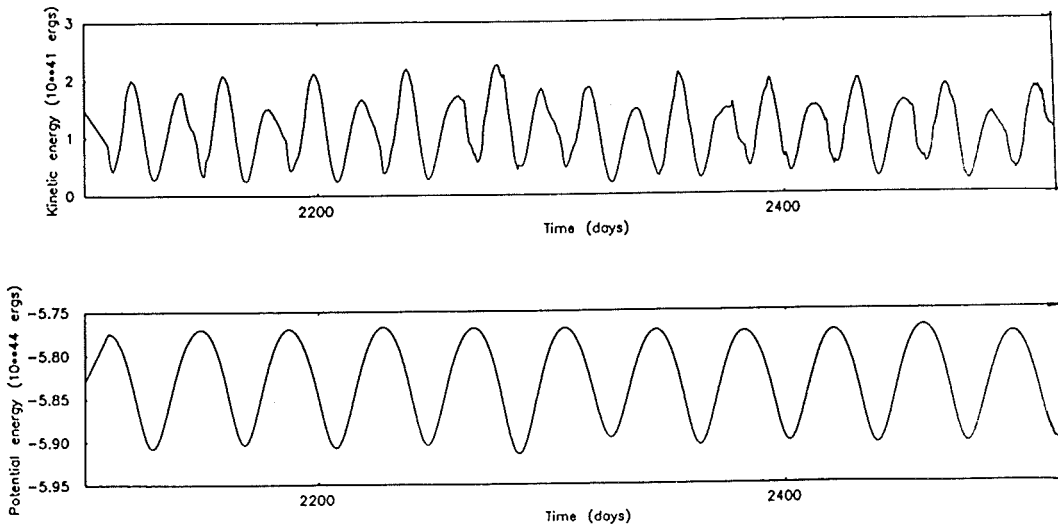


Figure 8.56 : Shows the kinetic (top) and potential (bottom) energy curves of the RY Sgr model for periods 54 to 64.

NON-LINEAR NON-ADIABATIC RESULTS

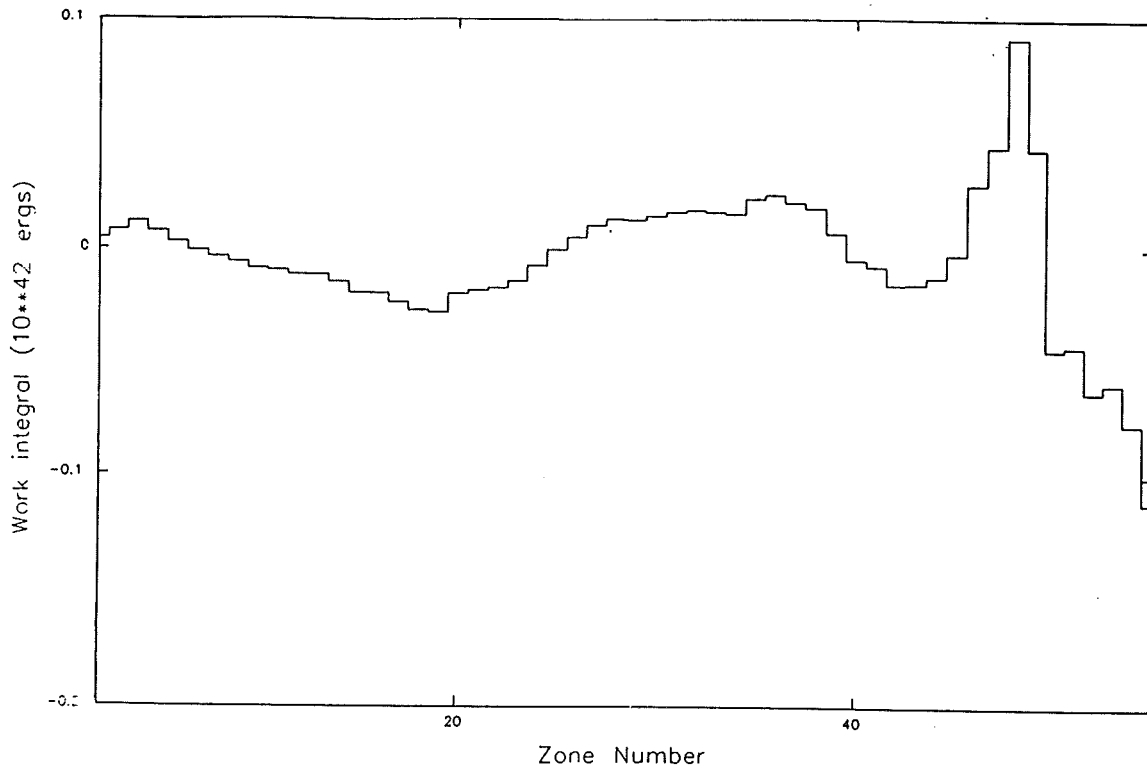


Figure 8.58 : Shows Periods and luminosity, velocity and fractional radius amplitudes of the RY Sgr model versus period number.

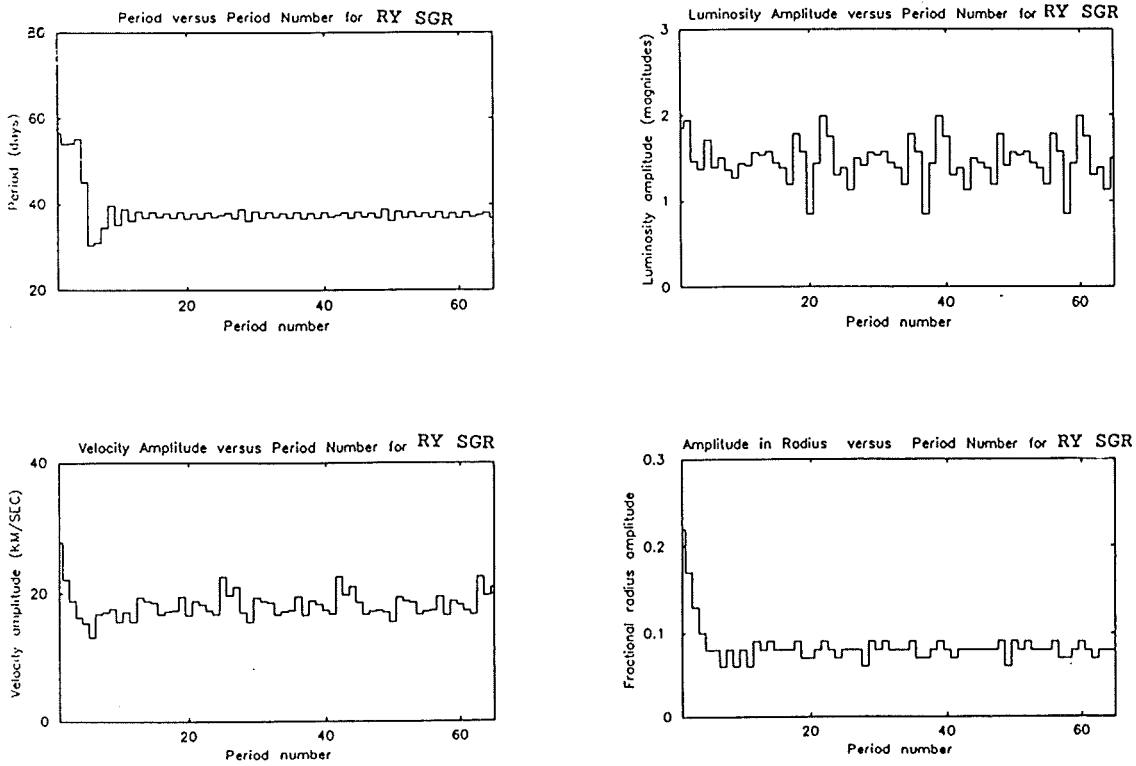
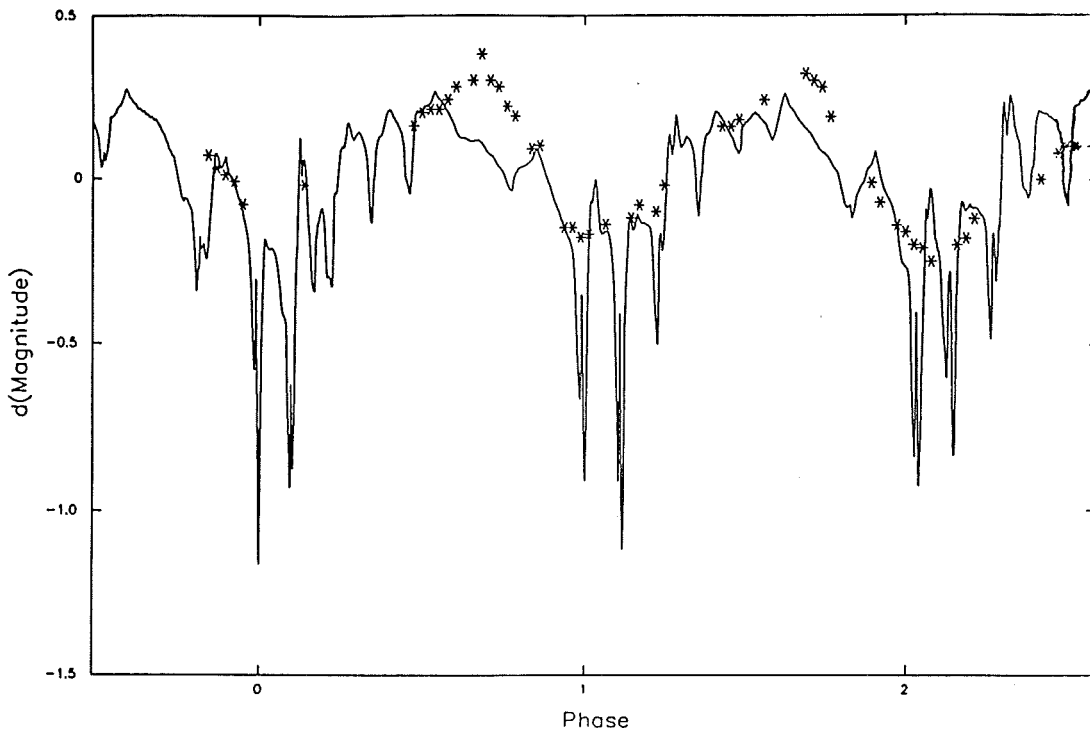


Figure 8.57 : Shows the work integral versus zone number for period 64 of the RY Sgr model.

NON-LINEAR NON-ADIABATIC RESULTS

Comparison of Theoretical Model with Observation



Comparison of Theoretical Model with Observation

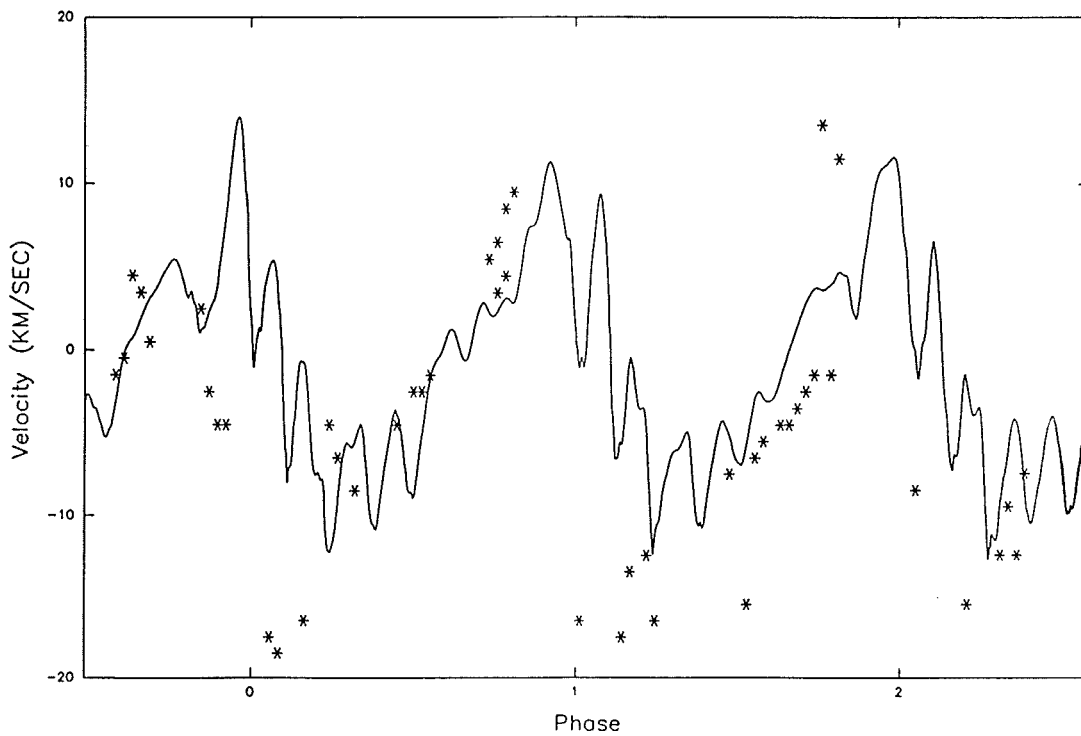


Figure 8.59 : This shows a rough comparison of the observed (asterisks) luminosity (top graph) and velocity (bottom graph) curves taken from Alexander et al (1972) with those curves found from the theoretical RY Sgr model (solid lines).

NON-LINEAR NON-ADIABATIC RESULTS

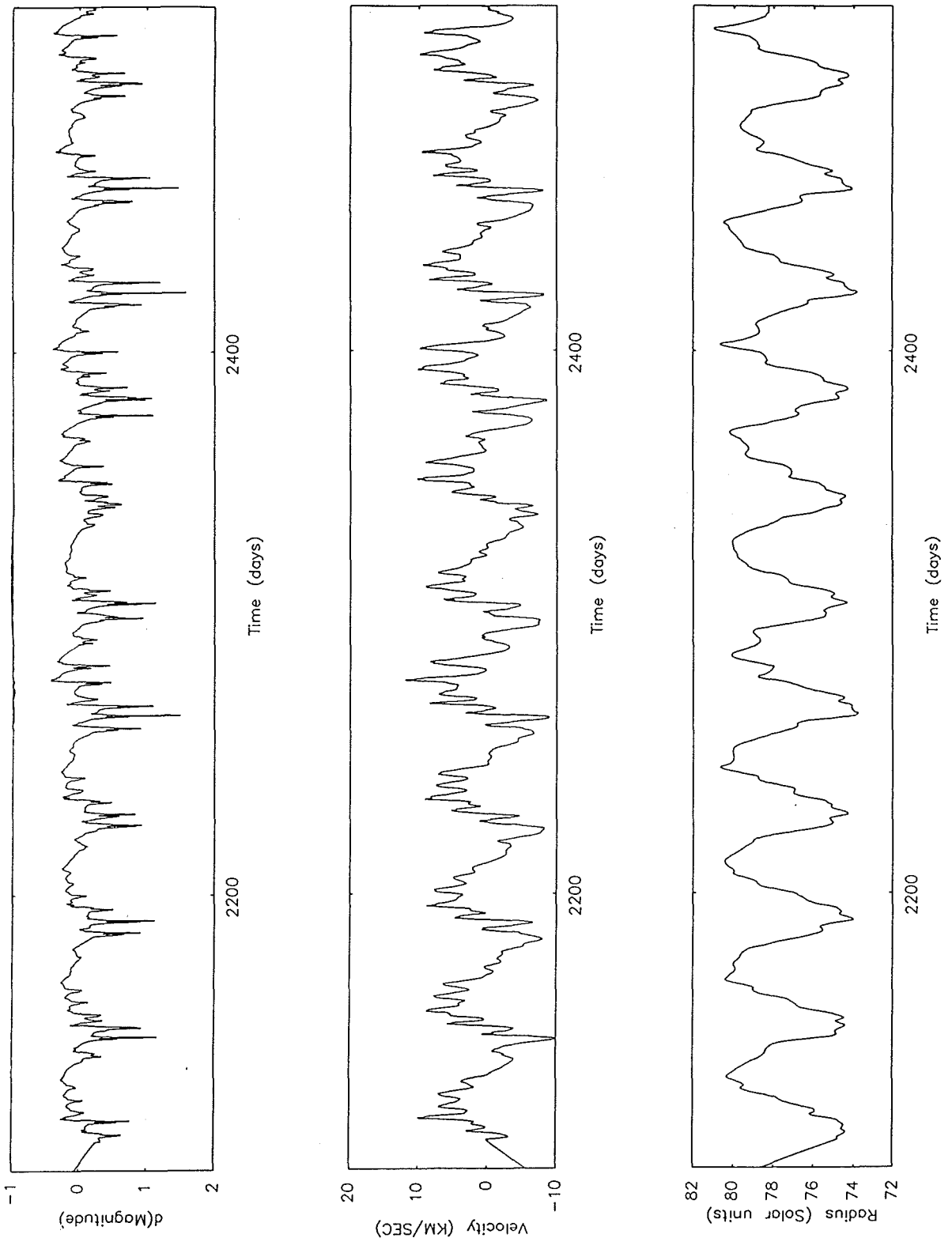


Figure 8.60 : This Figure shows M_{Bol} , Velocity (km/sec) and radius (solar radii) curves for periods 54-64 of the RY Sgr model.

NON-LINEAR NON-ADIABATIC RESULTS

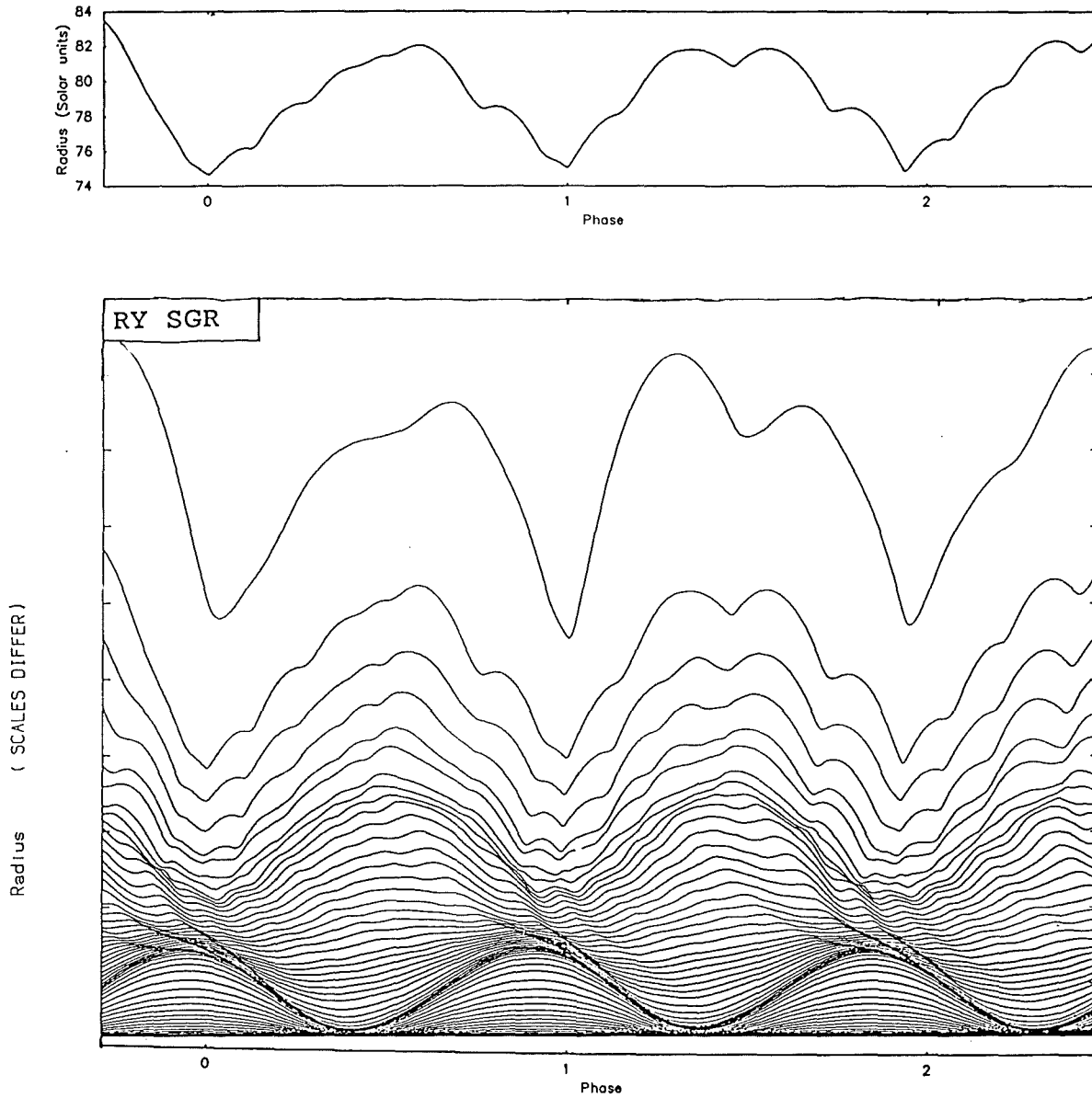


Figure 8.61 : This Figure shows the radial (dR/R) history for all zones of the RCB star model: RY Sgr.

NON-LINEAR NON-ADIABATIC RESULTS

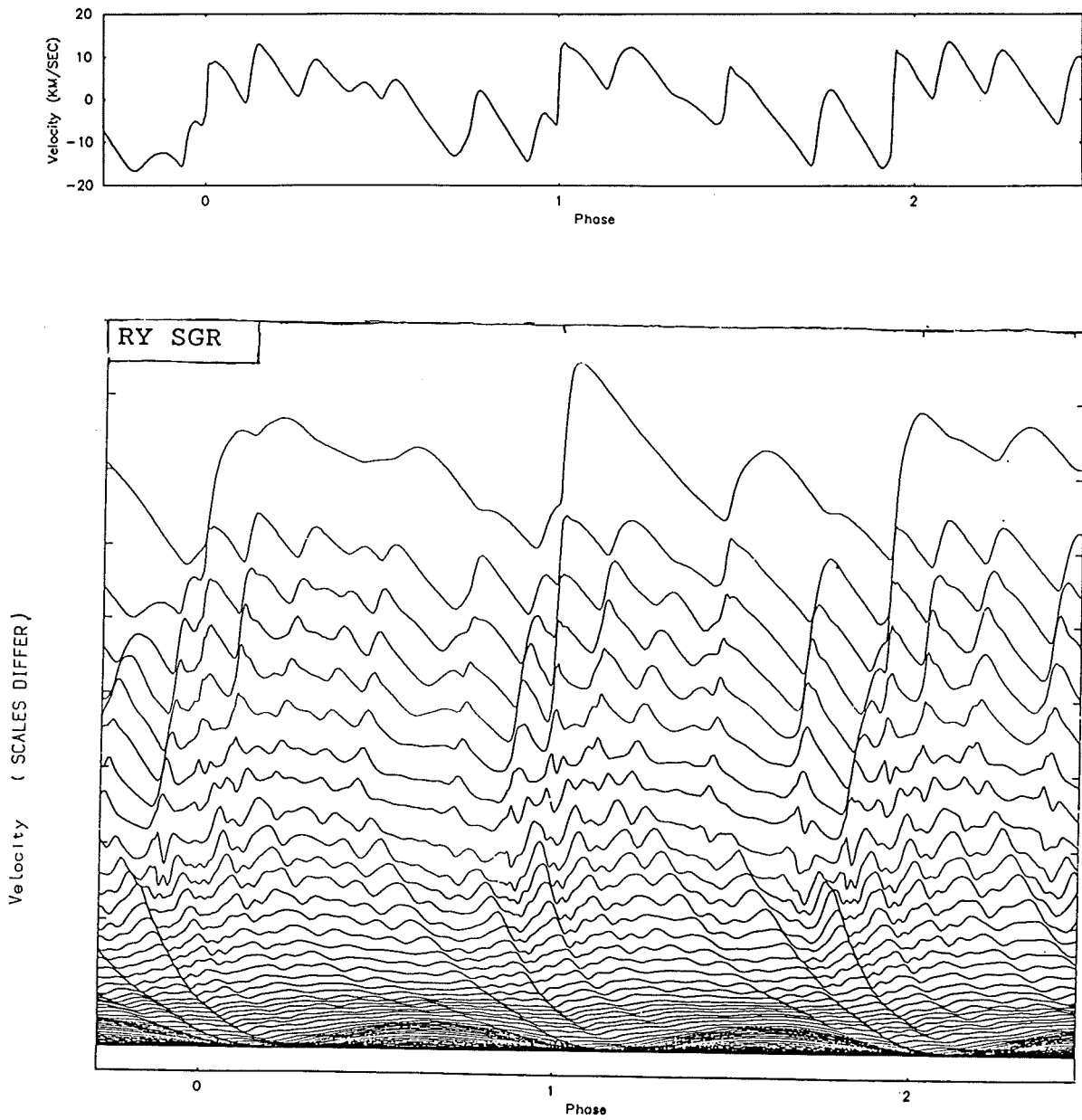


Figure 8.62 : This Figure shows the velocity history for all zones of the RCB star model: RY Sgr.

NON-LINEAR NON-ADIABATIC RESULTS

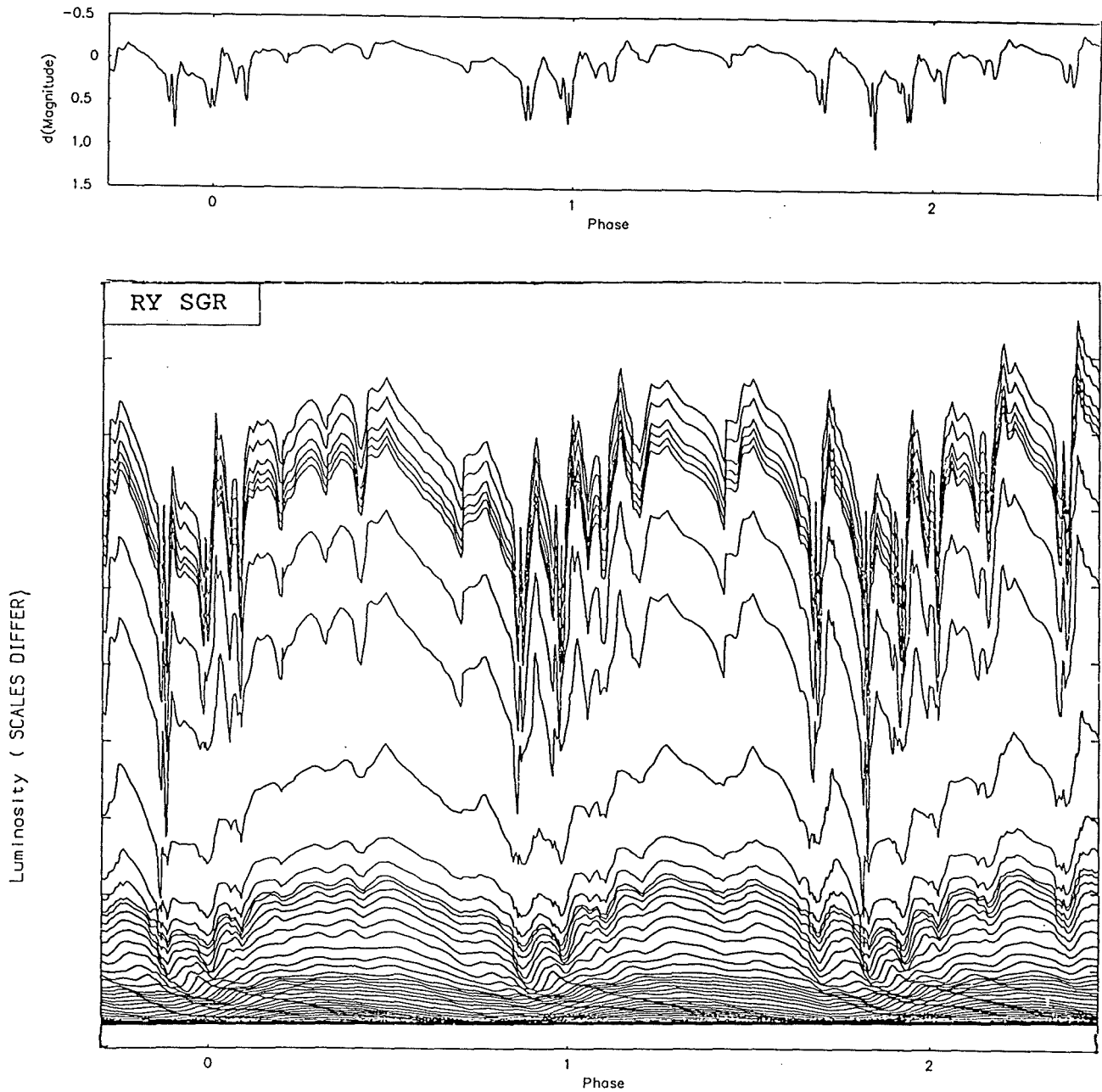


Figure 8.63 : This Figure shows the luminosity (dL/L) history for all zones of the RCB star model: RY Sgr.

NON-LINEAR NON-ADIABATIC RESULTS

shock ϵ -mechanism seen in the cooler models, and results in an outward travelling shock and luminosity wave. The luminosity is partially due to the release of 'dammed' radiation caused by the compression, and partially due to the radiative loss following the shock heating of the zone gases. The deep 'minima' naturally occur when the largest shocks occur, causing the greatest change in opacity, although not pushing it over the opacity peak. This is the reverse effect to that seen in the DXIX opacity table models, where the opacity sometimes decreased with such compressions, resulting in the luminosity spikes seen in those models.

This result then gives us a good indication that our choice of BD9C opacity table was correct, since irregular drops of a few tenths to several magnitude are known to occur in the RCB group of stars. To model such drops would require a far better treatment of the outer atmosphere and also the production of low temperature and density opacity tables, allowing for the effects of carbon grain formation.

8.4.2.2 The R Coronae Borealis Model -

This is the last model that will be presented in this thesis, and perhaps the most peculiar. In Figure 8.64, we can see that for about the first 5 periods the model behaved in a roughly regular way, the light curve being cyclic with a period around 33 days. Beyond this, a major drop in luminosity took place ($\sim 7^m$) followed by a ragged climb back to maximum light. Subsequently the variations in the light curve become much subdued, being only $0.^m1 - 0.^m2$ in size. The model was soon abandoned after this point as the time step increment plummeted to about 10 seconds, which meant that it would take too much processor time for the variations to grow back to their initial amplitude (as they seem to be doing, in the velocity curve). Time was very short

and there was no time to study this phenomenon further. This however is the only model, amongst all the models made, to show such a large drop in luminosity. It is doubtful whether the pre-drop curve represents any known star, especially not R Coronae Borealis. After the luminosity drop this could well represent R Cr B, though the period is only about 20 days, contrary to that observed for the real star or that predicted by the linear theory of the previous chapter. It would appear that the peculiar nature of this light curve is due to non-linearity caused by the high luminosity.

In Figure 8.65, the work integral for the period just before the drop in luminosity is shown, from which we can see that, except for a driving region just below the helium radiative damping zone, it looks quite normal. This inner driving region is not unexpected, as a similar region was seen in the RY Sgr model. Again, we find no outer zone dissipation of shock energy, and generally there is nothing to indicate why the model envelope should undergo such a large and traumatic drop in its luminosity. To try and get a better understanding of this drop, zonal histories of dR/R , velocity and dL/L are shown in Figures 8.66 - 8.68. Figure 8.66 seems to indicate that all the outer zones are undergoing continuous expansion, with only the lower zones being pulled back by gravitational effects of the star. It is also worth noting that there does not appear to be the usual heavy compression of the outer zones which was the cause of the shocks in previous models. In Figure 8.67 we can see the shallow shock of the previous period moving outward from the L.H.S. to about 330 days. The inward travelling shock and its reflection can also be seen between 260 and 300 days. Both these shocks seem normal and do not seem to account for the powerful shock that follows at 358 days. The large shock seems to be due to the amalgamation of the reflections of

two large inward shocks (caused by changes in the helium ionisation zone pressure) meeting with a third outward moving shock. The resultant outward moving shock then causes the envelope to expand rapidly with a high velocity and prevents gravity bringing the outer zones back, quickly suppressing the natural period in the photospheric curve. If we now look at Figure 8.68, we find that the history is even more peculiar, as the deep drop in luminosity does not occur at the large shock front but 20 days earlier, in the helium ionisation zones. The abrupt change in luminosity seen here then moves very rapidly (in less than two time steps or about 1.5 hours) inward towards the core and outward towards the surface. This outward moving luminosity step causes the luminosity of the outer zones to remain constant until the large outward moving shock decreases the zone opacities, after which the luminosities of the outer zones rapidly return to their pre-minimum value. Once the shock has passed, we can see that the opacity gradually rises and the shock heating of zones causes the luminosity to drop back towards its normal value. Beyond this, the luminosity variation is very small, with a period of around 20 days. The shallowness of the luminosity curve is due to the continual expansion of the outer zones. In time, the variations should build in amplitude back to the large value they had before the 'deep minimum' unless of course, another deep minimum occurs.

To try to understand what is really happening during the deep drop, a further set of 'snapshots' of dR/R , velocity and dL/L are shown in Figures 8.69 - 8.71. The 'snapshots' start at 337 days, proceeding in steps of 2 days down the page and end at 369 days. The radius 'snapshots' (Figure 8.69) show that at the onset of the rapid luminosity drop, the radius of the inner zones starts to expand, reaching a maximum after 12 days in the helium ionisation region of

the envelope before collapsing again. Throughout the whole of this time the outer zones are only barely affected and so would appear to have little to do with the cause and subsequent development of the very large shock. Figure 8.70 shows quite well the coming together of all the shocks, culminating in the large outward moving shock that signals the end of this deep luminosity minimum. Again we can see that there is a sharp change in the luminosity between 337 and 339 days, after which the luminosity remains constant until the large shock wave passes causing the luminosity to rise rapidly. This, as stated above, is due to the large changes in temperature and density causing large changes in the opacity, and also to the post shock radiation of excess heat from the shock zones.

Although the model does not look too much like the star it was modelled on, it does show some of the more peculiar characteristics of the star in question, such as a luminosity drop of $>7^m$ in its light curve. Now, as the radius did not increase greatly throughout the deep luminosity minimum, we can also surmise that the effective temperature of the model must have dropped significantly, possibly causing reddening (not unlike that seen in the real object during its deep minima). The post minimum expansion of the atmosphere may also allow the outer zones to move out far enough and for long enough to allow grain formation. This is hard to tell from the model presented here, as the atmosphere of the star was treated in a very rough manner which did not attempt to model the NLTE conditions that would reign in such tenuous regions. With more time a better treatment of the atmosphere could have been attempted, possibly with the inclusion

NON-LINEAR NON-ADIABATIC RESULTS

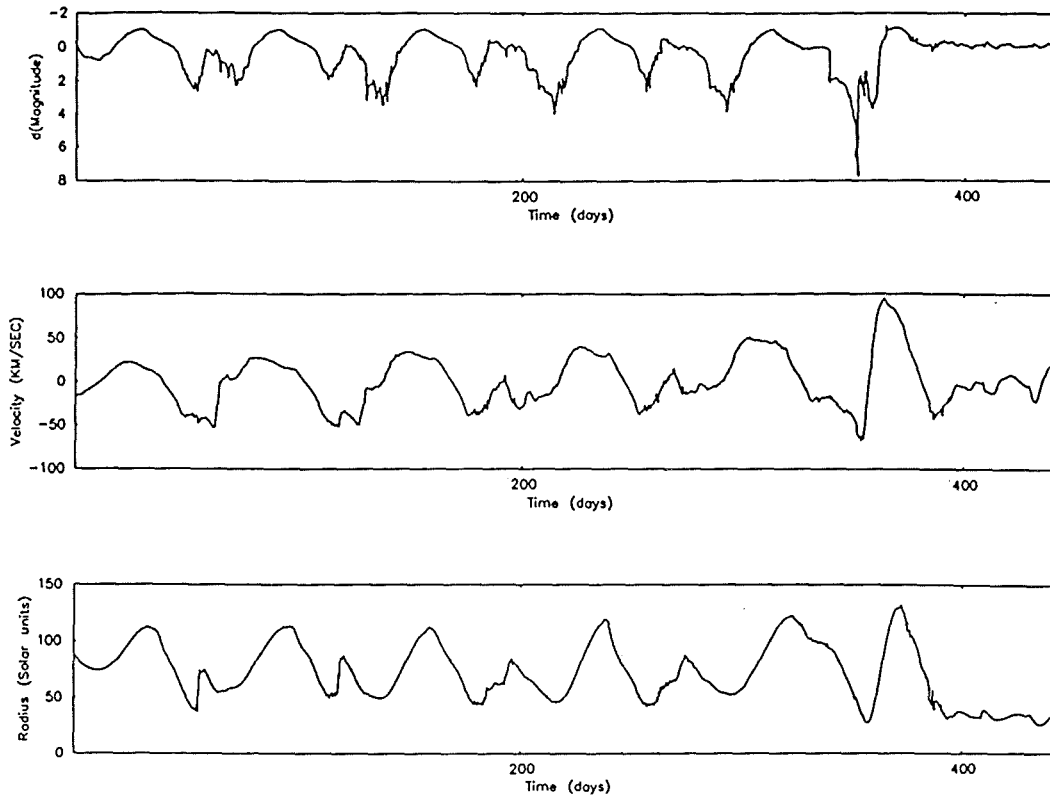


Figure 8.64 : Shows the luminosity in magnitudes, velocity in km/sec and the radius in solar radii versus time in days for model R Cr B.

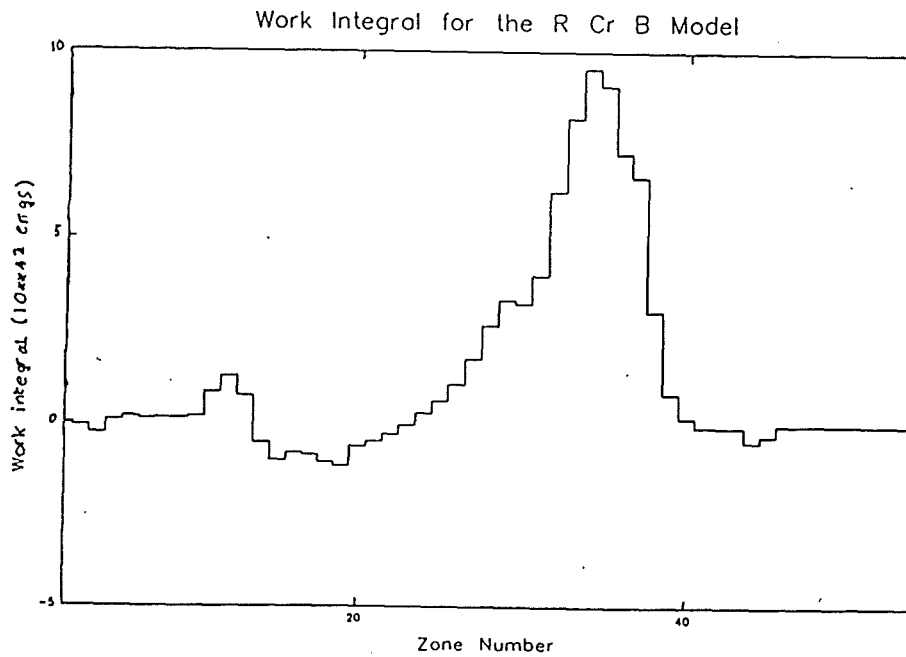


Figure 8.65 : Shows the work integral versus zone number for period 5 of model R Cr B.

NON-LINEAR NON-ADIABATIC RESULTS

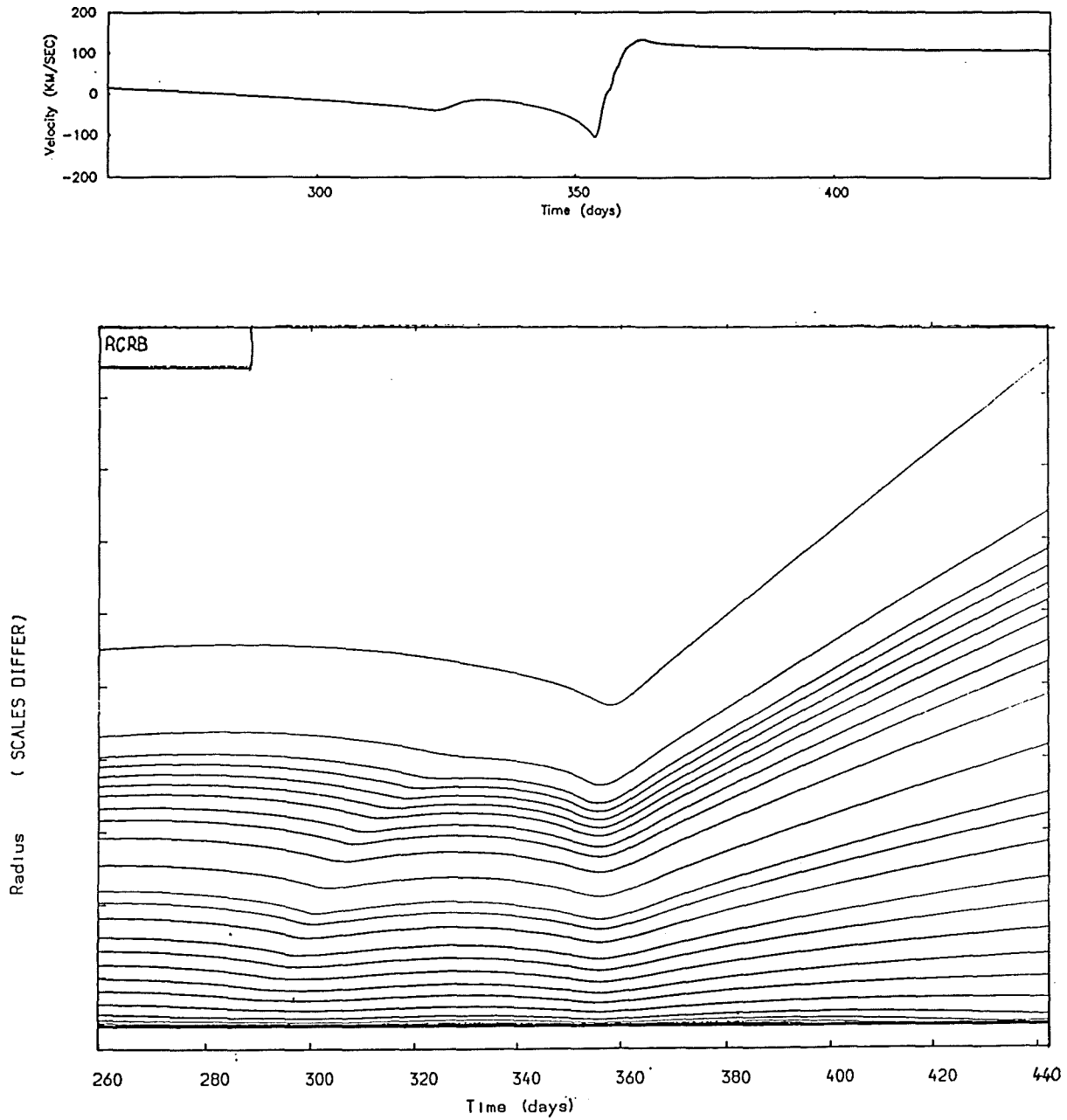


Figure 8.66 : This figure shows the radial (dR/R) history for all zones of the RCB star model: R Cr B.

NON-LINEAR NON-ADIABATIC RESULTS

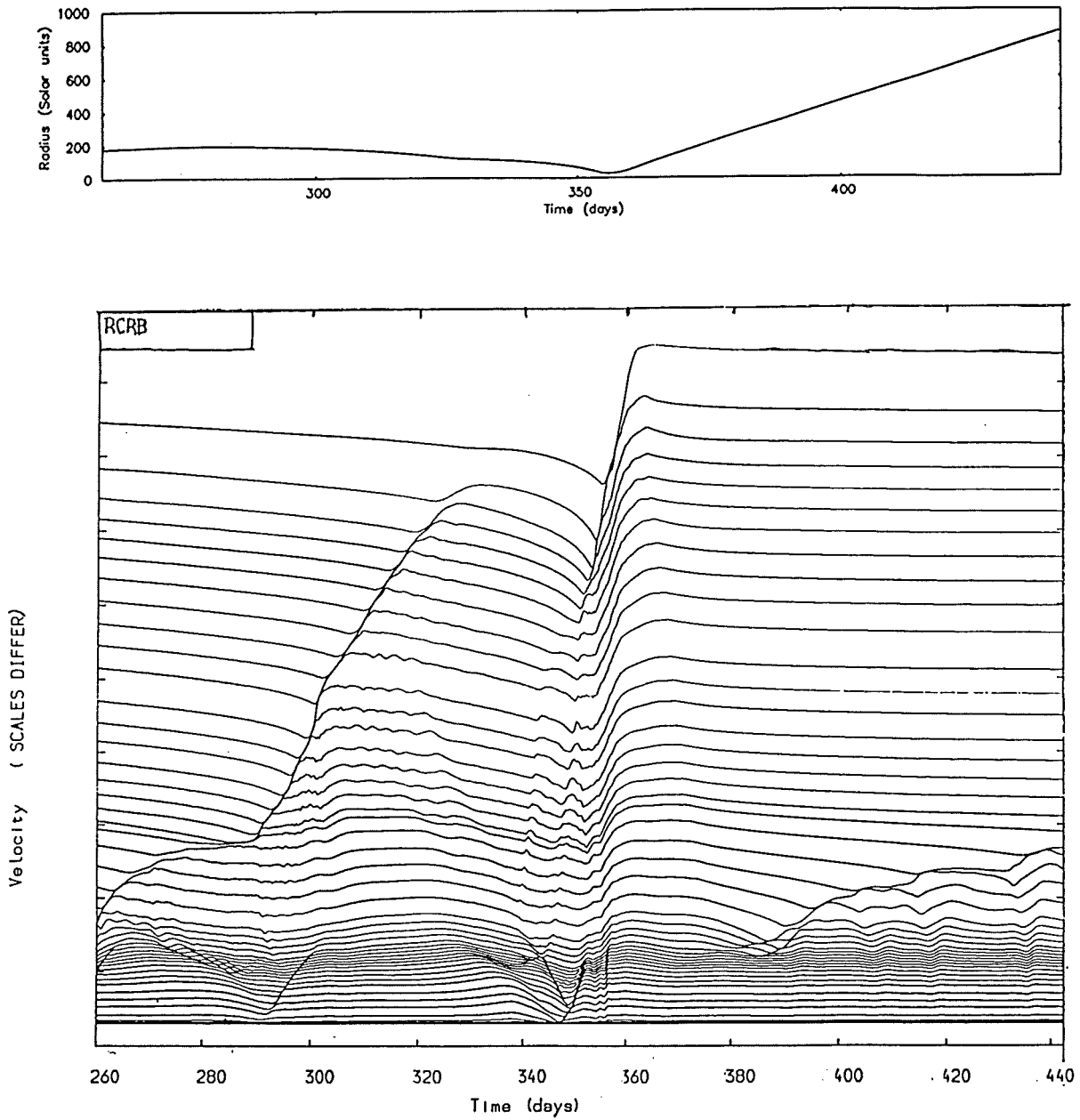


Figure 8.67 : This figure shows the velocity history for all zones of the RCB star model: R Cr B.

NON-LINEAR NON-ADIABATIC RESULTS

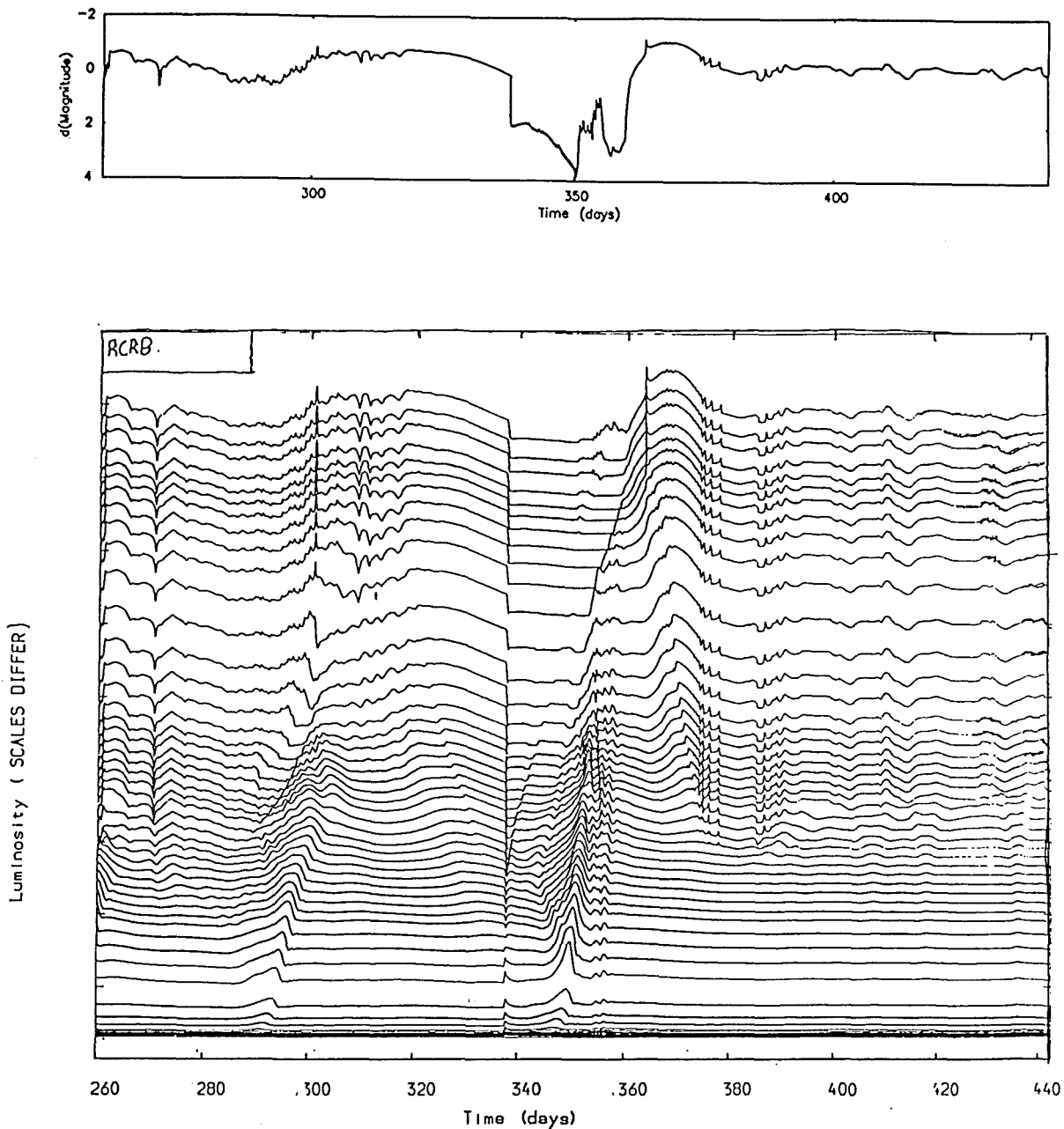


Figure 8.68 : This figure shows the luminosity (dL/L) history for all zones of the RCB star model: R Cr B.

NON-LINEAR NON-ADIABATIC RESULTS

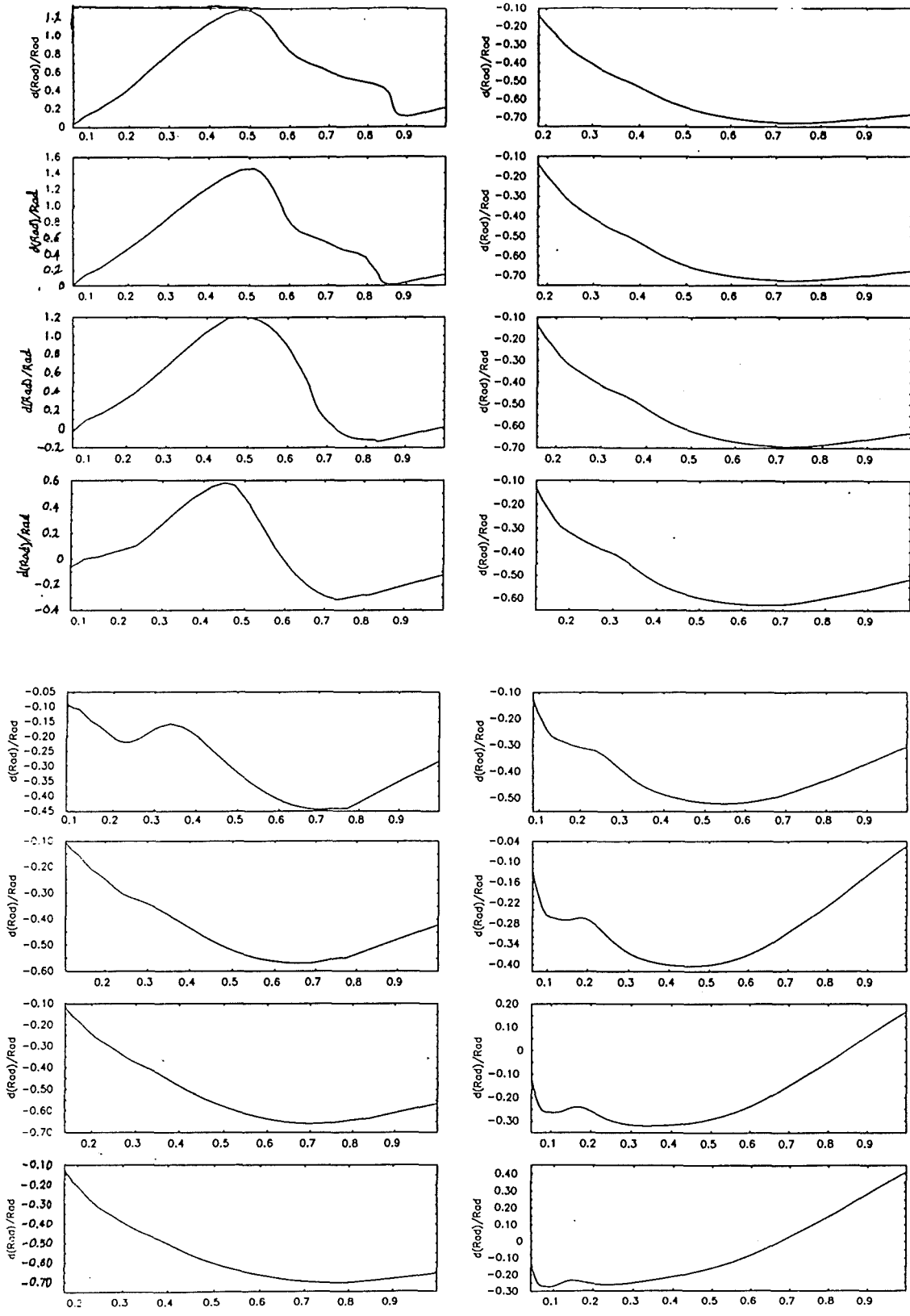


Figure 8.69 : Shows 'snapshots' of dR/R versus fractional radius for model R Cr B, with the time between 'snapshots' being 2 days . The sequence starts at top L.H.S (337 days) working down the page and then continues at the top R.H.S., ending at the bottom of the page at 369 days.

NON-LINEAR NON-ADIABATIC RESULTS

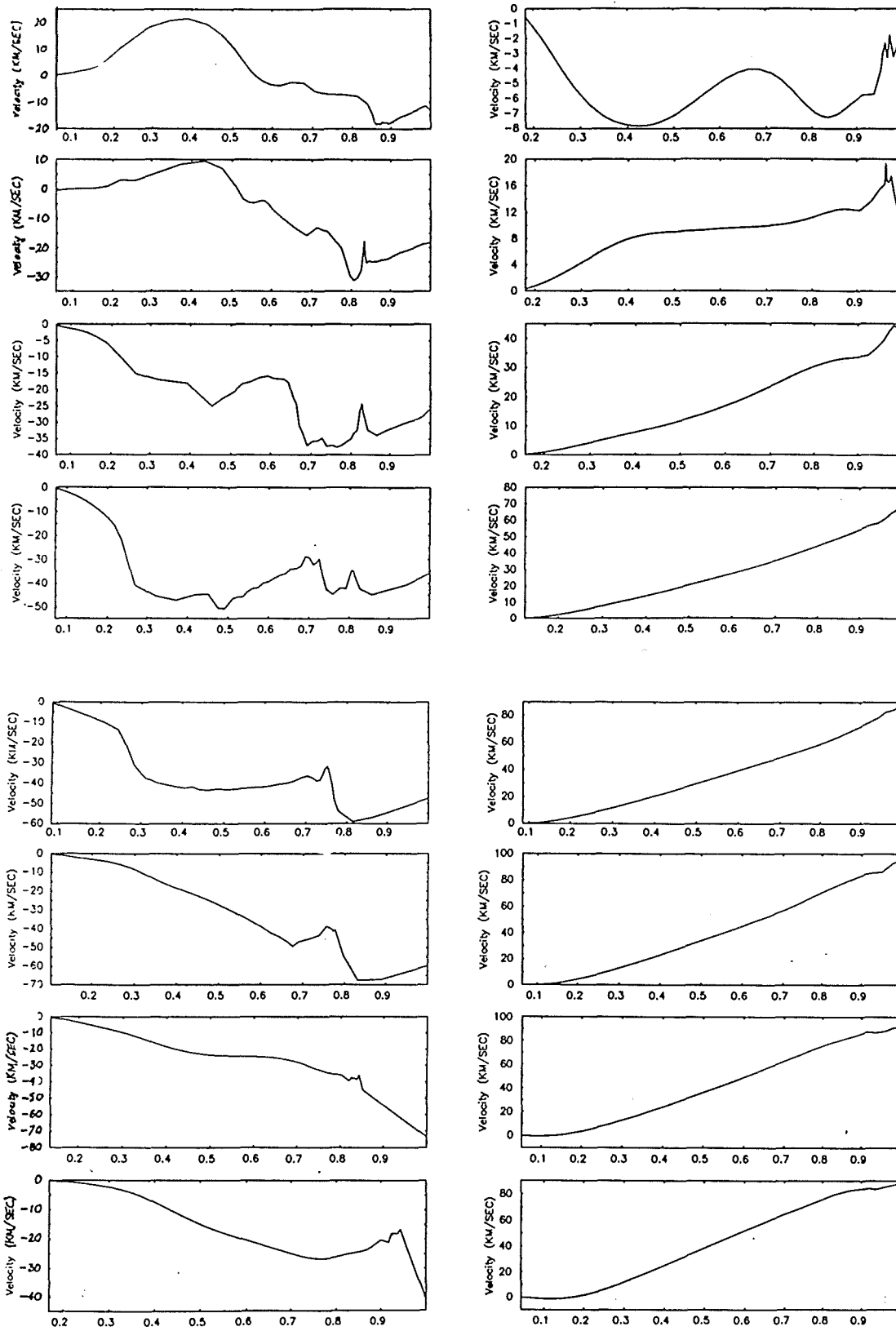


Figure 8.70 : Shows 'snapshots' of velocity versus fractional radius for model R Cr B, with the time between 'snapshots' being 2 days . The sequence starts at top L.H.S (337 days) working down the page and then continues at the top R.H.S., ending at the bottom of the page at 369 days.

NON-LINEAR NON-ADIABATIC RESULTS

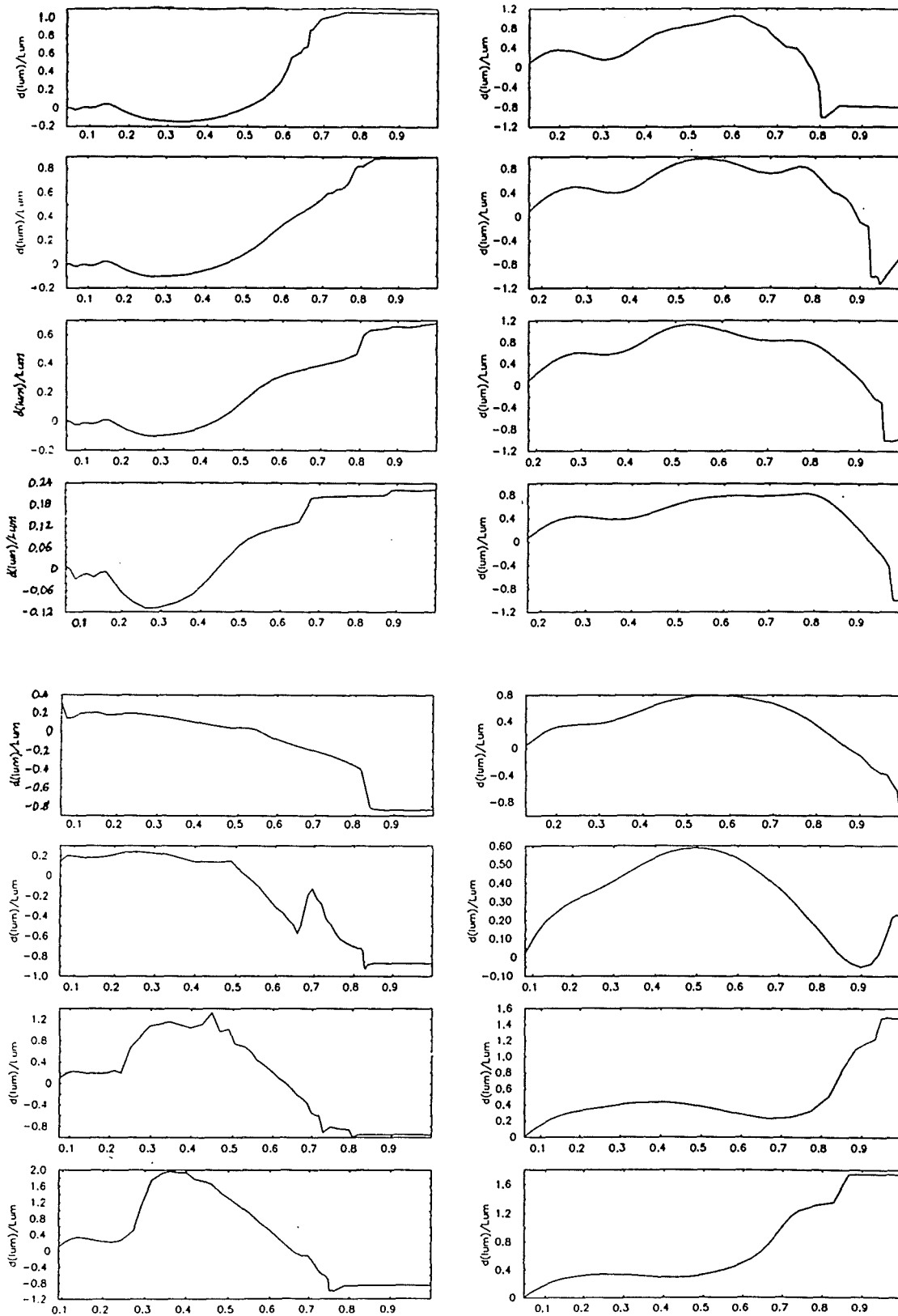


Figure 8.71 : Shows 'snapshots' of dL/L versus fractional radius for model R Cr B, with the time between 'snapshots' being 2 days. The sequence starts at top L.H.S (337 days) working down the page and then continues at the top R.H.S., ending at the bottom of the page at 369 days.

of Carbon grain formation. As it now stands, we can only show that in at least one model the deep minima seen in the RCB group of stars were producible (though it should be stressed that the model does not appear to be representative of the star it models) without resorting to ejection of matter or occultation of the underlying star by the ejection. As the deep minimum seen in this model appears to be the result of three shocks amalgamating (as well as some unknown cause of the sharp luminosity change seen in the lower zones), it can be concluded that it is a rare event and not predictable. Its occurrence may thus explain the irregular nature of the deep minima seen in the RCB group of stars. Indeed, it was fortuitous to have seen the event at all, as the RY Sgr model was followed for over 60 periods (about 7 years) without showing any such deep minima. Then again it may be due to the very high luminosity (resulting in extremely non-adiabatic behaviour) of this model, combined with effects due to non-linearity.

8.5 SUMMARY OF RESULTS

In this chapter we have seen that the major difference between the two opacity tables used is that the DXIX opacity table produces large luminosity spikes in most of the models produced using it, while the BD9C opacity table generally does not. The spikes are attributable to the shallowness of the opacity gradient in the outer zones of the models. For this reason, and because the light curves of the 7,000K models appear to be stable to pulsation, the table was rejected in the final modelling of the RCB stars. However, although the table was rejected and it looks as if the Carson opacities may be better at modelling this kind of object, it must be stressed that no firm proof has been found to reject the Los Alamos based opacity table generation method, as the 7000K models produced using opacity table BD9C are

subject to deep minima of the reverse nature to the luminosity spikes seen in the models made with the DXIX opacity table. The BD9C opacity table was only chosen because the periods in the nonlinear regime were in agreement with those of the real stars, they were unstable to pulsation and, more importantly, the 'spikes' were minima which had a similar appearance to some of the shallow irregular drops in luminosity seen in the light curves of real RCB stars. Thus, although the BD9C opacity table has been preferred to that of the DXIX opacity table, no firm conclusion can be made upon which table and hence opacity generation method is nearer reality. To answer this question, each method would have to produce opacity tables, using the best known abundances of the RCB group of stars, and the non-linear models presented in this thesis repeated. Another good reason for not being able to confirm or refute one of the opacity tables is that the BD9C table is a smoothed interpolation of the original Carson opacities, and hence is probably subject to large errors in places, as the number of original tables were sparse in Z_c and the opacity changes quite significantly with increasing Z_c for low Z_c .

The 5,000K and 6,000K models were a little disappointing in that they all had amplitudes that were far too large when compared with the observed values in Table 8.3. This can perhaps be put down to the effective temperatures given for the stars in the literature being too low. If they all had effective temperatures nearer that of RY Sgr and R Cr B, then the amplitude would be smaller (if luminosity minimum spikes are ignored) and would approach a value more in line with observations. From models not presented in this thesis, it has been found that the amplitude of the light curves seems to diminish for 7,000K models as the luminosity approaches the critical luminosity at which the 'dog-leg' occurs in the blue edges of the stability strip

seen in the linear results of Chapter 7. The required increase in effective temperature is quite feasible as the present effective temperatures were found using two black body fits of broad band photometry at maximum light of the star (Kilkenny, 1978) and its circumstellar shell, which allows quite a large margin of error in the estimates.

Finally, we can see that, in the RY Sgr model, the small cyclic variation has about the right size (ignoring luminosity drops) and period. When the observed data given in Alexander et al (1972) are overlaid, the periods are not too dissimilar. Although the radial velocity had to be shifted by +10 km/sec, to allow for the stars radial velocity. This then leaves us the R CrB model which does not initially look anything like R CrB having enormous variations in its light curves as well as a period that is about 2/3 of what it should be. It has been included because it was the only model to show a deep drop in its luminosity curve of the order seen in the deep minima of some RCB stars. It also appears to have a much reduced amplitude in its light curve after the deep minimum with a period which is roughly half the period of R CrB given in the literature. This then lets us speculate as to whether the deep minima are due to intrinsic variability of the star itself, instead of having to evoke non-uniform ejections of dust grains that then travel out in random directions and occasionally obscure the underlying star. Alternatively, these intrinsic deep minima could be the pre-cursors to grain formation, brought about by lifting the outer zones away from the stellar surface (reducing their temperature) and reducing the incident radiation as well. There is plenty of scope here for further research, especially into these 7,000K high luminosity stars with luminosities near that of the 'dog-leg' critical luminosity seen in linear blue edges.

CONCLUSIONS

CHAPTER 9

CONCLUSIONS

9.1 OVERALL SUMMARY

From the review of the literature carried out in Chapter 2, it soon became evident that little was known about the majority of the stars classed as RCB. Of the seven picked for study in this thesis, only two had been studied in any detail, giving us some hope of fixing their mass and luminosity. Of these two, only RY Sgr had a simultaneous luminosity and radial velocity curve (Alexander et al, 1972) of more than a few random points. From the literature, it was soon discovered that there were only two serious efforts to understand these objects theoretically, one using linear theory (Saio, 1984) and the other evolutionary modelling (Weiss, 1987). Saio (1984) placed some constraint upon the mass using the criterion of instability, and Weiss (1987) further constrained the masses by showing that for stars to evolve through this region of the HR diagram, they must have masses in the range $(0.9-1.0)M_{\odot}$. The results found in Chapter 7 for RY Sgr and R CrB which gave masses of $(0.96 \pm 0.07)M_{\odot}$ and $(0.95 \pm 0.06)M_{\odot}$ respectively, agree quite well with the above mass range found from Weiss's evolutionary work. It was also found that the linear results gave luminosities around those predicted by Weiss, although this time they were more sensitive to which opacity table was used. RY Sgr was found to have a luminosity in the range $(9,000 - 13,000)L_{\odot}$ and R CrB a luminosity in the range $(9,500 - 16,500)L_{\odot}$.

CONCLUSIONS

From the above results it seemed likely that all RCB stars would probably have mass around $1M_{\odot}$, and so this is the mass adopted for the other 5 RCB stars considered in this study (see table 8.3 for luminosity limitations).

Also in Chapter 7, we tried to see if we could decide which opacity table gave the better results, i.e., Cox & Tabor's Demarque XIX table or Carson's BD9C table. The results were inconclusive, though the DXIX opacity table survey found that the 7,000K models were stable to pulsation (or marginally stable depending upon the mass). As this is not the case, it indicates that perhaps the BD9C opacity table is a better choice for modelling these Helium-Carbon type objects. In the non-linear analysis of Chapter 8, the difference between the BD9C and DXIX opacity tables was further demonstrated by the striking difference in the behaviour of the models produced using both tables but otherwise identical input parameters. The models made using the DXIX opacity table have large luminosity spikes which are not observed in real stars and also do not appear in any of the BD9C opacity table models. Their cause seems to be attributable to the steeper opacity gradients and high opacities found in the DXIX models' outer zones, which lessen the 'freezing in' effect found in the BD9C models, and allow the massive change in luminosity seen as a 'spike' by allowing a large change in the opacity as the shock passes. This then indicates that, as the luminosity spikes are not seen in real stars and are also not seen in the BD9C opacity table models, the BD9C opacity table should be preferred over the DXIX opacity table when modelling helium-carbon objects. It must be stressed, however, that this is not conclusive and further models need to be made as well as a purpose-built Carson opacity table instead of the present smoothed interpolation.

CONCLUSIONS

From the non-linear models of the 5,000K and 6,000K RCB variables, it was generally found that the amplitudes of the luminosity and velocity curves were too large. This could not be alleviated by changing the opacity table, and indicates that the effective temperatures quoted in the literature are probably too low. This is quite possible, as nearly all the effective temperatures come from two sources (Kilkenny, 1972 and Walker, 1985), both of which use broad band photometry of the objects and black body fits. As the objects all have large infra-red excesses this complicates the fits further and could mean that the effective temperatures are 2,000K hotter than quoted in the literature. This could at least be the case for UW Cen, RS Tel and GU Sgr, which have periods similar to RY Sgr and R CrB. This would also bring the luminosities found in Chapter 7 up to the values generally expected for RCB stars, and make the class less heterogeneous and perhaps easier to understand from an evolutionary point of view.

Finally, the non-linear models for the 6,900K RCB variables have been shown to have about the right period and amplitude of variation in the light curves for the RY Sgr model. The light curves of the RY Sgr model also had roughly the same phasing as the observed light curve (Alexander et al, 1972). This along with the semi-regular behaviour, indicates that the model is reasonably good, allowing for the approximations used and coarseness of model zoning. The only set-back to the model was the appearance of inverted luminosity spikes, which may or may not be real. Certainly they are not present in the observed light curve, though due to the small number of points in this curve, and the lack of any other published light curve (as far as the author knows), it is hard to say whether these inverted luminosity 'spikes' are due to spurious opacity table effects or not.

CONCLUSIONS

The other 6,900K model R CrB, probably does not represent any known RCB star, as its initial amplitude of variation is far too large. Its final amplitude is not inconsistent with RCB stars, however, and it is hard to say whether the amplitude of the pulsation will grow back to the original large value or not (although it seems very likely that once the outer zones have returned, this will be the case). This model is interesting as it was the only model to show an irregular deep minimum of the order of those seen in the RCB group of stars. The cause is uncertain, but appears to be the appearance of a luminosity bump at the lower edge of the helium ionisation zone which passes very rapidly inward and outward. This luminosity 'edge' has the effect of causing two large shocks, which amalgamate with a third, which then causes a massive upsurge of all the outer zones, resulting in the observed reduction in pulsation amplitude and period. This is the first time in the author's knowledge that such a deep minimum as been seen in a non-linear model. However with the uncertainties in the opacity table and the unpredictable effects of non-linearity, the result should be treated carefully until a lot more modelling has been done to find the cause of this deep minimum. No such minima were observed in the RY Sgr or cooler RCB models made during the study for this thesis, which in total have an accumulative model time exceeding 100 years. The lifting of the outer zones seen here, could be the pre-cursor of carbon grain formation, resulting in the spectral changes observed in the RCB group of stars, during their deep minima.

Thus, from the work carried out in this study and from previous work by other researchers (see review in Chapter 2), it seems likely that the 'hot' RCB objects form a distinct group away from the main RCB group. This 'hot' group consists of the stars DY Cen, MV Sgr and V348 Sgr.

CONCLUSIONS

The linear results further indicate that the effective temperature of the 'cooler' RCB objects have been underestimated by about 2,000K, although this conclusion is based upon scanty light curve data and dubious periods.

From the above discussion, and taking account of the good non-linear model for RY Sgr, it seems that most of the real RCB stars will be semi-regular variables with periods around 40 days, with the following parameters: $T_{\text{eff}} \simeq 7,000\text{K}$, $L/L_{\odot} \simeq 10^4$ and $M/m_{\odot} \simeq 1.0$.

9.2 FUTURE DEVELOPEMENTS

Future work on the RCB stars should proceed in two stages: the first being observational, and the second theoretical. On the observational front, a detailed spectral analysis of as many of the member stars as is possible would be useful to obtain reasonable values of the effective temperature, $\text{Log}(g)$ and abundance. Only four stars of the group have had high dispersion spectroscopy carried out on them, of which only RY Sgr (Searle, 1961) and R CrB (Schonberner, 1975) have had $\text{Log}(g)$ values found for them, to date. Also more broad band photometry (including infra-red) at maximum light combined with better 'dust models' would be useful in obtaining a better estimate of the effective temperature.

A longer and more desirable project would be to carry out simultaneous spectroscopy and photometry on at least some of the stars, to obtain light curves and, more importantly, radial velocity curves. This would be a great asset, as in the literature only RY Sgr (Alexander, 1972) has had such simultaneous spectroscopy and photometry carried out on it for any length of time. Finally, on the observational front continuous observations of the variable stars,

CONCLUSIONS

over several years, would be useful to determine the periods more accurately, which, combined with other stellar parameters and theory, would help to fix the mass and luminosity of these stars.

On the theoretical front, there is still much to be done. Firstly, the radiation transfer equations could be altered to a form that would be more valid in an extended stellar atmosphere, as the proposed mechanism of 'carbon grain ejection' (deep minima) and their subsequent collation into a circumstellar cloud could be modelled. In particular, it would be interesting to see if the the periodicity observed in the infra-red (and hence circumstellar cloud) is connected in any way with the radial pulsations of the underlying star. This would, of course, mean the calculation of very low temperature opacity tables, and the inclusion of grain formation in the outer regions of the extended atmosphere. The inclusion of convection would also be an advantage, although this will have to wait until a good theory of convection has been formulated, and not the present ad hoc 'mixing length' methods.

Finally, more evolutionary work needs to be carried out, so that a good understanding of how the RCB stars and similar objects form, i.e., from which stellar objects do they originate, and how do they evolve into the RCB group. Where do they evolve too (after passing out of the RCB group)? These and many other questions need to be answered before we can state with confidence that our knowledge of these objects is complete. I hope this gives any future researcher, anticipating doing research in this field, whether observational or theoretical, an indication of work that still needs to be done.

REFERENCES

REFERENCES

- Aleshin (1959).....Aleshin,V.I. - Russian A. J. 36, 468
- Alexander et al (1972).....Alexander,J.B., Andrews,P.J.,
Catchpole,R.M. ,Feast,M.W.,Lloyd-Evans,T.,
Menzies,J.W. ,Wisse,P.N.J., and Wisse,M. -
MNRAS 158,305
- Alexander (1982).....Alexander,J.B. - MNRAS 201,579
- Allen et al (1982).....Allen,D.A., Baines,D.W.T., Blades,J.C.
and Whittet,D.C.B. - MNRAS 199, 1017
- Ashby (1976).....Ashby,R.M. - Sky and Telescope 52, 260
- Baker & Kippenhahn (1962)...Baker,N. and Kippenhahn,R. -
Z. Astrophys. 54, 114
- Baker & Kippenhahn (1967)...Baker,N. and Kippenhahn,R. -
Z. Astrophys. 67, 271
- Bateson (1972).....Bateson,P.M. - RASNZ Circ. No. 185
- Bateson & Jones (1972).....Bateson,P.M. and Jones,A.F. -
Circ. RASNZ Var. Star Sect. NO. 185, 1
- Bateson (1974).....Bateson,P.M. -
Publ. Var. Star Sect. RASNZ No. 1, 33
- Bateson (1975).....Bateson,P.M. -
Publ. Var. Star Sect. RASNZ No. 3, 1
- Bateson (1978).....Bateson,P.M. -
Publ. Var. Star Sect. RASNZ No. 6, 39
- Berman (1935).....Berman,L. - Ap. J. 81, 369
- Bidelman (1948).....Bidelman,W.P. - Ap. J. 107, 413
- Bidelman (1951).....Bidelman,W.P. - Ap. J. 113, 304
- Bidelman (1953).....Bidelman,W.P. - Ap. J. 117, 25
- Bond et al (1979).....Bond,H.E., Luck,R.E. and Newman,M.J. -
Ap. J. 233, 205

REFERENCES

- Borghesi et al (1985).....Borghesi,A., Bussoletti,E. and
Colangeli,L. - Astr. Astrophys. 142, 225
- Bridger (1983).....Bridger,A. - Ph. D Thesis
(St. Andrews, U.K.)
- Campbell & Jacchia (1946)...Campbell,L. and Jacchia,L. - "The Story
of Variable Stars", Harv. Mono.
Blackiston, Mass.
- Carson et al (1967).....Carson,T.R.,Mayers,D.F. and Stibbs, D.W.N.
MNRAS 140, 483
- Carson &Carson,T.R. and Hollingworth,H.M. -
Hollingworth (1968) MNRAS 141, 77
- Carson (1976).....Carson,T.R. -
Ann. Rev. Astr. Astrophys. 14,95
- Carson & Stothers (1976)....Carson,T.R. and Stothers,R. -
Ap. J. 204, 461
- Carson et al (1981).....Carson,T.R., Stothers,R. and vemury,S.K. -
Ap. J. 244, 230
- Carson & Stothers (1982)....Carson,T.R. and Stothers,R.- Ap. J 259, 40
- Carson et al (1984).....Carson,T.R., Huebner,W.F., Magee,N.H. and
Merts,A.L. - Ap. J. 283,468
- Carter et al (1979).....Carter,B.S., Roberts,G. and Feast,M.W. -
IAU Inf. Bull. Var. Stars 1640
- Castor (1971).....Castor,J.I. - Ap. J. 166, 109
- Chandrasekhar (1968).....Chandrasekhar,S. - "Radiative Transfer",
Dover publications, inc., New York.
- Christy (1962).....Christy,R.F. - Ap. J. 136, 887
- Christy (1966a).....Christy,R.F. - Ap. J. 144, 108
- Christy (1966b).....Christy,R.F. - Ap. J. 145, 337
- Christy (1967).....Christy,R.F. - Methods in Computational
Science 7, 191
- Cottrell & Lambert (1982)...Cottrell,P.L. and Lambert,D.I. -
Ap. J. 261, 595
- Coyne & Shawl (1973).....Coyne,G.V. and Shawl,S.J. -
Ap. J. 186, 961
- Cox & Whitney (1958).....Cox,J.P, and Whitney,C.A. - Ap. J. 127,561
- Cox (1963).....Cox,J.P. - Ap. J. 138, 487
- Cox et al (1965).....Cox,A.N. and Stewart,J.N. and
Eilers,D.D. - Ap. J. suppl. 11, 1

REFERENCES

- Cox et al (1966).....Cox,A.N., Brownlee,R.R. and Eilers,D.D. -
Ap. J. 144, 1024
- Cox & Giuli (1969).....Cox,J.P. and Giuli,R.T. - "Principles of
Stellar Structure", Gordan and Breach,
New York.
- Cox (1974).....Cox,J.P. - Rep. Prog. Phys 37, 563
- Cox & Tabor (1976).....Cox,A.N. and Tabor,J.E. -
Ap. J. Suppl 31, 271
- Cox (1980).....Cox,J.P. - "Theory of Stellar Pulsations",
Princeton University Press, Princeton,N.J.
- Cox & Stellingwerf (1980)...Cox,J.P. and Stellingwerf,R.F. -
PASP 91,319
- Danziger (1965).....Danziger,I.J. - MNRAS 130, 199
- D'Esterre (1913).....D'Esterre,L.R. - A. N. 4697, 301
- Deupree (1975).....Deupree,R.G. - Ap. J. 198, 419
- Deupree (1976).....Deupree,R.G. - Ap. J. 205, 286
- Deupree (1977).....Deupree,R.G. - Ap. J. 211, 509
- Drilling & Hill (1986).....Hill,P.W. and Drilling,J.S. -
IAU Coll. 87, "Hydrogen Deficient Stars
and Related Objects",499
- Drilling et al (1984a).....Drilling,J.S., Schonberner,D., Heber,U.
and Lynas-Gray,A.E. - Ap. J. 278, 224
- Drilling et al (1984b).....Drilling,J.S., Landolt,A.U., and
Schonberner,D. - Ap. J. 279, 748
- Eddington (1918a).....Eddington,A.S. - MNRAS 79, 2
- Eddington (1918B).....Eddington,A.S. - MNRAS 79, 177
- Eddington (1926).....Eddington,A.S.- "The Internal Constitution
of the Stars", Cambridge University Press.
- Eddington (1941).....Eddington,A.S. - MNRAS 101, 182
- Eggen (1965).....Eggen,O.J. - Observatory 85, 191
- Eggen (1969).....Eggen,O.J. - PASP 81, 553
- Epstein (1950).....Epstein,R.E. - Ap. J. 112, 6
- Fadeyev (1986).....Fadeyev,Y.A. - IAU Coll. 87,"Hydrogen
Deficient Stars and Related Objects", 441
- Feast (1956).....Feast,M.W. - MNRAS 116, 583
- Feast (1965).....Feast,M.W. - Inf. Bull. Var. Stars 87

REFERENCES

- Feast (1970).....Feast,M.W. - Ap. J. 162, L11
- Feast (1972).....Feast,M.W. - MNRAS 158, 11p
- Feast & Glass (1973).....Feast,M.W. and Glass,I.S.- MNRAS 161, 293
- Feast (1975).....Feast,M.W. - IAU Symp. 67, "Variable Stars
and Stellar Evolution", 129
- Feast et al (1977).....Feast,M.W., Catchpole,R.M., Lloyd,T.E. ,
Robertson,B.S.C., Dean,J.F. and
Bywater,.R.A. - MNRAS 178, 415
- Feast (1979).....Feast,M.W. - "Changing Trends in Variable
Star research", IAU Coll. 46, 246, eds.
Bateson,F.M. University of Waikato, New
Zealand.
- Feast (1986).....Feast,M.W. - IAU Coll. 87, "Hydrogen
Deficient Stars and Related Objects",186
- Fernie (1971).....Ferne,J.D. - Q. J. RAS 13, 81
- Fernie et al (1972).....Ferne,J.D. ,Sherwood,V. and Dupuy,P.L. -
Ap. J. 172, 383
- Fernie (1982).....Ferne,J.D. - PASP 94, 172
- Forrest et al (1971).....Forrest,W.J., Gillett,F.C. and Stein,W.A.-
Ap. J 170, L29
- Forrest et al (1972).....Forrest,W.J., Gillett,F.C. and Stein,W.A.-
Ap. J (lett.) 178, L129
- Freidjung & Viutti (1976)...Freidjung,M. and Viutti,R. -
Astr. Astrophys. 46, 303
- Geisel (1970).....Geisel,S.L. - Ap. J. 161, L105
- Gillett et al (1970).....Gillett,F.C., Hyland,A.R. and Stein,W.A. -
Ap. J. 162, L21
- Gillett & Stein (1971).....Gillett,F.C. and Stein,W.A. -
Ap. J. 164, 77
- Giridhar & Rao (1986).....Giridhar,S. and Rao,N.K. -
IAU Coll. 87, "Hydrogen Deficient
Stars and Related Objects", 177
- Glasby (1978).....Glasby,J.S. - Variable Stars, p217
Constable London.
- Glass (1972).....Glass,I.S. - MNRAS 168, 249
- Glass (1978).....Glass,I.S. - MNRAS 185, 23
- Habets (1985).....Habets,G.M.H.J., -
Astron. Astrophys. 167, 61

REFERENCES

- Hansen (1978).....Hansen,C.J. -
Ann. Rev. Astr. Astrophys. 16, 15
- Heber & Schonberner (1981)..Heber,U. and Schonberner,D. -
Astr. Astrophys. 102, 73
- Heck et al (1981).....Heck,A., Houziaux,L. and Manfroid,J. -
IAU Inf. Bull. Var. Stars 2184
- Hecht et al (1984).....Hecht,J.H., Holm,A.V., Donn,B. and
Wu Chi-Chao - Ap. J. 280, 228
- Herbig (1949).....Herbig,G.H. - Ap. J. 110, 143
- Herbig (1963).....Herbig,G.H. - Ap. J. 140, 203
- Herbig (1975).....Herbig,G.H. - Ap. J. 199, 702
- Herbig (1967).....Herbig,G.H. - Trans. IAU A13, 530
- Hill et al (1981).....Hill,P.W., Kilkenny,D., Schonberner,D.
and Walker,H.J. - MNRAS 197, 81
- Hoffliet (1958).....Hoffliet,D. - Astr. J. 63, 30
- Houziaux (1968).....Houziaux,L. -
Bull. Astr. Inst. Czech. 19, 265
- Howarth (1976).....Howarth,I.D. -
Publ. Var. Star Sect. RASNZ No. 4, 4
- Howarth (1977).....Howarth,I.D. - Acta astron. 27, 65
- Hubbard & Lampe (1968).....Hubbard,W.B. and Lampe,M. -
Ap. J. suppl. 18, 297
- Humphreys & Ney (1974).....Humphreys,R.M. and Ney,E.P. -
Ap. J. 187, L75
- Hunger (1975).....Hunger,K. - "Problems in Stellar
Atmospheres and Envelopes" (N.Y. Springer
& Verlag 57), Ed. Baschek,B. ,Kegel,W.H.
and Traving,G., 1
- Innes (1903).....Innes,R.T.A. - Ann. Cape Obs. 9, 135B
- Innes (1907).....Innes,R.T.A. - Astron. Nachr. 175, 127
- Jacchia (1933).....Jacchia,L. - P. Oss. Ast. U. Bol. 2, 173
- Joy & Humason (1923).....Joy,A.H. and Humason,M.L. - PASP 35, 325
- Keenan & Greenstein (1963)..Keenan,P.L. and Greenstein,J.L. - Mount
Wilson and Palomar observatory re-print
- Kilkenny (1978).....Kilkenny,D. - MNRAS 182, 629
- Kilkenny (1982).....Kilkenny,D. - MNRAS 200, 1019

REFERENCES

- Kilkenny (1983a).....Kilkenny,D. - MNRAS 203, 19
- Kilkenny (1983b).....Kilkenny,D. - MNRAS 205, 907
- Kilkenny & Whittet (1984)...Kilkenny,D. and Whittet,D.C.B. -
MNRAS 208, 25
- King et al (1980).....King,D.S., Wheeler,J.C., Cox,J.P.,
Cox,A.N. and Hodson,S.W. - "Nonradial
and Nonlinear Stellar Pulsation", p161,
Ed. Springer-Verlag, Berlin-Heidelberg
(New York).
- Kukarkin & Paranago (1963)..Kukarkin,B.V., Paranago,P.P. - In Basic
Astronomical Data, Chap. 18, Ed.
K. Aa Strands, University of Chicargo
Press, Chicargo.
- Kukarkin et al (1969).....Kukarkin,B.V., Kholopov,P.N., Efremov,Y.N.
Kukarkina,N.P., Kurochkin,N.E.,
Medvedeva,G.I., Perova,N.B., Frolov,M.S.,
Fedorovich,V.P. - Gen. Cat. Var. Stars I
- Kukarkin et al (1970).....Kukarkin,B.V., Kholopov,P.N., Efremov,Y.N.
Kukarkina,N.P., Kurochkin,N.E.,
Medvedeva,G.I., Perova,N.B., Frolov,M.S.,
Fedorovich,V.P. - Gen. Cat. Var. Stars II
- Lambert (1986).....Lambert,D.L. - IAU Coll. 87, "Hydrogen
Deficient Stars and Related Objects", 127
- Landolt (1968).....Landolt,A.U. - PASP 80, 318
- Law (1982).....Law,W.Y. - Astron. Astrophys. 108, 118
- Ledoux & Walraven (1958)....Ledoux,P. and Walraven,T. - Handbuch der
Physik 51, 353
- Lee & Feast (1969).....Lee,T.A. and Feast,M.W. - Ap. J. 157, L173
- Loreta & O'Keefe (1939).....Loreta,M. and O'Keefe,J.A - Ap. J. 90, 294
- Low (1970).....Low,F.J. - AFCRL TECH.REP - AFCRL-70-0179
- Ludendorf (1906).....Ludendorf,H. - A. N. 173
- Ludendorf (1919).....Ludendorf,H. - A. N. 5010, 281
- Malaney (1985).....Malaney,R. - Ph. D. Thesis
(St. Andrews, U.K.)
- Mayall (1960).....Mayall,M.W. - J. R. Astr. Soc. Can. 54,193
- Mayall (1972).....Mayall,M.W. - J. R. Astr. Soc. Can. 66,233
- Menzies (1985).....Menzies,J.W., 1985 - Unpublished
- Mihalas (1978).....Mihalas,D. - "Stellar Atmospheres",2 edn.,
W.H. Freeman and Co., San Fransisco.

REFERENCES

- Morraco & Milesi (1982).....Morraco,H.G and Milesi,G.E. -
Astr. J. 87, 1775
- MorrisonMorrison,K. and Willingale,G.P.H. -
& Willingale (1987) MNRAS 228, 819
- Myerscough (1968).....Myerscough,V.P. - Ap. J. 153, 421
- Nandy & Rao (1986).....Nandy,K., Rao,N.K. and Morgan,D.H. -
IAU Coll. 87, "Hydrogen Deficient
Stars and Related Objects", 203
- O'Keefe (1939).....O'Keefe,J.A. - Ap. J. 90,294
- Orlov & Rodriguez (1974)....Orlov,M,Ya. and Rodriguez,M.H. -
Astr. Astrophys. 31, 203
- Paczynski (1971).....Paczynski,B. - Acta Astron. 21, 1
- Parenago (1931).....Parenago,P.P. - Variable Stars 3, 113
- Parsons (1971).....Parsons,S.B. -Bull. Am. Astr. Soc. 3, 402
- Payne-GaposchkinPayne-Gaposchkin,L. and Gaposchkin,M. -
& Gaposchkin (1938) Variable Stars, 1938.
- Payne-Gaposchkin (1963).....Payne-Gaposchkin,L. - Ap. J. 138, 320
- Pickering (1908).....Pickering,E.C. - Harv. Circ. 140
- Pollacco (1987).....Private communication.
- Pollacco (1988).....Private communication.
- Pugach (1977).....Pugach,A.F. - Info. Bull. Var. Stars 1277
- Querci & Querci (1978).....Querci,M. and Querci,F. -
Astr. Astrophys. 70, 145
- Rao et al (1980).....Rao,N.K., Ashok,N.M. and Kulkarni,P.V. -
J. Ap. Astr. 1, 71
- Rao et al (1986).....Rao,N.K., Vasundhara,R. and Ashoka,B.N. -
IAU Coll. 87, "Hydrogen Deficient Stars
and Related Objects", 185
- Roche & Aitken (1984).....Roche,P.F. and Aitken,D.K.- MNRAS 200, 401
- Roser (1975).....Roser,M. - Astr. Astrophys. 45, 335
- Rosseland (1949).....Rosseland,S. - "The Pulsation Theory of
Variable Stars", Dover, New York.
- Saio (1982).....Saio,H. - Ap. J. 256, 717
- Saio & Wheeler (1983).....Saio,H. and Wheeler,J.C. - Ap. J. 272, L25
- Saio et al (1984).....Saio,H., Wheeler,J.C. and Cox,J.P. -
Ap. J 281, 318

REFERENCES

- Saio & Wheeler (1985).....Saio,H. and Wheeler,J.C. - Ap. J. 295, 38
- Schajn (1929).....Schajn,P. - Astron. Nachr. 235, 413
- Schonberner (1975).....Schonberner,D. - Astr. Astrophys. 44, 383
- Schonberner (1977).....Schonberner,D. - Astr. Astrophys. 57, 437
- Schonberner (1979).....Schonberner,D. - Astr. Astrophys. 79, 108
- Searle (1961).....Searle,L. - Ap. J. 133, 531
- Shapley (1914).....Shapley,H. - Ap. J. 40, 448
- Shapley & Swope (1934).....Shapley,H. and Swope,H.H.- Harv. Ann. 90,5
- Shenavrin et al (1979).....Shenavrin,V.I., Taranova,O.G., Moroz,V.I.
and Grigor'ev,A.V. - Sov. Astr. 23, 567
- Spite & Spite (1974).....Spite,F. and Spite,M. -
Astr. Astrophys. 40, 141
- Spite & Spite (1979).....Spite,F. and Spite,M. -
Astr. Astrophys. 80, 61
- Stein et al (1969).....Stein,W.A., Gaustad,J.E. and Gillett,F.C.-
Ap. J (lett.) 155, L3
- Stellingwerf (1975).....Stellingwerf,R.F. - Ap. J. 195, 441
- Stellingwerf (1978).....Stellingwerf,R.F. - Astron. J. 83, 1183
- Stellingwerf (1979).....Stellingwerf,R.F. - Ap. J. 227, 935
- Stephenson (1978).....Stephenson,C.B. -
IAU Inf. Bull. Var. stars No. 1453
- Sterne (1935).....Sterne,T.E. - Harv. Bull. No. 896
- Stobie (1969).....Stobie,R.S - MNRAS 144, 485
- Stothers (1974a).....Stothers,R. - Ap. J. 194, 695
- Stothers (1974b).....Stothers,R. - Ap. J. 194, 651
- Stothers & Vemury (1981)....Stothers,R. and Vemury,S.K. -
Ap. J. 244, 230
- Strecker (1975).....Strecker,D.W. - Astr. J. 80, 451
- Stromgren (1932).....Stromgren,B. - Z. Astrophys. 4 118
- Totochava (1973).....Totochava,A.G. - Astron. Tsirk. No. 791, 7
- Totochava (1975).....Totochava,A.G. - IAU Symp. 67, "Variable
Stars and Stellar Evolution", 161; Ed.
Sherwood and plaut.

REFERENCES

- Trimble & Paczynski (1971)..Trimble,V. and Paczynski,B. -
Bull. Am. Astr. Soc. 3, 402
- Trimble (1972).....Trimble,V. - MNRAS 156, 411
- Unno (1967).....Unno,W. - PASJ 19, 140
- Usher & Whitney (1968).....Usher,P.D. and Whitney,C.A. -
Ap. J. 154, 203
- Vemury & Stothers (1977)....Vemury,S.K. and Stothers,R. -
Ap. J. 214, 809
- Vemury & Stothers (1978)....Vemury,S.K. and Stothers,R. -
Ap. J. 225, 939
- Walker (1985).....Walker,H.J. - Astr. Astrophys. 152, 583
- Wallerstein et al (1984)....Wallerstein,G., Pilachowski,C.A. and
Harris,H.C - PASP 96
- Warner (1967).....Warner,B. - MNRAS 137, 119
- Waters (1966).....Waters,B.H.J. - RASNZ Circ. 119
- Weber (1966).....Weber,R. - Bull. Stat. Astr. Mainterne
- Wheeler (1978).....Wheeler,J.C. - Ap. J. 225, 212
- Webster & Glass (1974).....Webster,L.B. and Glass,I.S.-MNRAS 166, 491
- Weiss (1986).....Weiss,A. - Thesis, Munchen
- Weiss (1987).....Weiss,A. - Astr. _Astrophys. 185, 165
- Whitford (1967).....Whitford,A.E. - Astr. J. 72, 1084
- Wickramasinghe (1973).....Wickramasinghe,N.C. - "Light Scattering
Functions for Small Particles with
Application in Astronomy", Adam Hilger,
London.
- Wisniewski & Johnson (1968).Wisniewski,W.Z. and Johnson,H.L. -
Com. Lunar Planetary obs. 7, 57
- Wood (1976).....Wood,P.R. - MNRAS 174, 531
- Wood (1978).....Wood,P.R. - Ap. J 227, 220
- Woods (1926).....Woods,I.E - Harv. Bull. No. 838
- Worrell (1985).....Worrell,J.K. - Ph.D. Thesis
(St. Andrews, U.K.)
- Yashmita (1974).....Yashmita,Y. - PASJ 26, 159
- Yuin (1948).....Yuin,C. - Ap. J. 107, 413

REFERENCES

- Zavatti & Burchi (1975).....Zavatti,F. and Burchi,R. -
IAU Bull. Var. Stars 1027
- Zhevakin (1963).....Zhevarkin,S.A. - Russian A. J. 30, 161
- Zirin (1982).....Zirin,H. - Ap. J. 260, 655

APPENDICES

APPENDIX A

ABBREVIATIONS USED IN REFERENCES

A. N.	- Annuals of Nature
Acta. Astron.	- Acta Astronomica
Ann. Cape Obs.	- Annual Report of the Cape Observatory
Ann. Rev. Astr. Astrophys.	- Annual Review of Astronomy and Astrophysics
Ap. J.	- The Astrophysical Journal
Ap. J. Suppl.	- The Astrophysical Journal Supplement Series
Astr. J.	- The Astronomical Journal
Astr. & Astrophys.	- Astronomy and Astrophysics
Astron. Nachr.	- Astronomische Nachrichten
Astron. Tsirk.	- Astronomicheskij Tsirkulyar
Bull. Am. Astr. Soc.	- Bulletin of The American Astronomical Society
Bull. Astr. Inst. Czech.	- Bulletin of the Astronomical Institutes of Czechoslovakia
Bull. Stat. Astr.	- Bulletin of States Astronomy
Com. Lunar Planetary Obs.	- Communication of Lunar and Planetary Observations
Gen. Cat. Var. Stars	- General Catalogue of Variable Stars
Harv Bull.	- Harvard Bulletin
Harv. Circ.	- Harvard Circular
IAU Inf. Bull. Var. Stars	- IAU Information Bulletin on Variable Stars
J. Ap. Astr.	- Journal of Astrophysics and Astronomy

ABBREVIATIONS USED IN REFERENCES

J. R. Astr. Soc. Can.	- The Journal of the Royal Astronomical Society of Canada
MNRAS	- Monthly Notices of the Royal Astronomical Society
P. Oss. Ast. U. Bol.	- Pubblicazione Osservazioni e Astrofisico, Universita Bologna
PASJ	- Publications of the Astronomical Society of Japan
PASP	- Publications of the Astronomical Society of the Pacific
Q. J. RAS	- Quarterly Journal of the Royal Astronomical Society
RASNZ	- Publications of the Royal Astronomical Society of New Zealand
Rep. Prog. Phys.	- Reports on Progress in Physics
Russian A. J.	- Russian Astronomical Journal
Sov. Astr.	- Soviet Astronomy
Z. Astrophys.	- Zeitschrift fur Astrophysik

APPENDIX B

OPACITY TABLES

OPACITY TABLES

		log(Opaclty cm^2/gm)							
log(T)	log(D)	I	I+1	I+2	I+3	I+4	I+5	I+6	I+7
3.18	-12	-7.0301	-7.3072	-7.4763	-7.4510	-7.3002	-7.1002	-6.8697	-6.6003
3.40	-12	-5.1029	-5.2581	-5.3645	-5.2865	-4.9281	-4.4168	-3.8962	-3.3862
3.48	-12	-4.2581	-4.5528	-4.8386	-4.9208	-4.5200	-3.7696	-3.0711	-2.4949
3.60	-12	-3.8182	-3.8508	-3.6289	-3.0132	-2.6904	-2.4283	-2.0600	-1.4962
3.70	-12	-3.2441	-3.4034	-3.4921	-2.9586	-1.9914	-1.2168	-0.7167	-0.2933
3.78	-12	-2.8239	-3.0339	-3.0762	-2.7282	-2.0250	-1.1537	-0.1979	0.5694
3.85	-11	-2.6655	-2.7190	-2.4737	-1.7799	-1.0434	-0.2175	0.7853	1.6580
3.90	-11	-2.4868	-2.4711	-2.1580	-1.5702	-0.8477	-0.0804	0.7910	1.8312
3.95	-11	-2.3747	-2.3686	-2.0348	-1.3401	-0.6556	0.0899	0.9571	1.8645
4.00	-10	-2.2255	-2.0101	-1.2588	-0.4401	0.3075	1.1335	1.9350	2.8082
4.08	-10	-1.3799	-1.3716	-1.0232	-0.3179	0.5658	1.4150	2.1335	2.8531
4.18	-10	-0.6635	-0.2581	0.0828	0.4409	0.9713	1.6785	2.4166	3.0414
4.30	-10	-0.8210	-0.2604	0.6365	1.3997	2.0253	2.4928	2.9763	3.4533
4.48	-10	-0.7258	-0.5918	0.0212	0.9590	2.1514	3.0792	3.6911	4.1004
4.70	-9	-0.4001	0.2529	1.2380	2.0086	2.7152	3.6042	4.3522	5.0628
4.85	-9	-0.5784	-0.2000	0.6785	1.7202	2.7945	3.6096	4.2625	4.9191
5.00	-8	-0.4145	0.2068	1.1847	2.3010	3.3997	4.2648	4.5441	4.7388
5.30	-8	-0.6308	-0.3458	0.3692	1.3909	2.5077	3.4955	3.9370	3.8293
5.70	-7	-0.6819	-0.5784	-0.1308	0.7910	1.8998	2.6637	2.9079	3.0719
6.00	-6	-0.6737	-0.5901	-0.2118	0.6693	1.6325	2.3766	2.7118	3.0000
6.30	-5	-0.6778	-0.5670	-0.1605	0.6857	1.6875	2.2967	2.4099	2.5753
6.70	-4	-0.6990	-0.6676	-0.4660	0.1703	0.8639	1.2279	1.4378	1.9258
7.00	-3	-0.7011	-0.6799	-0.5751	-0.2020	0.3139	0.6532	1.0645	1.5999
7.30	-2	-0.7167	-0.6968	-0.5969	-0.2832	0.0755	0.3139	0.7938	1.3820
7.70	-1	-0.7447	-0.7423	-0.7258	-0.6478	-0.4815	-0.1720	0.2695	1.0599
8.00	0	-0.7878	-0.7852	-0.7773	-0.7375	-0.6073	-0.3391	0.0792	1.3962
8.30	1	-0.8601	-0.8601	-0.8539	-0.8210	-0.7144	-0.5287	0.0569	1.8965
8.70	2	-1.0119	-1.0119	-1.0092	-0.9957	-0.9393	-0.8268	-0.1024	2.2148
9.00	3	-1.1752	-1.1752	-1.1739	-1.1681	-1.1543	-1.0747	-0.2518	4.5729

Opacity table DXIX : X = 0.0, Y = 0.90, Z = 0.10

OPACITY TABLES

		log(Opaclty $\text{cm}^2/\text{g.m}$)										
log(T)	log(D)	I	I	I+1	I+2	I+3	I+4	I+5	I+6	I+7	I+8	I+9
3.30	-12	-4.4437	-4.4442	-4.4442	-4.4440	-4.4438	-4.4435	-4.4427	-4.4369	-4.3932	-4.0692	
3.40	-12	-4.4261	-4.4265	-4.4264	-4.4262	-4.4260	-4.4257	-4.4250	-4.4209	-4.3919	-4.1798	
3.50	-12	-4.4188	-4.4184	-4.4181	-4.4179	-4.4176	-4.4173	-4.4167	-4.4139	-4.3936	-4.2358	
3.60	-11	-4.3657	-4.3654	-4.3651	-4.3647	-4.3643	-4.3637	-4.3614	-4.3478	-4.2414	-3.3912	
3.70	-11	-4.3326	-4.3327	-4.3326	-4.3326	-4.3326	-4.3323	-4.3308	-4.3203	-4.2381	-3.5863	
3.80	-11	-4.1836	-4.1884	-4.1894	-4.1887	-4.1859	-4.1784	-4.1587	-3.9828	-3.7686	-3.1037	
3.90	-11	-3.6398	-3.8380	-3.9240	-3.9335	-3.5319	-3.1004	-2.5678	-2.3938	-2.1538	-1.5677	
4.00	-11	-2.2535	-2.6384	-2.7717	-2.5062	-2.0355	-1.4950	-0.9115	-0.7558	-0.5753	-0.2408	
4.10	-10	-1.3046	-1.3164	-1.0518	-0.6351	-0.1213	0.4563	0.5970	0.7308	0.9549	1.5696	
4.20	-10	-0.8398	-0.4326	0.1163	0.5489	1.0309	1.5892	1.7166	1.8192	1.9502	2.2601	
4.30	-10	-0.9252	-0.6268	0.0234	0.6797	1.0830	1.3465	1.6963	2.1468	2.7987	2.8224	
4.40	-10	-0.9363	-0.7782	-0.3182	0.5028	1.4387	2.0070	2.5004	2.9432	3.5398	3.3063	
4.50	-10	-0.6235	-0.5087	-0.2375	0.3168	1.2733	2.1207	2.9576	3.5531	4.1193	3.2798	
4.60	-9	-0.1854	0.3768	0.8330	1.3972	1.9995	3.0599	3.9914	4.6657	4.0790	4.6729	
4.70	-9	-0.4198	0.3262	1.2684	1.9436	2.3738	2.9859	4.1676	5.0086	4.7532	5.2283	
4.80	-9	-0.5928	-0.1804	0.8267	1.9881	2.8627	3.4125	4.2768	5.1172	5.2118	5.4504	
4.90	-9	-0.6216	-0.4131	0.2593	1.3676	2.5786	3.6000	4.4659	5.1103	5.2751	5.3814	
5.00	-9	-0.6255	-0.4771	-0.0004	0.9507	2.1350	3.4088	4.5035	5.0268	5.1713	5.1954	
5.20	-8	-0.5929	-0.2578	0.4751	1.5305	2.7318	3.7974	4.3563	4.6725	4.7020	5.1038	
5.40	-8	-0.6859	-0.5908	-0.2257	0.4991	1.4240	2.8192	3.2505	3.8597	4.0603	4.4696	
5.60	-7	-0.6843	-0.5998	-0.3069	0.3053	2.0685	2.1558	3.0409	3.3310	3.8181	4.5715	
5.80	-7	-0.6972	-0.6825	-0.6080	-0.1366	1.4289	1.1565	2.2803	2.5700	3.1392	3.8543	
6.00	-7	-0.6992	-0.6963	-0.6809	-0.4758	0.8398	0.3351	0.9063	1.7966	2.4412	3.2463	
6.20	-6	-0.6993	-0.6955	-0.6242	0.2890	-0.2243	0.2506	1.0339	1.7324	2.6317	3.0478	
6.40	-6	-0.7002	-0.6981	-0.6771	-0.6695	-0.5527	-0.2652	0.3421	1.0253	1.9716	2.4757	
6.60	-5	-0.7012	-0.6978	-0.6917	-0.6485	-0.5321	-0.1728	0.3749	1.2756	1.9167	1.9340	
6.80	-5	-0.7029	-0.6984	-0.6971	-0.6876	-0.6472	-0.4753	-0.1299	0.6016	1.3352	1.8266	
7.00	-5	-0.7054	-0.7054	-0.7053	-0.7038	-0.6956	-0.6352	-0.4490	0.0337	0.7326	1.2413	
7.20	-4	-0.7094	-0.7094	-0.7092	-0.7091	-0.6905	-0.6150	-0.3588	0.1655	0.7113	-0.4473	
7.40	-4	-0.7156	-0.7156	-0.7156	-0.7154	-0.7117	-0.6876	-0.5776	-0.2698	0.2278	0.5699	
7.60	-3	-0.7250	-0.7250	-0.7252	-0.7249	-0.7187	-0.6805	-0.5366	-0.2000	0.0580	-0.5060	
7.80	-3	-0.7392	-0.7392	-0.7392	-0.7394	-0.7383	-0.7279	-0.6746	-0.4988	-0.2755	-0.8131	
8.00	-3	-0.7601	-0.7601	-0.7601	-0.7603	-0.7602	-0.7580	-0.7428	-0.6724	-0.5382	-0.7332	
8.20	-2	-0.7898	-0.7898	-0.7899	-0.7899	-0.7896	-0.7866	-0.7653	-0.7083	-0.6929	-0.9374	
8.40	-2	-0.8302	-0.8302	-0.8302	-0.8302	-0.8302	-0.8299	-0.8255	-0.8079	-0.8102	-1.0308	
8.60	-1	-0.8822	-0.8822	-0.8822	-0.8822	-0.8823	-0.8820	-0.8788	-0.8920	-1.0548	-1.1051	
8.80	-1	-0.9456	-0.9456	-0.9456	-0.9456	-0.9456	-0.9459	-0.9461	-0.9545	-0.9972	-1.1619	
9.00	-1	-1.0196	-1.0196	-1.0196	-1.0196	-1.0196	-1.0197	-1.0202	-1.0244	-1.0591	-1.1805	

Opacity table R040 : X = 0.0, Y = 1.00, Z = 0.00

OPACITY TABLES

		log(Opaclty cm^2/gm)										
log(T)	log(D)	I	I	I+1	I+2	I+3	I+4	I+5	I+6	I+7	I+8	I+9
3.30	-12	-3.7216	-4.0595	-4.2943	-4.4625	-4.5322	-4.5523	-4.5514	-4.5455	-4.4998	-4.1594	
3.40	-12	-3.3926	-3.4533	-3.4436	-3.6060	-3.9250	-4.2310	-4.4200	-4.5141	-4.4822	-4.2506	
3.50	-12	-3.2763	-3.3467	-3.3136	-3.3357	-3.3825	-3.4895	-3.7400	-4.0519	-4.1473	-4.1175	
3.60	-11	-3.1931	-3.1906	-3.2154	-3.2420	-3.2447	-3.1609	-2.8795	-2.4260	-2.5653	-1.3867	
3.70	-11	-2.6423	-2.8434	-2.9283	-2.8364	-2.5147	-2.0366	-1.4545	-0.7813	-0.8453	-0.0724	
3.80	-11	-1.9470	-2.2051	-2.2722	-1.9547	-1.4374	-0.8838	-0.2867	0.3947	0.2060	0.9275	
3.90	-11	-1.8867	-1.8757	-1.6424	-1.1739	-0.5089	0.1312	0.7384	1.4215	1.2348	1.9290	
4.00	-11	-1.7863	-1.7490	-1.4894	-0.7162	0.1704	0.9053	1.5327	2.2963	2.1916	2.5113	
4.10	-10	-1.2702	-1.2126	-0.5870	0.2654	1.3214	2.1513	3.0073	2.9476	3.0130	4.0388	
4.20	-10	-0.8837	-0.5100	0.0695	0.6470	1.5098	2.4478	3.4561	3.3875	3.4436	3.9655	
4.30	-10	-0.9137	-0.6538	-0.0365	0.6499	1.2125	1.6677	2.4781	3.2886	4.0761	3.9811	
4.40	-10	-0.7310	-0.1739	0.5936	1.3986	2.2005	2.8539	3.5628	3.5628	4.2783	3.9422	
4.50	-10	0.3201	-0.4271	0.2311	0.7272	1.5774	2.1590	3.2387	3.9455	4.6114	3.8905	
4.60	-9	0.4925	1.1843	1.2504	1.8132	2.5990	3.2918	4.2474	4.9234	4.3768	6.3836	
4.70	-9	0.4014	0.9651	1.3079	2.2861	2.6648	3.3418	4.3600	5.1223	4.8067	5.9701	
4.80	-9	0.1747	0.8805	1.1248	2.6175	3.1891	3.7123	4.4192	5.1353	5.1419	5.6730	
4.90	-9	-0.6649	-0.1816	0.7958	2.4639	3.1566	3.8775	4.5209	5.0782	5.2071	5.4785	
5.00	-9	-0.6669	-0.5354	-0.1134	1.4056	2.4743	3.6868	4.5063	4.9679	5.0859	5.2082	
5.20	-8	-0.6339	-0.3366	0.3345	1.3841	2.6080	3.6823	4.2954	4.5983	4.6708	5.1964	
5.40	-8	-0.6970	-0.6195	-0.2994	0.3893	1.3014	2.6501	3.2462	3.9029	4.1279	4.4949	
5.60	-7	2.2035	2.1365	-0.0982	0.4176	1.2165	2.2429	3.2291	3.6708	3.8327	4.6785	
5.80	-7	1.2818	1.3402	1.4578	1.6266	1.8136	1.7843	2.6423	3.3079	3.3858	4.0240	
6.00	-7	0.2868	0.3391	0.4224	0.5984	1.1554	1.1748	2.5734	3.1369	3.1277	3.5088	
6.20	-6	-0.2904	-0.2641	-0.1934	0.3418	0.1995	1.4125	2.4280	2.7421	2.9639	3.4058	
6.40	-6	-0.5868	-0.5754	-0.5516	-0.4982	-0.3602	0.1359	1.4211	2.0227	2.3548	2.8760	
6.60	-5	-0.6736	-0.6681	-0.6611	-0.5865	-0.4159	0.4487	1.1615	1.6931	2.3320	2.2175	
6.80	-5	-0.6980	-0.6971	-0.6992	-0.6744	-0.5983	-0.1743	0.3647	1.0055	1.7316	2.0867	
7.00	-5	-0.7048	-0.7047	-0.7042	-0.7009	-0.6870	-0.5238	-0.2068	0.3524	1.0802	1.5325	
7.20	-4	-0.7094	-0.7094	-0.7088	-0.7059	-0.6719	-0.5202	-0.1641	0.4345	0.9940	-0.3293	
7.40	-4	-0.7156	-0.7156	-0.7156	-0.7145	-0.7087	-0.6570	-0.4853	-0.0958	0.4683	0.8166	
7.60	-3	-0.7250	-0.7250	-0.7250	-0.7245	-0.7106	-0.6458	-0.4450	-0.0216	0.2946	-0.2189	
7.80	-3	-0.7392	-0.7392	-0.7393	-0.7394	-0.7364	-0.7171	-0.6346	-0.3901	-0.0846	-0.6823	
8.00	-3	-0.7601	-0.7601	-0.7602	-0.7602	-0.7602	-0.7599	-0.7552	-0.7284	-0.6187	-0.4108	-0.5586
8.20	-2	-0.7893	-0.7898	-0.7899	-0.7899	-0.7899	-0.7890	-0.7823	-0.7440	-0.6395	-0.5705	-0.5581
8.40	-2	-0.8303	-0.8303	-0.8303	-0.8303	-0.8302	-0.8290	-0.8187	-0.7777	-0.7347	-0.8670	
8.60	-1	-0.8822	-0.8822	-0.8823	-0.8823	-0.8821	-0.8802	-0.8680	-0.8550	-0.9845	-0.4011	
8.80	-1	-0.9456	-0.9456	-0.9456	-0.9456	-0.9456	-0.9454	-0.9429	-0.9397	-0.9470	-0.8540	
9.00	-1	-1.0196	-1.0196	-1.0196	-1.0196	-1.0196	-1.0196	-1.0195	-1.0198	-1.0393	-1.0520	

Opacity table R631 : X = 0.0, Y = 0.75, Z = 0.25

OPACITY TABLES

log(τ) log(D)	log(Opaclty cm^2/gm)										
	I	I	I+1	I+2	I+3	I+4	I+5	I+6	I+7	I+8	I+9
3.30	-12	-3.5437	-3.9748	-4.2805	-4.5372	-4.6640	-4.7046	-4.7037	-4.6975	-4.6495	-4.2843
3.40	-12	-3.0943	-3.1831	-3.1933	-3.4209	-3.8085	-4.2222	-4.4760	-4.6494	-4.6149	-4.3565
3.50	-12	-2.9714	-3.0663	-3.0307	-3.0513	-3.1085	-3.2623	-3.5880	-3.9880	-4.1747	-4.2019
3.60	-11	-2.9197	-2.9088	-2.9316	-2.9658	-2.9903	-2.9489	-2.8115	-2.4743	-2.6417	-1.5482
3.70	-11	-2.4219	-2.6111	-2.6980	-2.6640	-2.4079	-1.9729	-1.4091	-0.7538	-0.8497	-0.2084
3.80	-11	-1.6478	-2.0015	-2.1732	-1.9507	-1.4609	-0.9103	-0.3204	0.3511	0.1532	0.8443
3.90	-11	-1.5894	-1.5891	-1.4224	-1.1149	-0.5138	0.1359	0.7317	1.3898	1.2814	2.0703
4.00	-11	-1.5201	-1.4690	-1.2817	-0.4958	0.1600	1.0073	1.5566	2.3137	2.3470	2.6895
4.10	-10	-1.2408	-1.1332	-0.4462	0.4279	1.5454	2.2254	3.0541	3.1619	3.1892	4.1834
4.20	-10	-0.9441	-0.6321	-0.0232	0.6896	1.6725	2.6153	3.5038	3.6113	4.0966	4.3224
4.30	-10	-0.9302	-0.7163	-0.1554	0.5415	1.2246	1.8698	2.8938	3.6505	4.3531	4.2732
4.40	-10	-0.6452	-0.6376	-0.1501	0.5462	1.2557	2.2185	3.0183	3.9506	4.5997	4.1659
4.50	-10	0.4370	0.1104	0.4022	0.8503	1.6246	2.0416	3.2993	4.1440	4.8702	4.1258
4.60	-9	0.6562	1.3765	0.8175	1.9224	2.7289	3.2999	4.3596	5.0533	4.4708	6.2164
4.70	-9	0.6263	1.0925	1.2122	2.4278	2.7345	3.4230	4.4199	5.1396	4.7790	6.1338
4.80	-9	0.3543	1.1263	1.1385	2.7659	3.3083	3.8353	4.4626	5.0985	5.0537	5.6884
4.90	-9	-0.7132	-0.2543	0.8496	2.6692	3.2566	3.9783	4.5236	5.0068	5.0957	5.3773
5.00	-9	-0.7099	-0.5997	-0.2561	1.4975	2.4953	3.7397	4.4611	4.8806	4.9679	5.1202
5.20	-3	-0.6786	-0.4255	0.1722	1.2093	2.4072	3.5245	4.2291	4.5125	4.6585	5.1473
5.40	-8	-0.7094	-0.6515	-0.3828	0.2401	1.1289	2.4344	3.2462	3.8575	4.0765	4.4805
5.60	-7	2.4742	2.4576	0.0146	0.4276	1.1256	2.1179	3.1465	3.7695	3.8345	4.7467
5.80	-7	1.5703	1.6328	1.7520	1.9232	1.9165	1.8084	2.7099	3.4315	3.4635	4.1331
6.00	-7	0.5152	0.5756	0.6679	0.8637	1.3107	1.4099	2.7920	3.3792	3.2909	3.6595
6.20	-6	-0.1655	-0.1225	-0.0379	0.4001	0.3250	1.6182	2.7058	2.9952	3.1456	3.6023
6.40	-6	-0.5355	-0.5204	-0.4874	-0.4088	-0.1123	0.2657	1.6956	2.2865	2.5522	3.0814
6.60	-5	-0.6579	-0.6499	-0.6362	-0.5377	-0.3710	0.6749	1.4191	1.8990	2.5417	2.3986
6.80	-5	-0.6946	-0.6932	-0.6967	-0.6585	-0.5566	-0.0121	0.5779	1.2081	1.9360	2.2476
7.00	-5	-0.7044	-0.7042	-0.7033	-0.6986	-0.6832	-0.4583	-0.0725	0.5275	1.2710	1.7075
7.20	-4	-0.7094	-0.7094	-0.7082	-0.7032	-0.6575	-0.4565	-0.0433	0.5975	1.1654	-0.2826
7.40	-4	-0.7156	-0.7156	-0.7156	-0.7136	-0.7068	-0.6334	-0.4207	0.0207	0.6206	0.9702
7.60	-3	-0.7251	-0.7251	-0.7249	-0.7242	-0.7042	-0.6188	-0.3777	0.0979	0.4452	-0.2190
7.80	-3	-0.7393	-0.7393	-0.7393	-0.7393	-0.7348	-0.7080	-0.6030	-0.3124	0.0430	-0.6822
8.00	-3	-0.7601	-0.7602	-0.7602	-0.7602	-0.7596	-0.7527	-0.7162	-0.5774	-0.3202	-0.4639
8.20	-2	-0.7899	-0.7899	-0.7899	-0.7898	-0.7885	-0.7784	-0.7265	-0.5874	-0.4865	-0.5582
8.40	-2	-0.8303	-0.8303	-0.8303	-0.8304	-0.8302	-0.8280	-0.8127	-0.7533	-0.6789	-0.8671
8.60	-1	-0.8823	-0.8823	-0.8823	-0.8823	-0.8819	-0.8785	-0.8587	-0.8260	-0.9830	-0.4012
8.80	-1	-0.9456	-0.9456	-0.9457	-0.9457	-0.9456	-0.9451	-0.9400	-0.9275	-0.9210	-0.8540
9.00	-1	-1.0196	-1.0196	-1.0196	-1.0196	-1.0196	-1.0196	-1.0189	-1.0158	-1.0292	-1.0520

Opacity table R622 : X = 0.0, Y = 0.50, Z = 0.50

OPACITY TABLES

		log(Opaclty cm^2/gcm)										
log(T)	log(D)	I	I	I+1	I+2	I+3	I+4	I+5	I+6	I+7	I+8	I+9
3.30	-12	-3.4306	-3.9275	-4.2877	-4.6432	-4.8699	-4.9582	-4.9573	-4.9505	-4.8977	-4.4827	
3.40	-12	-2.9029	-3.0202	-3.0506	-3.3144	-3.7377	-4.2128	-4.5588	-4.8775	-4.8380	-4.5294	
3.50	-12	-2.7781	-2.8976	-2.8621	-2.8793	-2.9442	-3.1324	-3.4997	-3.9554	-4.2451	-4.3663	
3.60	-11	-2.7559	-2.7401	-2.7595	-2.7972	-2.8357	-2.8367	-2.8202	-2.6401	-2.8364	-1.8457	
3.70	-11	-2.2957	-2.4699	-2.5592	-2.5419	-2.3815	-1.9967	-1.4522	-0.8358	-0.9223	-0.4943	
3.80	-11	-1.4723	-1.8950	-2.1642	-2.0982	-1.6623	-1.1216	-0.5380	0.1222	-0.0807	0.6019	
3.90	-11	-1.4136	-1.4258	-1.3442	-1.2489	-0.7023	-0.0318	0.5564	1.2022	1.1983	2.1156	
4.00	-11	-1.3495	-1.3012	-0.8898	-0.4799	0.0092	0.8907	1.4155	2.2261	2.4100	3.3051	
4.10	-10	-1.2084	-0.9248	-0.4575	0.3822	1.5717	2.1950	3.0177	3.2489	3.7966	4.2067	
4.20	-10	-1.0153	-0.7048	-0.1813	0.5495	1.6665	2.5863	3.4956	3.6604	4.2447	4.4297	
4.30	-10	-0.9507	-0.7942	-0.3430	0.3503	1.1986	1.9666	3.0286	3.8627	4.5297	4.4031	
4.40	-10	-0.5836	-0.6189	-0.1765	0.4519	1.2668	2.1997	3.1650	4.1604	4.7926	4.3602	
4.50	-10	0.4592	0.1804	0.3971	0.9008	1.6541	1.7865	3.3182	4.3178	4.9405	4.3525	
4.60	-9	0.3915	1.5385	0.7280	1.9832	2.8041	3.1927	4.4155	5.1207	4.5991	6.3701	
4.70	-9	0.8769	1.1643	1.0499	2.5254	2.7755	3.4135	4.4326	5.0908	4.8179	5.8816	
4.80	-9	0.4479	1.2628	1.4279	2.8501	3.3661	3.8560	4.4605	4.9867	4.9466	5.3006	
4.90	-9	-0.7672	-0.4788	0.8453	2.7350	2.8558	4.0000	4.4846	4.8820	4.8931	5.2199	
5.00	-9	-0.7587	-0.6773	-0.4120	1.5016	2.4537	3.7466	4.3785	4.7563	4.7922	5.1298	
5.20	-8	-0.7284	-0.5443	-0.0577	0.9279	2.0503	3.4386	4.1269	4.3866	4.5115	5.0806	
5.40	-8	-0.7226	-0.6805	-0.4948	0.0381	0.8939	2.0985	3.1670	3.7863	4.2340	4.4598	
5.60	-7	2.6327	2.6377	0.0919	0.4253	1.5495	1.9358	3.0421	3.8268	3.8456	4.7971	
5.80	-7	1.7415	1.7928	1.9251	2.0993	1.9862	1.8531	2.7343	3.5760	3.5375	4.2129	
6.00	-7	0.6594	0.7232	0.8210	1.0263	1.4142	1.3017	2.9241	3.5187	3.4056	3.7517	
6.20	-6	-0.0749	-0.0265	0.0676	0.4517	0.4237	1.7248	2.8681	3.1499	3.2713	3.7453	
6.40	-6	-0.4977	-0.4800	-0.4403	-0.3432	0.0157	0.2486	1.8576	2.4480	2.3918	3.2258	
6.60	-5	-0.6454	-0.6354	-0.6157	-0.4976	-0.2585	0.8245	1.5755	2.0361	2.6859	2.5424	
6.80	-5	-0.6918	-0.6900	-0.6948	-0.6450	-0.5200	0.0452	0.7165	1.3441	2.0762	2.3654	
7.00	-5	-0.7040	-0.7036	-0.7025	-0.6963	-0.6760	-0.4326	0.0234	0.6495	1.4040	1.8340	
7.20	-4	-0.7094	-0.7093	-0.7074	-0.7007	-0.6469	-0.4068	0.0461	0.7156	1.2892	-0.2373	
7.40	-4	-0.7157	-0.7157	-0.7157	-0.7128	-0.7049	-0.6137	-0.3699	0.1097	0.7329	1.0852	
7.60	-3	-0.7251	-0.7251	-0.7248	-0.7239	-0.6983	-0.5962	-0.3235	0.1890	0.5574	-0.2192	
7.80	-3	-0.7393	-0.7393	-0.7393	-0.7393	-0.7332	-0.6999	-0.5762	-0.2507	0.1402	-0.6822	
8.00	-3	-0.7602	-0.7602	-0.7602	-0.7601	-0.7593	-0.7505	-0.7054	-0.5433	-0.2486	-0.3842	
8.20	-2	-0.7900	-0.7900	-0.7900	-0.7899	-0.7881	-0.7750	-0.7113	-0.5444	-0.4183	-0.5583	
8.40	-2	-0.8303	-0.8304	-0.8304	-0.8304	-0.8301	-0.8270	-0.8073	-0.7322	-0.6320	-0.8671	
8.60	-1	-0.8823	-0.8823	-0.8823	-0.8823	-0.8817	-0.8769	-0.8504	-0.8007	-0.9815	-0.4013	
8.80	-1	-0.9457	-0.9457	-0.9457	-0.9457	-0.9456	-0.9447	-0.9373	-0.9163	-0.8978	-0.8541	
9.00	-1	-1.0196	-1.0196	-1.0196	-1.0196	-1.0196	-1.0195	-1.0183	-1.0120	-1.0197	-1.0521	

Opacity table R613 : X = 0.0, Y = 0.25, Z = 0.75

OPACITY TABLES

log(T)		log(Opaicity cm^2/gm)									
log(D)	I	I	I+1	I+2	I+3	I+4	I+5	I+6	I+7	I+8	I+9
3.30	-12	-4.0896	-4.2543	-4.3679	-4.4447	-4.4740	-4.4818	-4.4809	-4.4751	-4.4307	-4.1011
3.40	-12	-3.9245	-3.9529	-3.9454	-4.0219	-4.1795	-4.3255	-4.4157	-4.4531	-4.4229	-4.2039
3.50	-12	-3.8613	-3.8948	-3.8777	-3.8893	-3.9122	-3.9621	-4.0831	-4.2333	-4.2622	-4.1642
3.60	-11	-3.7888	-3.7883	-3.8013	-3.8140	-3.8126	-3.7637	-3.5990	-3.3427	-3.3607	-2.3295
3.70	-11	-3.4801	-3.5861	-3.6300	-3.5753	-3.4001	-3.1462	-2.8406	-2.4833	-2.4733	-1.7428
3.80	-11	-3.0565	-3.1815	-3.2043	-3.0275	-2.7539	-2.4620	-2.1412	-1.7013	-1.6955	-0.9975
3.90	-11	-2.7639	-2.8520	-2.7640	-2.5056	-1.9594	-1.4205	-0.8478	-0.4060	-0.3973	0.2336
4.00	-11	-2.0425	-2.2095	-2.1298	-1.6018	-0.8872	-0.2591	0.3566	0.8292	0.8448	1.1689
4.10	-10	-1.2902	-1.2720	-0.8270	-0.1863	0.6020	1.3208	1.8447	1.8578	2.0040	2.8362
4.20	-10	-0.8554	-0.4582	0.1031	0.5948	1.2604	2.0156	2.6154	2.6079	2.6404	3.1079
4.30	-10	-0.9172	-0.6333	0.0065	0.6772	1.1489	1.4893	2.0530	2.6971	3.4297	3.3899
4.40	-10	-0.8398	-0.7617	-0.2460	0.5557	1.4350	2.1055	2.6645	3.2189	3.8853	3.6101
4.50	-10	-0.1469	-0.5308	-0.0144	0.5154	1.4258	2.1547	3.0965	3.7333	4.3441	3.5691
4.60	-9	0.1475	0.7736	1.1020	1.6004	2.2957	3.1795	4.1111	4.7841	4.2226	5.5825
4.70	-9	-0.0198	0.6431	1.3004	2.1047	2.5168	3.1612	4.2605	5.0656	4.7043	5.5944
4.80	-9	-0.2153	0.3418	0.9801	2.2976	3.0181	3.5536	4.3456	5.1310	5.1860	5.5643
4.90	-9	-0.6383	-0.2840	0.5318	1.9130	2.8672	3.7322	4.4942	5.1022	5.2531	5.4440
5.00	-9	-0.6419	-0.4997	-0.0420	1.1762	2.3089	3.5470	4.5104	5.0066	5.1411	5.2126
5.20	-8	-0.6089	-0.2881	0.4215	1.4753	2.6915	3.7565	4.3326	4.6442	4.6873	5.1578
5.40	-8	-0.6902	-0.6019	-0.2540	0.4599	1.3809	2.7572	3.2483	3.8876	4.1014	4.4845
5.60	-7	0.7849	0.7845	-0.2119	0.3625	1.6364	2.2161	3.1487	3.4959	3.8255	4.6190
5.80	-7	0.2973	0.3342	0.4309	0.7447	1.6166	1.4801	2.4604	2.9329	3.2581	3.9295
6.00	-7	-0.2139	-0.1863	-0.1366	0.0509	0.9853	0.7435	1.7854	2.4654	2.7786	3.3647
6.20	-6	-0.5068	-0.4882	-0.4188	0.3095	-0.0190	0.8301	1.7255	2.2270	2.7826	3.2104
6.40	-6	-0.6474	-0.6409	-0.6195	-0.5912	-0.4823	-0.0722	0.8702	1.5121	2.1472	2.6592
6.60	-5	-0.6887	-0.6845	-0.6788	-0.6221	-0.4771	0.1232	0.7530	1.4680	2.1075	2.0597
6.80	-5	-0.7008	-0.6982	-0.6985	-0.6826	-0.6268	-0.3382	0.1017	0.7873	1.5168	1.9425
7.00	-5	-0.7051	-0.7051	-0.7048	-0.7026	-0.6916	-0.5851	-0.3392	0.1784	0.8905	1.3717
7.20	-4	-0.7094	-0.7094	-0.7091	-0.7078	-0.6826	-0.5733	-0.2721	0.2858	0.8377	-0.3915
7.40	-4	-0.7156	-0.7156	-0.7156	-0.7150	-0.7104	-0.6745	-0.5374	-0.1933	0.3346	0.6798
7.60	-3	-0.7250	-0.7250	-0.7251	-0.7247	-0.7153	-0.6657	-0.4970	-0.1216	0.1630	-0.3567
7.80	-3	-0.7392	-0.7392	-0.7393	-0.7394	-0.7375	-0.7234	-0.6576	-0.4516	-0.1915	-0.7451
8.00	-3	-0.7601	-0.7601	-0.7602	-0.7602	-0.7601	-0.7568	-0.7368	-0.6494	-0.4828	-0.6538
8.20	-2	-0.7898	-0.7898	-0.7899	-0.7899	-0.7893	-0.7848	-0.7563	-0.6788	-0.6393	-0.7402
8.40	-2	-0.8303	-0.8303	-0.8303	-0.8302	-0.8302	-0.8296	-0.8227	-0.7951	-0.7776	-0.9456
8.60	-1	-0.8822	-0.8822	-0.8823	-0.8823	-0.8822	-0.8813	-0.8743	-0.8762	-1.0184	-0.7390
8.80	-1	-0.9456	-0.9456	-0.9456	-0.9456	-0.9456	-0.9457	-0.9448	-0.9483	-0.9742	-1.0018
9.00	-1	-1.0196	-1.0196	-1.0196	-1.0196	-1.0196	-1.0196	-1.0199	-1.0225	-1.0500	-1.1137

Opacity table K610 : X = 0.0, Y = 0.90, Z = 0.10

OPACITY TABLES

		log(Opaclty $\text{cm}^2/\text{g}\tau$)										
log(T)	log(D)	I	I	I+1	I+2	I+3	I+4	I+5	I+6	I+7	I+8	I+9
3.30	-12	-4.2363	-4.2559	-4.2737	-4.2835	-4.1987	-3.8559	-3.3490	-2.8297	-2.2538	-1.3420	
3.40	-12	-4.1620	-4.1937	-4.1807	-4.1684	-3.9666	-3.5620	-1.2901	-2.5146	-1.9385	-1.0361	
3.50	-12	-4.0575	-4.0900	-4.0677	-4.0371	-3.7807	-3.3483	-1.4816	-2.3284	-1.7995	-1.0220	
3.60	-11	-3.9683	-3.9396	-3.8390	-3.4866	-3.0385	-2.5600	-2.0712	-1.5833	-0.9792	-0.1225	
3.70	-11	-3.7438	-3.7921	-3.7053	-3.3342	-2.8167	-2.3211	-1.7806	-1.3413	-0.9133	-0.2547	
3.80	-11	-3.4078	-3.4792	-3.3963	-3.0748	-2.6038	-2.0787	-1.4983	-1.0644	-0.6840	-0.0657	
3.90	-11	-3.0124	-3.0549	-3.0114	-2.6735	-2.0393	-1.3905	-0.7053	-0.3277	0.0209	0.5625	
4.00	-11	-2.1531	-2.3701	-2.2740	-1.5887	-1.0417	-0.1273	0.4637	1.2184	0.9876	1.5901	
4.10	-10	-1.2868	-1.2860	-0.8778	-0.3463	0.4790	1.1164	1.7321	1.5987	1.9092	2.7132	
4.20	-10	-0.8370	-0.4383	0.1093	0.5797	1.1683	1.7916	2.2394	2.2602	2.4646	3.0054	
4.30	-10	-0.9149	-0.6172	0.0439	0.7010	1.1362	1.4520	2.0252	2.4318	3.1436	3.2913	
4.40	-10	-0.9106	-0.7512	-0.2679	0.5689	1.4731	2.0842	2.6313	3.0778	3.6883	3.5337	
4.50	-10	-0.5175	-0.4825	-0.1396	0.4436	1.3791	2.2008	3.0469	3.6362	4.2071	3.5013	
4.60	-9	-0.1379	0.4835	0.9112	1.5001	2.1828	3.1617	4.1101	4.4081	3.9763	2.6496	
4.70	-9	-0.1650	0.4853	1.2984	1.9965	2.6299	3.2515	4.2286	4.6967	4.8027	2.9796	
4.80	-9	-0.3773	0.2404	0.9268	2.0939	2.9447	3.5074	4.3061	4.9278	5.1814	3.3262	
4.90	-9	-0.4580	-0.1266	0.5487	1.6342	2.6768	3.6450	4.4899	4.9805	5.2223	3.7799	
5.00	-9	-0.3758	-0.4005	0.2939	1.2246	2.2583	3.4326	4.4989	4.9484	3.5843	4.2503	
5.20	-8	-0.2775	-0.1763	0.5663	1.7209	2.8409	3.8099	4.3507	4.3066	4.2647	1.9506	
5.40	-8	-0.6291	-0.2910	-0.1417	0.6640	1.8219	2.8790	3.3346	3.8559	3.9069	2.5890	
5.60	-7	-0.5610	-0.2249	-0.0906	0.6406	2.1246	2.3906	3.1244	3.2684	3.3610	0.8097	
5.80	-7	-0.4878	-0.4449	-0.2276	0.1026	1.2349	1.5687	2.3683	2.7539	2.8932	1.4170	
6.00	-7	-0.5573	-0.5478	-0.4754	-0.0857	0.6049	0.8593	1.6011	2.2386	2.5893	2.2991	
6.20	-6	-0.6165	-0.6093	-0.5032	0.1785	0.2572	0.9726	1.7052	2.0871	2.4663	0.2239	
6.40	-6	-0.6578	-0.6580	-0.6409	-0.5497	-0.1764	0.3158	1.1082	1.5596	2.0860	0.8681	
6.60	-5	-0.6759	-0.6787	-0.6657	-0.5467	-0.1819	0.4479	1.0406	1.5040	1.5856	-0.9519	
6.80	-5	-0.6866	-0.6855	-0.6893	-0.6705	-0.5470	-0.1297	0.4485	0.7433	1.2746	-0.3558	
7.00	-5	-0.6964	-0.6973	-0.6955	-0.6988	-0.6773	-0.5243	-0.1653	0.1965	0.7419	0.5508	
7.20	-4	-0.7082	-0.7077	-0.7063	-0.7021	-0.6537	-0.4555	-0.1235	0.3034	0.6084	-1.5894	
7.40	-4	-0.7154	-0.7154	-0.7153	-0.7145	-0.7051	-0.6327	-0.4119	-0.1246	0.2849	-0.9146	
7.60	-3	-0.7249	-0.7249	-0.7251	-0.7240	-0.7113	-0.6348	-0.4249	-0.1310	-0.2441	-2.7522	
7.80	-3	-0.7392	-0.7392	-0.7392	-0.7393	-0.7374	-0.7184	-0.6400	-0.4580	-0.3321	-2.1498	
8.00	-3	-0.7601	-0.7601	-0.7601	-0.7603	-0.7600	-0.7550	-0.7339	-0.6567	-0.5287	-1.2141	
8.20	-2	-0.7898	-0.7898	-0.7899	-0.7899	-0.7894	-0.7831	-0.7580	-0.7172	-1.0062	-3.3483	
8.40	-2	-0.8302	-0.8302	-0.8302	-0.8302	-0.8302	-0.8268	-0.8232	-0.8112	-0.9566	-2.6608	
8.60	-1	-0.8822	-0.8822	-0.8822	-0.8822	-0.8822	-0.8810	-0.8816	-0.9555	-1.8108	-4.5435	
8.80	-1	-0.9456	-0.9456	-0.9456	-0.9456	-0.9457	-0.9451	-0.9481	-1.0309	-1.6096	-3.8884	
9.00	-1	-1.0196	-1.0196	-1.0196	-1.0196	-1.0196	-1.0198	-1.0212	-1.0592	-1.4442	-2.7621	

Opacity table BD9C : X = 0.0, Y = 0.90, Z = 0.10

APPENDIX C

EQUILIBRIUM MODEL

APPENDIX C

INITIAL STATIC EQUILIBRIUM MODEL

C.1 CALCULATING THE EQUILIBRIUM MODEL

This Appendix gives a brief description of how the initial static equilibrium model required for the solution of the hydrodynamic and thermal equations can be calculated. The four basic equations needed for the static model are (3.9), (3.20), (3.36), and (3.39) with the time derivative in (3.20) equal to zero. Thus we have:

$$\frac{dm_r}{dr} = 4\pi r^2 \rho, \quad (\text{C.1})$$

$$\frac{dP}{dr} = -\frac{G\rho m_r}{r^2}, \quad (\text{C.2})$$

$$\frac{dT}{dr} = -\frac{3\kappa\rho L_r}{4ac(4\pi r^2)T^3}, \quad (\text{C.3})$$

$$\frac{dL_r}{dm_r} = \epsilon. \quad (\text{C.4})$$

To increase accuracy and keep the gradients to manageable sizes, it is usually better to use logarithmic gradients (as Schwarzschild did), rather than those given in (C.1) - (C.4) above. Now, r and m_r are

INITIAL STATIC EQUILIBRIUM MODEL

slow moving variables in the stellar atmosphere, and T is virtually constant. This leaves P as the only choice for the independent variable ($\ln(P)$ being roughly linear with depth and fast moving in comparison to r and m_r). Thus we can now write the logarithmic forms of gradients (C.1)-(C.4) w.r.t. $\ln(P)$ as:

$$\frac{d \ln(m_r)}{d \ln(P)} = -\frac{4\pi r^4 P}{G m_r^2}, \quad (\text{C.5})$$

$$\frac{d \ln(r)}{d \ln(P)} = -\frac{r P}{G \rho m_r}, \quad (\text{C.6})$$

$$\frac{d \ln(T)}{d \ln(P)} = \frac{\eta \cdot L_r \cdot P}{16\pi \rho G m_r T^4}, \quad (\text{C.7})$$

$$\frac{d \ln(L)}{d \ln(P)} = -\frac{4\pi \epsilon_r \cdot r^4 \cdot P}{G m_r}, \quad (\text{C.8})$$

In this study, the stellar envelope being modelled is assumed to be non-rotating, non-magnetic, homogeneous and in thermal equilibrium. So, for a given chemical composition, opacity table (energy generation table if $\epsilon \neq 0$) and outer boundary condition, only 3 stellar parameters L_* , M_* and T_{eff} are needed to calculate the static equilibrium model.

Throughout this study, no energy generation ($\epsilon=0$) is assumed, which means that the luminosity is constant throughout the stellar envelope. So to calculate the stellar envelope we only need to know the photospheric pressure, which can be found by using one of the boundary conditions for P_{tot} (3.40) - (3.42) in conjunction with boundary condition (3.43). The grey atmosphere approximation has $T = T_{\text{eff}}$

at $\tau = 2/3$ and gives the following temperature distribution in the stellar atmosphere:

$$T^4 = 3T_{\text{eff}}^4 (\tau + q(\tau)) / 4, \quad (\text{C.9})$$

where $q(\tau)$ is the Hopf function and is $\sim 2/3$ in the Eddington approximation (see Mihalas, 1978). In the atmosphere, m_r and r are approximately constant, which when combined with the definition of optical depth ($d\tau = -\kappa\rho dr$) allows us to rewrite equation (C.1) as:

$$\frac{dP}{d\tau} = \frac{GM_*}{\kappa r^2}. \quad (\text{C.10})$$

Thus, for a small increment in optical depth, we can expand the pressure about τ using a Taylor series, and hence find the pressure at zone $i-1$ from that at zone i :

$$P_{i-1} = P_i + \left. \frac{dP}{d\tau} \right|_{\tau_i} d\tau. \quad (\text{C.11})$$

Equations (C.9), (C.10), (C.11) and the ideal gas law are then used iteratively to find the pressure, P_i at each subsequent zone until we reach $\tau=2/3$ and have the required photospheric pressure. The increment in τ is found by dividing $2/3$ by the number of zones in the atmosphere (generally about 40 - 50 zones). We can now use the ideal gas law to find the density of the gas at the photosphere which, combined with the other photospheric quantities, gives us the starting point for the envelope integrations.

INITIAL STATIC EQUILIBRIUM MODEL

The group of logarithmic differential equations (C.5) - (C.8) can now be solved using numerical quadrature. A fourth order Runge Kutta integration method will be used here for simplicity. So, for a system of differential equations:

$$f_i(Y_i, x) = \frac{dY_i}{dx}, \quad \text{for } i = 1 \text{ to } 4, \quad (\text{C.12})$$

where x is the independent variable. To integrate from point x_j to point $x_{j+1} = x_j + h$, we have:

$$Y_{i,j+1} = Y_{i,j} + (K_1 + 2K_2 + 2K_3 + K_4)h/6, \quad (\text{C.13})$$

where:

$$\begin{aligned} K_1 &= f_i(Y_{i,j}, x_j), \\ K_2 &= f_i(Y_{i,j} + hK_1/2, x_j + h/2), \\ K_3 &= f_i(Y_{i,j} + hK_2/2, x_j + h/2), \\ K_4 &= f_i(Y_{i,j} + hK_3, x_j + h) \end{aligned}$$

in which we have: $x = \ln(P)$, $Y_1 = \ln(r)$, $Y_2 = \ln(m_r)$, $Y_3 = \ln(T)$, $Y_4 = \ln(L)$ and the step h is given by:

$$h = \frac{\alpha}{N} \ln(P_{\text{cen}}/P_{\text{eff}}). \quad (\text{C.14})$$

P_{eff} is the photospheric pressure, N is the approximate number of zones in the stellar envelope, α is either equal to unity or the maximum gradient of previous zone, and P_{cen} is an estimate of the pressure at the bottom of the envelope. α is required to allow finer zoning in regions of steep gradients so that discontinuities do not occur. P_{cen} can be found by multiplying the equation of the lower

INITIAL STATIC EQUILIBRIUM MODEL

limit of P_{cen} found in Chandrasekhar (1968) by $P_{\text{factor}} \sim 10$. This then gives us:

$$P_{\text{cen}} = \frac{3}{8\pi G} \frac{GM_*^2}{r^2} P_{\text{factor}} \quad (\text{C.15})$$

Starting at $\tau = 2/3$, the envelope is integrated inwards until some preset criterion is met, e.g., $r = 0.1 R_*$ is reached, or until the temperature of the innermost zone reaches $1.5 \times 10^6 \text{ K}$. If the atmosphere is to be kept it should be re-integrated outwards from the photosphere using the above numerical quadrature. This is necessary as the atmosphere will be treated in the same way as the rest of the envelope. The number of zones in the stellar envelope should be between 500 and 700.

As the core is ignored in these models some combinations of the stellar parameters M_* , L_* and T_{eff} will result in unrealistic solutions, i.e., some of the models may not represent real stellar objects. This can be overcome by integrating a few steps out from the centre and making the inward and outward integrations meet.

All the calculations are performed in double precision and the variables L and m_r are scaled to prevent numerical overflow during the computations. Care is also needed in the order of calculation, so that the computer's limits are not exceeded. For the VAX/VMS system these limits are 10^{-37} and 10^{+37} .

C.2 REZONING THE EQUILIBRIUM MODEL

The finely zoned static equilibrium model produced in Section C.1 contains far too many zones to use in the non-linear dynamic codes. To overcome this problem a coarse model must be produced containing N_c

INITIAL STATIC EQUILIBRIUM MODEL

(usually about 50-60) zones, found by aggregating several of the finer static zones together. There are two ways of producing this coarser and hence more manageable static equilibrium model. The first is to make all the zones in the coarser model of constant mass ratio, and the second way is to make all the zones have equal sound travel time. The latter method is preferred as it allows a larger time step to be used in the time integrations, hence saving computational time.

The coarse zoning using constant sound travel times is found by first finding the total time for sound to travel across the whole envelope. This total time is then divided by N_c to give the travel time across a coarse zone. The coarse zones are then aggregated from the surface inwards in groups of fine zones whose total sound travel time is approximately equal to the required coarse sound travel time. The boundaries of the new zones are the outer boundaries of the aggregated fine zones.

The coarse zoning using constant mass ratio is found in a similar way, except that the zones are now linked together by mass rather than sound travel times. The masses of coarse zones are linked by:

$$\Delta M_i = \alpha \Delta M_{i-1}, \quad (C.16)$$

with

$$\alpha = \text{mass ratio} = \left(\frac{\Delta M_{\text{phot}}}{\Delta M_1} \right)^{1/N_c}, \quad (C.17)$$

where ΔM_i is the mass of zone i , and ΔM_{phot} is the mass of the zone directly below the photosphere. This method gives a few zones more if the atmosphere is included. It may be necessary to alter α in the inner zones as the sound travel times may become quite short, resulting in small time increments.

C.3 RELAXATION OF THE REZONED EQUILIBRIUM MODEL

The equilibrium model found above is not generally a solution of the difference equations and so must be 'relaxed' onto them. This is done by 'relaxing' the coarse equilibrium model found above onto a modified form of the difference equations. The difference equations are modified so that all time variances are ignored, the zonal velocities are set equal to zero, and the luminosity is held constant throughout the entire envelope. This then reduces the momentum (5.10) and energy (5.18) difference equations to:

$$P_{i-1/2} = P_{i+1/2} - \frac{GM_i \Delta M_i}{4\pi R_i^4}, \quad (C.18)$$

$$L_i = L_{*} = (4\pi R_i^2)^2 (W_{i-1/2} - W_{i+1/2}) 2F_i. \quad (C.19)$$

From (C.18) $P_{i-1/2}$ can be found using values of M and R found in the coarse equilibrium model. Having found $P_{i-1/2}$, (C.19) can be solved iteratively to give $W_{i-1/2}$ and hence the specific volume $V_{i-1/2}$ which can then be used in the continuity difference equation (5.9) to find R_{i-1} . Therefore, providing we have a boundary condition defining P and $W (=T^4)$ at the surface, we can 'relax' the whole envelope onto the difference equations. In this study the boundary conditions given in Chapter 5 (5.13 - 5.15) were used to fix P and W at the outer surface. The whole relaxation scheme above is repeated in a grand iteration until the r.m.s. of the changes in the zone boundary radii, between grand iterations, is less than some pre-set value (usually about 10^{-6}).

INITIAL STATIC EQUILIBRIUM MODEL

This is only one of many methods that can be used. It was invariably found that if a coarse model was used without some form of 'relaxation', temperature or luminosity inversion between zones would occur at some point during the time integration.

APPENDIX D

SOME MATHEMATICAL NOMENCLATURE

APPENDIX D
MATHEMATICAL NOMENCLATURE

D.1 A FEW ESSENTIAL DEFINITIONS

In this brief description of tensors, a basic knowledge of tensor calculus is assumed. Throughout this Appendix the summation convention will be used, and un-paired indices will indicate that the expression is valid for all values of the indices in question, i.e., A^i will represent A^1, A^2, \dots , etc.

The first tensor to be defined is the FUNDAMENTAL TENSOR which, as the name implies, is the most fundamental and important of all the tensors:

$$g_{\mu\nu} = \frac{\partial r}{\partial x^\mu} \cdot \frac{\partial r}{\partial x^\nu} = \frac{\partial y^i}{\partial x^\mu} \cdot \frac{\partial y^i}{\partial x^\nu}, \quad (\text{D.1})$$

where we are transforming from co-ordinates x^i to co-ordinates y^i , and $\underline{r} = \underline{r}(y^1, y^2, \dots)$. Then, if we represent the determinant of $g_{\mu\nu}$ by g , and the co-factor of element $g^{\mu\nu}$ by $G^{\mu\nu}$, we can define $g^{\mu\nu}$ as:

$$g^{\mu\nu} = \frac{G^{\mu\nu}}{g}. \quad (\text{D.2})$$

The tensors defined in (D.1) and (D.2) can be used to lift or drop tensor indices, as shown below:

$$A_\nu = g_{\nu\mu} A^\mu, \quad (\text{D.3})$$

$$A^\nu = g^{\nu\mu} A_\mu. \quad (\text{D.4})$$

MATHEMATICAL NOMENCLATURE

To complete this section, definitions of an inner product (contraction) and double dot product (double contraction) of two second rank tensors (Dyads), are given below:

$$\underline{A} \cdot \underline{B} = A^\mu B_\mu, \quad (\text{D.5})$$

$$\underline{A} : \underline{B} = A^{\mu k} B_{\mu k}. \quad (\text{D.6})$$

D.2 COVARIANT DERIVATIVES USED IN THIS WORK

Throughout the next two sections we define: Φ has a scalar function, \underline{A} has a vector, \underline{B} has a tensor and ∇ has its usual meaning. Having defined the symbols, we can now quote the tensorial form of the the covariant derivatives:

$$\nabla \Phi = \frac{\partial \Phi}{\partial x^k}, \quad (\text{D.7})$$

$$\nabla^2 \Phi = \frac{1}{\sqrt{g}} \frac{\partial}{\partial x^k} \left(\sqrt{g} g^{kr} \frac{\partial \Phi}{\partial x^r} \right), \quad (\text{D.8})$$

$$\nabla \cdot \underline{A} = \frac{1}{\sqrt{g}} \frac{\partial}{\partial x^k} \left(\sqrt{g} A^k \right), \quad (\text{D.9})$$

$$\nabla \underline{A} = \frac{\partial A^\mu}{\partial x^k}, \quad (\text{D.10})$$

$$\nabla \cdot \underline{B} = \frac{1}{\sqrt{g}} \frac{\partial}{\partial x^k} \left(\sqrt{g} B^{\mu k} \right). \quad (\text{D.11})$$

Using the above formulae, we can now derive the two expressions quoted in Chapter 3, i.e., the expansion of $\underline{\nabla} \cdot (\Phi \underline{A})$ and $\underline{B} \cdot (\underline{\nabla} \underline{A})$:

$$\begin{aligned} \underline{\nabla} \cdot (\Phi \underline{A}) &= \frac{1}{\sqrt{g}} \frac{\partial}{\partial x^k} \left(\sqrt{g} \Phi A^k \right) = \frac{\Phi}{\sqrt{g}} \frac{\partial}{\partial x^k} \left(\sqrt{g} A^k \right) + A^k \frac{\partial \Phi}{\partial x^k} \\ &= \Phi \underline{\nabla} \cdot \underline{A} + \underline{A} \cdot (\underline{\nabla} \Phi), \end{aligned} \quad (D.12)$$

and

$$\begin{aligned} \underline{B} \cdot (\underline{\nabla} \underline{A}) &= B^{\mu k} \frac{\partial A_k}{\partial x^\mu} \\ &= B^{\mu k} \frac{\partial A_k}{\partial x^\mu} + \frac{A_k}{\sqrt{g}} \frac{\partial}{\partial x^\mu} \left(\sqrt{g} B^{\mu k} \right) - \frac{A_k}{\sqrt{g}} \frac{\partial}{\partial x^k} \left(\sqrt{g} B^{\mu k} \right) \\ &= B^{\mu k} \frac{\partial A_k}{\partial x^\mu} + \frac{A_k}{\sqrt{g}} \frac{\partial}{\partial x^\mu} \left(\sqrt{g} B^{\mu k} \right) - \underline{A} \cdot (\underline{\nabla} \cdot \underline{B}) \\ &= \frac{1}{\sqrt{g}} \frac{\partial}{\partial x^k} \left(\sqrt{g} A_\mu B^{\mu k} \right) - \underline{A} \cdot (\underline{\nabla} \cdot \underline{B}) \\ &= \underline{\nabla} \cdot (\underline{A} \cdot \underline{B}) - \underline{A} \cdot (\underline{\nabla} \cdot \underline{B}) . \end{aligned} \quad (D.13)$$

To complete this section, the general divergence theorem is given by:

$$\int_v \underline{\nabla} \cdot \underline{B} d\tau = \int_v B^{\mu k}_{,k} d\tau = \int_s B^{\mu k} \nu_k dS = \int_s \underline{B} \cdot \underline{\nu} dS , \quad (D.14)$$

in which ν_k are the components of the unit vector normal to the surface element dS .

D.3 THE COVARIANT DERIVATIVES IN SPHERICAL CO-ORDINATES

To transform to spherical polar co-ordinates, we must first of all find $g^{\mu k}$ and g :

$$g^{11} = 1, \quad (D.15)$$

$$g^{22} = 1/r^2, \quad (D.16)$$

$$g^{33} = 1/r^2 \sin^2(\theta), \quad (D.17)$$

$$g^{\mu k} = 0 \quad \forall \mu \neq k, \quad (D.18)$$

$$g = r^4 \sin^2(\theta), \quad (D.19)$$

Using equations (D.15 - D.19) above, the covariant derivatives quoted in equations (D.7 - D.9) can be transformed into spherical polar co-ordinates as follows:

$$\underline{\nabla} \hat{\Phi} = \frac{\partial \hat{\Phi}}{\partial r} \hat{r} + \frac{\partial \hat{\Phi}}{\partial \theta} \hat{\theta} + \frac{\partial \hat{\Phi}}{\partial \phi} \hat{\phi}, \quad (D.20)$$

$$\underline{\nabla}^2 \hat{\Phi} = \frac{1}{r^2} \frac{\partial}{\partial r} \left(r^2 \frac{\partial \hat{\Phi}}{\partial r} \right) + \frac{1}{r^2 \sin(\theta)} \frac{\partial}{\partial \theta} \left(\sin(\theta) \frac{\partial \hat{\Phi}}{\partial \theta} \right) + \frac{1}{r^2 \sin^2(\theta)} \frac{\partial^2 \hat{\Phi}}{\partial \phi^2}, \quad (D.21)$$

$$\underline{\nabla} \cdot \underline{\hat{A}} = \frac{1}{r^2} \frac{\partial}{\partial r} (r^2 \hat{A}_r) + \frac{1}{\sin(\theta)} \frac{\partial}{\partial \theta} \left(\sin(\theta) \frac{\partial \hat{A}_\theta}{\partial \theta} \right) + \frac{\partial \hat{A}_\phi}{\partial \phi^2}. \quad (D.22)$$

The derivatives in equations (D.20 - D.22) above can be further reduced to their radial components, which is the form in which they are used throughout this thesis:

$$\underline{\nabla} \hat{\Phi} = \frac{\partial \hat{\Phi}}{\partial r}, \quad (D.23)$$

$$\underline{\nabla}^2 \hat{\Phi} = \frac{1}{r^2} \frac{\partial}{\partial r} \left(r^2 \frac{\partial \hat{\Phi}}{\partial r} \right), \quad (D.24)$$

$$\underline{\nabla} \cdot \underline{\hat{A}} = \frac{1}{r^2} \frac{\partial}{\partial r} (r^2 \hat{A}_r). \quad (D.25)$$

APPENDIX E

TABULATION OF LINEAR RESULTS

RESULTS FOR OPACITY TABLE R040

TABLES OF LINEAR RESULTS

TABLE OF NON-ADIABATIC PERIODS

MODE : 0 Opacity table : R040 Mass : 0.8 Solar masses

Luminosity (solar luminosities)						
Teff	1,000	3,000	6,000	10,000	15,000	20,000
5,000	---	---	---	---	---	---
5,500	---	---	---	---	---	---
6,000	---	---	---	---	---	---
6,500	---	---	---	---	---	---
7,000	---	---	---	---	89.720	115.200
7,500	---	---	---	37.440	69.400	106.700
8,000	---	---	18.880	38.360	70.510	100.400
9,000	2.900	7.840	16.870	30.460	48.280	59.190
10,000	1.730	4.800	9.910	17.660	35.210	33.680
12,000	0.860	2.460	5.270	10.380	16.760	23.160
15,000	0.440	1.160	2.470	4.700	7.830	12.200
20,000	0.180	0.410	0.820	1.510	2.690	3.810
25,000	0.860	0.200	0.350	0.470	1.110	1.650
30,000	0.470	0.120	0.190	0.300	0.980	0.880

TABLE OF ADIABATIC PERIODS

MODE : 0 Opacity table : R040 Mass : 0.8 Solar masses

Luminosity (solar luminosities)						
Teff	1,000	3,000	6,000	10,000	15,000	20,000
5,000	---	---	---	---	---	---
5,500	---	---	---	---	---	---
6,000	---	---	---	---	---	---
6,500	---	---	---	---	---	---
7,000	---	---	---	---	90.580	118.300
7,500	---	---	---	37.560	70.990	119.800
8,000	---	---	18.900	38.650	76.580	130.500
9,000	2.910	7.840	17.170	32.050	57.620	95.900
10,000	1.720	4.810	9.910	18.250	33.090	54.320
12,000	0.860	2.340	4.550	8.280	14.470	22.450
15,000	0.440	1.110	2.150	3.680	6.110	9.170
20,000	0.180	0.410	0.760	1.260	1.970	2.810
25,000	0.860	0.200	0.350	0.570	0.870	1.190
30,000	0.470	0.120	0.190	0.300	0.450	0.620

TABLES OF LINEAR RESULTS

TABLE OF NON-ADIABATIC Q VALUES

MODE : 0 Opacity table : R040 Mass : 0.8 Solar masses

Luminosity (solar luminosities)						
Teff	1,000	3,000	6,000	10,000	15,000	20,000
5,000	---	---	---	---	---	---
5,500	---	---	---	---	---	---
6,000	---	---	---	---	---	---
6,500	---	---	---	---	---	---
7,000	---	---	---	---	0.100	0.104
7,500	---	---	---	0.075	0.102	0.127
8,000	---	---	0.064	0.088	0.119	0.138
9,000	0.053	0.063	0.080	0.099	0.115	0.115
10,000	0.045	0.054	0.067	0.081	0.119	0.092
12,000	0.039	0.048	0.063	0.083	0.098	0.110
15,000	0.037	0.043	0.054	0.070	0.086	0.108
20,000	0.036	0.037	0.044	0.055	0.072	0.083
25,000	0.351	0.036	0.038	0.034	0.059	0.072
30,000	0.336	0.036	0.036	0.038	0.090	0.067

TABLE OF ADIABATIC Q VALUES

MODE : 0 Opacity table : R040 Mass : 0.8 Solar masses

Luminosity (solar luminosities)						
Teff	1,000	3,000	6,000	10,000	15,000	20,000
5,000	---	---	---	---	---	---
5,500	---	---	---	---	---	---
6,000	---	---	---	---	---	---
6,500	---	---	---	---	---	---
7,000	---	---	---	---	0.101	0.107
7,500	---	---	---	0.075	0.105	0.143
8,000	---	---	0.064	0.089	0.130	0.179
9,000	0.053	0.063	0.072	0.104	0.138	0.186
10,000	0.044	0.054	0.067	0.084	0.112	0.148
12,000	0.039	0.046	0.054	0.066	0.085	0.107
15,000	0.037	0.041	0.047	0.055	0.067	0.081
20,000	0.036	0.037	0.041	0.046	0.053	0.061
25,000	0.351	0.036	0.037	0.041	0.046	0.052
30,000	0.336	0.036	0.036	0.038	0.042	0.046

TABLES OF LINEAR RESULTS

TABLE OF NON-ADIABATIC GROWTH RATES

MODE : 0 Opacity table : R040 Mass : 0.8 Solar masses

Teff	Luminosity (solar luminosities)					
	1,000	3,000	6,000	10,000	15,000	20,000
5,000	---	---	---	---	---	---
5,500	---	---	---	---	---	---
6,000	---	---	---	---	---	---
6,500	---	---	---	---	---	---
7,000	---	---	---	---	0.289	0.682
7,500	---	---	---	0.169	0.803	2.194
8,000	---	---	0.556	0.414	1.766	3.313
9,000	0.244	0.884	0.360	1.358	2.382	2.420
10,000	0.571	-0.757	-0.448	-0.599	-0.734	-0.180
12,000	-0.945	-0.764	-1.424	-1.114	-0.327	0.429
15,000	-0.210	-0.326	-0.588	-0.604	-0.206	-0.312
20,000	-0.453	-0.941	-0.359	-0.468	-0.379	-0.281
25,000	-0.343	-0.498	-0.371	-0.351	-1.109	-0.563
30,000	-0.261	-0.235	-0.258	-0.667	-0.842	-1.094

TABLE OF NON-ADIABATIC PHI

MODE : 0 Opacity table : R040 Mass : 0.8 Solar masses

Teff	Luminosity (solar luminosities)					
	1,000	3,000	6,000	10,000	15,000	20,000
5,000	---	---	---	---	---	---
5,500	---	---	---	---	---	---
6,000	---	---	---	---	---	---
6,500	---	---	---	---	---	---
7,000	---	---	---	---	178.600	178.400
7,500	---	---	---	178.700	178.500	178.400
8,000	---	---	178.600	178.400	178.300	177.800
9,000	177.900	177.700	177.400	177.400	175.100	173.300
10,000	178.000	165.900	141.100	125.200	99.400	115.300
12,000	-8.500	-51.900	-67.200	-74.600	-30.200	10.600
15,000	-18.300	-53.200	-68.200	-71.800	-59.000	-32.700
20,000	2.800	-11.600	-39.900	-51.800	-55.100	-34.200
25,000	3.100	-4.800	-15.000	-32.000	-36.200	-34.100
30,000	1.200	-11.300	-24.400	-35.500	-33.800	-35.200

TABLES OF LINEAR RESULTS

TABLE OF NON-ADIABATIC PERIODS

MODE : 1 Opacity table : R040 Mass : 0.8 Solar masses

Teff	Luminosity (solar luminosities)					
	1,000	3,000	6,000	10,000	15,000	20,000
5,000	---	---	---	---	---	---
5,500	---	---	---	---	---	---
6,000	---	---	---	---	---	---
6,500	---	---	---	---	---	---
7,000	---	---	---	---	37.370	42.380
7,500	---	---	---	18.740	24.680	29.030
8,000	---	---	10.910	15.500	19.920	23.010
9,000	1.750	3.970	6.760	9.960	13.070	24.960
10,000	1.170	2.850	5.380	9.010	12.740	15.850
12,000	0.650	1.710	3.190	3.190	4.490	8.610
15,000	0.340	0.870	1.640	1.720	2.450	3.080
20,000	0.130	0.340	0.610	1.010	1.520	1.350
25,000	0.590	0.160	0.290	0.640	0.750	1.010
30,000	0.330	0.850	0.160	0.300	0.580	0.680

TABLE OF ADIABATIC PERIODS

MODE : 1 Opacity table : R040 Mass : 0.8 Solar masses

Teff	Luminosity (solar luminosities)					
	1,000	3,000	6,000	10,000	15,000	20,000
5,000	---	---	---	---	---	---
5,500	---	---	---	---	---	---
6,000	---	---	---	---	---	---
6,500	---	---	---	---	---	---
7,000	---	---	---	---	37.420	42.420
7,500	---	---	---	18.740	24.670	28.990
8,000	---	---	10.920	15.490	19.910	23.040
9,000	1.750	3.960	6.800	10.030	13.340	15.060
10,000	1.170	2.850	5.090	7.630	9.910	11.070
12,000	0.650	1.580	2.830	4.430	5.960	6.980
15,000	0.340	0.800	1.450	2.290	3.210	3.890
20,000	0.130	0.320	0.540	0.850	1.260	1.620
25,000	0.590	0.160	0.270	0.400	0.570	0.760
30,000	0.330	0.840	0.150	0.230	0.310	0.390

TABLES OF LINEAR RESULTS

TABLE OF NON-ADIABATIC Q VALUES

MODE : 1 Opacity table : R040 Mass : 0.8 Solar masses

Luminosity (solar luminosities)						
Teff	1,000	3,000	6,000	10,000	15,000	20,000
5,000	---	---	---	---	---	---
5,500	---	---	---	---	---	---
6,000	---	---	---	---	---	---
6,500	---	---	---	---	---	---
7,000	---	---	---	---	0.042	0.038
7,500	---	---	---	0.038	0.036	0.035
8,000	---	---	0.037	0.036	0.034	0.032
9,000	0.032	0.032	0.032	0.032	0.031	0.048
10,000	0.030	0.032	0.036	0.041	0.043	0.043
12,000	0.029	0.033	0.038	0.025	0.026	0.041
15,000	0.029	0.032	0.036	0.025	0.027	0.027
20,000	0.026	0.030	0.033	0.037	0.041	0.029
25,000	0.241	0.028	0.032	0.047	0.040	0.044
30,000	0.231	0.265	0.031	0.038	0.053	0.052

TABLE OF ADIABATIC Q VALUES

MODE : 1 Opacity table : R040 Mass : 0.8 Solar masses

Luminosity (solar luminosities)						
Teff	1,000	3,000	6,000	10,000	15,000	20,000
5,000	---	---	---	---	---	---
5,500	---	---	---	---	---	---
6,000	---	---	---	---	---	---
6,500	---	---	---	---	---	---
7,000	---	---	---	---	0.042	0.038
7,500	---	---	---	0.038	0.036	0.035
8,000	---	---	0.037	0.036	0.034	0.032
9,000	0.032	0.032	0.032	0.033	0.032	0.029
10,000	0.030	0.032	0.034	0.035	0.033	0.030
12,000	0.029	0.031	0.034	0.035	0.035	0.033
15,000	0.028	0.029	0.031	0.034	0.035	0.034
20,000	0.026	0.029	0.029	0.031	0.034	0.035
25,000	0.241	0.028	0.029	0.029	0.031	0.033
30,000	0.232	0.262	0.029	0.029	0.028	0.029

TABLES OF LINEAR RESULTS

TABLE OF NON-ADIABATIC GROWTH RATES

MODE : 1 Opacity table : R040 Mass : 0.8 Solar masses

Luminosity (solar luminosities)						
Teff	1,000	3,000	6,000	10,000	15,000	20,000
5,000	---	---	---	---	---	---
5,500	---	---	---	---	---	---
6,000	---	---	---	---	---	---
6,500	---	---	---	---	---	---
7,000	---	---	---	---	0.138	0.200
7,500	---	---	---	0.104	0.213	0.308
8,000	---	---	0.623	0.160	0.275	0.293
9,000	0.325	0.578	0.103	-0.365	-0.935	0.293
10,000	-0.161	-0.160	-1.153	-1.491	-0.282	1.790
12,000	-0.306	-0.712	-0.484	-0.698	-0.211	-0.451
15,000	-0.158	-0.424	-0.197	-0.418	-0.557	-0.418
20,000	-0.803	-0.257	-0.262	-0.379	-1.019	-1.137
25,000	-0.585	-0.347	-0.290	-0.729	-0.720	-1.808
30,000	-0.286	-0.402	-0.654	-0.667	-1.084	-1.611

TABLE OF NON-ADIABATIC PHI

MODE : 1 Opacity table : R040 Mass : 0.8 Solar masses

Luminosity (solar luminosities)						
Teff	1,000	3,000	6,000	10,000	15,000	20,000
5,000	---	---	---	---	---	---
5,500	---	---	---	---	---	---
6,000	---	---	---	---	---	---
6,500	---	---	---	---	---	---
7,000	---	---	---	---	180.300	180.100
7,500	---	---	---	---	179.600	179.300
8,000	---	---	179.700	179.600	179.400	178.800
9,000	178.900	178.800	178.600	177.500	178.300	181.200
10,000	177.900	170.300	116.400	187.700	163.300	165.200
12,000	-19.800	-84.800	---	120.200	111.300	113.900
15,000	-36.400	-83.200	-157.200	97.000	82.300	90.200
20,000	-15.600	-46.500	-114.200	167.800	149.000	57.600
25,000	-7.300	-20.400	-69.600	184.300	136.200	138.600
30,000	---	-27.500	-36.300	135.800	123.500	130.800

TABLES OF LINEAR RESULTS

TABLE OF NON-ADIABATIC PERIODS

MODE : 0 Opacity table : R040 Mass : 1.0 Solar masses

Luminosity (solar luminosities)						
Teff	1,000	3,000	6,000	10,000	15,000	20,000
5,000	---	---	---	---	---	---
5,500	---	---	---	---	---	---
6,000	---	---	---	---	---	---
6,500	---	---	---	---	---	---
7,000	---	---	---	---	---	98.790
7,500	---	---	---	30.530	49.700	77.020
8,000	---	---	16.270	28.300	51.760	78.050
9,000	---	6.670	13.450	23.730	37.860	56.520
10,000	1.460	4.150	7.760	13.730	25.020	33.040
12,000	---	---	---	---	---	---
15,000	0.360	0.930	1.790	3.250	5.580	8.530
20,000	0.150	0.380	0.660	1.160	1.960	2.970
25,000	0.740	0.190	0.310	0.500	0.830	1.210
30,000	0.340	0.930	0.150	0.230	0.360	0.950

TABLE OF ADIABATIC PERIODS

MODE : 0 Opacity table : R040 Mass : 1.0 Solar masses

Luminosity (solar luminosities)						
Teff	1,000	3,000	6,000	10,000	15,000	20,000
5,000	---	---	---	---	---	---
5,500	---	---	---	---	---	---
6,000	---	---	---	---	---	---
6,500	---	---	---	---	---	---
7,000	---	---	---	---	---	99.630
7,500	---	---	---	30.560	49.950	78.700
8,000	---	---	16.280	28.350	52.570	84.610
9,000	---	6.670	13.580	24.280	41.350	62.930
10,000	1.460	4.160	7.910	13.930	23.540	36.000
12,000	---	---	---	---	---	---
15,000	0.360	0.920	1.640	2.720	4.280	6.100
20,000	0.150	0.380	0.640	1.030	1.570	2.160
25,000	0.740	0.190	0.310	0.470	0.700	0.950
30,000	0.350	0.930	0.150	0.220	0.320	0.420

TABLES OF LINEAR RESULTS

TABLE OF NON-ADIABATIC Q VALUES

MODE : 0 Opacity table : R040 Mass : 1.0 Solar masses

Luminosity (solar luminosities)						
Teff	1,000	3,000	6,000	10,000	15,000	20,000
5,000	---	---	---	---	---	---
5,500	---	---	---	---	---	---
6,000	---	---	---	---	---	---
6,500	---	---	---	---	---	---
7,000	---	---	---	---	---	0.100
7,500	---	---	---	0.068	0.082	0.103
8,000	---	---	0.061	0.073	0.098	0.120
9,000	---	0.057	0.072	0.086	0.101	0.122
10,000	0.042	0.051	0.058	0.070	0.094	0.101
12,000	---	---	---	---	---	---
15,000	0.036	0.039	0.047	0.058	0.073	0.090
20,000	0.035	0.037	0.040	0.047	0.059	0.072
25,000	0.339	0.036	0.037	0.041	0.050	0.058
30,000	0.315	0.357	0.036	0.037	0.043	0.051

TABLE OF ADIABATIC Q VALUES

MODE : 0 Opacity table : R040 Mass : 1.0 Solar masses

Luminosity (solar luminosities)						
Teff	1,000	3,000	6,000	10,000	15,000	20,000
5,000	---	---	---	---	---	---
5,500	---	---	---	---	---	---
6,000	---	---	---	---	---	---
6,500	---	---	---	---	---	---
7,000	---	---	---	---	---	0.101
7,500	---	---	---	0.068	0.082	0.105
8,000	---	---	0.061	0.073	0.099	0.130
9,000	---	0.057	0.072	0.088	0.110	0.136
10,000	0.042	0.051	0.060	0.071	0.089	0.110
12,000	---	---	---	---	---	---
15,000	0.036	0.039	0.043	0.048	0.056	0.065
20,000	0.035	0.037	0.038	0.042	0.047	0.052
25,000	0.340	0.036	0.037	0.038	0.042	0.046
30,000	0.316	0.357	0.036	0.036	0.038	0.041

TABLES OF LINEAR RESULTS

TABLE OF NON-ADIABATIC GROWTH RATES

MODE : 0 Opacity table : R040 Mass : 1.0 Solar masses

Teff	Luminosity (solar luminosities)					
	1,000	3,000	6,000	10,000	15,000	20,000
5,000	---	---	---	---	---	---
5,500	---	---	---	---	---	---
6,000	---	---	---	---	---	---
6,500	---	---	---	---	---	---
7,000	---	---	---	---	---	0.262
7,500	---	---	---	0.523	0.247	0.780
8,000	---	---	0.140	0.124	0.651	1.690
9,000	---	0.320	0.232	0.733	1.842	2.053
10,000	0.142	-0.600	-0.183	-0.616	-1.588	-0.813
12,000	---	---	---	---	---	---
15,000	-0.584	-0.161	-0.488	-0.648	-0.534	-0.181
20,000	-0.198	-0.344	-0.234	-0.440	-0.487	-0.416
25,000	-0.172	-0.188	-0.159	-0.554	-0.727	-0.718
30,000	-0.143	-0.836	-0.541	-0.487	-1.159	-0.589

TABLE OF NON-ADIABATIC PHI

MODE : 0 Opacity table : R040 Mass : 1.0 Solar masses

Teff	Luminosity (solar luminosities)					
	1,000	3,000	6,000	10,000	15,000	20,000
5,000	---	---	---	---	---	---
5,500	---	---	---	---	---	---
6,000	---	---	---	---	---	---
6,500	---	---	---	---	---	---
7,000	---	---	---	---	---	178.600
7,500	---	---	---	178.600	178.500	178.400
8,000	---	---	178.600	178.200	178.300	178.200
9,000	---	177.800	177.700	177.700	177.100	173.700
10,000	177.600	168.700	151.100	130.600	92.500	108.600
12,000	---	---	---	---	---	---
15,000	-12.500	-43.500	-61.000	---	-72.700	-67.000
20,000	6.900	-5.300	-30.600	-48.500	-54.300	-53.400
25,000	4.600	-2.700	-11.600	-25.800	-33.800	-36.400
30,000	3.500	-5.300	-18.600	-29.200	-32.100	-35.000

TABLES OF LINEAR RESULTS

TABLE OF NON-ADIABATIC PERIODS

MODE : 1 Opacity table : R040 Mass : 1.0 Solar masses

Luminosity (solar luminosities)						
Teff	1,000	3,000	6,000	10,000	15,000	20,000
5,000	---	---	---	---	---	---
5,500	---	---	---	---	---	---
6,000	---	---	---	---	---	---
6,500	---	---	---	---	---	---
7,000	---	---	---	---	---	41.770
7,500	---	---	---	17.570	22.630	27.150
8,000	---	---	10.120	14.090	18.480	21.900
9,000	---	3.660	5.960	8.970	12.180	14.470
10,000	1.050	2.570	4.440	7.420	11.420	14.550
12,000	---	---	---	---	---	---
15,000	0.270	0.730	1.290	2.080	1.990	2.650
20,000	0.110	0.300	0.530	0.840	1.270	1.660
25,000	0.510	0.140	0.250	0.400	0.600	0.820
30,000	0.250	0.640	0.120	0.200	0.280	0.530

TABLE OF ADIABATIC PERIODS

MODE : 1 Opacity table : R040 Mass : 1.0 Solar masses

Luminosity (solar luminosities)						
Teff	1,000	3,000	6,000	10,000	15,000	20,000
5,000	---	---	---	---	---	---
5,500	---	---	---	---	---	---
6,000	---	---	---	---	---	---
6,500	---	---	---	---	---	---
7,000	---	---	---	---	---	41.820
7,500	---	---	---	17.580	22.630	27.130
8,000	---	---	10.120	14.090	18.470	21.900
9,000	---	3.660	5.980	9.040	12.270	14.870
10,000	1.050	2.580	4.440	6.790	9.310	11.040
12,000	---	---	---	---	---	---
15,000	0.270	0.690	1.140	1.810	2.630	3.310
20,000	0.110	0.300	0.490	0.720	1.050	1.380
25,000	0.510	0.140	0.240	0.360	0.490	0.630
30,000	0.250	0.640	0.110	0.180	0.240	0.290

TABLES OF LINEAR RESULTS

TABLE OF NON-ADIABATIC Q VALUES

MODE : 1 Opacity table : R040 Mass : 1.0 Solar masses

Luminosity (solar luminosities)						
Teff	1,000	3,000	6,000	10,000	15,000	20,000
5,000	---	---	---	---	---	---
5,500	---	---	---	---	---	---
6,000	---	---	---	---	---	---
6,500	---	---	---	---	---	---
7,000	---	---	---	---	---	0.042
7,500	---	---	---	0.039	0.037	0.036
8,000	---	---	0.038	0.036	0.035	0.034
9,000	---	0.032	0.032	0.033	0.033	0.031
10,000	0.030	0.031	0.033	0.038	0.043	0.044
12,000	---	---	---	---	---	---
15,000	0.027	0.031	0.034	0.037	0.026	0.041
20,000	0.025	0.029	0.032	0.034	0.038	0.040
25,000	0.233	0.027	0.030	0.033	0.036	0.040
30,000	0.224	0.247	0.028	0.032	0.033	0.037

TABLE OF ADIABATIC Q VALUES

MODE : 1 Opacity table : R040 Mass : 1.0 Solar masses

Luminosity (solar luminosities)						
Teff	1,000	3,000	6,000	10,000	15,000	20,000
5,000	---	---	---	---	---	---
5,500	---	---	---	---	---	---
6,000	---	---	---	---	---	---
6,500	---	---	---	---	---	---
7,000	---	---	---	---	---	0.042
7,500	---	---	---	0.039	0.037	0.036
8,000	---	---	0.038	0.036	0.035	0.034
9,000	---	0.032	0.032	0.033	0.033	0.032
10,000	0.030	0.031	0.033	0.035	0.035	0.034
12,000	---	---	---	---	---	---
15,000	0.027	0.029	0.030	0.032	0.034	0.035
20,000	0.025	0.029	0.029	0.029	0.032	0.034
25,000	0.234	0.027	0.029	0.029	0.029	0.030
30,000	0.225	0.246	0.027	0.029	0.029	0.028

TABLES OF LINEAR RESULTS

TABLE OF NON-ADIABATIC GROWTH RATES

MODE : 1 Opacity table : R040 Mass : 1.0 Solar masses

Luminosity (solar luminosities)						
Teff	1,000	3,000	6,000	10,000	15,000	20,000
5,000	---	---	---	---	---	---
5,500	---	---	---	---	---	---
6,000	---	---	---	---	---	---
6,500	---	---	---	---	---	---
7,000	---	---	---	---	---	0.129
7,500	---	---	---	0.611	0.130	0.208
8,000	---	---	0.346	0.945	0.194	0.265
9,000	---	0.334	0.137	-0.465	-0.591	-1.037
10,000	0.132	-0.848	-0.407	-1.691	-0.852	1.048
12,000	---	---	---	---	---	---
15,000	-0.874	-0.387	-0.272	-0.276	-0.454	-0.584
20,000	-0.404	-0.201	-0.313	-0.203	-0.558	-1.011
25,000	-0.211	-0.243	-0.424	-0.256	-0.488	-1.079
30,000	-0.922	-0.190	-0.652	-0.544	-0.271	-1.185

TABLE OF NON-ADIABATIC PHI

MODE : 1 Opacity table : R040 Mass : 1.0 Solar masses

Luminosity (solar luminosities)						
Teff	1,000	3,000	6,000	10,000	15,000	20,000
5,000	---	---	---	---	---	---
5,500	---	---	---	---	---	---
6,000	---	---	---	---	---	---
6,500	---	---	---	---	---	---
7,000	---	---	---	---	---	180.200
7,500	---	---	---	179.800	179.700	179.600
8,000	---	---	179.600	179.500	179.500	179.300
9,000	---	178.800	178.900	178.000	177.600	178.300
10,000	177.800	173.700	153.000	178.100	177.300	169.300
12,000	---	---	---	---	---	---
15,000	-29.300	-68.300	---	181.300	89.400	74.400
20,000	-8.400	-32.500	-76.700	212.000	157.700	-205.200
25,000	-3.200	-15.500	-34.200	249.800	162.500	-223.900
30,000	-4.700	-25.100	-32.700	299.600	183.100	-236.600

TABLES OF LINEAR RESULTS

TABLE OF NON-ADIABATIC PERIODS

MODE : 0 Opacity table : R040 Mass : 1.2 Solar masses

Teff	Luminosity (solar luminosities)					
	1,000	3,000	6,000	10,000	15,000	20,000
5,000	---	---	---	---	---	---
5,500	---	---	---	---	---	---
6,000	---	---	---	---	---	---
6,500	---	---	---	---	---	---
7,000	---	---	---	---	---	---
7,500	---	---	---	---	39.800	58.580
8,000	---	---	---	23.060	39.880	60.750
9,000	---	5.730	11.240	19.480	31.430	42.440
10,000	1.290	3.570	6.610	11.230	18.580	34.240
12,000	---	---	---	---	---	---
15,000	0.330	0.820	1.490	2.610	4.350	6.330
20,000	0.140	0.340	0.570	0.950	1.550	2.290
25,000	0.650	0.170	0.280	0.420	0.660	0.960
30,000	0.300	0.830	0.140	0.200	0.290	0.420

TABLE OF ADIABATIC PERIODS

MODE : 0 Opacity table : R040 Mass : 1.2 Solar masses

Teff	Luminosity (solar luminosities)					
	1,000	3,000	6,000	10,000	15,000	20,000
5,000	---	---	---	---	---	---
5,500	---	---	---	---	---	---
6,000	---	---	---	---	---	---
6,500	---	---	---	---	---	---
7,000	---	---	---	---	---	---
7,500	---	---	---	---	39.870	58.920
8,000	---	---	---	23.070	40.040	62.080
9,000	---	5.730	11.260	19.760	32.450	47.500
10,000	1.290	3.570	6.650	11.420	18.520	27.070
12,000	---	---	---	---	---	---
15,000	0.330	0.810	1.420	2.310	3.530	4.890
20,000	0.140	0.340	0.570	0.890	1.330	1.790
25,000	0.660	0.170	0.280	0.420	0.600	0.800
30,000	0.300	0.830	0.140	0.200	0.280	0.360

TABLES OF LINEAR RESULTS

TABLE OF NON-ADIABATIC Q VALUES

MODE : 0 Opacity table : R040 Mass : 1.2 Solar masses

Teff	Luminosity (solar luminosities)					
	1,000	3,000	6,000	10,000	15,000	20,000
5,000	---	---	---	---	---	---
5,500	---	---	---	---	---	---
6,000	---	---	---	---	---	---
6,500	---	---	---	---	---	---
7,000	---	---	---	---	---	---
7,500	---	---	---	---	0.072	0.086
8,000	---	---	---	0.065	0.083	0.102
9,000	---	0.054	0.066	0.078	0.092	0.101
10,000	0.041	0.048	0.055	0.063	0.077	0.115
12,000	---	---	---	---	---	---
15,000	0.036	0.038	0.043	0.051	0.062	0.073
20,000	0.035	0.036	0.037	0.042	0.051	0.061
25,000	0.328	0.036	0.036	0.038	0.043	0.051
30,000	0.301	0.349	0.036	0.036	0.038	0.044

TABLE OF ADIABATIC Q VALUES

MODE : 0 Opacity table : R040 Mass : 1.2 Solar masses

Teff	Luminosity (solar luminosities)					
	1,000	3,000	6,000	10,000	15,000	20,000
5,000	---	---	---	---	---	---
5,500	---	---	---	---	---	---
6,000	---	---	---	---	---	---
6,500	---	---	---	---	---	---
7,000	---	---	---	---	---	---
7,500	---	---	---	---	0.072	0.086
8,000	---	---	---	0.065	0.083	0.104
9,000	---	0.054	0.066	0.079	0.095	0.113
10,000	0.041	0.048	0.055	0.064	0.077	0.091
12,000	---	---	---	---	---	---
15,000	0.036	0.038	0.041	0.045	0.051	0.057
20,000	0.035	0.036	0.037	0.040	0.044	0.048
25,000	0.328	0.036	0.036	0.037	0.039	0.042
30,000	0.302	0.349	0.036	0.036	0.036	0.038

TABLES OF LINEAR RESULTS

TABLE OF NON-ADIABATIC GROWTH RATES

MODE : 0 Opacity table : R040 Mass : 1.2 Solar masses

Luminosity (solar luminosities)

Teff	1,000	3,000	6,000	10,000	15,000	20,000
5,000	---	---	---	---	---	---
5,500	---	---	---	---	---	---
6,000	---	---	---	---	---	---
6,500	---	---	---	---	---	---
7,000	---	---	---	---	---	---
7,500	---	---	---	---	0.962	0.294
8,000	---	---	---	0.441	0.258	0.779
9,000	---	0.978	0.148	0.371	1.092	2.190
10,000	0.149	-0.394	-0.117	-0.409	-0.981	-2.324
12,000	---	---	---	---	---	---
15,000	-0.225	-0.777	-0.395	-0.631	-0.652	-0.429
20,000	-0.106	-0.151	-0.960	-0.315	-0.510	-0.449
25,000	-0.104	-0.862	-0.534	-0.331	-0.686	-0.778
30,000	-0.911	-0.442	-0.202	-0.139	-0.830	-1.191

TABLE OF NON-ADIABATIC PHI

MODE : 0 Opacity table : R040 Mass : 1.2 Solar masses

Luminosity (solar luminosities)

Teff	1,000	3,000	6,000	10,000	15,000	20,000
5,000	---	---	---	---	---	---
5,500	---	---	---	---	---	---
6,000	---	---	---	---	---	---
6,500	---	---	---	---	---	---
7,000	---	---	---	---	---	---
7,500	---	---	---	---	178.500	178.400
8,000	---	---	---	178.400	178.100	178.200
9,000	---	177.900	177.800	177.800	177.600	177.300
10,000	177.300	171.900	159.300	134.900	111.200	67.000
12,000	---	---	---	---	---	---
15,000	-7.200	-34.200	-54.500	-64.600	-71.100	-72.300
20,000	7.200	0.600	-17.700	-42.000	-52.100	-52.700
25,000	6.600	-2.600	-4.200	-18.000	-31.800	-38.300
30,000	3.500	-2.400	-12.100	-25.300	-31.300	-36.700

TABLES OF LINEAR RESULTS

TABLE OF NON-ADIABATIC PERIODS

MODE : 1 Opacity table : R040 Mass : 1.2 Solar masses

Luminosity (solar luminosities)						
Teff	1,000	3,000	6,000	10,000	15,000	20,000
5,000	---	---	---	---	---	---
5,500	---	---	---	---	---	---
6,000	---	---	---	---	---	---
6,500	---	---	---	---	---	---
7,000	---	---	---	---	---	---
7,500	---	---	---	---	21.100	25.340
8,000	---	---	---	13.000	17.140	20.620
9,000	---	3.340	5.380	8.140	11.250	13.830
10,000	0.960	2.310	3.950	6.310	9.780	13.020
12,000	---	---	---	---	---	---
15,000	0.240	0.650	1.120	1.800	2.640	2.280
20,000	0.950	0.260	0.470	0.730	1.090	1.460
25,000	0.460	0.120	0.220	0.350	0.510	0.680
30,000	0.220	0.570	0.100	0.170	0.250	0.310

TABLE OF ADIABATIC PERIODS

MODE : 1 Opacity table : R040 Mass : 1.2 Solar masses

Luminosity (solar luminosities)						
Teff	1,000	3,000	6,000	10,000	15,000	20,000
5,000	---	---	---	---	---	---
5,500	---	---	---	---	---	---
6,000	---	---	---	---	---	---
6,500	---	---	---	---	---	---
7,000	---	---	---	---	---	---
7,500	---	---	---	---	21.100	25.330
8,000	---	---	---	13.000	17.130	20.600
9,000	---	3.340	5.380	8.200	11.300	13.920
10,000	0.960	2.310	3.950	6.090	8.530	10.520
12,000	---	---	---	---	---	---
15,000	0.240	0.630	1.020	1.580	2.310	2.980
20,000	0.960	0.260	0.450	0.650	0.910	1.190
25,000	0.460	0.120	0.210	0.330	0.440	0.550
30,000	0.220	0.570	0.990	0.160	0.220	0.270

TABLES OF LINEAR RESULTS

TABLE OF NON-ADIABATIC Q VALUES

MODE : 1 Opacity table : R040 Mass : 1.2 Solar masses

Luminosity (solar luminosities)						
Teff	1,000	3,000	6,000	10,000	15,000	20,000
5,000	---	---	---	---	---	---
5,500	---	---	---	---	---	---
6,000	---	---	---	---	---	---
6,500	---	---	---	---	---	---
7,000	---	---	---	---	---	---
7,500	---	---	---	---	0.038	0.037
8,000	---	---	---	0.037	0.036	0.035
9,000	---	0.031	0.031	0.032	0.033	0.033
10,000	0.030	0.031	0.033	0.035	0.040	0.044
12,000	---	---	---	---	---	---
15,000	0.026	0.030	0.032	0.035	0.038	0.026
20,000	0.240	0.028	0.031	0.033	0.036	0.039
25,000	0.229	0.026	0.029	0.032	0.033	0.036
30,000	0.218	0.239	0.026	0.030	0.033	0.033

TABLE OF ADIABATIC Q VALUES

MODE : 1 Opacity table : R040 Mass : 1.2 Solar masses

Luminosity (solar luminosities)						
Teff	1,000	3,000	6,000	10,000	15,000	20,000
5,000	---	---	---	---	---	---
5,500	---	---	---	---	---	---
6,000	---	---	---	---	---	---
6,500	---	---	---	---	---	---
7,000	---	---	---	---	---	---
7,500	---	---	---	---	0.038	0.037
8,000	---	---	---	0.037	0.035	0.035
9,000	---	0.031	0.031	0.033	0.033	0.033
10,000	0.030	0.031	0.033	0.034	0.035	0.035
12,000	---	---	---	---	---	---
15,000	0.026	0.029	0.029	0.031	0.033	0.035
20,000	0.240	0.028	0.029	0.029	0.030	0.032
25,000	0.230	0.026	0.028	0.029	0.029	0.029
30,000	0.220	0.239	0.259	0.028	0.029	0.029

RESULTS FOR OPACITY TABLE DXIX

TABLES OF LINEAR RESULTS

MODE : 0

Opacity table : DXIX

Mass : 0.8 Solar masses

Luminosity (solar luminosities)

Teff	1,000	3,000	6,000	10,000	15,000	20,000
5,000	19.710	58.450	101.900	---	---	---
5,500	13.790	38.630	67.470	---	---	---
6,000	10.520	29.370	51.320	74.110	---	---
6,500	7.410	20.690	38.910	53.940	---	---
7,000	5.780	16.210	31.450	50.300	0.800	---
7,500	4.200	11.780	23.150	37.430	10.260	---
8,000	3.590	9.990	21.820	34.630	114.400	0.210
9,000	2.440	6.850	14.950	26.420	33.260	0.390
10,000	1.670	4.670	10.230	18.570	23.200	23.960
12,000	0.910	2.550	5.300	9.930	15.020	16.060
15,000	0.460	1.240	2.580	4.480	6.960	8.620
20,000	0.180	0.450	0.910	1.650	2.810	3.520
25,000	0.870	0.210	0.400	0.760	1.020	2.630
30,000	0.490	0.120	0.210	0.390	0.420	1.130

TABLE OF ADIABATIC PERIODS

MODE : 0

Opacity table : DXIX

Mass : 0.8 Solar masses

Luminosity (solar luminosities)

Teff	1,000	3,000	6,000	10,000	15,000	20,000
5,000	19.650	65.410	185.600	---	---	---
5,500	13.810	44.530	115.500	---	---	---
6,000	10.650	33.720	83.560	245.600	---	---
6,500	7.590	23.510	55.610	136.500	---	---
7,000	5.930	18.030	41.570	94.550	410.400	---
7,500	4.290	12.740	28.450	60.340	154.300	---
8,000	3.650	10.730	23.610	48.670	111.300	217.000
9,000	2.460	7.030	14.970	29.200	58.000	119.000
10,000	1.670	4.660	9.650	18.120	33.400	57.540
12,000	0.910	2.480	4.840	8.860	15.500	24.060
15,000	0.460	1.200	2.340	4.050	6.660	9.960
20,000	0.180	0.440	0.840	1.410	2.240	3.210
25,000	0.870	0.210	0.380	0.650	1.020	1.420
30,000	0.490	0.120	0.210	0.350	0.540	0.750

TABLES OF LINEAR RESULTS

TABLE OF NON-ADIABATIC Q VALUES

MODE : 0 Opacity table : DXIX Mass : 0.8 Solar masses

Luminosity (solar luminosities)

Teff	1,000	3,000	6,000	10,000	15,000	20,000
5,000	0.064	0.083	0.086	---	---	---
5,500	0.059	0.073	0.075	---	---	---
6,000	0.055	0.068	0.071	0.069	---	---
6,500	0.051	0.063	0.071	0.067	---	---
7,000	0.049	0.061	0.070	0.076	0.001	---
7,500	0.047	0.058	0.068	0.075	0.015	1.643
8,000	0.046	0.057	0.074	0.080	0.094	---
9,000	0.045	0.055	0.071	0.086	0.080	0.001
10,000	0.043	0.053	0.069	0.085	0.079	0.065
12,000	0.041	0.050	0.063	0.079	0.088	0.076
15,000	0.038	0.045	0.056	0.067	0.076	0.076
20,000	0.036	0.040	0.049	0.060	0.076	0.076
25,000	0.354	0.038	0.044	0.055	0.054	0.114
30,000	0.347	0.037	0.040	0.050	0.039	0.085

TABLE OF ADIABATIC Q VALUES

MODE : 0 Opacity table : DXIX Mass : 0.8 Solar masses

Luminosity (solar luminosities)

Teff	1,000	3,000	6,000	10,000	15,000	20,000
5,000	0.064	0.093	0.157	---	---	---
5,500	0.059	0.084	0.129	---	---	---
6,000	0.056	0.078	0.115	0.230	---	---
6,500	0.053	0.072	0.101	0.169	---	---
7,000	0.051	0.068	0.093	0.144	0.460	---
7,500	0.048	0.063	0.084	0.121	0.228	---
8,000	0.047	0.061	0.080	0.112	0.189	4.408
9,000	0.045	0.056	0.071	0.095	0.139	0.230
10,000	0.043	0.053	0.065	0.083	0.113	0.157
12,000	0.041	0.049	0.057	0.071	0.091	0.114
15,000	0.038	0.044	0.051	0.060	0.073	0.088
20,000	0.036	0.040	0.045	0.052	0.060	0.070
25,000	0.354	0.038	0.042	0.047	0.054	0.062
30,000	0.348	0.037	0.039	0.044	0.050	0.057

TABLES OF LINEAR RESULTS

TABLE OF NON-ADIABATIC GROWTH RATES

MODE : 0 Opacity table : DXIX Mass : 0.8 Solar masses

Teff	Luminosity (solar luminosities)					
	1,000	3,000	6,000	10,000	15,000	20,000
5,000	0.223	2.295	3.565	---	---	---
5,500	0.346	1.706	2.708	---	---	---
6,000	0.384	1.159	1.259	2.172	---	---
6,500	0.228	0.613	0.166	0.544	---	---
7,000	0.627	0.209	-0.865	-1.590	0.250	-5.478
7,500	-0.566	-0.284	-0.790	-0.693	0.384	-1.243
8,000	-0.964	-0.397	-1.523	-0.656	6.970	-0.230
9,000	-0.165	-0.680	-1.477	-1.355	0.641	-0.303
10,000	-0.170	-0.778	-1.327	-1.410	0.577	1.133
12,000	-0.104	-0.650	-1.074	-1.056	0.233	0.819
15,000	-0.397	-0.395	-0.953	-1.013	-0.704	0.934
20,000	-0.128	-0.181	-0.675	-1.285	-1.422	0.703
25,000	-0.419	-0.112	-0.442	-0.804	-0.487	0.499
30,000	-0.167	-0.475	-0.324	-0.559	-0.742	0.548

TABLE OF NON-ADIABATIC PHI

MODE : 0 Opacity table : DXIX Mass : 0.8 Solar masses

Teff	Luminosity (solar luminosities)					
	1,000	3,000	6,000	10,000	15,000	20,000
5,000	173.000	170.100	158.800	---	183.500	---
5,500	176.800	158.300	153.800	---	181.200	---
6,000	167.400	142.600	135.500	139.600	182.100	---
6,500	143.200	123.400	105.300	121.900	181.000	---
7,000	116.400	96.500	75.900	70.600	---	---
7,500	89.800	67.900	63.800	79.900	96.200	---
8,000	71.400	58.400	11.700	71.900	137.100	103.270
9,000	31.100	14.300	-14.600	11.700	102.900	100.200
10,000	0.600	-14.000	-34.900	-28.000	104.500	104.600
12,000	-17.600	-34.600	-46.500	-47.900	112.800	99.200
15,000	-16.800	-40.700	-52.000	-38.900	-40.700	105.700
20,000	-12.400	-28.500	-52.000	-55.500	-65.800	146.800
25,000	---	-22.300	-43.600	-64.300	96.500	-90.700
30,000	-2.000	-18.200	-32.300	-57.400	122.900	-109.800

TABLES OF LINEAR RESULTS

TABLE OF NON-ADIABATIC PERIODS

MODE : 1 Opacity table : DXIX Mass : 0.8 Solar masses

Luminosity (solar luminosities)						
Teff	1,000	3,000	6,000	10,000	15,000	20,000
5,000	10.680	24.380	39.140	---	71.910	78.290
5,500	7.920	18.270	29.790	---	123.100	67.150
6,000	6.380	14.850	24.660	19.230	53.560	57.330
6,500	4.700	11.170	19.460	19.690	43.270	44.930
7,000	3.720	8.900	11.530	27.650	58.080	38.530
7,500	2.740	6.770	8.910	12.700	25.590	22.500
8,000	2.360	5.860	10.680	70.850	41.290	17.620
9,000	1.640	4.250	7.730	8.020	6.300	18.270
10,000	1.150	3.020	5.610	5.630	10.220	399.700
12,000	0.650	1.730	3.180	4.740	4.510	2.760
15,000	0.340	0.880	1.690	2.610	7.050	2.960
20,000	0.130	0.340	0.640	1.060	1.690	2.200
25,000	0.640	0.160	0.300	0.500	0.810	1.300
30,000	0.360	0.920	0.170	0.270	0.700	0.700

TABLE OF ADIABATIC PERIODS

MODE : 1 Opacity table : DXIX Mass : 0.8 Solar masses

Luminosity (solar luminosities)						
Teff	1,000	3,000	6,000	10,000	15,000	20,000
5,000	10.590	24.270	39.850	---	74.720	91.380
5,500	7.870	18.480	30.680	---	57.660	70.250
6,000	6.360	15.100	25.260	35.910	47.510	57.900
6,500	4.770	11.510	19.460	27.770	36.660	44.680
7,000	3.830	9.360	15.970	22.850	30.150	36.760
7,500	2.850	7.070	12.220	17.610	23.170	28.250
8,000	2.450	6.130	10.670	15.450	20.310	24.730
9,000	1.680	4.270	7.550	11.070	14.560	17.660
10,000	1.150	2.950	5.300	7.910	10.470	12.640
12,000	0.640	1.630	2.920	4.550	6.190	7.410
15,000	0.340	0.820	1.500	2.360	3.320	4.070
20,000	0.130	0.320	0.560	0.890	1.300	1.690
25,000	0.640	0.160	0.270	0.420	0.610	0.800
30,000	0.360	0.900	0.160	0.230	0.330	0.430

TABLES OF LINEAR RESULTS

TABLE OF NON-ADIABATIC Q VALUES

MODE : 1 Opacity table : DXIX Mass : 0.8 Solar masses

Luminosity (solar luminosities)						
Teff	1,000	3,000	6,000	10,000	15,000	20,000
5,000	0.035	0.035	0.033	---	0.031	0.027
5,500	0.034	0.034	0.033	---	---	0.030
6,000	0.034	0.034	0.034	0.018	0.037	0.032
6,500	0.033	0.034	0.035	0.024	0.039	0.033
7,000	0.032	0.033	0.026	0.042	0.065	0.035
7,500	0.031	0.033	0.026	0.025	0.038	0.027
8,000	0.031	0.033	0.036	0.163	0.070	0.024
9,000	0.030	0.034	0.037	0.026	0.015	0.035
10,000	0.030	0.034	0.038	0.026	0.035	1.093
12,000	0.029	0.034	0.038	0.038	0.026	0.020
15,000	0.028	0.032	0.037	0.039	0.077	0.026
20,000	0.027	0.030	0.034	0.038	0.045	0.048
25,000	0.263	0.029	0.033	0.036	0.043	0.056
30,000	0.253	0.286	0.032	0.034	0.065	0.053

TABLE OF ADIABATIC Q VALUES

MODE : 1 Opacity table : DXIX Mass : 0.8 Solar masses

Luminosity (solar luminosities)						
Teff	1,000	3,000	6,000	10,000	15,000	20,000
5,000	0.034	0.035	0.034	---	0.032	0.031
5,500	0.034	0.035	0.034	---	0.032	0.032
6,000	0.034	0.035	0.035	0.034	0.033	0.032
6,500	0.033	0.035	0.035	0.034	0.033	0.033
7,000	0.033	0.035	0.036	0.035	0.034	0.033
7,500	0.032	0.035	0.036	0.035	0.034	0.034
8,000	0.032	0.035	0.036	0.036	0.034	0.034
9,000	0.031	0.034	0.036	0.036	0.035	0.034
10,000	0.030	0.033	0.036	0.036	0.035	0.035
12,000	0.029	0.032	0.035	0.036	0.036	0.035
15,000	0.028	0.030	0.033	0.035	0.036	0.036
20,000	0.027	0.029	0.030	0.033	0.035	0.037
25,000	0.263	0.029	0.029	0.030	0.033	0.035
30,000	0.254	0.281	0.029	0.029	0.031	0.032

TABLES OF LINEAR RESULTS

TABLE OF NON-ADIABATIC GROWTH RATES

MODE : 1 Opacity table : DXIX Mass : 0.8 Solar masses

Luminosity (solar luminosities)						
Teff	1,000	3,000	6,000	10,000	15,000	20,000
5,000	0.113	0.315	-0.305	---	-0.137	1.064
5,500	0.176	0.364	-0.951	---	---	0.518
6,000	0.289	0.248	-0.383	-1.677	-0.435	0.402
6,500	0.367	0.188	-0.356	-0.754	0.771	0.642
7,000	0.258	0.243	-1.420	0.320	2.204	0.760
7,500	0.767	-0.287	-0.598	-0.635	1.775	0.936
8,000	-0.256	-0.394	-0.582	-3.921	1.167	-1.264
9,000	-0.312	-0.657	-0.830	0.217	-0.995	0.185
10,000	-0.469	-0.671	-0.735	0.398	1.574	-13.600
12,000	-0.399	-0.609	-0.538	-0.628	0.789	-2.575
15,000	-0.191	-0.563	-0.336	-0.769	-7.215	-0.961
20,000	-0.913	-0.399	-0.298	-0.327	-1.451	-0.441
25,000	-0.517	-0.348	-0.362	-0.932	-0.369	-0.470
30,000	-0.256	-0.287	-0.377	-0.197	-0.694	-0.946

TABLE OF NON-ADIABATIC PHI

MODE : 1 Opacity table : DXIX Mass : 0.8 Solar masses

Luminosity (solar luminosities)						
Teff	1,000	3,000	6,000	10,000	15,000	20,000
5,000	171.100	169.100	158.700	---	154.800	147.000
5,500	176.100	162.200	157.900	---	---	142.700
6,000	174.300	152.200	153.100	174.100	151.700	139.900
6,500	158.900	141.000	159.100	145.600	144.300	135.700
7,000	138.000	117.800	163.400	144.300	124.800	130.800
7,500	113.600	78.800	140.800	130.900	133.800	124.700
8,000	93.700	61.500	173.500	230.700	111.600	126.600
9,000	43.000	-27.300	-150.300	122.600	157.500	94.500
10,000	-4.100	-55.400	---	111.700	116.900	188.600
12,000	-31.200	-71.000	-148.000	160.700	105.300	87.100
15,000	-35.100	-71.300	-143.200	173.800	104.700	124.500
20,000	-22.000	-58.100	-113.800	157.900	112.700	94.900
25,000	-19.500	-41.600	-92.300	172.200	112.000	87.300
30,000	-14.200	-34.100	-71.500	212.200	-75.700	92.900

TABLES OF LINEAR RESULTS

TABLE OF NON-ADIABATIC PERIODS

MODE : 0 Opacity table : DXIX Mass : 1.0 Solar masses

Luminosity (solar luminosities)						
Teff	1,000	3,000	6,000	10,000	15,000	20,000
5,000	16.160	48.210	89.360	131.400	37.150	83.200
5,500	11.420	32.190	60.420	87.890	40.770	67.370
6,000	8.790	24.280	45.860	66.480	87.830	59.860
6,500	6.250	17.200	33.030	47.700	0.460	47.910
7,000	4.900	13.460	26.200	41.060	65.420	0.190
7,500	3.570	9.750	19.180	35.430	46.080	56.630
8,000	3.060	8.330	16.900	29.120	41.860	0.220
9,000	2.080	5.680	11.360	22.320	32.820	16.400
10,000	1.420	3.870	7.830	14.700	21.150	25.680
12,000	0.780	2.110	---	7.670	12.280	0.340
15,000	0.400	1.030	2.040	3.680	9.250	18.180
20,000	0.160	0.380	0.730	1.280	2.120	3.090
25,000	0.760	0.180	---	0.580	1.000	1.470
30,000	0.430	0.100	---	0.300	0.520	0.860

TABLE OF ADIABATIC PERIODS

MODE : 0 Opacity table : DXIX Mass : 1.0 Solar masses

Luminosity (solar luminosities)						
Teff	1,000	3,000	6,000	10,000	15,000	20,000
5,000	16.130	50.100	121.000	328.700	---	---
5,500	11.420	34.650	80.310	187.100	---	---
6,000	8.820	26.480	59.880	130.600	415.100	---
6,500	6.320	18.670	41.080	84.390	195.500	---
7,000	4.960	14.430	31.180	62.070	131.000	376.700
7,500	3.610	10.290	21.760	41.820	80.990	162.200
8,000	3.080	8.710	18.230	34.470	64.600	119.400
9,000	2.090	5.780	11.780	21.520	38.130	62.630
10,000	1.420	3.860	7.710	13.710	23.350	36.450
12,000	0.780	2.080	---	6.920	11.440	16.810
15,000	0.400	1.020	1.940	3.250	5.130	7.350
20,000	0.160	0.380	0.710	1.160	1.780	2.480
25,000	0.760	0.180	---	0.530	0.820	1.120
30,000	0.430	0.100	---	0.290	0.440	0.600

TABLES OF LINEAR RESULTS

TABLE OF NON-ADIABATIC Q VALUES

MODE : 0 Opacity table : DXIX Mass : 1.0 Solar masses

Luminosity (solar luminosities)

Teff	1,000	3,000	6,000	10,000	15,000	20,000
5,000	0.059	0.077	0.085	0.085	0.018	0.032
5,500	0.055	0.068	0.075	0.075	0.026	0.034
6,000	0.052	0.063	0.070	0.070	0.068	0.037
6,500	0.049	0.059	0.067	0.066	---	0.039
7,000	0.047	0.056	0.065	0.070	0.082	---
7,500	0.045	0.054	0.063	0.079	0.076	0.076
8,000	0.044	0.053	0.064	0.075	0.079	---
9,000	0.043	0.051	0.061	0.081	0.088	0.035
10,000	0.041	0.049	0.059	0.075	0.080	0.078
12,000	0.039	0.046	---	0.068	0.080	0.002
15,000	0.037	0.042	0.050	0.061	0.113	0.180
20,000	0.036	0.038	0.044	0.052	0.064	0.075
25,000	0.348	0.037	---	0.048	0.060	0.071
30,000	0.339	0.036	---	0.043	0.054	0.073

TABLE OF ADIABATIC Q VALUES

MODE : 0 Opacity table : DXIX Mass : 1.0 Solar masses

Luminosity (solar luminosities)

Teff	1,000	3,000	6,000	10,000	15,000	20,000
5,000	0.059	0.080	0.115	0.212	---	---
5,500	0.055	0.073	0.100	0.159	---	---
6,000	0.052	0.068	0.092	0.137	0.321	---
6,500	0.049	0.064	0.083	0.117	0.199	---
7,000	0.047	0.060	0.078	0.105	0.164	0.381
7,500	0.045	0.057	0.072	0.094	0.134	0.216
8,000	0.045	0.055	0.069	0.089	0.123	0.183
9,000	0.043	0.052	0.063	0.078	0.102	0.136
10,000	0.041	0.049	0.058	0.070	0.088	0.111
12,000	0.039	0.045	---	0.062	0.075	0.089
15,000	0.037	0.042	0.047	0.054	0.063	0.073
20,000	0.036	0.038	0.042	0.047	0.054	0.060
25,000	0.349	0.037	---	0.043	0.049	0.054
30,000	0.340	0.036	---	0.041	0.045	0.050

TABLES OF LINEAR RESULTS

TABLE OF NON-ADIABATIC GROWTH RATES

MODE : 0 Opacity table : DXIX Mass : 1.0 Solar masses

Luminosity (solar luminosities)						
Teff	1,000	3,000	6,000	10,000	15,000	20,000
5,000	0.824	1.346	2.804	3.934	0.493	-0.128
5,500	0.146	1.131	1.806	2.886	-1.486	-0.571
6,000	0.191	0.878	1.409	1.923	3.083	-0.275
6,500	0.134	0.344	0.551	-0.298	0.674	0.681
7,000	0.467	0.655	-0.309	-0.763	-0.905	-0.448
7,500	-0.262	-0.195	-0.499	-2.188	-0.195	0.993
8,000	-0.577	-0.285	-0.783	-1.472	-0.149	0.608
9,000	-0.889	-0.467	-0.908	-1.714	-0.729	1.836
10,000	-0.773	-0.527	-0.976	-1.073	-0.322	0.711
12,000	-0.442	-0.408	---	-0.926	-0.708	0.191
15,000	-0.171	-0.196	-0.677	-1.068	-1.984	0.132
20,000	-0.425	-0.830	-0.408	-1.000	-1.444	-1.817
25,000	-0.139	-0.376	---	-0.674	-1.021	-1.219
30,000	-0.705	-0.140	---	-0.428	-0.626	-0.461

TABLE OF NON-ADIABATIC PHI

MODE : 0 Opacity table : DXIX Mass : 1.0 Solar masses

Luminosity (solar luminosities)						
Teff	1,000	3,000	6,000	10,000	15,000	20,000
5,000	169.700	171.600	162.100	157.900	124.800	155.900
5,500	176.500	159.600	148.600	151.300	139.900	155.700
6,000	172.300	149.500	139.400	140.900	145.600	154.300
6,500	148.000	124.100	114.900	115.400	---	144.600
7,000	120.700	101.600	85.400	82.200	84.300	---
7,500	90.800	71.900	64.600	15.100	94.700	110.200
8,000	71.300	---	35.300	30.900	90.100	---
9,000	32.900	15.000	9.200	-30.100	51.600	127.100
10,000	5.400	-12.400	-19.900	-38.900	59.800	107.900
12,000	-12.300	-32.600	---	-45.900	-26.400	---
15,000	-13.200	-33.500	-46.100	-51.000	---	-90.600
20,000	-11.000	-19.700	-43.100	-51.100	-56.000	-61.600
25,000	-6.900	-15.400	---	-54.400	-70.200	-77.100
30,000	1.900	-13.400	---	-43.900	-67.800	-80.600

TABLES OF LINEAR RESULTS

TABLE OF NON-ADIABATIC PERIODS

MODE : 1 Opacity table : DXIX Mass : 1.0 Solar masses

Luminosity (solar luminosities)						
Teff	1,000	3,000	6,000	10,000	15,000	20,000
5,000	9.400	22.100	36.230	50.170	63.200	48.690
5,500	6.930	16.550	27.340	24.370	58.460	48.620
6,000	5.570	13.290	22.270	20.560	32.380	38.460
6,500	4.110	9.820	16.980	17.710	51.250	28.980
7,000	3.260	7.880	13.400	22.640	20.730	38.210
7,500	2.400	5.890	10.210	11.920	15.390	18.690
8,000	2.060	5.090	9.230	10.410	20.210	31.480
9,000	1.430	3.650	6.680	10.280	13.660	11.600
10,000	1.000	2.590	4.840	7.330	7.090	11.400
12,000	0.570	1.470	---	4.290	3.810	6.100
15,000	0.300	0.750	1.410	2.320	3.200	2.630
20,000	0.120	0.290	0.540	0.880	1.350	1.870
25,000	0.560	0.140	---	0.420	0.630	1.120
30,000	0.310	0.790	---	0.230	0.340	0.660

TABLE OF ADIABATIC PERIODS

MODE : 1 Opacity table : DXIX Mass : 1.0 Solar masses

Luminosity (solar luminosities)						
Teff	1,000	3,000	6,000	10,000	15,000	20,000
5,000	9.350	21.850	36.520	51.890	68.380	83.170
5,500	6.900	16.540	27.970	39.990	52.730	64.170
6,000	5.560	13.460	22.920	32.960	43.430	52.880
6,500	4.150	10.200	17.560	25.430	33.530	40.740
7,000	3.320	8.260	14.340	20.920	27.560	33.510
7,500	2.460	6.200	10.890	16.060	21.240	25.710
8,000	2.120	5.360	9.470	14.050	18.640	22.540
9,000	1.450	3.700	6.640	9.990	13.370	16.210
10,000	1.000	2.540	4.620	7.060	9.610	11.640
12,000	0.560	1.400	---	3.980	5.590	6.840
15,000	0.300	0.710	1.280	2.030	2.900	3.690
20,000	0.120	0.280	0.490	0.760	1.100	1.440
25,000	0.560	0.140	---	0.360	0.520	0.670
30,000	0.310	0.780	---	0.210	0.280	0.360

TABLES OF LINEAR RESULTS

TABLE OF NON-ADIABATIC Q VALUES

MODE : 1 Opacity table : DXIX Mass : 1.0 Solar masses

Luminosity (solar luminosities)						
Teff	1,000	3,000	6,000	10,000	15,000	20,000
5,000	0.034	0.035	0.034	0.032	0.030	0.019
5,500	0.033	0.035	0.034	0.021	0.037	0.025
6,000	0.033	0.034	0.034	0.022	0.025	0.024
6,500	0.032	0.033	0.034	0.024	0.052	0.024
7,000	0.031	0.033	0.033	0.038	0.026	0.039
7,500	0.030	0.033	0.034	0.027	0.025	0.025
8,000	0.030	0.032	0.035	0.027	0.038	0.048
9,000	0.029	0.033	0.036	0.037	0.037	0.025
10,000	0.029	0.033	0.036	0.038	0.027	0.035
12,000	0.028	0.032	---	0.038	0.025	0.032
15,000	0.028	0.031	0.034	0.039	0.039	0.026
20,000	0.027	0.029	0.032	0.036	0.041	0.045
25,000	0.255	0.028	---	0.034	0.038	0.054
30,000	0.243	0.274	---	0.033	0.035	0.047

TABLE OF ADIABATIC Q VALUES

MODE : 1 Opacity table : DXIX Mass : 1.0 Solar masses

Luminosity (solar luminosities)						
Teff	1,000	3,000	6,000	10,000	15,000	20,000
5,000	0.034	0.035	0.035	0.034	0.033	0.032
5,500	0.033	0.035	0.035	0.034	0.033	0.033
6,000	0.033	0.035	0.035	0.035	0.034	0.033
6,500	0.032	0.035	0.036	0.035	0.034	0.034
7,000	0.032	0.035	0.036	0.036	0.035	0.034
7,500	0.031	0.034	0.036	0.036	0.035	0.034
8,000	0.031	0.034	0.036	0.036	0.035	0.035
9,000	0.030	0.033	0.035	0.036	0.036	0.035
10,000	0.029	0.032	0.035	0.036	0.036	0.036
12,000	0.028	0.031	---	0.036	0.037	0.036
15,000	0.028	0.029	0.031	0.034	0.036	0.037
20,000	0.027	0.029	0.029	0.031	0.033	0.035
25,000	0.256	0.028	---	0.029	0.031	0.032
30,000	0.244	0.272	---	0.029	0.029	0.031

TABLES OF LINEAR RESULTS

TABLE OF NON-ADIABATIC GROWTH RATES

MODE : 1 Opacity table : DXIX Mass : 1.0 Solar masses

Luminosity (solar luminosities)

Teff	1,000	3,000	6,000	10,000	15,000	20,000
5,000	0.723	0.235	0.329	-0.279	-0.782	0.483
5,500	0.123	0.395	0.284	-0.896	-2.313	-0.707
6,000	0.196	0.492	0.172	-1.216	-0.643	-0.798
6,500	0.277	0.422	0.101	-1.897	3.549	-0.978
7,000	0.206	0.215	-0.154	-0.613	-0.607	1.198
7,500	0.646	-0.672	-0.525	-0.510	-0.455	-0.171
8,000	-0.381	-0.255	-0.768	-0.435	1.136	3.942
9,000	-0.218	-0.568	-0.847	-0.556	0.602	-0.148
10,000	-0.276	-0.695	-0.710	-0.563	0.441	1.692
12,000	-0.210	-0.681	---	-0.597	0.408	1.401
15,000	-0.100	-0.523	-0.453	-0.492	-1.098	2.159
20,000	-0.438	-0.284	-0.445	-0.221	-0.532	-1.663
25,000	-0.214	-0.211	---	-0.278	-0.780	-0.643
30,000	-0.113	-0.149	---	-0.337	-0.101	-0.588

TABLE OF NON-ADIABATIC PHI

MODE : 1 Opacity table : DXIX Mass : 1.0 Solar masses

Luminosity (solar luminosities)

Teff	1,000	3,000	6,000	10,000	15,000	20,000
5,000	169.600	171.100	164.400	157.400	154.500	102.800
5,500	174.900	167.800	157.000	168.500	179.600	143.500
6,000	176.000	162.900	151.200	172.000	146.000	146.900
6,500	162.200	146.000	143.500	175.200	146.400	141.100
7,000	140.600	125.800	117.500	168.300	---	142.000
7,500	113.200	92.300	81.600	129.500	131.800	153.600
8,000	92.900	70.900	-10.200	126.900	135.300	127.400
9,000	44.300	0.900	-81.800	170.800	131.000	122.600
10,000	5.300	-32.900	-106.500	182.600	112.300	118.000
12,000	-22.700	-54.300	---	198.500	105.500	103.800
15,000	-26.800	-59.200	-96.600	198.800	197.500	78.600
20,000	-18.300	-41.300	-79.400	210.700	142.700	114.200
25,000	-16.000	-29.300	---	243.600	148.700	94.600
30,000	-8.900	-27.300	---	263.500	182.700	105.300

TABLES OF LINEAR RESULTS

TABLE OF NON-ADIABATIC PERIODS

MODE : 0 Opacity table : DXIX Mass : 1.2 Solar masses

Luminosity (solar luminosities)

Teff	1,000	3,000	6,000	10,000	15,000	20,000
5,000	13.860	40.870	78.900	119.900	159.500	171.700
5,500	9.880	27.690	53.150	79.510	107.500	136.600
6,000	7.630	20.980	40.620	60.980	80.280	99.780
6,500	5.460	14.810	29.080	45.860	61.700	80.540
7,000	4.290	11.580	22.700	35.710	58.910	65.110
7,500	3.130	8.460	16.390	27.910	43.640	57.360
8,000	2.690	7.220	14.380	25.590	50.910	27.160
9,000	1.830	4.890	9.660	17.160	28.600	16.690
10,000	1.250	3.340	6.540	11.850	19.660	23.860
12,000	0.690	1.820	3.480	6.210	10.400	13.890
15,000	0.360	0.900	1.730	2.970	4.620	6.180
20,000	0.140	0.340	0.620	1.060	1.680	2.370
25,000	0.680	0.170	0.290	0.480	0.790	1.150
30,000	0.380	0.940	0.160	0.260	0.410	0.600

TABLE OF ADIABATIC PERIODS

MODE : 0 Opacity table : DXIX Mass : 1.2 Solar masses

Luminosity (solar luminosities)

Teff	1,000	3,000	6,000	10,000	15,000	20,000
5,000	13.850	41.210	92.630	201.200	669.900	2543.540
5,500	9.870	28.730	62.960	128.300	298.000	1120.420
6,000	7.630	22.080	47.580	93.880	195.500	558.100
6,500	5.490	15.670	33.110	63.130	121.000	240.200
7,000	4.320	12.180	25.360	47.440	87.380	156.500
7,500	3.150	8.750	17.890	32.660	57.680	95.810
8,000	2.700	7.430	15.070	27.180	47.180	76.140
9,000	1.840	4.960	9.860	17.330	29.020	44.330
10,000	1.250	3.340	6.520	11.230	18.310	27.130
12,000	0.690	1.810	3.380	5.780	9.220	13.070
15,000	0.360	0.890	1.680	2.760	4.240	5.920
20,000	0.140	0.340	0.610	0.990	1.500	2.050
25,000	0.690	0.170	0.290	0.460	0.700	0.930
30,000	0.380	0.940	0.160	0.250	0.370	0.500

TABLES OF LINEAR RESULTS

TABLE OF NON-ADIABATIC Q VALUES

MODE : 0 Opacity table : DXIX Mass : 1.2 Solar masses

Luminosity (solar luminosities)						
Teff	1,000	3,000	6,000	10,000	15,000	20,000
5,000	0.055	0.071	0.082	0.085	0.083	0.072
5,500	0.052	0.064	0.073	0.074	0.074	0.076
6,000	0.049	0.059	0.068	0.070	0.068	0.068
6,500	0.046	0.055	0.065	0.069	0.069	0.073
7,000	0.045	0.053	0.062	0.066	0.081	0.072
7,500	0.043	0.051	0.059	0.068	0.079	0.084
8,000	0.043	0.050	0.059	0.072	0.106	0.046
9,000	0.041	0.048	0.056	0.068	0.084	0.040
10,000	0.040	0.046	0.054	0.067	0.082	0.080
12,000	0.038	0.044	0.051	0.061	0.074	0.081
15,000	0.036	0.040	0.046	0.054	0.062	0.067
20,000	0.035	0.037	0.041	0.047	0.055	0.063
25,000	0.343	0.036	0.038	0.043	0.052	0.061
30,000	0.330	0.356	0.037	0.040	0.047	0.056

TABLE OF ADIABATIC Q VALUES

MODE : 0 Opacity table : DXIX Mass : 1.2 Solar masses

Luminosity (solar luminosities)						
Teff	1,000	3,000	6,000	10,000	15,000	20,000
5,000	0.055	0.072	0.096	0.142	0.350	1.764
5,500	0.052	0.066	0.086	0.120	0.205	0.774
6,000	0.049	0.063	0.080	0.108	0.166	0.381
6,500	0.047	0.058	0.073	0.096	0.135	0.216
7,000	0.045	0.056	0.069	0.088	0.120	0.174
7,500	0.044	0.053	0.064	0.080	0.104	0.140
8,000	0.043	0.052	0.062	0.077	0.098	0.128
9,000	0.041	0.049	0.058	0.069	0.085	0.105
10,000	0.040	0.046	0.054	0.063	0.076	0.091
12,000	0.038	0.043	0.049	0.056	0.066	0.076
15,000	0.036	0.040	0.045	0.050	0.057	0.064
20,000	0.035	0.037	0.040	0.044	0.049	0.054
25,000	0.344	0.036	0.038	0.041	0.045	0.050
30,000	0.332	0.357	0.037	0.039	0.042	0.046

TABLES OF LINEAR RESULTS

TABLE OF NON-ADIABATIC GROWTH RATES

MODE : 0 Opacity table : DXIX Mass : 1.2 Solar masses

Luminosity (solar luminosities)

Teff	1,000	3,000	6,000	10,000	15,000	20,000
5,000	0.322	0.814	2.093	3.088	4.202	0.501
5,500	0.733	0.792	1.480	2.151	3.402	3.784
6,000	0.886	0.542	1.071	0.870	1.418	-0.102
6,500	0.877	0.318	0.649	-0.287	0.161	0.461
7,000	0.358	0.114	-0.353	-0.367	-1.676	0.746
7,500	-0.147	-0.183	-0.278	-1.076	-0.760	-0.355
8,000	-0.338	-0.209	-0.672	-1.438	-5.001	3.326
9,000	-0.485	-0.298	-0.704	-1.192	-1.271	2.290
10,000	-0.431	-0.340	-0.761	-1.210	-1.128	0.438
12,000	-0.227	-0.238	-0.652	-0.950	-0.899	-0.561
15,000	-0.758	-0.111	-0.420	-0.894	-0.809	-0.480
20,000	-0.175	-0.364	-0.216	-0.721	-1.275	-1.802
25,000	-0.606	-0.146	-0.108	-0.440	-0.881	-0.119
30,000	-0.370	-0.534	-0.523	-0.277	-0.569	-0.585

TABLE OF NON-ADIABATIC PHI

MODE : 0 Opacity table : DXIX Mass : 1.2 Solar masses

Luminosity (solar luminosities)

Teff	1,000	3,000	6,000	10,000	15,000	20,000
5,000	167.500	175.200	162.600	156.200	156.800	121.700
5,500	175.300	163.400	151.300	149.800	152.600	145.400
6,000	175.000	145.900	137.100	131.100	137.100	145.900
6,500	155.900	131.600	101.400	96.200	115.900	114.200
7,000	127.300	109.800	92.800	91.500	58.800	112.700
7,500	92.300	66.100	69.400	46.700	71.500	90.500
8,000	69.600	55.100	29.900	7.800	-62.300	113.000
9,000	35.700	23.500	8.400	-9.500	-12.400	127.900
10,000	8.000	-9.200	-13.400	-36.000	-38.700	83.200
12,000	-10.200	-25.200	-35.800	-42.600	-48.900	-21.300
15,000	-9.500	-27.900	-42.200	-45.000	-34.500	-5.100
20,000	-8.300	-13.700	-32.200	-48.400	-47.700	-41.000
25,000	-4.100	-13.600	-23.400	-45.500	-61.000	-67.100
30,000	3.500	-8.900	-17.800	-33.600	-56.100	-69.500

TABLES OF LINEAR RESULTS

TABLE OF NON-ADIABATIC PERIODS

MODE : 1 Opacity table : DXIX Mass : 1.2 Solar masses

Luminosity (solar luminosities)

Teff	1,000	3,000	6,000	10,000	15,000	20,000
5,000	8.440	20.160	33.620	47.800	61.020	70.060
5,500	6.180	15.090	25.140	36.080	30.680	46.200
6,000	4.970	12.070	20.520	29.610	23.280	36.880
6,500	3.670	8.890	15.210	23.050	22.320	48.200
7,000	2.910	7.080	12.220	18.670	30.420	23.060
7,500	2.140	5.290	9.240	10.920	14.740	17.940
8,000	1.850	4.580	8.270	12.800	19.670	8.850
9,000	1.280	3.190	5.970	9.220	8.920	8.690
10,000	0.900	2.260	4.250	6.690	6.180	10.750
12,000	0.510	1.280	2.370	3.870	5.390	6.470
15,000	0.270	0.660	1.230	2.020	2.870	3.530
20,000	0.100	0.260	0.470	0.760	1.130	1.550
25,000	0.500	0.130	0.220	0.360	0.540	0.720
30,000	0.270	0.700	0.130	0.200	0.300	0.380

TABLE OF ADIABATIC PERIODS

MODE : 1 Opacity table : DXIX Mass : 1.2 Solar masses

Luminosity (solar luminosities)

Teff	1,000	3,000	6,000	10,000	15,000	20,000
5,000	8.410	19.940	33.740	48.500	63.840	77.450
5,500	6.160	15.040	25.710	37.290	49.150	59.700
6,000	4.960	12.200	21.010	30.660	40.490	49.170
6,500	3.690	9.190	16.010	23.580	31.270	37.890
7,000	2.950	7.410	13.010	19.320	25.700	31.150
7,500	2.180	5.530	9.830	14.750	19.790	23.960
8,000	1.880	4.770	8.520	12.860	17.340	21.010
9,000	1.300	3.280	5.930	9.070	12.380	15.150
10,000	0.900	2.250	4.100	6.340	8.800	10.860
12,000	0.510	1.240	2.210	3.530	5.040	6.300
15,000	0.270	0.640	1.130	1.780	2.570	3.310
20,000	0.100	0.260	0.440	0.670	0.960	1.250
25,000	0.500	0.130	0.220	0.330	0.460	0.580
30,000	0.270	0.700	0.120	0.190	0.260	0.320

TABLES OF LINEAR RESULTS

TABLE OF NON-ADIABATIC Q VALUES

MODE : 1 Opacity table : DXIX Mass : 1.2 Solar masses

Luminosity (solar luminosities)						
Teff	1,000	3,000	6,000	10,000	15,000	20,000
5,000	0.034	0.035	0.035	0.034	0.032	0.030
5,500	0.032	0.035	0.034	0.034	0.021	0.026
6,000	0.032	0.034	0.035	0.034	0.020	0.025
6,500	0.031	0.033	0.034	0.035	0.025	0.043
7,000	0.030	0.033	0.033	0.035	0.042	0.026
7,500	0.030	0.032	0.033	0.027	0.027	0.026
8,000	0.029	0.032	0.034	0.036	0.041	0.015
9,000	0.029	0.031	0.035	0.037	0.026	0.021
10,000	0.028	0.031	0.035	0.038	0.026	0.036
12,000	0.028	0.031	0.034	0.038	0.039	0.038
15,000	0.027	0.030	0.033	0.037	0.039	0.038
20,000	0.026	0.028	0.031	0.034	0.037	0.041
25,000	0.248	0.028	0.030	0.032	0.035	0.038
30,000	0.235	0.265	0.029	0.032	0.033	0.035

TABLE OF ADIABATIC Q VALUES

MODE : 1 Opacity table : DXIX Mass : 1.2 Solar masses

Luminosity (solar luminosities)						
Teff	1,000	3,000	6,000	10,000	15,000	20,000
5,000	0.033	0.035	0.035	0.034	0.033	0.033
5,500	0.032	0.035	0.035	0.035	0.034	0.033
6,000	0.032	0.035	0.035	0.035	0.034	0.034
6,500	0.031	0.034	0.036	0.036	0.035	0.034
7,000	0.031	0.034	0.036	0.036	0.035	0.035
7,500	0.030	0.033	0.035	0.036	0.036	0.035
8,000	0.030	0.033	0.035	0.036	0.036	0.035
9,000	0.029	0.032	0.035	0.036	0.036	0.036
10,000	0.029	0.031	0.034	0.036	0.036	0.036
12,000	0.028	0.030	0.032	0.034	0.036	0.037
15,000	0.027	0.029	0.030	0.032	0.034	0.036
20,000	0.026	0.028	0.029	0.030	0.032	0.033
25,000	0.249	0.027	0.029	0.029	0.030	0.031
30,000	0.236	0.265	0.028	0.029	0.029	0.030

TABLES OF LINEAR RESULTS

TABLE OF NON-ADIABATIC GROWTH RATES

MODE : 1 Opacity table : DXIX Mass : 1.2 Solar masses

Teff	Luminosity (solar luminosities)					
	1,000	3,000	6,000	10,000	15,000	20,000
5,000	0.452	0.214	0.377	0.416	-0.460	5.469
5,500	0.844	0.363	0.433	-0.163	-1.354	-1.284
6,000	0.122	0.431	0.292	-0.157	-2.252	3.490
6,500	0.211	0.462	0.160	-0.297	-1.545	0.534
7,000	0.168	0.319	-0.395	-0.144	-0.283	-0.455
7,500	0.428	-0.115	-0.349	-0.754	-0.646	-0.163
8,000	-0.345	-0.199	-0.808	-0.818	1.077	-0.421
9,000	-0.139	-0.444	-0.796	-0.830	0.343	-0.771
10,000	-0.171	-0.654	-0.749	-0.754	0.386	0.608
12,000	-0.121	-0.626	-0.605	-0.551	-0.587	-0.353
15,000	-0.541	-0.404	-0.549	-0.380	-0.584	-0.707
20,000	-0.222	-0.172	-0.449	-0.366	-0.253	-0.822
25,000	-0.104	-0.126	-0.346	-0.425	-0.140	-1.387
30,000	-0.610	-0.749	-0.302	-0.418	-0.282	-0.851

TABLE OF NON-ADIABATIC PHI

MODE : 1 Opacity table : DXIX Mass : 1.2 Solar masses

Teff	Luminosity (solar luminosities)					
	1,000	3,000	6,000	10,000	15,000	20,000
5,000	169.200	173.800	165.900	158.000	156.000	156.100
5,500	173.100	171.200	159.400	156.100	171.800	137.800
6,000	176.800	161.400	---	149.700	176.800	145.800
6,500	167.600	150.500	127.600	149.900	---	148.600
7,000	145.700	132.700	112.200	147.900	154.200	131.700
7,500	113.900	83.600	76.400	141.500	126.600	130.300
8,000	89.300	67.600	1.000	-144.800	139.500	---
9,000	49.100	23.600	-46.500	-131.600	127.100	131.700
10,000	9.800	-20.700	-67.800	-131.200	115.000	125.800
12,000	-17.700	-41.800	-77.900	-136.700	-179.700	139.200
15,000	-19.500	-49.300	-75.300	-129.400	-168.800	173.400
20,000	-14.100	---	-61.800	-100.400	-175.400	145.300
25,000	-12.600	-24.400	-46.500	-82.800	-154.200	143.100
30,000	-5.900	-21.000	-34.400	-67.400	-118.800	170.400

TABLE OF NON-ADIABATIC PERIODS

RESULTS FOR OPACITY TABLE BD9C

TABLES OF LINEAR RESULTS

MODE : 0

Opacity table : BD9C

Mass : 0.8 Solar masses

Luminosity (solar luminosities)

Teff	1,000	3,000	6,000	10,000	15,000	20,000
5,000	---	56.430	118.600	267.600	76.250	86.110
5,500	---	40.220	102.200	171.300	---	---
6,000	9.330	34.910	71.460	100.100	37.080	76.360
6,500	7.810	27.330	49.350	68.580	82.200	---
7,000	6.490	20.010	33.900	46.840	56.410	64.610
7,500	4.480	13.110	21.590	28.430	42.940	---
8,000	3.730	10.730	17.200	22.510	39.050	27.760
9,000	2.410	7.010	14.590	13.240	38.770	32.330
10,000	1.610	4.890	11.280	23.990	11.030	---
12,000	0.870	2.550	6.300	12.820	18.790	6.180
15,000	0.410	1.200	2.650	5.600	10.340	9.350
20,000	0.170	0.450	0.960	1.960	3.460	4.600
25,000	0.850	0.210	0.850	0.820	1.530	2.020
30,000	0.410	0.100	0.840	0.690	0.940	1.620

TABLE OF ADIABATIC PERIODS

MODE : 0

Opacity table : BD9C

Mass : 0.8 Solar masses

Luminosity (solar luminosities)

Teff	1,000	3,000	6,000	10,000	15,000	20,000
5,000	---	56.520	---	363.900	---	---
5,500	---	40.230	107.800	334.500	---	---
6,000	9.340	35.130	85.680	234.600	---	---
6,500	7.810	28.150	65.750	172.800	1521.320	---
7,000	6.490	21.440	49.600	124.200	744.600	1023.190
7,500	4.490	14.790	33.630	80.010	254.700	---
8,000	3.760	12.300	27.670	64.260	180.600	487.540
9,000	2.450	7.820	17.060	37.440	88.280	231.600
10,000	1.620	5.010	10.590	22.150	47.310	---
12,000	0.860	2.400	4.990	10.140	20.290	35.310
15,000	0.410	1.110	2.140	4.060	7.740	13.500
20,000	0.170	0.440	0.800	1.410	2.530	3.640
25,000	0.850	0.210	0.370	0.610	1.040	1.640
30,000	0.410	0.100	0.170	0.280	0.450	0.710

TABLES OF LINEAR RESULTS

TABLE OF NON-ADIABATIC Q VALUES

MODE : 0 Opacity table : BD9C Mass : 0.8 Solar masses

Luminosity (solar luminosities)

Teff	1,000	3,000	6,000	10,000	15,000	20,000
5,000	---	0.077	0.101	0.155	0.032	0.030
5,500	---	0.073	0.114	0.130	---	---
6,000	0.053	0.083	0.105	0.101	0.027	0.077
6,500	0.054	0.080	0.089	0.085	0.025	---
7,000	0.055	0.072	0.076	0.071	0.063	0.058
7,500	0.051	0.062	0.063	0.057	0.063	---
8,000	0.048	0.059	0.058	0.052	0.066	0.038
9,000	0.044	0.054	0.070	0.043	0.093	0.063
10,000	0.042	0.053	0.076	0.110	0.100	---
12,000	---	0.050	0.075	0.102	0.110	0.029
15,000	0.037	0.045	0.062	0.089	0.121	0.089
20,000	0.036	0.039	0.051	0.072	0.093	0.100
25,000	0.348	0.037	0.091	0.060	0.082	0.088
30,000	0.332	0.036	0.180	0.051	0.100	0.140

TABLE OF ADIABATIC Q VALUES

MODE : 0 Opacity table : BD9C Mass : 0.8 Solar masses

Luminosity (solar luminosities)

Teff	1,000	3,000	6,000	10,000	15,000	20,000
5,000	---	0.077	0.102	0.210	---	---
5,500	---	0.073	0.120	0.255	---	---
6,000	0.053	0.084	0.126	0.236	---	---
6,500	0.054	0.082	0.119	0.213	1.723	---
7,000	0.055	0.077	0.111	0.189	0.832	2.031
7,500	0.051	0.070	0.099	0.160	0.375	---
8,000	0.049	0.067	0.093	0.148	0.305	0.903
9,000	0.045	0.060	0.081	0.122	0.211	0.448
10,000	0.042	0.055	0.071	0.102	0.160	---
12,000	---	0.047	0.059	0.081	0.119	0.168
15,000	0.037	0.042	0.050	0.065	0.091	0.128
20,000	0.036	0.038	0.043	0.052	0.068	0.079
25,000	0.349	0.037	0.039	0.045	0.056	0.071
30,000	0.333	0.036	0.037	0.040	0.048	0.061

TABLES OF LINEAR RESULTS

TABLE OF NON-ADIABATIC GROWTH RATES

MODE : 0 Opacity table : BD9C Mass : 0.8 Solar masses

Luminosity (solar luminosities)

Teff	1,000	3,000	6,000	10,000	15,000	20,000
5,000	---	0.700	0.680	4.334	0.455	0.626
5,500	---	0.168	1.804	5.277	---	---
6,000	0.545	0.536	2.872	4.754	0.404	5.961
6,500	0.174	0.950	3.025	4.474	-1.358	---
7,000	0.846	1.154	2.649	3.536	-1.546	0.216
7,500	0.962	0.851	1.435	2.191	-1.773	---
8,000	0.115	0.255	0.573	2.398	-0.822	1.136
9,000	-0.686	-0.993	0.198	1.423	-1.240	0.513
10,000	-0.194	-1.587	-4.025	-3.364	0.159	---
12,000	---	-1.251	-2.048	-1.968	-1.170	0.233
15,000	-0.408	-0.880	-1.313	-1.160	-1.099	0.272
20,000	-0.111	-0.305	-0.725	-0.720	-0.137	0.426
25,000	-0.566	-0.140	-0.704	-0.756	-0.144	0.354
30,000	-0.247	-0.506	-0.449	-0.984	0.373	-5.989

TABLE OF NON-ADIABATIC PHI

MODE : 0 Opacity table : BD9C Mass : 0.8 Solar masses

Luminosity (solar luminosities)

Teff	1,000	3,000	6,000	10,000	15,000	20,000
5,000	---	171.600	172.700	172.700	174.500	170.100
5,500	---	173.400	172.200	176.200	---	---
6,000	171.100	171.400	175.800	175.200	175.300	175.500
6,500	170.900	174.900	175.100	173.300	177.800	---
7,000	171.500	173.700	169.500	165.000	166.200	161.700
7,500	176.000	156.100	153.700	153.900	121.000	---
8,000	164.200	132.600	143.600	152.600	107.200	150.100
9,000	94.500	51.700	144.400	145.000	137.700	108.100
10,000	24.900	-19.600	-60.800	-50.400	-36.300	---
12,000	---	-46.800	-69.800	-65.900	-49.400	123.600
15,000	-13.000	-55.500	-68.400	-71.300	-52.300	75.200
20,000	-3.000	-37.100	-61.000	-64.400	-40.700	65.900
25,000	-9.700	-21.600	-104.700	-52.500	-38.800	59.300
30,000	-6.400	-32.400	-155.100	-42.800	-76.100	3.300

TABLES OF LINEAR RESULTS

TABLE OF NON-ADIABATIC PERIODS

MODE : 1 Opacity table : BD9C Mass : 0.8 Solar masses

Luminosity (solar luminosities)						
Teff	1,000	3,000	6,000	10,000	15,000	20,000
5,000	---	30.480	44.750	62.630	49.830	85.540
5,500	---	20.840	32.380	43.030	---	---
6,000	6.390	14.630	22.080	29.050	35.300	49.430
6,500	4.820	11.230	17.200	21.980	27.290	---
7,000	3.660	9.080	13.610	17.360	21.900	28.230
7,500	2.790	6.800	9.860	13.250	33.000	---
8,000	2.410	5.790	8.310	11.800	15.650	16.010
9,000	1.640	3.810	8.930	8.080	36.480	11.730
10,000	1.140	3.190	3.820	5.340	5.660	---
12,000	0.660	1.770	3.140	3.040	4.320	5.250
15,000	0.320	0.900	1.580	1.690	2.030	1.440
20,000	0.130	0.380	0.670	1.080	0.670	0.900
25,000	0.610	0.170	0.580	0.540	0.970	0.940
30,000	0.290	0.790	0.710	0.350	0.630	0.880

TABLE OF ADIABATIC PERIODS

MODE : 1 Opacity table : BD9C Mass : 0.8 Solar masses

Luminosity (solar luminosities)						
Teff	1,000	3,000	6,000	10,000	15,000	20,000
5,000	---	30.500	44.650	62.230	75.680	85.130
5,500	---	20.800	32.210	42.680	---	---
6,000	6.390	14.580	21.980	29.270	36.030	41.210
6,500	4.820	11.220	17.230	22.700	28.040	---
7,000	3.650	9.110	13.930	18.220	22.380	25.780
7,500	2.790	6.970	10.760	14.110	17.250	---
8,000	2.420	6.090	9.480	12.520	15.280	17.440
9,000	1.680	4.310	6.880	9.270	11.460	13.140
10,000	1.160	3.020	4.930	6.810	8.560	---
12,000	0.650	1.620	2.810	4.100	5.300	6.220
15,000	0.310	0.810	1.400	2.130	2.850	3.410
20,000	0.130	0.340	0.580	0.920	1.330	1.370
25,000	0.610	0.160	0.280	0.440	0.650	0.850
30,000	0.290	0.760	0.130	0.200	0.290	0.380

TABLES OF LINEAR RESULTS

TABLE OF NON-ADIABATIC Q VALUES

MODE : 1 Opacity table : BD9C Mass : 0.8 Solar masses

Luminosity (solar luminosities)						
Teff	1,000	3,000	6,000	10,000	15,000	20,000
5,000	---	0.042	0.038	0.036	0.021	0.029
5,500	---	0.038	0.036	0.033	---	---
6,000	0.036	0.035	0.033	0.029	0.019	0.030
6,500	0.033	0.033	0.031	0.027	0.018	---
7,000	0.031	0.033	0.030	0.026	0.024	0.026
7,500	0.031	0.032	0.029	0.027	0.019	---
8,000	0.031	0.032	0.028	0.027	0.026	0.022
9,000	0.030	0.029	0.027	0.026	0.028	0.023
10,000	0.030	0.035	0.026	0.025	0.037	---
12,000	---	0.035	0.037	0.024	0.025	0.025
15,000	0.028	0.034	0.037	0.027	0.024	0.014
20,000	0.026	0.033	0.036	0.039	0.018	0.020
25,000	0.248	0.030	0.062	0.039	0.052	0.041
30,000	0.238	0.273	0.152	0.037	0.067	0.076

TABLE OF ADIABATIC Q VALUES

MODE : 1 Opacity table : BD9C Mass : 0.8 Solar masses

Luminosity (solar luminosities)						
Teff	1,000	3,000	6,000	10,000	15,000	20,000
5,000	---	0.042	0.038	0.036	0.032	0.029
5,500	---	0.038	0.036	0.033	---	---
6,000	0.036	0.035	0.032	0.029	0.027	0.025
6,500	0.033	0.033	0.031	0.028	0.025	---
7,000	0.031	0.033	0.031	0.028	0.025	0.023
7,500	0.031	0.033	0.032	0.028	0.025	---
8,000	0.031	0.033	0.032	0.029	0.026	0.024
9,000	0.031	0.033	0.033	0.030	0.027	0.025
10,000	0.030	0.033	0.033	0.031	0.029	---
12,000	---	0.032	0.033	0.033	0.031	0.030
15,000	0.028	0.031	0.033	0.034	0.033	0.032
20,000	0.026	0.029	0.031	0.034	0.036	0.030
25,000	0.248	0.028	0.030	0.032	0.035	0.037
30,000	0.239	0.263	0.028	0.029	0.031	0.033

TABLES OF LINEAR RESULTS

TABLE OF NON-ADIABATIC GROWTH RATES

MODE : 1 Opacity table : BD9C Mass : 0.8 Solar masses

Luminosity (solar luminosities)

Teff	1,000	3,000	6,000	10,000	15,000	20,000
5,000	---	0.742	0.191	0.335	-0.298	0.912
5,500	---	0.102	0.272	0.311	---	---
6,000	0.194	0.186	0.204	-0.525	-0.222	-3.571
6,500	0.384	0.189	0.132	-0.444	-0.156	---
7,000	0.681	0.176	-0.208	-0.914	-0.996	-5.030
7,500	0.736	0.226	-0.573	-0.413	-1.501	---
8,000	0.116	0.846	-0.445	-0.267	-0.183	2.607
9,000	-0.313	-1.199	-0.370	0.951	-1.989	1.678
10,000	-0.394	-1.595	0.247	0.840	1.847	---
12,000	---	-0.777	-0.570	-0.444	3.602	1.680
15,000	-0.269	-0.429	-0.514	-0.676	2.327	0.461
20,000	-0.138	-0.417	-0.220	-1.154	2.550	-0.147
25,000	-0.798	-0.539	-0.824	-0.908	-3.111	0.376
30,000	-0.276	-0.623	-0.471	-0.589	-1.240	0.945

TABLE OF NON-ADIABATIC PHI

MODE : 1 Opacity table : BD9C Mass : 0.8 Solar masses

Luminosity (solar luminosities)

Teff	1,000	3,000	6,000	10,000	15,000	20,000
5,000	---	174.800	175.800	174.400	158.700	200.900
5,500	---	175.700	174.800	174.800	---	---
6,000	172.800	173.700	175.500	175.700	169.100	183.400
6,500	173.100	174.700	177.100	174.900	166.600	---
7,000	172.900	177.700	174.200	170.400	175.700	164.700
7,500	177.700	167.100	159.400	165.700	156.100	---
8,000	173.100	149.900	154.100	163.000	160.700	150.400
9,000	116.000	117.700	164.300	153.400	145.200	140.800
10,000	29.300	-91.000	137.700	137.300	129.300	---
12,000	---	-103.200	173.100	113.600	123.600	116.500
15,000	-32.900	-104.000	170.800	125.900	94.100	129.400
20,000	-20.600	-72.600	185.000	147.700	125.100	113.100
25,000	-19.100	-43.000	59.400	136.500	169.500	101.300
30,000	-21.600	-46.400	86.100	143.300	133.700	90.400

TABLES OF LINEAR RESULTS

TABLE OF NON-ADIABATIC PERIODS

MODE : 0 Opacity table : BD9C Mass : 1.0 Solar masses

Luminosity (solar luminosities)						
Teff	1,000	3,000	6,000	10,000	15,000	20,000
5,000	---	---	86.780	186.000	331.100	84.800
5,500	---	29.670	73.100	148.900	199.400	58.100
6,000	---	25.840	63.350	105.900	134.900	---
6,500	6.630	20.660	42.250	63.610	79.970	92.120
7,000	5.380	15.570	29.770	44.230	55.320	62.780
7,500	3.740	10.410	18.980	27.470	33.440	48.100
8,000	3.120	8.560	15.540	21.420	26.190	29.000
9,000	2.040	5.560	10.550	12.140	16.590	---
10,000	1.370	3.730	8.320	17.830	30.480	---
12,000	0.750	2.020	4.590	9.470	17.070	21.800
15,000	0.390	0.990	2.190	4.360	8.020	---
20,000	0.150	0.370	0.730	1.440	2.630	---
25,000	0.740	0.180	0.310	0.600	1.100	1.650
30,000	0.410	0.100	0.170	0.300	0.540	0.820

TABLE OF ADIABATIC PERIODS

MODE : 0 Opacity table : BD9C Mass : 1.0 Solar masses

Luminosity (solar luminosities)						
Teff	1,000	3,000	6,000	10,000	15,000	20,000
5,000	---	---	86.990	194.600	605.400	---
5,500	---	29.670	73.570	178.800	547.200	---
6,000	---	25.830	65.610	146.900	411.800	---
6,500	6.640	20.790	47.480	103.400	260.400	1683.390
7,000	5.380	15.860	35.980	77.380	182.400	706.400
7,500	3.740	10.990	24.680	51.880	113.500	273.000
8,000	3.130	9.170	20.450	42.390	90.140	195.300
9,000	2.060	5.900	12.830	25.670	51.220	---
10,000	1.380	3.830	8.100	15.680	29.770	---
12,000	0.750	1.980	3.920	7.420	13.630	22.110
15,000	0.390	0.960	1.870	3.350	5.840	---
20,000	0.150	0.370	0.660	1.110	1.830	---
25,000	0.740	0.180	0.310	0.500	0.790	1.160
30,000	0.410	0.100	0.170	0.270	0.420	0.600

TABLES OF LINEAR RESULTS

TABLE OF NON-ADIABATIC Q VALUES

MODE : 0 Opacity table : BD9C Mass : 1.0 Solar masses

Luminosity (solar luminosities)						
Teff	1,000	3,000	6,000	10,000	15,000	20,000
5,000	---	---	0.082	0.120	0.158	0.033
5,500	---	0.062	0.091	0.127	0.125	0.029
6,000	---	0.067	0.097	0.111	0.104	---
6,500	0.052	0.070	0.086	0.088	0.081	0.076
7,000	0.051	0.065	0.074	0.075	0.069	0.064
7,500	0.047	0.058	0.062	0.062	0.055	0.062
8,000	0.045	0.054	0.059	0.055	0.050	0.044
9,000	0.042	0.050	0.056	0.044	0.044	---
10,000	0.040	0.047	0.063	0.091	0.115	---
12,000	0.037	0.044	0.061	0.084	0.112	0.066
15,000	0.036	0.041	0.053	0.072	0.098	---
20,000	0.035	0.037	0.044	0.059	0.079	---
25,000	0.339	0.036	0.038	0.049	0.066	0.080
30,000	0.324	0.036	0.037	0.042	0.056	0.069

TABLE OF ADIABATIC Q VALUES

MODE : 0 Opacity table : BD9C Mass : 1.0 Solar masses

Luminosity (solar luminosities)						
Teff	1,000	3,000	6,000	10,000	15,000	20,000
5,000	---	---	0.082	0.126	0.289	---
5,500	---	0.062	0.092	0.152	0.344	---
6,000	---	0.067	0.101	0.154	0.318	---
6,500	0.052	0.071	0.096	0.143	0.265	1.435
7,000	0.051	0.066	0.090	0.131	0.229	0.715
7,500	0.047	0.061	0.081	0.116	0.188	0.364
8,000	0.045	0.058	0.077	0.109	0.171	0.299
9,000	0.042	0.053	0.068	0.093	0.137	---
10,000	0.040	0.049	0.061	0.080	0.113	---
12,000	0.037	0.043	0.052	0.066	0.089	0.117
15,000	0.036	0.040	0.046	0.056	0.072	---
20,000	0.035	0.037	0.040	0.045	0.055	---
25,000	0.340	0.036	0.038	0.041	0.047	0.056
30,000	0.325	0.036	0.037	0.038	0.043	0.050

TABLES OF LINEAR RESULTS

TABLE OF NON-ADIABATIC GROWTH RATES

MODE : 0 Opacity table : BD9C Mass : 1.0 Solar masses

Teff	Luminosity (solar luminosities)					
	1,000	3,000	6,000	10,000	15,000	20,000
5,000	---	---	0.213	1.561	5.390	0.417
5,500	---	0.459	0.579	3.244	5.733	0.268
6,000	---	0.104	1.322	3.796	5.482	---
6,500	0.363	0.383	1.982	3.520	5.042	4.995
7,000	0.280	0.516	1.591	2.937	3.369	4.095
7,500	0.443	0.485	0.815	1.374	2.580	5.670
8,000	0.678	0.220	0.185	1.170	2.232	2.777
9,000	-0.200	-0.487	-2.155	0.472	1.291	---
10,000	-0.622	-0.743	-2.714	-4.223	-2.847	---
12,000	-0.471	-0.786	-1.749	-2.461	-1.826	-1.274
15,000	-0.157	-0.442	-1.236	-1.371	-0.718	---
20,000	-0.419	-0.796	-0.557	-0.866	-0.637	---
25,000	-0.233	-0.377	-0.314	-0.666	-0.698	-0.313
30,000	-0.137	-0.181	-0.186	-0.770	-1.081	-1.046

TABLE OF NON-ADIABATIC PHI

MODE : 0 Opacity table : BD9C Mass : 1.0 Solar masses

Teff	Luminosity (solar luminosities)					
	1,000	3,000	6,000	10,000	15,000	20,000
5,000	---	---	172.100	173.000	174.000	175.000
5,500	---	173.600	171.900	173.800	176.200	174.000
6,000	---	171.800	174.300	175.900	176.300	---
6,500	169.700	173.200	175.800	173.400	175.000	168.000
7,000	169.700	175.200	165.700	164.700	163.400	162.900
7,500	176.400	156.100	147.200	149.100	155.300	165.800
8,000	172.000	136.200	128.600	147.200	153.500	153.800
9,000	104.600	62.200	20.600	147.400	139.600	---
10,000	48.300	7.600	-45.200	-67.600	-40.800	---
12,000	1.200	-35.300	-62.000	---	-67.000	-11.800
15,000	-9.200	-43.800	-65.200	-71.300	-72.600	---
20,000	0.900	-18.100	-53.600	-61.700	-63.700	---
25,000	-4.200	-11.600	-26.700	-50.100	-49.800	-28.500
30,000	-5.200	-23.900	-33.700	-36.100	-34.000	-9.900

TABLES OF LINEAR RESULTS

TABLE OF NON-ADIABATIC PERIODS

MODE : 1 Opacity table : BD9C Mass : 1.0 Solar masses

Luminosity (solar luminosities)						
Teff	1,000	3,000	6,000	10,000	15,000	20,000
5,000	---	---	40.900	58.600	74.400	52.810
5,500	---	18.180	29.780	40.950	50.700	37.380
6,000	---	13.990	22.410	30.750	37.750	---
6,500	4.260	9.650	15.980	21.440	26.140	29.860
7,000	3.210	7.820	12.830	16.780	21.360	25.950
7,500	2.440	5.880	9.480	12.080	16.920	37.750
8,000	2.110	5.020	8.040	10.470	14.820	21.140
9,000	1.450	3.410	5.190	7.170	10.270	---
10,000	1.010	2.460	5.010	7.660	6.670	---
12,000	0.570	1.500	2.770	2.880	3.280	11.670
15,000	0.300	0.790	1.480	1.560	2.160	---
20,000	0.110	0.300	0.570	0.930	1.300	---
25,000	0.530	0.140	0.270	0.440	0.690	0.870
30,000	0.290	0.740	0.140	0.250	0.390	0.660

TABLE OF ADIABATIC PERIODS

MODE : 1 Opacity table : BD9C Mass : 1.0 Solar masses

Luminosity (solar luminosities)						
Teff	1,000	3,000	6,000	10,000	15,000	20,000
5,000	---	---	40.890	58.390	73.880	84.190
5,500	---	18.170	29.660	40.700	50.400	57.670
6,000	---	13.960	22.310	30.580	37.870	---
6,500	4.250	9.630	15.990	21.770	26.880	31.110
7,000	3.210	7.830	13.010	17.560	21.560	24.850
7,500	2.440	5.970	---	13.610	16.690	19.110
8,000	2.120	5.190	8.770	12.040	14.780	16.970
9,000	1.470	3.640	6.270	8.820	11.000	---
10,000	1.020	2.520	4.440	6.390	8.130	---
12,000	0.570	1.410	2.480	3.760	4.970	5.900
15,000	0.290	0.730	1.310	2.020	2.780	---
20,000	0.110	0.280	0.500	0.790	1.140	---
25,000	0.530	0.130	0.240	0.370	0.540	0.720
30,000	0.290	0.730	0.130	0.210	0.290	0.370

TABLES OF LINEAR RESULTS

TABLE OF NON-ADIABATIC Q VALUES

MODE : 1 Opacity table : BD9C Mass : 1.0 Solar masses

Luminosity (solar luminosities)						
Teff	1,000	3,000	6,000	10,000	15,000	20,000
5,000	---	---	0.039	0.038	0.035	0.020
5,500	---	0.038	0.037	0.035	0.032	0.019
6,000	---	0.036	0.034	0.032	0.029	---
6,500	0.033	0.033	0.032	0.030	0.027	0.025
7,000	0.031	0.033	0.032	0.029	0.027	0.026
7,500	0.031	0.032	0.031	0.027	0.028	0.050
8,000	0.031	0.032	0.030	0.027	0.028	0.032
9,000	0.030	0.031	0.028	0.026	0.028	---
10,000	0.029	0.031	0.038	0.039	0.025	---
12,000	0.029	0.033	0.037	0.026	0.021	0.062
15,000	0.028	0.032	0.036	0.026	0.026	---
20,000	0.025	0.030	0.034	0.038	0.039	---
25,000	0.242	0.027	0.033	0.036	0.041	0.042
30,000	0.233	0.257	0.030	0.035	0.040	0.055

TABLE OF ADIABATIC Q VALUES

MODE : 1 Opacity table : BD9C Mass : 1.0 Solar masses

Luminosity (solar luminosities)						
Teff	1,000	3,000	6,000	10,000	15,000	20,000
5,000	---	---	0.039	0.038	0.035	0.032
5,500	---	0.038	0.037	0.035	0.032	0.029
6,000	---	0.036	0.034	0.032	0.029	---
6,500	0.033	0.033	0.032	0.030	0.027	0.026
7,000	0.031	0.033	0.032	0.030	0.027	0.025
7,500	0.031	0.033	0.033	0.030	0.028	0.025
8,000	0.031	0.033	0.033	0.031	0.028	0.026
9,000	0.030	0.033	0.033	0.032	0.029	---
10,000	0.029	0.032	0.033	0.033	0.031	---
12,000	0.029	0.031	0.033	0.034	0.032	0.031
15,000	0.027	0.030	0.032	0.034	0.034	---
20,000	0.025	0.028	0.030	0.032	0.034	---
25,000	0.242	0.027	0.029	0.030	0.032	0.035
30,000	0.234	0.255	0.028	0.029	0.030	0.031

TABLES OF LINEAR RESULTS

TABLE OF NON-ADIABATIC GROWTH RATES

MODE : 1 Opacity table : BD9C Mass : 1.0 Solar masses

Luminosity (solar luminosities)

Teff	1,000	3,000	6,000	10,000	15,000	20,000
5,000	---	---	0.110	0.266	0.374	0.404
5,500	---	0.512	0.193	0.306	0.236	0.228
6,000	---	0.947	0.249	0.185	0.663	---
6,500	0.166	0.160	0.157	-0.189	-0.670	-1.473
7,000	0.362	0.161	0.110	-0.583	-1.224	-1.460
7,500	0.493	0.251	-0.232	-0.495	-0.670	3.049
8,000	0.829	0.217	-0.984	-0.200	0.761	-7.930
9,000	0.306	-0.443	-0.261	0.303	1.116	---
10,000	-0.148	-1.247	-1.177	0.293	1.471	---
12,000	-0.223	-0.978	-0.628	-0.160	-0.729	-7.190
15,000	-0.152	-0.611	-0.377	-0.190	-0.859	---
20,000	-0.630	-0.442	-0.228	-0.564	-1.419	---
25,000	-0.274	-0.354	-0.393	-0.279	-1.470	-4.017
30,000	-0.139	-0.295	-0.682	-0.217	-1.204	-0.932

TABLE OF NON-ADIABATIC PHI

MODE : 1 Opacity table : BD9C Mass : 1.0 Solar masses

Luminosity (solar luminosities)

Teff	1,000	3,000	6,000	10,000	15,000	20,000
5,000	---	---	174.900	176.000	174.800	155.500
5,500	---	175.400	175.000	174.100	174.500	162.200
6,000	---	174.300	175.200	175.300	175.700	---
6,500	171.900	173.700	177.300	175.800	175.100	175.400
7,000	172.000	177.100	174.100	169.200	169.800	173.800
7,500	176.200	168.100	159.000	161.200	167.100	154.800
8,000	177.000	153.200	145.100	157.600	164.300	212.700
9,000	123.500	84.100	139.000	147.500	152.600	---
10,000	59.900	-31.000	-148.000	144.000	140.800	---
12,000	-8.000	-69.700	-147.000	110.200	124.800	227.100
15,000	-24.900	-71.000	-153.700	98.700	94.600	---
20,000	-14.800	-49.400	-112.300	154.900	162.500	---
25,000	-11.700	-28.500	-69.500	180.200	136.600	202.000
30,000	-15.500	-38.900	-43.000	212.300	119.400	97.400

TABLES OF LINEAR RESULTS

TABLE OF NON-ADIABATIC PERIODS

MODE : 0 Opacity table : BD9C Mass : 1.2 Solar masses

Luminosity (solar luminosities)

Teff	1,000	3,000	6,000	10,000	15,000	20,000
5,000	---	---	74.200	137.500	265.800	373.100
5,500	---	27.230	56.560	118.900	187.600	220.200
6,000	---	21.300	50.750	93.000	127.800	149.400
6,500	6.140	17.290	35.880	57.110	77.360	89.990
7,000	4.690	13.150	25.860	39.910	53.480	62.070
7,500	3.250	8.930	16.990	25.460	33.150	37.820
8,000	2.720	7.390	14.030	20.440	26.290	29.660
9,000	1.790	4.800	9.020	18.420	15.230	18.410
10,000	1.210	3.220	6.510	13.560	26.370	32.880
12,000	0.670	1.730	3.550	7.450	13.870	18.860
15,000	---	0.860	1.730	3.440	6.050	9.110
20,000	---	0.330	0.600	1.110	1.990	3.190
25,000	0.660	0.160	0.280	0.480	0.830	1.280
30,000	0.360	0.920	0.160	0.250	0.420	0.920

TABLE OF ADIABATIC PERIODS

MODE : 0 Opacity table : BD9C Mass : 1.2 Solar masses

Luminosity (solar luminosities)

Teff	1,000	3,000	6,000	10,000	15,000	20,000
5,000	---	---	74.290	138.700	304.500	813.300
5,500	---	27.240	56.610	124.700	280.700	746.700
6,000	---	21.290	51.150	106.100	223.800	550.100
6,500	6.150	17.310	37.640	75.190	156.400	333.200
7,000	4.690	13.250	28.590	56.870	115.600	228.000
7,500	3.250	9.190	19.720	38.680	76.130	139.300
8,000	2.720	7.690	16.410	31.860	61.680	109.700
9,000	1.800	4.980	10.410	19.690	36.580	61.460
10,000	1.210	3.270	6.660	12.250	21.970	35.370
12,000	0.670	1.720	3.280	5.930	10.300	15.860
15,000	---	0.850	1.600	2.730	4.550	6.900
20,000	---	0.330	0.580	0.940	1.480	2.150
25,000	0.660	0.160	0.280	0.430	0.660	0.920
30,000	0.360	0.920	0.160	0.240	0.350	0.480

TABLES OF LINEAR RESULTS

TABLE OF NON-ADIABATIC Q VALUES

MODE : 0 Opacity table : BD9C Mass : 1.2 Solar masses

Luminosity (solar luminosities)

Teff	1,000	3,000	6,000	10,000	15,000	20,000
5,000	---	---	0.077	0.097	0.138	0.157
5,500	---	0.063	0.077	0.111	0.129	0.122
6,000	---	0.060	0.085	0.107	0.108	0.102
6,500	0.052	0.065	0.080	0.086	0.086	0.081
7,000	0.049	0.060	0.071	0.074	0.073	0.069
7,500	0.045	0.054	0.061	0.062	0.060	0.055
8,000	0.043	0.051	0.058	0.058	0.054	0.050
9,000	0.040	0.047	0.053	0.073	0.045	0.044
10,000	0.038	0.045	0.054	0.076	0.109	0.110
12,000	0.037	0.041	0.052	0.073	0.099	0.110
15,000	---	0.038	0.046	0.062	0.081	0.099
20,000	---	0.037	0.039	0.050	0.065	0.085
25,000	0.330	0.036	0.037	0.042	0.054	0.068
30,000	0.313	0.349	0.036	0.038	0.048	0.083

TABLE OF ADIABATIC Q VALUES

MODE : 0 Opacity table : BD9C Mass : 1.2 Solar masses

Luminosity (solar luminosities)

Teff	1,000	3,000	6,000	10,000	15,000	20,000
5,000	---	---	0.077	0.098	0.158	0.443
5,500	---	0.063	0.077	0.116	0.193	0.415
6,000	---	0.060	0.086	0.122	0.189	0.376
6,500	0.052	0.065	0.084	0.114	0.174	0.300
7,000	0.049	0.061	0.078	0.106	0.158	0.253
7,500	0.045	0.056	0.071	0.095	0.137	0.204
8,000	0.043	0.053	0.068	0.090	0.128	0.184
9,000	0.040	0.049	0.061	0.078	0.107	0.146
10,000	0.038	0.045	0.055	0.069	0.091	0.118
12,000	0.037	0.041	0.048	0.058	0.074	0.092
15,000	---	0.038	0.043	0.050	0.061	0.075
20,000	---	0.037	0.038	0.042	0.049	0.057
25,000	0.331	0.036	0.037	0.039	0.043	0.049
30,000	0.314	0.349	0.036	0.037	0.040	0.044

TABLES OF LINEAR RESULTS

TABLE OF NON-ADIABATIC GROWTH RATES

MODE : 0 Opacity table : BD9C Mass : 1.2 Solar masses

Luminosity (solar luminosities)

Teff	1,000	3,000	6,000	10,000	15,000	20,000
5,000	---	---	0.845	0.572	2.892	5.753
5,500	---	0.133	0.227	1.633	4.407	5.864
6,000	---	0.384	0.594	2.453	4.477	5.564
6,500	0.807	0.176	1.190	2.592	4.030	4.697
7,000	0.889	0.288	1.163	2.492	2.877	3.825
7,500	0.326	0.294	0.551	1.651	2.075	1.759
8,000	0.265	0.133	-0.971	0.727	1.587	2.078
9,000	-0.978	-0.269	-0.962	-5.107	1.058	1.290
10,000	-0.324	-0.492	-1.882	-3.570	-4.221	-1.668
12,000	-0.189	-0.425	-1.454	-2.416	-2.234	-1.092
15,000	---	-0.185	-1.041	-1.280	-1.156	-0.482
20,000	---	-0.305	-0.360	-0.774	-0.745	-0.563
25,000	-0.120	-0.168	-0.125	-0.640	-0.858	-0.667
30,000	-0.753	-0.792	-0.654	-0.541	-0.917	0.102

TABLE OF NON-ADIABATIC PHI

MODE : 0 Opacity table : BD9C Mass : 1.2 Solar masses

Luminosity (solar luminosities)

Teff	1,000	3,000	6,000	10,000	15,000	20,000
5,000	---	---	171.300	171.800	172.600	174.500
5,500	---	172.200	172.600	172.000	175.500	176.600
6,000	---	172.900	172.800	175.300	175.600	175.300
6,500	169.800	170.900	175.700	171.100	172.200	171.700
7,000	170.800	175.300	167.400	167.300	161.500	165.900
7,500	174.400	157.900	143.900	155.500	150.200	---
8,000	174.500	134.200	117.800	142.000	146.000	150.100
9,000	112.600	70.200	61.500	-58.300	143.800	137.900
10,000	45.200	8.900	-28.900	-60.800	-73.400	5.200
12,000	2.800	-25.800	-53.500	-69.600	-76.600	-62.200
15,000	---	-32.400	-57.100	-68.900	-71.200	-72.100
20,000	---	-7.700	-45.500	-61.400	-64.500	-67.800
25,000	-3.400	-12.800	-19.200	-44.300	-46.800	-47.000
30,000	-2.400	-18.900	-30.400	-38.700	-43.100	-82.100

TABLES OF LINEAR RESULTS

TABLE OF NON-ADIABATIC PERIODS

MODE : 1 Opacity table : BD9C Mass : 1.2 Solar masses

Luminosity (solar luminosities)

Teff	1,000	3,000	6,000	10,000	15,000	20,000
5,000	---	---	39.840	54.660	71.580	83.460
5,500	---	17.430	27.530	38.740	49.220	56.700
6,000	---	12.790	20.800	29.080	36.840	42.160
6,500	3.840	8.730	14.810	20.740	25.420	29.450
7,000	2.890	7.060	11.970	16.490	19.980	24.950
7,500	2.200	5.320	8.890	12.120	15.230	13.690
8,000	1.900	4.550	7.550	10.230	31.150	17.360
9,000	1.310	3.100	4.920	10.870	9.020	11.820
10,000	0.910	2.200	4.380	4.660	4.990	7.760
12,000	0.510	1.300	2.450	3.830	3.550	3.780
15,000	---	0.680	1.300	2.040	1.990	1.760
20,000	---	0.260	0.500	0.800	1.470	1.450
25,000	0.470	0.120	0.230	0.390	0.580	0.780
30,000	0.260	0.650	0.120	0.220	0.320	0.620

TABLE OF ADIABATIC PERIODS

MODE : 1 Opacity table : BD9C Mass : 1.2 Solar masses

Luminosity (solar luminosities)

Teff	1,000	3,000	6,000	10,000	15,000	20,000
5,000	---	---	39.850	54.500	71.240	82.840
5,500	---	17.430	27.460	38.570	48.890	56.390
6,000	---	12.780	20.730	28.960	36.770	42.410
6,500	3.840	8.710	14.820	20.870	26.050	30.190
7,000	2.890	7.070	12.090	16.910	20.970	24.190
7,500	2.200	5.380	9.260	13.060	16.280	18.690
8,000	1.900	4.670	8.080	11.500	14.430	16.600
9,000	1.320	3.250	5.720	8.320	10.650	12.370
10,000	0.920	2.250	4.010	5.960	7.790	9.170
12,000	0.510	1.260	2.210	3.440	4.670	5.600
15,000	---	0.650	1.160	1.810	2.550	3.170
20,000	---	0.250	0.450	0.690	1.010	1.310
25,000	0.470	0.120	0.210	0.330	0.470	0.620
30,000	0.260	0.650	0.120	0.180	0.260	0.320

TABLES OF LINEAR RESULTS

TABLE OF NON-ADIABATIC Q VALUES

MODE : 1 Opacity table : BD9C Mass : 1.2 Solar masses

Luminosity (solar luminosities)						
Teff	1,000	3,000	6,000	10,000	15,000	20,000
5,000	---	---	0.041	0.039	0.037	0.035
5,500	---	0.040	0.038	0.036	0.034	0.032
6,000	---	0.036	0.035	0.033	0.031	0.029
6,500	0.033	0.033	0.033	0.031	0.028	0.027
7,000	0.030	0.032	0.033	0.031	0.027	0.028
7,500	0.030	0.032	0.032	0.030	0.027	0.020
8,000	0.030	0.032	0.031	0.029	0.027	0.029
9,000	0.029	0.030	0.029	0.043	0.026	0.028
10,000	0.029	0.031	0.036	0.026	0.025	0.026
12,000	0.028	0.031	0.036	0.037	0.025	0.022
15,000	---	0.031	0.035	0.037	0.027	0.026
20,000	---	0.028	0.033	0.036	0.048	0.039
25,000	0.237	0.026	0.030	0.035	0.038	0.041
30,000	0.227	0.249	0.028	0.033	0.036	0.057

TABLE OF ADIABATIC Q VALUES

MODE : 1 Opacity table : BD9C Mass : 1.2 Solar masses

Luminosity (solar luminosities)						
Teff	1,000	3,000	6,000	10,000	15,000	20,000
5,000	---	---	0.041	0.039	0.037	0.035
5,500	---	0.040	0.038	0.036	0.034	0.031
6,000	---	0.036	0.035	0.033	0.031	0.029
6,500	0.033	0.033	0.033	0.032	0.029	0.027
7,000	0.030	0.032	0.033	0.031	0.029	0.027
7,500	0.030	0.033	0.033	0.032	0.029	0.027
8,000	0.030	0.032	0.033	0.032	0.030	0.028
9,000	0.030	0.032	0.033	0.033	0.031	0.029
10,000	0.029	0.031	0.033	0.034	0.032	0.031
12,000	0.028	0.030	0.032	0.034	0.033	0.033
15,000	---	0.029	0.031	0.033	0.034	0.034
20,000	---	0.028	0.029	0.031	0.033	0.035
25,000	0.238	0.026	0.028	0.030	0.031	0.033
30,000	0.229	0.248	0.027	0.028	0.029	0.030

TABLES OF LINEAR RESULTS

TABLE OF NON-ADIABATIC GROWTH RATES

MODE : 1 Opacity table : BD9C Mass : 1.2 Solar masses

Teff	Luminosity (solar luminosities)					
	1,000	3,000	6,000	10,000	15,000	20,000
5,000	---	---	0.751	0.177	0.316	0.369
5,500	---	0.350	0.130	0.264	0.319	0.248
6,000	---	0.586	0.201	0.266	0.102	0.290
6,500	0.739	0.112	0.198	0.303	-0.410	-0.892
7,000	0.180	0.145	0.194	-0.118	-0.880	-1.569
7,500	0.428	0.214	0.157	-0.343	-0.608	-1.014
8,000	0.322	0.179	-0.616	-0.381	-0.177	-0.387
9,000	0.121	-0.242	-0.531	-0.802	0.745	1.160
10,000	-0.100	-0.880	-1.748	0.103	0.732	1.834
12,000	-0.129	-0.874	-0.759	-0.509	-0.418	2.499
15,000	---	-0.590	-0.436	-0.558	-0.384	-0.152
20,000	---	-0.295	-0.453	-0.198	-0.852	-1.157
25,000	-0.125	-0.216	-0.527	-0.226	-0.684	-1.953
30,000	-0.699	-0.127	-0.647	-0.330	-0.368	-1.149

TABLE OF NON-ADIABATIC PHI

MODE : 1 Opacity table : BD9C Mass : 1.2 Solar masses

Teff	Luminosity (solar luminosities)					
	1,000	3,000	6,000	10,000	15,000	20,000
5,000	---	---	174.200	175.100	175.200	174.600
5,500	---	174.100	175.100	174.000	174.700	175.100
6,000	---	174.800	174.700	175.200	175.400	175.100
6,500	172.000	172.300	176.600	175.900	173.800	173.000
7,000	173.000	175.800	175.400	172.700	167.100	170.200
7,500	174.800	169.500	158.600	159.200	161.200	170.800
8,000	178.000	151.700	139.200	148.800	159.000	162.700
9,000	128.200	91.900	129.200	163.500	151.700	150.600
10,000	55.200	-8.300	-103.900	135.100	139.900	141.300
12,000	-4.600	-51.900	-113.300	174.300	111.300	125.900
15,000	---	-55.600	-113.100	-175.000	92.800	121.400
20,000	---	-35.900	-75.800	-168.900	117.100	166.600
25,000	-8.800	-25.300	-46.600	-117.500	145.000	142.900
30,000	-11.000	-32.300	-40.200	-81.800	163.200	109.600

APPENDIX F
STABILITY EDGES OF LINEAR SURVEYS

TABLES OF LINEAR STABILITY EDGES

F.2 LINEAR STABILITY EDGES FOR OPACITY TABLE DXIX

OPACITY TABLE : DXIX

MASS : $0.8M_{\odot}$

Luminosity L/L_{\odot}	Fundamental Blue Edge	First overtone edges			
		Red 1	Blue 1	Red 2	Blue 2
1,000	3.861	---	3.816	---	---
3,000	3.857	---	3.857	---	---
6,000	3.815	---	3.676	---	---
10,000	3.817	3.829	3.854	3.946	4.032
15,000	4.103	3.784	3.929	3.967	4.089
20,000	4.670	3.699	3.888	3.942	3.950

OPACITY TABLE : DXIX

MASS : $1.0M_{\odot}$

Luminosity L/L_{\odot}	Fundamental		First overtone Blue Edge
	Red Edge	Blue Edge	
1,000	---	3.867	3.850
3,000	---	3.872	3.893
6,000	---	3.830	3.821
10,000	---	3.804	3.670
15,000	3.749	3.821	4.103
20,000	3.783	4.179	4.243

OPACITY TABLE : DXIX

MASS : $1.2M_{\odot}$

Luminosity L/L_{\odot}	Fundamental Blue Edge	First overtone	
		Red Edge	Blue Edge
1,000	3.867	---	3.891
3,000	3.852	---	3.867
6,000	3.831	---	3.818
10,000	3.800	---	3.729
15,000	3.813	3.887	4.031
20,000	4.032	3.975	4.051

TABLES OF LINEAR STABILITY EDGES

F.3 LINEAR STABILITY EDGES FOR OPACITY TABLE BD9C

OPACITY TABLE : BD9C

MASS : $0.8M_{\odot}$

Luminosity L/L_{\odot}	Fundamental		First overtone	
	Red Edge	Blue Edge	Red edge	Blue Edge
1,000	---	3.906	---	3.913
3,000	---	3.911	---	3.921
6,000	---	3.953	3.974	4.026
10,000	---	3.966	3.911	4.054
15,000	3.786	4.427	3.975	4.345
20,000	3.686	4.405	3.879	4.746

OPACITY TABLE : BD9C

MASS : $1.0M_{\odot}$

Luminosity L/L_{\odot}	Fundamental Blue Edge	First overtone edges		
		Blue 1	Red 1	Blue 2
1,000	3.938	3.984	---	---
3,000	3.915	3.915	---	---
6,000	3.902	3.852	---	---
10,000	3.955	3.795	3.918	4.059
15,000	3.966	3.791	3.889	4.054
20,000	4.024	3.750	3.853	3.885

OPACITY TABLE : BD9C

MASS : $1.2M_{\odot}$

Luminosity L/L_{\odot}	Fundamental Blue Edge	First overtone edges		
		Blue 1	Red 1	Blue 2
1,000	3.912	3.978	---	---
3,000	3.916	3.921	---	---
6,000	3.887	3.886	---	---
10,000	3.906	3.832	3.994	4.015
15,000	3.961	3.778	3.910	4.048
20,000	3.973	3.780	3.913	4.164